UNIVERSIDAD NACIONAL AUTÓNOMA DE MÉXICO

Maestría y Doctorado en Ciencias Bioquímicas

IDENTIFICACIÓN DEL HIDROXIMETILOMA DURANTE LA DIFERENCIACIÓN DE HEPATOCITOS, UN INDICIO EN EL ESTUDIO DEL CÁNCER HEPÁTICO

TESIS

QUE PARA OPTAR POR EL GRADO DE:

Doctor en Ciencias

PRESENTA:
M. en C. JESÚS RAFAEL RODRÍGUEZ AGUILERA

TUTORES

DRA. VICTORIA CHAGOYA HAZAS
Instituto de Fisiología Celular, UNAM
DR. HÉCTOR HERNÁNDEZ VARGAS
Centre de Recherche en Cancérologie de Lyon, INSERM

MIEMBROS DEL COMITÉ TUTOR

DR. FÉLIX RECILLAS TARGA
Instituto de Fisiología Celular, UNAM
DR. EMILIO ROJAS DEL CASTILLO
Instituto de Investigaciones Biomédicas, UNAM

Ciudad Universitaria, Cd.Mx., marzo, 2020

AGRADECIMIENTOS ACADÉMICOS

El presente trabajo fue elaborado en el Instituto de Fisiología Celular de la UNAM, en los laboratorios de la Dra. Victoria Chagoya Hazas y del Dr. Félix Recillas Targa, así como en el grupo de epigenética de la Agencia Internacional de Investigación en Cáncer (EGE-IARC) bajo la supervisión del Dr. Héctor Hernández Vargas, con los apoyos de DGAPA-UNAM IN208915 y el donativo de Vela Advisor SA de CV para VCS; *Agence Nationale de Recherches sur le SIDA et les Hépatites Virales* ANRS, Referencia No. ECTZ47287 y ECTZ50137, *Institut National du Cancer* AAP PLBIO 2017 (proyecto: *T cell tolerance to microbiota and colorectal cancers*) *La Ligue Nationale Contre Le Cancer Comité d'Auvergne-Rhône-Alpes* AAP 2018 para HHV. Agradezco a los Doctores la confianza, el apoyo, la contribución al conocimiento y a mi formación académica.

Los estudios del M. en C. Jesús Rafael Rodríguez Aguilera se realizaron con el apoyo de la beca de Doctorado del Consejo Nacional de Ciencia y Tecnología (CONACyT CVU 508509), el apoyo a ayudante de investigador del Sistema Nacional de Investigadores (SNI-CONACyT EXP. INV. 12666 EXP. AYTE. 7507), la beca mixta del CONACyT (CVU 508509), un complemento de estipendio de IARC (Ref. STU. 2052), la *Aide au logement* de CAF (No Allocataire: 4384941 W) y el apoyo para manutención en el extranjero por parte de la Dra. María de Lourdes Rodríguez Aguilera.

Agradezco y reconozco al comité tutor que asesoró esta tesis, el cual estuvo integrado por:

Dra. Victoria Eugenia Chagoya Hazas	Instituto de Fisiología Celular
Dr. Félix Recillas Targa	Instituto de Fisiología Celular
Dr. Emilio Rojas del Castillo	Instituto de Investigaciones Biomédicas

Asesorías fundamentales para la realización de éste trabajo fueron proporcionadas por la Dra. Szilvia Ecsedi, la Dra. Chloe Goldsmith, la Dra. Marie-Pierre Cros, la Biol. Nuria Guerrero Celis, la Dra. Rebeca Pérez Cabeza de Vaca, la Dra. Mariana Domínguez López, la Dra. Isabelle Chemin, el Dr. Pedro Valencia Mayoral, el Dr. Ramón González García-Conde, la Dra. Mayra Furlan-Magaril y el Dr. Rodrigo Arzate Mejía.

Agradezco el apoyo técnico brindado por el Dr. Cyrille Cuenin, la Dra. Severine Croze, la Dra. Florence Le Calvez-Kelm, el Dr. Geoffroy Durand, el Dr. Zdenko Herceg, la Dra. Aurelie Salle, la Biól. Georgina Guerrero Avendaño, la Dra. Rosario Pérez Molina, la Dra. Nora Gabriela Velasco Loyden y el Dr. Enrique Chávez. Así mismo se reconoce el trabajo de los laboratoristas Jesús Salgado Cortés, Gianelli Cortés González y Xóchitl Castrejón Galindo, así como el de las secretarias Rosario Villaseñor Ávila y Gabriela Valdés Silva.

Gracias por el apoyo durante los experimentos a la QFB Mónica Liliana Guzmán López; gracias también a la Lic. María Elena Rodríguez Aguilera y a la Dra. Luz Lazos Ramírez por sus observaciones y comentarios sobre el escrito de la Tesis.

Mi agradecimiento a la Unidad de Bilogía Molecular del Instituto de Fisiología Celular por el apoyo brindado de la Dra. Laura Ongay, la Dra. Minerva Cabrera Mora y la Dra. María Guadalupe Códiz Huerta; así como a la Unidad de Cómputo, Ing. Ivett Rosas Arciniega e Ing. Juan Manuel Barbosa Castillo.

Agradezco al "Programa de Apoyo a los Estudios del Posgrado" (PAEP) por los recursos brindados para realizar una estancia de Investigación en la IARC, Lyon, Francia.

Finalmente mi gratitud a los miembros del Jurado que revisaron y enriquecieron este trabajo con sus observaciones y comentarios.

PRESIDENTE	Dr. José Pedraza Chaverri	(FQ-UNAM)
VOCAL	Dra. Viviana Valadez Graham	(IBT-UNAM)
VOCAL	Dr. Julio Isael Pérez Carreón	(INMEGEN)
VOCAL	Dr. Víctor Julián Valdés Rodríguez	(IFC-UNAM)
SECRETARIO	Dra. Mayra Furlan Magaril	(IFC-UNAM)

A la UNAM por adoptarme y ser mi segunda casa desde hace 13.5 años.

“Espero que, por fortuna, las células HepaRG no hayan revelado completamente todos sus secretos biológicos, principalmente aquellos relacionados con sus propiedades de troncalidad y que continúen emocionando a los científicos durante mucho tiempo”

Dra. Christiane Guguen-Guillouzo

AGRADECIMIENTOS PERSONALES/ PERSONAL ACKNOWLEDGMENTS / REMERCIEMENTS PERSONNELS / AGRADECIMENTOS PESSOAIS

A Dios porque que sin El no puedo hacer nada.

A mi mamá María Elena Aguilera Mendieta †, a mi papá Jesús Rodríguez Flores † y a mis hermanas María Elena y María de Lourdes por todo el amor, consejos y apoyo.

A mis amigos que siempre están presentes.

A la Dra. Norma Silvia Sánchez Sánchez por introducirme al mundo de la investigación.

A la M. en C. Lucía Yáñez Maldonado, a la Biól. Susana Vidrio Gómez † y a la M. en C. Lidia Martínez Pérez †, por todo su apoyo en mi formación en el laboratorio y por su amistad.

Al Dr. Héctor Hernández Vargas, por la confianza, apoyo y dirección en la realización de este proyecto.

A la Dra. Victoria Eugenia Chagoya Hazas y al Dr. Félix Recillas Targa por permitirme formar parte de su equipo de investigación.

Gracias Rebe, Nu, Carlos, Adrián, Charis, Paco, Rodri, Geito, Karina, Jessi, Franco, Marianita, Brendita, César, Ana, Marco, Aldo, Ceci, Marlene, Helivier, Pablo, Chayito y Gaby, por compartir su amistad, cariño y las excelentes experiencias en el laboratorio y más allá.

Merci beaucoup, Marie-Pierre Cros, pour ta patience, ton soutien et ton amitié.

Cirmi and Chloé, thanks so much for your help, advice and for being aware of the progress of the project.

To Athena Sklias and Andrea Halaburkova for all the support to going ahead.

Annita, Anne-Claire, Oscar, Bele, Gaby, Whyara, Jessica, Erika and Miguel, thanks for your friendship and good moments shared in France. Mercie beaucoup. Muito obrigado. Mil gracias.

Carol et Jean-Jacques, merci beaucoup de m'avoir adopté lors de mon séjour en France.

Ángeles y Susi, muchas gracias por hacerme sentir como si estuviera en México, durante mi estancia en Francia.

To Dr. Bilal Sheikh from "Helmholtz Institute for Metabolism, Obesity and Vascular Research", for giving me the opportunity to take the next step in my professional career.

A mis sobrinos Lulú, Pedro y Sebastián como aliciente en sus estudios.

ÍNDICE

ABREVIATURAS

Abreviatura	Significado
2-HG	2-hidroxiglutarato
5caC	5-carboxilcitosina
5fC	5-formilcitosina
5hmC	5-hidroximetilcitosina
5mC	5-metilcitosina
AFP	Alfa feto proteína
ALB	Albumina
ALDOB	Aldolasa B
APC	Gen supresor de tumores *Adenomatous polyposis coli*
AR	Receptor de andrógenos
BER	Sistema de reparación de DNA por escisión de bases
BS	Conversión de DNA con bisulfito de sodio
C	Citosina
CCl4	Tetracloruro de carbono
CD	Dominio cut
CD49F	Integrina alfa 6
Cdx-2	Proteína caudal homeobox 2
CEP85	Proteína centrosomal 85
Cfp1	Proteína 1 con subunidad conservada con dedo CXXC
CGI	Isla CpG
ChIP	Imnunoprecipitación de la cromatina
ChromHMM	Segmentación del estado de la cromatina por el modelo *Hidden Markov*
CK	Citoqueratina
Col2a1	Gen de la colágena 1 alfa 1
CpG	Dinucleótido citosina guanina
CPT2	Carnitina O-palmitoiltransferasa 2
CTCF	Factor de unión a CCCTC
CXXC	Dominio rico en cisteína implicado en las secuencias de unión a DNA que contienen dinucleótidos CpG
CYP3A4	Citocromo P450 3A4
DBD	Dominio de unión a DNA
DD	Dominio de dimerización
DEG	Gen diferencialmente expresado
DEN	Dietilnitrosamina
DhMP	Posición diferencialmente hidroximetilada
DMOG	Glicina dimetiloxalílica
DMP	Posición diferencialmente metilada
DMSO	Dimetilsulfóxido

Continuación Abreviaturas

Abreviatura	Significado
DNMT1	DNA metiltransferasa 1
DNMT3A	DNA metiltransferasa 3A
DNMT3B	DNA metiltransferasa 3B
DTT	Ditiotreitol
ESC	Célula troncal embrionaria
FOX	Proteínas *Forkhead box*
G	Guanina
GATA1	Factor de unión 1 a la secuencia GATA
GDF7	Factor de diferenciación de crecimiento 7
GEO	*Gene Expression Omnibus*
GSTA	Glutatión S-transferasa alfa
GSTP1	Glutatión S-transferasa P1
H3K4me2	Dimetilación de la lisina 4 de la histona H3
HBV	Virus de la hepatitis B
HCC	Carcinoma hepatocelular
HClO4	Ácido perclórico
HCV	Virus de la hepatitis C
HD	Homeodominio divergente
HDAC4	Desacetilasa de histonas 4
HNF	Factor nuclear hepático
HNF4A	Factor nuclear hepático 4A
HPLC	Cromatografía líquida de alta resolución acoplada a espectrometría de masas
IDH	Isocitrato deshidrogenasa
IDH3G	Isocitrato deshidrogenasa (NAD (+)) Subunidad 3 no catalítica Gamma
IFC-305	Aspartato de adenosina
INSERM	Instituto Nacional de Investigación Médica y de Salud de Francia
JBP1	Proteína 1 de unión a JAK o Proteína metiltransferasa de arginina 5
JBP2	Proteína 2 de unión a JAK
K2CO3	Carbonato de potasio
Kdm2	Desmetilasa de lisina 2
LBD	Dominio de unión a ligando
LINE	Elementos nucleares largos intercalados
MBD	Proteína de unión a DNA metilado
MeCP2	Proteína 2 de unión a CpG metilado
MET	Proteína tirosina cinasa Met
Met	Metionina
Mimk	*Myomarker*
MLE	*Maximum Likelihood Estimation*
Myf6	Factor miogénico 6

Continuación Abreviaturas

Abreviatura	Significado
Myog	Miogenina
NFE2L2	Factor 2 relacionado con el factor nuclear eritroide 2
NH4H2PO4	Difosfato de amonio
OC	ONECUT / HNF6
OxBS	Conversión de DNA oxidante con bisulfito de sodio
p16	Inhibidor 2A de cinasa dependiente de ciclina
PBS	Solución reguladora de pH salina de fosfatos
PCR	Reacción en cadena de la polimerasa
PolII	RNA polimerasa II
PPARγ	Receptor gama activado por proliferadores de peroxisomales
PTPRK	Proteína tirosina fosfatasa kapa de tipo receptor
RAB7A	Proteína relacionada con RAS 7ª
RASSF1A	Proteína 1 que contiene el dominio de asociación Ras
Runx2	Factor de transcripción 2 relacionado con Runt
SAM	S-adenosilmetionina
SBNO2	Strawberry Notch Homolog 2
SERPINA1	Alfa 1-antitripsina
SFRS4	Factor 4 de empalme rico en serina y arginina
siRNA	RNA de silenciamiento
SOX	Factor de transcripción SOX
STB box	Región enriquecida en serina/treonina/prolina
TCHP	Proteína de unión a filamentos de queratina tricopleína
TDG	Glucosilasa de timina de DNA
TET	Dioxigenas de citosina modificada Tet Eleven Translocation
TOF	Cromatografía líquida de interacción hidrofílica de cuadrupolo
TSS	Sitio de inicio de la transcripción
UBE2I	Pequeño modificador similar a la ubiquitina (SUMO)- enzima conjugadora E2I
α-KG	Alfa cetoglutarato / 2-oxoglutarato

RESUMEN

Una pregunta básica relacionada con los patrones diferenciales de expresión génica es: ¿cómo se obtienen diferentes tipos celulares en un organismo, a pesar de contener el mismo templado de DNA? Desde que la 5-hidroximetilcitosina (5hmC) surgió como un metabolito intermediario en la desmetialción activa del DNA, se han incrementado los esfuerzos para dilucidar su función como una modificación estable en el genoma, incluyendo su papel en el establecimiento de patrones de expresión de genes específicos de tejido. En este trabajo se estudia la distribución de la 5hmC a nivel de genoma completo en un estado temprano de la diferenciación *in vitro* de células humanas tipo hepatocito. Se observó un incremento global de 5hmC así como una reducción de 5-metilcitosina a una semana de la diferenciación *in vitro* de progenitores bipotenciales, al tiempo en el que el programa de transcripción hepático ya se ha establecido; estos datos correlacionan con el enriquecimiento, recientemente descrito, de 5hmC mediado por TET1 sobre la región promotora del regulador maestro de la diferenciación de hepatocitos *HNF4A*, la cual precede la diferenciación de células hepáticas progenitoras adultas *in vitro*. La 5hmC se encontró, en general, más elevada en los cuerpos de genes sobreexpresados. Además se observó que al incrementar los niveles de S-adenosilmentionina a través de un derivado de adenosina, se disminuye el enriquecimiento de 5hmC, conduciendo a una menor adquisición de marcadores de identidad celular. Estos resultados sugieren que la 5hmC puede ser un marcador de la identidad celular, así como un biomarcador útil en condiciones asociadas con la desdiferenciación celular como en el cáncer hepático.

ABSTRACT

A basic question linked to differential patterns of gene expression is how cells reach different fates despite using the same DNA template. Since 5-hydroxymethylcytosine (5hmC) emerged as an intermediate metabolite in active DNA demethylation, there have been increasing efforts to elucidate its function as a stable modification of the genome, including a role in establishing such tissue-specific patterns of expression. Recently it has been described a TET1-mediated enrichment of 5hmC on the promoter region of the master regulator of hepatocyte identity, *HNF4A*, which precedes differentiation of liver adult progenitor cells *in vitro*. This work assessed the genome-wide distribution of 5hmC at early *in vitro* differentiation of human hepatocyte-like cells. A global increase in 5hmC as well as a reduction of 5-methylcytosine were found after one week of *in vitro* differentiation from bipotent progenitors, at a time when the liver transcript program is already established. 5hmC was overall higher at the bodies of overexpressed genes. Furthermore, increasing S-adenosylmethionine levels through an adenosine derivative we decrease 5hmC enrichment, triggering an impaired acquisition of hepatic identity markers. These results suggest that 5hmC could be a marker of cell identity, as well as a useful biomarker in conditions associated with cell de-differentiation such as liver cancer.

RÉSUMÉ

Une des questions fondamentales liée aux schémas différentiels d'expression des gènes est de savoir comment les cellules parviennent à des destinées différentes malgré l'utilisation de la même matrice d'ADN. Depuis que la 5-hydroxyméthylcytosine (5hmC) a été identifiée en tant que métabolite intermédiaire dans la déméthylation active de l'ADN, des efforts croissants ont été déployés pour élucider sa fonction en tant que modification stable du génome, notamment pour établir de tels modes d'expression spécifiques à un tissu. Récemment, il a été décrit un enrichissement de 5hmC médié par TET1 sur la région promotrice du gène régulateur principal de l'identité des hépatocytes, HNF4A, qui précède la différenciation in vitro des cellules progénitrices adultes du foie. Ce travail a évalué la distribution à l'échelle du génome de 5hmC au début de la différenciation in vitro de cellules ressemblant à des hépatocytes humains. Une augmentation globale de 5hmC ainsi qu'une réduction de la 5-méthylcytosine ont été observées après une semaine de différenciation in vitro des progéniteurs bipotents, à un moment où le programme de transcription du foie est déjà établi. 5hmC était globalement plus élevé au niveau de la partie transcriptionnelle des gènes surexprimés. De plus, en augmentant les taux de S-adénosylméthionine par le biais d'un dérivé de l'adénosine, nous diminuons l'enrichissement de 5hmC, ce qui entraîne une acquisition altérée des marqueurs d'identité hépatiques. Ces résultats suggèrent que 5hmC pourrait être un marqueur d'identité cellulaire, ainsi qu'un biomarqueur utile des conditions associées à la dédifférenciation cellulaire, comme le cancer du foie.

1. INTRODUCCIÓN

La historia de la epigenética está ligada al estudio de la evolución y el desarrollo. Durante los últimos 50 años, el significado del término “epigenética” ha evolucionado en paralelo con el dramático incremento del conocimiento de los mecanismos moleculares que coordinan la regulación de la expresión genética en eucariontes. Las definiciones actuales de epigenética reflejan nuestro entendimiento referente a que el DNA es esencialmente el mismo en todas las células somáticas de un organismo, que los patrones de expresión génica difieren en gran medida entre los diferentes tipos de células y que estos patrones pueden ser heredados clonalmente. Esto ha conducido a una definición de trabajo para epigenética como “el estudio de cambios mitótica y/o meióticamente heredables de la función génica, que no pueden ser explicados por cambios en la secuencia de DNA”. Más recientemente agregado a esta definición, se encuentra la restricción en torno a que el inicio del nuevo estado epigenético implica un mecanismo transitorio separado del requerido para mantenerlo. Considerando que la definición de epigenética ha evolucionado para ajustarse al avance del conocimiento, es importante tener en mente que la pregunta original era: ¿cómo puede un óvulo fertilizado individual originar a un organismo complejo con células con diferentes fenotipos? [Felsenfeld, 2014].

Una vez que Fleming descubrió la existencia de los cromosomas en 1879, varios investigadores continuaron sobre la línea, incluidos Wilson y Boveri, que proveyeron evidencia sólida de que el programa de desarrollo residía en los cromosomas. Desde ese punto hubo un gran avance en torno al estudio de estas estructuras, sin embargo la pregunta de la “epigénesis” clásica continuaba: ¿qué moléculas dentro del cromosoma acarrean la información genética? ¿cómo es que dirigen el programa de desarrollo embrionario? y ¿cómo es que la información es transmitida durante la división celular? Ya era claro que tanto los ácidos nucleicos como las proteínas estaban presentes en los

cromosomas, pero su contribución relativa no era obvia; ciertamente, nadie creía que únicamente los ácidos nucleicos pudieran contener toda la información para el desarrollo y aún se mantenían preguntas en torno a la posible contribución del citoplasma. Este debate cambió dramáticamente por la identificación del DNA como el responsable de contener la información genética. En última instancia, este evento también fue útil para redefinir a la epigenética y distinguir entre las modificaciones heredables atribuibles a cambios en la secuencia de DNA, de los que no podían asociarse a este tipo de cambios [Felsenfeld, 2014].

En años recientes, el estudio de la epigenética se ha enfocado en definir mecanismos de transmisión de la información no codificada en el DNA. La definición del término epigenética ha cambiado, pero la pregunta sobre los mecanismos de desarrollo abordados por las generaciones tempranas de investigadores en el campo son ahora nuevamente el centro de atención. Los epigenéticos contemporáneos aún abordan estas preguntas centrales y con la llegada de este conocimiento, actualmente se puede afirmar que los mecanismos epigenéticos son, de hecho, responsables de una considerable parte del fenotipo de organismos complejos [Felsenfeld, 2014].

1.1. Regulación de la transcripción

El control de los programas de transcripción está mediado por tres principales mecanismos que actúan en conjunto (Figura 1). El primero se basa en los factores de transcripción que se unen a secuencias específicas y que regulan un conjunto particular de genes. El segundo involucra mecanismos que tienen que ver con la metilación del DNA y las modificaciones post-traduccionales de histonas que en su conjunto proveen la memoria epigenética que ayuda a estabilizar el estado de diferenciación de una célula y su progenie y el tercero está

relacionado con la organización nuclear de la cromatina. A gran escala, el plegamiento de la cromatina puede afectar la expresión génica a través de localizar los genes en subcompartimentos nucleares específicos que son estimulantes o inhibitorios de la transcripción [Peric-Hupkes et al., 2010].

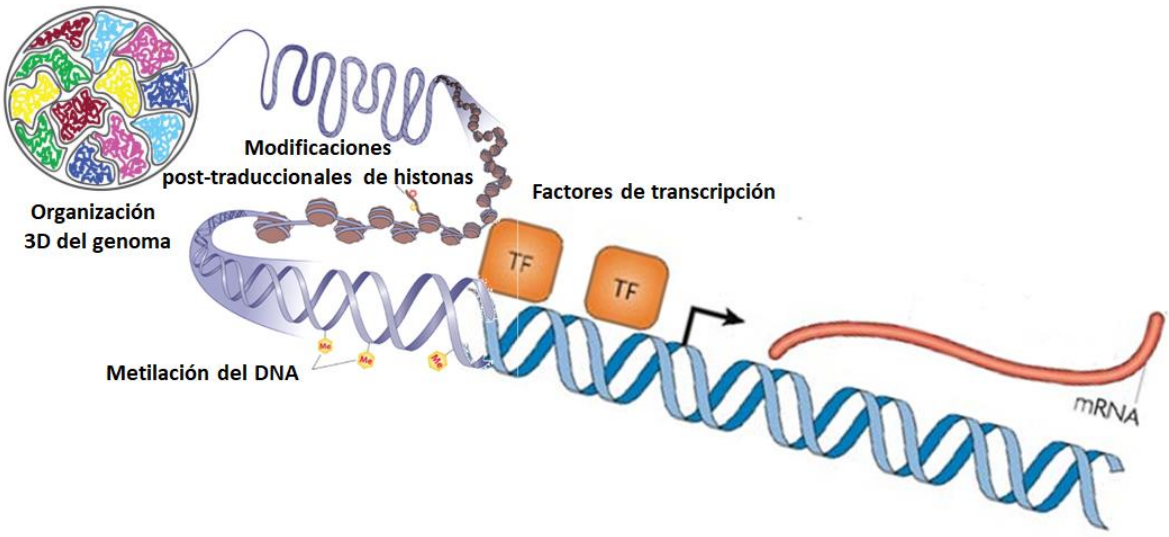

Fig. 1. Mecanismos que regulan los programas de transcripción. Esquema donde se ilustran los tres principales niveles de regulación de la transcripción. 1. Factores de transcripción (TF). 2. Dinámica de la metilación del DNA y modificaciones post-traduccionales de histonas y 3. Topología de la cromatina y organización tridimensional dentro del núcleo. Modificado de [Gericke et al., 2017; Matharu and Ahituv, 2015; Nelson and Cox, 2008]

Con los avances en el entendimiento de la organización de la cromatina en el genoma eucarionte, se ha hecho evidente que no sólo la genética sino también la epigenética influye tanto en la biología normal como en las enfermedades [Recillas-Targa, 2014]. Es por esto que los factores de transcripción y las modificaciones epigenéticas se han estudiado extensamente estudiados en diferentes procesos, desde la diferenciación hasta las enfermedades [Rodríguez-Aguilera, 2015].

1.1.1. La dinámica de la metilación del DNA

La metilación del DNA es uno de los procesos epigenéticos más estudiados durante el desarrollo de los organismos y la diferenciación celular [Bird, 2002]. Consiste en la incorporación de un grupo metilo en la posición 5 de la citosina del dinucleótido CpG [Bird and Wolffe, 1999]. Existe evidencia que sustenta el papel de esta modificación en el mantenimiento de la estabilidad genómica, manteniendo la estructura de la cromatina con una configuración estable en cuanto a elementos móviles, como transposones y otras secuencias repetidas [Cordaux and Batzer, 2009; Smith and Meissner, 2013]. La 5-metilcitosina (5mC) es una base poco abundante en el DNA de mamífero, constituye ~1% de todas las bases del DNA y es casi exclusivamente como metilación simétrica del dinucleótido CpG [Ehrlich and Wang, 1981; Li and Zhang, 2014].

El descubrimiento de la DNA metiltransferasa de mantenimiento (DNMT1), proporcionó un mecanismo por el cual el patrón de metilación se puede mantener a lo largo de generaciones celulares. La actividad de metiltransferasa de DNA de mamífero responsable de la replicación semiconservativa de la metilación del DNA fue detectada en extractos celulares y purificada como una proteína de 200 kDa [Bestor and Ingram, 1983]. Esta enzima es específica para CpG y tiene actividad significativa contra DNA no metilado en ensayos bioquímicos. Sin embargo, su sustrato preferido es el DNA hemimetilado (metilado en CpG en una de las dos cadenas) (Figura 2). Estudios genéticos subsecuentes indicaron que la inactivación de Dnmt1 en células troncales embrionarias de ratón conduce a una pérdida genómica de la metilación de CpG [Li et al., 1992]. Esta evidencia concuerda con la observación de que la Dnmt1 mantiene la metilación del DNA en las CpGs completando los sitios hemimetilados, lo que valida la hipótesis propuesta originalmente por los grupos de Pugh y Riggs en 1975 [Holliday and Pugh, 1975; Li and Zhang, 2014; Riggs, 1975].

Las metiltransferasas (de DNA) *de novo* fueron descubiertas al buscar una homología de secuencia con las metiltransferasas de citosina procariotas, utilizando bases de datos de expresión de secuencias. Estas metiltrasferasas procariotas comparten un conjunto de motivos proteicos conservados [Posfai et al., 1989], características que se encontraron en la DNA metiltransferasa de mantenimiento, Dnmt1. La búsqueda de homología identificó tres genes que podían codificar potencialmente DNA metiltransferasas nuevas (Figura 2). Una proteína candidata, Dnmt2, mostró una actividad de DNA metiltransferasa mínima *in vitro* y su ausencia no tuvo un efecto discernible sobre la metilación del DNA *de novo* o de mantenimiento [Okano et al., 1998b]. Los otros dos genes, *Dnmt3a* y *Dnmt3b*, codificaron polipéptidos catalíticamente activos relacionados que no presentaron preferencia para metilar DNA hemimetilado *in vitro*, a diferencia de Dnmt1 [Okano et al., 1998a]. La inactivación tanto de Dnmt3a como Dnmt3b por selección de genes en ESC confirmó que estos genes constituían a las DNA metiltransferasas *de novo,* ya que ESC y embriones carentes de ambas proteínas no son capaces de metilar *de novo* a los genomas provirales y elementos repetitivos [Li and Zhang, 2014; Okano et al., 1999].

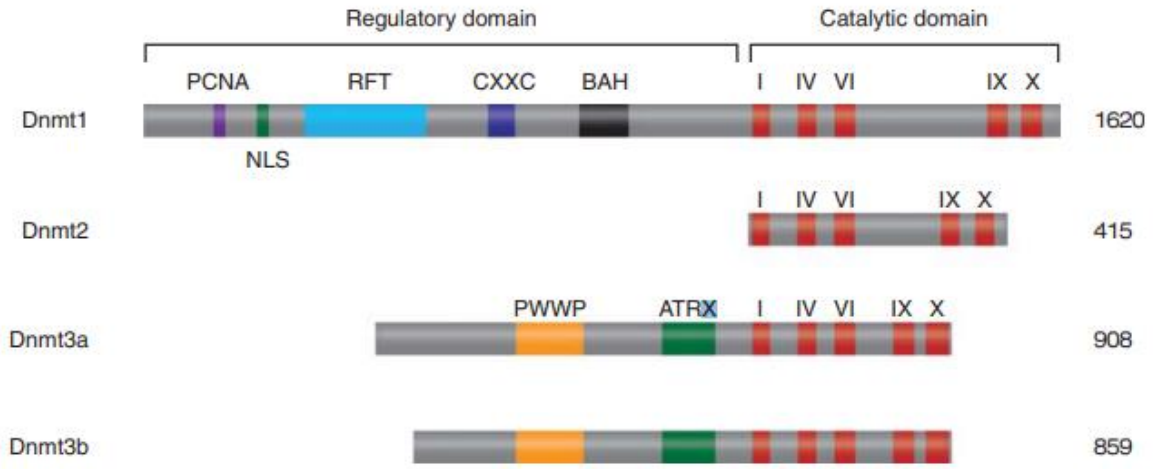

Fig. 2. DNA metiltransferasas de mamífero. Los dominios catalíticos de las Dnmt1, Dnmt2 y de los miembros de la familia Dnmt3 están conservados (los motivos I, IV, VI, IX y X son los más conservados en todas las metiltransferasas de citosina), pero hay poca similitud entre sus dominios regulatorios amino-terminales. PCNA, dominio de interacción con el antígeno nuclear de células en proliferación (PCNA); NLS, señal de localización nuclear; RFT, dominio de focalización de replicación; CXXC, dominio rico en cisteína implicado en las secuencias de unión a DNA que contienen dinucleótidos CpG; BAH, dominio de homología bromo adyacente implicado en las interacciones proteína-proteína; PWWP, dominio que contiene un motivo altamente conservado de "prolina-triptófano-triptófano-prolina" involucrado en la asociación con heterocromatina; ATRX, región rica en cisteína relacionada con la helicasa dependiente de ATP (ATRX) que contiene un dedo de zinc C2-C2; PHD, dominio atípico implicado en interacciones proteína-proteína. Tomado de [Li and Zhang, 2014].

Las enzimas DNMTs transfieren el grupo metilo a la posición 5 de la citosina en el dinucleótido CpG a partir de la S-adenosilmetionina (SAM) convirtiéndola a S-adenosilhocisteina (SAH) (Figura 3). La SAM es generada a partir de metionina a través de la adenilación de este aminoácido catalizada por las adenosilmetiltransferasas de metionina (MAT) [Finkelstein, 1990; Tehlivets et al., 2013; Zhang, 2018]. Más adelante se profundizará entre la relación del metabolismo y la regulación epigenética, donde se detallarán las reacciones que dan origen a la SAM.

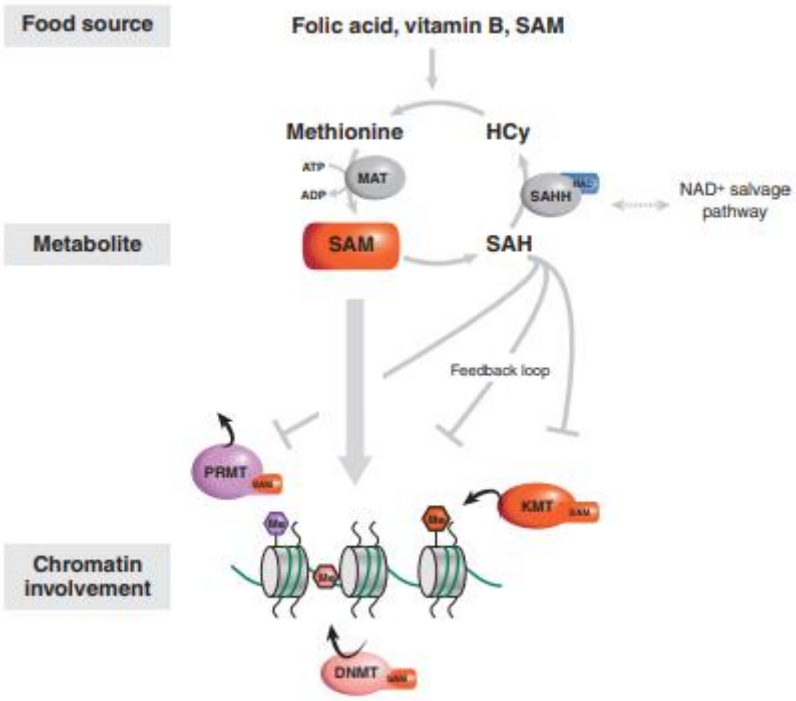

Fig. 3. Ruta de biosíntesis de S-adenosilmetionina (SAM) y su relación con procesos relacionados con la cromatina. La SAM es un co-factor esencial para las enzimas modificadoras de la cromatina como las proteínas metiltransferasas de arginina (PRMT), metiltransferasas de DNA (DNMT) y metiltransferasas de lisina (KMT). Esta ruta está metabólicamente influenciada por la ruta de recuperación de NAD en virtud de que la enzima SAH hidrolasa (SAHH) en su ruta de biosíntesis usa al dinucleótido de nicotinamida adenina (NAD). El principal producto del metabolismo de la SAM es la SAH, la cual tiene efectos inhibitorios sobre los complejos modificadores de la cromatina dependientes de SAM. HCy, homocisteina. Tomado de [Berger and Sassone-Corsi, 2016].

El DNA a lo largo del genoma de tejidos somáticos de mamífero se encuentra metilado en un 70-80% e todos los sitios CpG. Con los continuos avances en la tecnología ha habido un refinamiento constante en el nivel de detalle en el que se puede medir la metilación del DNA a una resolución de un sólo sitio CpG en un tipo celular dado. Estudios de trazado de mapas a lo largo del genoma indican que secuencias altamente metiladas incluyen DNAs satélite, elementos repetidos (incluyendo transposones y sus reliquias inertes), DNA intergénico no repetitivo y exones de genes. Muchas secuencias se encuentran metiladas de acuerdo a su frecuencia de dinucleótidos CpG. Excepciones clave a esta metilación global en el genoma de mamífero son las islas CpG (CGI) [Li and Zhang, 2014].

Las CGIs son secuencias ricas en CG de aproximadamente 1 kb de longitud. Generalmente se encuentran no metiladas en células germinales, embriones tempranos y en varios tejidos somáticos [Bird et al., 1985]. Fue en los primeros estudios de trazado de mapas de promotores individuales de genes donde se identificaron estas regiones ricas en CG [McKeon et al., 1982] (Figura 4A). Actualmente es evidente que muchas (aunque no todas) las CGIs marcan los promotores en la región 5' de los genes. De hecho, aproximadamente 60% de los genes humanos presentan promotores CGI [Li and Zhang, 2014].

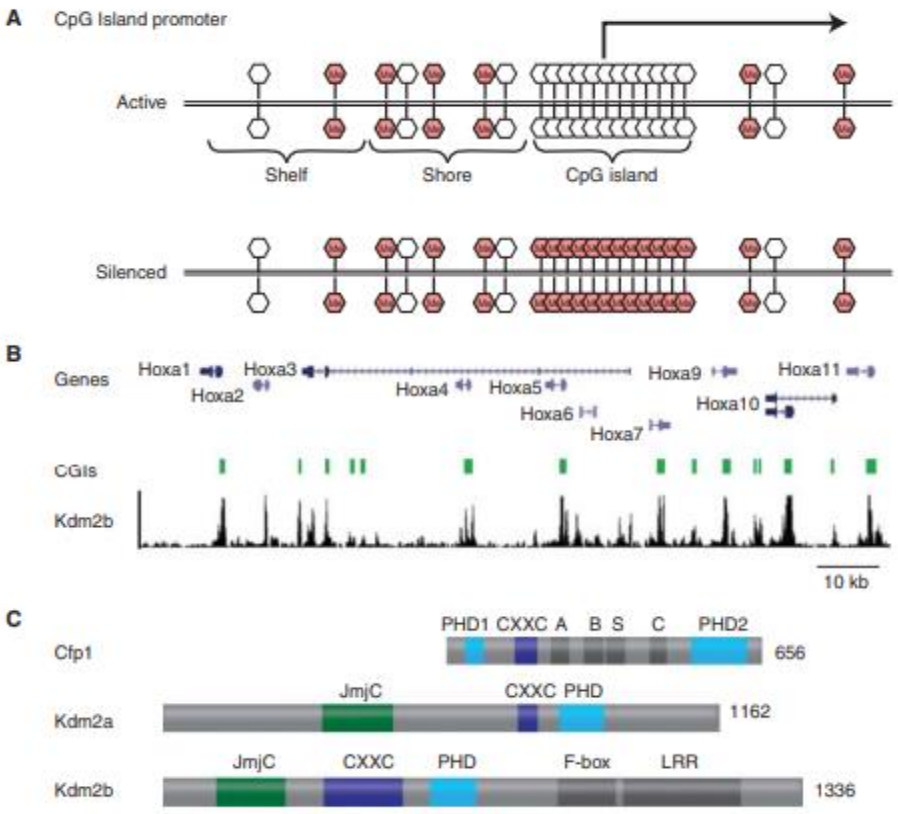

Fig. 4. Islas CpG (CGIs). (A) Las CGIs son regiones de la densidad de CpG (>50%), usualmente de 200 pb – 2 kb de longitud que carecen de metilación de DNA, y se encuentran en promotores de muchos genes humanos. Un silenciamiento de largo plazo de un gen puede atribuirse a la metilación de la región CGI. Por ejemplo, genes en el cromosoma X inactivo y ciertos genes improntados son silenciados de esta manera. También en células tumorales, ciertos genes son silenciados aberrantemente por metilación de CGIs. Las *shores* son regiones del genoma que residen 2 kb río arriba de las CGIs, mientras que las *shelves* se encuentran de 2 – 4 kb de distancia de las CGIs. (B) El Análisis de inmunoprecipitación de la cromatina (IP) de los sitios de unión de Kdm2b muestra que la proteína está enriquecida en CpGs del *locus Hox* donde se localizan CGIs sin metilación

(barras verdes). (C) Las proteínas Cfp1, Kdm2a, y Kdm2b comparten un dominio común CXXC que se une específicamente a sitios CpG no metilados. La longitud de la proteína se indica a la derecha de cada una. Abreviaciones de otros dominios incluyen PHD, plat homeodominio; A, dominio acídico; B, dominio básico; S, dominio de integración Set1; C, dominio *coiled coil*; LRR, dominio de repetidas ricas en leucina. Tomado de [Li and Zhang, 2014].

Los genes con promotores CGI que se expresan de manera específica de tejido se expresan usualmente en embriones tempranos y después en el soma. Un patrón distinto de metilación del DNA se encuentra en el cromosoma X inactivo en hembras, donde contrario a la norma, las CGIs se metilan *de novo* en un gran número durante el proceso embrionario de inactivación del cromosoma X en la placenta [Wolf et al., 1984]. Este proceso es determinante para evitar la expresión de genes en el cromosoma inactivado, lo cual es crucial para la compensación de dosis, es por ello que ratones o células deficientes en metilación del DNA muestran frecuentemente reactivación transcripcional de genes relacionados al cromosoma X [Brockdorff and Turner, 2015; Li and Zhang, 2014].

Los estudios sobre los patrones de metilación se han enfocado en la pregunta ¿cómo la expresión génica es regulada por la metilación del DNA? Las CGIs normalmente permanecen sin metilar y diversos mecanismos están involucrados en su protección contra la metilación *de novo* por las DNMT3A y DNMT3B. El descubrimiento de dos proteínas que contienen un dominio de unión a DNA CXXC, Cfp1 y Kdm2 (Figura 4 B y C), que son capaces de unirse específicamente a CpGs no metiladas dentro de las CGIs [Blackledge et al., 2013; Thomson et al., 2010], ha mostrado una forma de cómo el DNA no metilado puede contribuir en la creación de un ambiente de cromatina transcripcionalmente competente y protegerse así de la metilación de DNA *de novo* [Cheng, 2014; Deaton and Bird, 2011], es decir, la unión de Cfp1 y Kdm2 en sitios no metilados de CGIs previene la metilación en esta región.

El incremento de resolución con la cual se han analizado los metilomas de tipos celulares específicos ha comenzado a revelar patrones de metilación de DNA asociados al desarrollo

normal en comparación con estados patológicos como el cáncer o estados como el de envejecimiento. Los detalles han resultado en la caracterización de diferentes tipos de CGIs conteniendo un sitio de inicio de la transcripción (TSS) y comparando contra CGIs huérfanas que pueden estar localizadas intra- o intergénicamente. Los estudios han revelado también otras regiones diferencialmente metiladas denominadas *shores* (localizadas 2 kb río arriba de la CGI) y *shelves* (localizada entre 2-4 kb de la CGI [Irizarry et al., 2009] (Figura 4A). Un estudio ha propuesto que el estado de metilación del DNA en el primer exón de un gen es un mejor indicador de la represión transcripcional que las CGIs [Brenet et al., 2011]. La relevancia que estas categorías de regiones que contienen CpGs en el genoma con el ambiente cromatínico, el control de la transcripción así como su represión y el desarrollo de patologías o su asociación, aun es materia de análisis [Li and Zhang, 2014].

Uno de los aspectos más atractivos de la epigenética ha sido, hasta hace poco, el intenso debate sobre la reversibilidad de la metilación del DNA [Recillas-Targa, 2014]. En años recientes, la desmetilación activa del DNA ha surgido como una novedosa y reversible manera de regulación epigenética, en particular a través de la modificación de la 5mC en 5-hidroximetilcitosina (5hmC) como parte de la cascada enzimática que conduce a la recuperación de una citosina sin modificar [Hahn et al., 2014]. La presencia de 5hmC en el genoma es conocida desde 1972, cuando Yura R. y colaboradores propusieron un método que permitía identificar esta modificación en el DNA de cerebro e hígado de rata [Penn et al., 1972], pero fue hasta 2009 cuando dos grupos independientes describieron la presencia de esta citosina oxidada en las neuronas de Purkinje y en células troncales embrionarias (ESCs, por sus siglas en inglés) [Kriaucionis and Heintz, 2009; Tahiliani et al., 2009] y pocos años después, fueron descritas otras formas más oxidadas que la 5hmC (5-formilcitoisna

(5fC), y 5-carboxilcitosina (5caC)), así como las enzimas que catalizan las reacciones de oxidación de la 5mC (Dioxigenasas TET (TET)) [Ito et al., 2011] (Figura 5).

El descubrimiento de la hidroximetilación de la citosina sugirió una forma simple y activa de desmetilación de DNA y activación de genes. Sin embargo, diferentes estudios han revelado un proceso inesperado y complejo que implica tanto al mecanismo de desmetilación pasivo del DNA como al mecanismo activo y los estudios subsecuentes asociaron a tres familias enzimáticas al proceso activo de desmetilación (Figura 6): la familia TET que modifica a las citosinas metiladas primero por hidroxilación y después por oxidaciones subsecuentes; la activación inducida de la familia de la citidina desaminasa (AID/APOBEC), que desamina la base (tanto 5mC como 5hmC); y finalmente a la familia de glucosilasas involucradas en la reparación de DNA por escisión de bases (BER) [Bhutani et al., 2011]. Rutas bioquímicas ya validadas podrían estar participando en la modificación de la citosina dentro del DNA. Brevemente, el grupo metilo incorporado a la citosina por las metiltransferasas de DNA (DNMTs), enzimas que utilizan al donador universal de grupos metilo S-adenosilmetionina (SAM), genera a la 5mC. Esta citosina modificada puede oxidarse iterativamente hacia 5hmC, 5fC y 5caC (Figura 6). En la ruta de desmetilación pasiva, la 5hmC se diluye en un proceso dependiente de la replicación para generar una citosina sin modificación. Esto significaría que la pérdida pasiva de 5fC y 5caC altamente oxidados no es significativa. En la ruta de desmetilación activa, la cual es seguida de una restauración igualmente activa, la 5fC o 5caC son escindidas por la glucosilasa de timina de DNA (TDG), generando un sitio sin base como parte del sistema de reparación de DNA por escisión de bases que genera una citosina sin modificar [Kohli and Zhang, 2013] (Figura 6).

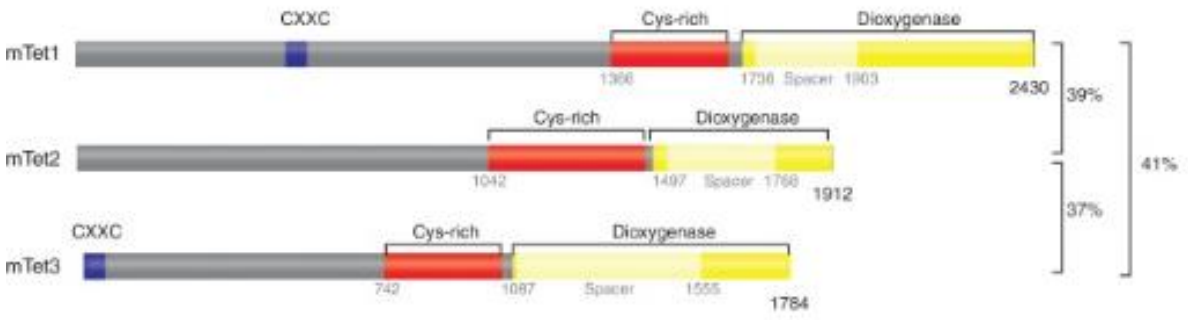

Fig. 5. Estructura de los dominios de la familia de proteínas Tet en ratón. Diagramas esquemáticos de las estructuras predichas de los dominios conservados en las tres proteínas Tet de ratón. Los dominios conservados incluyen al dominio *zinc binding* CXXC, el dominio rico en cisteína, y la doble hélice β (DSHB) encontradas en los miembros de la Superfamilia de dioxigenasas. Tanto el dominio rico en Cys y el DSBH han mostrado ser críticos para la actividad enzimática. Los números indican el número de aminoácidos. Tomado de [Li and Zhang, 2014].

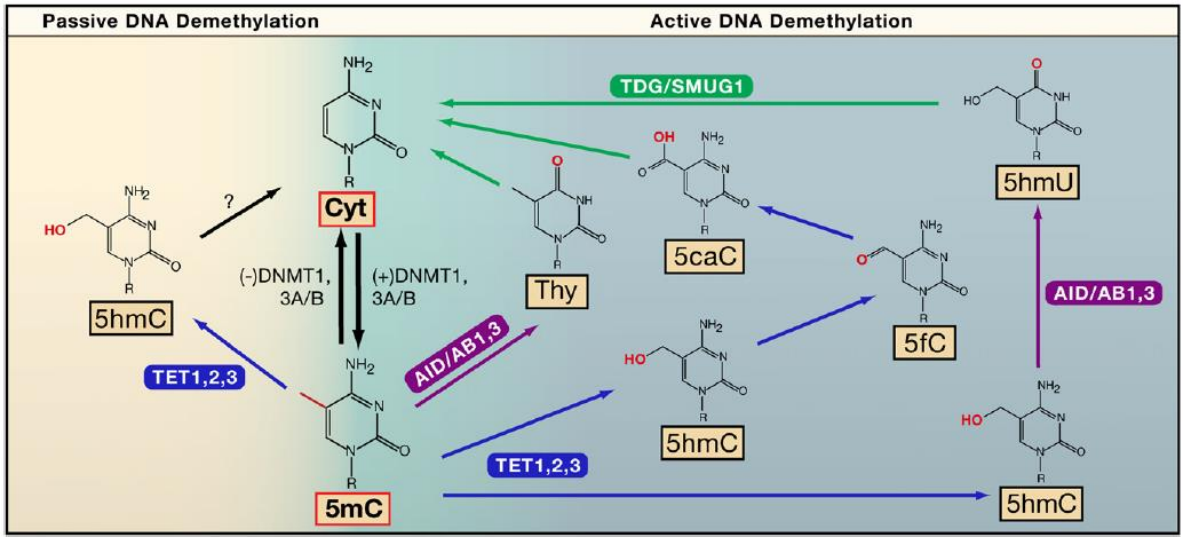

Fig. 6. Proceso de desmetilación del DNA. Desde hace mucho tiempo se sabe que la desmetilación pasiva del DNA ocurre por una reducción en la actividad o ausencia de metiltransferasas de DNA (DNMTs) (flechas negras). Las DNMT3A y 3B son responsables de la metilación de DNA *de novo*, mientras que la DNMT1 mantiene los patrones de metilación del DNA a través de las sucesivas rondas de división celular. Tres familias enzimáticas están implicadas en la desmetilación activa del DNA a través de la reparación del DNA. (1) La 5-metilcitosina (5mC) puede ser oxidada por la familia de las dioxigenasas ten-eleven translocation (TET) (flechas azules) hacia 5-hidroximetilcitosina (5hmC), la cual puede ser oxidada sucesivamente hacia 5-formilcitosina (5fC) y 5-carboxilcitosina (5caC). (2) La 5mC (o la 5hmC) pueden ser desaminadas por los miembros de la familia Desaminasa de Citosina Inducida por Activación / Enzima editora de la apolipoproteína B mediante mRNA semejante al polipéptido catalítico (AID/APOBEC) (flechas moradas) para formar al 5-metiluracilo (5mU) o 5-hidroximetiluracilo (5hmU). (3) El reemplazo de estos intermediarios (por ejemplo 5mU, 5hmU o 5caC) es iniciado por la familia de la glucosilasa de uracilo de DNA de las glucosilasas de reparación por escisión de base (flechas verdes) como La glucosilasa de timina de DNA (TDG) o la glucosilasa de uracilo de DNA monofuncional selectiva monocatenaria (SMUG1), culminando en el reemplazo de la citosina y desmetilación del DNA. Tomado de [Bhutani et al., 2011].

En la actualidad existen varios esfuerzos para elucidar las funciones epigenéticas de la 5hmC. El descubrimiento de esta modificación del DNA generó una gran expectativa al ser capaz de incrementar fácilmente la expresión reprimida por 5mC en promotores de varios genes [Bhutani et al., 2011; Pastor et al., 2011], por lo que se establece que la función de la 5hmC es claramente diferente a la de la 5mC.

Algunos de los esfuerzos por entender la función de la 5hmC han demostrado que la conversión de 5mC en 5hmC reduce considerablemente la afinidad de proteínas de unión a dominios de DNA metilado (MBDs) en ensayos *in vitro* [Valinluck et al., 2004], sin embargo, más recientemente se describió que MeCP2, una proteína MBD, presenta la capacidad de unirse a regiones de cromatina abierta enriquecida en 5hmC promoviendo la activación de genes [Mellen et al., 2012]. Otros estudios identificaron que la 5hmC se encuentra de manera abundante en el genoma de las ESCs y en el linaje neural [Ruzov et al., 2011] y que juega un papel importante en la autorenovación de ESCs [Ito et al., 2010]. Esto concuerda con el conocimiento en relación a que en ESCs, la cromatina se encuentra globalmente descompactada, enriquecida en marcas de histonas de activación en comparación con una célula diferenciada que presenta regiones de forma de heterocromatina compacta y acumulación de marcas de histonas de silenciamiento [Meshorer and Misteli, 2006]. (Figura 7).

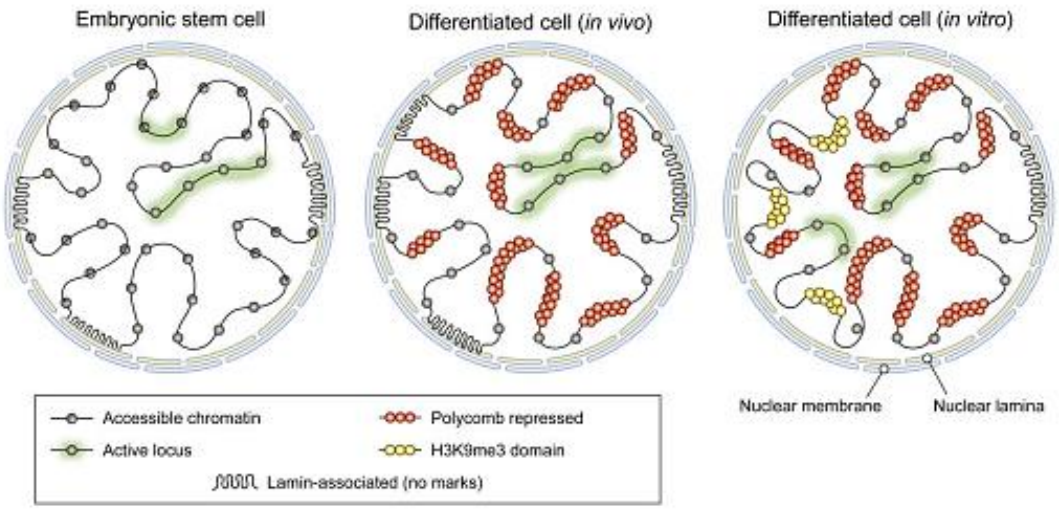

Fig.7. Modelo a gran escala de las transiciones de los estados de la cromatina. La ilustración muestra los patrones de la cromatina a gran escala y su presencia relativa en células de diferente estado de desarrollo o ambiente. Aunque la cantidad de secuencia del genoma que participa en la actividad reguladora del gen es relativamente constante, la configuración de cromatina de las regiones inactivas varía considerablemente. En células troncales embrionarias (izquierda), las regiones inactivas están enriquecidas difusamente para los marcadores de intercambio de cromatina y accesibilidad. En células diferenciadas *in vivo* (centro), los *loci* inactivos, en su lugar, tienden a adoptar un estado de cromatina reprimida por Polycomb. En células diferenciadas *in vitro* (derecha), hay grandes dominios enriquecidos para la marca de heterocromatina H3K9me3 que emergen en regiones asociadas a la lamina nuclear. Tomado de [Zhu et al., 2013].

1.1.2. Las enzimas TETs como responsables de la formación de 5hmC

Las enzimas TET originalmente llamadas *Ten-eleven translocation proteins* al haber sido identificadas fusionadas con la proteína MLL1 en leucemia mieloide aguda [Ono et al., 2002] son las responsables de la oxidación de la 5mC, y son los homólogos mamíferos de las proteínas de tripanosoma JBP1 y JBP2 a quién se les ha atribuido la función de oxidar al grupo 5-metilo de la timina [Tahiliani et al., 2009]. Estas enzimas se encuentran distribuidas en diferentes tejidos. Recientemente el grupo de Rao analizó la expresión de las tres 5mC-oxidasas en tejidos murinos y encontró que *Tet1* y *Tet2* son los dos principales transcritos de *Tet* expresadas en células embrionarias de ratón, mientras que *Tet3* se expresa escasamente; por otra parte, *Tet2* y *Tet3* son los principales transcritos *Tet* expresadas en tejidos diferenciados (Figura 8) [Tsagaratou and Rao, 2014].

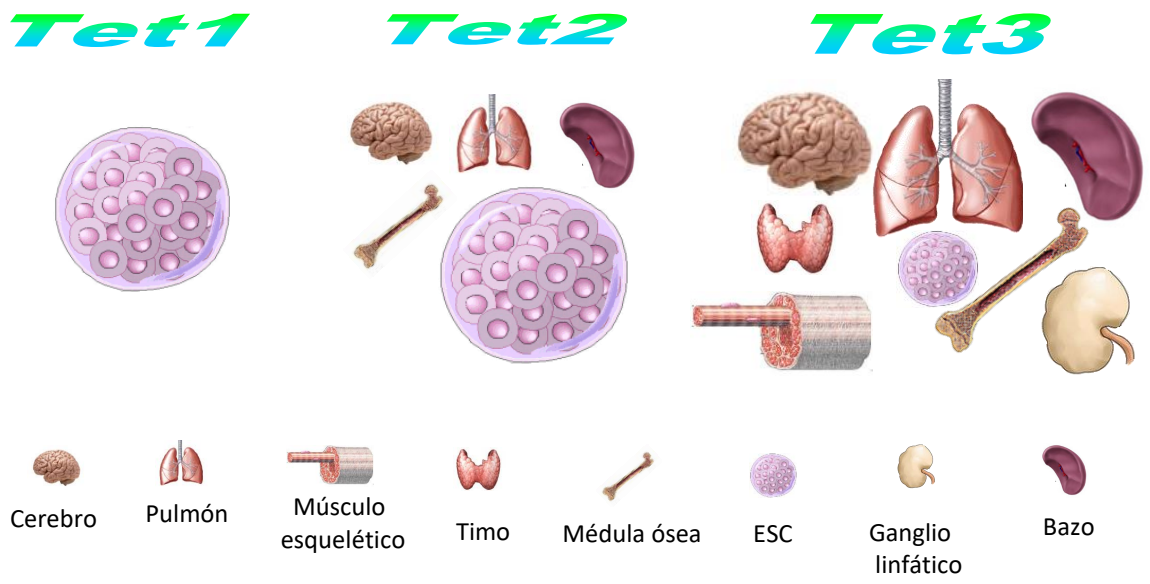

Fig. 8. Tejidos con mayor expresión de los transcritos que codifican a las dioxigenasas TET en ratón. Células troncales embrionarias de ratón (ESC) expresan principalmente *Tet1* y *Tet2; Tet3* se expresa escasamente en ESC pero es abundante en células diferenciadas. Basado en análisis de northern blot de [Tsagaratou and Rao, 2014].

Las enzimas TET son miembros de las dioxigenasas dependientes de Fe^{2+}/α-cetoglutarato, las cuales pueden ser inhibidas competitivamente por la pérdida o ganancia de actividades que involucren la producción de α-cetoglutarato (α-KG) y 2-hidroxiglutarato (2-HG) respectivamente [Dang et al., 2009; Zhao et al., 2009] porque el 2-HG funciona como un antagonista del α-KG ya que se une en el mismo punto del sitio catalítico de la enzima TET [Xu et al., 2011]. El cambio en la producción de α-KG puede ser originado por mutaciones en genes que codifican para las enzimas isocitrato deshidrogenasas (*IDH1* e *IDH2).* Tales mutaciones se han reportado en algunos tipos de neoplasias como la leucemia mieloide aguda [Mardis et al., 2009], el glioma [Parsons et al., 2008], el condrosarcoma [Amary et al., 2011a], el encondroma [Amary et al., 2011b; Pansuriya et al., 2011], en carcinomas de tiroides [Hemerly et al., 2010] y el colangiocarcinoma [Wang et al., 2019]. En este punto es importante mencionar que el grupo de Shi ha descrito un papel de IDH2 como supresor de

tumor en el carcinoma hepatocelular (HCC) [Liu et al., 2014], sin embargo la expresión de IDH2 mutada y el papel preciso de IDH2 en HCC aún se encuentra en investigación.

Esta información resalta la relevancia de las enzimas TET así como de la 5hmC en la regulación y mantenimiento de la homeostasis en los diferentes tejidos.

1.1.3. Abundancia de la 5hmC en diferentes tejidos

Desde que se describió la presencia de la 5hmC, la investigación se ha enfocado en evaluar la función de esta modificación en el sistema nervioso, quizá por su relativa abundancia en este tejido, pero la 5hmC está presente en diferentes linajes celulares. Diferentes tejidos de ratón, evaluados con un método de cromatografía líquida de alta resolución acoplada a espectrometría de masas (HPLC-MS) basado en isótopos ultra sensible y preciso, revelaron el nivel de 5hmC, el cual se clasificó dependiendo de su abundancia relativa en altos (5hmC de 0.3 – 0.7%), medios (5hmC de 0.15 a 0.17%) y bajos (5hmC de 0.03 – 0.06%) (Tabla 1) [Globisch et al., 2010]. Estos valores indican que la 5hmC se encuentra extensamente distribuida en los tejidos de ratón, lo cual abre la puerta a un nuevo mundo de regulación de manera específica de tejido.

Tabla 1. Cantidad de 5hmC en tejido de ratón. Datos tomados de [Globisch et al., 2010]

Tejido	% 5hmC/dG
Corteza cerebral	0.3-0.7
Tronco cerebral	
Médula espinal	
Cerebelo	
Riñón	0.15-0.17
Epitelio nasal	
Vejiga	
Corazón	
Músculo esquelético	
Pulmón	
Hígado	0.03-0.06
Bazo	
Testículos	
Hipófisis	

Con respecto al ser humano, se ha desarrollado un inmunoensayo de alta sensibilidad que permite la distinción entre 5mC y 5hmC. Los tejidos con mayor porcentaje de 5hmC (0.45 – 0.68 %) incluyen al cerebro, recto, hígado y colon (Tabla 2) [Li and Liu, 2011]. Este dato revela una notoria diferencia entre los tejidos de humano y ratón desde el punto de vista de la cantidad relativa de 5hmC. Esto pudiera sugerir que la 5hmC juega un papel importante y diferente en la dinámica de metilación del DNA, la remodelación de la cromatina y la expresión génica de manera órgano, tejido o célula específica y probablemente con variaciones entre las especies.

Tabla 2. Porcentaje de 5hmC en tejidos humanos. Datos tomados de [Li and Liu, 2011].

Tejido									
% <u>5hmC</u> gDNA	0.68	0.57	0.46	0.45	0.38	0.14	0.06	0.05	0.05

Considerando la amplia distribución de la 5hmC y la variabilidad en la cantidad relativa dependiendo del tejido estudiado, es importante, desde el punto de vista biomédico, desarrollar más estudios para determinar la importancia y la función de esta modificación epigenética tanto en un estado homeostático como en los diferentes estados de enfermedad.

1.1.4. Distribución genómica de 5mC y 5hmC

Utilizando un modelo carcinogénico no genotóxico en hígado roedor utilizando fenobarbital, el grupo de Meehan realizó ensayos de inmunoprecipitación de 5mC y 5hmC, encontrando una disminución de 5mC después de 28 días de exposición a fenobarbital. La distribución de 5hmC a lo largo de las regiones y genes afectados tiende a residir en el cuerpo de genes (68.4% en el cuerpo de genes, 56% en regiones intrónicas y 12.4% en regiones exónicas), mientras que únicamente 6.3% de todos los picos se encontraron en regiones promotoras

(-1 kb a + 250 pb). De manera similar, hay un enriquecimiento de los picos de 5mC dentro del cuerpo de los genes, lo cual posiblemente sugiere que la marca de metilación juega un papel dual y que cuando está presente en el *core* del gen, esté relacionada con la expresión del mismo [Thomson et al., 2012].

Este grupo [Thomson et al., 2012] expandió el análisis para estudiar el enriquecimiento de 5hmC en regiones enhancer dentro del genoma y encontró que de las 23 556 sondas del microarreglo que cubrían enhancers definidos, el 15.4% sobrelapaba con picos de 5hmC, mientras que solo 1.5% lo hacía con picos de 5mC. Un análisis más profundo reveló que una región de 1 kb de largo en una región enhancer, presentaba significativamente más 5hmC que la que se encontraba sobre regiones promotoras definidas. Por otra parte, no se observaron diferencias en este sentido para el caso de la marca de 5mC, lo cual sugiere que la regulación de 5hmC se extiende más allá de la región promotora e influye en elementos regulatorios distales. Con respecto a las regiones satelitales principales, los *Long Interspersed Nuclear Elements* (LINEs) y las partículas A intracisternales, secuencias retrovirales endógenas, se encontraron enriquecidos de 5mC pero no de 5hmC, lo que posiblemente hable de que la fracción genómica de 5hmC se encuentra limitada a regiones no repetitivas.

En este mismo estudio [Thomson et al., 2012], el nivel de 5hmC sobre promotores y cuerpos de genes correlacionaron con la actividad transcripcional en el hígado de ratón. Este grupo encontró que los promotores de genes expresados se encontraban marcados con altos niveles de 5hmC, la cual se encontraba directamente sobre el TSS (TSS ± 1.5 kb), lo cual indica que la distribución de 5hmC en promotores de hígado de ratón, está asociada con niveles relativos de actividad transcripcional. Además, los elementos regulatorios localizados en la proximidad del TSS y enriquecidos en 5hmC están relacionados con genes involucrados en patrones de expresión tejido específicos. Adicionalmente, estas regiones

corresponden a áreas con densidad de CpGs intermedia (de 1 a 5 CpGs por cada 100 pb). A pesar de que las principales islas CGIs del hígado se encuentran no metiladas, un subconjunto contenía al menos un pico de 5hmC (601 picos alineados con los CGI). De esta, la vasta mayoría (78%) se encontró que correspondía a CGIs intragénicas, las cuales están asociadas con regiones promotoras. Resultados similares fueron encontrados en regiones río arriba de las CGIs (CGI *shores*), las cuales se han visto involucradas en metilación diferencial entre tejidos sanos, así como en tejidos neoplásicos [Irizarry et al., 2009].

La relación entre las modificaciones de histonas y la modificación de 5hmC también fue evaluada por este grupo [Thomson et al., 2012]. El promedio de las señales de la marca de histona H3K4me2 reveló una correlación con los valores de 5hmC en promotores; por su parte, hay una menor correlación en cuerpos de genes, en los que la marca de histona H3K36me3 está enriquecida. Como estas marcas de histonas se encuentran típicamente asociadas con regiones de eucromatina, esto puede indicar que la 5hmC está asociada con cromatina transcripcionalmente activa, tanto en promotores como en el cuerpo de los genes. Además se encontró una correlación inversamente proporcional entre los niveles de 5hmC en los promotores de genes y la marca de histona H3K27me3 en los cuerpos de los mismos. Aunque las señales de 5mC en promotores presentan una correlación mucho más débil con las modificaciones de las histonas, son opuestas a la observada para la modificación de 5hmC, indicando que estas dos marcas (5mC y 5hmC) son funcionalmente distintas, la primera asociada a represión y la segunda favoreciendo la transcripción.

Estos hallazgos revelan una diferencia tanto en el contexto de compactación como en el funcional en la cromatina hepática entre ambas citosinas modificadas, lo cual va de acuerdo con las funciones de cromatina activa descritas para la 5hmC en el sistema nervioso central [Mellen et al., 2012].

1.2. Dinámica global de la metilación del DNA en el hígado humano fetal y adulto

Considerando las diferencias en la distribución y en la función de la 5mC y 5hmC, cobra trascendencia el proceso de adquisición de estas citosinas modificadas a lo largo de la biogénesis del hígado. Un estudio acerca de la dinámica de metilación del DNA durante el desarrollo del hígado humano fue realizado por el grupo de Ingelman-Sundberg [Ivanov et al., 2013], en dicho estudio se describió que el contenido medio de 5mC era de 4.2% con respecto al total de citosinas en hígado fetal, mientras que en hígado adulto era de 5.3%. Por el contrario, se encontraron niveles mucho menos abundantes de 5hmC en hígado fetal comparado contra el adulto. La muestras fetales presentaron un contenido de 5hmC menor a 0.125% mientras que la señal de muestras adultas estuvo alrededor del 0.2%.

Para explorar la distribución de 5hmC en el hígado, el grupo [Ivanov et al., 2013] realizó inmunotinciones de secciones de tejido hepático humano para ambas citosinas modificadas y no encontró diferencias significativas referentes a la localización internuclear entre 5mC y 5hmC, pero el análisis tridimensional de las secciones además reveló una abundante distribución de 5hmC en la mayoría de los hepatocitos.

Con el interés de conocer la función de los genes sobrerrepresentados con ocupación de 5hmC, los investigadores analizaron la distribución de esta modificación a nivel de genoma completo [Ivanov et al., 2013]. En general las muestras de hígado fetal presentaron significativamente menos picos de 5hmC, cubriendo una porción pequeña del genoma (de 10 a 40 Mb) comparada con las muestras adultas (de 80 a 203 Mb). Además, los picos de 5hmC se encuentran distribuidos de forma desigual entre los cromosomas, estando sobrerrepresentados los cromosomas 16, 17, 19 y 22 y subrepresentados en los cromosomas sexuales.

Las diferencias observadas tanto en el contenido global de 5hmC como en el número de picos de 5hmC entre las muestras de hígado del feto y del adulto sugieren que la distribución de esta marca se modifica significativamente durante el desarrollo del hígado en todo el genoma. Comparando los hidroximetilomas fetal y adulto, este grupo [Ivanov et al., 2013] encontró 5 038 intervalos genómicos continuos que denominó “bloques de 5hmC” donde la 5hmC se detectó únicamente en el hígado fetal, mientras que las muestras de hígado adulto presentaron 96 097 bloques. Los genes que se encontraban en dichos bloques se clasificaron en 5 grupos que se presentan en la Tabla 3.

Los bloques de 5hmC específicos del hígado fetal estuvieron enriquecidos de genes que se expresan en este estado (grupos I y II) pero fueron escasos para genes no relacionados con el desarrollo (grupo III) así como para genes específicos de adulto (grupos IV y V). Por su parte, los bloques específicos de hígado adulto presentaron subrepresentación de genes exclusivos del hígado fetal (grupo I), pero presentaron un enriquecimiento para genes que se expresan únicamente en hígados adultos (grupos IV y V). Es así que los patrones de desarrollo de 5hmC correlacionan con los patrones transcriptómicos del hígado de seres humanos [Ivanov et al., 2013]; estos cambios sugieren una función diferencial en los genes regulados por la marca de hidroximetilación en ambos estados.

Tabla 3. Clasificación de los bloques de 5hmC durante el desarrollo del hígado humano. Datos tomados de [Ivanov et al., 2013].

Clasificación		Número de genes
I.	Genes fetales específicos	464
II.	Genes expresados en muestras fetales por lo menos dos veces más que en muestras adultas	805
III.	Genes no expresados durante el desarrollo	8 731
IV.	Genes expresados en muestras adultas por lo menos dos veces más que en muestras fetales	1 079
V.	Genes adultos específicos	306

Los genes que adquieren 5hmC en el estado adulto están involucrados en procesos catabólicos, transporte de carbohidratos, oxidación de ácidos grasos y oxidación de lípidos, lo cual está en línea con las funciones del hígado adulto. Mientras que los genes asociados con una alta presencia de 5hmC en el estado fetal están relacionados con vías que están involucradas con la diferenciación celular y el desarrollo como la regulación de la diferenciación celular, el desarrollo de células troncales, y el establecimiento y mantenimiento de la polaridad celular. Los 10 principales procesos biológicos para ambos estados se presentan en la Tabla 4.

Tabla 4. Anotación funcional de las regiones de 5hmC exclusivas del hígado fetal e hígado adulto. Datos tomados de [Ivanov et al., 2013]

Clasificación	Proceso Biológico
Grupo V	**Genes enriquecidos en bloques de 5hmC exclusivos del hígado adulto**
	Procesamiento catabólico de mRNA transcrito nuclearmente
	Procesamiento catabólico de mRNA
	Procesamiento de carbohidratos
	Localización vesicular
	Oxidación de ácidos grasos
	Oxidación de lípidos
	Procesamiento de la terminación 3´ de RNAm
	Procesamiento de ácidos monocarboxílicos
	Procesamiento de la terminación 3´ de RNA
	Procesamiento catabólico de ácidos grasos
Clasificación	**Genes enriquecidos en bloques de 5hmC exclusivos del hígado fetal**
Grupo I	Regulación de la diferenciación de granulocitos
	Regulación de la diferenciación de células mieloides
	Inducción de apoptosis por señales extracelulares
	Regulación positiva del procesamiento metabólico de esteroides
	Desarrollo de células troncales
	Establecimiento y mantenimiento de la polaridad celular
	Regulación de la unión de proteínas
	Mantenimiento de la troncalidad celular
	Mantenimiento de la troncalidad celular somática
	Regulación negativa de la depuración de partículas lipoprotéicas

Además este grupo analizó los cambios en el enriquecimiento de 5hmC tanto en hígado fetal como en hígado adulto y su relación con la expresión de *TET*s e *IDH*s. Se evaluó a través de qPCR la expresión de las enzimas dependientes de Fe^{2+}/α-KG que oxidan a la 5mC así como la expresión de *IDHs* y se encontró una disminución significativa de la expresión de los genes de *TET* en hígados adultos comparados con los fetales [Ivanov et al., 2013]. Sin embargo, un ligero incremento en la expresión de *IDH1* e *IDH2* en muestras adultas puede potencialmente explicar el incremento total del contenido de 5hmC en estos

hígados comparando contra el nivel fetal de 5hmC, porque la IDH es una enzima que cataliza la formación de α-KG desde el D-isocitrato y el incremento en la producción de α-KG conduce a un incremento en la función de TETs (Figura 9).

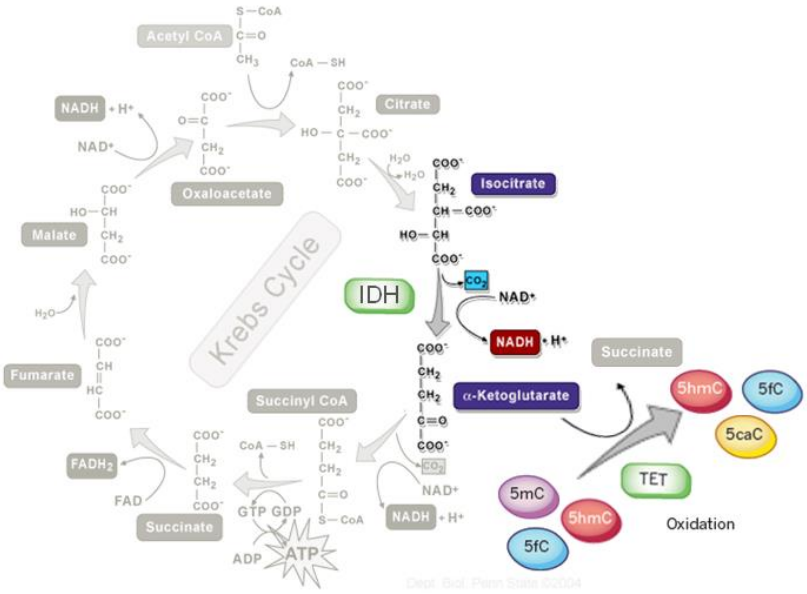

Fig 9. Interconexión entre el ciclo de Krebs y la oxidación de 5mC. El esquema resume la reacción de oxidación de las diferentes citosinas modificadas y señala la influencia de la IDH en la producción de α-KG, uno de los cofactores de las TETs.
El ciclo de Krebs al fondo fue tomado y modificado del sitio en la red https://wikispaces.psu.edu/download/attachments/46695632/Krebs_cycle.jpg

1.3. Los tumores hepáticos presentan niveles reducidos de 5hmC

El carcinoma hepatocelular (HCC) es el carcinoma primario más común en el hígado. Más del 85% de los casos de HCC provienen de una inflamación crónica y la subsecuente aparición de cirrosis [Bosch et al., 2005]. De acuerdo a las bases de datos de GLOBOCAN-IARC [The, 2018], el cáncer de hígado se estima en la séptima posición en incidencia de cáncer y en la cuarta causa de muerte por cáncer en 2018.

Considerando a la cirrosis como un preludio de HCC, es entendible que muchos cánceres hepáticos sigan un patrón patológico de evolución, empezando por una cirrosis (caracterizada por nódulos regenerativos), hasta nódulos displásicos de bajo grado,

nódulos displásicos de alto grado, HCC temprano, progresión hacia HCC y finalmente HCC avanzado. Además este progreso de la enfermedad involucra un evidente desbalance entre los factores genéticos y epigenéticos; con respecto a los factores genéticos, los nódulos displásicos tempranos presentan un genoma con muy limitada variación génica, mientras que el HCC avanzado tiene un genoma heterogéneo con un intervalo de 72 a 182 mutaciones [Castelli et al., 2017; Marquardt et al., 2014; Rodríguez-Aguilera et al., 2019].

Por otra parte, concerniente a los aspectos epigenéticos, se ha descrito una hipometilación de DNA en HCC, la cual puede ser indicativo de un mal pronóstico de supervivencia [Miyata et al., 2018]. En el mismo sentido se ha descrito una metilación aberrante en genes diferencialmente expresados que están relacionados con el progreso del ciclo celular, la proteína supresora de tumores y guardián del genoma p53 y la vía de señalización de las proteínas cinasas activadas por mitógenos (MAPK) en HCC [Fan et al., 2018; Rodríguez-Aguilera et al., 2019].

La metilación de CGIs en genes relacionados con tumores como *APC, GSTP1, RASSF1A, p16, COX-2* y *E-cadherin,* es un evento temprano y frecuente y se acumulan durante la hepatocarcinogénesis [Lee et al., 2003].

Por otra parte, la reducción en los niveles de 5hmC se ha asociado con la progresión de HCC [Liu et al., 2013]. Las alteraciones en el estado de metilación en HCC pueden ser explicadas por la subexpresión de las dioxigenesas TET con la subsecuente reducción de los niveles de 5hmC [Yang et al., 2013]. En tejido sano hay una diferencia característica entre regiones de eucromatina y heterocromatina que se pierde en cáncer; se ha sugerido que esta pérdida puede estar generada por una reducción de los niveles de 5hmC los cuales son de alrededor del 70%. Es importante comentar que la relación específica entre la 5hmC y las marcas de histonas del tejido sano se pierde en tumores y puede asociarse con

alteraciones en la estructura de la cromatina y en la desregulación de la expresión génica durante la tumorigénesis [Li et al., 2016b; Rodríguez-Aguilera et al., 2019].

Se han analizado muestras de tumores y de tejido sano para conocer el comportamiento de la 5hmC en diferentes tejidos tumorales y se encontró que el tejido sano y peritumoral desplegaban niveles equivalentes de 5hmC, pero existe una disminución global de 5hmC tanto en adenoma hepático como en HCC si se compara con hígado sano. Resultados similares se encontraron en tumores de mama, pulmón, páncreas y próstata. Coincidentemente con la disminución de 5hmC todos los tejidos neoplásicos tienen una fuerte señal de la proteína Ki67, un marcador celular de proliferación, comparado con tejidos sanos [Haffner et al., 2011; Yang et al., 2013].

En este mismo sentido, una reducción de 69% en el nivel de 5hmC se ha encontrado en tejidos de pacientes con HCC comparados contra tejidos no tumorales; además se ha descrito que bajos niveles de 5hmC están significativamente asociados con la edad (≥50 años), género (masculino), tamaño de tumor (≥5 cm) y al nivel de α-fetoproteína (>400 ng/mL) y con una supervivencia en general significativamente más corta que aquellos con alto nivel de 5hmC; por otro lado, no hubo correlación entre la abundancia de 5hmC en tejidos no tumorales y el parámetro clínico-patológico. En contraste, altos niveles de 5mC en tejidos con HCC correlacionaron significativamente con un una corta supervivencia [Liu et al., 2013].

Utilizando cromatografía líquida de interacción hidrofílica de cuadrupolo (TOF) y espectrometría de masas, el grupo de Yuang obtuvo resultados equivalentes que se resumen en la Tabla 5. Este grupo encontró que el contenido de 5hmC correlaciona significativamente con la progresión del tumor. Sin embargo, no existe correlación con respecto a la edad, el género, los estados de inflación hepática, los estados de cirrosis, el

consumo de alcohol o los parámetros de función hepática. Adicionalmente, la 5mC no estuvo asociada con ningún parámetro evaluado por este grupo [Chen et al., 2013b].

Tabla 5. Abundancia de 5mC y 5hmC en tejidos tumorales y no tumorales. Datos tomados de [Chen et al., 2013b].

Muestra	Contenido de 5mC	Contenido de 5hmC
Tejido tumoral	5.57%	0.37%
Tejido adyacente al tumor	5.97%	1.72%
DNA genómico de tejidos tumorales emparejados por pares	6.00%	0.42%
DNA genómico de tejido adyacente al tumor	5.97%	1.72%

Estos resultados en conjunto, sugieren que la 5hmC es un posible biomarcador, cuya disminución está asociada de manera amplia y estrecha con el desarrollo del tumor y puede ser una herramienta útil en pacientes con acceso a una biopsia para el establecimiento de un pronóstico clínico.

Las enfermedades hepáticas, incluido el HCC, se han abordado también desde el punto de vista de la ciencia básica. Se han desarrollado modelos animales para el estudio de estas patologías; uno de estos modelos es el de daño hepático crónico inducido con dietilnitrosamina (DEN), que reproduce la cirrosis y la progresión hacia HCC, como lo que ocurre en pacientes, ya que genera un proceso inflamatorio que se vuelve crónico, conduciendo a la fibrosis, generación de cirrosis y finalmente desarrollo de HCC [Schiffer et al., 2005]. En este modelo se ha descrito que los niveles de 5hmC disminuyen gradualmente en el hígado, durante el periodo de inducción de daño con DEN si se comparan contra el tejido sano, el cual presenta un nivel elevado de 5hmC [Liu et al., 2013], lo cual concuerda con los hallazgos que se han descrito en muestras tumorales humanas.

En conjunto, los datos que se han descrito en pacientes así como en el modelo animal, demuestran que es importante y esencial conocer cuál es el contenido de 5hmC tanto en hígado sano como en las diversas enfermedades hepáticas, así como a lo largo del desarrollo, para identificar la dinámica de metilación en este tejido y cómo las alteraciones en esta dinámica pueden conducir al establecimiento del fenotipo patológico.

Otro punto importante que debe considerarse, es la asociación de los niveles de 5hmC con el pronóstico del paciente. Un primer esfuerzo para determinar esta asociación ha sido la evaluación de la correlación entre los niveles de 5hmC y la historia clínica del paciente, donde el grupo de Shi encontró que bajos niveles de 5hmC correlacionan con el tamaño del tumor y con una expectativa de vida corta [Liu et al., 2014]. Este hallazgo puede estar relacionado, de acuerdo con los autores, al hecho de que las características histopatológicas agresivas, incluyendo niveles de α-feto proteína (AFP) altos eran significativamente más frecuentes en pacientes que presentaban niveles de 5hmC bajos que en aquellos con mayor abundancia. Además, asociado a los niveles de AFP altos se encontraba un mayor número de tumores y una mayor tinción positiva para metástasis nodo-tumoral avanzada. Este grupo además identificó correlaciones significativas entre bajos niveles de IDH2 y un fondo de antígeno de superficie de hepatitis B y un alto nivel de AFP con bajo grado de diferenciación tumoral. Otro dato importante de este estudio fue que altos niveles de 5hmC y elevada cantidad de IDH2 por separado y en combinación, correlacionaban significativamente con una mayor supervivencia y mayor tiempo a la reincidencia [Liu et al., 2014].

Estos hallazgos están de acuerdo con el hecho de que la actividad de TETs y por lo tanto el enriquecimiento de 5hmC están enlazados a la actividad de IDH que actúa como productor de α-KG en el ciclo de Krebs y que se requiere para el funcionamiento de las dioxigenasas dependientes de Fe^{2+} / α-cetoglutarato.

1.4. La subexpresión de TETs está relacionada con cáncer

El posible mecanismo que involucra la disminución de 5hmC en el cáncer de hígado ha sido abordado mediante la evaluación de los niveles de expresión de los genes que codifican a las enzimas TET, y se ha reportado una disminución significativa en el HCC así como en adenoma hepático cuando se compara contra el tejido normal [Yang et al., 2013]. El gen *TET1* muestra la reducción más significativa en la expresión seguido de *TET2* y *TET3;* esto podría reflejar una diferencia en la importancia de TET1 en humano comparado contra ratón, ya que en este último la expresión de esta 5mC dioxigenasa es detectada exclusivamente en ESC (Figura 8) [Tsagaratou and Rao, 2014].

Considerando que la proteína es la molécula relevante en el proceso catalítico, y considerando el conocimiento en los cambios del estado transcripcional, es importante determinar si la reducción global de 5hmC en HCC es debido a la disminución de la cantidad de TET en muestras de cáncer. El grupo de Quian abordó esta pregunta y encontró que la enzima TET1 estaba significativamente disminuida en tejidos con HCC y no encontró diferencias significativas para el caso de TET2 y TET3 [Liu et al., 2013]. Por lo anterior es posible que la diminución en la cantidad de TET1 represente uno de los mecanismos moleculares por los cuales ocurre la reducción de 5hmC en HCC.

Estos hallazgos son relevantes porque definen posibles biomarcadores para cáncer y abren un nuevo horizonte en el área de fármacos epigenéticos que tengan como blanco la estimulación de TETs y sus reguladores, para mantener los niveles saludables de 5hmC.

2. La 5hmC, un marcador de identidad en la diferenciación de células progenitoras adultas

La 5hmC ha sido asociada con la diferenciación en células de todas las capas germinales:

- Endodermo

El endodermo da origen a varios de los tipos celulares que forman el tracto gastrointestinal y los órganos relacionados. Se ha descrito una acumulación estable de 5hmC durante la diferenciación de enterocitos en sitios descritos para la unión de factores de transcripción y blancos involucrados en este proceso [Chapman et al., 2015; Kim et al., 2016]. De manera interesante, la redistribución de 5hmC va acompañada de una disminución de 5mC. Además, la pérdida de expresión génica en las células comprometidas se correlacionó con una disminución significativa en los niveles de 5hmC del cuerpo del gen (Figura 10) [Ecsedi et al., 2018].

- Mesodermo

Dada la existencia de aproximaciones relativamente sencillas para realizar diferenciación y selección *in vitro* de tipos celulares hematopoyéticos bien caracterizados, datos sustanciales favorecen la hipótesis de que la 5hmC juega un papel en el programa transcripcional mieloide y linfoide durante la diferenciación [Ecsedi et al., 2018].

Globalmente, se ha descrito una disminución en los niveles de 5hmC durante la diferenciación de células troncales hematopoyéticas [Tsagaratou and Rao, 2014]. A pesar de esta reducción global, la 5hmC permanece enriquecida en *loci* particulares, coincidiendo su distribución con promotores y cuerpos de genes. Adicionalmente, se ha descrito enriquecimiento de 5hmC en enhancers [Caron et al., 2015; Garcia-Gomez et al., 2017; Lio et al., 2016; Montagner et al., 2016; Tekpli et al., 2016; Tsagaratou and Rao, 2014] y sitios de unión a factores de transcripción específicos de linaje [Ichiyama et al., 2015; Madzo et

al., 2014]. En línea con lo anterior, los cambios en 5hmC están sobrerrepresentados en genes altamente transcritos [Ecsedi et al., 2018].

Además de las células sanguíneas, se ha sugerido que la 5hmC juega un papel importante en la diferenciación de condrocitos. Un incremento global de 5hmC fue observado en el primer estado de diferenciación, seguido de una disminución en estados más tardíos [Taylor et al., 2016]. De manera similar a lo descrito para células del sistema inmune, el incremento de 5hmC fue más evidente en el cuerpo de genes de factores específicos de linaje condrogénico (*Sox9*, *5* y *6*, *Runx2* y *Col2a1*) y se asoció con activación transcripcional [Ecsedi et al., 2018].

Se ha descrito un enriquecimiento global y localizado de 5hmC durante el desarrollo de miocitos [Zhong et al., 2017] y cardiomiocitos [Greco et al., 2016; Kranzhofer et al., 2016]. El enriquecimiento de 5hmC se encuentra principalmente en el cuerpo de los genes y en las regiones regulatorias distales, marcando a los genes enriquecidos por la ocupación de Pol II, así como por marcas activas de histonas. La transición del corazón embrionario a adulto se caracteriza por picos de 5hmC en genes relacionados al desarrollo cardiaco (Figura 10), como los procesos basados en el filamento de actina y la regulación de la contracción cardiaca. Adicionalmente Tet2 se ha visto implicada tanto en el desarrollo de miocitos como de cardiomiocitos. El *knockdown* de *Tet2,* más no el de *Tet1*, significativamente reduce la expresión de genes miocíticos (*Myog*, *Myf6* y *Mymk*) y altera la diferenciación de mioblastos [Ecsedi et al., 2018; Zhong et al., 2017].

Por su parte, durante el desarrollo de adipocitos, en un modelo de preadipocitos 3T3-L1 (Figura 10), la proteína arquitectónica CTCF se encontró interactuando con las enzimas TET para promover la deposición de 5hmC en enhancers transcripcionales adipogénicos

[Dubois-Chevalier et al., 2014]. Además, las proteínas TET (en particular TET2) se requieren para la adipogénesis al incrementar 5hmC en el *locus* de *PPARG* con la consecuente inducción de su expresión [Yoo et al., 2017].

En un estudio reciente se ha demostrado que la 5hmC también se redistribuye en las células de Sertoli, células mesodérmicas que se requieren para la espermatogénesis. Se observó una reducción de 5mC asociada a la pubertad y un incremento de 5hmC [Landfors et al., 2017]. Los picos de 5hmC ganados durante la maduración se relacionaron con el transporte celular, procesos catabólicos, función mitocondrial y endocitosis, lo cual va de la mano con el hecho de que las células de Sertoli presentan un metabolismo diverso y elevado con abundantes mitocondrias [Ecsedi et al., 2018].

- Ectodermo

Al tiempo que se redescubrió la 5hmC, se identificó que esta citosina modificada constiyuye 0.6% del total de nucleótidos en las células de Purkinje [Kriaucionis and Heintz, 2009]. Siendo altamente abundante en el cerebro, se sugirió que la 5hmC tiene un papel en el control genómico de las funciones neurales. Es así que en conjunto con las células troncales embrionarias, varios tipos de neuronas, su localización anatómica y sus niveles de diferenciación han sido de los tipos celulares más estudiados en términos del contenido de 5mC/5hmC, su distribución y su función [Ecsedi et al., 2018].

De manera similar a otros tipos de tejidos, la 5hmC está enriquecida en el cuerpo de los genes altamente transcritos en neuronas postmitóticas, y se acumula en regiones que enmarcan enhancers y sitios de factores de transcripción [Mellen et al., 2017; Wen and Tang, 2014; Yu et al., 2012]. Adicionalmente se ha encontrado que la 5hmC está enriquecida en neuronas adultas mientras ocurre la sinaptogénesis, aunque su contenido y distribución varía entre diferentes tipos de neuronas [Tekpli et al., 2016]. En línea con lo

anterior, las tres proteínas TET se expresan en el cerebro de mamífero, y todas están involucradas en la neurogénesis y la fisiología del cerebro [Wen and Tang, 2014]. Particularmente, se ha descrito que las células progenitoras neurales (NPC) están afectadas con la ausencia de TET1 con consecuencias a nivel funcional, incluyendo el aprendizaje y la memoria [Rudenko et al., 2013; Zhang et al., 2013]. De manera similar, se ha demostrado que la reducción de TET2 conduce a una reducción de los niveles de 5hmC (particularmente en genes neurogénicos) y parcialmente bloquea la ganancia de 5hmC durante la diferenciación. También se ha demostrado que FOXO3A interactúa físicamente con TET2 y regula la expresión de genes relacionados con la troncalidad neural/proliferación de progenitores [Li et al., 2017] (Figura 10). Por lo tanto, la 5hmC y las TETs controlan la expresión de genes y vías relacionadas con los programas neurales, varios de los cuales son regulados durante el desarrollo [Spiers et al., 2017]. Un enriquecimiento específico de 5hmC se ha observado en secuencias adyacentes a sitio de p300 en genes críticos para la diferenciación neuronal [Hahn et al., 2013] o de la vía Notch y Wnt en la neurogénesis de retina [Ecsedi et al., 2018; Seritrakul and Gross, 2017].

Otro hecho que incrementa el interés en la 5hmC es la posibilidad de unión de la proteína 2 de unión a metilcitosina (MeCP2) como un lector de esta modificación [Williams et al., 2011] además de que esta proteína se ha asociado previamente con desórdenes en el neurodesarrollo [Amir et al., 1999]. Además, recientemente se ha demostrado que la distribución de 5hmC en CG y en dinucleótidos no CpG es distinta y refleja la unión específica y la ocupación genómica de MeCP2 [Mellen et al., 2017]. Adicionalmente, la pérdida de MeCP2 conduce a una reducción de la señal de 5hmC en regiones hidroximetiladas dinámicas intergénicas no-CpGs, involucradas en la activación génica [Ecsedi et al., 2018; Szulwach et al., 2011].

Los altos niveles de 5hmC en las neuronas adultas (y su capacidad de incrementar), y su distribución específica a lo largo de los tipos celulares y las regiones cerebrales, indican un papel funcional importante relacionado con la preservación de la identidad celular [Ecsedi et al., 2018].

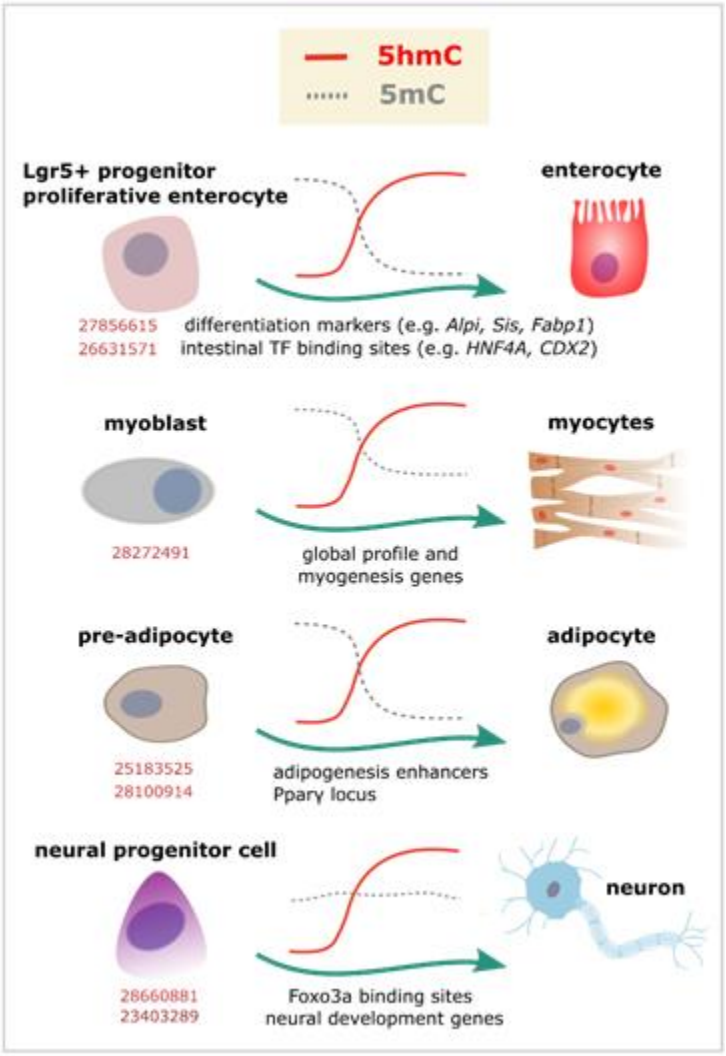

Fig. 10. Dinámica de la 5hmC durante la diferenciación. Evidencia de cambios dinámicos en la 5mC (líneas grises) o la 5hmC (líneas rojas) en los *loci* indicados, asociados con el compromiso de linaje. Las líneas punteadas representan evidencia adicional. 5mC, 5-metilcitosina; 5hmC, 5-hidroximetilcitosina. Se muestran en rojo los correspondientes PMIDs de PubMed para cada estudio. Modificado de [Ecsedi et al., 2018].

Estos estudios relacionan el proceso de diferenciación con un enriquecimiento de 5hmC, sugiriendo que hay un cambio general en la distribución de 5hmC el cual puede asociarse con la sobreexpresión de genes que definen el estado celular.

1.6. HepaRG, la línea celular troncal hepática

En esta sección se presenta el relato de la Dra. Christiane Gugen-Guillouzo (tomada del sitio web de la línea celular HepaRG [Biopredic]), donde narra cómo se obtuvo la línea celular HepaRG. Esta narración nos permite comprender por qué esta línea celular facilita el estudio de los hepatocitos, al conservar muchas de las características de un cultivo primario células parenquimales de hígado:

En las décadas de los 80s y 90s, un grupo de la universidad de Rennes era uno de los líderes mundiales de la comunidad científica que trabajaba con cultivos de hepatocitos primarios humanos. Este grupo, consciente de la problemática relacionada con las enfermedades hepáticas infecciosas y tomando ventaja de sus cultivos primarios de hepatocitos humanos diferenciados, asumió el reto de realizar una infección *in vitro* de los cultivos primarios, utilizando virus de hepatitis.

Philippe Gripon, estudiante de Doctorado, tuvo éxito al infectar hepatocitos humanos maduros con alta eficiencia, utilizando suero de pacientes infectados con virus de hepatitis B (HBV). Sin embargo, la infección para el caso del virus de hepatitis C (HCV) fue más problemática. Por lo anterior se propuso obtener células hepáticas ya infectadas con HCV a partir de pacientes (*in vivo*).

En este punto, el grupo consideró que podrían tener más posibilidades de éxito, al combinar la experiencia y los esfuerzos del grupo de Rennes con algunos colegas de la universidad de Lyon, quienes tenían experiencia en la virología de la hepatitis. Se estableció la colaboración y Sylvie Rumin asumió el reto del proyecto y sirviendo de puente entre Rennes (donde obtuvo su Doctorado y experiencia en el cultivo de hepatocitos) y Lyon, donde comenzó a trabajar como investigadora postdoctoral.

Fue en 1999 que Sylvie Rumin obtuvo la pieza de tumor que posteriormente dio origen a la línea HepaRG años más tarde.

De acuerdo al protocolo experimental, el tumor tuvo su origen en una paciente que sufría de infección por HCV y fue operada en Lyon por ablación tumoral. La paciente dio el consentimiento de usar sus células con propósitos de investigación. Desafortunadamente, para el propósito del proyecto de Rennes, la infección por HCV gradualmente desapareció en conjunto con el desprendimiento y muerte de los hepatocitos normales que rodeaban el tumor y encontrando en los platos de cultivo, únicamente hepatocitos normales (no las células transformadas). Sin embargo, permanecieron vivas poblaciones mixtas de células del tumor.

A pesar de que estas células fueron negativas para marcadores de HCV, se tomó la decisión de no desecharlas, porque Sylvie Rumin estaba intrigada desde un comienzo debido a que esas células a baja confluencia presentaban una morfología que mimetizaba una forma epitelial hepática. Posteriormente ella decidió proporcionar viales de dichas células a investigadores de ambos equipos, quienes podían estar interesados en caracterizarlas a mayor profundidad.

Nuevamente Philippe Gripon aceptó tomar el reto, el cual implicó un esfuerzo de un año hasta obtener una población enriquecida de hepatocitos.

Como recompensa por la importante contribución de ambos jóvenes científicos, la Dra. Christiane Gugen-Guillouzo decidió utilizar la primera letra de sus apellidos para identificar a las células, por lo que actualmente se conocen como HepaRG (por Rumin y Gripon).

Posteriormente siguió un periodo con observaciones entusiastas, donde se encontró que todas las funciones específicas del hígado estaban altamente expresadas en las células HepaRG, principalmente aquellas asociadas con la desintoxicación y metabolismo y demostrando que las células son susceptibles a la infección por HBV y soportan la replicación viral.

Fue la primera vez en la que se demostró una infección por HBV en una línea celular estabilizada y se proporcionó una fuerte evidencia de que las células HepaRG pudieron llegar a una completa diferenciación de hepatocitos.

Los resultados descritos se publicaron en la revista *Proceedings of the National Academy of Sciences* (PNAS) en 2002 en conjunto con la primera descripción de la línea celular [Gripon et al., 2002] y el Instituto Nacional Francés de Investigación en Salud y Medicina (INSERM) inició simultáneamente el proceso de patentado que en la actualidad cubre varios países a nivel mundial.

La empresa Biopredic compró la licencia en 2003 e inmediatamente se hizo cargo del banco celular de trabajo y de preservación para preservar la estabilidad de la línea celular hasta el día de hoy.

Tomó más tiempo evidenciar el mantenimiento no predecible de los progenitores hepáticos y en identificar la propiedad biológica de *trans*-diferenciación publicada por [Cerec et al., 2007], que hacen a la línea celular HepaRG un modelo hepático único, al compartir junto con las células troncales altas propiedades de plasticidad.

Y finalmente fue en 2011 cuando estos grupos obtuvieron las condiciones para hacer susceptible a la línea HepaRG a la infección por HCV [Biopredic].

1.6.1. Diferenciación de las células HepaRG en hepatocitos y células biliares

Entre las líneas celulares humanas derivadas de hepatoma, las células HepaRG aisladas de un tumor diferenciado grado 1 de Edmonson secundario a una infección crónica por HCV, exhiben características únicas; presentan un cariotipo pseudodiploide. De manera constitutiva y sincrónica, muestran un fenotipo similar tanto a hepatocitos como a células biliares cuando se encuentran en confluencia, lo que indica que poseen características de progenitor bipotencial [Gripon et al., 2002; Parent et al., 2004]. Cuando se diferencian de manera óptima soportan la infección por HBV [Gripon et al., 2002] y expresan un gran panel

de genes específicos de hígado, incluyendo aquellos que expresan enzimas metabólicas [Aninat et al., 2006; Cerec et al., 2007].

Cuando las células HepaRG diferenciadas y confluentes se resiembran a baja confluencia en presencia de insulina y corticoesteroides, son capaces de originar células indiferenciadas que proliferan activamente por 3 a 4 días y se comprometen a vías de diferenciación de hepatocitos y células bliares justo después de alcanzar confluencia al día 5 (Figura 11 A y B). Las células se organizan en células epiteliales planas claras o en cordones de células poligonales granulares (Figura 11C). La máxima diferenciación celular se alcanza después de dos semanas de exposición al dimetilsulfóxido (DMSO). Las células tipo hepatocito exhiben un fenotipo muy cercano al de hepatocitos humanos (Figura 11D), con estructuras similares a canalículos biliares funcionales (Figura 11D). Las células tipo hepatocito son positivos para el citocromo P450 3A4 (CYP3A4), mientras que las células epiteliales aplanadas que las rodean son negativas (Figura 11F). Asimismo, ambas células presentan la citoquetarina 18 (CK18), siendo más abundante en hepatocitos que en células biliares (Figura 11G). En contraste, la citoqueratina 19 (CK19) y la integrina α6 (CD49F) están presentes únicamente en células biliares (Figura 11H) y CD49a (Integrina α1) está limitada a hepatocitos (Figura 11 I-J).

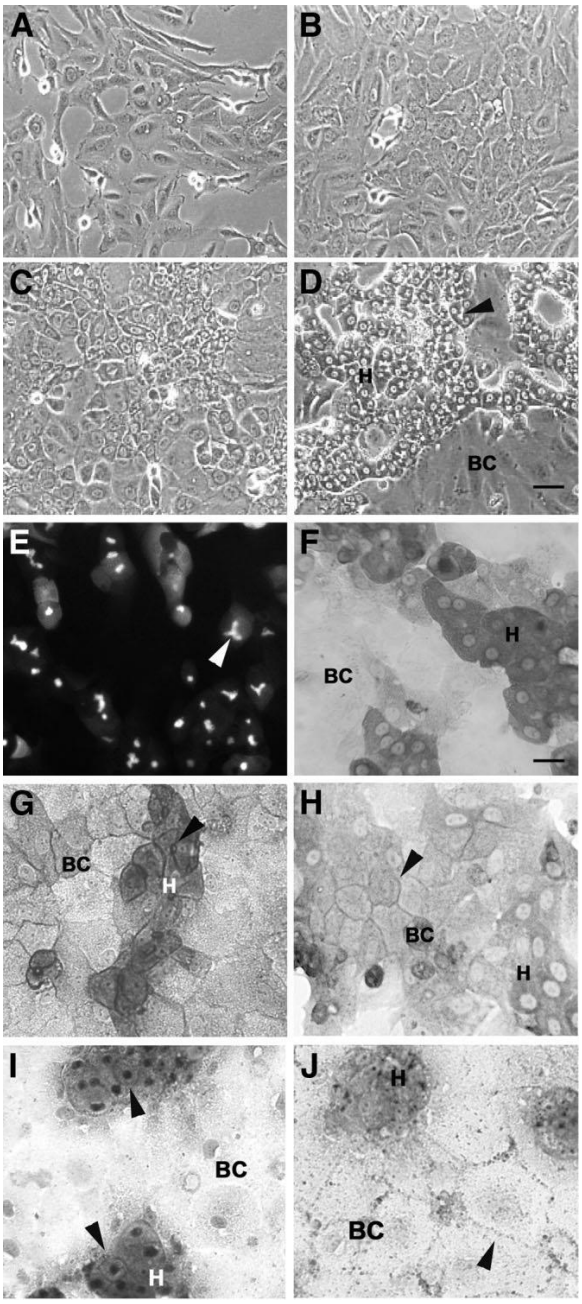

Fig. 11. Morfología de las células HepaRG y expresión de marcadores de diferenciación durante este proceso. Fotografías de contraste de fase de las células HepaRG a (A) 2, (B) 5, (C) 15 y (D) 30 días después de la siembra. A los 15 días el medio se suplementó con DMSO al 2% y las células se cultivan por 15 días más. La barra representa 60 μm. Las flechas negras señalan la estructura tipo canalículo biliar. (E) Micrografía de la tinción de diacetato de fluoresceína donde se observa la excreción de esta molécula, lo que evidencia la funcionalidad del canalículo. Inmunolocalización de (F) CYP3A4, citoqueratina (G) 18 y (H) 19, (I) integrina α1 y (J) α6 en las células HepaRG diferenciadas al día 30. La barra representa 30 μm. H, hepatocito, BC célula biliar. Las flechas negras indican tinción positiva. Tomado de [Cerec et al., 2007].

En cuanto a la expresión de factores nucleares hepáticos, durante los 2 a 3 días iniciales de proliferación activa, las células HepaRG en estado de progenitor presentan el factor nuclear de hepatocitos 3 β (HNF3β). Su expresión disminuye drásticamente en el día 4 y está completamente ausente en las células diferenciadas En contraste el factor nuclear de hepatocitos 4α (HNF4α) es poco abundante en progenitores, progresivamente se acumula hasta alcanzar su máxima expresión en células diferenciadas. Por su parte HNF1α exhibe un perfil estable durante la diferenciación (Figura 12).

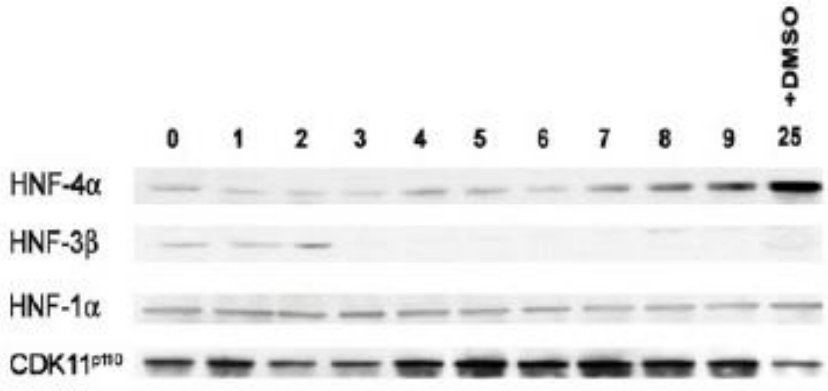

Fig. 9. Niveles de los factores transcripción hepáticos durante la diferenciación de las células HepaRG. Análisis por inmunoblot de los factores nucleares hepáticos HNF4α, HNF3β, y HNF1α a los diferentes tiempos de cultivo. La proteína cinasa 11 ($CDK11^{p110}$) se utilizó como control de carga. Tomado de [Cerec et al., 2007].

Por lo anterior es posible afirmar que las células HepaRG presentan plasticidad celular y soportan transiciones *in vitro* de células indiferenciadas hacia los linajes hepático y biliar [Cerec et al., 2007].

1.7. Factores nucleares hepáticos (HNFs)

Los factores nucleares hepáticos (HNFs) están presentes en una gran variedad de tejidos y órganos incluyendo el hígado, el páncreas y el riñón. La manera espacio-temporal en la

que se los HNFs se expresan, regula el desarrollo embrionario y subsecuentemente el desarrollo de múltiples tejidos durante la edad adulta [Lau et al., 2018].

Algunos estudios han identificado los motivos de unión de HNFs en diferentes familias y dichos motivos no parecen ser exclusivamente activos en el hígado. Una variedad de genes hepáticos y extra hepáticos contienen los motivos de HNFs en su promotor y en regiones enhancer, lo que sugiere la presencia de múltiples redes regulatorias involucrando a estos factores de transcripción, y que no están restringidas al desarrollo y función del hígado [Lau et al., 2018], sin embargo, en el presente trabajo resaltaremos las propiedades hepáticas en las que están involucrados estos factores transcripcionales.

Los HNFs se clasifican en cuatro familias, las cuales son HNF1, *Forkhead box A* ([FOXA] o HNF3), HNF4 y *One cut* ([OC] o HNF6), cada una caracterizada por distintos dominios funcionales (Figura 13A). La familia HNF1 comprende a HNF1α y HNF1β, cuyo dominio de unión a DNA (DBD) se une a la secuencia consenso palindrómica GTTAATNATTANC. El dominio de dimerización (DD) en el dominio N-terminal permite tanto a HNF1α como a HNF1β formar homodímeros o heterodímeros [De Simone et al., 1991; Rey-Campos et al., 1991]. Los genes que codifican ambos genes presentan tres isoformas (A, B y C) con funciones específicas de tejido [Bach and Yaniv, 1993; Harries et al., 2006; Lau et al., 2018].

FOXA (formalmente conocido como HNF3) pertenece a la subfamilia de las proteínas *Forkhead box* (FOX), que comprende a FOXA, FOXA2 y FOXA3 [Kaestner et al., 2000; Lai et al., 1991]. La familia de proteínas FOXA contiene una estructura de hélice alada (*winged helix* (WH) o también conocida como el dominio *forkhead*) enmarcada por secuencias requeridas para la localización nuclear (Figura 13B) [Friedman and Kaestner, 2006]. Estos factores de transcripción también comparten un DBD altamente conservado y se unen a su DNA blanco como monómero [Rausa et al., 1997]. Los dominios N- y C- terminal de las

proteínas FOXA están conservados y se ha descrito que actúan como dominios de transactivación (TAD) [Lau et al., 2018; Pani et al., 1992; Qian and Costa, 1995].

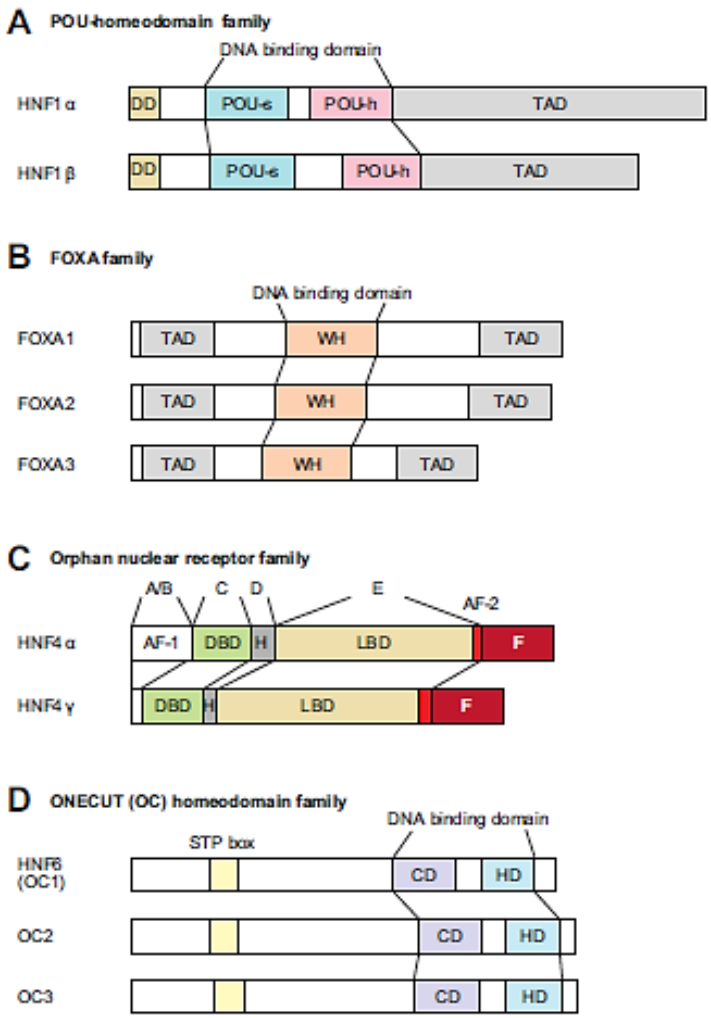

Fig. 13. Dominios estructurales de las familias de HNF. (A) Diagrama esquemático de HNF1α y HNF1β. El N-terminal consiste del DD. El DBD de la familia consiste del homeodominio POU-s u POU-h. El C-terminal contiene al TAD, el cual es menos conservado entre los dos miembros de la familia HNF1. (B) Diagrama esquemático representando a los miembros de la subfamilia *Forkhead box* que son FOXA1, FOXA2 y FOXA3. Los dos TADs enmarcan cada extremo de estos factores de transcripción. El DBD de la familia consiste de una estructura WH con secuencias para la localización nuclear. (C) Diagrama esquemático de la familia de receptores nucleares huérfanos HNF4 que comprende a HNF4α y a HNF4γ. El dominio A/B contiene a la AF-1 en el N-terminal, el dominio C contiene al DBD altamente conservado, el dominio D se refiere a la región bisagra (*hinge region* (H)) que conecta a los dominios C y E, mientras que el dominio E contiene al dominio de unión a ligando (LBD) con dos dedos de zinc que reconocen y se unen a motivos específicos en el DNA. El LBD también contiene a la AF-2. Las proteínas HBF4 también tienen una región represora (dominio F) en el C-terminal. (D) diagrama esquemático de los miembros de la familia ONECUT HNF6 (OC1), OC2 y OC3. Una region STB *box* se localiza cerca del extremo N-terminal de las proteínas OC. En conjunto el dominio cut (CD) y el homeodominio divergente (HD) forman el DBD bipartita cerca del extremo C-terminal. Los esquemas están realizados a escala. AF-1/2, función activadora 1/2; CD, dominio *cut*; DBD, dominio de unión a DNA; DD, dominio de dimerización; FOXA, *forkhead box* A; HD, homeodominio; HNF, factor nuclear de hepatocito; LBD, dominio de unión a ligando; OC, ONECUT; POU-s, dominio POU específico; POU-h, homeodominio POU; TAD, dominio de transactivación; WH, *winged helix*. Tomado de [Lau et al., 2018].

El HNF4 pertenece a la familia de receptores nucleares huérfanos y comprende a HNF4α y HNF4γ (Figura 13C). Contienen dos dominios con función transactivadora, función transactivadora 1 y 2 (AF-1 y AF-2), localizada en los dominios N- y C-terminal respectivamente, y activan la transcripción de manera independiente del tipo celular. Un dominio de unión a ligando (LBD) se localiza adyacente a AF-2 y transactiva genes de manera dependiente de ligando, proveyendo un punto de control adicional para la regulación de la actividad de la proteína. Además, las proteínas HNF4 contienen también un dominio represor, región F, con funciones inhibitorias [Hadzopoulou-Cladaras et al., 1997] que no han sido caracterizadas en otras familias de HNF.

El HNF4α regula la expresión de muchos genes involucrados en varios procesos, como el desarrollo [DeLaForest et al., 2011], el metabolismo [Xu et al., 2015], y transición epitelio-mesénquima [Santangelo et al., 2011]. El HNF4α también juega un papel crucial en el desarrollo del endodermo, tal que el *knockout* en ratón resulta en letalidad embrionaria [Chen et al., 1994]. Mutaciones polimórficas del gen *HNF4A* se han asociado con un amplio espectro de enfermedades, incluyendo la diabetes de la adolescencia [Anuradha et al., 2011], la enfermedad de Crohn [Marcil et al., 2012] y el síndrome inflamatorio del intestino [Chahar et al., 2014] y se ha observado que las isoformas de HNF4α (HNF4α 1/2/3/7/8/9) difieren en su habilidad para activar el promotor *core* del virus de hepatitis B, afectando así la eficiencia de la replicación viral [Ko et al., 2017; Ko et al., 2019].

El *HNF4A* está codificado por dos promotores regulados de acuerdo a la etapa de desarrollo (P1 y P2) y el uso diferencial de promotores y el *splicing* alternativo generan 12 isoformas (Figura 14), P1 dirige a *HNF4A1-6* y P2 a *HNF4A7-12*), que son expresadas de manera específica de acuerdo al tiempo y al tejido [Drewes et al., 1996; Huang et al., 2009; Lau et al., 2018; Sladek et al., 1999; Thomas et al., 2001]. Con la excepción de HNF4α4 y HNF4α6,

el resto de las isoformas han sido validadas (Figura 14B) y se ha encontrado expresión diferencial en una variedad de tejidos. Las 12 isoformas difieren solamente en las regiones N- y C- terminal, que son los responsables de activar [Briancon and Weiss, 2006] y reprimir [Ruse et al., 2002] la trascripción, respectivamente. Sin embargo, una expresión aberrante de las isoformas resulta en la alteración de los perfiles de expresión genética asociado con enfermedades como el carcinoma hepatocelular [Tanaka et al., 2006], cáncer de colon [Schwartz et al., 2009] y diabetes mellitus [Anuradha et al., 2011], y se reconoce que cada isoforma desarrolla una función distinta para regular un subconjunto específico de genes de manera específica de tejido [Li et al., 2006; Torres-Padilla and Weiss, 2003]. Por ejemplo, se ha descrito que HNF4α2 está enriquecido en el hígado y actúa como supresor tumoral, cuya pérdida se asocia con carcinoma hepatocelular, mientras que HNF4α8 se expresa altamente en colon y controla la expresión de genes promotores del crecimiento [Ko et al., 2019; Vuong et al., 2015].

Se ha descrito a HNF4α como homodímero [Jiang and Sladek, 1997; Lu et al., 2008] que comprende 2 cadenas polipeptídicas idénticas. Se sabe que los monómeros de HNF4α dimerizan con otros receptores nucleares. Se han encontrado combinaciones que generan alta o baja actividad transcripcional, indicando que la coexpresión de 2 isoformas genera heterodímeros de isoformas que son funcionalmente distintos de su correspondiente homodímero de isoformas [Ko et al., 2019]. A lo largo del presente trabajo haremos referencia a HNF4α y a sus promotores P1 y P2.

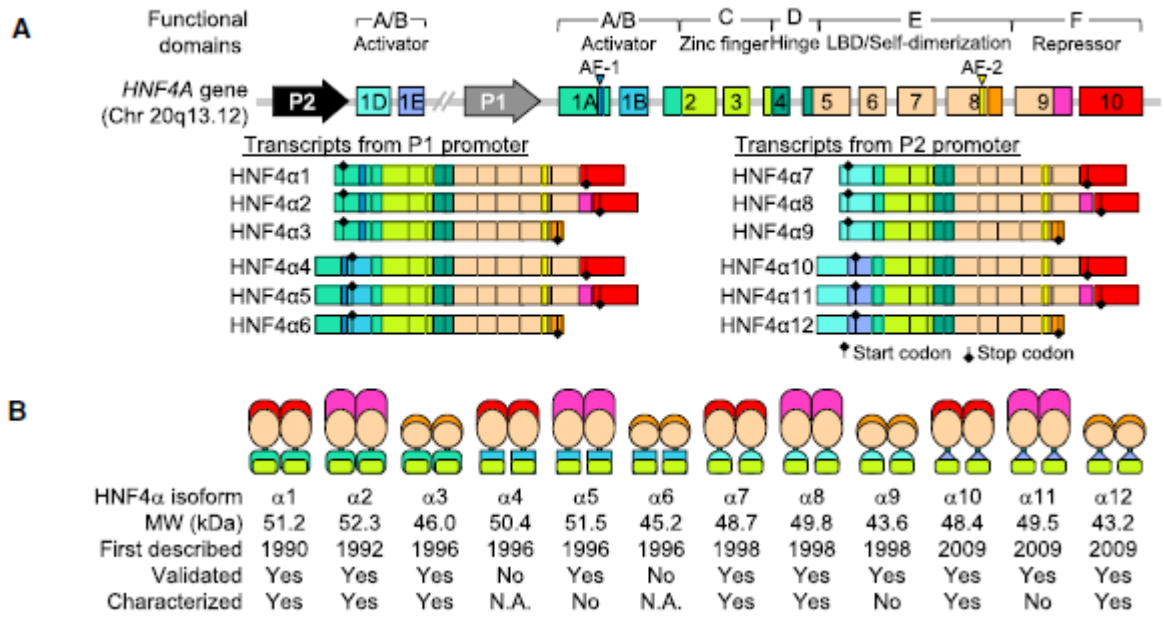

Fig. 14. HNF4α humano se expresa como 12 isoformas funcionales distintas. (A) El esquema muestra la estructura del gen de *HNF4A* humano y sus 12 transcritos, generados por el uso alternativo de los promotores P1 o P2, y por *splicing* alternativo en los extremos N- y C- terminal. (B) Esquema que representa los homodímeros de las isoformas del factor nuclear hepático HNF4a con diferentes combinaciones de N y C-terminales. Tomado de [Ko et al., 2019]

OC1 (o HNF6) pertenece a la familia de genes *one cut homeobox.* Consiste en un solo dominio *cut* (CD) y un homeodominio divergente (HD) (Figura 13D) que forma el DBD bipartita [Iyaguchi et al., 2007; Lemaigre et al., 1996]. El HD contiene secuencias que median la localización nuclear y la activación transcripcional, en conjunto con la región enriquecida en serina/treonina/prolina) (STB *box*) [Lannoy et al., 2000; Rausa et al., 1997]. Los miembros de esta familia son OC1 y sus dos parálogos OC2 [Jacquemin et al., 1999] y OC3 [Lau et al., 2018; Vanhorenbeeck et al., 2002].

Con la información anterior es posible notar que los miembros de la familia albergan características comunes como las capacidades de unión y transactivación de DNA, las cuales están ampliamente definidas por dominios estructurales definidos que explican su diversidad funcional. Además, las múltiples isoformas dentro de cada subfamilia, confieren

mayor complejidad a su potencial regulatorio de las funciones celulares y tisulares [Lau et al., 2018].

1.7.1. Perfil de expresión de HNFs durante el desarrollo embrionario hepático y la etapa adulta

Los patrones de expresión de los miembros de la familia de HNF durante el desarrollo embrionario de mamíferos ha sido mejor caracterizado en roedores que en humanos. Es sabido que el hígado, el páncreas y el riñón exhiben altos niveles de varios miembros de la familia de HNF y que la desregulación de estas proteínas está implicada en varias enfermedades [Lau et al., 2018].

En el ratón, la expresión de *Hnf1b* se detecta por primera vez en el endodermo primitivo en el día embrionario E4.5 y se requiere para la especificación del linaje primitivo endodermal [Barbacci et al., 1999; Cereghini et al., 1992].La expresión de *Hnf1b* precede a *Hnf1a* durante la embriogénesis, es así que los trascritos de *Hnf1a* se detectan por primera vez en el saco vitelino en el día E8.5 [Cereghini et al., 1992]. *Hnf4a* se expresa en el endodermo visceral desde el día E4.5 [Chen et al., 1994; Duncan et al., 1994; Li et al., 2000; Parviz et al., 2003; Taraviras et al., 1994] y subsecuentemente se detecta en el brote del hígado y en el intestino posterior a partir del día E8.5 [Chen et al., 1994; Duncan et al., 1994; Li et al., 2000; Nammo et al., 2008; Parviz et al., 2003; Taraviras et al., 1994]. Por otra parte, *Foxa1, Foxa2* y *Foxa3* tienen patrones temporales de expresión distintos y aparecen en dominios parcialmente traslapantes del endodermo definitivo y del notocordio [Lau et al., 2018].

Los transcritos de *Hnf1b* son detectados subsecuentemente en el endodermo del intestino anterior en el día E9, a partir del cual se desarrollan el hígado y el páncreas. Durante el desarrollo del hígado, tanto los transcritos de *Hnf1a* como *Hnf1b* pueden ser detectados en el primordio hepático al día E10.5 y continúan presentes en el hígado a lo largo de la vida

embrionaria [Ott et al., 1991]. En el día E9.5, *Foxa1* y *Foxa2* se encuentran altamente expresados durante la formación del brote del hígado, mientras que *Foxa3* se expresa a bajos niveles. Posteriormente, la expresión de *Foxa1* y *Foxa2* disminuye entre los días E12.5 y E15.5 antes de incrementar nuevamente en el hígado adulto. En contraste *Foxa3*, que inicialmente se expresa poco, incrementa su expresión en el día E10.5 y permanece elevado durante el desarrollo hepático [Monaghan et al., 1993]. De manera similar al patrón observado para *Foxa1* y *Foxa2*, *Oc1* se detecta al día E9, cuando la diferenciación hepática ocurre, luego disminuye de manera transitoria entre los días E12.5 y E15, antes de continuar una expresión estable dentro del sistema biliar extrahepático y durante el desarrollo del hígado [Barbacci et al., 1999; Landry et al., 1997; Lau et al., 2018; Rausa et al., 1997].

En contraste con *Foxa* y *Oc1,* altos niveles de los transcritos de *Hnf4* se localizan en la periferia del hígado donde se desarrollan los hepatocitos del día E11.5 al E16, pero no en el centro, donde las células hematopoyéticas se diferencian [Taraviras et al., 1994]. En el hígado de ratón hay un *switch* controlado del promotor P2 (distal) hacia el promotor P1 (proximal) que dirigen la transcripción de *Hnf4a* de la vida fetal hacia el nacimiento, y los transcritos dirigidos por P1 continúan su expresión a niveles significativos en el hígado adulto [Dean et al., 2010]. La activación temprana de *Hnf1b, Foxa1, Foxa2, Hnf4a* y *OC1* en el desarrollo del hígado entre los días E8.5-E9.5 sugiere su importancia en el compromiso temprano hacia el linaje de hepatoblasto [Lau et al., 2018].

Durante la etapa adulta, *Hnf1a* y *Hnf1b* se expresan en tejidos como el hígado, el páncreas, el riñón y el intestino. *Hnf1b* puede tener papeles regulatorios más amplios, ya que se expresa en órganos que carecen de *Hnf1a*, como el timo, el pulmón, los testículos y los ovarios [Cereghini, 1996; Reber and Cereghini, 2001]. *Foxa1* y *Foxa2* se expresan de manera elevada, principalmente en células epiteliales del hígado y páncreas desarrollados.

Los transcritos de *Hnf4* se expresan de manera más abundante en el hígado, riñón e intestinos adultos, con relativamente baja expresión observada en el páncreas, la piel y el estómago [Cattin et al., 2009; Miquerol et al., 1994; Sladek et al., 1990]. En el ratón adulto, solo *Oc1* se detecta en altos niveles en el páncreas y en muy bajos niveles en los testículos. Tanto los transcritos de *Oc1* como de *Oc2* se expresan altamente en el hígado [Davidson, 2006; Lau et al., 2018; Vanhorenbeeck et al., 2002].

1.7.2. Regulación diferencial de las isoformas de HNF4α en hígado y páncreas

Las múltiples isoformas de *HNF4A* generadas a través de *splicing* alternativo destacan la complejidad de la expresión y función de *HNF4.* El consenso es que las isoformas derivadas del promotor P1 se expresan predominantemente en el hígado adulto (aunque también en el riñón), mientras que las isoformas reguladas por el promotor P2 son activas tanto en el hígado embrionario como en las células β pancreáticas (Figura 15). Se han descrito sitios de unión para HNF1, OC1 y el factor de transcripción 6 que se une a la secuencia GATA (GATA6) en el promotor P1 [Kyrmizi et al., 2006]. En el hígado embrionario, se ha sugerido que HNF1β coopera con GATA6 para activar la expresión de *HNF4A1* [Hatzis and Talianidis, 2001] (Figura 15). Sin embargo en el hígado adulto, el sinergismo entre FOXA2 y OC1 dirige la expresión de *HNF4A1* [Kyrmizi et al., 2006; Lau et al., 2018] (Figura 15).

El promotor alternativo P2, que da origen a *HNF4A7*, puede dirigir la activación de HNF1β y OC1 en el hígado embrionario [Kyrmizi et al., 2006]. Mientras que en el páncreas, el promotor P2 se activa por los factores de transcripción pancreáticos HNF1α, OC1 y *Pancreatic and Duodenal Homeobox 1* (PDX1) [Lau et al., 2018] (Figura 15).

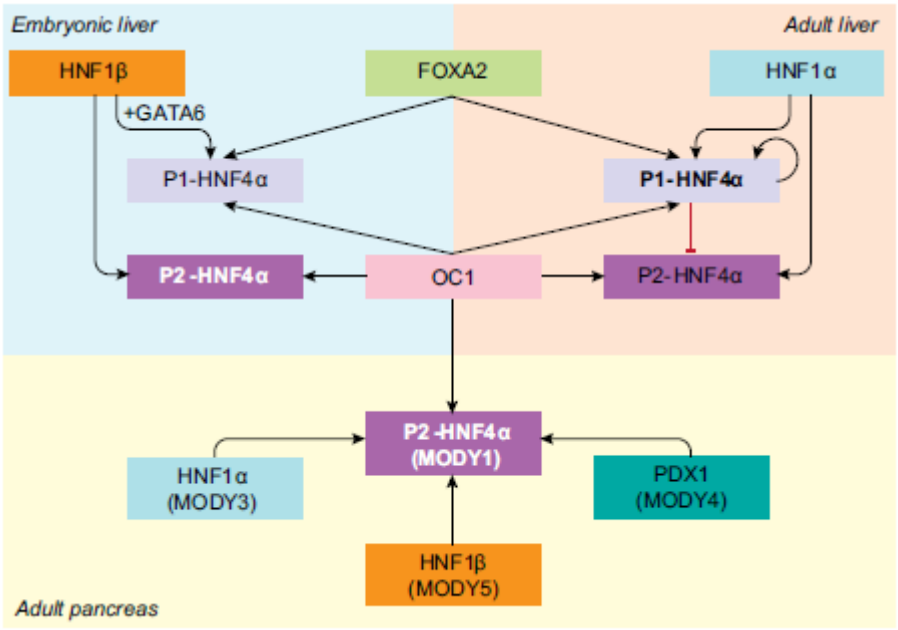

Fig. 15. Regulación diferencial de las isoformas de *HNF4A* en el hígado y páncreas. HNF1, OC1, GATA6 y FOXA2 están involucrados en activar la expresión de las isoformas reguladas por el promotor P1 de HNF4α en el hígado embrionario. HNF1β coopera con GATA6 para activar a P1-*HNF4A*, mientras que el hígado adulto, el sinergismo entre FOXA2 y OC1 dirige la expresión de P1-*HNF4A*. De manera similar, la expresión de P2-*HNF4A* es dirigida por OC1, HNF1β (hígado embrionario) y HNF1α (hígado adulto). El promotor P2 de *HNF4A* contiene sitios de unión para factores de transcripción en donde sus mutaciones conducen a diabetes de la adolescencia (MODY), nombrada HNF1α (MODY3), HNF1β (MODY5) y PDX1 (MODY4). FOXA, *forkhead box A;* HNF, factor nuclear de hepatocitos; OC, ONECUT. Tomada de [Lau et al., 2018].

Una vez revisada la red de regulación mediada por los HNFs, se puede entender que la variación en su expresión influya en el estado del desarrollo y diferenciación celular así como en el establecimiento de patologías.

2. ANTECEDENTES

2.1. *HNF4A* es desmetilado progresivamente durante la diferenciación de los progenitores hepáticos adultos HepaRG

Recientemente se han descrito los cambios que ocurren a nivel de la dinámica de metilación de DNA en el *locus* de *HNF4A* durante el proceso de diferenciación de la línea celular humana HepaRG. En un modelo *in vitro,* el progenitor hepático HepaRG se ha cultivado en condiciones de diferenciación durante 1 mes, encontrando que cambios en el estado de metilación e hidroximetilación del promotor P1 del gen *HNF4A* podrían ser los responsables del desencadenamiento de la diferenciación [Ancey et al., 2017].

En este estudio se aisló el DNA genómico en cada una de las semanas del mes de diferenciación y se realizó un análisis de metilación diferencial, encontrando que la mayor disminución en el estado de metilación correspondía al promotor P1 de *HNF4A* además, entre los sitios que progresivamente se hipometilan se encontraban blancos de HNF4α como *GDF7, CEP85, UBE2I, F2, SERPINA1, SBNO2, HDAC4, MET, CPT2* y *PTPRK.* Asimismo, los autores subrayan que no se encontraron cambios en la metilación del DNA en otros genes que incrementan su expresión durante la diferenciación, tales como *ALB, ALDOB, GSTA1* y *CYP3A4* [Ancey et al., 2017].

2.2. La desmetilación se asocia con un *switch* reversible de la expresión de las isoformas reguladas por el promotor 1 de *HNF4A*

Al estudiar el efecto de la desmetilación de *HNF4A* P1 a nivel de expresión, los investigadores [Ancey et al., 2017] encontraron que las isoformas dependientes del promotor P1 aumentaron su expresión, la cual correlacionaba negativamente con la desmetilación de la región, comparada con la expresión del promotor P2 (Figura 16).

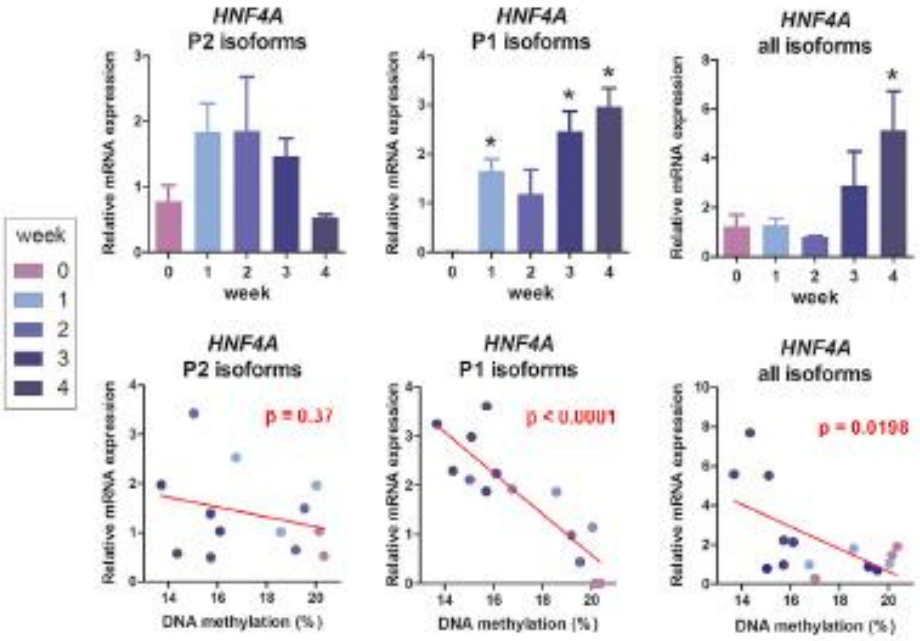

Fig. 16. Correlación entre la expresión de las isoformas reguladas por los promotores P1 y P2 de *HNF4A* a lo largo del proceso de diferenciación de la línea celular HepaRG. Los valores de expresión se muestran normalizados al tiempo 0 de la diferenciación para cada RT-qPCR. Los valores de P para cada correlación (Pearson) se muestran en los paneles inferiores. Tomado de [Ancey et al., 2017].

Cuando las células completamente diferenciadas se resembraron a baja confluencia para inducir una desdiferenciación, protocolo previamente descrito [Dubois-Pot-Schneider et al., 2014], los programas de transcripción vuelven a mostrar un patrón asociado al estado de progenitor a las 24 h del resembrado. Las isoformas reguladas por el promotor P1 de *HNF4A* revelaron un silenciamiento progresivo de su expresión, mientras que las isoformas dirigidas por el promotor P2 se reexpresaron (Figura 17), patrón opuesto al que caracterizó al proceso de diferenciación [Ancey et al., 2017].

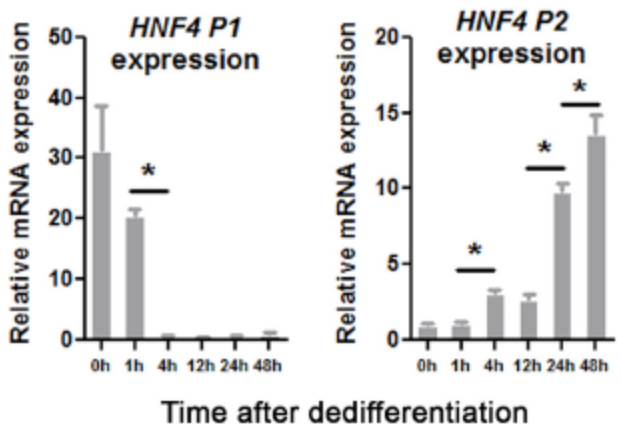

Fig. 17. Inversión del patrón de expresión de las isoformas de *HNF4A* en la desdiferenciación. Hepatocitos diferenciados durante 1 mes se resembraron a baja confluencia para inducir la desdiferenciación y la expresión de las isoformas reguladas por los promotores P1 y P2 fue evaluada por RT-qPCR. Los datos muestras el promedio ± DE. Tomado de [Ancey et al., 2017].

Con esta información los autores demostraron que existe un *switch* en la expresión de las isoformas reguladas por los promotores P2 y P1 de *HNF4A* en los progenitores HepaRG detectable a 1 semana del proceso de diferenciación hacia hepatocitos, y reversible a 1 día después de iniciada la desdiferenciación [Ancey et al., 2017].

2.3. La hidroximetilación del promotor P1 de *HNF4A* precede la diferenciación terminal de los hepatocitos

Como se describió en la sección introductoria, la desmetilación puede ser el resultado de una adición deficiente del grupo metilo en las cadenas nacientes de DNA durante la división celular (desmetilación pasiva) o la consecuencia de una oxidación progresiva de las citosinas metiladas, la cual es mediada por las dioxigenasas TET (desmetilación activa) [Kriaucionis and Heintz, 2009; Schubeler, 2015; Tahiliani et al., 2009]. Cuando los progenitores hepáticos HepaRG, se cultivan en estado de confluencia durante una semana, divisiones celulares adicionales no pueden llevarse a cabo (la proliferación se encuentra limitada). Lo anterior sugeriría que la desmetilación que los autores observaron durante el proceso de diferenciación no estaría ocurriendo de manera pasiva al no haber división celular, sino más bien, la desmetilación podría asociarse a un proceso activo.

En este estudio, los investigadores encontraron que la expresión de *TET1* y *TET2* se encuentra incrementada a una semana de diferenciación (Figura 18), lo cual correlacionaba con la mayor expresión de las isoformas reguladas por el promotor P1 de *HNF4A* [Ancey et al., 2017].

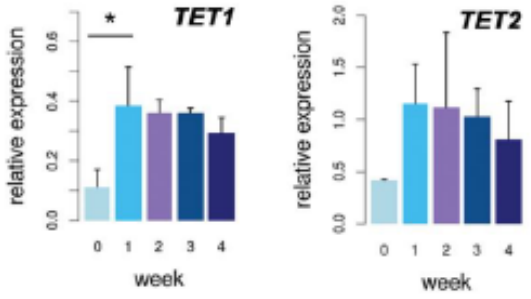

Fig. 18. Expresión de *TET1* y *TET2* durante la diferenciación de hepatocitos. Expresión de *TET1* (panel izquierdo) y *TET2* (panel derecho) evaluada por RT-qPCR a cada semana del proceso de diferenciación de la línea celular HepaRG. *Indica un valor de p menor a 0.05 en la prueba de t student. Tomado de [Ancey et al., 2017]

De igual manera, se encontró un incremento de 5hmC en el promotor P1 de *HNF4A* después de una semana de la diferenciación del progenitor hepático. Sin embargo, se observó una menor ocupación de 5hmC en las semanas subsecuentes de la diferenciación hasta alcanzar el estado de hepatocito maduro a los 30 días. (Figura 19). Este enriquecimiento de 5hmC alcanza el nivel más bajo a las 24 h de resembrar a baja confluencia los hepatocitos diferenciados por 30 días (Figura 19).

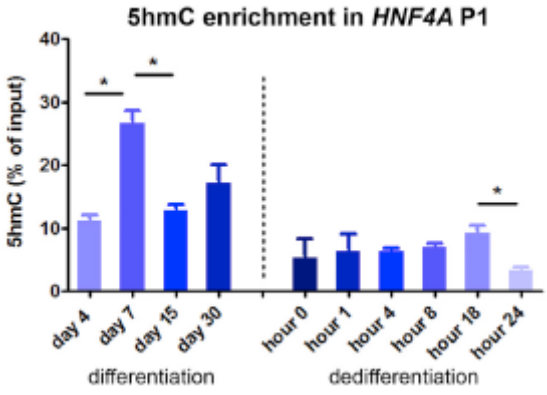

Fig. 19. El promotor P1 de *HNF4A* se enriquece en 5hmC durante la diferenciación de hepatocitos. La cinética de 5hmC fue evaluada a través de hMeDIP para el promotor P1 de *HNF4A* hasta la completa diferenciación de los hepatocitos (panel izquierdo) y seguida también durante la desdiferenciación (panel derecho). Los datos muestran el promedio ± DS de tres experimentos independientes. * $p < 0.05$ en la prueba de t de student. Tomado de [Ancey et al., 2017].

Con estos datos los autores señalan que hay un enriquecimiento en 5hmC que precede a la expresión de las isoformas reguladas por el promotor P1 de *HNF4A* durante la

diferenciación de progenitores hepáticos, por lo que se puede sugerir que esta zona diferencialmente hidroximetilada representa una región de regulación [Ancey et al., 2017].

2.4. El factor de transcripción pionero FOXA2 colocaliza con TET1 en el promotor de *HNF4A*

Los datos descritos en los párrafos anteriores sugieren un modelo en el que los progenitores bipontenciales hepáticos se encuentran enriquecidas en 5hmC en el promotor P1 de *HNF4A*, lo cual estaría determinado por las enzimas TET en un estado temprano de la diferenciación terminal de los hepatocitos. Sin embargo, estas enzimas dioxigenasas requieren de cofactores para ser reclutadas a sitios específicos del genoma. Los autores identificaron que en el *locus* de *HNF4A* se encuentra un sitio de unión para el factor pionero de hepatocitos FOXA2 entre -306 y -7 bp río arriba del TSS regulado por P1 y validaron la unión de este factor de transcripción tanto en el estado de progenitor como a una semana de diferenciación, así como la unión de TET1 en este sitio en las células con una semana de diferenciación (Figura 20) mientras que no se encontraron cambios significativos en el caso de TET2. La ocupación de FOXA2 se detectó, pero no presentó cambios en el promotor P1, de manera consistente con su papel de pionero. No hubo cambios significativos en ninguna de las tres proteínas en el promotor P2 [Ancey et al., 2017].

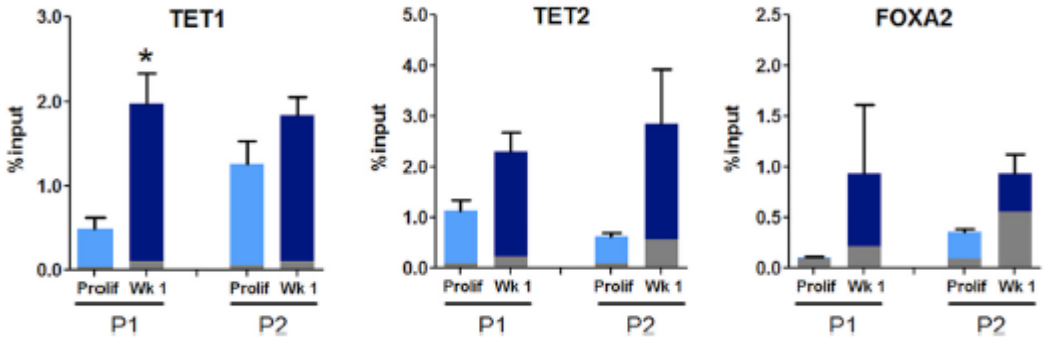

Figura 20. TET1 y FOXA2 colocalizan en el *locus* P1 de *HNF4A.* Se realizó inmunoprecipitación de la cromatina (ChIP) con anticuerpos anti-dioxigenasas TET y contra FOXA2 en el estado de progenitor (Prolif) y después de una semana de diferenciación (Wk 1). qPCRs fueron realizadas para los promotores P1 y P2 de *HNF4A*. Las barras grises representan la señal de fondo de IgG. Se realizaron tres réplicas biológicas. Se muestran resultados representativos. Los datos muestran el promedio ± DE. * $p < 0.05$ en la prueba de t de student. Tomado de [Ancey et al., 2017].

2.5. FOXA2 y TETs son requeridos para el *switch* de expresión en *HNF4A* relacionado con 5hmC

Utilizando RNAs de interferencia pequeños (siRNAs), el grupo de Hernández-Vargas demostró que la inducción de la expresión de las isoformas coordinadas por el promotor P1 de *HNF4A* a la semana de diferenciación fue significativamente afectada después del silenciamiento de TET1/TET1 (Figura 21), esta afectación fue aún más drástica al silenciar FOXA2 (Figura 21), mientras que las isoformas reguladas por P2 no presentaron cambios con estos silenciamientos (Figura 21). Por su parte, la inducción de la expresión de las isoformas reguladas por P1 correlaciona con un pico de 5hmC en el promotor P1 (Figura 21); de manera equivalente, este enriquecimiento se vio afectado después de silenciar las TETs y FOXA2, sin cambios significativos en el promotor P2 (Figura 21) [Ancey et al., 2017].

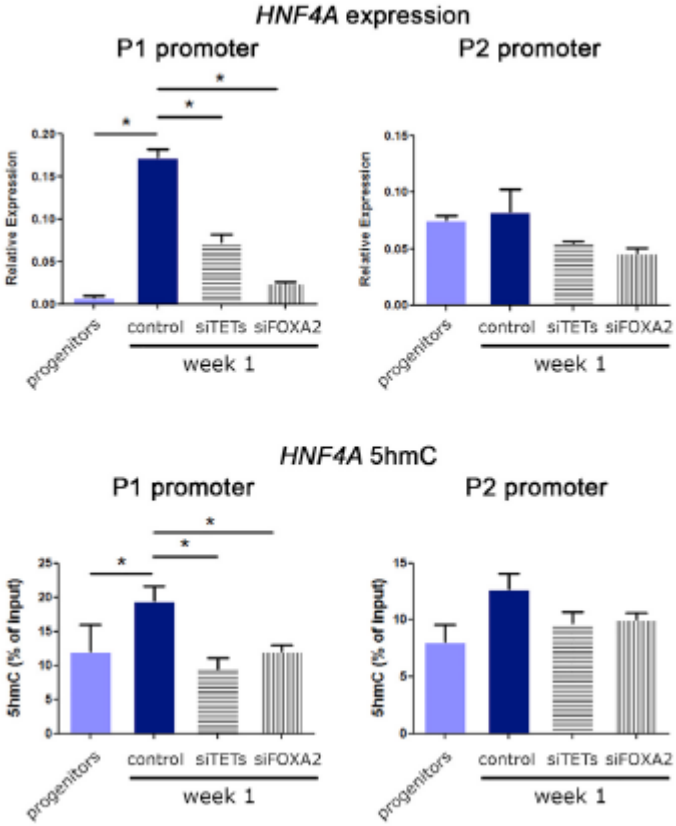

Fig. 21. TET1 y FOXA2 se requieren para el switch de 5hmC y las isoformas de *HNF4A*. Después de una semana de diferenciación expuestas a los RNAs de interferencia siTETs y siFOXA2, se extrajo el RNA para evaluar las isoformas dirigidas por los promotores P1 (panel superior izquierdo) y P2 (panel superior derecho) por RT-qPCR. Bajo las mismas condiciones de silenciamiento, se extrajo DNA para cuantificar la 5hmC utilizando hMeDIP sobre los promotores P1 (panel inferior izquierdo) y P2 (panel inferior derecho). Los ensayos se realizaron por triplicado. Los resultados muestran el promedio ± DE. * $p < 0.05$ en la prueba de t de student. Tomado de [Ancey et al., 2017].

Al realizar una inmunoprecipitación de cromatina (ChIP) durante la primera semana de diferenciación (cuando ocurre el mayor enriquecimiento de 5hmC), los autores comprobaron que TET1 se enriquece en el promotor P1 (Figura 22) y que este incremento no ocurre en presencia del siRNA contra FOXA2 (Figura 22), demostrando que el incremento de 5hmC se ve eliminado al silenciar TETs o FOXA2 y que este efecto es limitado a la región del promotor P1 de *HNF4A* [Ancey et al., 2017].

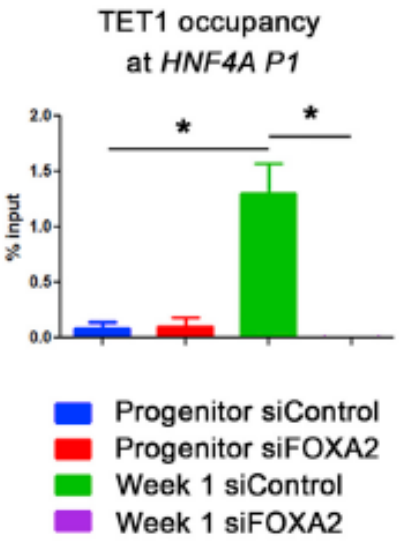

Fig. 22. El reclutamiento de TET1 al promotor P1 de *HNF4A* depende de la presencia de FOXA2. Ocupación de TET1 en el promotor P1 de *HNF4A* evaluado por ChIP en condiciones control (siControl) o después del silenciamiento de FOXA2 (siFOXA2)**.** Los resultados muestran el promedio ± DE. * $p < 0.05$ en la prueba de t de student. Tomado de [Ancey et al., 2017].

En conclusión, el trabajo de Ancey y colaboradores revela que tanto la enzima dioxigenasa TET1 como el factor pionero FOXA2 se requieren para el *switch* de expresión de *HNF4A* mediado por el enriquecimiento de 5hmC y que marca un paso inicial de la diferenciación de progenitor hepático bipotencial HepaRG.

2.6. Interrelación entre el metabolismo y la cromatina ¿Podría la modulación farmacológica de metabolitos intervenir en la expresión tanto fisiológica como patológica de genes?

Un área relevante en la investigación epigenética que ha surgido en años recientes relaciona cómo el metabolismo celular regula varios eventos involucrados en la remodelación de la cromatina. Las células perciben estos cambios en el ambiente y las traducen como modulaciones específicas en el epigenoma a través de una gran variedad de componentes de señalización, algunos de los cuales son proteínas con actividad enzimática de modificadores de histonas y de DNA. Las enzimas que llevan a cabo estas modificaciones dependen críticamente de la disponibilidad de grupos fosfato, acetilo y metilo, por mencionar algunos. Esto constituye un enlace entre el metabolismo celular y el control epigenético. Sin embargo aún es incierta la especificidad y el grado de cambio en

que los niveles de los metabolitos celulares puedan influir en el epigenoma [Berger and Sassone-Corsi, 2016].

En este trabajo haremos énfasis en la regulación de los niveles de la S-adenosilmetionina (SAM), el sustrato requerido para la metilación del DNA, por un derivado de adenosina y su papel como metabolito capaz de influir en la regulación epigenética, en particular de la hidroximetilación del DNA.

La metilación del DNA (así como la de histonas y otras proteínas no histónicas) requiere del metabolito SAM como fuente de grupos metilo. La SAM es un co-sustrato involucrado en la transferencia de grupos metilo y se obtiene a partir de ATP durante el ciclo de la metionina por las enzimas metionina adenosiltransferasas (MATs) (Figura 23) [Grillo and Colombatto, 2008]. El grupo metilo (CH_3-) en la SAM es reactivo y es donado al aceptor de sustratos por *trans*-metilación. Después de esta reacción, SAM se convierte en S-adenosilhomocisteina (SAH), que es un potencial inhibidor de las metiltrasferasas. Se ha caracterizado una gran variedad de metiltransferasas que están involucradas en el control epigenético, incluyendo las DNMTs. Ya que la fuente de la SAM es el ATP y la metionina, la concentración intracelular de ATP así como su sublocalización puede influir en la disponibilidad de SAM para las reacciones de metilación [Berger and Sassone-Corsi, 2016].

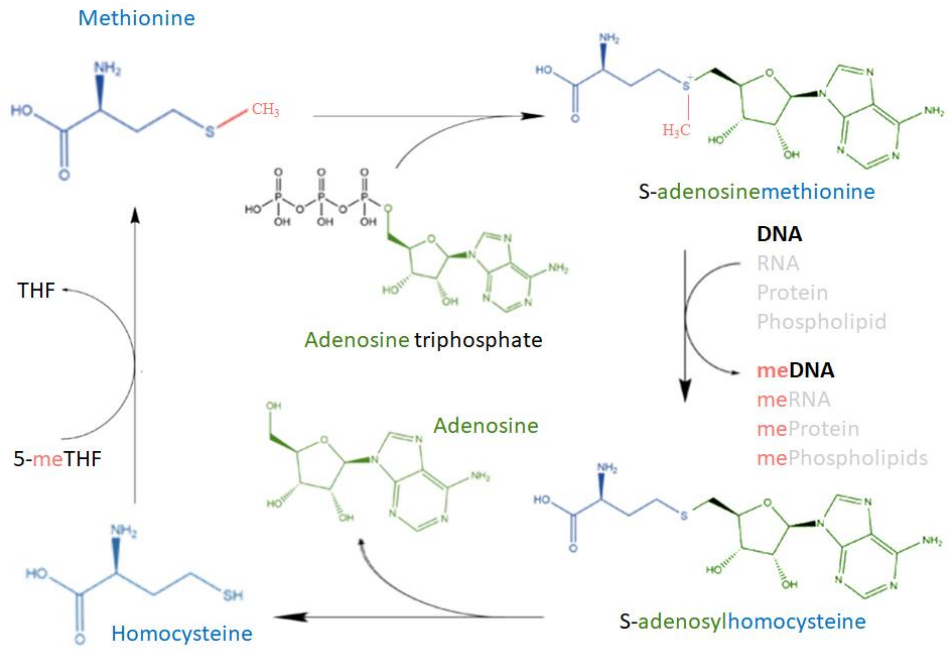

Fig. 23. Síntesis de SAM a partir de metionina y ATP. Esquema que representa el ciclo de la metionina donde se destacan las reacciones de *trans*-metilación biológicas mediadas por la S-adenosilmetionina (SAM). Cada componente del ciclo esta denotado por colores: adenosina en verde, metionina y su precursor homocisteina en azul, fosfatos en negro y el grupo metilo en rojo.

Como se muestra en la figura 23, la adenosina, que es una molécula fisiológica, constituye una parte de la estructura de carbono de SAM, y se incorpora a la metionina a través de las enzimas MAT que toman el nucleósido a partir del ATP.

La capacidad del sistema adenilato para modular los niveles energéticos (ATP) de la célula ha sido propuesta previamente [Atkinson, 1968]. Nuestro grupo ha evaluado los efectos farmacológicos de la adenosina, entre los cuales se encontró que el nucleósido genera un incremento de la carga energética del hígado después de su administración intraperitoneal en ratas sanas, lo cual se denota por un incremento en los niveles de ATP [Chagoya de Sanchez et al., 1972]. Este cambio metabólico puede ser explicado de acuerdo a la hipótesis de Atkinson, la cual propone que la carga de energía controla la velocidad y la dirección de una secuencia metabólica [Atkinson, 1968]. Un efecto equivalente se encontró cuando la adenosina se administró en un modelo de hepatotoxicidad inducida por etanol [Hernandez-

Munoz et al., 1978] y tetracloruro de carbono (CCl_4) [Hernandez-Munoz et al., 1990] en ratas y más recientemente este efecto se reprodujo usando una sal derivada de la adenosina, denominada IFC-305 (Patente UNAM 207422), en un modelo de intoxicación hepática crónica por dietilnitrosamina [Chavez et al., 2017].

Considerando la capacidad de la adenosina para incrementar la carga energética de la célula, a través del incremento de los niveles de ATP, en el laboratorio se ha propuesto que el IFC-305 es capaz de estimular la síntesis de SAM al ser una reacción dependiente de ATP. En un contexto fisiológico se encontró un pico endógeno en la concentración de adenosina que correlaciona con un incremento de SAM durante la evaluación de los ritmos circadianos de estas moléculas (Figura 24A) [Chagoya de Sanchez et al., 1991]. Por otra parte, la administración de IFC-305 favorece la recuperación de los niveles de SAM en la cirrosis inducida con CCl_4 (Figura 25A) [Rodriguez-Aguilera et al., 2018], y en un modelo de intoxicación crónica con dietilnitrosamina (Figura 25B) [Lozano-Rosas et al., 2019]. Además la regulación de la capacidad metilante (SAM/SAH) mediada por adenosina, se puede relacionar con la metilación endógena de fosfolípidos (Figura 24B) [Chagoya de Sanchez et al., 1991] y con los niveles de metilación y de hidroximetilación de DNA durante la recuperación de la cirrosis (Figura 25C) [Rodriguez-Aguilera et al., 2018].

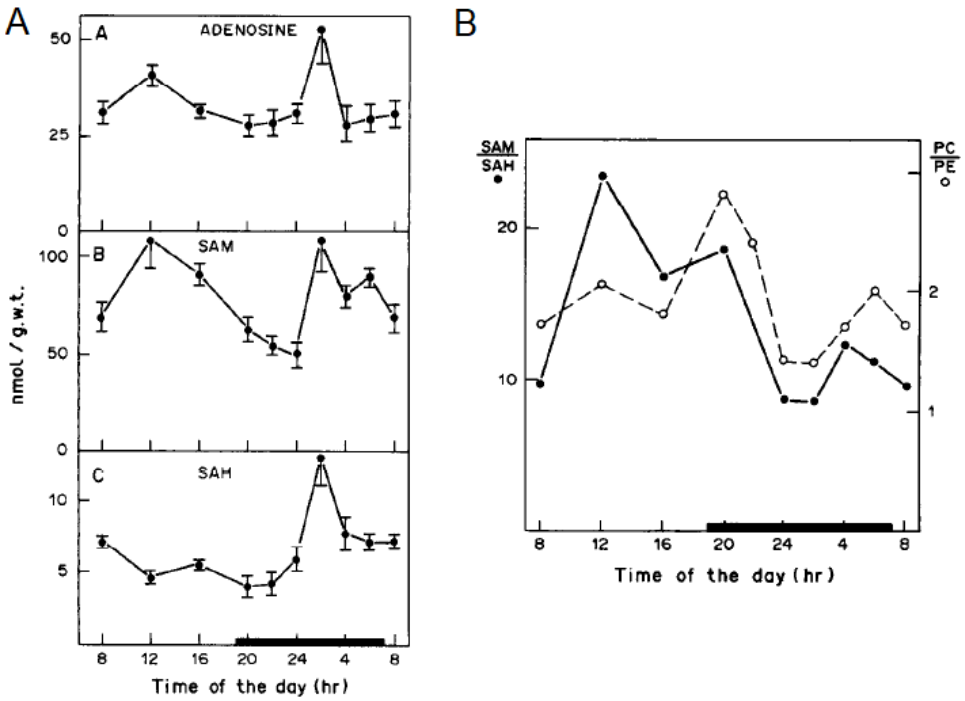

Fig. 24. Variaciones de los sustratos y productos de las reacciones de *trans*-metilación en el hígado de rata durante 24 h. (A) Se muestran los cambios de adenosina, S-adenosilmetionina (SAM) y S-adenosilhomocisteina (SAH) a lo largo del día. El eje de las abscisas indica las horas del día, la región en negro representa el periodo de oscuridad. Los valores muestran el promedio ± DE de 5 animales. De acuerdo con la prueba de Mann-Whitney en el panel superior, comparando el valor de la adenosina a las 2 h vs las 24 h tiene un valor de $p < 0.05$; para 12 h vs 24 h $p < 0.01$, para 12 h vs 8 h $p < 0.02$. En el panel intermedio, los valores de SAM a las 12 h y 2 h vs 24 h tienen un valor de $p < 0.01$ y 0.02 respectivamente. En el panel inferior, los valores de SAH son significativamente diferentes; para 2 h vs 24 h $p < 0.02$ y para 2 h vs 4 h $p < 0.05$. (B) Variaciones de la actividad metilante en el hígado de rata a lo largo del día. El eje de las abscisas indica el tiempo del día, con la región negra representando el periodo de oscuridad. Las ordenadas representan la relación SAM/SAH (línea continua) y la relación fosfatidil colina/fosfatidil etanolamina (PC/PE), que indica la metilación de fosfolípidos (línea discontinua). Se observa una correlación entre el pico de adenosina con el pico de SAM y de SAM/SAH a las 12 h, lo que indica un efecto de la adenosina sobre la actividad metilante y por otro lado una correlación entre el pico de SAM/SAH y de PC/PE a las 12 h, por lo que se puede asociar la actividad metilante con la metilación de fosfolípidos a este tiempo. Tomado de [Chagoya de Sanchez et al., 1991].

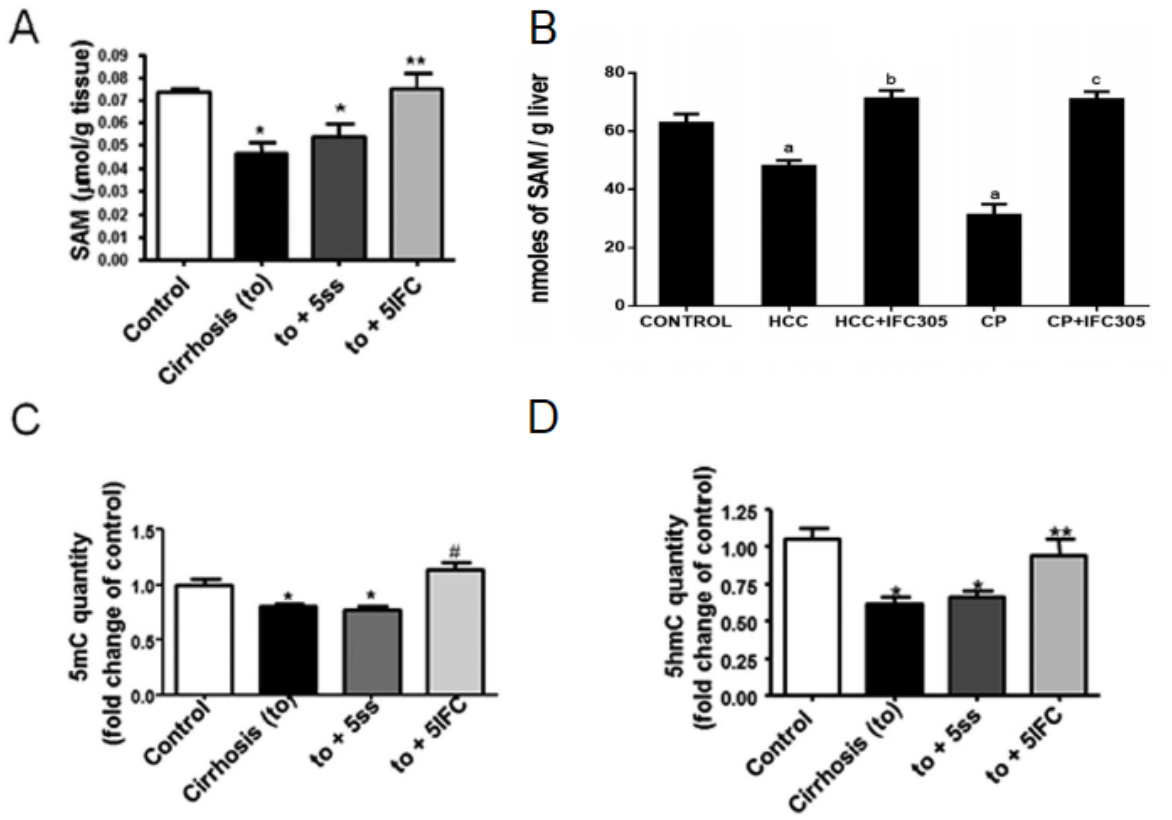

Fig. 25. El derivado de adenosina IFC-305 regula los niveles de SAM y la dinámica de metilación del DNA en el estado patológico. Cuantificación de SAM (A) en cirrosis inducida por CCl_4 y en (B) carcinoma hepatocelular inducido por dietilnitrosamina. (C) Cuantificación de la metilación global del DNA en cirrosis. (D) Cuantificación de la hidroximetilación global del DNA en cirrosis. Los datos representan el promedio ± DEM de tres ratas/grupo. *Diferencia estadística ($p < 0.05$) comparado contra grupo control. **Diferencia estadística ($p < 0.05$) comparada contra cirrosis (to). $^{\#}$Diferencia estadística ($p < 0.05$) comparada contra cirrosis (to) y to + 5ss. Para el panel B: a indica diferencia estadística contra el grupo control, b indica diferencia estadística contra el grupo de carcinoma hepatocelular (HCC) y c indica diferencia estadística contra el grupo de progresión de cáncer (CP). ($p < 0.05$). Tomado de [Lozano-Rosas et al., 2019; Rodriguez-Aguilera et al., 2018].

Esta propiedad de la adenosina y de su derivado, el IFC-305, de modular los niveles de SAM podría ser el origen de los diferentes efectos que presentan estos compuestos, al estar modulando la expresión génica a través de mecanismo epigenéticos. Dichos efectos se revisan a detalle en [Rodríguez-Aguilera et al., 2019] y están relacionados con la reducción de la fibrosis y un mejoramiento de la función hepática a través de cambios en el

transcriptoma [Perez-Carreon et al., 2010], la promoción de la recuperación del ciclo celular en el hígado cirrótico [Chagoya de Sanchez et al., 2012], la polarización hacia macrófagos antiinflamatorios en cirrosis [Perez-Cabeza de Vaca et al., 2018], la prevención de la activación de células estelares hepáticas [Velasco-Loyden et al., 2010], además de presentar propiedades antineoplásicas [Chavez et al., 2017; Lian et al., 2019; Lozano-Rosas et al., 2019; Velasco-Loyden et al., 2017].

Con los datos anteriores, podemos sugerir que el metabolismo celular puede influir en el estado de diferenciación de las células al regular metabolitos implicados en el control epigenético. El estado energético directamente afecta a los reguladores de la cromatina que modulan la transcripción, alterando la disponibilidad de metabolitos celulares como SAM entre otros cofactores de enzimas modificadoras de la cromatina. Dado que la reserva local de energía puede influir en el estado epigenético de las células [Harvey et al., 2019], una reprogramación metabólica podría considerarse una herramienta potencial para estudiar los diferentes estados de diferenciación, así como la influencia del estado metabólico sobre modificaciones epigenéticas como la hidroximetilación del DNA, que a su vez puede relacionarse con la identidad celular. Además, tanto la reprogramación metabólica como epigenética pudieran ser utilizadas también en patologías relacionadas con la regeneración tisular y como medida de intervención temprana para enfermedades donde ocurre una desdiferenciación celular, como en el cáncer.

3. JUSTIFICACIÓN

A pesar de que la distribución de la 5hmC durante la diferenciación de células progenitoras adultas se ha evaluado en diferentes tejidos (revisado en [Ecsedi et al., 2018]), hay una carencia de información de cómo ocurre este proceso en el hígado. Previamente se describió un cambio específico de 5hmC en el *locus* de *HNF4A,* que ocurre a una semana de cultivo celular lo cual conduce a la diferenciación de progenitores hepáticos [Ancey et al., 2017]. Este hallazgo fue una motivación para realizar un mapa más detallado de 5hmC en el modelo *in vitro* de diferenciación de progenitores hepáticos.

Hasta donde tenemos conocimiento, no existe un análisis de 5hmC, con una resolución a nivel de nucleótido, durante la diferenciación de progenitores hepáticos bipotenciales putativos hacia hepatocitos. A pesar de las limitaciones, este modelo ofrece la ventaja de estudiar los hepatocitos en aislamiento, lo cual es más problemático con aproximaciones *in vivo* en tejido hepático completo.

Al momento de la redacción de éste documento ya ha habido varias revisiones sobre la distribución y la función de 5hmC [Cimmino and Aifantis, 2017; Ecsedi et al., 2018; Laird et al., 2013; Liang et al., 2016; Lopez et al., 2017; Shi et al., 2017; Szyf, 2016; Zhu et al., 2018] y se ha descrito la distribución de 5hmC en el hígado sano, demostrando que ésta sufre cambios durante el desarrollo del carcinoma hepatocelular [Li et al., 2016b]. Además se sabe que hay un incremento de 5hmC en el hígado adulto humano comparado contra el hígado fetal, con una ocupación sobrerrepresentada en genes involucrados en procesos catabólicos y metabólicos [Ivanov et al., 2013]. Otro estudio ha relacionado los patrones de metilación del DNA y los ha relacionado con la edad del tejido hepático en el ratón, encontrando que la mayoría de los cambios ocurren entre los días postnatales 5 y 20 [Cannon et al., 2016], sin embargo este estudio no distinguió entre 5mC y 5hmC.

Por otra parte, las aproximaciones que se han realizado en modelos *in vitro* sobre la diferenciación de hepatocitos, han utilizado células troncales humanas mesenquimales, donde se ha inhibido la metilación del DNA y se ha observado un incremento en la eficiencia de diferenciación [Chaker et al., 2018; Lee et al., 2017; Seeliger et al., 2013]. Además, otro reporte describe una acumulación transitoria de 5-carboxilcitosina, otro intermediario en el proceso de desmetilación activa del DNA durante la diferenciación de células pluripotenciales troncales humanas inducibles a hepatocitos [Lewis et al., 2017].

4. PLANTEAMIENTO DEL PROBLEMA

Algunos estudios han descrito los cambios en la distribución genómica de la 5hmC durante el desarrollo hepático humano y de ratón. También se ha sugerido que en procesos patológicos como el cáncer hepático, hay una pérdida de esta citosina modificada. Sin embargo, aún no hay información relacionada con la abundancia, localización genómica y función de la 5hmC durante el proceso de diferenciación de progenitores hepáticos adultos en humano. Es por ello que el presente estudio plantea la evaluación de la distribución de 5hmC a lo largo del genoma, a una semana de diferenciación, como posible marcador de identidad celular de hepatocitos.

5. HIPÓTESIS

La diferenciación de progenitores hepáticos adultos humanos hacia hepatocitos, involucra un enriquecimiento genómico de 5hmC asociado con la activación de genes relacionados con la fisiología hepática.

6. OBJETIVO GENERAL

Identificar los dinucleótidos CpGs hidroximetilados a nivel genómico durante la diferenciación del progenitor hepático HepaRG, así como el efecto de la modificación del estado metabólico por un derivado de adenosina, sobre la adquisición de la hidroximetilación del DNA y de marcadores hepáticos en este proceso.

7. OBJETIVOS PARTICULARES

1. Identificar los genes diferencialmente expresados entre el estado de progenitor hepático y las células con una semana de diferenciación.
2. Analizar la distribución de 5hmC durante la diferenciación del progenitor hepático HepaRG.
3. Asociar las CpGs diferencialmente hidroximetiladas con genes diferencialmente expresados y correlacionarlos con la función hepática.
4. Evaluar la viabilidad de la línea celular HepaRG en respuesta a la exposición con el derivado de adenosina, inductor de SAM, IFC-305.
5. Determinar si la intervención metabólica con el derivado de adenosina puede influir en la dinámica de metilación de DNA y por consecuencia en el proceso de diferenciación.

8. MÉTODOS

8.1. Sustancias químicas

Los reactivos fueron adquiridos con Sigma Chemical Co. (St. Louis, MO). El IFC-305 es la sal de aspartato de adenosina: 2-aminosuccinic acid-2-(6-amino-9*H*-purin-9-il)-5-(hidroxmetil) tetrahidrofuran-3,4-diol (1:1), y se sintetizó en el laboratorio de acuerdo con la patente UNAM 207422.

8.2. Cultivo de la línea celular HepaRG

Las células HepaRG (Biopredic) se cultivaron a 37°C y CO_2 al 5% de la siguiente manera. La células en diferenciación ($4.4 \times 10^4/cm^2$) se crecieron por una semana en medio William's E (Gibco 12551-032) y se suplementó con suero fetal bovino al 10% (Eurobio CVFSVF0001), penicilina/estreptomicina 1x (Gibco 10378016), insulina 5 µg/mL (Sigma I9278) e hidrocortisona 3×10^{-5} mM (Sigma H0888) en placas de cultivo de 6 pozos (Figura 26), el medio fue reemplazado 24 h después del sembrado y una vez más después de 3 días. Para la condición proliferante, las células se sembraron a baja confluencia, para evitar el contacto célula-célula y, con esto, la diferenciación.

El tratamiento con IFC-305 comenzó 24 h después del sembrado celular, y las células se trataron nuevamente a los 3 días de cultivo, cuando el medio se reemplazó (Figura 26); las células expuestas a la glicina dimetiloxalílica (DMOG (Biotechne CAS# 89464-63-1)) siguieron el mismo esquema de tratamiento que las células expuestas al IFC-305, a las concentraciones correspondientes; las células expuestas a la S-adenosilmetionina (SAM) en su forma de p-toluensulfonato [Cabrales-Romero Mdel et al., 2006; Li et al., 2015; Stiuso et al., 2016; Tomasi et al., 2012] (Sigma A-2408) fueron tratadas cada 24 h con una concentración de 1 mM en medio fresco, la cual es equivalente a la concentración utilizada

para IFC-305, el tratamiento inició 24 h después del sembrado de las células y continuó hasta el día 6. Los tres compuesto se solubilizaron directamente en el medio William's E.

Por otra parte, una mezcla de siRNAs contra *TET1, TET2* y *TET3* o siRNA control (siRNA CTRL) (Dharmacon, On-Target Plus siRNA) fue transfectada en la células HepaRG (4.4 x $10^4/cm^2$), sembradas 24 h previas a la transfección, en placas de cultivo de 12 pozos, a una concentración de 20 nM utilizando Lipofectamina 2000 (Invitrogen 11668) utilizando 3 µL por reacción en 350 µL de Medio William´s sin suplementar, mezclando de acuerdo a las instrucciones del fabricante. La mezcla de lipofectamina + siRNA se incubó a temperatura ambiente por 15 min y se agregaron, por goteo, 50 µL de la mezcla a los pozos correspondientes. La transfección se incubó durante 12 h a 37°C y CO_2 5%. Transcurrido este tiempo, se cambió el medio de cultivo y se reemplazó por 3 mL de medio William's suplementado, y se siguió el esquema de los tratamientos químicos para diferenciar durante una semana. Las células se recuperaron 7 días después de la siembra para obtener el material biológico necesario para cada ensayo.

8.3. Análisis del transcriptoma

El RNA se aisló directamente del cultivo utilizando TRIzol (Invitrogen 15596018) y tratado con DNAsa (Invitrogen 18068-015) como se describe a continuación:

Preparación de la muestra

En la placa de cultivo de 6 pozos:

- Lavar las células con 5 mL de solución reguladora de fosfatos (PBS) 1x.
- Adicionar 300 µL de TRIzol por pozo, las células se despegarán inmediatamente, utilizando la micropipeta, lavar varias veces con la mezcla TRIzol-células y transferir el volumen a un tubo de mricrocentrífuga de 1.5 mL.
- En este punto, la muestra puede congelarse inmediatamente a -70°C.

Extracción

- Descongelar el tubo con la mezcla TRIzol-células, en hielo.
- Centrifugar a 12 000 *g* por 10 min a 4°C para remover el material insoluble.
- Transferir el sobrenadante a un tubo de microcentrífuga de 1.5 mL, nuevo y libre de RNasas.
- Incubar la muestra durante 5 min a temperatura ambiente.
- Agregar 0.2 mL de cloroformo por cada 1 mL de TRIzol (60 µL para 300 µL de TRIzol).
- Mezclar vigorosamente por 30 s e incubar a temperatura ambiente de 2 – 15 min.
- Centrifugar a 12 000 *g* por 15 min a 4°C.

Aislamiento de RNA

- Transferir la fase acuosa a un tubo nuevo.
- Agregar 0.5 mL de isopropanol 100% por cada 1 mL de TRIzol (150 µL para 300 µL de TRIzol), mezclar.
- Incubar la muestra a temperatura ambiente de 5 – 10 min.
- Centrifugar a 12 000 *g* por 10 min a 4°C (Mantener siempre en hielo los tubos que contienen el RNA).
- Remover el sobrenadante y lavar el botón de RNA adicionando 1 mL de etanol 75% por cada 1 mL de TRIzol (300 µL para 300 µL de TRIzol).
- Mezclar en vortex y centrifugar a 7 500 *g* por 5 min a 4°C.
- Secar brevemente (no completamente) el botón de RNA invirtiendo el tubo en una servitoalla a temperatura ambiente.
- Adicionar 30 µL de agua inyectable (nunca utilizar agua DEPC ya que inhibe la reacción de retrotranscriptasa).

- Medir la concentración de RNA y la relación de densidad óptica 260/280, la cual debe ser cercana a 2.
- Verificar la integridad del RNA en un gel de agarosa al 1% con 1 µL de RNA.
- Almacenar a -70°C.

Tratamiento con DNasa

Para 1 µg de RNA:

1 µL de solución reguladora (*buffer*) de reacción de DNasa I

1 µL de DNasa I Amp Grade, 1 U/µL

cbp 10 µL H_2O inyectable

- Incubar la mezcla por 15 min a temperatura ambiente
- Calentar a 65°C por 10 min.

Obtención del Transcriptoma

Utilizando el estuche Illumina ToatlPrep-96 RNA Amp (Ambion 4393543), 500 ng de RNA fueron transcritos inversamente a cDNA, se sintetiza una segunda cadena para actual como templado de la RNA polimersa T7 y ser etiquetada con biotina-UTP.

2 000 ng de cDNA etiquetado se hibridaron en el microarreglo Illumina HumanHT-12 v3 (Illumina) y se procedió de acuerdo a las instrucciones del fabricante. Las laminillas se leyeron inmediatamente utilizando el Illumina BeadStation iScan (Illumina). Los ensayos se realizaron por duplicado con dos cultivos independientes por condición.

8.4. RT-PCR cuantitativa

La síntesis de cDNA se realizó con 2 µg de RNA total utilizando la M-MLV transcriptasa inversa (Invitrogen 28025-013) y *random primers*.

1 µL *Random primers* 250 µg/µL.

1 µL dNTPs mix 10 mM.

cbp 12 µL H_2O inyectable.

2 µg RNA.

Incubar la mezcla a 65°C por 5 min y enfriar rápidamente en hielo. Centrifugar brevemente y adicionar:

4 µL *First-Srand* solución reguladora 5x

2 µL Ditiotreitol (DTT) 0.1 M

Mezclar el contenido de tubo suavemente e incubar el tubo a 25°C por 2 min.

Adicionar 1 µL (200 U) de M-MLV RT y mezclar con la micropipeta suavemente hacia arriba y hacia abajo.

Incubar a 37°C durante 50 min.

Inactivar la reacción calentando a 70°C por 15 min.

Todos los ensayos de PCR cuantitativa se realizaron independientemente utilizando 3 cultivos por condición en duplicado. Se utilizó el estuche Mesa Green qPCR 2x Master Mix Plus (Eurogentec 05-SY2X-06+WOU) en el sistema CF96 PCR (Bio-Rad). Los oligonucleótidos fueron descritos previamente [Ancey et al., 2017] y se muestran en la Tabla 6. La expresión relativa fue calculada de acuerdo al método ΔΔCt como se describe a continuación: Nivel de expresión = 2^-(ΔΔ Ct), dónde ΔCt = (promedio Ct $_{\text{gen evaluado}}$ – promedio Ct $_{\text{gene housekeeping}}$), y ΔΔCt = ΔCt - Promedio ΔCt $_{\text{Condición control}}$). La normalización se realizó contra las células proliferantes, que fueron consideradas como condición control para comparar los niveles de expresión y *SFRS4* fue utilizado como gene *housekeeping*.

Tabla 6. Lista de oligonucleótidos utilizada en RT-PCR cuantitativa.

Región	Secuencia
SFRS4	Fw (5'-GGCTACGGGAAGATCCTGGA-3')
	Rv (5'-TGCATCACGCAGATCATCAA-3')
ALDOB	Fw (5'-TGTTCACACGGGTTCTTCTG-3')
	Rv (5'-CGGGCATTGGACCCTAGTA-3')
GSTA	Fw (5'-GGGAGAGAACTATTGAGAGGAACA-3')
	Rv (5'-TTAAACGCTGTCACCGTCCT-3')
ALB	Fw (5'-GCTTATTCCAGGGGTGTGTTT-3')
	Rv (5'-CTGAGCAAAGGCAATCAACA-3')
HNF4A P1	Fw (5'-ATGGACATGGCCGACTACAGTGCT-3')
	Rv (5'-CGAATGTCGCCGTTGATC-3')
HNF4A P2	Fw (5'-CTTGGCCATGGTCAGCGTGAACG-3')
	Rv (5'-CGAATGTCGCCGTTGATC-3')
TET1	Fw (5'-GCTATACACAGAGCTCACAG-3')
	Rv (5'-GCCAAAAGAGAATGAAGCTCC-3')
TET2	Fw (5'-CTTTCCTCCCTGGAGAACAGCTC-3')
	Rv (5'-TGCTGGGACTGCTGCATGACT-3')
IDH1	Fw (5'-CGGAACCCAAAAGGTGACAT-3')
	Rv (5'-TGGCAACACCACCACCTTCT-3')
IDH2	Fw (5'-CACGGCCTCAGCAATGTG-3')
	Rv (5'-TCGAGGAAGTCCGTGGTGTT-3')
DNMT1	Fw (5'-GATGTGGCGTCTGTGAGGT-3')
	Rv (5'-CCTTGCAGGCTTTACATTTCC-3')
DNMT3A	Fw (5'-CCTGAAGCCTCAAGAGCAGT-3')
	Rv (5'-TGGTCTCCTTCTGTTCTTTGC-3')
DNMT3B	Fw (5'-CAAATGGCTTCAGATGTTGC-3')
	Rv (5'-TCCTGCCACAAGACAAACAG-3')
MAT1A	Fw (5'-GGGCAGGAGATCAGGGTTTG-3')
	Rv (5'-GCCCTGATGACTTGCTCCTT-3')
MAT2A	Fw (5'-CTACGAGTAGAACGCTGTCCG-3')
	Rv (5'-CCAGTTTTAGCAACAGTTTCACA-3')

8.5. Evaluación de la supervivencia celular

Las células HepaRG en diferenciación y en diferenciación expuestas al IFC-305 por 1 semana, se trataron con tripsina y se contaron utilizando un contador automatizado TC20 (Bio-Rad) en laminillas de doble cámara y azul tripano (Bio-Rad 1450003). El número de células totales y células vivas se determinó automáticamente y el porcentaje de supervivencia se determinó comparando las células vivas de cada condición con el promedio de las células no tratadas, el cual se consideró como 100%.

8.6. Inmunofluorescencia

Se sembraron 400 000 células HepaRG por pozo en placas de 6 pozos con 4 cubreobjetos redondos por pozo y se trataron de acuerdo al modelo de diferenciación con o sin IFC-305. Se sembraron 100 000 células en las mismas condiciones durante 24 h, las que se designaron como proliferantes. A diferentes tiempos, las células se lavaron con PBS 1x, se fijaron con formaldehido al 4% y se lavaron dos veces con PBS 1x. Los anticuerpos utilizados fueron anti-HNF4α (Cell signalling 3113S) diluido 1:200 y anti-5hmC (Active motif 39769) diluido 1:400. Los cubreobjetos se incubaron toda la noche a 4°C. En seguida los cubreobjetos se incubaron durante 1 h a temperatura ambiente con anti-conejo Alexa Fluor 488 IgG de cabra (Invitrogen) y con anti-conejo Alexa Fluor 568 IgG de cabra (Invitrogen) respectivamente. Después de la incubación, los cubreobjetos se lavaron y se montaron sobre un portaobjetos con medio de montaje con 2-(4-amidinofenil)-1H-indol-6-carboxamidina (DAPI Vectashield). La fluorescencia se visualizó con un microscopio invertido Olympus modelo IX71 y las imágenes se capturaron con una cámara digital Evolution/QImaging utilizando el programa Image Pro Plus (Media Cybernetics). Los controles negativos se realizaron sin exponer los cubreobjetos al anticuerpo primario. La

configuración para la adquisición de imágenes fue la siguiente: *gain 8, gamma 1, offset -1000; White balance: R 1.240, G 1.000, B 1.40;* para DAPI (azul), el tiempo de exposición fue de 50 ms; para Alexa 488 (verde), el tiempo de exposición fue de 800 ms; para Alexa 568 (rojo), el tiempo de exposición fue de 4.5 s. El análisis de datos se realizó utilizando la herramienta *measure* y el *plugin integrative 3D surface plot* en ImageJ (National Institutes of Health, http://imagej.nih.gov).

8.7. Inmunoblot

Cantidades equivalentes de lisados de proteína (30 µg) se separaron por electroforesis en un gel de poliacrilamida-dodecilsulfato de sodio (SDS-PAGE) y se transfirieron a una membrana de Immobilion-P (Millipore). Se utilizaron los anticuerpos primarios específicos para las isoformas reguladas por los promotores P1 y P2 de *HNF4A* (R&D Systems).

8.8. Bisulfito oxidante y obtención del hidroximetiloma

Para el aislamiento de DNA genómico, se añadieron 500 µL de solución reguladora de lisis (Tris-HCl 50 mM pH 8, EDTA 100 mM, NaCl 100 mM, SDS 1% y proteinasa K 0.5 mg/mL) a cada pozo de la placa de 6, previamente lavados dos veces con PBS 1x. Las células se despegaron utilizando la micropipeta y la suspensión se incubó 2 h a 55°C. Se agregaron 200 µL de NaCl 6 M, la muestra se mezcló y se centrifugó 10 min a máxima velocidad en una microcentrífuga Eppendorf 5415D. El sobrenadante se recuperó y el DNA se precipitó con 500 µL de isopropanol. Se centrifugó nuevamente a máxima velocidad y el botón se lavó con 500 µL de etanol 70% y se secó en servitoalla invirtiendo el tubo. El DNA se resuspendió con 25 µL de H_2O inyectable. Se convirtieron por bisulfito convencional y oxidante 1 000 ng de DNA utilizando el estuche TrueMethyl Seq (Cambridge Epigenetix) de acuerdo a las instrucciones del fabricante. El bisulfito oxidante permite la distinción entre

5mC y 5hmC al oxidar esta última a 5fC, que es leída como timina (la citosina no modificada y la 5mC son leídas como timina y citosina respectivamente, como en el bisulfito convencional), ambas conversiones se realizan simultáneamente y mientras el bisulfito oxidante informa de la 5mC real, la sustracción entre ambas conversiones permite identificar a la 5hmC [Booth et al., 2013].

El DNA convertido fue analizado con la plataforma MethylationEPC (Illumina), utilizando los protocolos recomendados por el fabricante, para la amplificación, etiquetado, hibridación y lectura del microarreglo. Para las células proliferantes y en diferenciación, cada análisis de metilación se realizó con dos cultivos independientes, mientras que para el tratamiento con IFC-305 el análisis se realizó con cultivos en triplicado.

El bisulfito oxidante seguido de PCR específica para metilación (oxBS-qMSP) se realizó como previamente fue descrito [Hernández-Vargas and Goldsmith, 2019], utilizando oligonucleótidos específicos para los promotores P1 y P2 de *HNF4A* (Tabla 7).

Tabla 7. Lista de oligonucleótidos utilizados para hidroximetilación por bisulfito oxidante y PCR cuantitativa específica para metilación

Región	Secuencia
	Metilado
HNF4A P1	Fw (5'-TGAGTTAAGGGTTAAATGAGTGTTC-3')
	Rv (5'-CGCCGATAAATAAACTAAACGAA-3')
HNF4A P2	Fw (5'-GAGATTTAAAATTGAGATAAAAGAAACG-3')
	Rv (5'-CAAAATCATCCTATCTAACGTCT-3')
	No metilado
HNF4A P1	Fw (5'-GTGAGTTAAGGGTTAAATGAGTGTTT-3')
	Rv (5'-CCCACCAATAAATAAACTAAACAAA-3')
HNF4A P2	Fw (5'-ATTTAAAATTGAGATAAAAGAAATGGG-3')
	Rv (5'-AACAAAATCATCCTATCTAACATCT-3')

8.9. Análisis bioinformático

Los datos crudos de expresión y metilación se importaron y procesaron utilizando la paquetería bioinformática de R/Bioconductor para *Illumina bead arrays* [Du et al., 2008]. La calidad de los datos se inspeccionó utilizando gráficas de cajas (*boxplots*) para la distribución de señales de expresión y para la relación entre muestras se utilizaron gráficas de escalamiento multidimensional y agrupamiento no supervisado.

Para los datos de metilación, se removieron las sondas con baja calidad con un valor de detección $p > 0.01$ en más del 10% de las muestras. Se procedió con una normalización de swan (subconjunto de cuantiles dentro del microarreglo) [Maksimovic et al., 2012] implementada en el programa minfi [Aryee et al., 2014], los "picos" de 5hmC se identificaron por la substracción de la señal del bisulfito oxidante de la señal del bisulfito convencional. En seguida se realizó una estimación de máxima verosimilitud (*Maximum Likelihood Estimation,* MLE) de 5mC y 5hmC (oxBS.MLE) con el programa ENmix [Xu et al., 2016]. Utilizando un modelo binomial en cada *locus* CpG de cada muestra, el oxBS.MLE arroja una matriz de MLEs de los niveles de 5mC y una matriz de MLEs de los niveles de 5hmC, configurando como NA cada valor negativo.

Para definir los genes diferencialmente expresados (DEGs), las posiciones diferencialmente metiladas (DMPs) y las posiciones diferencialmente hidroximetiladas (DhMPs), se modelaron condiciones experimentales como variables categóricas en una regresión lineal utilizando una aproximación empírica de Bayesian [Smyth, 2004]. Las regiones diferencialmente metiladas e hidroximetiladas (DMRs y DhMRs, respectivamente) se identificaron con el programa DMRcate utilizando los criterios recomendados de proximidad [Peters et al., 2015]. Las comparaciones de *false discovery rate* (FDR) con un valor de P ajustado menor a 0.05 para un fueron consideradas como estadísticamente significativas. Adicionalmente, sólo los DhMPs con al menos 10% de cambio en 5hmC se consideraron

significativos para cada comparación dada, lo cual ha sido sugerido como un límite de sensibilidad para esta técnica [Skvortsova et al., 2017]. Los DEGs, DhMPs y DhMRs se analizaron para determinar el enriquecimiento funcional utilizando EnrichR [Chen et al., 2013a].

Las anotaciones del contexto genómico, incluidos los estado de la cromatina (ChromHMM) se realizaron a través de los programas ChIPseeker [Yu et al., 2015] y Annotatr [Cavalcante and Sartor, 2017]. El programa EnrichedHearmap [Gu et al., 2018] se utilizó para realizar los mapas de calor que resumen el contexto genómico. Una lista de genes *housekeeping* se descargó de https://m.tau.ac.il/~elieis/HKG/ [Eisenberg and Levanon, 2013].

8.10. Inmunoprecipitación de DNA

Se sonicaron 80 µL de DNA genómico acuoso (100 ng/µL) en un *microTUBE AFA Fiber Pre-Slit Snap-Cap* 6x16mm Covaris en un sonicador S220 (Covaris) para obtener fragmentos entre 400-800 pb (Temperatura < 7°C, *peak power* 105.0, *duty factor* 5.0, *Cycles/Burst* 200 y tiempo de 40 s). Se utilizaron 130 ng de DNA por inmunoprecipitación empleando el estuche Auto hMeDIP (Diagenode C02010033) de acuerdo a las instrucciones del fabricante. Brevemente, la precipitación se ajustó de la siguiente manera: 15 h para la mezcla a 4°C a una velocidad media de mezclado; para los lavados el tiempo de 8 min a 4°C y una velocidad media de mezclado. Las inmunoprecipitaciones se realizaron en tres cultivos independientes por condición. Se analizaron 5 µL del DNA hidroximetilado inmunoprecipitado para las regiones enriquecidas en 5hmC de acuerdo a los datos de oxBS (regiones con al menos 3 CpGs conteniendo un DhMPs con 10% de diferencia entre células proliferantes y diferenciadas (Delta 10%)), el promotor del gen *Splicing factor, arginine/serine-rich 4 (SFRS4)* se utilizó como control de una región sin enriquecimiento de 5hmC. Todos los ensayos de PCR cuantitativa se realizaron por

duplicado con Mesa Green qPCR 2x MasterMix Plus (Eurogentec 05-SY2X-06+WOU) en un sistema CFX96 PCR (Bio-Rad), utilizando los oligonucleótidos indicados en la Tabla 8. El enriquecimiento de 5hmC se determinó como % (hmeDNA-IP/ Total input) de la siguiente forma: % (hmeDNA-IP/ Input total) = 2^[($Ct_{(10\% \text{ input})}$ - 3.32) - $Ct_{(hmeDNA\text{-}IP)}$]x 100%, dónde 2 es la eficiencia de amplificación, $Ct_{(10\% \text{ input})}$ y $Ct_{(hmeDNA\text{-}IP)}$ son los valores límite obtenidos de la fase exponencial de la qPCR para el input y el DNA hidroximetilado, respectivamente; el factor compensatorio (3.32) es utilizado para considerar la dilución 1:10 del *input*.

Tabla 8. Lista de oligonucleótidos utilizados para hMedIP.

Región	Sequencia	Localización (hg19)
SFRS4 P	Fw (5'-CCTCTTTCGCCCTCCTCA-3')	chr1:29508139-
	Rv (5′-TGTAGGCTGGGTCCAGTG-3′)	29508338
HNF4A P1	Fw (5′-ATCTTCCCAGAGGACGGTTT-3′)	chr20:43029881-
	Rv (5′-TGTAGGCTGGGTCCAGTG-3′)	43030082
TCHP	Fw (5'-GCCAGGTTCTCTGCATCAT-3')	chr12:110352469-
	Rv (5'-ATGGCATGTACCTCGTAGAAAG-3')	110352877
RAB7A	Fw (5'-TCTGAGTCCTGGTGGTAGTT-3')	chr3:128483808-
	Rv (5'-GTTGTGGGTAGCAGAGACATT-3')	128484074

8.11. Cuantificación de adenosina, S-adenosilmetionina y S-adenosilhomocisteina por HPLC

Los niveles de adenosina, SAM y SAH se determinaron modificando protocolos previamente descritos [Hernandez-Munoz et al., 1984; Korinek et al., 2013]. Brevemente, se sembraron 10 $x10^6$ células HepaRG proliferantes en platos de Petri de 15 cm; 24 h después del sembrado, las células se cultivaron con y sin IFC-305 por una semana para permitir la diferenciación, o colectadas en condiciones de células proliferantes. En seguida las células se congelaron con nitrógeno líquido y se preservaron a -70°C.

Las células congeladas se cosecharon con 1.5 mL de ácido trifluoroacético al 0.03% en metanol al 90%. Las muestras se incubaron a temperatura ambiente durante 10 min a

temperatura ambiente y en seguida se pasaron a través de un homogenizador Dounce para romper mecánicamente a las células. Las soluciones obtenidas se sonicaron dos veces durante un minuto en un sonicador Bransonic 220 y se centrifugaron a 16 000 *g* por 13 min a 4°C. Los sobrenadantes se recuperaron y se centrifugaron a sequedad en un concentrador Eppendorf 5301 a 45°C. Las muestras se reconstituyeron con 200 µL de agua MilliQ y se determinó la concentración de proteína por el método de Bradford. Las muestras se diluyeron para obtener una concentración de 1.2 µg/µL de proteína en un volumen de 300 µL y se agregaron 100 µL de $HClO_4$ 1.6 M para obtener una concentración final de 0.4 M y la muestra se incubó por 10 min en hielo. Se añadieron 10 µL de K_2CO_3 5 M a las muestras y estas se incubaron una vez más en hielo por 10 min. Las muestras diluidas se centrifugaron a 14 000 rpm durante 5 min en una microcentrífuga Eppendorf 5415C. Se recuperaron los sobrenadantes y se filtraron utilizando filtros de jeringa Phenex PFTE de 4 mm. A 95 µL de la muestra filtrada se le añadieron 5 µL de una mezcla de los estándares de adenosina 400 mM y SAM 400 mM, estos 100 µL se analizaron en un equipo de cromatografía líquida de alta resolución HPLC Knauer E4310 (El estándar de SAM contenía contaminación de SAH, la cual de determinó utilizando una curva estándar de SAH). Las muestras se separaron en una columna ACE 5 C 18 (150 x 4.6 mm) (Advanced Chromatography Technologies LTD) utilizando una fase móvil consistente en heptanosulfonato de sodio 8 mM, $NH_4H_2PO_4$ 40 mM y metanol isocrático al 15% a pH 3, con un flujo de 1 mL/min. La detección se realizó a una absorbancia de 254 nm y el tiempo total de separación fue de 60 min. Los picos se analizaron con el programa EUROCHROME para Windows versión 3.05 (Knauer GmbH).

8.12. Análisis estadístico

La paquetería de R/Bioconductor se utilizó para el análisis de los microarreglos, como se describió previamente en esta sección. Los gráficos fueron generados utilizando Graph Pad Prism 5.0 (Graph Pad Software, Inc., La Jolla CA) para Windows. La prueba de Wilcoxon para análisis no pareado fue utilizada para comparar el promedio entre condiciones y se realizó en RStudio 1.1.463 (RStudio, Inc.). Los valores de $P < 0.05$ fueron considerados estadísticamente significativos.

8.13. Disponibilidad de datos y materiales

Todos los datos de expresión y metilación se han depositado en el repositorio Gene Expression Omnibus (SuperSeries GSE130849, SubSeries GSE130844 y GSE130848).

9. RESULTADOS

9.1. Las Células HepaRG en diferenciación por una semana expresan marcadores hepáticos

Las células HepaRG son progenitores hepáticos bipotenciales que pueden diferenciarse *in vitro* después de 4 semanas tanto en hepatocitos como en colangiocitos, estas células se cultivaron durante una semana en presencia de insulina e hidrocortisona para inducir la diferenciación hacia hepatocitos. Para determinar el perfil de expresión génica a una semana de cultivo celular (Figura 26A), el RNA total fue aislado de células en diferenciación y células proliferantes y se realizó un análisis de transcriptoma. Se encontraron 4175 DEGs (Figura 26B) de los cuales los genes subexpresados (n=2066 sondas, correspondientes a 1772 genes anotados en hg19) estuvieron relacionados con linfoblastos y células endoteliales (Figura 26C), y asociados con el programa de transcripción de *E2F4* (Figura 27E), las vías de señalización involucradas en la progresión del ciclo celular, procesos biológicos relacionados con el metabolismo del DNA y replicación y funciones moleculares implicadas en la actividad de DNA dependiente de ATPasa (Figura 27F-H). En contraste, los genes sobreexpresados (2109 sondas, correspondientes a 1822 genes anotados en hg19) estuvieron altamente asociados con hígado e hígado fetal (Figura 26D) y estuvieron enriquecidos en genes blancos del programa de transcripción de *HNF4A* (Figura 27A). Las vías y ontologías relacionadas con genes sobreexpresados incluyeron oxidaciones biológicas y metabolismo (ácidos grasos, regulación de lípidos, homeostasis de triglicéridos y actividades de oxidoreductasa, endopeptidasa y alcohol deshidrogenasa) (Figura 27B-D). Para validar estos datos, se evaluaron los niveles de expresión de marcadores hepáticos sobreexpresados en el transcriptoma, confirmando que las isoformas derivadas del promotor P1 de *HNF4A, GSTA y ALDOB* se encuentran sobreexpresados a una semana

de diferenciación (Figuras 26E-H). Las regiones analizadas para el promotor P1 de *HNF4A* se presentan en la figura 28.

Estos resultados en conjunto, indican que después de una semana de diferenciación, las células HepaRG se encuentran expresando un programa de transcripción tipo hepatocito, mientras que los genes relacionados con el estado proliferante, se silencia progresivamente.

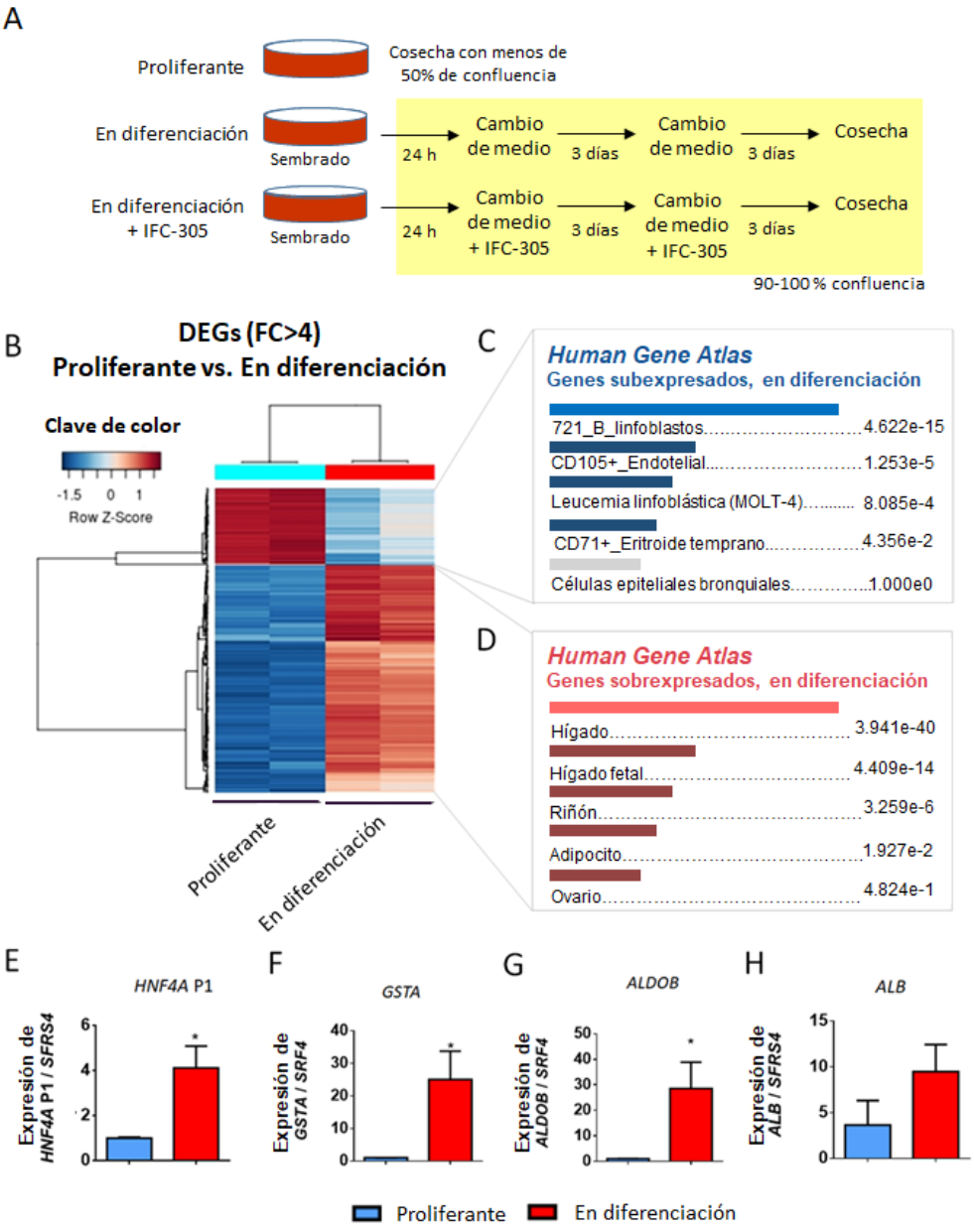

Fig. 26. El programa de transcripción de hígado se expresa en las células HepaRG a una semana de diferenciación. (A) Modelo de diferenciación de HepaRG. Para la condición proliferante (progenitor), las células fueron sembradas y tratadas con tripsina antes de alcanzar 50% de confluencia; para la condición de diferenciación, las células fueron sembradas a 70-80% de confluencia para que alcance el 100% de confluencia 24 h después de ser sembradas. (B) El transcriptoma fue analizado en ambas condiciones. Mapa de calor que representa los genes diferencialmente expresados (DEGs) con más de cuatro veces de cambio. Las células o tejidos asociados con genes subexpreados (C) y sobrexpresados (D) en las células en diferenciación (EnrichR), se muestran los valores de p ajustados. (E-H) La expresión de los marcadores de hepatocitos fue valida por RT-qPCR, los datos representan el promedio ± DEM de 3 cultivos independientes/condición; *Diferencia estadística ($p < 0.05$).

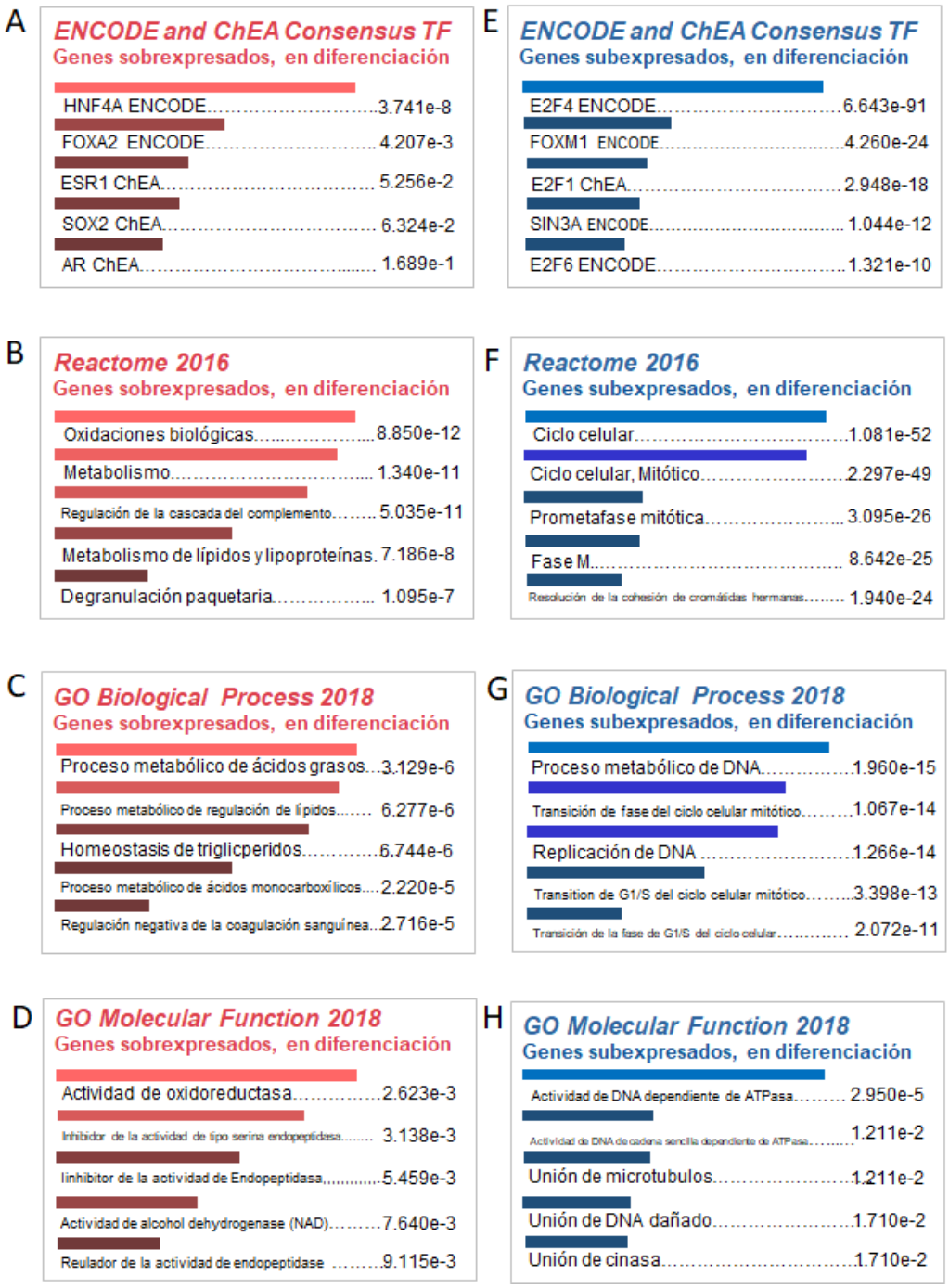

Fig. 27. Enriquecimiento funcional de las células en diferenciación. (A y E) Factores de transcripción consenso de la enciclopedia de elementos de DNA (ENCODE) y análisis de enriquecimiento de ChIP-X (ChEA) de los genes sobreexpresados y subexpresados en células en diferenciación. (B-D) ontologías relacionadas con genes sobreexpresados en células en diferenciación. (F-H) Ontologías relacionadas con genes subexpresados en células en diferenciación. Los datos fueron obtenidos a través de EnrichR, los números muestran el valor de p ajustado del tejido asociado.

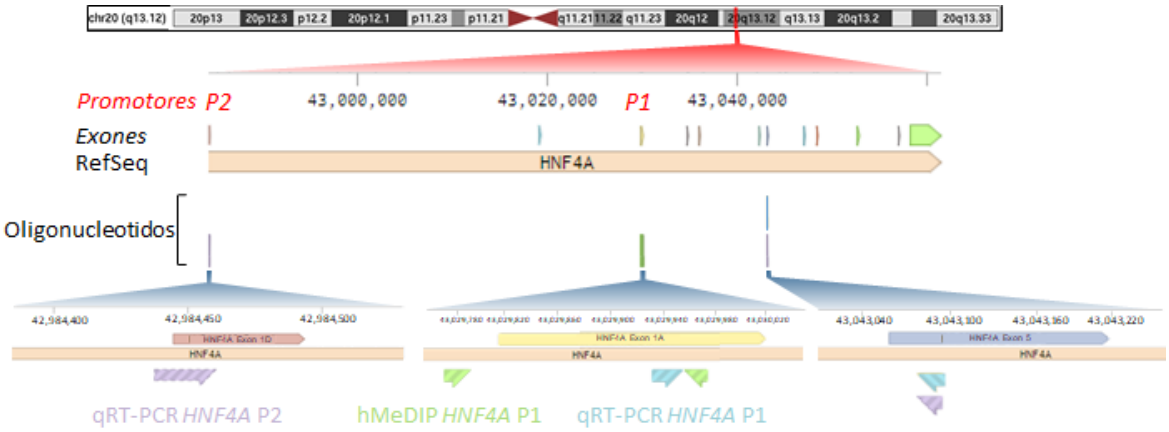

Fig. 28. Regiones analizadas sobre *HNF4A.* El mapa muestra un acercamiento del cromosoma 20 (q13.12) donde se localiza el *locus* de *HNF4A*, Los promotores P1 y P2 están indicados en rojo. Los exones de *NHF4A* se denotan con cajas de colores sobre la RefSeq de *HNF4A* (simbolizada por un pentágono rosa). Los pares de oligonucleótidos para la qRT-PCR y para hMeDIP están representados por cajas de colores debajo de la RefSeq de *HNF4A*. Se muestra un acercamiento de las regiones donde los oligonucleótidos fueron diseñados, los pare de oligos para las isoformas controladas por el promotor P2 de *HNF4A* se denotan por medias flechas moradas, los pares de oligos para las isoformas controladas por el promotor P1 de *HNF4A* están representadas por medias flechas azules y los pares para hMeDIP sobre la región promotora P1 de *HNF4A* se simbolizan con medias flechas verdes. El esquema fue armado con información de *UCSC Genome Browser* [2018] y construido con la plataforma Benchling (http://benchling.com).

9.2. La diferenciación temprana de HepaRG se asocia con un incremento global de 5hmC

Considerando que a una semana de diferenciación hay un enriquecimiento de 5hmC en el promotor P1 de *HNF4A* mediado por TET1 [Ancey et al., 2017] y que el transcriptoma refleja un perfil tipo hepatocito a este tiempo, se escogió este punto para evaluar los niveles de 5hmC en la línea celular HepaRG comparado con su estado proliferante. La inmunotinción contra 5hmC revela la presencia de esta citosina modificada en las células en diferenciación, en contraste con su prácticamente ausencia en las células proliferantes (Figura 29A y Figura 30).

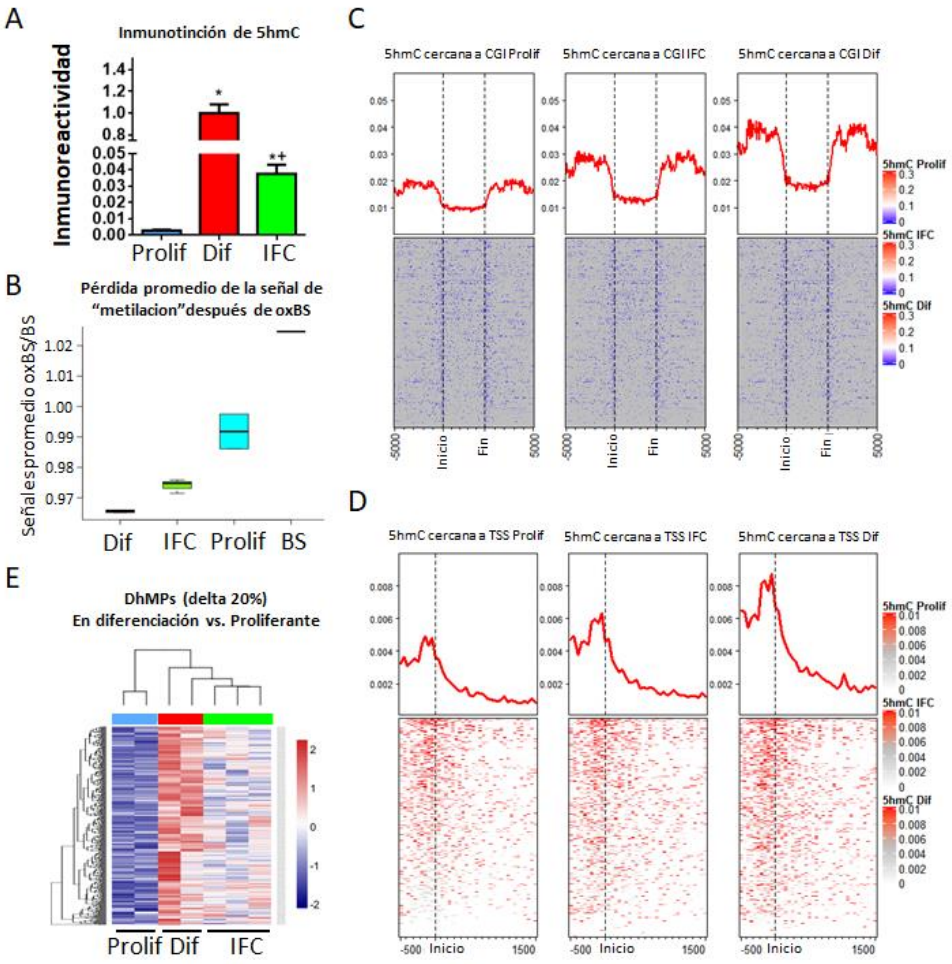

Fig. 29. Enriquecimiento de 5hmC a lo largo del genoma durante la diferenciación de hepatocitos. (A) Inmunofluorescencia de 5hmC en células HepaRG proliferantes (Prolif), en diferenciación (dif) y en diferenciación + IFC-305 (IFC). Las barras de cuantificación de la señal de 5hmC están basadas en el promedio ± DEM de 3 campos/grupo. *Diferencia estadística ($p < 0.05$) comparada con células proliferantes, o *+ ($p < 0.05$) comparada con células proliferantes u en diferenciación. (B) Las mismas condiciones fueron analizadas para 5mC/5hmC a resolución de nucleótido, utilizando bisulfito clásico (BS) y bisulfito oxidante (OxBS) seguido de una hibridación en microarreglos EPIC (ver métodos). La proporción de la pérdida de la señal después de la oxidación (promedio de la señal de OxBS/ promedio de la señal de BS) se usó como una estimación de la 5hmC global en cada condición. BS representa la variación entre dos réplicas técnicas. Distribución global de la 5hmC para una muestra representativa de cada condición, de acuerdo con las islas CpG (CGI) (C) y con los sitios de inicio de la trascripción (TSS) (D). En ambos casos, los niveles de 5hmC están promediados a través de todas las regiones genómicas anotadas de hg19. (E) Mapa de calor mostrando la comparación del hidroximetiloma entre las células en diferenciación y las proliferantes. Las posiciones diferencialmente hidroximetiladas (DhMPs) se filtraron por la magnitud del cambio de metilación (delta beta) de al menos 20% con un valor de p ajustado < 0.05. Dos cultivos independientes se utilizaron para las células proliferantes y en diferenciación, y tres cultivos independientes para las células en diferenciación expuestas al IFC-305 1 mM.

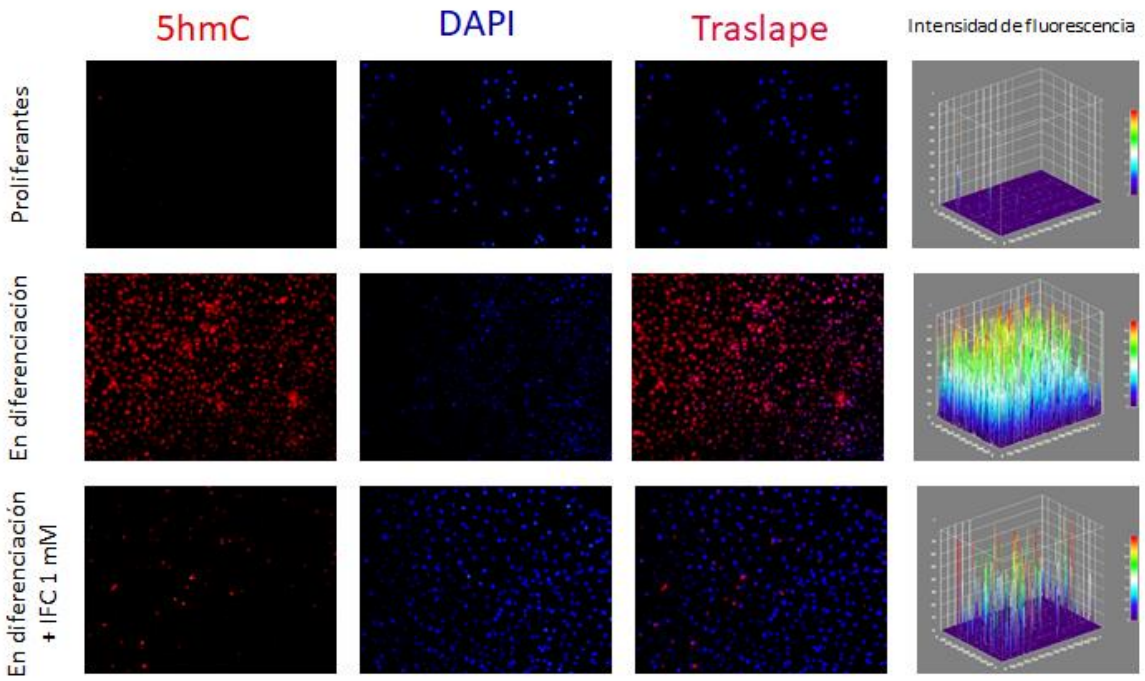

Fig. 30. La 5hmC surge en las células en diferenciación. Inmunofluorescencia contra 5hmC en células proliferantes (panel superior), en diferenciación (panel intermedio) y en diferenciación + IFC-305 (panel inferior). Se muestran imágenes representativas de 3 campos por condición, así como la medición de la intensidad de fluorescencia.

En seguida se procedió a evaluar el hidroximetiloma a resolución de nucleótido. En este punto es importante mencionar que la conversión de DNA con bisulfito de sodio tradicional (BS) no es capaz de distinguir entre 5mC y 5hmC. Una alternativa para evaluar ambas modificaciones de manera independiente, es el uso de bisulfito oxidante (oxBS); el cual permite la identificación de 5mC a través de la oxidación de 5hmC hacia 5-formilcitosina (5fC) con KO_4Ru [Booth et al., 2013]. Por lo que se aisló DNA de células proliferantes y en diferenciación y se realizó BS y oxBS utilizando el estuche TrueMethyl Seq (Cambridge Epigenetix), seguido de hibridación en microarreglos Infinitum EPIC.

Una vez realizado el proceso de oxidación, el protocolo del estuche TrueMethyl Seq señala que el sobrenadante en los tubos de reacción debe permanecer en color anaranjado debido a que hay un remanente de reactivo oxidante y que la reacción de oxidación se ha

completado, es decir, que el color de la solución es indicativo del éxito de la oxidación. Si la solución se torna en un color diferente al anaranjado (verde, café/negro) (Figura 31A), implica que la reacción del oxidante ocurrió en presencia de trazas de otros compuestos en la solución de oxidación (por ejemplo, Tris, etanol, etc.) y señala que la reacción de oxidación pudiera estar comprometida. Esto puede conducir a una conversión incompleta de 5hmC a uracilo y a la variabilidad en los resultados.

Una vez ocurrida la reacción de oxidación ya descrita, se obtuvo una suspensión color gris que una vez centrifugada dio paso a un botón y sobrenadante color anaranjado (Figura 31B), señalando que la conversión de 5hmC a uracilo se completó exitosamente, por lo que se procedió a la conversión con BS.

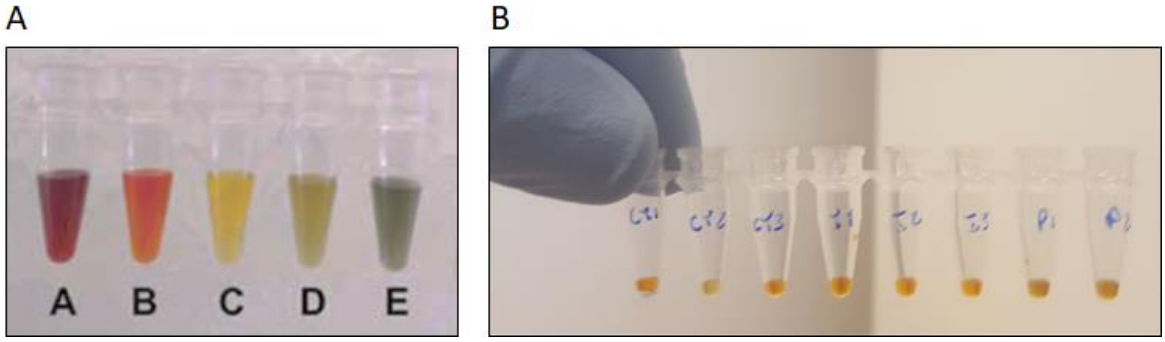

Fig. 31. Colores en la solución de oxidación. (A) posibles cambios de color en la solución de oxidación. A, solución de oxidación concentrada suministrada en el estuche TrueMethyl Seq de Cambridge Epigenetix, si esta solución presenta un color amarillo oscuro con precipitados blancos considerables, indica que el reactivo se ha expuesto a contaminantes o CO_2; B, Solución de oxidación diluida 10 veces en la solución alcalina; C, Concentración de trabajo de la solución oxidante (WOC), la solución debe presentar este color después de la reacción de oxidación; D, Exceso de WOC:etanol en una relación molar 5:1, este color es indicativo de una descomposición parcial del oxidante, sin embargo la oxidación de la muestra puede ser adecuada; E, Exceso de etanol:WOC en una relación molar 20:1, este color indica que es probable que el oxidante se haya consumido completamente por una reacción secundaria con especies contaminantes, en esta circunstancia, es probable que la oxidación del ADN sea subóptima. (B) Los tubos de las muestras analizadas, mostraron un color anaranjado, indicando que la reacción de oxidación se llevó acabo correctamente.

Después de realizar la conversión con BS, se procedió a la evaluación cualitativa de la oxidación de 5hmC y la conversión con bisulfito antes de proceder a la hibridación en microarreglos Infinitum EPIC.

El estuche TrueMethyl Seq de Cambridge Epigenetix contiene secuencias de DNA control que se añaden a las muestras y que permiten realizar esta evaluación. La secuencia que funciona como control de digestión contiene un sitio de restricción para la enzima Taqᵅ1 (5'-TCGA-3'). La citosina dentro de este motivo en el control de digestión es 5hmC. Una completa conversión de esta base a uracilo durante el proceso con el estuche TrueMethyl, hará que el motivo sea resistente a la digestión por la TaqᵅI. El motivo será digerido después de una conversión incompleta o una falla en el proceso de oxidación. En la figura 32 se presenta un gel de agarosa al 2% donde se analizaron las digestiones de las muestras estudiadas y se encontró una oxidación y conversiones eficientes, por lo que se procedió análisis del metiloma e hidroximetiloma utilizando microarreglos Infinitum EPIC.

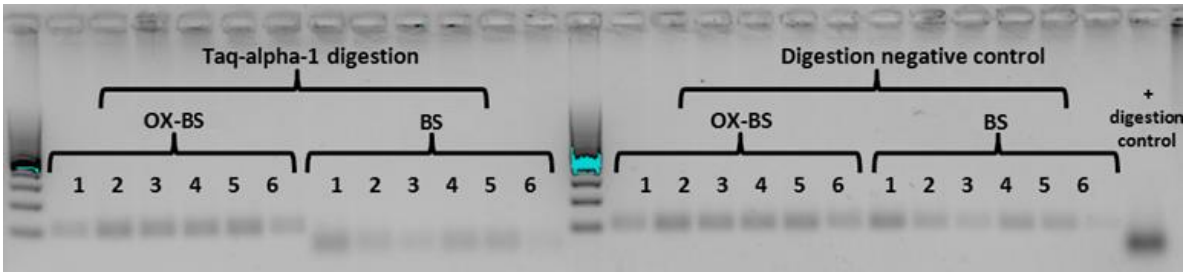

Fig. 32. Digestión con TaqᵅI del amplicón del control de digestión en las muestras analizadas. Muestras BS, el sitio de corte de TaqᵅI se mantiene durante la conversión con bisulfito, la enzima corta el amplicón de 100 pb del control de digestión generando dos bandas de 40 y 60 pb respectivamente (en el gel de agarosa al 2% estas bandas no se resuelven y aparecen como una sola banda). Muestras oxBS, el sitio de corte de TaqᵅI se ha convertido de TCGA a TTGA durante la oxidación y conversión con bisulfito por lo que la enzima no es capaz de cortar el amplicón de 100 pb del control de digestión. 1-2, En diferenciación; 3-5, en diferenciación + IFC-305; 6, proliferante.

Utilizando únicamente la señal de oxBS (que corresponde al contenido "real" de 5mC), se observó la esperada distribución de 5mC en islas CpG (CGIs) y en los inicios de la

transcripción (TSS) (Figura 33). Aunque no se observaron diferencias globales entre las condiciones analizadas, se identificaron 3351 DMPs mostrando menor metilación después de una semana de diferenciación (Figura 34A).

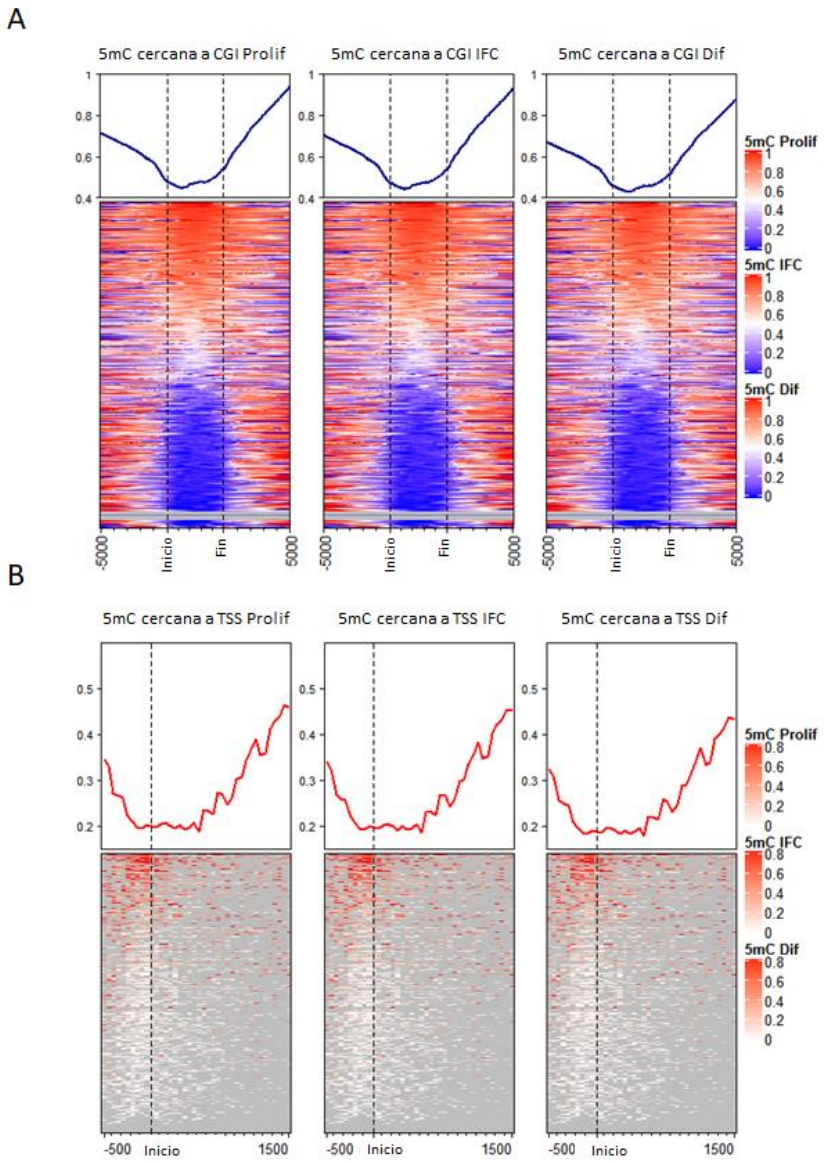

Fig. 33. Distribución de 5mC sobre las islas CpG y los inicios de la transcripción durante la diferenciación de hepatocitos. Distribución global de 5hmC para una muestra representativa de cada condición, se acuerdo a las islas CpG (A) y en los sitios de inicio dela transcripción (B). En ambos casos, los niveles de 5mC están promediados a través de todas las regiones genómicas anotadas de hg19. Dos cultivos independientes se utilizaron para las células proliferantes (Prolif) y en diferenciación (Dif), y tres cultivos independientes para las células en diferenciación expuestas al IFC-305 1 mM (IFC).

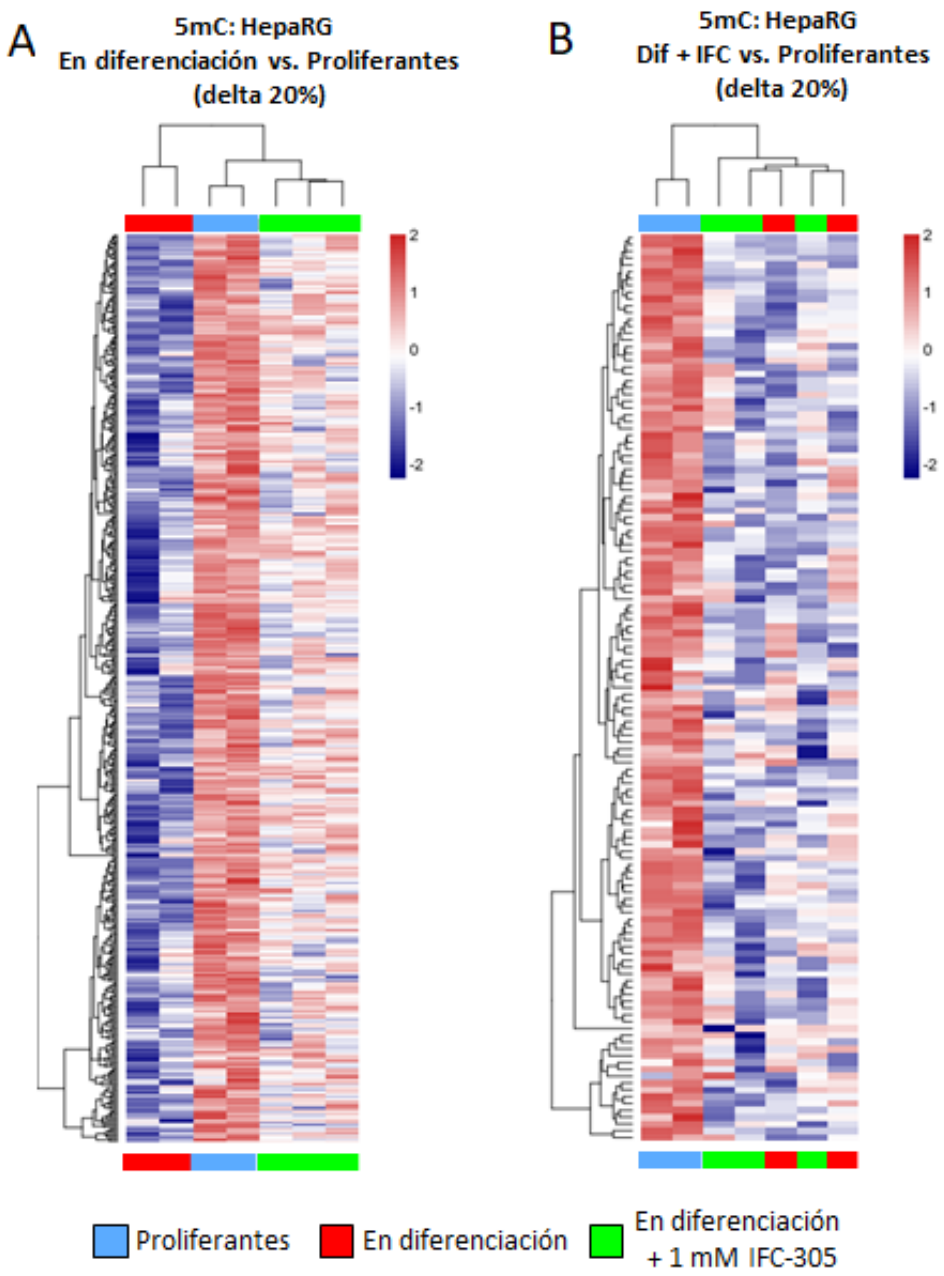

Fig. 34. El proceso de diferenciación involucra desmetilación a lo largo del genoma. (A) Mapa de calor presentando la comparación del metiloma entre las células en diferenciación y las células proliferantes**.** (B) Mapa de calor presentando la comparación entre el metiloma de las células en diferenciación expuestas al IFC-305 y las células proliferantes. Las posiciones diferencialmente metiladas (DMPs) fueron filtradas por la magnitud del cambio de metilación (delta beta) de al menos 20% con un valor de p ajustado < 0.05. Se utilizaron dos cultivos independientes fueron utilizados para las células proliferantes y en diferenciación y tres cultivos independientes para las células en diferenciación expuestas a 1 mM de IFC-305.

Una pérdida de señal después de oxBS relativo a BS indica la presencia de 5hmC. Mientras que en las células proliferantes el análisis genómico reveló que casi no hay una pérdida de señal entre ambas conversiones, en las células en diferenciación hay una pérdida global y significativa, sugiriendo una ganancia global de 5hmC durante la primera semana de diferenciación (Figura 29B). Esta ganancia de 5hmC fue consistente, independientemente de la ubicación relativa en CGIs y TSS (Figura 29 C-D).

Enseguida estudiamos la 5hmC a través de la comparación directa de los datos de oxBS y BS. Si bien no se observaron diferencias significativas en las células proliferantes (Figure 29B), se identificó una ganancia de 5hmC en 11766 sitios en células en diferenciación, definidos por una reducción significativa de la señal de metilación después del oxBS de, al menos, 10% (“picos” de 5hmC). La evaluación de hidroximetilación diferencial, reveló 6952 posiciones diferencialmente hidroximetiladas (DhMPs) entre las células proliferantes y diferenciadas (Figura 29E). Adicionalmente, se identificaron 2482 regiones diferencialmente hidroximetiladas (DhMRs). Entre estas, se identificó una región con 3 CpGs sobre *HNF4A* así como una región con 21 CpGs, una con 5 CpGs y dos con 3 CpGs sobre los genes *IDH3G, TET1, y TET3* respectivamente (Estos *loci* pueden observarse a través de la sesión del UCSC Genome Browser [2018] y en las Figuras 35-39). Es de destacar que estos genes se encuentran involucrados en el establecimiento de la 5hmC.

Estos resultados revelan que mientras la 5hmC es escasa en el estado de progenitor, esta modificación se enriquece en múltiples posiciones genómicas al iniciar la diferenciación de hepatocitos.

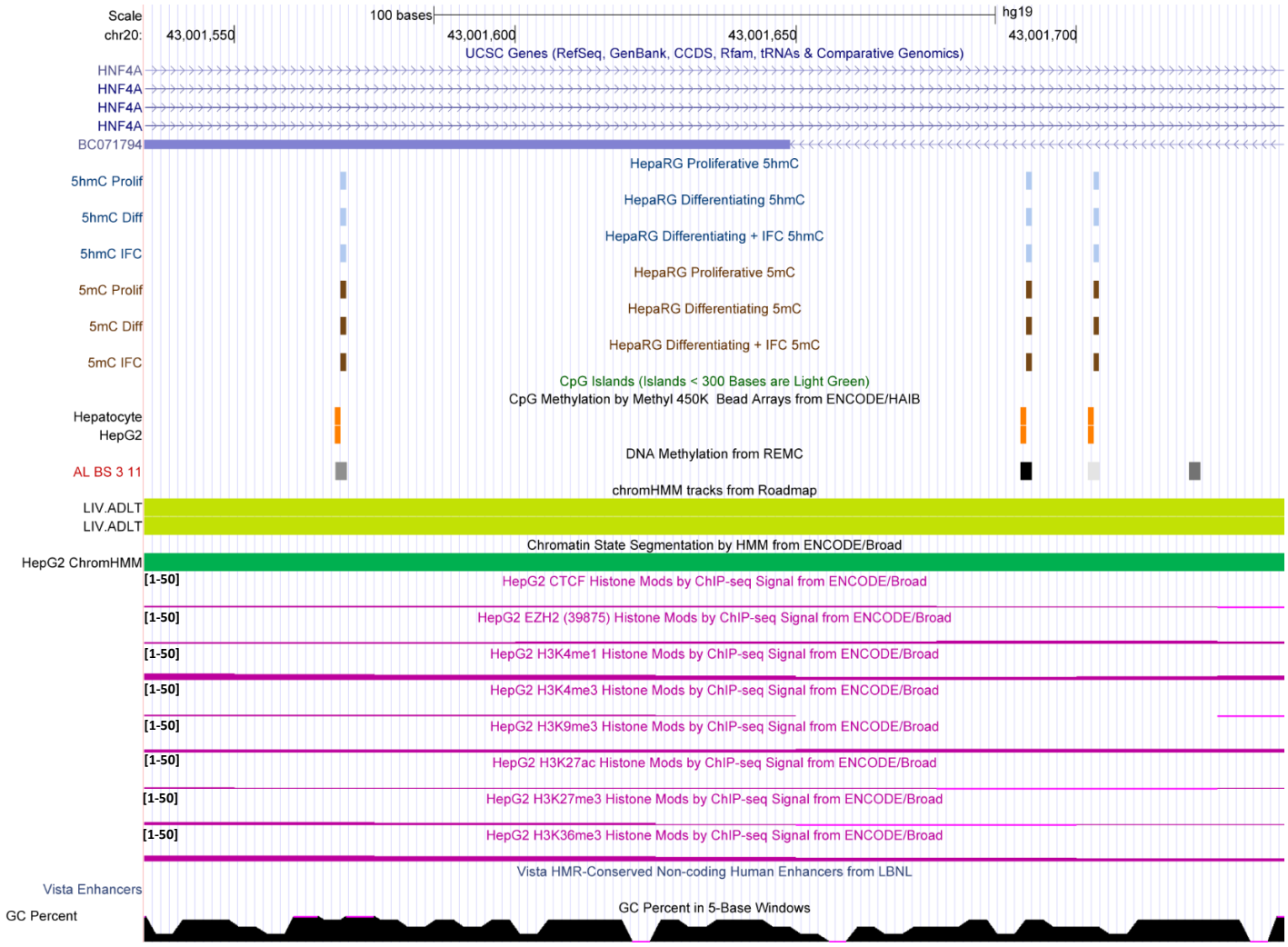

Fig. 35. Región de 5hmC sobre *HNF4A*. Pantalla de la sesión del UCSC Genome Browser [2018] presentando la región chr20: 43001569-43001703, que enmarca los 3 sitios CpG enriquecidos en 5hmC sobre el gen de *HNF4A*. Los datos de 5hmC están mostrados en azul y los de 5mC en café; la intensidad del color es proporcional al grado de enriquecimiento. Células proliferantes (Prolif), en diferenciación (Diff) y en diferenciación + IFC-305 (IFC). Se muestran algunos *tracks* adicionales: Islas CpG < 300 pb; metilación de CpGs por el microarreglo 450K de ENCODE/HAIB para hepatocitos y la línea celular HepG2; metilación de DNA por el consorcio *Roadmap Epigenomics Mapping (REMC)* por secuenciación de bisulfito en hígado adulto (AL BS), la intensidad de grises es proporcional al grado de enriquecimiento; Segmentación del estado de la cromatina por el modelo *Hidden Markov (ChromHMM)* de hígado adulto (LIV ADLT) y la línea celular HepG2; *tracks* de las proteína arquitectónica CTCF, EZH2 y las marcas de histonas H3K4me1 (*enhancers*), H3k36me3 (elongación), H3K9me3 y H3K27me3 (marcas de cromatina cerrada) y H3K27ac (marca de cromatina abierta) de ENCODE/Broad; *Vista enhancer Handbook and Methods (HMR) at the Lawrence Berkeley National Laboratory (LBNL),* los picos denotan enriquecimieno; y *CG percent*, los picos denotan abundancia. El código de color para cada *track* se muestra en la Figura 40.

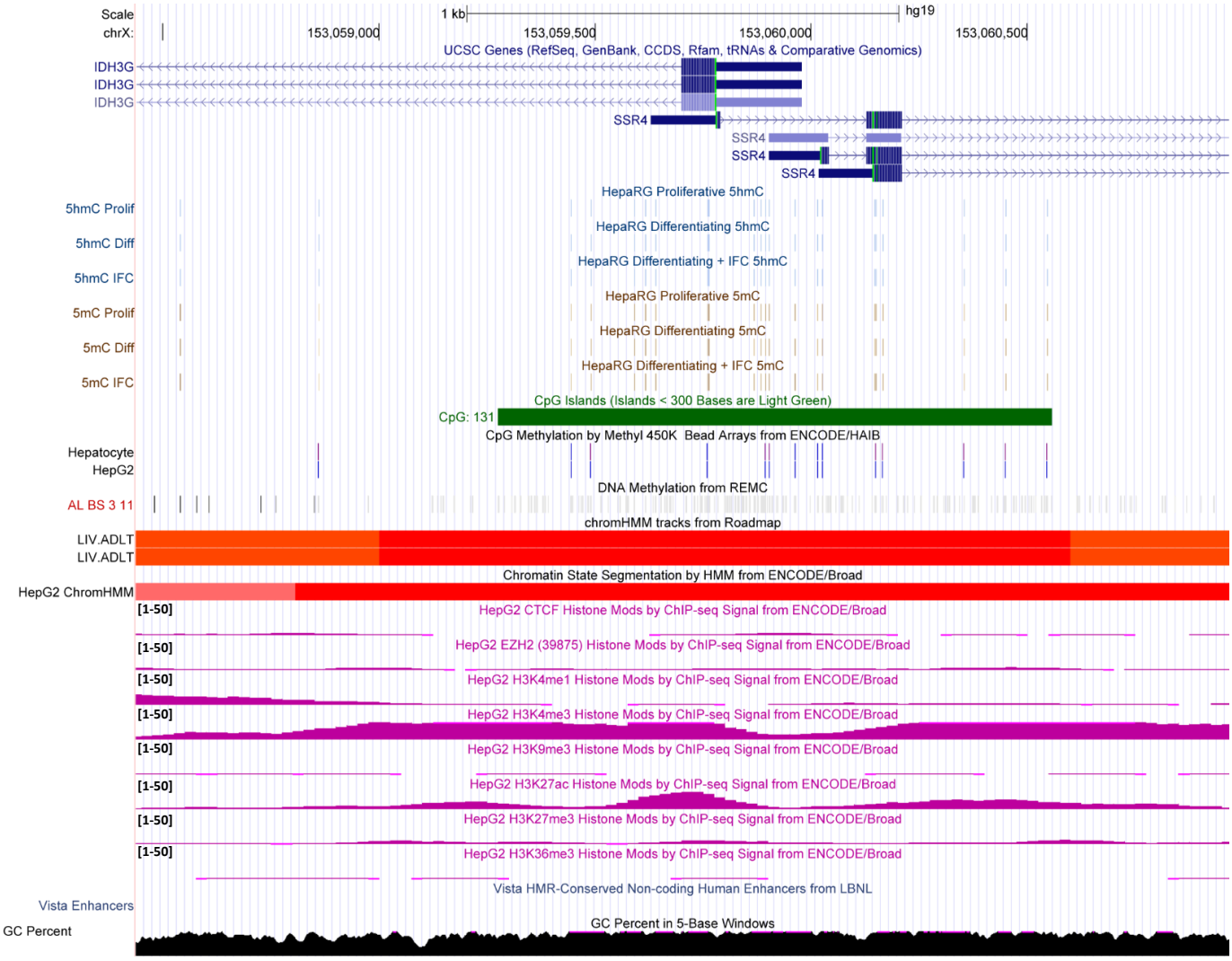

Fig. 36. Región de 5hmC sobre *IDH3G*. Pantalla de la sesión del UCSC Genome Browser [2018] presentando la región chrX:153058860-153060546, que enmarca los 21 sitios CpG enriquecidos en 5hmC sobre el gen de *IDH3G*. Los datos de 5hmC están mostrados en azul y los de 5mC en café; la intensidad del color es proporcional al grado de enriquecimiento. Células proliferantes (Prolif), en diferenciación (Diff) y en diferenciación + IFC-305 (IFC). Se muestran algunos *tracks* adicionales: Islas CpG < 300 pb; metilación de CpGs por el microarreglo 450K de ENCODE/HAIB para hepatocitos y la línea celular HepG2; metilación de DNA por el consorcio *Roadmap Epigenomics Mapping (REMC)* por secuenciación de bisulfito en hígado adulto (AL BS), la intensidad de grises es proporcional al grado de enriquecimiento; Segmentación del estado de la cromatina por el modelo *Hidden Markov (ChromHMM)* de hígado adulto (LIV ADLT) y la línea celular HepG2; *tracks* de las proteína arquitectónica CTCF, EZH2 y las marcas de histonas H3K4me1 (*enhancers*), H3k36me3 (elongación), H3K9me3 y H3K27me3 (marcas de cromatina cerrada) y H3K27ac (marca de cromatina abierta) de ENCODE/Broad; *Vista enhancer Handbook and Methods (HMR) at the Lawrence Berkeley National Laboratory (LBNL),* los picos denotan enriquecimieno; y *CG percent*, los picos denotan abundancia. El código de color para cada *track* se muestra en la Figura 40.

Fig. 37. Región de 5hmC sobre *TET1*. Pantalla de la sesión del UCSC Genome Browser [2018] presentando la región chr10:70457799-70458175, que enmarca los 5 sitios CpG enriquecidos en 5hmC sobre el gen de *TET1*. Los datos de 5hmC están mostrados en azul y los de 5mC en café; la intensidad del color es proporcional al grado de enriquecimiento. Células proliferantes (Prolif), en diferenciación (Diff) y en diferenciación + IFC-305 (IFC). Se muestran algunos *tracks* adicionales: Islas CpG < 300 pb; metilación de CpGs por el microarreglo 450K de ENCODE/HAIB para hepatocitos y la línea celular HepG2; metilación de DNA por el consorcio *Roadmap Epigenomics Mapping (REMC)* por secuenciación de bisulfito en hígado adulto (AL BS), la intensidad de grises es proporcional al grado de enriquecimiento; Segmentación del estado de la cromatina por el modelo *Hidden Markov (ChromHMM)* de hígado adulto (LIV ADLT) y la línea celular HepG2; *tracks* de las proteína arquitectónica CTCF, EZH2 y las marcas de histonas H3K4me1 (*enhancers*), H3k36me3 (elongación), H3K9me3 y H3K27me3 (marcas de cromatina cerrada) y H3K27ac (marca de cromatina abierta) de ENCODE/Broad; *Vista enhancer Handbook and Methods (HMR) at the Lawrence Berkeley National Laboratory (LBNL),* los picos denotan enriquecimieno; y *CG percent*, los picos denotan abundancia. El código de color para cada *track* se muestra en la Figura 40.

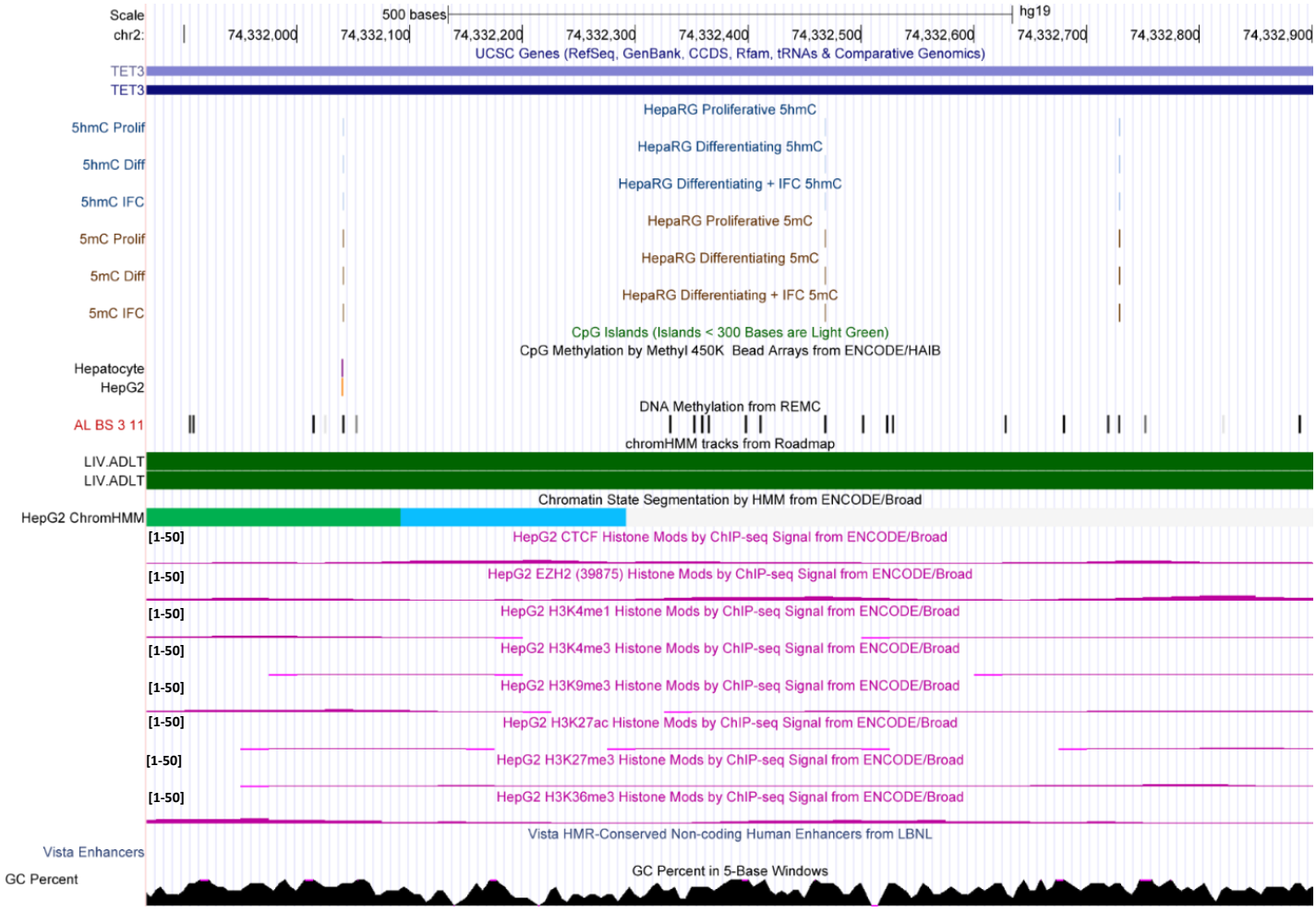

Fig. 38. Primera región de 5hmC sobre *TET3*. Pantalla de la sesión del UCSC Genome Browser [2018] presentando la región chr2:74332041-74332729, que enmarca los 5 sitios CpG enriquecidos en 5hmC sobre el gen de *TET3*. Los datos de 5hmC están mostrados en azul y los de 5mC en café; la intensidad del color es proporcional al grado de enriquecimiento. Células proliferantes (Prolif), en diferenciación (Diff) y en diferenciación + IFC-305 (IFC). Se muestran algunos *tracks* adicionales: Islas CpG < 300 pb; metilación de CpGs por el microarreglo 450K de ENCODE/HAIB para hepatocitos y la línea celular HepG2; metilación de DNA por el consorcio *Roadmap Epigenomics Mapping (REMC)* por secuenciación de bisulfito en hígado adulto (AL BS), la intensidad de grises es proporcional al grado de enriquecimiento; Segmentación del estado de la cromatina por el modelo *Hidden Markov (ChromHMM)* de hígado adulto (LIV ADLT) y la línea celular HepG2; *tracks* de las proteína arquitectónica CTCF, EZH2 y las marcas de histonas H3K4me1 (*enhancers*), H3k36me3 (elongación), H3K9me3 y H3K27me3 (marcas de cromatina cerrada) y H3K27ac (marca de cromatina abierta) de ENCODE/Broad; *Vista enhancer Handbook and Methods (HMR) at the Lawrence Berkeley National Laboratory (LBNL),* los picos denotan enriquecimieno; y *CG percent*, los picos denotan abundancia. El código de color para cada *track* se muestra en la Figura 40.

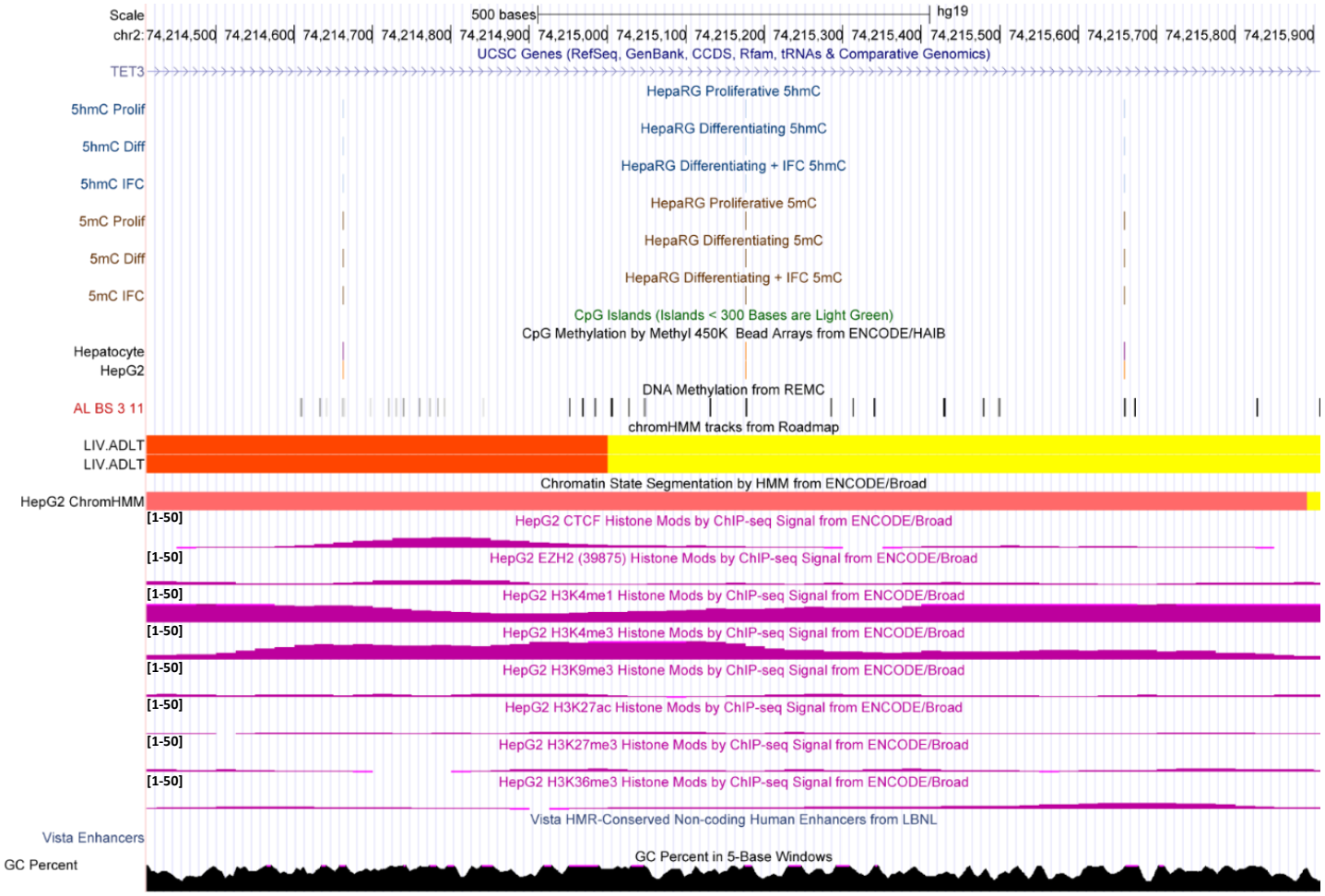

Fig. 39. Segunda región de 5hmC sobre *TET3*. Pantalla de la sesión del UCSC Genome Browser [2018] presentando la región chr2:74214662-74215659, que enmarca los 5 sitios CpG enriquecidos en 5hmC sobre el gen de *TET3*. Los datos de 5hmC están mostrados en azul y los de 5mC en café; la intensidad del color es proporcional al grado de enriquecimiento. Células proliferantes (Prolif), en diferenciación (Diff) y en diferenciación + IFC-305 (IFC). Se muestran algunos *tracks* adicionales: Islas CpG < 300 pb; metilación de CpGs por el microarreglo 450K de ENCODE/HAIB para hepatocitos y la línea celular HepG2; metilación de DNA por el consorcio *Roadmap Epigenomics Mapping (REMC)* por secuenciación de bisulfito en hígado adulto (AL BS), la intensidad de grises es proporcional al grado de enriquecimiento; Segmentación del estado de la cromatina por el modelo *Hidden Markov (ChromHMM)* de hígado adulto (LIV ADLT) y la línea celular HepG2; *tracks* de las proteína arquitectónica CTCF, EZH2 y las marcas de histonas H3K4me1 (*enhancers*), H3K36me3 (elongación), H3K9me3 y H3K27me3 (marcas de cromatina cerrada) y H3K27ac (marca de cromatina abierta) de ENCODE/Broad; *Vista enhancer Handbook and Methods (HMR) at the Lawrence Berkeley National Laboratory (LBNL),* los picos denotan enriquecimieno; y *CG percent*, los picos denotan abundancia. El código de color para cada *track* se muestra en la Figura 40.

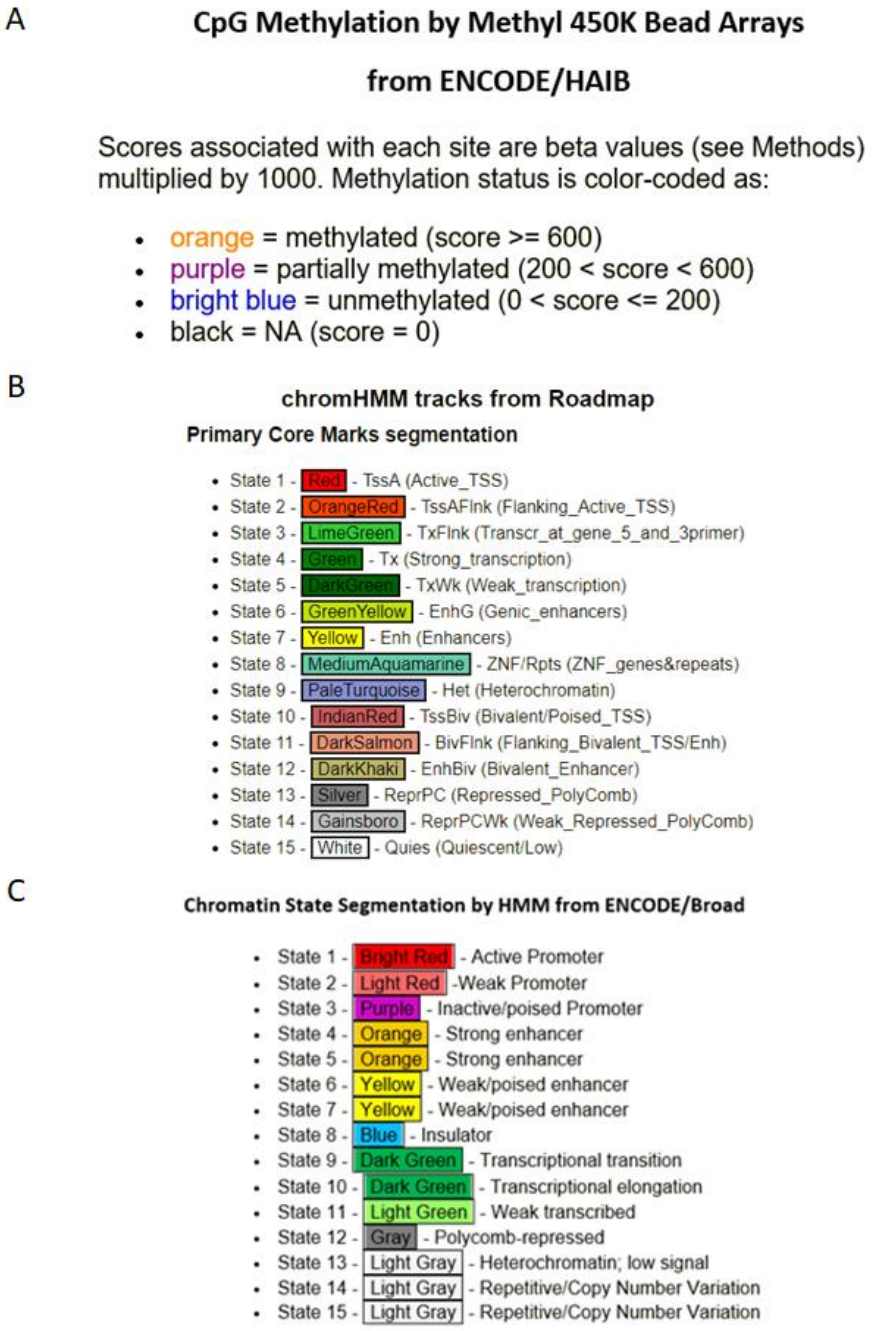

Fig. 40. Código de color de cada *track* mostrado en las pantallas del UCSC Genome Browser. (A) Metilación de CpGs por microarreglos Methyl 450K de ENCODE/HAIB de hepatocitos y la línea celular HepG2 [UCSC-Genome-Browser, 2018a]. Segmentación de los estados de la cromatina por el modelo *Hidden Markov (ChromHMM)* de hígado adulto (LIV ADLT) y de la línea celular HepG2 (B [UCSC-Genome-Browser, 2018c] y C [UCSC-Genome-Browser, 2018b] respectivamente).

9.3. Contexto genómico y funcional de los sitios diferencialmente hidroximetilados asociados con la diferenciación temprana de hepatocitos

Con el interés de saber si existe una relación entre el enriquecimiento de 5hmC y la expresión génica, se comparó la asociación el gen más próximo a los DhMPs con los DEGs asociados a una semana de diferenciación. Se encontraron 6952 DhMPs asociados a genes, 522 y 482 sobre y subexpresados respectivamente (Figura 41A). Los DhMPs asociados con un incremento de la expresión génica se relacionaron con células hepáticas y células hepáticas fetales y estuvieron enriquecidos en vías involucradas con los programas transcripcionales regulados por el receptor de andrógenos (*AR*) y el factor nuclear eritroide 2 relacionado con el factor 2 (*NFE2L2*) así como con rutas metabólicas (Figuras 42 A–C). Los DhMPs asociados con genes subexpresados se relacionaron con linfoblastos B y estuvieron enriquecidos en vías involucradas en el control del ciclo celular, como el programa de transcripción regulado por *E2F2* (Figura 42 D-F).

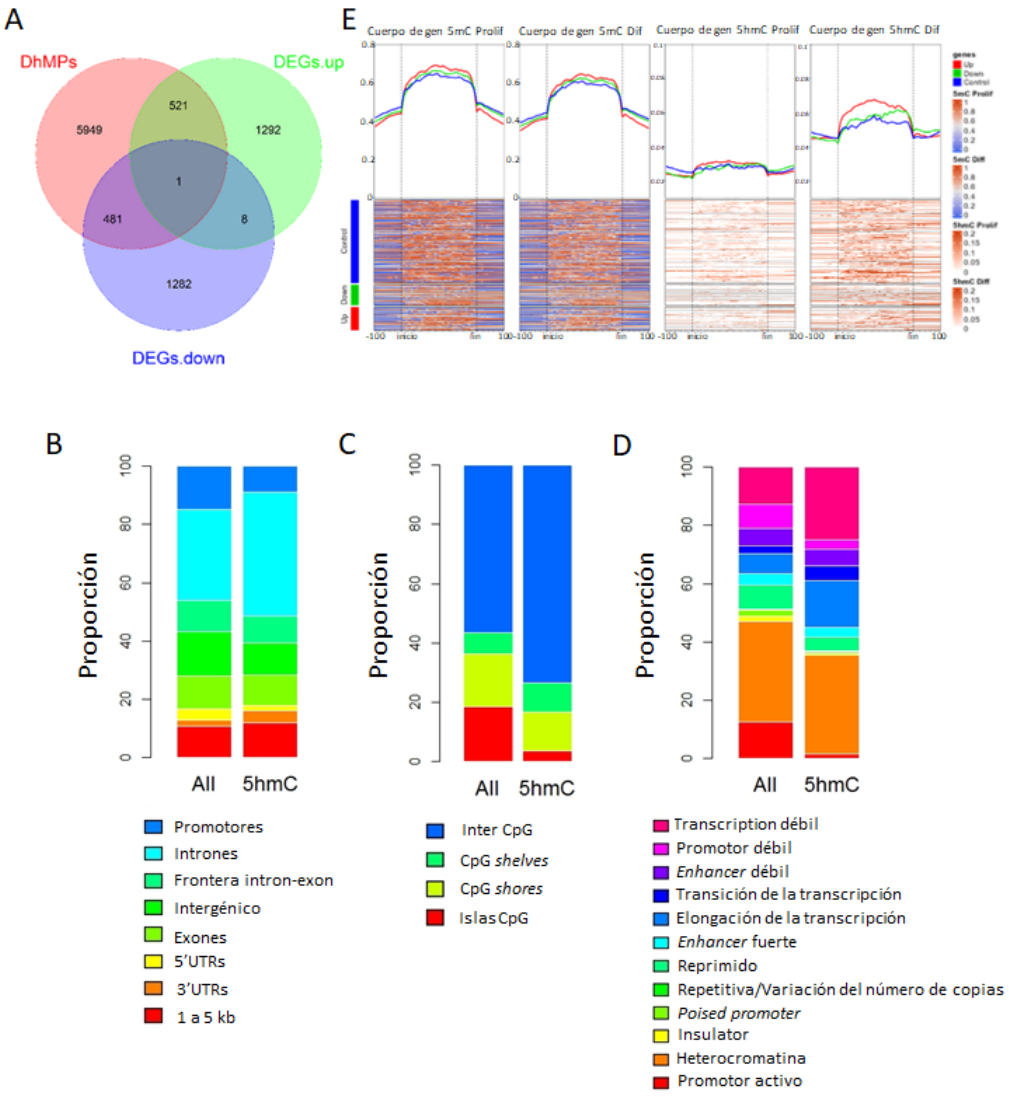

Fig. 41. Asociación entre la 5hmC y la expresión diferencial. (A) Diagrama de Venn representando los traslapes entre las posiciones diferencialmente hidroximetiladas (DhMPs) y los genes diferencialmente expresados (DEGs). Para este análisis, las DhMPs se anotaron a su gen más cercano. Los niveles de 5hmC están promediados a lo largo de las regiones genómicas anotadas en hg19, a su vez dividido en genes control, sobrexpresados y subexpresados. Las DhMPs fueron también anotadas de acuerdo a las características génicas (B), distribución de acuerdo a las CGIs (C), y a los estados de cromatina de la línea celular HepG2 (ChromHMM) (D). Para cada contexto genómico, la distribución se muestra de manera separada pata todos los DhMPs y para todas las sondas en el microarreglo EPIC como control. (E) Mapas de calor metagénicos mostrando la distribución de 5mC (dos paneles izquierdos) y 5hmC (dos paneles derechos) en células HepaRG proliferantes y diferenciadas por una semana. Todos los paneles muestran el promedio de la distribución de los valores de 5mC/5hmC en el cuerpo de genes sobreexpresados (rojo), subexpresados (verde) después de una semana de diferenciación. Los genes *housekeeping* que no muestran un cambio significativo se muestran en azul. Dos cultivos independientes fueron utilizados para las células proliferantes y en diferenciación.

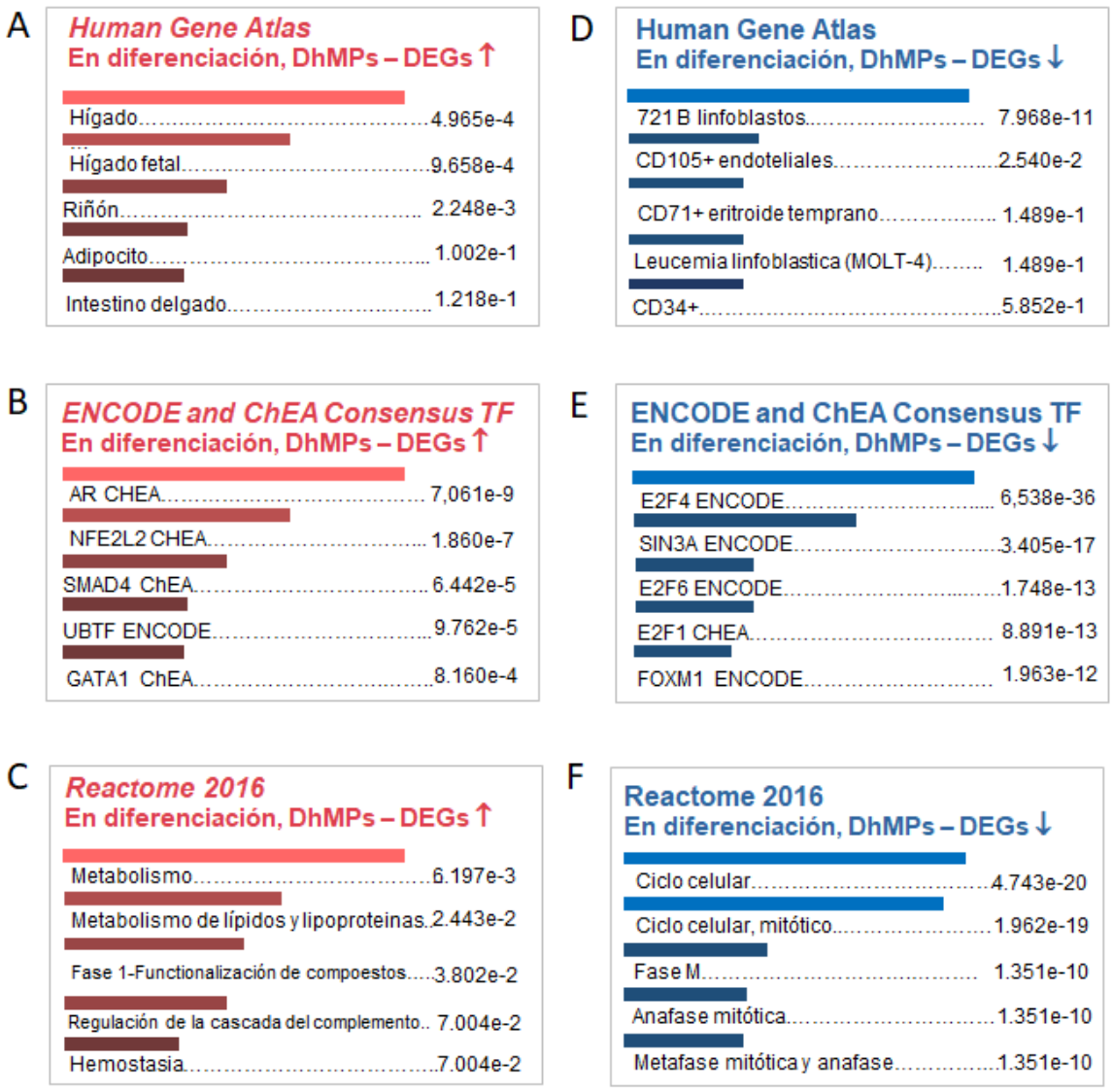

Fig. 42. Enriquecimiento funcional de los traslapes entre DhMPs y DEGs. (A) Células/tejidos asociados con las posiciones enriquecidas en 5hmC en células en diferenciación y los genes sobreexpresados comparando células en diferenciación vs. Células proliferantes. (B) Factores transcripcionales (TF) conceso de ENCODE ChEA de las posiciones enriquecidas en 5hmC de células en diferenciación y genes sobreexpresados. (C) Ontologías relacionadas con las posiciones enriquecidas en 5hmC en células en diferenciación y genes sobrexpresados. (D) Células/tejidos asociados con las posiciones enriquecidas en 5hmC en células en diferenciación y los genes subexpresados comparando células en diferenciación vs. Células proliferantes. (E) Factores transcripcionales (TF) consenso de ENCODE ChEA de las posiciones enriquecidas en 5hmC de células en diferenciación y genes subexpresados. (F) Ontologías relacionadas con las posiciones enriquecidas en 5hmC en células en diferenciación y genes subexpresados. Datos de EnrichR, el número muestra el valor de p ajustado asociado al tejido.

Enseguida, para explorar un papel menos evidente del enriquecimiento de 5hmC en la expresión génica, se comparó la distribución de DhMPs relativa a diferentes localizaciones genómicas anotadas. Los DhMPs están enriquecidos en regiones intrónicas y están ausentes en promotores y CGIs (Figura 41 B-C). Además, cuando se evaluaron características genómicas anotadas para células hepáticas HepG2 y se compararon contra los datos obtenidos en HepaRG, se encontró una sobrerrepresentación de DhMPs en *loci* relacionados con transcripción débil y elongación de la transcripción (Figura 41D). Enseguida, se analizó el enriquecimiento de 5mC y 5hmC en los cuerpos de los genes tanto en células HepaRG proliferantes como en células con una semana de diferenciación. El contenido de 5mC fue mayor en los genes regulados al alza incluso a nivel proliferativo, con una reducción general después de iniciada la diferenciación (Figura 41E). Además se encontró un incremento de 5hmC. A pesar de los bajos niveles de 5hmC, el incremento es evidente en el subconjunto de genes sobreexpresados después de una semana de diferenciación (Figura 41E). En resumen, estos datos indican que únicamente 14% del enriquecimiento de 5hmC en la diferenciación temprana de HepaRG puede asociarse directamente con genes que muestran un cambio en la expresión y que se encuentran vecinos al sitio de enriquecimiento. Sin embargo, el contenido de 5hmC es en general más alto en los cuerpos genéticos de los genes regulados al alza, lo cual concuerda con otros análisis realizados con una resolución a nivel de nucleótido y que relacionan a genes altamente expresados con la presencia de 5hmC [revisado por [Ecsedi et al., 2018]].

9.4. La exposición al derivado de adenosina y la inhibición de TET tiene repercusiones en la diferenciación de hepatocitos

Considerando el incremento de 5hmC a nivel de genoma completo desde la diferenciación temprana de HepaRG, se evaluó si la estimulación metabólica de las reacciones de *trans*-metilación pudiera impactar en los niveles de 5hmC, conduciendo a una modificación en el proceso de diferenciación de hepatocitos. Para abordar esta pregunta, se utilizó un derivado de adenosina previamente descrito, IFC-305, que es capaz de regular los flujos metabólicos favoreciendo la disponibilidad de SAM y modulando la dinámica de metilación de DNA [Rodriguez-Aguilera et al., 2018].

En primer lugar se evaluó la viabilidad de las células HepaRG en respuesta a la exposición con IFC-305 y se encontró que la viabilidad no se afecta en concentraciones por debajo de 1 mM durante 1 semana de diferenciación (Figura 43).

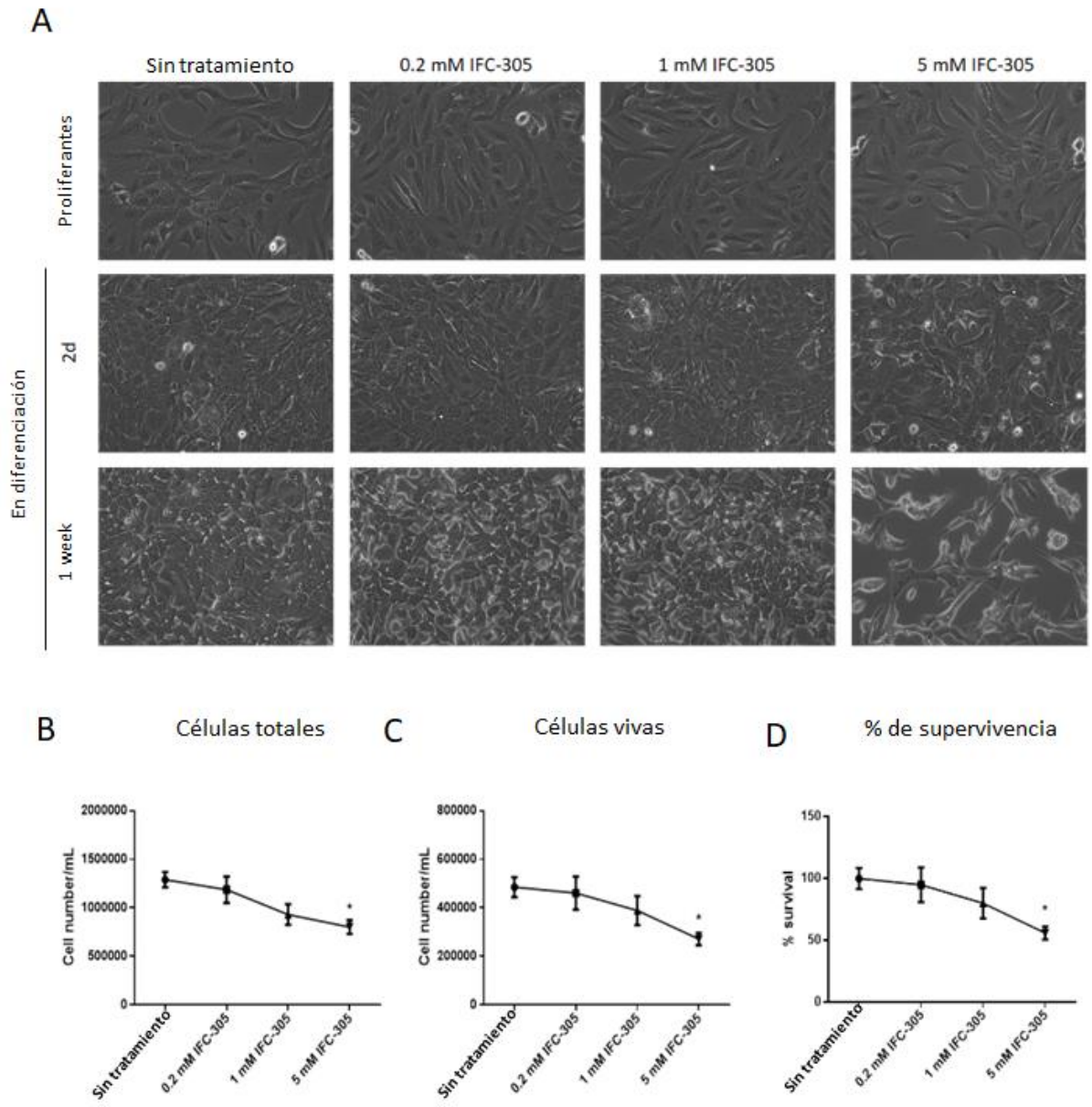

Fig. 43. Bajas concentraciones del derivado de adenosina no alteran la viabilidad de la línea celular HepaRG. (A) Fenotipo de la línea HepaRG durante 1 semana de diferenciación. Se muestran imágenes representativas a un aumento de 20x de cada grupo. Es posible observar que el tratamiento con IFC-305 5 mM retine el fenotipo elongado propio de células proliferantes y que las concentraciones de 0.2 y 1 mM no modifican el fenotipo celular comparado con las células en diferenciación sin tratamiento. (B) Número total de células. (C) Número de células viables. (D) Porcentaje de supervivencia. Los datos representan el promedio ± DEM de siete cultivos independientes. Diferencia estadística ($p < 0.05$) comparado con las células en diferenciación sin tratamiento.

Se analizó la expresión de marcadores hepáticos en respuesta a diferentes dosis de IFC-305 y notamos que 1 mM del compuesto produce valores menores de *ALDOB* y *GSTA* en comparación con células en diferenciación no tratadas (Figura 44A). La expresión de albúmina no presentó cambios en las células sin tratamiento ni en las tratadas con IFC-305, excepto por la reducción en la expresión con IFC-305 5 mM (Figura 44A) comparada con células proliferantes. Con respecto a las isoformas reguladas por el promotor P1 de *HNF4A*, su expresión presentó el mismo incremento con IFC-305 0.2 y 1 mM que en células en diferenciación no tratadas, mientras que una concentración de 5 mM de IFC-305 generó una sobreexpresión de estas isoformas comparadas con células proliferantes y diferenciadas (Figura 44B). Por otra parte, las isoformas reguladas por el promotor P2 de *HNF4A* incrementaron su expresión solo con IFC-305 0.2 y 1 mM comparadas con células proliferantes (Figura 44B). A nivel de proteína, el IFC-305 a 1 mM se asoció con una reducción de la inmunoreactividad nuclear de HNF4α en células en diferenciación comparadas con las células en diferenciación sin tratamiento (Figura 45).

Este comportamiento de la expresión de marcadores de hepatocitos sugiere que la exposición de HepaRG al IFC-35 durante la diferenciación influye en la maduración de hepatocitos. Explorando esta posibilidad, extendimos el modelo de diferenciación a un periodo más largo (20 días). A 13 días, las células en diferenciación no tratadas presentaron una morfología similar a la de hepatocitos, mostrando pequeñas células poligonales con granularidad incrementada y organizados en trabéculas bien delineadas, separadas por estructuras brillantes similares a canalículos (Figura 46). El IFC-305 retrasa la aparición de este fenotipo de manera dependiente de la concentración, con 1 mM de IFC-305, las células tratadas muestran un fenotipo retrasado de al menos una semana, y 5 mM de IFC-305 retiene un fenotipo similar al de células proliferantes incluso a 20 días de diferenciación (Figura 44C y Figura 46). Esta variación del fenotipo, reduce los niveles de marcadores de

hepatocitos (por ejemplo las isoformas reguladas por el promotor P1 de *HNF4A*, *ALDOB* y *GSTA*) e incrementa la expresión de las isoformas reguladas por el promotor P2 de *HNF4A*, así como una tendencia a la reducción de la expresión de *TET1* (Figura 47A), sugiriendo que el IFC-305 es capaz de retrasar la diferenciación de hepatocitos a concentraciones de 1 y 5 mM.

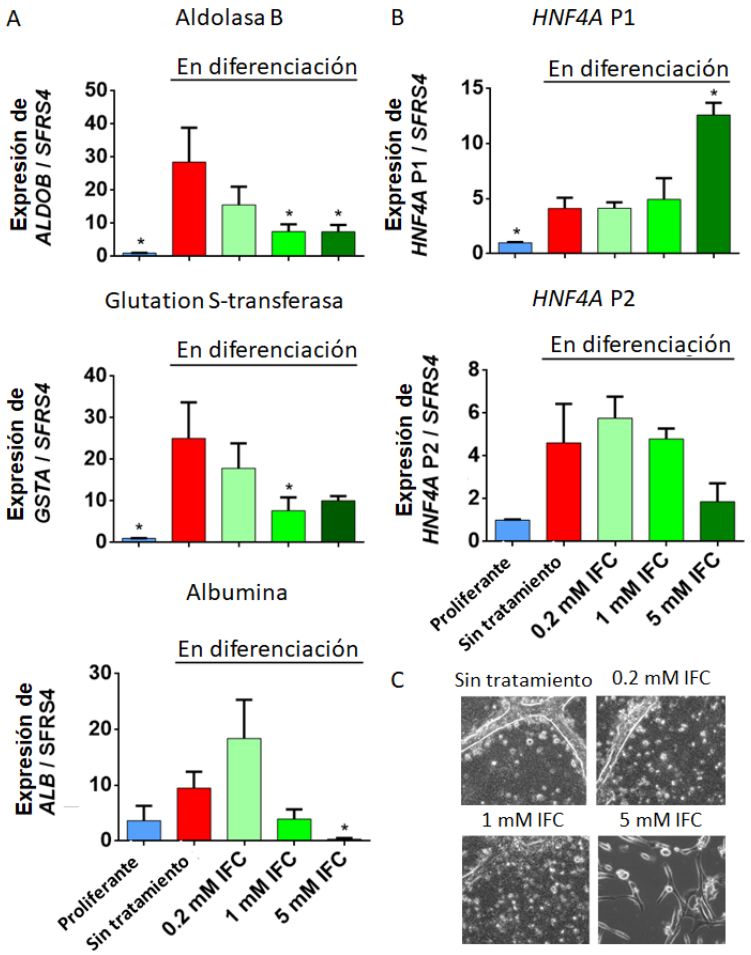

Fig. 44. Alteración de la expresión de marcadores de hepáticos tras la exposición al derivado de adenosina. (A) La expresión de marcadores de hepatocitos se evaluó por RT-qPCR, los datos representan el promedio ± DEM de tres cultivos independientes/condición. (B) Se evaluó la expresión de las isoformas reguladas por los promotores P1 y P2 de *HNF4A* por RT-qPCR, los datos representan el promedio ± DEM de tres cultivos independientes/condición. (C) Imágenes de contraste de fases mostrando el fenotipo de las células HepaRG durante 20 días de exposición a un gradiente de concentraciones crecientes de IFC-305. Se muestran imágenes representativas a un aumento de 20x de siete cultivos independientes. *Diferencia estadística ($p < 0.05$) cuando se compara con células en diferenciación sin tratamiento.

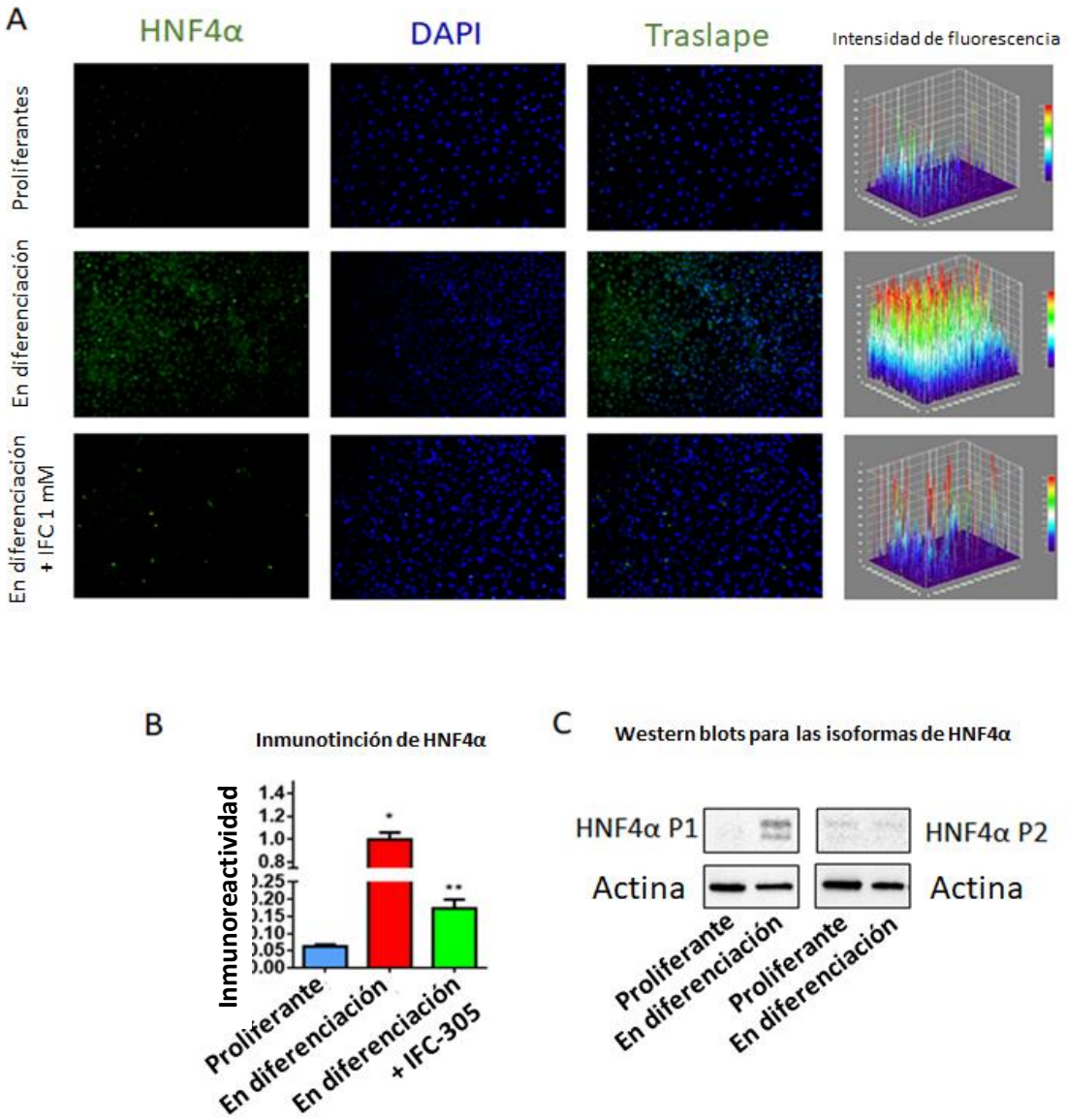

Fig. 45. HNF4α incrementa en células en diferenciación. (A) Inmunofluorescencia de HNF4α en células proliferantes (panel superior), en diferenciación (panel intermedio) y en diferenciación expuestas al IFC-305 (panel inferior). Imágenes representativas de 3 campos/condición. (B) Cuantificación de la señal positiva de inmunofluorescencia para HNF4α. Los datos representan el promedio ± DEM de 3 campos/grupo. *Diferencia significativa ($p < 0.05$) cuando se compara con las células proliferantes. **Diferencia estadística ($p < 0.05$) comparada con las células en diferenciación. (C) Western blots con anticuerpos específicos contra cada las isoformas codificadas por los promotores P1 y P2 de HNF4α en proteínas totales de células HepaRG proliferantes y en diferenciación. Se utilizó actina como control de carga.

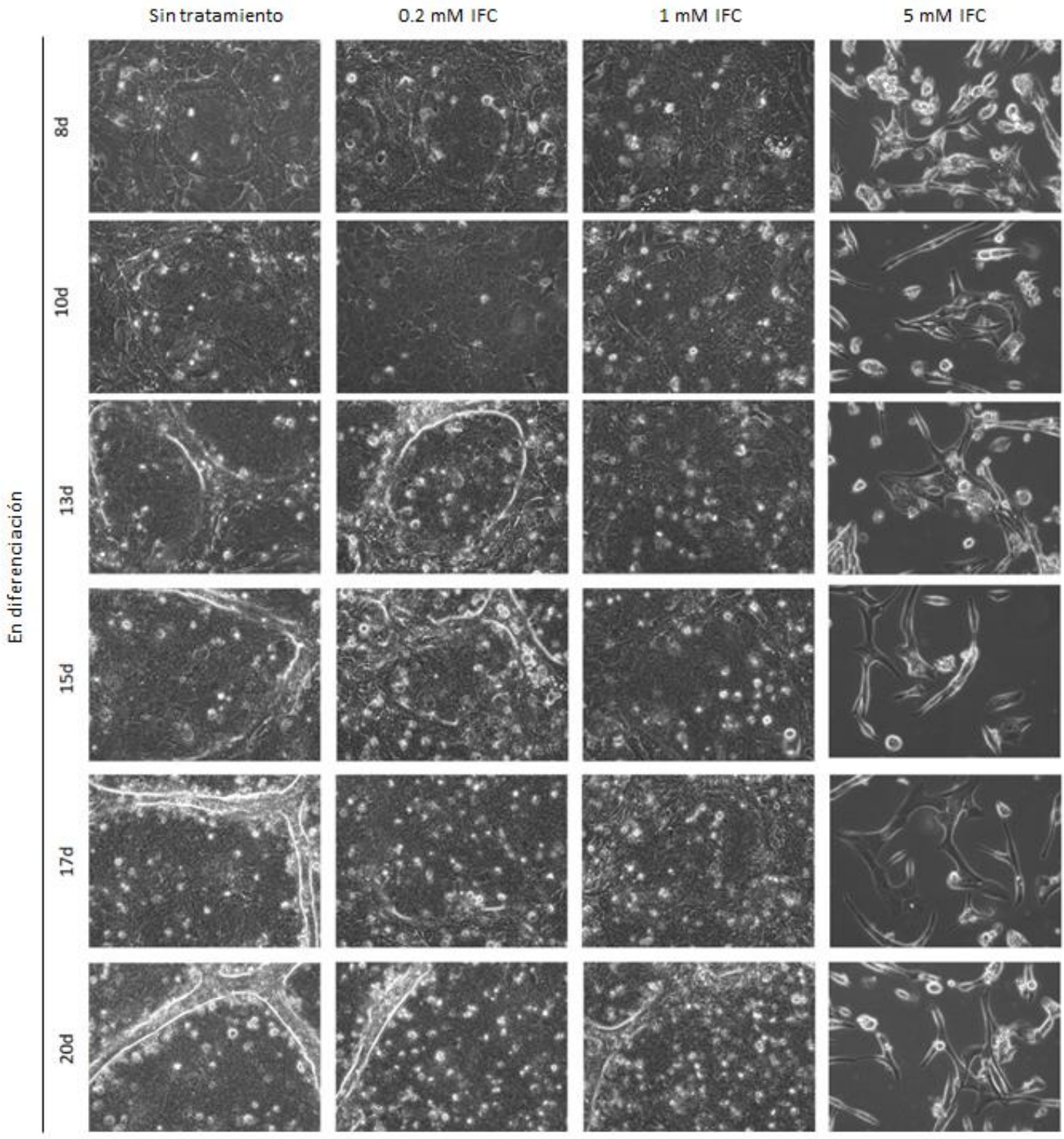

Fig. 46. Las células en diferenciación expuestas a IFC-305 1 mM presentan un fenotipo menos diferenciado. Imágenes mostrando el fenotipo de células en diferenciación durante un lapso de 20 días con un gradiente de concentración creciente de IFC-305. Se muestran imágenes representativas a un aumento de 20x de siete cultivos independientes por condición.

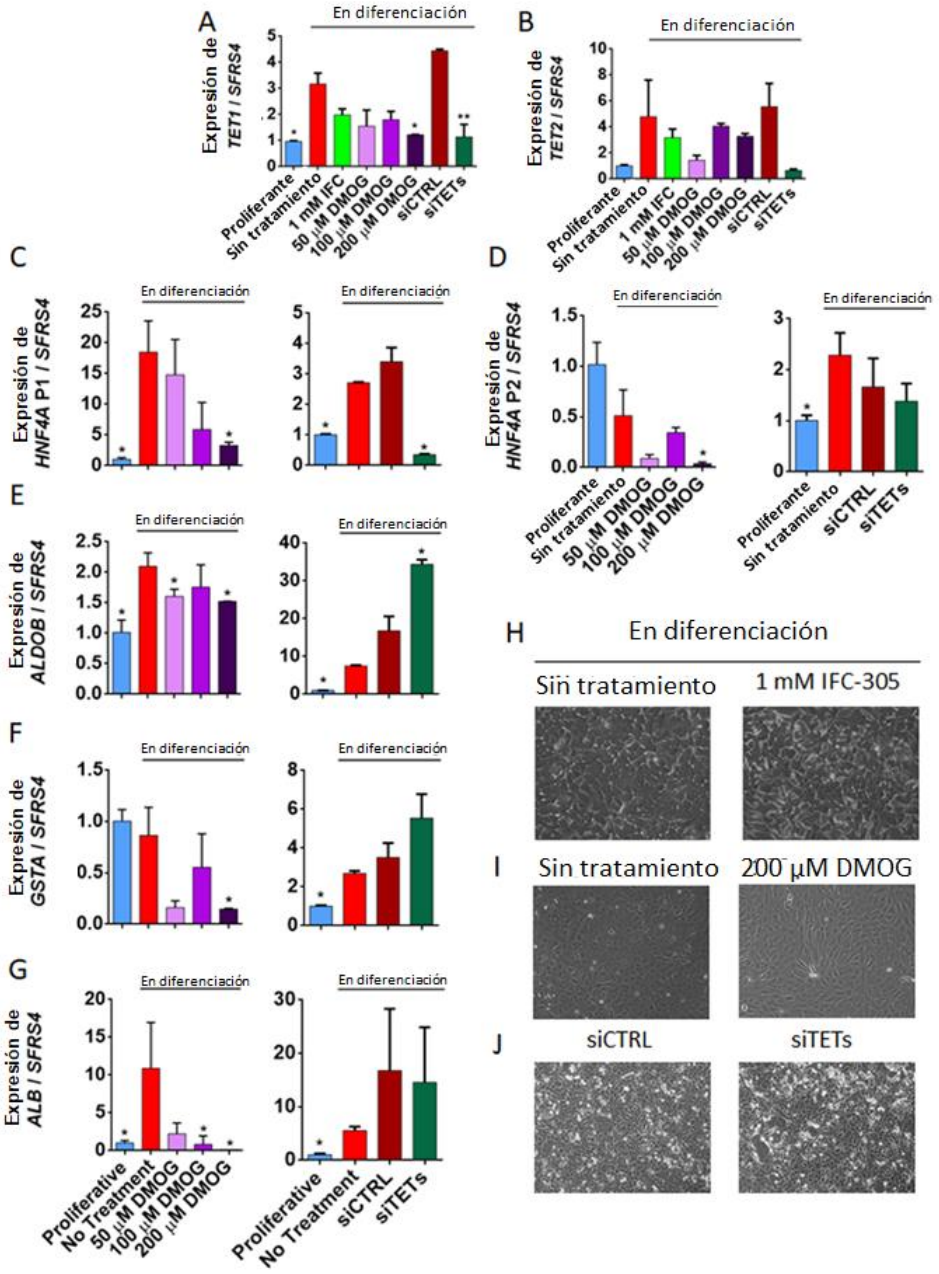

Fig. 47. Alteración de la expresión de marcadores de hepáticos tras la disminución transcripcional de TETs. Expresión de *TET1* (A) y *TET2* (B) después de la exposición de las células HepaRG al IFC-305, a la DMOG o a los siTETs durante una semana de diferenciación; (C-G) Expresión modificada de marcadores hepáticos en respuesta a la exposición a la DEMOG y a los siTETs, durante una semana de diferenciación de las células HepaRG. Los datos representan el promedio ± DEM de3 cultivos independientes/condición. *Diferencia estadística ($p < 0.05$) cuando se compara con las células en diferenciación sin tratamiento. **Diferencia estadística ($p < 0.05$) cuando se compara con la exposición a siCTRL. Fenotipo de las células HepaRG no tratadas expuestas al IFC-305 1 mM (H) o a DMOG 200 µM (I) y entre siCTRL y siTETs (J) a una semana de diferenciación; se muestran imágenes representativas a 20x de aumento de 3 cultivos independientes.

Con el interés de saber si la diferenciación es regulada por la adquisición de 5hmC a una semana de la diferenciación de las células HepaRG, se evaluaron los efectos de inhibidores químicos y transcripcionales de TETs a concentraciones que no afectan la viabilidad celular. Las células HepaRG fueron expuestas a la DMOG, un derivado de la N-oxalilglicina (NOG), que es capaz de penetrar a las células y que inhibe a las dioxigenasas dependientes de Fe^{2+}/2-oxoglutarato como las enzimas TET [Rose et al., 2011] o transfectadas con una mezcla de siRNAs contra *TET1* y *TET2.* La DMOG a 200 μM es capaz de reducir la expresión de *TET1* cuando se compara contra las células no tratadas (Figura 47A). Un comportamiento similar es observado para los siTETs, como era de esperarse. Por lo tanto, el inhibidor químico como el transcripcional de TETs reducen la expresión de *TET1* a una semana de diferenciación de la línea celular HepaRG. En ambas condiciones (DMOG a 200 μM y siTETs), la expresión del regulador maestro de la diferenciación de hepatocitos regulada por su promotor P1 *HNF4A* se reduce en comparación con las células no tratadas y con el siCTRL, respectivamente (Figura 47C). Lo anterior indica que una inhibición específica de *TET1* reduce los niveles esperados de expresión de *HNF4A* P1 a una semana de diferenciación. Previamente se ha demostrado que esta reducción de *HNF4A* P1 correlaciona con la ausencia de 5hmC en el promotor P1 [Ancey et al., 2017]. Estos resultados en su conjunto sugieren que la interferencia con los niveles de expresión de *TETs*, alteran la regulación del programa de transcripción de hepatocitos desde *HNF4A locus*.

El análisis de los marcadores de expresión de hepatocitos indicó que la DMOG a 200 μM presenta un comportamiento similar al IFC-305: reduce marcadamente la expresión de *ALDOB, GSTA* y *ALB.* Mientras que los siTETs incrementan la expresión de *ALDOB,* presentan una tendencia similar en *GSTA* y no inducen cambios de expresión en *ALB* (Figura 47 E-G). No se observó algún efecto fenotípico con ninguno de los dos tratamientos

(DMOG y siTETs) a una semana de diferenciación de HepaRG (Figura 47 H-J). Con los datos anteriores es posible sugerir que ambos inhibidores de TET afectan en forma diferente la expresión de los marcadores hepáticos a una semana del proceso de diferenciación de HepaRG, posiblemente porque la DMOG al igual que el IFC-305 es un regulador metabólico, mientras que los siTETs inhiben directamente al mensajero de TETs.

A pesar de que el IFC-305 no es inhibidor específico de las TETs, se escogió a este análogo de nucleósido para los siguientes experimentos, ya que representa una forma de contrarrestar la carencia del donador de grupos metilo que ocurre en varias patologías como la cirrosis [Rodriguez-Aguilera et al., 2018] y el carcinoma hepatocelular [Lozano-Rosas et al., 2019], propiedades que lo sustentan como un compuesto no tóxico para el hígado.

9.5. El cambio en el ambiente metabólico por el derivado de adenosina modifica el paisaje de 5hmC asociado a la diferenciación de hepatocitos

Las Células HepaRG proliferantes fueron expuestas a IFC-305 1 mM en condiciones de diferenciación durante 1 semana. Bajo estas condiciones, la reducción de 5 mC y la acumulación de 5hmC se afectan (Figuras 29 A-B). De manera similar, solo una fracción de DhMPs relacionados con la diferenciación se detectaron en presencia de IFC-305 utilizando microarreglos de metilación con resolución de nucleótido (Figura 29E). Como se describió anteriormente, se aprecia un cambio en 5hmC durante la diferenciación de hepatocitos, el cual es particularmente evidente en el cuerpo de los genes sobreexpresados (Figura 48A, panel izquierdo). En contraste, las células que crecieron expuestas al IFC-305 desplegaron una acumulación intermedia de 5hmC (Figura 48A, panel derecho). A pesar de este fenotipo atenuado, fue posible detectar hidroximetilación diferencial en 8460 en CpGs asociadas a genes (Figura 48B) y 1890 regiones, en comparación con células proliferantes. Comparando estos genes con DEGs sobreexpresados en células en diferenciación,

encontramos un empalme de 173 genes, los cuales están altamente asociados con expresión hepática, de acuerdo con la base de datos ARCH4 (Figura 49).

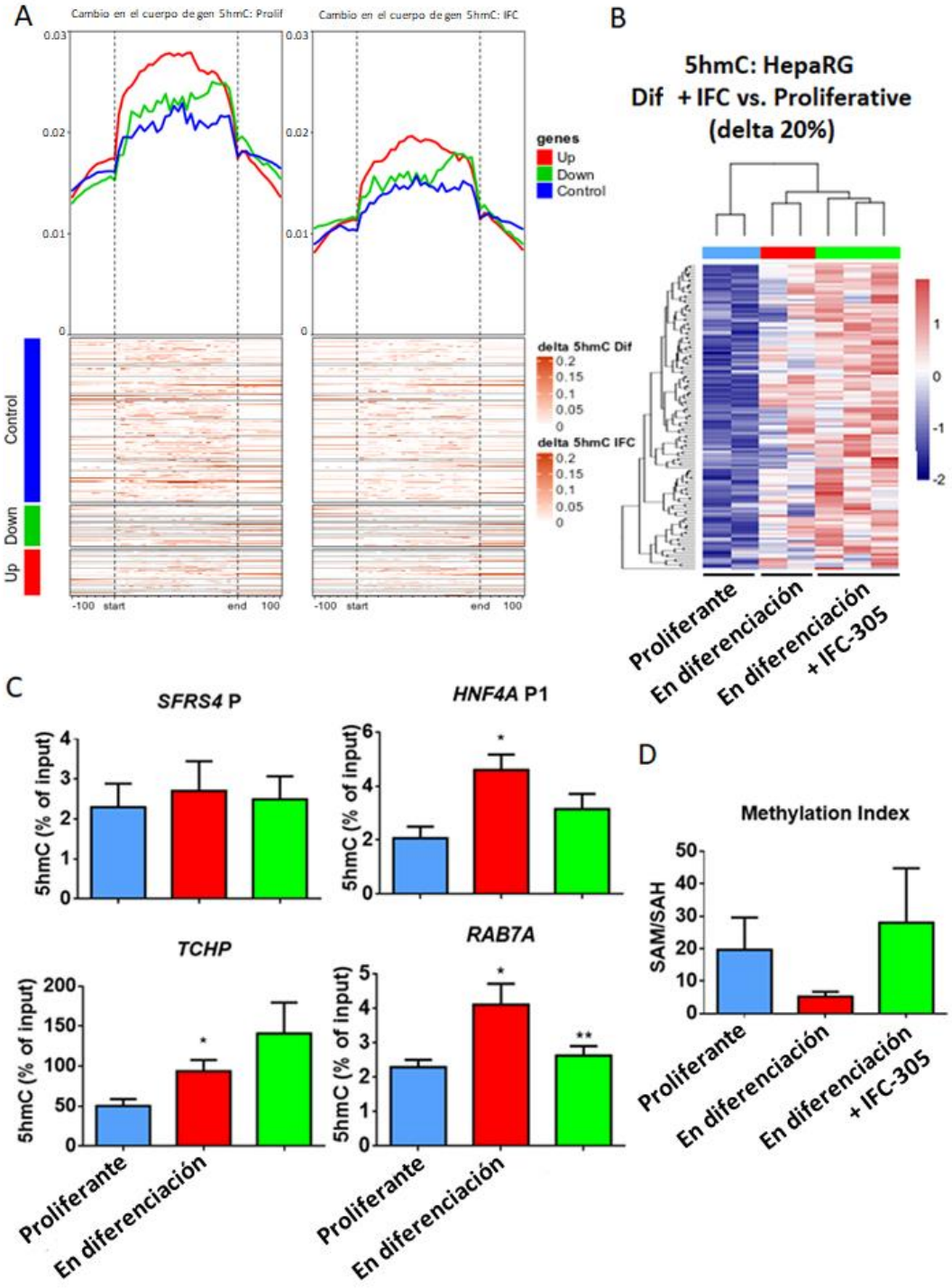

Figura 48. La perturbación de los niveles del donador de grupos metilo reduce el enriquecimiento de 5hmC. 5hmC en células proliferantes, en diferenciación y en diferenciación expuestas al IFC-305, evaluadas a través de BS y OxBS seguido de hibridación en microarreglos EPIC (ver métodos y Figura 26). (A) Mapa de calor metagénico mostrando el cambio en el contenido de 5hmC después de una semana de diferenciación de las células HepaRG en condiciones control (panel izquierdo) o después de ser expuestas al derivado de adenosina IFC-305 (panel derecho). Se trazaron gráficas por separado para el incremento en el contenido de 5hmC en cuerpos de genes sobre (rojo) o sub (verde) expresados después de una semana de diferenciación. Los genes *housekeeping* que no mostraron cambio significativo se muestran en azul. (B) Mapa de calor mostrando la comparación del hidroximetiloma entre las células en diferenciación expuestas al IFC-305 y las células proliferantes. Las posiciones diferencialmente hidroximetiladas (DhMPs) se filtraron por la magnitud del cambio de metilación (delta beta) de al menos 20% con un valor de p ajustado < 0.05. Dos cultivos independientes se utilizaron para las células proliferantes y tres cultivos independientes para las células en diferenciación expuestas a IFC-305 1 mM. (C) Validación de cambios en 5hmC. El enriquecimiento de 5hmC fue evaluado por hMeDIP y qPCR; El promotor del gen *SFRS4* fue usado como control de una región no enriquecida de 5hmC, el promotor P1 del gen *HNF4A* se usó como control positivo de enriquecimiento de 5hmC a una semana de diferenciación, los datos representan el promedio ± DEM de 3 cultivos independientes/condición; *Diferencia estadística ($p < 0.05$) comparado con células proliferantes. **Diferencia estadística ($p < 0.05$) comparada con células en diferenciación. (D) El contenido de S-adenosilhomocisteina (SAH) y S-adenosilmetionina (SAM) se evaluó utilizando HPLC en las diferentes condiciones experimentales, se utilizaron estándares internos en cada muestra. Las barras indican el índice de metilación, calculado como la relación SAM/SAH, promedio ± DEM de 4 cultivos/condición.

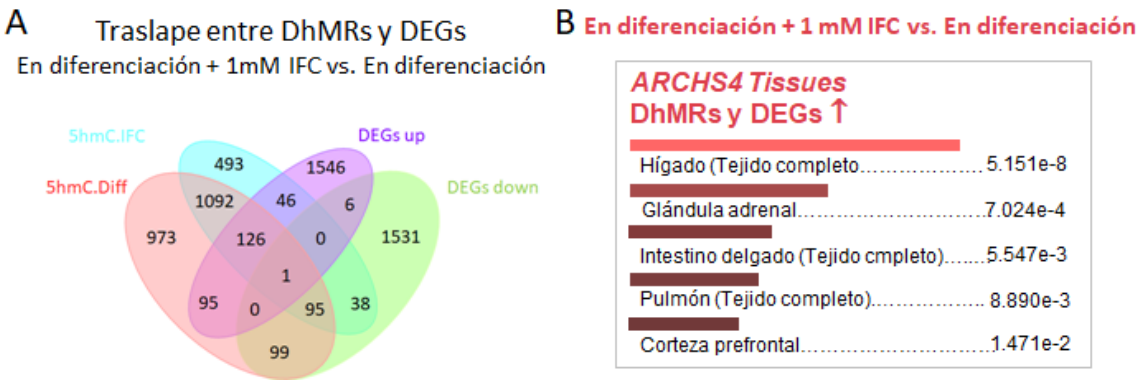

Fig. 49. Algunas regiones diferencialmente hidroximetiladas en las células en diferenciación tratadas con IFC-305 se relacionaron con genes diferencialmente expresados. (A) Comparación entre las regiones diferencialmente hidroximetiladas (DhMRs) en células expuestas al IFC-306 y los genes sobreexpresados en las células en diferenciación. (B) Enriquecimiento funcional relacionado con las regiones enriquecidas en 5hmC en las células en diferenciación expuesta al IFC-305 y los genes sobreexpresados en las células en diferenciación. Los datos fueron obtenidos utilizando EnrichR, el número indica el valor de p ajustado asociado al tejido.

Para validar el incremento de 5hmC durante el proceso de diferenciación, se utilizó el ensayo de inmunoprecipitación de DNA hidroximetilado (hMeDIP) en regiones con alto enriquecimiento de 5hmC. Se evaluaron dos regiones en la vecindad de *TCHP* y *RAB7A.* Además, evaluamos la región donde se da el switch de 5mC/5hmC en el promotor P1 de *HNF4A*, y se utilizó al promotor del gen *SFRS4* como región control. Pudimos observar un nivel constante de 5hmC sobre el promotor de *SFRS4* en células proliferantes y en diferenciación (Figura 48C). El promotor P1 de *HNF4A* presentó un incremento de 5hmC a una semana de diferenciación, como previamente se había encontrado [Ancey et al., 2017]. Este incremento se afectó por la exposición con IFC-305 y un comportamiento similar se observó en las regiones *TCHP* y *RAB7A* (Figura 48C).

A continuación, nos preguntamos ¿cómo el derivado de adenosina es capaz de modificar los niveles de 5hmC conduciendo a un retraso en la diferenciación de hepatocitos? Para abordar esta pregunta, evaluamos algunos componentes del ciclo de la metionina, el cual es la ruta metabólica responsable de las reacciones biológicas de *trans*-metilación [Kharbanda, 2007]. Estas reacciones, incluyendo la metilación del DNA, pueden ser modificadas por la disponibilidad de SAM, así como por los niveles de S-adenosilhomocisteína (SAH) [Auta et al., 2017; Garcea et al., 1989]. Previamente demostramos que la adenosina, así como el IFC-305, es capaz de modular los niveles de SAM, favoreciendo la metilación de fosfolípidos [Chagoya de Sanchez et al., 1991] y restaurando los niveles globales de metilación de DNA y 5mC en un modelo de cirrosis inducido con CCl_4 [Rodriguez-Aguilera et al., 2018]. Con este razonamiento, evaluamos el contenido de adenosina, SAM y SAH, a través de HPLC (Figura 50). Una tendencia hacia la disminución de SAM se observó en las células en diferenciación comparadas con las células proliferantes (Figura 50 A, B y E), consistente con la reducción global de 5mC a una semana de diferenciación (Figura 34A), con una tendencia no significativa al incremento de

SAH (Figura 50 A, B y F). El índice de metilación (relación SAM/SAH) derivado de estos datos, fue menor y menos variable en las células en diferenciación (Figura 48D). Un índice de metilación más alto y disperso se observó en células proliferantes y en diferenciación expuestas a IFC-305 los cuales correlacionan con elevada abundancia de 5mC a lo largo del genoma (Figura 34B). El contenido de adenosina fue mayor en las células en diferenciación comparadas con las células proliferantes, con los niveles más altos en las células en diferenciación expuesta a IFC-305 1 mM (Figura 50 A. B, C y G; un cromatograma de los estándares se muestra en la Figura 50D); un comportamiento similar se encontró para SAM, con el nivel más elevado observado en las células expuestas al IFC-305 (Figura 50 A, B, C y D).

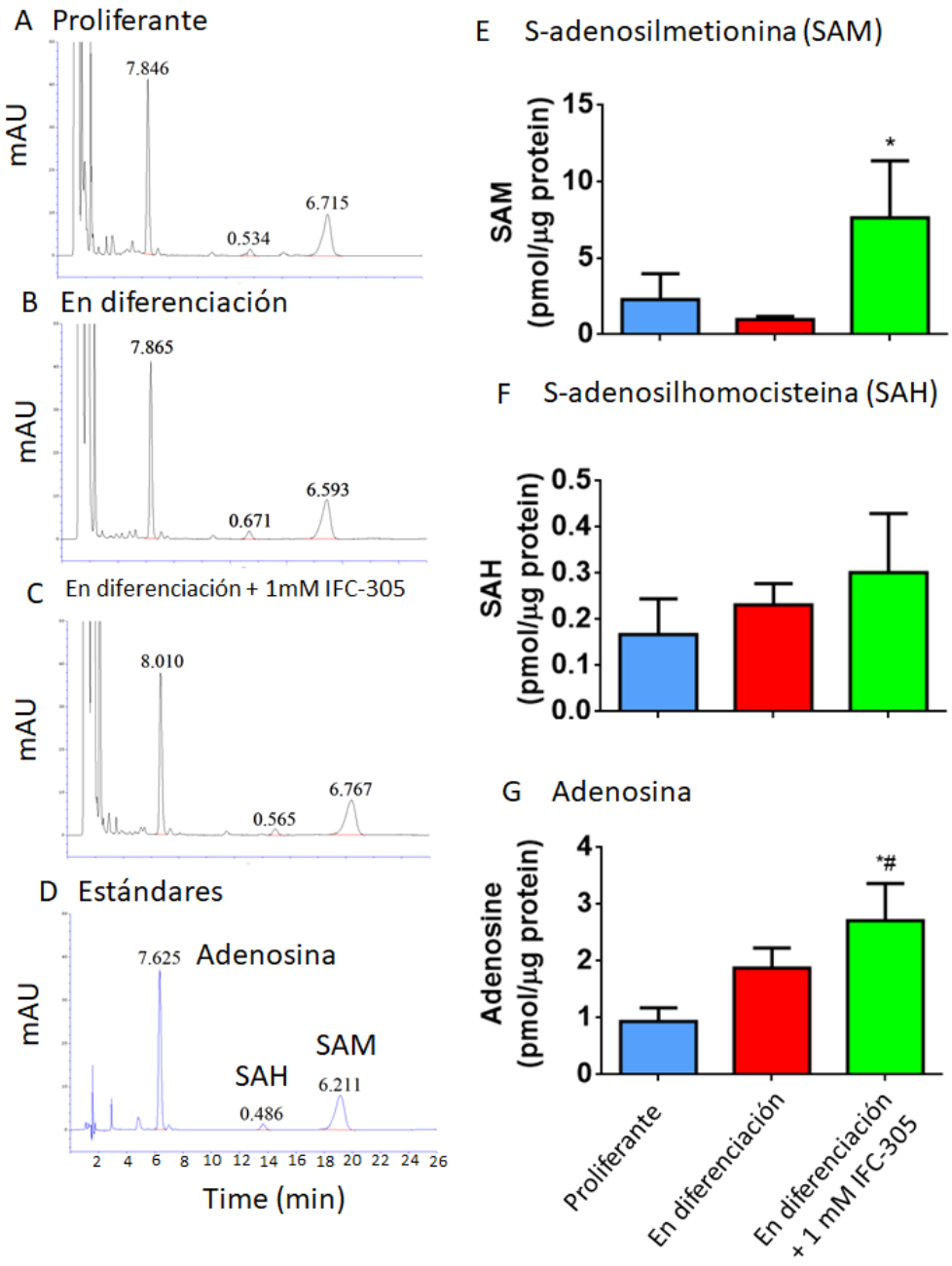

Fig. 50. La S-adenosilmetionina tiende a disminuir en la diferenciación temprana de las células HepaRG. (A-D) Cromatogramas representativos identificando adenosina, S-adenosilmetionina (SAM) y S-adenosilhomocisteina (SAH) a través de HPLC en las condiciones analizadas y generados con estándar interno, los números indican el área bajo la curva, se muestran los primeros 26 min del tiempo de separación. (E-G) Cuantificación de cada analito. Los datos representan el promedio ± DEM de 4 cultivos /condición. *Diferencia estadística ($p < 0.05$) cuando se compara con las células en diferenciación sin tratamiento. **Diferencia estadística ($p < 0.05$) cuando se compara con células proliferantes.

Estos resultados sugieren que el IFC-305 genera un ambiente metilante que compite con la ola de desmetilación asociada a la diferenciación de hepatocitos y subraya la importancia del enriquecimiento de 5hmC en este proceso.

Con el interés de determinar si los efectos del derivado de adenosina pueden ser atribuidos a su capacidad para incrementar el nivel de SAM, se expusieron las células HepaRG a SAM a una concentración de 1 mM durante una semana de diferenciación. Se observó una reducción en el número celular (Figura 51A), principalmente en la periferia del cultivo. Se observó una sobreexpresión de los transcritos codificados tanto por el promotor P1 como P2 de *HNF4A*, pero los marcadores hepáticos *ALDOB, GSTA,* y *ALB* se subexpresaron comparados con las células en diferenciación sin tratamiento (Figura 51C). La ruta de metilación de DNA también mostró una reducción, subexpresándose las DNA metiltransferasas (*DNMT1*, *DNMT3A* y *DNMT3B*), así como los transcritos correspondientes a las enzimas adenosiltransferasas (*MAT1A* y *MAT2A*) (Figura 51D). Analizando la expresión de la ruta de oxidación de la metilcitosina, se encontró un incremento del transcrito de *TET1* y una misma tendencia para el trascrito de *TET2*, así como una subexpresión de los transcritos de las enzimas isocitrato deshidrogenasas (*IDH1* e *IDH2*), enzimas que generan al α-cetoglutarato, metabolito requerido para el funcionamiento de TET (Figura 51E) y que pudiera estar relacionada con la reducción de 5hmC debida a la exposición a SAM (Figura 52). En cuanto a los efectos del IFC-305, se pudo observar una sobrexpresión de las DNA metiltransferasas, un mismo nivel del transcrito de *MAT2A,* se validó la subexpresión de *TET1* y *TET2,* y se observó un nivel intermedio de expresión de *IDH2,* comparando con las células en diferenciación sin tratamiento (Figura 51).

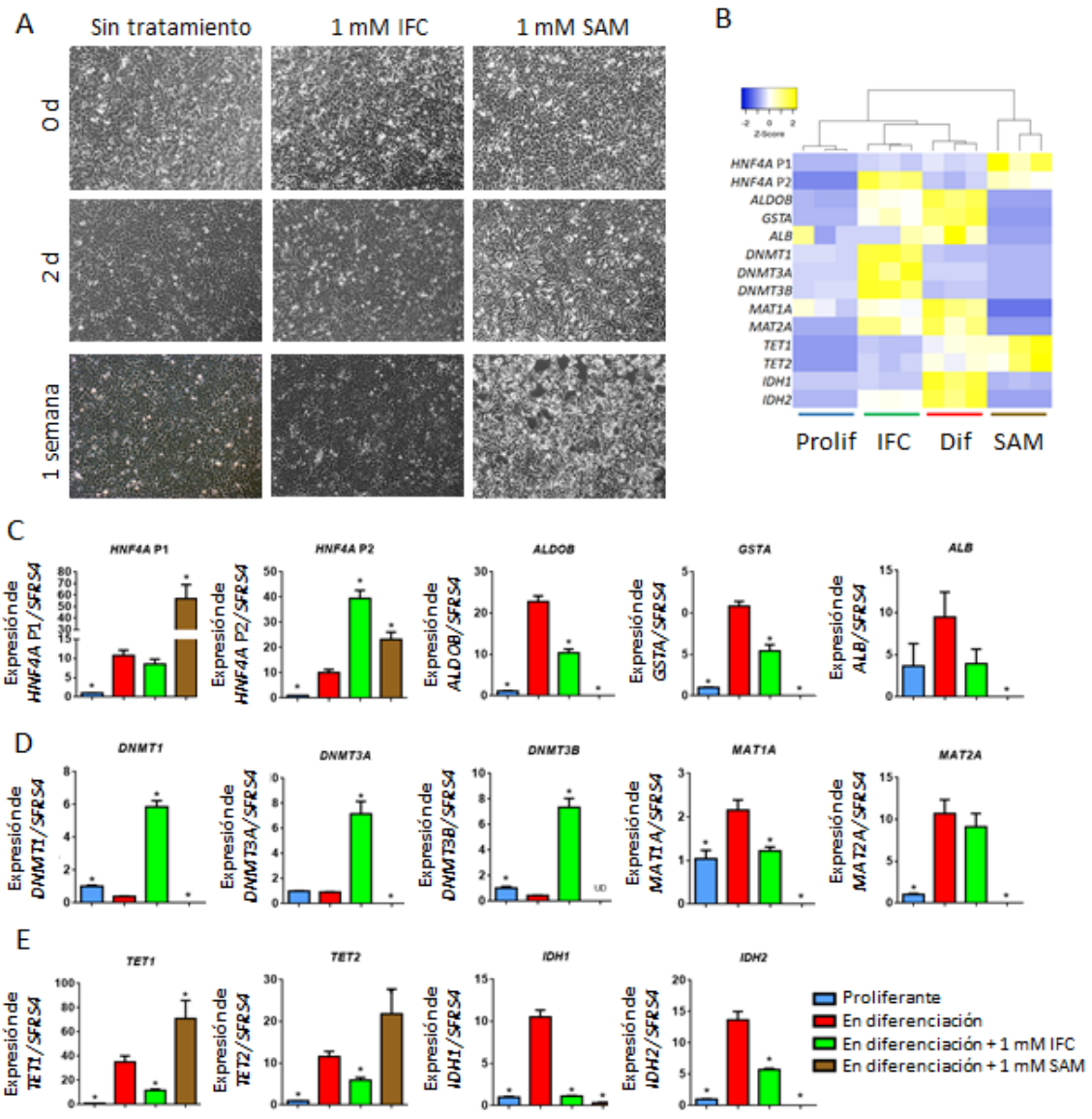

Fig. 51. Disminución de la expresión de marcadores hepáticos, rutas de metilación de DNA y de oxidación de citosinas después del tratamiento a la línea celular HepaRG con el derivado de adenosina y con S-adenosilmetionina. (A) Fenotipo celular de HepaRG a lo largo de una semana de diferenciación, se muestran imágenes representativas por grupo con un aumento de 10x. (B) El mapa de calor representa la expresión diferencial de los genes analizados y fue construido utilizando la plataforma (http://heatmapper.ca/). (C) Expresión de los marcadores de diferenciación de hepatocitos en respuesta a los diferentes tratamientos, a una semana de diferenciación. (D) Expresión de las metiltransferasas de DNA (*DNMTs*) y de las metionina adenosiltransferasas (*MATs*) después de una semana de exposición durante el proceso de diferenciación. (E) Expresión de los transcritos de las dioxigenasas TET y de las isocitrato deshidrogenasas (*IDHs*) después de una semana de diferenciación y el efecto de la exposición al IFC-305 y SAM. Los datos representan el promedio ± DEM de 3 cultivos independientes/condición. *Diferencia significativa ($p < 0.05$) cuando se compara contra las células en diferenciación sin tratamiento. UD: indetectable.

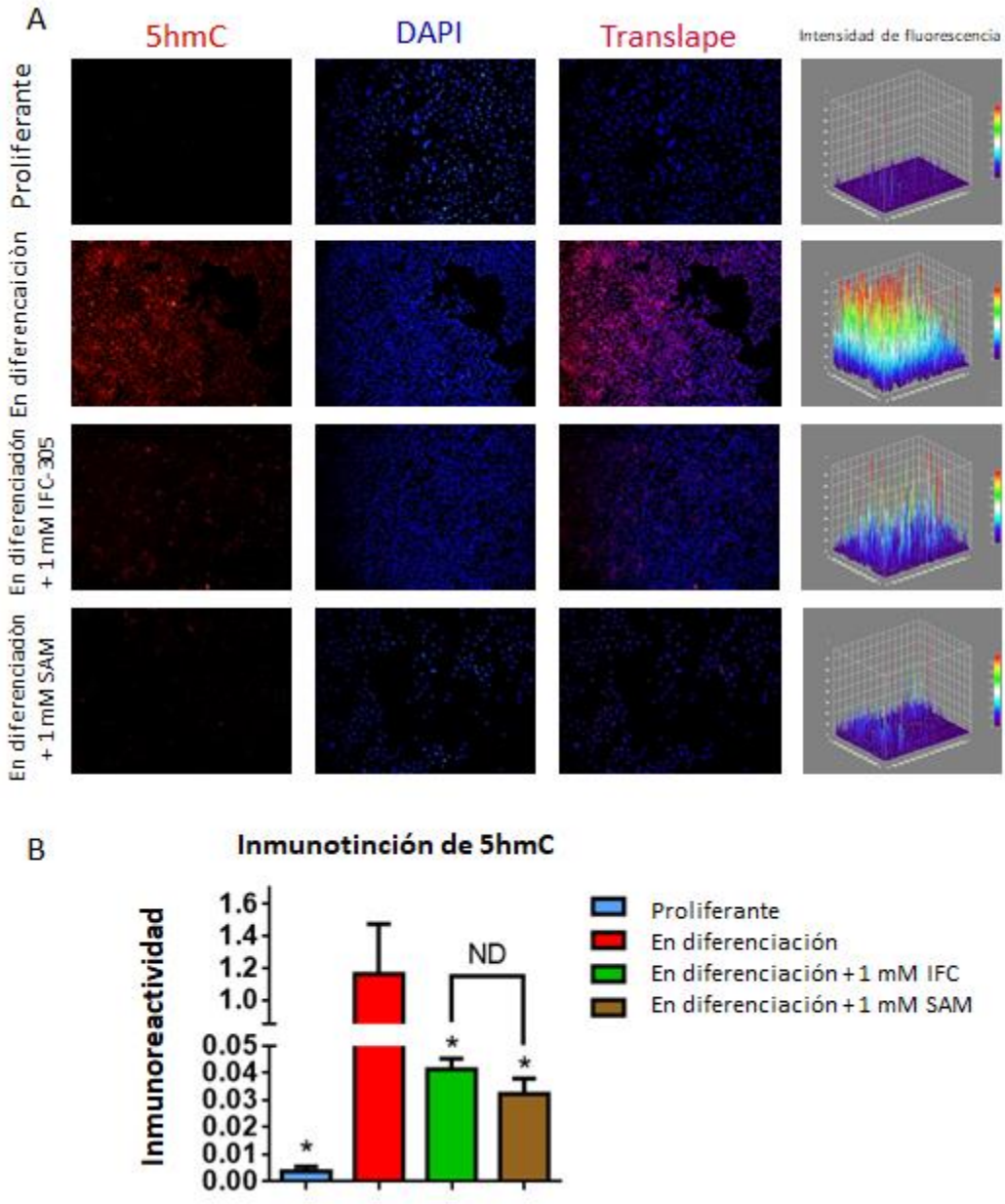

Fig. 52. El derivado de adenosina y la S-adenosilmetionina reducen el enriquecimiento de 5hmC a una semana de diferenciación de HepaRG. (A) Inmunofluorescencia de 5hmC en células proliferantes (panel superior), en diferenciación (panel superior intermedio), en diferenciación + IFc-305 (panel inferior intermedio) y en diferenciación + SAM (panel inferior). Se muestran imágenes representativas con un aumento de 10x de 3 cultivos independientes/condición, así como la medición de la intensidad de fluorescencia. (B) La gráfica de barras de la cuantificación de la señal de 5hmC se basa en el promedio ± DEM de 3 campos por grupo. * Diferencia significativa ($p < 0.05$), comparada con las células en diferenciación. ND: Sin diferencia comparando entre las células en diferenciación tratadas con IFC-305 y con SAM.

Considerando los resultados en su conjunto, es posible sugerir que la exposición a la SAM genera un fenotipo similar al que resulta de la exposición al IFC-305, en términos de la reducción en el enriquecimiento de 5hmC y la menor adquisición de expresión de marcadores hepáticos. La reducción de 5hmC por el derivado de adenosina puede estar mediada por la sobreexpresión de *DNMTs* y la subexpresión de *TETs*, mientras que la reducción de 5hmC en respuesta a la SAM, puede al menos estar parcialmente relacionada con la disminución en la expresión de *IDH.*

Desde un punto de vista más general, estos resultados pueden indicar que el estado metabólico es capaz de influir en la regulación de la diferenciación de la línea celular HepaRG, así como en los niveles de 5hmC durante este proceso.

10. DISCUSIÓN

En este trabajo, se evaluó la relación entre la dinámica de metilación del DNA y el establecimiento del programa de transcripción tipo hepatocito, a una semana del proceso de diferenciación de la línea celular HepaRG. Se encontró que a este tiempo se ha puesto en marcha el programa transcripcional de hepatocitos, mientras que existe una reducción de la metilación del DNA y la 5hmC emerge a lo largo del genoma. Se encontró una asociación de únicamente 14% de los DhMPs con los cambios de expresión génica en las células en diferenciación en comparación con las células proliferantes. Estos sitios con elevación de 5hmC estaban enriquecidos en intrones y fueron escasos en promotores y CGIs. En particular, el contenido de 5hmC en general fue más alto en el cuerpo de genes sobreexpresados, lo cual concuerda con estudios previos en torno a la distribución de 5hmC (revisado en [Pfeifer and Szabo, 2018]). Finalmente se encontró que la perturbación en el metabolismo de SAM utilizando un derivado de adenosina puede reducir el enriquecimiento de 5hmC asociado a la diferenciación. Esto además se relacionó con una reducción de la expresión de los marcadores hepáticos (Figura 53).

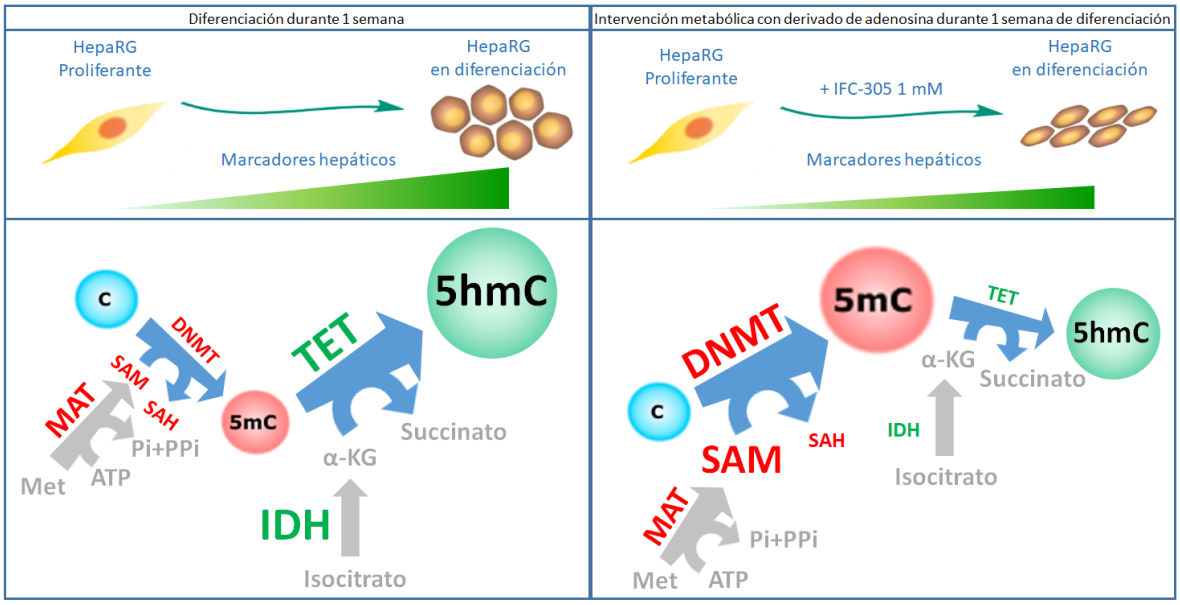

Fig. 53. Interrelación entre el metabolismo, el enriquecimiento de 5hmC y la identidad celular durante la diferenciación de progenitores hepáticos adultos *in vitro.* La diferenciación de células progenitoras hepáticas involucra un proceso de desmetilación del DNA así como un incremento de 5hmC en el genoma completo. El enriquecimiento de 5hmC durante la diferenciación es más evidente en el cuerpo de genes sobreexpresados. La intervención metabólica con un derivado de adenosina, el IFC-305 favorece un estado metilante que genera una reducción en el nivel de 5hmC y una menor expresión de marcadores hepáticos en células en diferenciación, además de presentar una atenuación del fenotipo diferenciado. Estos resultados sugieren un papel fisiológico de la adquisición de 5hmC, modulando la expresión de genes relacionados con la identidad celular. Met, metionina; MAT, metionina adenosiltransferasas; ATP, trifosfato de adenosina; Pi + PPi, Fosfato + Pirofosfato; SAM, S-adenosilmetionina; SAH, S-adenosilhomocisteina; C, Citosina, DNMT, metiltransferasas de DNA; 5mC, 5-metilcitosina; IDH, isocitrato deshidrogenasas; α-KG, alfa-cetoglutarato; TET, Dioxigenasas de citosina modificada; 5hmC, 5-hidroximetilcitosina.

Desde su redescubrimiento en 2009 [Kriaucionis and Heintz, 2009; Tahiliani et al., 2009], la 5hmC surgió como un intermediario para la desmetilación activa del DNA, sin embargo, evidencia que va en aumento ha considerado a esta citosina modificada como “la sexta base” debido a su estabilidad y a su funcionalidad característica y distinta a la de la 5mC. Independientemente de su significado funcional, los eventos de 5hmC correlacionan con pasos clave de la diferenciación en células de mamífero adultas [Ecsedi et al., 2018]. El análisis de BS y OxBS de las células HepaRG con una semana de diferenciación así como

la inmunotinción (Figuras 29 A-B y 30) revelan un incremento de esta citosina modificada a lo largo del genoma, que corresponde con hallazgos previos en el promotor P1 de *HNF4A* [Ancey et al., 2017]. Este comportamiento en el enriquecimiento de 5hmC ha sido descrito también en tejidos de cada capa germinal (por ejemplo enterocitos [Chapman et al., 2015; Kim et al., 2016], miocitos [Zhong et al., 2017], adipocitos [Dubois-Chevalier et al., 2014; Yoo et al., 2017] y neuronas [Hahn et al., 2013; Li et al., 2017]), lo que sugiere que se trata de un proceso general [Lin et al., 2017].

La especialización celular se acompaña por una transición dramática en el paisaje epigenético desde un único estado accesible en la pluripotencia, hacia configuraciones que incrementan su restricción en estados diferenciados [Zhu et al., 2013]. Sin embargo, la 5hmC se ha relacionado frecuentemente con genes con alta expresión, específicos de cada linaje celular [Li et al., 2016b; Lin et al., 2017]. Lo anterior va en línea con los hallazgos descritos en este trabajo, en los que hay una correlación con el enriquecimiento de 5hmC en y los programas de transcripción específicos de hepatocitos, como los relacionados con rutas metabólicas y con funciones hepáticas especializadas como en la síntesis de los componentes del complemento, la regulación del metabolismo de lípidos, la degranulación plaquetaria y la actividad de oxidoreductasa. Esto sugiere que la 5hmC puede operar en conjunto con mecanismos que generan una cromatina restrictiva que ocurriría en *loci* no relacionados con la función hepática. Además se encontraron DhMRs asociados con *TETs* e *IDH3G,* los cuales pueden estar relacionados con un asa de retroalimentación positiva de 5hmC para reforzar la diferenciación. En relación con estos hallazgos, recientemente se ha descrito que *TET1* es regulada a través de la metilación del DNA sobre su promotor [Li et al., 2016a].

Es importante mencionar que no podemos descartar a la posibilidad de que otros mecanismos epigenéticos (como las modificaciones post-traduccionales de histonas, los

remodeladores de cromatina dependientes de ATP, RNA no codificantes, la organización tridimensional y la topología de la cromatina, por mencionar algunos) tengan papeles importantes en este modelo al tiempo estudiado o incluso en etapas posteriores. Es posible que estos otros aspectos de la regulación de la cromatina puedan estar regulando algunos de los genes diferencialmente expresados, lo cuales no estuvieron directamente relacionados con un enriquecimiento de 5hmC en *cis* en la vecindad genética.

Se requieren más estudios para evaluar la estabilidad de la 5hmC durante la diferenciación de hepatocitos. En este sentido, es de destacar que utilizando bisulfito oxidante seguido de PCR cuantitativa específica para metilación, se confirmó que la acumulación de 5hmC en el *locus* de *HNF4A* P1 en las células HepaRG en diferenciación es transitoria (Figura 54). De manera similar, la 5hmC es prácticamente ausente en ese *locus* en hepatocitos humanos primarios terminalmente diferenciados (Figura 46). Sin embargo, si una cinética similar ocurre a nivel de genoma completo, será un tema de futuros análisis.

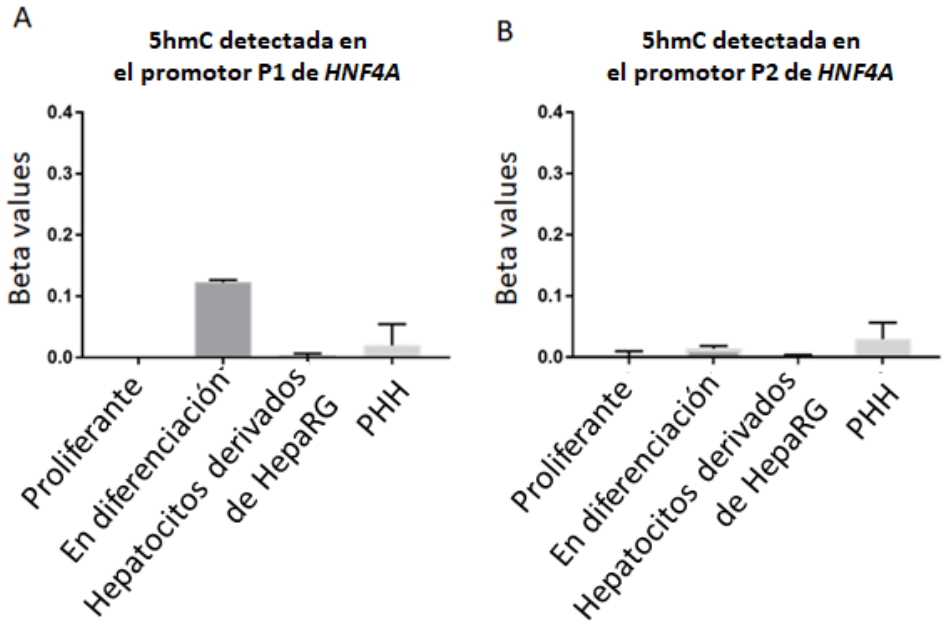

Fig. 54. **Cuantificación de 5hmC por OxBS-qMSP**, **en los promotores P1 (A) y P2 (B) del gen *HNF4A*.** PHH= hepatocitos primarios humanos

Se encontró un enriquecimiento de 5hmC en el cuerpo de los genes (intrones) durante la diferenciación, característica que concuerda parcialmente con un estudio en el hígado de ratón, el cual indica que la 5hmC se enriquece en regiones intergénicas [Lin et al., 2017]. Sin embargo un estudio anterior relacionado con la diferenciación de hepatocitos [Thomson et al., 2013] provee un modelo *in vivo* más cercano para contrastar estos resultados. En dicho trabajo, los autores encontraron que los patrones globales de 5hmC fueron suficientes para estratificar los hígados murinos de acuerdo a su edad, subrayando que la 5hmC es un identificador de tejido hepático y del estado celular. Cuando se compararon los genes diferencialmente hidroximetilados en las células HepaRG con las diferencias en hidroximetilación durante la maduración hepática de la publicación de Thomson, se encontró un traslape de 122 genes (40% más que los esperados al azar, utilizando una prueba hipergeométrica, $p < 4.8e-05$). De manera similar, en el hígado adulto sano, ha sido descrito un paisaje de 5hmC específico, el cual incluye una acumulación bimodal de 5hmC alrededor del TSS y un nivel incrementado a lo largo del cuerpo de los genes, con otro pico justo después de la terminación de la trascripción [Li et al., 2016b]. Además, se encontró que algunos DhMPs pueden estar relacionados con elementos regulatorios distales, tal puede ser el caso de la región rica en 5hmC asociada a *TET3* (Figura 34), la cual colocaliza con un enhancer en el hígado adulto y traslapa con las señales de marcas de histona H3K4me1 y de histona H3K27ac en células HepG2, de acuerdo con el Consorcio *Epigenome Road Map* y con ENCODE respectivamente. A pesar de esta correlación, no se encontró un traslape global entre el enriquecimiento de 5hmC intragénico y las marcas de histonas relacionadas con enhancers (Figura 55).

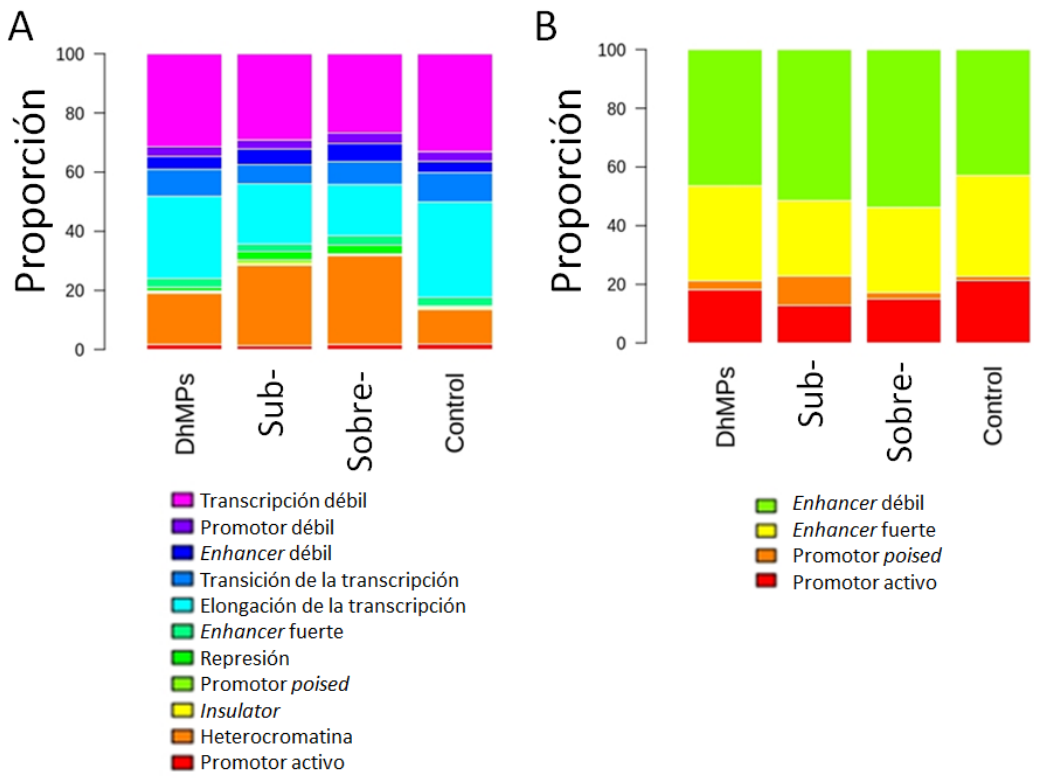

Fig. 55 Distribución de DhMPs en células HepaRG en diferenciación vs Proliferantes, relativa a marcas de histonas. Las regiones genómicas con 5hmC diferencial se anotaron utilizando las características de ChromHMM para HepG2. La anotación determina varios estados cromatínicos diferentes (A) enfatizando los correspondientes a las marcas de cromatina H3K4me1/H3K27ac (B). La figura presenta los DhMPs de los genes con señal de 5hmC, los genes sobre expresados (sobre-), subexpresados (sub-) y los que no tienen cambio (control/*housekeeping*).

El enriquecimiento de 5hmC hallado durante la diferenciación no puede ser atribuido a una subpoblación celular en particular. Será interesante analizar desde una aproximación unicelular si el incremento de 5hmC a una semana de diferenciación de la línea HepaRG correlaciona con la expresión de marcadores hepáticos. Adicionalmente, un problema que ha persistido durante largo tiempo en el campo, es la falta de evidencia causal de una relación directa entre la metilación del DNA y la expresión génica. Las nuevas herramientas de edición epigenética pudieran ser capaces de proveer este tipo de evidencia, sin embargo esto será tema de futuras investigaciones.

Con el propósito de entender la dinámica de 5hmC en respuesta a la perturbación del metabolismo, se evaluó el efecto de un derivado de adenosina, IFC-305, el cuál es capaz de modular los niveles de SAM, 5mC y 5hmC durante la cirrosis experimental [Rodriguez-Aguilera et al., 2018]. Se encontró que el hidroximetiloma de las células HepaRG expuestas al IFC-305 presenta un estado intermedio entre las células proliferantes y las células en diferenciación (Figuras 44 y 46). Esto puede ser explicado parcialmente por la capacidad del IFC-305 de incrementar los niveles de SAM (Figura 50E). Además, el IFC-305 influye en el ambiente de metilación a través de la sobreexpresión de *DNMTs* (Figura 51D), que favorece la metilación del DNA. Por otra parte, el derivado de adenosina genera la subexpresión de *TETs* (Figura 51E) disminuyendo las reacciones de oxidación de 5mC con la consecuente reducción de 5hmC a lo largo de genoma (Figuras 29 y 48). Es así que en esta condición es posible decir que el nivel de 5hmC está atenuado, pero es suficiente para permitir que las células entren al proceso de diferenciación.

Previamente se ha demostrado que la SAM es un metabolito clave que regula el crecimiento de los hepatocitos, la muerte y la diferenciación dependiendo de su concentración. Además, es altamente inestable, con una vida media corta y se convierte a metiltioadenosina rápidamente *in vitro* [Mato and Lu, 2007]. Debido a este efecto dual regulando el crecimiento y la muerte, el nivel hepático de SAM debe ser finamente regulado [Mato and Lu, 2007]. Es probable que al menos parte del efecto de la exposición al IFC-305, incluida la expresión reducida de los marcadores de hepatocitos, dependa de su capacidad para actuar como un estimulador de la disponibilidad fisiológica de SAM. Adicionalmente, se observó una menor expresión de *DNMTs* debido después de la exposición de a SAM (Figura 51D), lo cual concuerda con otro reporte donde se demostró que en la exposición *in vitro* de otras líneas celulares a SAM conduce a la subexpresión de *DNMTs* [Kar et al., 2014], y desde el punto de vista químico, es entendible que la expresión de enzimas requeridas para sintetizar SAM

(*MAT1A* y *MAT2A*) se encuentre disminuida (Figura 51D) si hay un exceso del producto que estas generan (SAM). Por otra parte, a pesar de la sobreexpresión de los transcritos de las enzimas TET (Figura 51E), la falta de expresión de *IDHs* (Figura 51E) podría no favorecer el enriquecimiento de 5hmC (Figura).

Contrario a nuestro enfoque donde las células son expuestas a un compuesto que estimula la producción de SAM, un modelo de ratón con una dieta deficiente de metionina y colina, el cual tiene como consecuencia la reducción de la disponibilidad de SAM, no causa una reducción los niveles de 5mC, en su lugar induce una sobreexpresión de *Tet2, Tet3,* timina DNA glucosilasa y de la endonucleasa 1 apurínica/apirimídica, e incrementa la expresión de *Dnmt1* y *Dnmt3a* [Takumi et al., 2015]. Entonces, mientras que la dinámica de metilación puede sobrellevar la deficiencia de SAM, un incremento de SAM conduce a una reducción del enriquecimiento de 5hmC asociado a un retraso en la diferenciación (Figura 46).

La posibilidad de modular la diferenciación a través de la regulación de la 5hmC representa una observación relevante. En efecto, algunos estudios indican que una de las alteraciones tempranas en el carcinoma hepatocelular es una reducción global y significativa de 5hmC [Liu et al., 2013], un comportamiento también observado en la infección con virus de hepatitis B [Liu et al., 2018], en cirrosis [Rodriguez-Aguilera et al., 2018] y durante la *tras*-diferenciación de HSCs a miofibroblastos [Page et al., 2016]. Patrones alterados de 5hmC no solo son detectados en pares tumor-tejido sano a partir de resecciones de biopsias, sino también en DNA circulante en pacientes con cáncer [Pfeifer and Szabo, 2018], sugiriendo que la 5hmC es un potencial biomarcador para la detección temprana de cáncer.

La posibilidad de modular la diferenciación a través de la regulación de 5hmC representa una herramienta relevante. En este sentido, algunos estudios indican que una de las alteraciones tempranas en HCC es una disminución significativa de la 5hmC global, un comportamiento que también se observa en la infección por virus de hepatitis B [Liu et al.,

2018], cirrosis [Rodriguez-Aguilera et al., 2018] y durante la *trans*-diferenciación de HSC a miofibrobalstos [Page et al., 2016]. Los patrones alterados de 5hmC no solo son detectables en pares de tejidos tumorales y normales de resecciones o biopsias, sino que también en DNA circulante de pacientes con cáncer [Pfeifer and Szabo, 2018] sugiriendo que la 5hmC es un potencial biomarcador para la detección temprana de esta patología. Además la posibilidad de modificar la identidad celular a través de la regulación de la distribución y los niveles de 5hmC representa un método farmacológico innovador para prevenir y revertir patologías relacionadas con procesos de desdiferenciación como el cáncer hepático.

11. CONCLUSIONES

1. A una semana de diferenciación *in vitro*, la línea celular de progenitores hepáticos HepaRG, ha encendido el programa de transcripción de hepatocitos.
2. Las células HepaRG a una semana de diferenciación, presentan una hipometilación a lo largo del genoma si se comparan contra las células en estado proliferante.
3. Un enriquecimiento de 5hmC se presenta a nivel de genoma completo a una semana de diferenciación del progenitor hepático HepaRG.
4. Particularmente el cuerpo de los genes sobreexpresados, se enriquece con 5hmC a una semana de diferenciación de la línea celular HepaRG.
5. Únicamente 14% de los sitios diferencialmente hidroximetilados entre las células proliferantes y en diferenciación, se asocian a genes diferencialmente expresados.
6. No se encontró una correlación global entre el enriquecimiento de 5hmC y las modificaciones de histonas H3K4me1 y H3K27ac, asociadas a *enhancers,* en la primera semana de diferenciación.
7. La intervención metabólica con el derivado de adenosina, IFC-305, genera una reducción en el enriquecimiento de 5hmC a una semana de diferenciación en la línea celular HepaRG.
8. La expresión del regulador maestro de la diferenciación de Hepatocitos *HNF4A* no se ve modificada con la exposición al IFC-305 a 1 mM, a una semana de diferenciación, sin embargo su proteína se encuentra reducida.
9. La exposición al derivado de adenosina durante una semana de diferenciación produce una menor expresión de marcadores hepáticos comparando contra las células sin tratamiento. Este efecto se ve reproducido al exponer a las células al inhibidor químico de las enzimas TET, DMOG, así como a la SAM.

10. La exposición de las células HepaRG al derivado de adenosina, IFC-305, conduce a un incremento fisiológico del nivel de SAM y una sobreexpresión de las DNA metiltransferasas que podrían favorecen un ambiente metilante, a una semana de diferenciación.
11. La expresión de los transcritos que codifican a las dioxigenasas TET1 y TET2 se encuentra reducida en respuesta a la exposición al IFC-305, al igual que los transcritos de las isocitrato deshidrogenasas IDH1 e IDH2, por lo que las reacciones de oxidación de la 5mC se encuentran desfavorecidas, a una semana de diferenciación.
12. El reducido nivel de expresión de marcadores hepáticos debido a la exposición de las células HepaRG al derivado de adenosina, puede ser entendido en parte, por la reducción en el enriquecimiento de la 5hmC a una semana de diferenciación. Enriquecimiento que se ve comprometido al competir una desfavorecida reacción de oxidación de citosinas modificadas contra el ambiente prometilante generado por el IFC-305.
13. La adquisición de un fenotipo diferenciado atenuado en conjunto con una reducción en el nivel de 5hmC durante el proceso de diferenciación, sugiere una relación de esta citosina modificada con la identidad celular.
14. Considerando que en procesos neoplásicos hay una reducción de la 5hmC, y que el nivel y la distribución de esta citosina modificada está relacionada con la adquisición del fenotipo hepático, la 5hmC pudiera ser considerada como un biomarcador para la identificación temprana de enfermedades relacionadas con la desdiferenciación celular como el cáncer hepático.
15. La posibilidad de modificar el nivel de 5hmC a través de la regulación del ambiente metabólico, proporciona una potencial herramienta para el desarrollo de fármacos antineoplásicos.

12. PERSPECTIVAS

Una vez definido el hidroximetiloma a una semana de diferenciación en la línea celular HepaRG, será interesante estudiar el nivel y distribución de la 5hmC una vez que se complete la diferenciación *in vitro*, para identificar si el patrón molecular adquirido al inicio de la diferenciación, es característico de este tiempo o se retiene en los hepatocitos maduros. Así mismo, será importante comparar la firma de hidroximetilación entre los hepatocitos derivados de HepaRG y hepatocitos primarios humanos o muestras de hígado humano adulto, ya que se ha descrito una gran similitud entre la fisiología de la línea celular una vez diferenciada y los hepatocitos adultos del ser humano.

Si se encontrara una analogía entre el hidroximetiloma de las células HepaRG diferenciadas y los hepatocitos humanos adultos, se estaría contando con un modelo que facilitaría el estudio biológico del hígado, ya que el material podría obtenerse fácilmente, al ser una línea celular.

Otro punto interesante sería la comparación del hidroximetiloma de hepatocitos humanos adultos, con el de muestras de cáncer hepático, para identificar las regiones diferencialmente hidroximetiladas en ambas condiciones, la función de estas regiones y con ello plantear estrategias que permitan un diagnóstico oportuno así como el desarrollo de terapias encaminadas al restablecimiento del patrón del 5hmC en el tejido.

En este sentido, la capacidad de las células HepaRG diferenciadas de recuperar el fenotipo de progenitor si se resiembran a baja confluencia, pudiera representar un modelo interesante para el estudio genómico del proceso de desdiferenciación, así como para la evaluación de fármacos que pudieran estar contribuyendo a la retención del fenotipo diferenciado, por ejemplo, modulando el nivel de 5hmC.

El derivado de adenosina, IFC-305, ha presentado efectos hepatoprotectores en un modelo experimental del cirrosis, favoreciendo la recuperación de la función y arquitectura hepática, mediados en parte, por el restablecimiento de los niveles globales de 5mC y 5hmC abrogados durante la patología, por lo que será interesante evaluar el efecto del fármaco en las células HepaRG completamente diferenciadas, así como durante el proceso de desdiferenciación.

Finalmente el estudio de los efectos del IFC-305 sobre líneas celulares de carcinoma hepatocelular, en particular sobre el transcriptoma e hidroximetiloma podrá revelar blancos farmacológicos de este compuesto, los cuales pudieran ser de utilidad para el desarrollo de estrategias terapéuticas.

13. REFERENCIAS

Amary MF, Bacsi K, Maggiani F, Damato S, Halai D, Berisha F, Pollock R, O'Donnell P, Grigoriadis A, Diss T, Eskandarpour M, Presneau N, Hogendoorn PC, Futreal A, Tirabosco R, Flanagan AM. 2011a. IDH1 and IDH2 mutations are frequent events in central chondrosarcoma and central and periosteal chondromas but not in other mesenchymal tumours. J Pathol 224:334-43.

Amary MF, Damato S, Halai D, Eskandarpour M, Berisha F, Bonar F, McCarthy S, Fantin VR, Straley KS, Lobo S, Aston W, Green CL, Gale RE, Tirabosco R, Futreal A, Campbell P, Presneau N, Flanagan AM. 2011b. Ollier disease and Maffucci syndrome are caused by somatic mosaic mutations of IDH1 and IDH2. Nat Genet 43:1262-5.

Amir RE, Van den Veyver IB, Wan M, Tran CQ, Francke U, Zoghbi HY. 1999. Rett syndrome is caused by mutations in X-linked MECP2, encoding methyl-CpG-binding protein 2. Nature Genetics 23:185-8.

Ancey PB, Ecsedi S, Lambert MP, Talukdar FR, Cros MP, Glaise D, Narvaez DM, Chauvet V, Herceg Z, Corlu A, Hernandez-Vargas H. 2017. TET-Catalyzed 5-Hydroxymethylation Precedes HNF4A Promoter Choice during Differentiation of Bipotent Liver Progenitors. Stem Cell Reports 9:264-278.

Aninat C, Piton A, Glaise D, Le Charpentier T, Langouet S, Morel F, Guguen-Guillouzo C, Guillouzo A. 2006. Expression of cytochromes P450, conjugating enzymes and nuclear receptors in human hepatoma HepaRG cells. Drug Metab lism and Disposition: The Biological Fate of Chemicals 34:75-83.

Anuradha S, Radha V, Mohan V. 2011. Association of novel variants in the hepatocyte nuclear factor 4A gene with maturity onset diabetes of the young and early onset type 2 diabetes. Clinical Genetics 80:541-9.

Aryee MJ, Jaffe AE, Corrada-Bravo H, Ladd-Acosta C, Feinberg AP, Hansen KD, Irizarry RA. 2014. Minfi: a flexible and comprehensive Bioconductor package for the analysis of Infinium DNA methylation microarrays. Bioinformatics 30:1363-9.

Atkinson DE. 1968. The energy charge of the adenylate pool as a regulatory parameter. Interaction with feedback modifiers. Biochemistry 7:4030-4.

Auta J, Zhang H, Pandey SC, Guidotti A. 2017. Chronic Alcohol Exposure Differentially Alters One-Carbon Metabolism in Rat Liver and Brain. Alcoholism, Clinical and Experimental Research 41:1105-1111.

Bach I, Yaniv M. 1993. More potent transcriptional activators or a transdominant inhibitor of the HNF1 homeoprotein family are generated by alternative RNA processing. EMBO Journal 12:4229-42.

Barbacci E, Reber M, Ott MO, Breillat C, Huetz F, Cereghini S. 1999. Variant hepatocyte nuclear factor 1 is required for visceral endoderm specification. Development 126:4795-805.

Berger SL, Sassone-Corsi P. 2016. Metabolic Signaling to Chromatin. Cold Spring Harb Perspect Biol 8.

Bestor TH, Ingram VM. 1983. Two DNA methyltransferases from murine erythroleukemia cells: purification, sequence specificity, and mode of interaction with DNA. Proceedings of the National Academy of Sciences of the United States of America 80:5559-63.

Bhutani N, Burns DM, Blau HM. 2011. DNA demethylation dynamics. Cell 146:866-72.

Biopredic. ORIGINS of the HepaRG cell line< https://www.heparg.com/rubrique-origins-of-the-heparg-cell-line>

Bird A. 2002. DNA methylation patterns and epigenetic memory. Genes Dev 16:6-21.

Bird A, Taggart M, Frommer M, Miller OJ, Macleod D. 1985. A fraction of the mouse genome that is derived from islands of nonmethylated, CpG-rich DNA. Cell 40:91-9.
Bird AP, Wolffe AP. 1999. Methylation-induced repression--belts, braces, and chromatin. Cell 99:451-4.
Blackledge NP, Thomson JP, Skene PJ. 2013. CpG island chromatin is shaped by recruitment of ZF-CxxC proteins. Cold Spring Harb Perspect Biol 5:a018648.
Booth MJ, Ost TW, Beraldi D, Bell NM, Branco MR, Reik W, Balasubramanian S. 2013. Oxidative bisulfite sequencing of 5-methylcytosine and 5-hydroxymethylcytosine. Nat Protoc 8:1841-51.
Bosch FX, Ribes J, Cleries R, Diaz M. 2005. Epidemiology of hepatocellular carcinoma. Clin Liver Dis 9:191-211, v.
Brenet F, Moh M, Funk P, Feierstein E, Viale AJ, Socci ND, Scandura JM. 2011. DNA methylation of the first exon is tightly linked to transcriptional silencing. PLoS One 6:e14524.
Briancon N, Weiss MC. 2006. In vivo role of the HNF4alpha AF-1 activation domain revealed by exon swapping. EMBO Journal 25:1253-62.
Brockdorff N, Turner BM. 2015. Dosage compensation in mammals. Cold Spring Harb Perspect Biol 7:a019406.
Cabrales-Romero Mdel P, Marquez-Rosado L, Fattel-Fazenda S, Trejo-Solis C, Arce-Popoca E, Aleman-Lazarini L, Villa-Trevino S. 2006. S-adenosyl-methionine decreases ethanol-induced apoptosis in primary hepatocyte cultures by a c-Jun N-terminal kinase activity-independent mechanism. World J Gastroenterol 12:1895-904.
Cannon MV, Pilarowski G, Liu X, Serre D. 2016. Extensive Epigenetic Changes Accompany Terminal Differentiation of Mouse Hepatocytes After Birth. G3 (Bethesda) 6:3701-3709.
Caron G, Hussein M, Kulis M, Delaloy C, Chatonnet F, Pignarre A, Avner S, Lemarie M, Mahe EA, Verdaguer-Dot N, Queiros AC, Tarte K, Martin-Subero JI, Salbert G, Fest T. 2015. Cell-Cycle-Dependent Reconfiguration of the DNA Methylome during Terminal Differentiation of Human B Cells into Plasma Cells. Cell Rep 13:1059-71.
Castelli G, Pelosi E, Testa U. 2017. Liver Cancer: Molecular Characterization, Clonal Evolution and Cancer Stem Cells. Cancers (Basel) 9.
Cattin AL, Le Beyec J, Barreau F, Saint-Just S, Houllier A, Gonzalez FJ, Robine S, Pincon-Raymond M, Cardot P, Lacasa M, Ribeiro A. 2009. Hepatocyte nuclear factor 4alpha, a key factor for homeostasis, cell architecture, and barrier function of the adult intestinal epithelium. Molecular and Cellular Biology 29:6294-308.
Cavalcante RG, Sartor MA. 2017. annotatr: genomic regions in context. Bioinformatics 33:2381-2383.
Cerec V, Glaise D, Garnier D, Morosan S, Turlin B, Drenou B, Gripon P, Kremsdorf D, Guguen-Guillouzo C, Corlu A. 2007. Transdifferentiation of hepatocyte-like cells from the human hepatoma HepaRG cell line through bipotent progenitor. Hepatology 45:957-67.
Cereghini S. 1996. Liver-enriched transcription factors and hepatocyte differentiation. FASEB Journal 10:267-82.
Cereghini S, Ott MO, Power S, Maury M. 1992. Expression patterns of vHNF1 and HNF1 homeoproteins in early postimplantation embryos suggest distinct and sequential developmental roles. Development 116:783-97.
Cimmino L, Aifantis I. 2017. Alternative roles for oxidized mCs and TETs. Current Opinion in Genetics and Development 42:1-7.

Cordaux R, Batzer MA. 2009. The impact of retrotransposons on human genome evolution. Nat Rev Genet 10:691-703.

Chagoya de Sanchez V, Brunner A, Pina E. 1972. In vivo modification of the energy charge in the liver cell. Biochem Biophys Res Commun 46:1441-5.

Chagoya de Sanchez V, Hernandez-Munoz R, Sanchez L, Vidrio S, Yanez L, Suarez J. 1991. Twenty-four-hour changes of S-adenosylmethionine, S-adenosylhomocysteine adenosine and their metabolizing enzymes in rat liver; possible physiological significance in phospholipid methylation. Int J Biochem 23:1439-43.

Chagoya de Sanchez V, Martinez-Perez L, Hernandez-Munoz R, Velasco-Loyden G. 2012. Recovery of the Cell Cycle Inhibition in CCl(4)-Induced Cirrhosis by the Adenosine Derivative IFC-305. Int J Hepatol 2012:212530.

Chahar S, Gandhi V, Yu S, Desai K, Cowper-Sal-lari R, Kim Y, Perekatt AO, Kumar N, Thackray JK, Musolf A, Hoffman A, Londono D, Vazquez BN, Serrano L, Shin H, Lupien M, Gao N, Verzi MP. 2014. Chromatin profiling reveals regulatory network shifts and a protective role for hepatocyte nuclear factor 4alpha during colitis. Molecular and Cellular Biology 34:3291-304.

Chaker D, Mouawad C, Azar A, Quilliot D, Achkar I, Fajloun Z, Makdissy N. 2018. Inhibition of the RhoGTPase Cdc42 by ML141 enhances hepatocyte differentiation from human adipose-derived mesenchymal stem cells via the Wnt5a/PI3K/miR-122 pathway: impact of the age of the donor. Stem Cell Res Ther 9:167.

Chapman CG, Mariani CJ, Wu F, Meckel K, Butun F, Chuang A, Madzo J, Bissonette MB, Kwon JH, Godley LA. 2015. TET-catalyzed 5-hydroxymethylcytosine regulates gene expression in differentiating colonocytes and colon cancer. Sci Rep 5:17568.

Chavez E, Lozano-Rosas MG, Dominguez-Lopez M, Velasco-Loyden G, Rodriguez-Aguilera JR, Jose-Nunez C, Tuena de Gomez-Puyou M, Chagoya de Sanchez V. 2017. Functional, metabolic, and dynamic mitochondrial changes in the rat cirrhosis-hepatocellular carcinoma model and the protective effect of IFC-305. Journal of Pharmacology and Experimental Therapeutics.

Chen EY, Tan CM, Kou Y, Duan Q, Wang Z, Meirelles GV, Clark NR, Ma'ayan A. 2013a. Enrichr: interactive and collaborative HTML5 gene list enrichment analysis tool. BMC Bioinformatics 14:128.

Chen ML, Shen F, Huang W, Qi JH, Wang Y, Feng YQ, Liu SM, Yuan BF. 2013b. Quantification of 5-methylcytosine and 5-hydroxymethylcytosine in genomic DNA from hepatocellular carcinoma tissues by capillary hydrophilic-interaction liquid chromatography/quadrupole TOF mass spectrometry. Clin Chem 59:824-32.

Chen WS, Manova K, Weinstein DC, Duncan SA, Plump AS, Prezioso VR, Bachvarova RF, Darnell JE, Jr. 1994. Disruption of the HNF-4 gene, expressed in visceral endoderm, leads to cell death in embryonic ectoderm and impaired gastrulation of mouse embryos. Genes and Development 8:2466-77.

Cheng X. 2014. Structural and functional coordination of DNA and histone methylation. Cold Spring Harb Perspect Biol 6.

Dang L, White DW, Gross S, Bennett BD, Bittinger MA, Driggers EM, Fantin VR, Jang HG, Jin S, Keenan MC, Marks KM, Prins RM, Ward PS, Yen KE, Liau LM, Rabinowitz JD, Cantley LC, Thompson CB, Vander Heiden MG, Su SM. 2009. Cancer-associated IDH1 mutations produce 2-hydroxyglutarate. Nature 462:739-44.

Davidson MH. 2006. Mechanisms for the hypotriglyceridemic effect of marine omega-3 fatty acids. American Journal of Cardiology 98:27i-33i.

De Simone V, De Magistris L, Lazzaro D, Gerstner J, Monaci P, Nicosia A, Cortese R. 1991. LFB3, a heterodimer-forming homeoprotein of the LFB1 family, is expressed in specialized epithelia. EMBO Journal 10:1435-43.
Dean S, Tang JI, Seckl JR, Nyirenda MJ. 2010. Developmental and tissue-specific regulation of hepatocyte nuclear factor 4-alpha (HNF4-alpha) isoforms in rodents. Gene Expression 14:337-44.
Deaton AM, Bird A. 2011. CpG islands and the regulation of transcription. Genes Dev 25:1010-22.
DeLaForest A, Nagaoka M, Si-Tayeb K, Noto FK, Konopka G, Battle MA, Duncan SA. 2011. HNF4A is essential for specification of hepatic progenitors from human pluripotent stem cells. Development 138:4143-53.
Drewes T, Senkel S, Holewa B, Ryffel GU. 1996. Human hepatocyte nuclear factor 4 isoforms are encoded by distinct and differentially expressed genes. Molecular and Cellular Biology 16:925-31.
Du P, Kibbe WA, Lin SM. 2008. lumi: a pipeline for processing Illumina microarray. Bioinformatics 24:1547-8.
Dubois-Chevalier J, Oger F, Dehondt H, Firmin FF, Gheeraert C, Staels B, Lefebvre P, Eeckhoute J. 2014. A dynamic CTCF chromatin binding landscape promotes DNA hydroxymethylation and transcriptional induction of adipocyte differentiation. Nucleic Acids Res 42:10943-59.
Dubois-Pot-Schneider H, Fekir K, Coulouarn C, Glaise D, Aninat C, Jarnouen K, Le Guevel R, Kubo T, Ishida S, Morel F, Corlu A. 2014. Inflammatory cytokines promote the retrodifferentiation of tumor-derived hepatocyte-like cells to progenitor cells. Hepatology 60:2077-90.
Duncan SA, Manova K, Chen WS, Hoodless P, Weinstein DC, Bachvarova RF, Darnell JE, Jr. 1994. Expression of transcription factor HNF-4 in the extraembryonic endoderm, gut, and nephrogenic tissue of the developing mouse embryo: HNF-4 is a marker for primary endoderm in the implanting blastocyst. Proceedings of the National Academy of Sciences of the United States of America 91:7598-602.
Ecsedi S, Rodríguez-Aguilera JR, Hernández-Vargas H. 2018. 5-Hydroxymethylcytosine (5hmC), or How to Identify Your Favorite Cell. Epigenomes 2:3.
Ehrlich M, Wang RY. 1981. 5-Methylcytosine in eukaryotic DNA. Science 212:1350-7.
Eisenberg E, Levanon EY. 2013. Human housekeeping genes, revisited. Trends in Genetics 29:569-74.
Fan G, Tu Y, Chen C, Sun H, Wan C, Cai X. 2018. DNA methylation biomarkers for hepatocellular carcinoma. Cancer Cell Int 18:140.
Felsenfeld G. 2014. A brief history of epigenetics. Cold Spring Harb Perspect Biol 6.
Finkelstein JD. 1990. Methionine metabolism in mammals. J Nutr Biochem 1:228-37.
Friedman JR, Kaestner KH. 2006. The Foxa family of transcription factors in development and metabolism. Cellular and Molecular Life Sciences 63:2317-28.
Garcea R, Daino L, Pascale R, Simile MM, Puddu M, Ruggiu ME, Seddaiu MA, Satta G, Sequenza MJ, Feo F. 1989. Protooncogene methylation and expression in regenerating liver and preneoplastic liver nodules induced in the rat by diethylnitrosamine: effect of variations of S-adenosylmethionine:S-adenosylhomocysteine ratio. Carcinogenesis 10:1183-92.
Garcia-Gomez A, Li T, Kerick M, Catala-Moll F, Comet NR, Rodriguez-Ubreva J, de la Rica L, Branco MR, Martin J, Ballestar E. 2017. TET2- and TDG-mediated changes are required for the acquisition of distinct histone modifications in divergent terminal differentiation of myeloid cells. Nucleic Acids Res 45:10002-10017.
Gericke N, McEwen B, Thörne K. 2017. EPIGENETIC LITERACY AND THE IMPLEMENTATION OF EPIGENETICS IN SCHOOL BIOLOGY Karlstad

University<https://www.kau.se/en/biology/research/biology-didactics-reasearch/epigenetic-literacy-and-implementation-epigenetics>.
Globisch D, Munzel M, Muller M, Michalakis S, Wagner M, Koch S, Bruckl T, Biel M, Carell T. 2010. Tissue distribution of 5-hydroxymethylcytosine and search for active demethylation intermediates. PLoS One 5:e15367.
Greco CM, Kunderfranco P, Rubino M, Larcher V, Carullo P, Anselmo A, Kurz K, Carell T, Angius A, Latronico MV, Papait R, Condorelli G. 2016. DNA hydroxymethylation controls cardiomyocyte gene expression in development and hypertrophy. Nat Commun 7:12418.
Grillo MA, Colombatto S. 2008. S-adenosylmethionine and its products. Amino Acids 34:187-93.
Gripon P, Rumin S, Urban S, Le Seyec J, Glaise D, Cannie I, Guyomard C, Lucas J, Trepo C, Guguen-Guillouzo C. 2002. Infection of a human hepatoma cell line by hepatitis B virus. Proceedings of the National Academy of Sciences of the United States of America 99:15655-60.
Gu Z, Eils R, Schlesner M, Ishaque N. 2018. EnrichedHeatmap: an R/Bioconductor package for comprehensive visualization of genomic signal associations. BMC Genomics 19:234.
Hadzopoulou-Cladaras M, Kistanova E, Evagelopoulou C, Zeng S, Cladaras C, Ladias JA. 1997. Functional domains of the nuclear receptor hepatocyte nuclear factor 4. Journal of Biological Chemistry 272:539-50.
Haffner MC, Chaux A, Meeker AK, Esopi DM, Gerber J, Pellakuru LG, Toubaji A, Argani P, Iacobuzio-Donahue C, Nelson WG, Netto GJ, De Marzo AM, Yegnasubramanian S. 2011. Global 5-hydroxymethylcytosine content is significantly reduced in tissue stem/progenitor cell compartments and in human cancers. Oncotarget 2:627-37.
Hahn MA, Qiu R, Wu X, Li AX, Zhang H, Wang J, Jui J, Jin SG, Jiang Y, Pfeifer GP, Lu Q. 2013. Dynamics of 5-hydroxymethylcytosine and chromatin marks in Mammalian neurogenesis. Cell Rep 3:291-300.
Hahn MA, Szabo PE, Pfeifer GP. 2014. 5-Hydroxymethylcytosine: A stable or transient DNA modification? Genomics 104:314-23.
Harries LW, Ellard S, Stride A, Morgan NG, Hattersley AT. 2006. Isomers of the TCF1 gene encoding hepatocyte nuclear factor-1 alpha show differential expression in the pancreas and define the relationship between mutation position and clinical phenotype in monogenic diabetes. Human Molecular Genetics 15:2216-24.
Harvey A, Caretti G, Moresi V, Renzini A, Adamo S. 2019. Interplay between Metabolites and the Epigenome in Regulating Embryonic and Adult Stem Cell Potency and Maintenance. Stem Cell Reports 13:573-589.
Hatzis P, Talianidis I. 2001. Regulatory mechanisms controlling human hepatocyte nuclear factor 4alpha gene expression. Molecular and Cellular Biology 21:7320-30.
Hemerly JP, Bastos AU, Cerutti JM. 2010. Identification of several novel non-p.R132 IDH1 variants in thyroid carcinomas. Eur J Endocrinol 163:747-55.
Hernandez-Munoz R, Diaz-Munoz M, Suarez J, Chagoya de Sanchez V. 1990. Adenosine partially prevents cirrhosis induced by carbon tetrachloride in rats. Hepatology 12:242-8.
Hernandez-Munoz R, Glender W, Diaz Munoz M, Adolfo J, Garcia-Sainz JA, Chagoya de Sanchez V. 1984. Effects of adenosine on liver cell damage induced by carbon tetrachloride. Biochem Pharmacol 33:2599-604.
Hernandez-Munoz R, Santamaria A, Garcia-Sainz JA, Pina E, Chagoya de Sanchez V. 1978. On the mechanism of ethanol-induced fatty liver and its reversibility by adenosine. Arch Biochem Biophys 190:155-62.

Hernández-Vargas H, Goldsmith C. 2019. Quantitative analysis of methylation and hydroxymethylation using oXBS-qMSP USA: Protocols.io< https://www.protocols.io/view/quantitative-analysis-of-methylation-and-hydroxyme-52bg8an>.

Holliday R, Pugh JE. 1975. DNA modification mechanisms and gene activity during development. Science 187:226-32.

Huang J, Levitsky LL, Rhoads DB. 2009. Novel P2 promoter-derived HNF4alpha isoforms with different N-terminus generated by alternate exon insertion. Experimental Cell Research 315:1200-11.

Ichiyama K, Chen T, Wang X, Yan X, Kim BS, Tanaka S, Ndiaye-Lobry D, Deng Y, Zou Y, Zheng P, Tian Q, Aifantis I, Wei L, Dong C. 2015. The methylcytosine dioxygenase Tet2 promotes DNA demethylation and activation of cytokine gene expression in T cells. Immunity 42:613-26.

Irizarry RA, Ladd-Acosta C, Wen B, Wu Z, Montano C, Onyango P, Cui H, Gabo K, Rongione M, Webster M, Ji H, Potash J, Sabunciyan S, Feinberg AP. 2009. The human colon cancer methylome shows similar hypo- and hypermethylation at conserved tissue-specific CpG island shores. Nature Genetics 41:178-186.

Ito S, D'Alessio AC, Taranova OV, Hong K, Sowers LC, Zhang Y. 2010. Role of Tet proteins in 5mC to 5hmC conversion, ES-cell self-renewal and inner cell mass specification. Nature 466:1129-33.

Ito S, Shen L, Dai Q, Wu SC, Collins LB, Swenberg JA, He C, Zhang Y. 2011. Tet proteins can convert 5-methylcytosine to 5-formylcytosine and 5-carboxylcytosine. Science 333:1300-3.

Ivanov M, Kals M, Kacevska M, Barragan I, Kasuga K, Rane A, Metspalu A, Milani L, Ingelman-Sundberg M. 2013. Ontogeny, distribution and potential roles of 5-hydroxymethylcytosine in human liver function. Genome Biol 14:R83.

Iyaguchi D, Yao M, Watanabe N, Nishihira J, Tanaka I. 2007. DNA recognition mechanism of the ONECUT homeodomain of transcription factor HNF-6. Structure 15:75-83.

Jacquemin P, Lannoy VJ, Rousseau GG, Lemaigre FP. 1999. OC-2, a novel mammalian member of the ONECUT class of homeodomain transcription factors whose function in liver partially overlaps with that of hepatocyte nuclear factor-6. Journal of Biological Chemistry 274:2665-71.

Jiang G, Sladek FM. 1997. The DNA binding domain of hepatocyte nuclear factor 4 mediates cooperative, specific binding to DNA and heterodimerization with the retinoid X receptor alpha. Journal of Biological Chemistry 272:1218-25.

Kaestner KH, Knochel W, Martinez DE. 2000. Unified nomenclature for the winged helix/forkhead transcription factors. Genes and Development 14:142-6.

Kar S, Sengupta D, Deb M, Shilpi A, Parbin S, Rath SK, Pradhan N, Rakshit M, Patra SK. 2014. Expression profiling of DNA methylation-mediated epigenetic gene-silencing factors in breast cancer. Clin Epigenetics 6:20.

Kharbanda KK. 2007. Role of transmethylation reactions in alcoholic liver disease. World J Gastroenterol 13:4947-54.

Kim R, Sheaffer KL, Choi I, Won KJ, Kaestner KH. 2016. Epigenetic regulation of intestinal stem cells by Tet1-mediated DNA hydroxymethylation. Genes and Development 30:2433-2442.

Ko HL, Lam TH, Ng H, Toh J, Wang LW, Ren EC. 2017. Identification of Slug and SOX7 as transcriptional repressors binding to the hepatitis B virus core promoter. Journal of Hepatology.

Ko HL, Zhuo Z, Ren EC. 2019. HNF4alpha Combinatorial Isoform Heterodimers Activate Distinct Gene Targets that Differ from Their Corresponding Homodimers. Cell Rep 26:2549-2557 e3.
Kohli RM, Zhang Y. 2013. TET enzymes, TDG and the dynamics of DNA demethylation. Nature 502:472-9.
Korinek M, Sistek V, Mladkova J, Mikes P, Jiracek J, Selicharova I. 2013. Quantification of homocysteine-related metabolites and the role of betaine-homocysteine S-methyltransferase in HepG2 cells. Biomedical Chromatography 27:111-21.
Kranzhofer DK, Gilsbach R, Gruning BA, Backofen R, Nuhrenberg TG, Hein L. 2016. 5'-Hydroxymethylcytosine Precedes Loss of CpG Methylation in Enhancers and Genes Undergoing Activation in Cardiomyocyte Maturation. PLoS One 11:e0166575.
Kriaucionis S, Heintz N. 2009. The nuclear DNA base 5-hydroxymethylcytosine is present in Purkinje neurons and the brain. Science 324:929-30.
Kyrmizi I, Hatzis P, Katrakili N, Tronche F, Gonzalez FJ, Talianidis I. 2006. Plasticity and expanding complexity of the hepatic transcription factor network during liver development. Genes and Development 20:2293-305.
Lai E, Prezioso VR, Tao WF, Chen WS, Darnell JE, Jr. 1991. Hepatocyte nuclear factor 3 alpha belongs to a gene family in mammals that is homologous to the Drosophila homeotic gene fork head. Genes and Development 5:416-27.
Laird A, Thomson JP, Harrison DJ, Meehan RR. 2013. 5-hydroxymethylcytosine profiling as an indicator of cellular state. Epigenomics 5:655-69.
Landfors M, Johansen J, Aronsen JM, Vagbo CB, Dore LC, He C, Sjaastad I, Saetrom P, Fedorcsak P, Dahl JA, Aanes H, Fusser M, Klungland A. 2017. Genome-wide profiling of DNA 5-hydroxymethylcytosine during rat Sertoli cell maturation. Cell Discov 3:17013.
Landry C, Clotman F, Hioki T, Oda H, Picard JJ, Lemaigre FP, Rousseau GG. 1997. HNF-6 is expressed in endoderm derivatives and nervous system of the mouse embryo and participates to the cross-regulatory network of liver-enriched transcription factors. Developmental Biology 192:247-57.
Lannoy VJ, Rodolosse A, Pierreux CE, Rousseau GG, Lemaigre FP. 2000. Transcriptional stimulation by hepatocyte nuclear factor-6. Target-specific recruitment of either CREB-binding protein (CBP) or p300/CBP-associated factor (p/CAF). Journal of Biological Chemistry 275:22098-103.
Lau HH, Ng NHJ, Loo LSW, Jasmen JB, Teo AKK. 2018. The molecular functions of hepatocyte nuclear factors - In and beyond the liver. Journal of Hepatology 68:1033-1048.
Lee CW, Huang WC, Huang HD, Huang YH, Ho JH, Yang MH, Yang VW, Lee OK. 2017. DNA Methyltransferases Modulate Hepatogenic Lineage Plasticity of Mesenchymal Stromal Cells. Stem Cell Reports 9:247-263.
Lee S, Lee HJ, Kim JH, Lee HS, Jang JJ, Kang GH. 2003. Aberrant CpG island hypermethylation along multistep hepatocarcinogenesis. Am J Pathol 163:1371-8.
Lemaigre FP, Durviaux SM, Truong O, Lannoy VJ, Hsuan JJ, Rousseau GG. 1996. Hepatocyte nuclear factor 6, a transcription factor that contains a novel type of homeodomain and a single cut domain. Proceedings of the National Academy of Sciences of the United States of America 93:9460-4.
Lewis LC, Lo PC, Foster JM, Dai N, Correa IR, Durczak PM, Duncan G, Ramsawhook A, Aithal GP, Denning C, Hannan NR, Ruzov A. 2017. Dynamics of 5-carboxylcytosine during hepatic differentiation: Potential general role for active demethylation by DNA repair in lineage specification. Epigenetics 12:277-286.

Li E, Bestor TH, Jaenisch R. 1992. Targeted mutation of the DNA methyltransferase gene results in embryonic lethality. Cell 69:915-26.
Li E, Zhang Y. 2014. DNA methylation in mammals. Cold Spring Harb Perspect Biol 6:a019133.
Li J, Ning G, Duncan SA. 2000. Mammalian hepatocyte differentiation requires the transcription factor HNF-4alpha. Genes and Development 14:464-74.
Li K, Zhang H, Wang Y, Feng M. 2006. Differential expression of HNF4alpha isoforms in liver stem cells and hepatocytes. Journal of Cellular Biochemistry 99:558-64.
Li L, Li C, Mao H, Du Z, Chan WY, Murray P, Luo B, Chan AT, Mok TS, Chan FK, Ambinder RF, Tao Q. 2016a. Epigenetic inactivation of the CpG demethylase TET1 as a DNA methylation feedback loop in human cancers. Sci Rep 6:26591.
Li TW, Peng H, Yang H, Kurniawidjaja S, Panthaki P, Zheng Y, Mato JM, Lu SC. 2015. S-Adenosylmethionine and methylthioadenosine inhibit beta-catenin signaling by multiple mechanisms in liver and colon cancer. Molecular Pharmacology 87:77-86.
Li W, Liu M. 2011. Distribution of 5-hydroxymethylcytosine in different human tissues. J Nucleic Acids 2011:870726.
Li X, Liu Y, Salz T, Hansen KD, Feinberg A. 2016b. Whole-genome analysis of the methylome and hydroxymethylome in normal and malignant lung and liver. Genome Research 26:1730-1741.
Li X, Yao B, Chen L, Kang Y, Li Y, Cheng Y, Li L, Lin L, Wang Z, Wang M, Pan F, Dai Q, Zhang W, Wu H, Shu Q, Qin Z, He C, Xu M, Jin P. 2017. Ten-eleven translocation 2 interacts with forkhead box O3 and regulates adult neurogenesis. Nat Commun 8:15903.
Lian B, Ren Y, Zhang H, Lin T, Wang Y. 2019. An adenosine derivative (IFC-305) reduced the risk of radiation-induced intestinal toxicity in the treatment of colon cancer by suppressing the methylation of PPAR-r promoter. Biomedicine and Pharmacotherapy 118:109202.
Liang J, Yang F, Zhao L, Bi C, Cai B. 2016. Physiological and pathological implications of 5-hydroxymethylcytosine in diseases. Oncotarget 7:48813-48831.
Lin IH, Chen YF, Hsu MT. 2017. Correlated 5-Hydroxymethylcytosine (5hmC) and Gene Expression Profiles Underpin Gene and Organ-Specific Epigenetic Regulation in Adult Mouse Brain and Liver. PLoS One 12:e0170779.
Lio CW, Zhang J, Gonzalez-Avalos E, Hogan PG, Chang X, Rao A. 2016. Tet2 and Tet3 cooperate with B-lineage transcription factors to regulate DNA modification and chromatin accessibility. Elife 5.
Liu C, Liu L, Chen X, Shen J, Shan J, Xu Y, Yang Z, Wu L, Xia F, Bie P, Cui Y, Bian XW, Qian C. 2013. Decrease of 5-hydroxymethylcytosine is associated with progression of hepatocellular carcinoma through downregulation of TET1. PLoS One 8:e62828.
Liu J, Jiang J, Mo J, Liu D, Cao D, Wang H, He Y. 2018. Global DNA 5-hydroxymethylcytosine and 5-formylcytosine contents are decreased in the early stage of hepatocellular carcinoma. Hepatology.
Liu WR, Tian MX, Jin L, Yang LX, Ding ZB, Shen YH, Peng YF, Zhou J, Qiu SJ, Dai Z, Fan J, Shi YH. 2014. High expression of 5-hydroxymethylcytosine and isocitrate dehydrogenase 2 is associated with favorable prognosis after curative resection of hepatocellular carcinoma. J Exp Clin Cancer Res 33:32.
Lopez V, Fernandez AF, Fraga MF. 2017. The role of 5-hydroxymethylcytosine in development, aging and age-related diseases. Ageing Res Rev 37:28-38.
Lozano-Rosas MG, Chavez E, Velasco-Loyden G, Dominguez-Lopez M, Martinez-Perez L, Chagoya De Sanchez V. 2019. Diminished S-adenosylmethionine biosynthesis

and its metabolism in a model of hepatocellular carcinoma is recuperated by an adenosine derivative. Cancer Biol Ther:1-14.
Lu P, Rha GB, Melikishvili M, Wu G, Adkins BC, Fried MG, Chi YI. 2008. Structural basis of natural promoter recognition by a unique nuclear receptor, HNF4alpha. Diabetes gene product. Journal of Biological Chemistry 283:33685-97.
Madzo J, Liu H, Rodriguez A, Vasanthakumar A, Sundaravel S, Caces DBD, Looney TJ, Zhang L, Lepore JB, Macrae T, Duszynski R, Shih AH, Song CX, Yu M, Yu Y, Grossman R, Raumann B, Verma A, He C, Levine RL, Lavelle D, Lahn BT, Wickrema A, Godley LA. 2014. Hydroxymethylation at gene regulatory regions directs stem/early progenitor cell commitment during erythropoiesis. Cell Rep 6:231-244.
Maksimovic J, Gordon L, Oshlack A. 2012. SWAN: Subset-quantile within array normalization for illumina infinium HumanMethylation450 BeadChips. Genome Biol 13:R44.
Marcil V, Sinnett D, Seidman E, Boudreau F, Gendron FP, Beaulieu JF, Menard D, Lambert M, Bitton A, Sanchez R, Amre D, Levy E. 2012. Association between genetic variants in the HNF4A gene and childhood-onset Crohn's disease. Genes Immun 13:556-65.
Mardis ER, Ding L, Dooling DJ, Larson DE, McLellan MD, Chen K, Koboldt DC, Fulton RS, Delehaunty KD, McGrath SD, Fulton LA, Locke DP, Magrini VJ, Abbott RM, Vickery TL, Reed JS, Robinson JS, Wylie T, Smith SM, Carmichael L, Eldred JM, Harris CC, Walker J, Peck JB, Du F, Dukes AF, Sanderson GE, Brummett AM, Clark E, McMichael JF, Meyer RJ, Schindler JK, Pohl CS, Wallis JW, Shi X, Lin L, Schmidt H, Tang Y, Haipek C, Wiechert ME, Ivy JV, Kalicki J, Elliott G, Ries RE, Payton JE, Westervelt P, Tomasson MH, Watson MA, Baty J, Heath S, Shannon WD, Nagarajan R, Link DC, Walter MJ, Graubert TA, DiPersio JF, Wilson RK, Ley TJ. 2009. Recurring mutations found by sequencing an acute myeloid leukemia genome. N Engl J Med 361:1058-66.
Marquardt JU, Seo D, Andersen JB, Gillen MC, Kim MS, Conner EA, Galle PR, Factor VM, Park YN, Thorgeirsson SS. 2014. Sequential transcriptome analysis of human liver cancer indicates late stage acquisition of malignant traits. Journal of Hepatology 60:346-353.
Matharu N, Ahituv N. 2015. Minor Loops in Major Folds: Enhancer-Promoter Looping, Chromatin Restructuring, and Their Association with Transcriptional Regulation and Disease. PLoS Genet 11:e1005640.
Mato JM, Lu SC. 2007. Role of S-adenosyl-L-methionine in liver health and injury. Hepatology 45:1306-12.
McKeon C, Ohkubo H, Pastan I, de Crombrugghe B. 1982. Unusual methylation pattern of the alpha 2 (I) collagen gene. Cell 29:203-10.
Mellen M, Ayata P, Dewell S, Kriaucionis S, Heintz N. 2012. MeCP2 binds to 5hmC enriched within active genes and accessible chromatin in the nervous system. Cell 151:1417-30.
Mellen M, Ayata P, Heintz N. 2017. 5-hydroxymethylcytosine accumulation in postmitotic neurons results in functional demethylation of expressed genes. Proceedings of the National Academy of Sciences of the United States of America 114:E7812-E7821.
Meshorer E, Misteli T. 2006. Chromatin in pluripotent embryonic stem cells and differentiation. Nat Rev Mol Cell Biol 7:540-6.
Miquerol L, Lopez S, Cartier N, Tulliez M, Raymondjean M, Kahn A. 1994. Expression of the L-type pyruvate kinase gene and the hepatocyte nuclear factor 4 transcription

factor in exocrine and endocrine pancreas. Journal of Biological Chemistry 269:8944-51.
Miyata T, Yamashita YI, Baba Y, Harada K, Yamao T, Umezaki N, Tsukamoto M, Kitano Y, Yamamura K, Arima K, Nakagawa S, Okabe H, Imai K, Hashimoto D, Chikamoto A, Shimokawa M, Baba H. 2018. Prognostic value of LINE-1 methylation level in 321 patients with primary liver cancer including hepatocellular carcinoma and intrahepatic cholangiocarcinoma. Oncotarget 9:20795-20806.
Monaghan AP, Kaestner KH, Grau E, Schutz G. 1993. Postimplantation expression patterns indicate a role for the mouse forkhead/HNF-3 alpha, beta and gamma genes in determination of the definitive endoderm, chordamesoderm and neuroectoderm. Development 119:567-78.
Montagner S, Leoni C, Emming S, Della Chiara G, Balestrieri C, Barozzi I, Piccolo V, Togher S, Ko M, Rao A, Natoli G, Monticelli S. 2016. TET2 Regulates Mast Cell Differentiation and Proliferation through Catalytic and Non-catalytic Activities. Cell Rep 15:1566-1579.
Nammo T, Yamagata K, Tanaka T, Kodama T, Sladek FM, Fukui K, Katsube F, Sato Y, Miyagawa J, Shimomura I. 2008. Expression of HNF-4alpha (MODY1), HNF-1beta (MODY5), and HNF-1alpha (MODY3) proteins in the developing mouse pancreas. Gene Expr Patterns 8:96-106.
Nelson D, Cox M. 2008. Lehninger Principles of Biochemistry. USA: Freeman and Company.
Okano M, Bell DW, Haber DA, Li E. 1999. DNA methyltransferases Dnmt3a and Dnmt3b are essential for de novo methylation and mammalian development. Cell 99:247-57.
Okano M, Xie S, Li E. 1998a. Cloning and characterization of a family of novel mammalian DNA (cytosine-5) methyltransferases. Nature Genetics 19:219-20.
Okano M, Xie S, Li E. 1998b. Dnmt2 is not required for de novo and maintenance methylation of viral DNA in embryonic stem cells. Nucleic Acids Res 26:2536-40.
Ono R, Taki T, Taketani T, Taniwaki M, Kobayashi H, Hayashi Y. 2002. LCX, leukemia-associated protein with a CXXC domain, is fused to MLL in acute myeloid leukemia with trilineage dysplasia having t(10;11)(q22;q23). Cancer Research 62:4075-80.
Ott MO, Rey-Campos J, Cereghini S, Yaniv M. 1991. vHNF1 is expressed in epithelial cells of distinct embryonic origin during development and precedes HNF1 expression. Mechanisms of Development 36:47-58.
Page A, Paoli P, Moran Salvador E, White S, French J, Mann J. 2016. Hepatic stellate cell transdifferentiation involves genome-wide remodeling of the DNA methylation landscape. Journal of Hepatology 64:661-73.
Pani L, Quian XB, Clevidence D, Costa RH. 1992. The restricted promoter activity of the liver transcription factor hepatocyte nuclear factor 3 beta involves a cell-specific factor and positive autoactivation. Molecular and Cellular Biology 12:552-62.
Pansuriya TC, van Eijk R, d'Adamo P, van Ruler MA, Kuijjer ML, Oosting J, Cleton-Jansen AM, van Oosterwijk JG, Verbeke SL, Meijer D, van Wezel T, Nord KH, Sangiorgi L, Toker B, Liegl-Atzwanger B, San-Julian M, Sciot R, Limaye N, Kindblom LG, Daugaard S, Godfraind C, Boon LM, Vikkula M, Kurek KC, Szuhai K, French PJ, Bovee JV. 2011. Somatic mosaic IDH1 and IDH2 mutations are associated with enchondroma and spindle cell hemangioma in Ollier disease and Maffucci syndrome. Nat Genet 43:1256-61.
Parent R, Marion MJ, Furio L, Trepo C, Petit MA. 2004. Origin and characterization of a human bipotent liver progenitor cell line. Gastroenterology 126:1147-56.

Parsons DW, Jones S, Zhang X, Lin JC, Leary RJ, Angenendt P, Mankoo P, Carter H, Siu IM, Gallia GL, Olivi A, McLendon R, Rasheed BA, Keir S, Nikolskaya T, Nikolsky Y, Busam DA, Tekleab H, Diaz LA, Jr., Hartigan J, Smith DR, Strausberg RL, Marie SK, Shinjo SM, Yan H, Riggins GJ, Bigner DD, Karchin R, Papadopoulos N, Parmigiani G, Vogelstein B, Velculescu VE, Kinzler KW. 2008. An integrated genomic analysis of human glioblastoma multiforme. Science 321:1807-12.

Parviz F, Matullo C, Garrison WD, Savatski L, Adamson JW, Ning G, Kaestner KH, Rossi JM, Zaret KS, Duncan SA. 2003. Hepatocyte nuclear factor 4alpha controls the development of a hepatic epithelium and liver morphogenesis. Nature Genetics 34:292-6.

Pastor WA, Pape UJ, Huang Y, Henderson HR, Lister R, Ko M, McLoughlin EM, Brudno Y, Mahapatra S, Kapranov P, Tahiliani M, Daley GQ, Liu XS, Ecker JR, Milos PM, Agarwal S, Rao A. 2011. Genome-wide mapping of 5-hydroxymethylcytosine in embryonic stem cells. Nature 473:394-7.

Penn NW, Suwalski R, O'Riley C, Bojanowski K, Yura R. 1972. The presence of 5-hydroxymethylcytosine in animal deoxyribonucleic acid. Biochem J 126:781-90.

Perez-Cabeza de Vaca R, Dominguez-Lopez M, Guerrero-Celis N, Rodriguez-Aguilera JR, Chagoya de Sanchez V. 2018. Inflammation is regulated by the adenosine derivative molecule, IFC-305, during reversion of cirrhosis in a CCl4 rat model. Int Immunopharmacol 54:12-23.

Perez-Carreon JI, Martinez-Perez L, Loredo ML, Yanez-Maldonado L, Velasco-Loyden G, Vidrio-Gomez S, Ramirez-Salcedo J, Hernandez-Luis F, Velazquez-Martinez I, Suarez-Cuenca JA, Hernandez-Munoz R, de Sanchez VC. 2010. An adenosine derivative compound, IFC305, reverses fibrosis and alters gene expression in a pre-established CCl(4)-induced rat cirrhosis. Int J Biochem Cell Biol 42:287-96.

Peric-Hupkes D, Meuleman W, Pagie L, Bruggeman SW, Solovei I, Brugman W, Graf S, Flicek P, Kerkhoven RM, van Lohuizen M, Reinders M, Wessels L, van Steensel B. 2010. Molecular maps of the reorganization of genome-nuclear lamina interactions during differentiation. Mol Cell 38:603-13.

Peters TJ, Buckley MJ, Statham AL, Pidsley R, Samaras K, R VL, Clark SJ, Molloy PL. 2015. De novo identification of differentially methylated regions in the human genome. Epigenetics Chromatin 8:6.

Pfeifer GP, Szabo PE. 2018. Gene body profiles of 5-hydroxymethylcytosine: potential origin, function and use as a cancer biomarker. Epigenomics 10:1029-1032.

Posfai J, Bhagwat AS, Posfai G, Roberts RJ. 1989. Predictive motifs derived from cytosine methyltransferases. Nucleic Acids Res 17:2421-35.

Qian X, Costa RH. 1995. Analysis of hepatocyte nuclear factor-3 beta protein domains required for transcriptional activation and nuclear targeting. Nucleic Acids Res 23:1184-91.

Rausa F, Samadani U, Ye H, Lim L, Fletcher CF, Jenkins NA, Copeland NG, Costa RH. 1997. The cut-homeodomain transcriptional activator HNF-6 is coexpressed with its target gene HNF-3 beta in the developing murine liver and pancreas. Developmental Biology 192:228-46.

Reber M, Cereghini S. 2001. Variant hepatocyte nuclear factor 1 expression in the mouse genital tract. Mechanisms of Development 100:75-8.

Recillas-Targa F. 2014. Interdependency between genetic and epigenetic regulatory defects in cancer. Methods Mol Biol 1165:33-52.

Rey-Campos J, Chouard T, Yaniv M, Cereghini S. 1991. vHNF1 is a homeoprotein that activates transcription and forms heterodimers with HNF1. EMBO Journal 10:1445-57.

Riggs AD. 1975. X inactivation, differentiation, and DNA methylation. Cytogenetics and Cell Genetics 14:9-25.

Rodríguez-Aguilera JR. 2015. Estudio de las modificaciones epigenéticas en un modelo de cirrosis experimental y su reversión por el hepatoprotector IFC-305editor^editors. Biología Celular y Desarrollo, Instituto de Fisiiología Celular. México: Universidad Nacional Autónoma de México.

Rodriguez-Aguilera JR, Guerrero-Hernandez C, Perez-Molina R, Cadena-Del-Castillo CE, Perez-Cabeza de Vaca R, Guerrero-Celis N, Dominguez-Lopez M, Murillo-de-Ozores AR, Arzate-Mejia R, Recillas-Targa F, Chagoya de Sanchez V. 2018. Epigenetic Effects of an Adenosine Derivative in a Wistar Rat Model of Liver Cirrhosis. Journal of Cellular Biochemistry 119:401-413.

Rodríguez-Aguilera JR, Pérez-Cabeza-de-Vaca R, Guerrero-Celis N, Velasco-Loyden G, Domínguez-López M, Recillas-Targa F, Chagoya-de-Sánchez V. 2019. Molecular and cellular aspects of cirrhosis and how an adenosine derivative could revert fibrosis. In Tsoulfas G, editor^editors. Liver Cirrhosis - Debates and Current Challenges. United Kingdom: InctechOpen.

Rose NR, McDonough MA, King ON, Kawamura A, Schofield CJ. 2011. Inhibition of 2-oxoglutarate dependent oxygenases. Chem Soc Rev 40:4364-97.

Rudenko A, Dawlaty MM, Seo J, Cheng AW, Meng J, Le T, Faull KF, Jaenisch R, Tsai LH. 2013. Tet1 is critical for neuronal activity-regulated gene expression and memory extinction. Neuron 79:1109-1122.

Ruse MD, Jr., Privalsky ML, Sladek FM. 2002. Competitive cofactor recruitment by orphan receptor hepatocyte nuclear factor 4alpha1: modulation by the F domain. Molecular and Cellular Biology 22:1626-38.

Ruzov A, Tsenkina Y, Serio A, Dudnakova T, Fletcher J, Bai Y, Chebotareva T, Pells S, Hannoun Z, Sullivan G, Chandran S, Hay DC, Bradley M, Wilmut I, De Sousa P. 2011. Lineage-specific distribution of high levels of genomic 5-hydroxymethylcytosine in mammalian development. Cell Res 21:1332-42.

Santangelo L, Marchetti A, Cicchini C, Conigliaro A, Conti B, Mancone C, Bonzo JA, Gonzalez FJ, Alonzi T, Amicone L, Tripodi M. 2011. The stable repression of mesenchymal program is required for hepatocyte identity: a novel role for hepatocyte nuclear factor 4alpha. Hepatology 53:2063-74.

Schiffer E, Housset C, Cacheux W, Wendum D, Desbois-Mouthon C, Rey C, Clergue F, Poupon R, Barbu V, Rosmorduc O. 2005. Gefitinib, an EGFR inhibitor, prevents hepatocellular carcinoma development in the rat liver with cirrhosis. Hepatology 41:307-14.

Schubeler D. 2015. Function and information content of DNA methylation. Nature 517:321-6.

Schwartz B, Algamas-Dimantov A, Hertz R, Nataf J, Kerman A, Peri I, Bar-Tana J. 2009. Inhibition of colorectal cancer by targeting hepatocyte nuclear factor-4alpha. International Journal of Cancer 124:1081-9.

Seeliger C, Culmes M, Schyschka L, Yan X, Damm G, Wang Z, Kleeff J, Thasler WE, Hengstler J, Stockle U, Ehnert S, Nussler AK. 2013. Decrease of global methylation improves significantly hepatic differentiation of Ad-MSCs: possible future application for urea detoxification. Cell Transplantation 22:119-31.

Seritrakul P, Gross JM. 2017. Tet-mediated DNA hydroxymethylation regulates retinal neurogenesis by modulating cell-extrinsic signaling pathways. PLoS Genet 13:e1006987.

Shi DQ, Ali I, Tang J, Yang WC. 2017. New Insights into 5hmC DNA Modification: Generation, Distribution and Function. Front Genet 8:100.

Skvortsova K, Zotenko E, Luu PL, Gould CM, Nair SS, Clark SJ, Stirzaker C. 2017. Comprehensive evaluation of genome-wide 5-hydroxymethylcytosine profiling approaches in human DNA. Epigenetics Chromatin 10:16.

Sladek FM, Ruse MD, Jr., Nepomuceno L, Huang SM, Stallcup MR. 1999. Modulation of transcriptional activation and coactivator interaction by a splicing variation in the F domain of nuclear receptor hepatocyte nuclear factor 4alpha1. Molecular and Cellular Biology 19:6509-22.

Sladek FM, Zhong WM, Lai E, Darnell JE, Jr. 1990. Liver-enriched transcription factor HNF-4 is a novel member of the steroid hormone receptor superfamily. Genes and Development 4:2353-65.

Smith ZD, Meissner A. 2013. DNA methylation: roles in mammalian development. Nat Rev Genet 14:204-20.

Smyth GK. 2004. Linear models and empirical bayes methods for assessing differential expression in microarray experiments. Stat Appl Genet Mol Biol 3:Article3.

Spiers H, Hannon E, Schalkwyk LC, Bray NJ, Mill J. 2017. 5-hydroxymethylcytosine is highly dynamic across human fetal brain development. BMC Genomics 18:738.

Stiuso P, Bagarolo ML, Ilisso CP, Vanacore D, Martino E, Caraglia M, Porcelli M, Cacciapuoti G. 2016. Protective Effect of Tyrosol and S-Adenosylmethionine against Ethanol-Induced Oxidative Stress of Hepg2 Cells Involves Sirtuin 1, P53 and Erk1/2 Signaling. Int J Mol Sci 17.

Szulwach KE, Li X, Li Y, Song CX, Wu H, Dai Q, Irier H, Upadhyay AK, Gearing M, Levey AI, Vasanthakumar A, Godley LA, Chang Q, Cheng X, He C, Jin P. 2011. 5-hmC-mediated epigenetic dynamics during postnatal neurodevelopment and aging. Nature Neuroscience 14:1607-16.

Szyf M. 2016. The elusive role of 5'-hydroxymethylcytosine. Epigenomics 8:1539-1551.

Tahiliani M, Koh KP, Shen Y, Pastor WA, Bandukwala H, Brudno Y, Agarwal S, Iyer LM, Liu DR, Aravind L, Rao A. 2009. Conversion of 5-methylcytosine to 5-hydroxymethylcytosine in mammalian DNA by MLL partner TET1. Science 324:930-5.

Takumi S, Okamura K, Yanagisawa H, Sano T, Kobayashi Y, Nohara K. 2015. The effect of a methyl-deficient diet on the global DNA methylation and the DNA methylation regulatory pathways. Journal of Applied Toxicology 35:1550-6.

Tanaka T, Jiang S, Hotta H, Takano K, Iwanari H, Sumi K, Daigo K, Ohashi R, Sugai M, Ikegame C, Umezu H, Hirayama Y, Midorikawa Y, Hippo Y, Watanabe A, Uchiyama Y, Hasegawa G, Reid P, Aburatani H, Hamakubo T, Sakai J, Naito M, Kodama T. 2006. Dysregulated expression of P1 and P2 promoter-driven hepatocyte nuclear factor-4alpha in the pathogenesis of human cancer. Journal of Pathology 208:662-72.

Taraviras S, Monaghan AP, Schutz G, Kelsey G. 1994. Characterization of the mouse HNF-4 gene and its expression during mouse embryogenesis. Mechanisms of Development 48:67-79.

Taylor SE, Li YH, Smeriglio P, Rath M, Wong WH, Bhutani N. 2016. Stable 5-Hydroxymethylcytosine (5hmC) Acquisition Marks Gene Activation During Chondrogenic Differentiation. Journal of Bone and Mineral Research 31:524-34.

Tehlivets O, Malanovic N, Visram M, Pavkov-Keller T, Keller W. 2013. S-adenosyl-L-homocysteine hydrolase and methylation disorders: yeast as a model system. Biochimica et Biophysica Acta 1832:204-15.

Tekpli X, Urbanucci A, Hashim A, Vagbo CB, Lyle R, Kringen MK, Staff AC, Dybedal I, Mills IG, Klungland A, Staerk J. 2016. Changes of 5-hydroxymethylcytosine distribution during myeloid and lymphoid differentiation of CD34+ cells. Epigenetics Chromatin 9:21.

The L. 2018. GLOBOCAN 2018: counting the toll of cancer. Lancet 392:985.
Thomas H, Jaschkowitz K, Bulman M, Frayling TM, Mitchell SM, Roosen S, Lingott-Frieg A, Tack CJ, Ellard S, Ryffel GU, Hattersley AT. 2001. A distant upstream promoter of the HNF-4alpha gene connects the transcription factors involved in maturity-onset diabetes of the young. Human Molecular Genetics 10:2089-97.
Thomson JP, Hunter JM, Lempiainen H, Muller A, Terranova R, Moggs JG, Meehan RR. 2013. Dynamic changes in 5-hydroxymethylation signatures underpin early and late events in drug exposed liver. Nucleic Acids Res 41:5639-54.
Thomson JP, Lempiainen H, Hackett JA, Nestor CE, Muller A, Bolognani F, Oakeley EJ, Schubeler D, Terranova R, Reinhardt D, Moggs JG, Meehan RR. 2012. Non-genotoxic carcinogen exposure induces defined changes in the 5-hydroxymethylome. Genome Biol 13:R93.
Thomson JP, Skene PJ, Selfridge J, Clouaire T, Guy J, Webb S, Kerr AR, Deaton A, Andrews R, James KD, Turner DJ, Illingworth R, Bird A. 2010. CpG islands influence chromatin structure via the CpG-binding protein Cfp1. Nature 464:1082-6.
Tomasi ML, Tomasi I, Ramani K, Pascale RM, Xu J, Giordano P, Mato JM, Lu SC. 2012. S-adenosyl methionine regulates ubiquitin-conjugating enzyme 9 protein expression and sumoylation in murine liver and human cancers. Hepatology 56:982-93.
Torres-Padilla ME, Weiss MC. 2003. Effects of interactions of hepatocyte nuclear factor 4alpha isoforms with coactivators and corepressors are promoter-specific. FEBS Letters 539:19-23.
Tsagaratou A, Rao A. 2014. TET Proteins and 5-Methylcytosine Oxidation in the Immune System. Cold Spring Harb Symp Quant Biol.
UCSC-Genome-Browser 2018. UCSC Genome Browser, session URL < http://genome-euro.ucsc.edu/cgi-bin/hgTracks?hgS_doOtherUser=submit&hgS_otherUserName=H%20Hernandez&hgS_otherUserSessionName=HepaRG%20oxBS>
UCSC-Genome-Browser. 2018a. CpG Methylation by Methyl 450K Bead Arrays from ENCODE/HAIB < http://genome-euro.ucsc.edu/cgi-bin/hgTrackUi?hgsid=233154903_5aNHhW6pbVvtdISvAsfMXcwYiXjh&g=wgEncodeHaibMethyl450>
UCSC-Genome-Browser. 2018b. Chromatin State Segmentation by HMM from ENCODE/Broad<http://genome-euro.ucsc.edu/cgi-bin/hgTrackUi?hgsid=233154903_5aNHhW6pbVvtdISvAsfMXcwYiXjh&g=wgEncodeBroadHmm>.
UCSC-Genome-Browser. 2018c. chromHMM tracks from Roadma< http://genome-euro.ucsc.edu/cgi-bin/hgTrackUi?hgsid=233154903_5aNHhW6pbVvtdISvAsfMXcwYiXjh&g=hub_1623_RoadmapConsolidatedHMM>
Valinluck V, Tsai HH, Rogstad DK, Burdzy A, Bird A, Sowers LC. 2004. Oxidative damage to methyl-CpG sequences inhibits the binding of the methyl-CpG binding domain (MBD) of methyl-CpG binding protein 2 (MeCP2). Nucleic Acids Res 32:4100-8.
Vanhorenbeeck V, Jacquemin P, Lemaigre FP, Rousseau GG. 2002. OC-3, a novel mammalian member of the ONECUT class of transcription factors. Biochemical and Biophysical Research Communications 292:848-54.
Velasco-Loyden G, Perez-Carreon JI, Aguero JF, Romero PC, Vidrio-Gomez S, Martinez-Perez L, Yanez-Maldonado L, Hernandez-Munoz R, Macias-Silva M, de

Sanchez VC. 2010. Prevention of in vitro hepatic stellate cells activation by the adenosine derivative compound IFC305. Biochem Pharmacol 80:1690-9.
Velasco-Loyden G, Perez-Martinez L, Vidrio-Gomez S, Perez-Carreon JI, Chagoya de Sanchez V. 2017. Cancer chemoprevention by an adenosine derivative in a model of cirrhosis-hepatocellular carcinoma induced by diethylnitrosamine in rats. Tumour Biology 39:1010428317691190.
Vuong LM, Chellappa K, Dhahbi JM, Deans JR, Fang B, Bolotin E, Titova NV, Hoverter NP, Spindler SR, Waterman ML, Sladek FM. 2015. Differential Effects of Hepatocyte Nuclear Factor 4alpha Isoforms on Tumor Growth and T-Cell Factor 4/AP-1 Interactions in Human Colorectal Cancer Cells. Molecular and Cellular Biology 35:3471-90.
Wang T, Drill E, Vakiani E, Pak LM, Boerner T, Askan G, Schvartzman JM, Simpson AL, Jarnagin WR, Sigel CS. 2019. Distinct histomorphological features are associated with IDH1 mutation in intrahepatic Cholangiocarcinoma. Human Pathology.
Wen L, Tang F. 2014. Genomic distribution and possible functions of DNA hydroxymethylation in the brain. Genomics 104:341-6.
Williams K, Christensen J, Helin K. 2011. DNA methylation: TET proteins-guardians of CpG islands? EMBO Rep 13:28-35.
Wolf SF, Jolly DJ, Lunnen KD, Friedmann T, Migeon BR. 1984. Methylation of the hypoxanthine phosphoribosyltransferase locus on the human X chromosome: implications for X-chromosome inactivation. Proceedings of the National Academy of Sciences of the United States of America 81:2806-10.
Xu W, Yang H, Liu Y, Yang Y, Wang P, Kim SH, Ito S, Yang C, Xiao MT, Liu LX, Jiang WQ, Liu J, Zhang JY, Wang B, Frye S, Zhang Y, Xu YH, Lei QY, Guan KL, Zhao SM, Xiong Y. 2011. Oncometabolite 2-hydroxyglutarate is a competitive inhibitor of alpha-ketoglutarate-dependent dioxygenases. Cancer Cell 19:17-30.
Xu Y, Zalzala M, Xu J, Li Y, Yin L, Zhang Y. 2015. A metabolic stress-inducible miR-34a-HNF4alpha pathway regulates lipid and lipoprotein metabolism. Nat Commun 6:7466.
Xu Z, Taylor JA, Leung YK, Ho SM, Niu L. 2016. oxBS-MLE: an efficient method to estimate 5-methylcytosine and 5-hydroxymethylcytosine in paired bisulfite and oxidative bisulfite treated DNA. Bioinformatics 32:3667-3669.
Yang H, Liu Y, Bai F, Zhang JY, Ma SH, Liu J, Xu ZD, Zhu HG, Ling ZQ, Ye D, Guan KL, Xiong Y. 2013. Tumor development is associated with decrease of TET gene expression and 5-methylcytosine hydroxylation. Oncogene 32:663-9.
Yoo Y, Park JH, Weigel C, Liesenfeld DB, Weichenhan D, Plass C, Seo DG, Lindroth AM, Park YJ. 2017. TET-mediated hydroxymethylcytosine at the Ppargamma locus is required for initiation of adipogenic differentiation. Int J Obes (Lond) 41:652-659.
Yu G, Wang LG, He QY. 2015. ChIPseeker: an R/Bioconductor package for ChIP peak annotation, comparison and visualization. Bioinformatics 31:2382-3.
Yu M, Hon GC, Szulwach KE, Song CX, Zhang L, Kim A, Li X, Dai Q, Shen Y, Park B, Min JH, Jin P, Ren B, He C. 2012. Base-resolution analysis of 5-hydroxymethylcytosine in the mammalian genome. Cell 149:1368-80.
Zhang N. 2018. Role of methionine on epigenetic modification of DNA methylation and gene expression in animals. Anim Nutr 4:11-16.
Zhang RR, Cui QY, Murai K, Lim YC, Smith ZD, Jin S, Ye P, Rosa L, Lee YK, Wu HP, Liu W, Xu ZM, Yang L, Ding YQ, Tang F, Meissner A, Ding C, Shi Y, Xu GL. 2013. Tet1 regulates adult hippocampal neurogenesis and cognition. Cell Stem Cell 13:237-45.

Zhao S, Lin Y, Xu W, Jiang W, Zha Z, Wang P, Yu W, Li Z, Gong L, Peng Y, Ding J, Lei Q, Guan KL, Xiong Y. 2009. Glioma-derived mutations in IDH1 dominantly inhibit IDH1 catalytic activity and induce HIF-1alpha. Science 324:261-5.

Zhong X, Wang QQ, Li JW, Zhang YM, An XR, Hou J. 2017. Ten-Eleven Translocation-2 (Tet2) Is Involved in Myogenic Differentiation of Skeletal Myoblast Cells in Vitro. Sci Rep 7:43539.

Zhu J, Adli M, Zou JY, Verstappen G, Coyne M, Zhang X, Durham T, Miri M, Deshpande V, De Jager PL, Bennett DA, Houmard JA, Muoio DM, Onder TT, Camahort R, Cowan CA, Meissner A, Epstein CB, Shoresh N, Bernstein BE. 2013. Genome-wide chromatin state transitions associated with developmental and environmental cues. Cell 152:642-54.

Zhu Q, Stoger R, Alberio R. 2018. A Lexicon of DNA Modifications: Their Roles in Embryo Development and the Germline. Front Cell Dev Biol 6:24.

Anexo 1. Catálogo histológico de un modelo de intoxicación hepática crónica con dietilnitrosamina en ratas wistar

De acuerdo con el trabajo del grupo de Rosmorduc [Schiffer et al., 2005], el tratamiento de ratas con dietilnitrosamina (DEN) permite tener un modelo experimental para inducir cirrosis y su progresión hacia carcinoma hepatocelular (HCC), es así que este modelo representa una herramienta válida para evaluar potenciales efectos antitumorales en el hígado. Los animales de experimentación reciben semanalmente una administración intraperitoneal de DEN (50 mg/kg) seguida de un período de lavado de 2 semanas; la cirrosis se presenta a las 14 semanas y el HCC multifocal a las 18 semanas.

Como parte de los objetivos con respecto a los efectos hepatoprotectores del IFC en cáncer, se replicó en el laboratorio el modelo de DEN en ratas Wistar de ~200 g, obteniendo muestras de tejido hepático a las 18 y 22 semanas de tratamiento, para contar con un estado neoplásico (18 semanas) y una evolución del mismo (22 semanas).

Con el interés de validar el modelo, se estableció una colaboración con el Dr. Pedro Valencia Mayoral, hepatopatólogo del Hospital Infantil de México “Federico Gómez”, quien realizó un diagnóstico doble ciego para cada muestra generada.

En seguida se presentan imágenes representativas de muestras clasificadas macroscópicamente como no tumorales y tumorales, fijadas con paraformaldehído al 4% y 300 mosM, a las que se les realizó una tinción de hematoxilina-eosina y posteriormente un diagnóstico histopatológico, basado en la identificación de cúmulos clónales de células alteradas que indicaran la presencia de HCC.

Tabla A1. Características fenotípicas de los hígados de ratas tratadas con dietilnitrosamina (DEN)

<table>
<tr><th>Fenotipo macroscópico</th><th colspan="3">Clasificación macroscópica y diagnóstico</th></tr>
<tr><td> 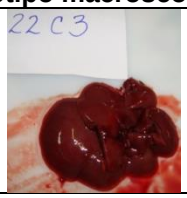
</td><td colspan="3"> 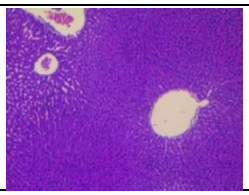
22 semanas - control 3
Sin alteración</td></tr>
<tr><td rowspan="2"> 
</td><td>Tumor</td><td colspan="2">No tumor</td></tr>
<tr><td> 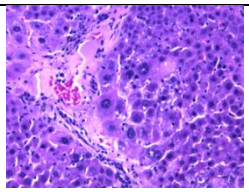
18 semanas - DEN 4
Displasia leve</td><td colspan="2"> 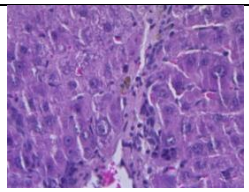
18 semanas-DEN 4
Displasia difusa leve</td></tr>
<tr><td rowspan="2"> 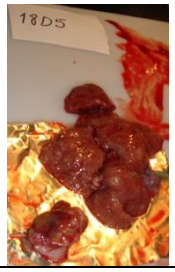
</td><td>Tumor</td><td>Tumor adherente</td><td>No tumor</td></tr>
<tr><td> 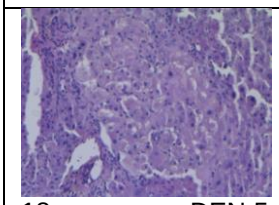
18 semanas - DEN 5
Displasia multinodular</td><td> 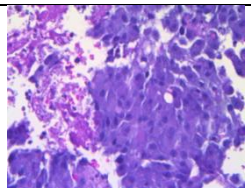
18 semanas – DEN 5
Hepatocarcinoma</td><td> 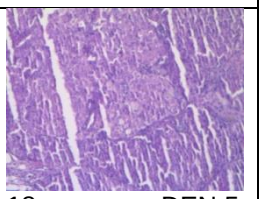
18 semanas-DEN 5
Displasia multinodular</td></tr>
</table>

<table>
<tr><th>Fenotipo macroscópico</th><th colspan="2">Clasificación macroscópica y diagnóstico</th></tr>
<tr><td rowspan="2"> 
</td><td>Tumor</td><td>No tumor</td></tr>
<tr><td> 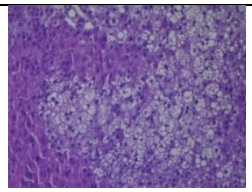
22 semanas - DEN 1
Displasia leve difusa</td><td> 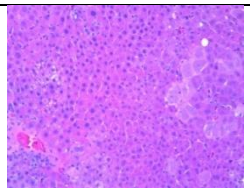
22 semanas -DEN 1
Displasia leve difusa</td></tr>
<tr><td> 
</td><td> 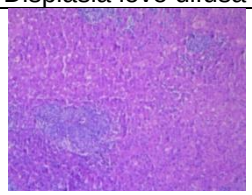
22 semanas - DEN 8
Hepatocarcinoma multinodular</td><td> 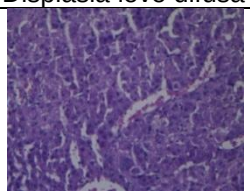
22 semanas - DEN 8
Displasia leve difusa</td></tr>
</table>

Se muestran imágenes representativas a una amplificación de 10x

La Tabla A2 condensa los diagnósticos encontrados por muestra.

Tabla A2. Diagnósticos histopatológicos por muestra

18 semanas

Tratamiento	Diagnostico	Tratamiento	Diagnostico
18 Control 1	Sin alteración	18 Control 4	Sin alteración
18 Control 2	Sin alteración	18 Control 5	Sin alteración
18 Control 3	Sin alteración	18 Control 6	Sin alteración

Tratamiento	Diagnostico	Tratamiento	Diagnóstico
18 DEN 1 T	Displasia nodular leve	18 DEN 1 NT	Displasia grave
18 DEN 3 T	Sin dato	18 DEN 3 NT	Displasia focal leve
18 DEN 4 T	Displasia leve	18 DEN 4 NT	Displasia difusa leve
18 DEN 5 T	Displasia multinodular leve	18 DEN 5 NT	Displasia multinodular
18 DEN 5 TA	HCC		
18 DEN 6 T	Displasia difusa moderada	18 DEN 6 NT	Displasia moderada
18 DEN 7 T	Displasia difusa leve	18 DEN 7 NT	Displasia leve
18 DEN 8 T	Displasia multinodular moderada	18 DEN 8 NT	Displasia multinodular leve
18 DEN 9 T	Displasia leve + posible HCC	18 DEN 9 NT	Displasia multinodular extensa

22 semanas

Tratamiento	Diagnostico	Tratamiento	Diagnostico
22 Control 1	Sin alteración	22 Control 4	Sin alteración
22 Control 2	Sin alteración	22 Control 5	Sin alteración
22 Control 3	Sin alteración	22 Control 6	Sin alteración

Tratamiento	Diagnostico	Tratamiento	Diagnóstico
22 DEN 1 T	Displasia leve difusa	22 DEN 1 NT	Displasia leve difusa
22 DEN 2 T	Displasia leve difusa	22 DEN 2 NT	Displasia leve difusa
22 DEN 2 TA	Tumor maligno vascularizado e indiferenciado		
22 DEN 4 T	Displasia leve difusa	22 DEN 4 NT	Displasia leve
22 DEN 5 T	Displasia nodular grave y extensa + HCC	22 DEN 5 NT	Displasia multinodular moderada
22 DEN 6 T	Displasia leve difusa	22 DEN 6 NT	Displasia leve difusa
22 DEN 8 T	HCC multinodular	22 DEN 8 NT	Displasia leve difusa
22 DEN 9 T	Displasia leve difusa + HCC	22 DEN 9 NT	Displasia leve

Clasificaci Macroscópica: T, tumor; NT, No tumor

En seguida se resumen los casos de neoplasias encontradas

Tabla A3. Resumen de muestras del modelo de Schiffer que presentaron neoplasias

Tratamiento	n	Tumor maligno vascularizado e indiferenciado		Carcinoma hepatocelular		Muerte durante el tratamiento
Clasificación Macroscópica		Tumor	No tumor	Tumor	No tumor	
18 Control	6	0	0	0	0	0
18 DEN	10	0	0	2	0	2
22 Control	6	0	0	0	0	0
22 DEN	10	1	0	2	0	2

El diagnóstico histopatológico del modelo analizado mostró que la mayoría de las muestras de hígados de rata tratadas con DEN presentan una gran variedad de displasias y muy pocos casos con características de carcinoma hepatocelular, al no observarse cúmulos clonales de células transformados. Como se comentó al inicio de esta sección, se ha descrito que este modelo presenta en una primera etapa cirrosis a las 14 semanas de evolución, sin embargo en las muestras tanto de 18 como de 22 semanas, no se observa la acumulación de colágena, que es característica de esta patología.

Con el interés de determinar el origen de la falta de reproducibilidad entre los datos previamente descritos por Schiffer y los obtenidos en el laboratorio, se decidió evaluar la efectividad de la DEN empleada a través de un ensayo de toxicidad aguda, utilizando una dosis de 220 mg/kg, correspondiente a la dosis letal 50 (DL50) reportada en la ficha de datos de seguridad del producto, comercializado por Sigma-Aldrich.

Se preparó una solución de DEN, en oscuridad para evitar la degradación por fotosensibilidad, a una concentración de 0.045 g/mL y se administraron volúmenes equivalentes a la dosis letal de DEN. Se utilizaron 6 ratas Wistar de ~200 g, con el carcinógeno y una rata control a la que únicamente se le administró solución salina.

Una vez realizada la administración, las ratas continuaron con alimentación y agua *ad libitum* y se les dio seguimiento durante 14 días. Todas los animales experimentales sobrevivieron, lo cual habla de una baja efectividad del compuesto carcinogénico. Es posible que el mismo se encuentre en un estado de degradación tal que no puede ejercer su efecto tóxico agudo, con este hecho es posible entender la variabilidad biológica encontrada en el modelo de Schiffer así como el reducido número de casos donde se presentó el carcinoma hepatocelular.

Transcurridos los 14 días de seguimiento, se sacrificaron los animales, se realizó la disección del hígado y se tomaron muestras para la evaluación histopatológica. En seguida se muestran imágenes de los cortes histológicos de cada tejido.

Tabla A4. Características fenotípicas de los hígados de ratas administradas con DL50 de DEN

Fenotipo macroscópico	Corte histológico y diagnóstico
 DEN 1	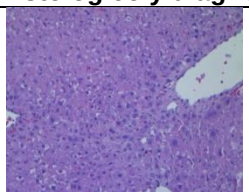 Displasia leve difusa
 DEN 2	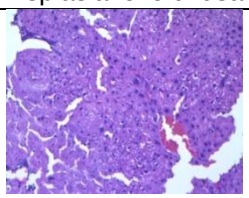 Cambios leves displásicos

Continuación Tabla A4

Fenotipo macroscópico	Corte histológico y diagnóstico
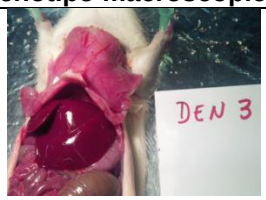 DEN 3	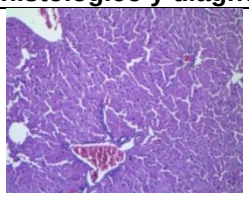 Cambios citoplásmicos y nucleares mínimos
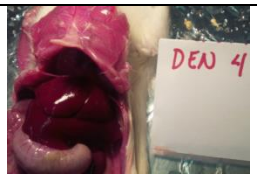 DEN 4	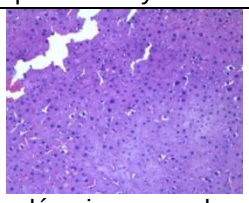 Cambios citoplásmicos y nucleares mínimos
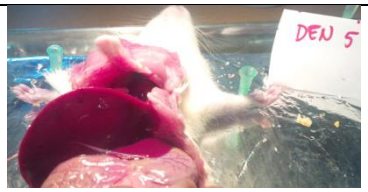 DEN 5	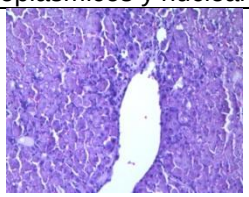 Cambios citoplásmicos y nucleares mínimos
 DEN 6	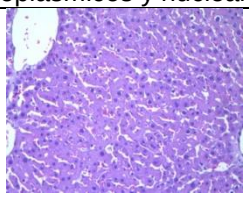 Cambios citoplásmicos y nucleares mínimos
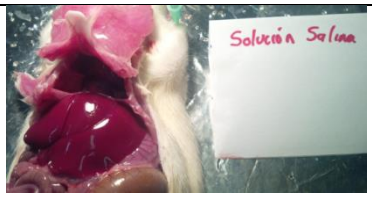 Control, solución salina	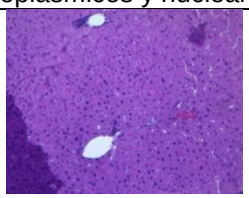 Cambios mínimos

Se muestran imágenes representativas a una amplificación de 10x

Estos resultados sugieren que la DEN utilizada presenta baja efectividad, al no observarse toxicidad aguda después de la administración de una dosis letal, lo que pudiera explicar la variabilidad obtenida en el modelo de inducción de HCC en rata. Se concluyó que en estas condiciones, el modelo obtenido no nos permitiría realizar la evaluación de los efectos antineoplásicos del IFC-305, ya que la DEN no estaba generando la patología.

Anexo 2. Publicaciones relacionadas al proyecto principal de tesis

ARTÍCULOS DIRECTOS

Rodríguez-Aguilera JR, Ecsedi S, Cros MP, Goldsmith C, Domínguez-López M, Guerrero-Celis N, Pérez-Cabeza de Vaca R, Chemin I, Recillas-Targa F, Chagoya de Sánchez V, Hernández-Vargas H. **Genome-wide 5-hydroxymethylcytosine (5hmC) emerges at early stage of *in vitro* hepatocyte differentiation.** Preprint, bioRxiv 629493; (2019), doi: https://doi.org/10.1101/629493

Ecsedi S*, **Rodríguez-Aguilera JR***, Hernandez-Vargas H*. 5-Hydroxymethylcytosine (5hmC), or How to Identify Your Favorite Cell. *Epigenomes*. (2018), 2(1):3. doi: https://doi.org/10.3390/epigenomes2010003 * Indica primeros autores en conjunto

ARTÍCULOS COLATERALES

Rodríguez-Aguilera JR, Guerrero-Hernández C, Pérez-Molina R, Cadena-del-Castillo CE, Pérez Cabeza de Vaca R, Guerrero-Celis N, Domínguez-López M, Murillo-de-Ozores AR, Arzate-Mejía R, Recillas-Targa F and Chagoya de Sánchez V, (2018) **Epigenetic effects of an adenosine derivative in a Wistar rat model of liver cirrhosis**. Journal of Cellular Biochemistry, 2018 Jan; 119(1):401-413. doi: 10.1002/jcb.26192

Pérez-Cabeza de Vaca R, Domínguez-López M, Guerrero-Celis N, **Rodríguez-Aguilera JR**, Chagoya de Sánchez V. **Inflammation is regulated by the adenosine derivative molecule, IFC-305, during reversion of cirrhosis in a CCl_4 rat model.** International Immunopharmacology, (2018) Jan; 54:12-23. doi: 10.1016/j.intimp.2017.10.019.

Chavez E, Lozano-Rosas MG, Dominguez-Lopez M, Velasco-Loyden G, **Rodriguez-Aguilera JR**, Jose-Nunez C, Tuena de Gomez-Puyou M y Chagoya de Sanchez V. **Functional, metabolic, and dynamic mitochondrial changes in the rat cirrhosis-hepatocellular carcinoma model and the protective effect of IFC-305**, The Journal of pharmacology and experimental therapeutics, (2017) May;361(2):292-302. doi: 10.1124/jpet.116.239301.

Murillo-de-Ozores AR* and **Rodríguez-Aguilera JR***, La N6-metiladenina: una potencial marca de regulación epigenética en eucariontes, *Revista de Educación Bioquímica*, 35(1): 11-17, (2016). * Indica primeros autores en conjunto

ARTÍCULOS EN COLABORACIÓN

Patil V, Cuenin C, Chung F; **Rodriguez-Aguilera JR**; Fernandez-Jimenez N; Romero-Garmendia I, Bilbao JR; Cahais V, Rothwell J and Herceg Z, **Human mitochondrial DNA is extensively methylated in a non-CpG context**, Nucleic Acids Research, (2019), doi: https://doi.org/10.1093/nar/gkz762

Álvarez EK, Cortés Hernández A, Alemán-Muench HR, Alverú J, **Rodríguez-Aguilera JR**, RecillasTarga F, Chagoya de Sánchez V, Cuevas E, Mancilla Urrea E, Perez-García M, Mondragón Ramírez G, Vilatová M, Bostock I, Hernández-Méndez E, De Rungs D, García Zepeda EA, y Soldevila G, **Methylation of FOXP3 TSDR underlies the impaired suppressive function of Tregs from long-term**

Belatacept-treated kidney transplant patients, Frontiers in Immunology, (2017) doi: 10.3389/fimmu.2017.00219

CAPÍTULO DE LIBRO

Rodríguez-Aguilera JR, Pérez-Cabeza de Vaca R, Guerrero-Celis N, Velasco-Loyden G, Domínguez-López M, Recillas-Targa F, Chagoya de Sánchez V. **Molecular and Cellular Aspects of Cirrhosis and How an Adenosine Derivative Could Revert Fibrosis**, Chapter 6, in Liver Cirrhosis - Debates and Current Challenges, IntechOpen, United Kingdom, (2019). doi: https://doi.org/10.5772/intechopen.83481

DIFUSIÓN DE LA CIENCIA

Tapia E, Lazos L, Reyes L, **Rodríguez-Aguilera JR.** Infografía: **El Cáncer**, Instituto de Fisiología Celular, UNAM, (2019). https://twitter.com/harry_brennan/status/1092631313251741698?s=19

Genome-wide 5-hydroxymethylcytosine (5hmC) emerges at early stage of *in vitro* hepatocyte differentiation

Jesús Rafael Rodríguez-Aguilera[1], Szilvia Ecsedi[2], Marie-Pierre Cros[3], Chloe Goldsmith[4], Mariana Domínguez-López[1], Nuria Guerrero-Celis[1], Rebeca Pérez-Cabeza de Vaca[1,5], Isabelle Chemin[6], Félix Recillas-Targa[7], Victoria Chagoya de Sánchez[1], Héctor Hernández-Vargas[4,8]

1. Department of Cellular Biology and Development, Instituto de Fisiología Celular, Universidad Nacional Autónoma de México (UNAM), Circuito Exterior s/n, Ciudad Universitaria, Coyoacán 04510, Cd. Mx., Mexico.
2. Institute of Biology Valrose (iBV), The National Center for Scientific Research (CNRS) - National Institute of Health and Medical Research (Inserm), Université Côte d'Azur, France.
3. Molecular Mechanisms and Biomarkers Group, International Agency for Research on Cancer (IARC), 150 Cours Albert Thomas, 69008 Lyon, France.
4. Department of Immunity, Virus and Inflammation. Cancer Research Centre of Lyon (CRCL), Inserm U 1052, CNRS UMR 5286, Université de Lyon, Centre Léon Bérard, 28 rue Laennec, 69373 Lyon CEDEX 08, France.
5. Coordination of Research, Centro Médico Nacional "20 de noviembre", ISSSTE, San Lorenzo 502, Benito Juárez 03100, Cd. Mx., Mexico.
6. INSERM U1052, CNRS UMR5286, Centre de Recherche en Cancérologie de Lyon Université Claude Bernard, Lyon, France.
7. Department of Molecular Genetics, Instituto de Fisiología Celular, Universidad Nacional Autónoma de México (UNAM), Circuito Exterior s/n, Ciudad Universitaria, Coyoacán 04510, Cd. Mx., Mexico.
8. Department of Translational Research and Innovation. Centre Léon Bérard, 28 rue Laennec, 69373 Lyon CEDEX 08, France.

Correspondence to:

VCS: vchagoya@ifc.unam.mx

HHV: hector.hernandez-vargas@lyon.unicancer.fr

Abstract

How cells reach different fates despite using the same DNA template, is a basic question linked to differential patterns of gene expression. Since 5-hydroxymethylcytosine (5hmC) emerged as an intermediate metabolite in active DNA demethylation, there have been increasing efforts to elucidate its function as a stable modification of the genome, including a role in establishing such tissue-specific patterns of expression. Recently we described TET1-mediated enrichment of 5hmC on the promoter region of the master regulator of hepatocyte identity, HNF4A, which precedes differentiation of liver adult progenitor cells *in vitro*. Here we asked whether 5hmC is involved in hepatocyte differentiation. We found a genome-wide increase of 5hmC as well as a reduction of 5-methylcytosine at early hepatocyte differentiation, a time when the liver transcript program is already established. Furthermore, we suggest that modifying s-adenosylmethionine (SAM) levels through an adenosine derivative could decrease 5hmC enrichment, triggering an impaired acquisition of hepatic identity markers. These results suggest that 5hmC is a regulator of differentiation as well as an imprint related with cell identity. Furthermore, 5hmC modulation could be a useful biomarker in conditions associated with cell de-differentiation such as liver malignancies.

Keywords: DNA methylation, differentiation, hepatocytes, hydroxymethylation, progenitor cells.

Graphical Abstract

It has been suggested that 5-hydroxymethylcytosine (5hmC) is an imprint of cell identity. Here we show that commitment to a hepatocyte transcriptional program is characterized by a demethylation process and emergence of 5hmC at multiple genomic locations. Cells exposed to an adenosine derivative during differentiation did not reach such 5hmC levels, and this was associated with a lower expression of hepatocyte-markers. These results suggest that 5hmC enrichment is an important step on the road to hepatocyte cell fate.

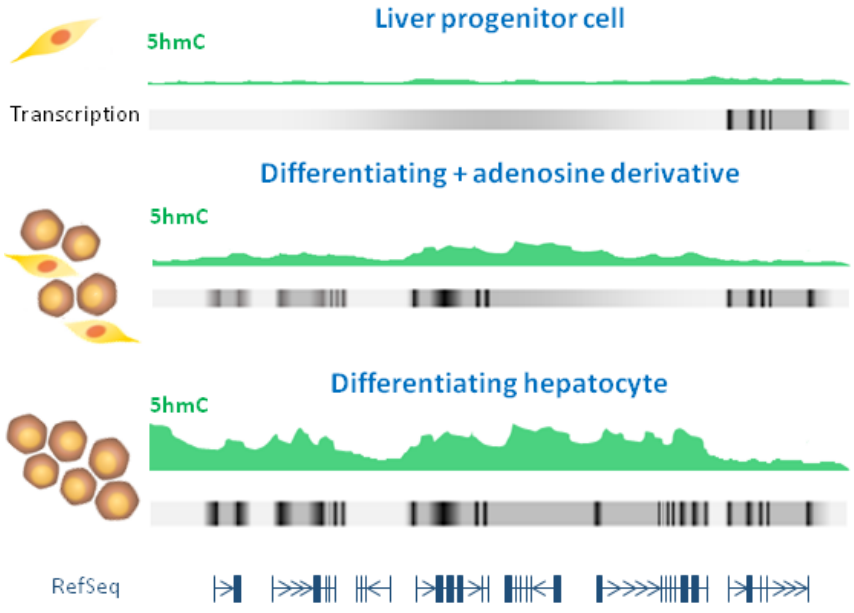

Introduction

Chronic liver disease comprises multiple different pathologies, such as non-alcoholic fatty liver disease, liver fibrosis and cirrhosis. Commonly these pathologies are the background to develop liver cancer [Sia et al., 2017], which encompass a heterogeneous group of malignant tumours with different histological features, and unfavourable prognosis. Hepatocellular carcinoma (HCC) and intrahepatic cholangiocarcinoma (iCCA) are the most common primary cancers of the liver [Ervik et al., 2016], which was estimated as the seventh in incidence and fourth highest cause of cancer-related death worldwide in 2018 [The, 2018].

Several studies point to adult hepatocytes as the cell of origin of liver cancer [Mu et al., 2015; Shin et al., 2016], through de-differentiation into hepatocyte precursor cells that later become HCC cells or through *trans*-differentiation into biliary-like cells, which give rise to iCCA [Sia et al., 2017]. In spite of their different aetiologies, chronic liver damage is a shared factor in HCC and iCCA development. This constant insult results in high cell turnover, and aberrant genetic and regulatory landscapes that favours liver cell transformation [Castelli et al., 2017]. As transformation takes place, progenitor-like cells accumulate, in a process known as ductular reaction [Mu et al., 2015] where cholangiocytes could also *trans*-differentiate into stress-resistant hepatocytes to help in liver repopulation of damaged regions [Manco et al., 2019]. This underscores the importance of understanding hepatocyte differentiation as a key process in chronic liver injury, where cell identity is lost.

With the advance on the understanding of chromatin organization of the eukaryotic genome it has been clear that epigenetics influences both, normal human biology and disease [Recillas-Targa, 2014], being DNA methylation one of the most studied epigenetic modifications. DNA methyl-transferases (DNMTs) establish 5-methylcytosine (5mC) from S-adenosylmethionine (SAM), the principal methylating agent in the body derived from the methionine cycle [Tehlivets et al., 2013]. In humans, the liver is the organ with the highest turnover of SAM and metabolism of methionine [Mato et al., 2002]. It has been suggested, that adenosine could be able to modulate SAM methylation in the liver, promoting either the metabolic flow of methyl group

transfer-reactions or their inhibition by inducing S-adenosylhomocysteine (SAH) accumulation [Chagoya de Sanchez et al., 1991].

As opposed to DNMTs, Tet Methylcytosine Dioxygenases (TET) are involved in the oxidation of methylated cytosine in DNA forming 5-hydroxymethylcytosine (5hmC) and together, with the base excision DNA repair machinery, leading to active cytosine demethylation [Kriaucionis and Heintz, 2009; Tahiliani et al., 2009]. Moreover, 5hmC is emerging as a stable modified base with unique functions that suggests that the dynamic distribution of 5hmC could be an acquired "imprint" of cell identity during adult progenitor cell differentiation in several tissues (reviewed in [Ecsedi et al., 2018]) including liver. Indeed, using an *in vitro* model of hepatocyte differentiation, we recently described a switch in 5mC/5hmC state of promoter 1 (P1) of the master transcription factor (TF) of hepatocyte identity *HNF4A* [Ancey et al., 2017].

The capacity to modulate epigenetic modifications, offers an opportunity to develop new strategies for the early prevention and treatment of diseases [Li et al., 2018]. An adenosine derivative, IFC-305 (UNAM Patent 207422), administered in a cirrhotic rat model has previously been able to recover SAM levels abrogated in cirrhosis which triggers the re-establishment of 5mC and 5hmC in this condition [Rodriguez-Aguilera et al., 2018]. IFC-305 also has several hepatoprotective properties (reviewed in [Rodríguez-Aguilera et al., 2019]), such as, reduction of fibrosis and amelioration of liver function through regulation of transcriptome [Perez-Carreon et al., 2010], promotion of cell cycle recovery in the liver [Chagoya de Sanchez et al., 2012], anti-inflammatory effects during cirrhosis [Perez-Cabeza de Vaca et al., 2018], prevention of hepatic stellate cells (HSCs) activation [Velasco-Loyden et al., 2010], and anti-carcinogenic effects [Velasco-Loyden et al., 2017].

Here, we asked whether 5hmC is present and/or redistributed in the genome of differentiating hepatocytes. We describe 5hmC genomic enrichment and its relationship with gene expression. Moreover, we show that 5hmC accumulation and hepatocyte differentiation are impaired by perturbing SAM metabolism using IFC-305.

Results

HepaRG cells differentiated for 1 week express hepatocyte markers

HepaRG cells are bipotent liver progenitor cells that differentiate *in vitro* after 4 weeks into either hepatocytes or cholangiocytes. Our group previously found a TET1-dependent switch from methylated to hydroxymetylated DNA status at *HNF4A* promoter P1 in HepaRG cells, triggering differentiation at one week of cell culture [Ancey et al., 2017]. In order to determine the gene expression profile at this stage of hepatocyte differentiation (Figure 1A), RNA was isolated and a transcriptome analysis was performed to identify differentially expressed genes (DEGs) (Figure 1B). We found 4175 DEGs upon one week of differentiation. While down-regulated genes (n=2066 probes, corresponding to 1772 hg19-annotated genes) were related to lymphoblasts and endothelial cells (Figure 1C), over-expressed genes (2109 probes, corresponding to 1822 hg19-annotated genes) were highly associated with liver and foetal liver cells (Figure 1D). In addition, we found that over-expressed genes were enriched in targets of the *HNF4A* transcription program (Supplementary Figure S1A). Pathways most related with these genes included biological oxidation and metabolism related signalling pathways (Supplementary Figure S1B). Gene ontologies revealed fatty acids, regulation of lipids, and triglyceride homeostasis, metabolic processes as well as oxidoreductase, and endopeptidase and alcohol dehydrogenase activities (Supplementary Figures S1C and S1D). On the other hand, down-regulated genes in differentiating cells are associated with *E2F4* transcriptional program (Supplementary Figure S1E), signalling pathways involved in cell cycle progression, biological process related with DNA metabolism and replication, and molecular functions implicated in DNA dependent ATPase activity (Supplementary Figures S1F - S1H). We assessed expression levels of hepatocyte markers over-expressed in transcriptome data and validated the overexpression of *HNF4A* P1 isoforms, *GSTA,* and *ALDOB* (Figures 1E- 1H).

Altogether, these results indicate that after 1 week of differentiation, HepaRG cells have turned on a hepatocyte-like expression program, while proliferative related genes become progressively silenced.

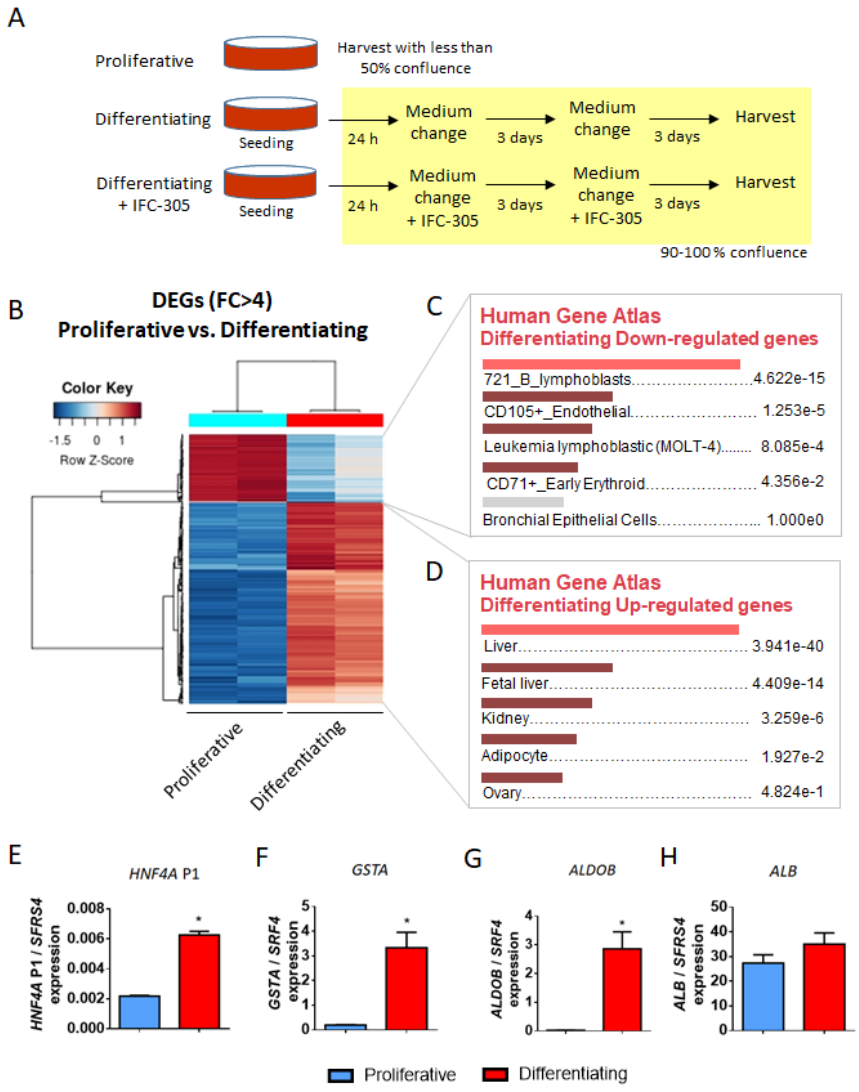

Figure 1. Liver transcription program is expressed in HepaRG cells at 1 week of differentiation. (A) HepaRG differentiation model. For proliferative (progenitor) condition, cells were seeded and trypsinized after reaching 50% confluence; for differentiating conditions, cells were seeded at 70-80% confluence in order to reach 100% confluence 24 h after seeding. (B) Transcriptome was analyzed in both conditions. Heatmap represents differentially expressed genes (DEGs) with fold change greater than four. Cell/tissues types associated with genes down-regulated (C) and up-regulated (D) in differentiating cells (EnrichR), adjusted p-values are shown. (E-H) Expression of hepatocyte markers was validated by RT-qPCR, data represent mean ± SEM 3 independent cultures/condition; *Statistical difference ($p < 0.05$).

HepaRG differentiation involves an early 5hmC landscape remodelling

Considering that at 1 week of HepaRG differentiation there is a TET1-mediated 5hmC enrichment on *HNF4A* promoter P1 [Ancey et al., 2017] and the transcriptome already reflects a hepatocyte-like profile, we chose this time point to assess 5hmC levels of the HepaRG cell line compared to its proliferative state. Immunostaining against 5hmC reveals the presence of this modified cytosine in differentiating cells, in contrast with its almost complete absence in proliferative HepaRG cells (Figure 2A and Supplementary Figure S2).

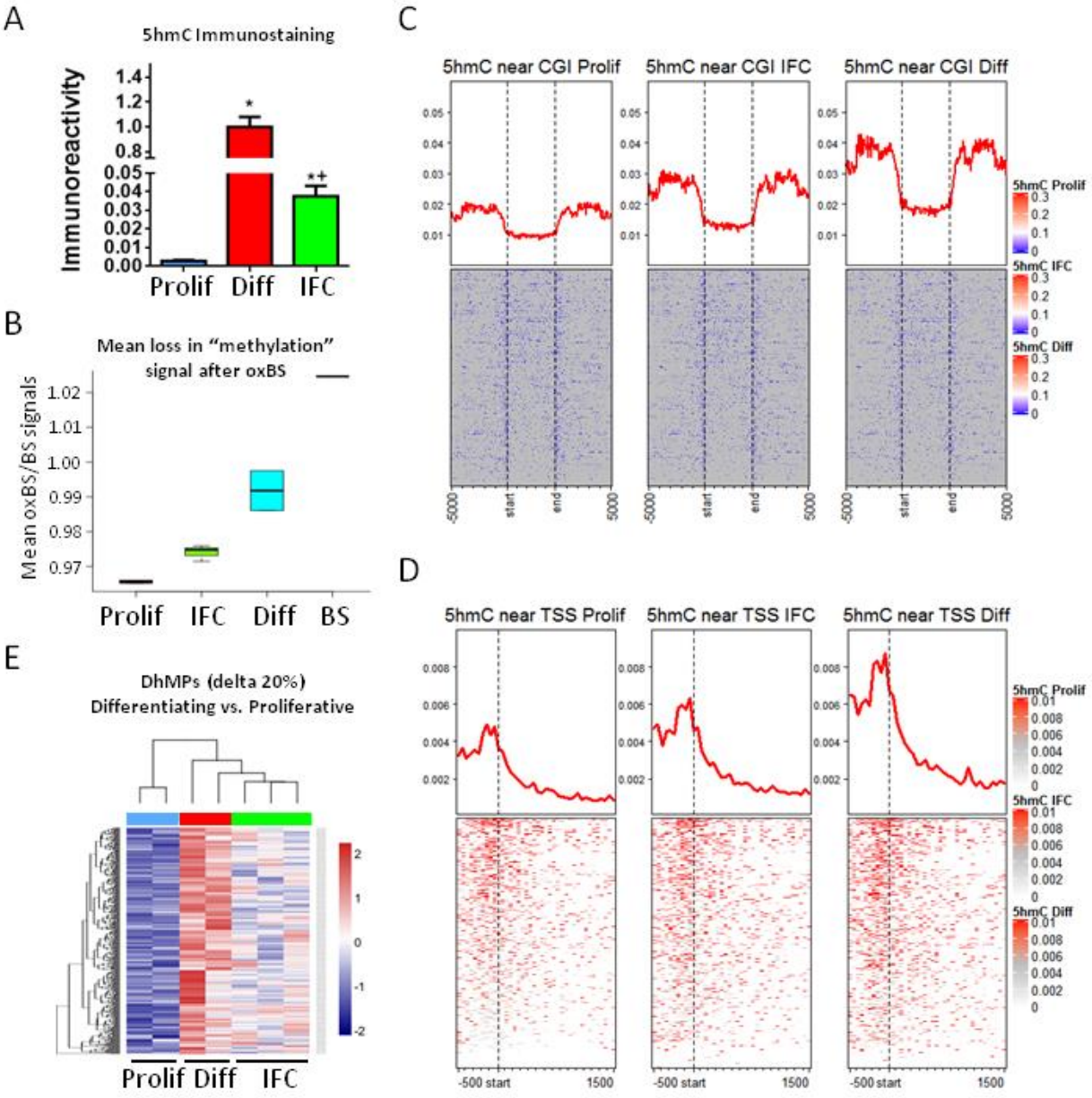

Figure 2. 5hmC genome-wide enrichment during hepatocyte differentiation. (A) Immunofluorescence of 5hmC in proliferative (Prolif), differentiating (Diff) and differentiating + IFC-305 (IFC) HepaRG cells. Quantification barplots of 5hmC signal are based on mean ± SEM from 3 fields/group. *Statistical difference ($p < 0.05$), or *+ ($p < 0.05$) when compared with proliferative and differentiating cells. (B) The same conditions were assessed for base-resolution 5mC/5hmC, using BS and OxBS followed by EPIC beadarray hybridization (see Methods). Proportion of signal loss after oxidation (mean oxBS signal / mean BS signal) was used as an estimation of global 5hmC in each condition. BS represents the variation between two BS technical replicates. (C) Global distribution of 5hmC for one representative sample of each condition, according to CpG islands (CGI) (C) and transcription start sites (TSS) (D). In both cases, 5hmC levels are averaged across all hg19-annotated genomic regions. (E) Heatmap showing hydroxymethylome comparison between differentiating and proliferative cells. Differentially hydroxymethylated positions (DhMPs) were filtered by the magnitude of change in methylation (delta beta) of at least 20% and p-adjusted value < 0.05. Two independent cultures were used for proliferative and differentiating cells, and three independent cultures for differentiating + 1 mM IFC-305.

Next, we proceeded to evaluate the hydroxymethylome at base resolution. At this point it is worth mentioning that conventional DNA bisulfite conversion is not able to distinguish 5mC and 5hmC. An alternative to evaluate both modifications independently, is the use of oxidative bisulfite; which allows for the identification of 5mC through the oxidation of 5hmC to 5-formylcytosine (5fC) with KO_4Ru [Booth et al., 2013]. Therefore, we isolated DNA from proliferative and differentiating HepaRG cells and performed oxidative and conventional bisulfite conversion (oxBS and BS, respectively), followed by hybridization on Infinium EPIC arrays.

Using only oxBS signal, we observed the expected distribution of 5mC in CpG islands (CGIs) and transcription start sites (TSS) (Supplementary Figure S3). Although no global differences were evident between conditions, we identified 3351 differential methylated positions (DMPs) displaying lower methylation after one week of differentiation (Supplementary Figure S4A).

Roughly, a loss of signal after oxBS relative to conventional BS indicates the presence of 5hmC. While analysis of genomic data showed almost no signal loss between oxBS and BS in proliferative cells, a significant global loss was evident in differentiating cells suggesting a global gain in 5hmC during the first week of differentiation (Figure 2B). Such gain in 5hmC was consistent, regardless of relative location across CGIs and TSS (Figure 2C and 2D).

Next, we studied 5hmC by directly comparing oxBS and BS data. While no significant global signal in 5hmC was observed in proliferative cells (Figure 2B), we identified a gain of 5hmC at 11766 sites in differentiating cells, defined by a significant reduction of methylation signal after oxBS of at least 10% (5hmC peaks). Differential hydroxymethylation performed at these sites revealed 6952 differentially hydroxymethylated positions (DhMPs) between proliferative and differentiating cells (Figure 2E). In addition, we identified 2482 differentially hydroxymethylated regions (DhMRs). Among these, a 3-CpGs region on *HNF4α* was identified as well as a 21-CpGs region, a 5-CpGs region and two 3-CpGs regions on *IDH3G, TET1* and *TET3* genes, respectively (Supplementary Figures S5 – S9). All of these genes are involved themselves in establishment of 5hmC.

Together, these results show that while 5hmC is poorly present at the HepaRG progenitor stage, it is enriched at multiple genomic locations upon entering hepatocyte differentiation.

Genomic context of differentially hydroxymethylated sites associated with early hepatocyte differentiation

In order to know whether there is a relationship between 5hmC enrichment and gene expression, we compared the nearest associated gene of DhMPs with DEGs associated with one week of differentiation (described above). Out of 6952 DhMP-associated genes, 522 and 482 fall near an up- or a down-regulated DEG, respectively (Figure 3A). Globally, however, there was no difference in the genomic 5hmC distribution in DEGs (up- or down-regulated) compared to control genes (Figure 3B).

DhMPs associated with increased gene expression were related with liver and fetal liver cell types, and enriched in pathways involved in androgen receptor (*AR)* and Nuclear Factor Erythroid 2-Related Factor 2 (*NFE2L2*) transcription programs as well as part of metabolism signalling pathways (Supplementary Figures S10A – S10C). DhMPs associated with down-regulated genes, were related with B lymphoblasts and enriched in pathways involved in cell cycle control, such as the *E2F4* transcription program (Supplementary Figures S10D - S10F).

Next, in order to explore a less evident role of 5hmC enrichment on gene expression, we compared distribution of DhMPs relative to different genomic annotations. DhMPs were enriched in intronic regions, and depleted from promoters and CGIs (Figure 3C and 3D). In addition, when we assessed genomic annotated features of liver HepG2 cells, we found an over-representation of DhMPs in weak transcription and transcription elongation loci (Figure 3E).

In summary, these results show that only 17% of 5hmC enrichment during HepaRG differentiation can be directly associated with gene expression changes at the neighbouring genomic location.

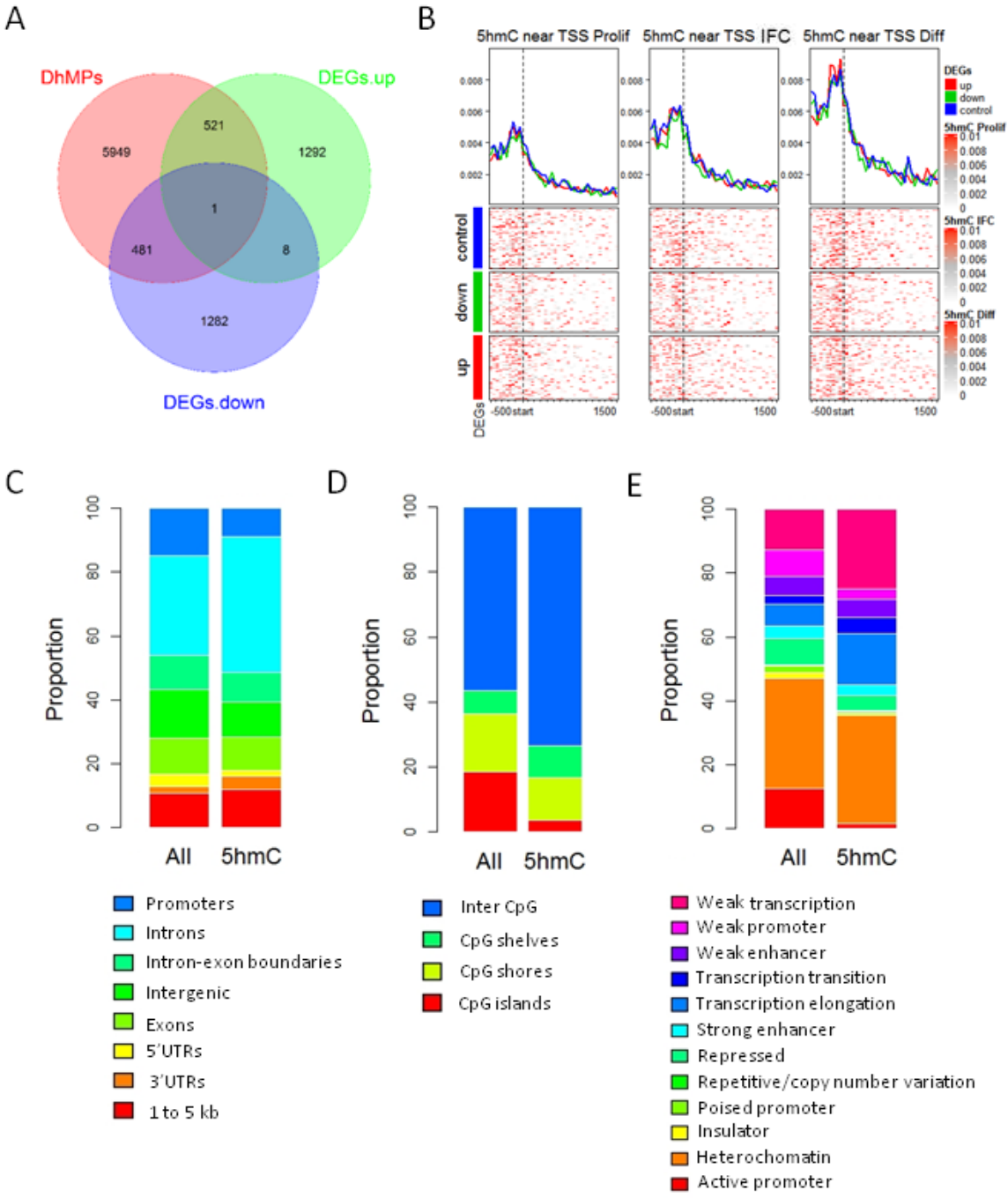

Figure 3. Association between 5hmC and differential expression. (A) Venn diagram representation of the overlaps between 5hmC differentiated positions (DhMPs) and differential expressed genes (DEGs). For this analysis, DhMPs were annotated to its nearest gene. (B) Global distribution of 5hmC according to transcription start sites. 5hmC levels are averaged across all hg19-annotated genomic regions, in turn divided into control, up-regulated, or down-regulated genes. DhMPs were also annotated according to gene features (C), distribution according to CpG islands (D), and HepG2 chromatin states (ChromHMM) (D). For each genomic context, distribution is shown separately for all DhMPs, and all EPIC beadarray probes, as a control. Two independent cultures were used for proliferative and differentiating cells, and three independent cultures for differentiating + 1 mM IFC-305.

Methyl-donor perturbation has repercussions for hepatocyte differentiation

Considering the genome-wide increase in 5hmC upon early HepaRG differentiation, we evaluated if a disruption in 5hmC levels could modify the hepatocyte differentiation process. To assess this question, we used a previously described adenosine derivative, IFC-305, which is able to ameliorate liver function and reduce collagen accumulation during cirrhosis. IFC-305 recovers both 5mC and 5hmC, abrogated during cirrhosis, improving SAM availability [Rodriguez-Aguilera et al., 2018].

Firstly, we evaluated HepaRG cell viability in response to IFC-305 exposure and we found that viability was not affected at concentrations of up to 1 mM for 1 week of differentiation (Supplementary Figure S11). With this maximum concentration, we analysed the expression of hepatocyte markers in response to different concentrations of IFC-305 and noticed 1 mM triggered lower values of *ALDOB* and *GSTA* in comparison with non-treated differentiating cells (Figure 4A). Albumin expression did not change, neither on differentiating non-treated cells nor after IFC-305 treatment, except for a reduction in expression levels with 5 mM IFC-305 (Figure 4A) compared with proliferative cells. Regarding *HNF4A* isoform regulated by P1 gene promoter, its expression showed the same increment level with 0.2 and 1 mM IFC-305 and non-treated differentiating cells, but a concentration of 5 mM generated an over-expression of this isoform compared with proliferative cells (Figure 4B). On the other hand, *HNF4A* isoforms regulated by P2 gene promoter increased its expression only with 0.2 and 1 mM IFC-305 on differentiating cells in comparison with proliferative cells (Figure 4B). However, at the protein level, 1 mM IFC-305 was associated with a reduced HNF4α nuclear immunoreactivity signal in differentiating cells compared with non-treated differentiating ones (Supplementary Figure S12).

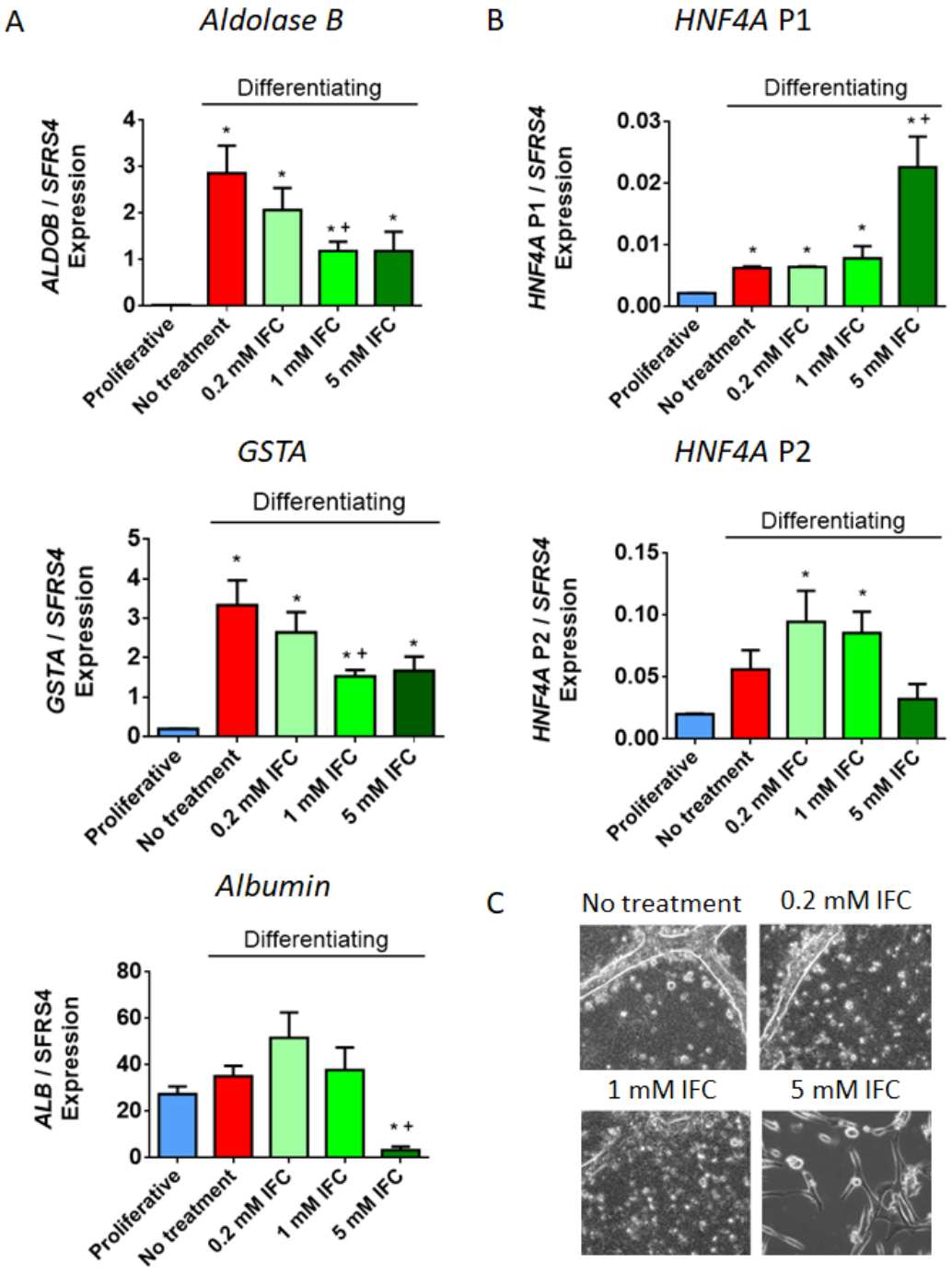

Figure 4. Impaired hepatocyte marker expression upon adenosine derivative exposure. (A) Expression of hepatocyte markers was assessed by RT-qPCR, data represent mean ± SEM 3 independent cultures/condition. (B) Expression of isoforms from HNF4A promoters 1 and 2 was assessed by RT-qPCR, data represent mean ± SEM 3 independent cultures/condition. (C) Phase contrast images showing HepaRG differentiated phenotype after 20 days of exposure to an increasing gradient of IFC-305. Representative 20x magnification images from seven independent cultures are shown. *Statistical difference ($p < 0.05$). *+Statistical difference ($p < 0.05$) when compared with proliferative and differentiating non-treated cells.

This pattern of expression of hepatocyte markers suggests that HepaRG exposure to IFC-305 during differentiation influences hepatocyte maturation. Exploring this possibility, we extended the differentiation model to a longer period (20 days). At 13 days, differentiating non treated cells show hepatocyte-like cell morphology, emergence of small polygonal cells with increased granularity and organized in well-delineated trabeculae, separated by bright canaliculi-like structures (Supplementary Figure S13). IFC-305 delays this phenotype in a concentration-dependent manner, with 1 mM IFC-305 treated cells showing a phenotypic delay of at least one week, and 5 mM IFC-305 retaining a proliferative-like phenotype up to day 20 of differentiation (Figure 4C and Supplementary Figure S13). Such phenotypic variation, reduced levels of hepatocyte markers (i.e. *HNF4A* isoforms regulated by P1 gene promoter, *AldoB* and *GSTA)* and increased expression of *HNF4A* isoforms regulated by P2 gene promoter, suggest that IFC-305 is able to delay hepatocyte differentiation.

Methyl-donor perturbation disrupts the 5hmC landscape associated with hepatocyte differentiation

Proliferative HepaRG cells were exposed to 1 mM IFC-305 in differentiating conditions during 1 week. Under these conditions, 5mC reduction and 5hmC accumulation are impaired, as assessed by IF and global oxBS and BS analyses (Figures 2A and 2B, #Supplementary Figure S4B). Similarly, only a fraction of differentiation-related DhMPs are detected in presence of IFC-305 using base-resolution methylation bead arrays (Figure 2E). Despite this attenuated phenotype, differential hydroxymethylation was identified at 8460 gene associated CpGs sites (Figure 5A), and 1890 regions, relative to proliferative cells. Comparing these genes with up-regulated DEGs in differentiating cells, we found an overlap of 173 genes which are highly associated with liver expression, according to the ARCHS4 Tissues data base (Supplementary Figure 14).

In order to validate the increment of 5hmC through the differentiation process, we performed hydroxymethylated DNA immunoprecipitation assays (hMeDIP) on selected regions with the highest 5hmC increase. We assessed two different regions in the vicinity of *TCHP and RAB7A.* Furthermore, we evaluated the region where a switch in 5mC/5hmC on *HNF4A* P1 occurs, using *SFRS4* promoter as a control region. We could observe a constant level of 5hmC on *SFRS4*

promoter in proliferative and differentiating cells (Figure 5B). *HNF4A P1* showed an increment of 5hmC at 1 week of differentiation as previously shown [Ancey et al., 2017]. A similar behaviour was found in *TCHP* and *RAB7A* regions (Figure 5B).

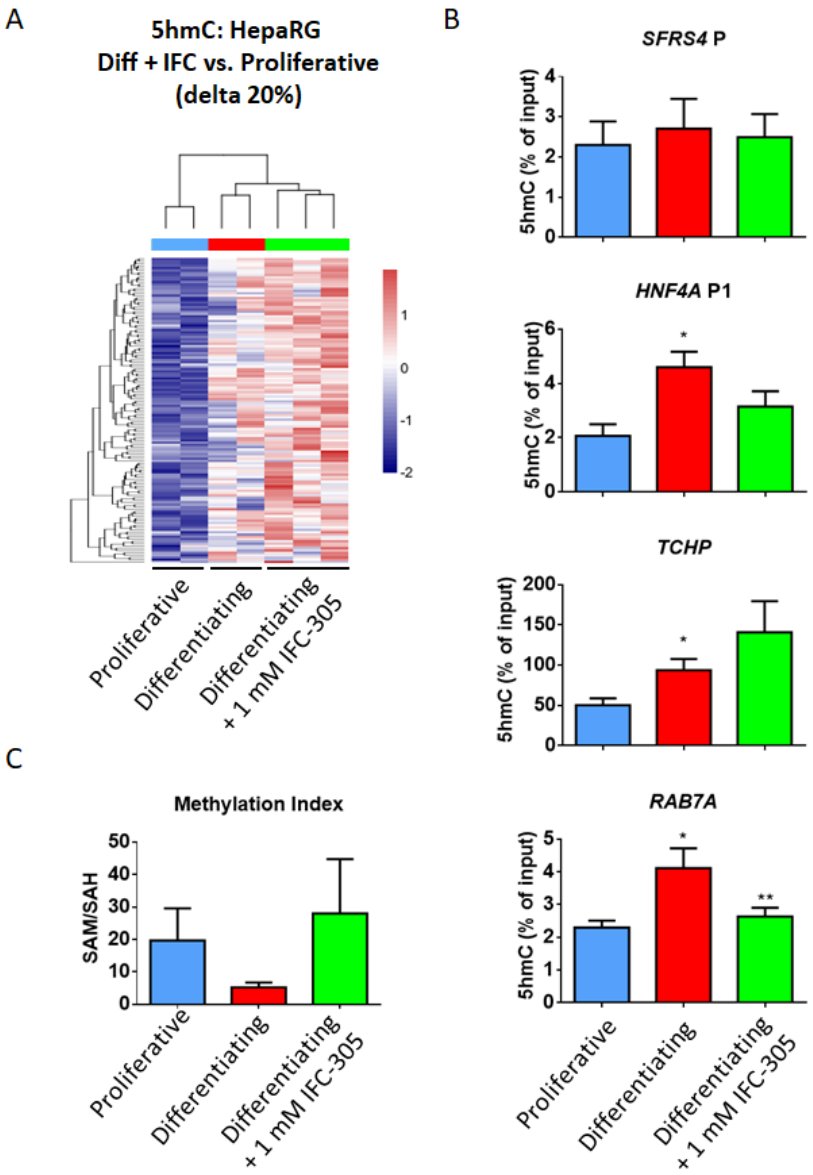

Figure 5. Reduced 5hmC enrichment under methyl-donor exposure. (A) 5hmC in proliferative, differentiating and differentiating + IFC-305 HepaRG cells, as assessed using BS and OxBS followed by EPIC beadarray hybridization (see methods and Figure 2). Heatmap showing hydroxymethylome comparison between differentiating + IFC-305 and proliferative cells. Differentially hydroxymethylated positions (DhMPs) were filtered by the magnitude of change in methylation (delta beta) of at least 20% and p-adjusted value < 0.05. Two independent cultures were used for proliferative and differentiating cells, and three independent cultures for differentiating + 1 mM IFC-305. (B) Validation of 5hmC changes. 5hmC enrichment was assessed by hMeDIP and qPCR; *SFRS4* gene promoter was used as non-5hmC enriched control region, HNF4A promoter P1 was used as 1 week differentiation 5hmC enrichment positive control, data represent mean ± SEM 3 independent cultures/condition; *Statistical difference ($p < 0.05$) compared with proliferative cells. **Statistical difference ($p < 0.05$) compared with differentiating cells. (C) Content of S-adenosylhomocysteine (SAH) and S-adenosylmethionine (SAM) was assessed using HPLC in different experimental conditions and generated by standards. Barplots indicate the methylation index, calculated as the SAM/SAH ratio, mean ± SEM from 4 cultures/condition.

Next we asked how an adenosine derivative is able to disturb 5hmC levels triggering a differentiation delay on hepatocytes. To address this question we evaluated several components of the methionine cycle, which is the metabolic pathway responsible for biological

trans-methylation reactions [Kharbanda, 2007]. Such reactions, including DNA methylation, could be modified by SAM availability as well as SAH levels [Auta et al., 2017; Garcea et al., 1989]. We previously showed that adenosine as well as IFC-305 are able to modulate SAM levels, favouring phospholipids methylation [Chagoya de Sanchez et al., 1991] and restoring global DNA methylation and 5hmC levels in a CCl_4-mediated cirrhosis model [Rodriguez-Aguilera et al., 2018]. With this rationale, we evaluated the content of adenosine, SAM and SAH, through HPLC (Supplementary Figure S15). A trend to reduced SAM levels was observed in differentiating cells (Supplementary Figures S15A, S15B and S15E), consistent with global 5mC reduction at 1 week of HepaRG differentiation (Supplementary Figure S4A), with a non-significant trend to increase in SAH levels (Supplementary Figures S15A, S15B and S15F). Methylation index (SAM/SAH ratio) derived from these data, was lower and less variable in differentiating cells (Figure 5C). Higher and dispersed methylation index was observed in proliferative and IFC-305 exposed cells and correlates with high 5mC abundance genome wide (Supplementary Figure S4B). Adenosine measurement showed an increment in differentiating compared with proliferative cells, with the highest levels observed in differentiating + 1 mM IFC-305 cells, although not statistically significant (Supplementary Figure S15A, S15B, S15C and S15G; standard chromatogram is shown in Supplementary Figure S15D).

These results suggest that IFC-305 generates a methylation environment which competes with the demethylation wave associated with hepatocyte differentiation and highlights the importance of 5hmC enrichment in this process.

Discussion

In this work, we have assessed the link between DNA methylation dynamics and the establishment of the hepatocyte-like transcription program after one week of HepaRG cells differentiation. We found that HepaRG cells at one week of differentiation have already triggered a hepatocyte transcriptional program, a time where there is a reduction of DNA methylation and 5hmC emerges genome-wide. While only 17% of DhMPs were associated to

changes in gene expression, they were enriched in introns and depleted from promoters and CGIs. Finally, we found that perturbation of S-adenosylmethionine metabolism through an adenosine derivative, can reduce 5hmC enrichment associated to differentiation, triggering reduced levels of expression of hepatocyte markers.

Since its rediscovery in 2009 [Kriaucionis and Heintz, 2009; Tahiliani et al., 2009], 5hmC emerged as an intermediate of active DNA demethylation, but increasing evidence considers this modified cytosine as the "sixth base" because of its stability and its distinct functionality. Furthermore, 5hmC events correlate with key differentiation steps in mammal adult progenitors cells [Ecsedi et al., 2018]. Analysis of BS and OxBS from one week differentiating HepaRG cells as well as 5hmC immunostaining (Figures 2A and 2B, Supplementary Figure S2), showed a genome wide increase of this modified cytosine which corresponded with our previous findings on the *HNF4A P1* gene promoter [Ancey et al., 2017]. This behaviour of 5hmC enrichment has been described also in tissues from every germ layer, for example: enterocytes [Chapman et al., 2015; Kim et al., 2016], myocytes [Zhong et al., 2017], adipocytes [Dubois-Chevalier et al., 2014; Yoo et al., 2017] and neurons [Hahn et al., 2013; Li et al., 2017]. Hence, we could suggest that 5hmC enrichment in the last stage of cell differentiation is a mechanism widely present in human tissues; besides that, distribution of this mark at specific genomic locations could be characteristic of each cell type as it is observed in adult tissues [Lin et al., 2017].

It has been described that cell specification is accompanied by a stark transition in epigenetic landscape from a uniquely accessible state in pluripotency, to increasingly restrictive configurations in differentiated stage [Zhu et al., 2013]. However, 5hmC is often related to highly expressed cell specific genes [Li et al., 2016b; Lin et al., 2017]; hence in the present study, it is potentially playing a role in opening chromatin regions involved in hepatocyte specific transcription programs like metabolic pathways and with liver specialized functions as synthesis of complement components, regulation of lipids metabolism, platelet degranulation and oxidoreductase activity (Supplementary Figure S1A-S1D). Furthermore, we validated 5hmC enrichment on *HNF4A* and found DhMRs associated with *TET*s, and *IDH3G* (Supplementary Figures S5-S9), which could be related with a 5hmC feedback loop to reinforce differentiation. In

line with these finding, it has been recently described that *TET1* is regulated through DNA methylation on its promoter [Li et al., 2016a]. This does not exclude that some other regulators could cooperate with this process or could also be generating restrictive chromatin context in non-hepatocyte related loci.

We found 5hmC enrichment in gene bodies (introns) and transcriptional features (Figure 3C and E) upon differentiation, features that partially agree with a report in adult mouse liver which indicates 5hmC is enriched in intragenic regions [Lin et al., 2017]. Similarly, in adult healthy liver, a specific 5hmC landscape has been described, which includes a bimodal 5hmC accumulation around TSS and an increased level along gene bodies, with another peak right after transcription termination [Li et al., 2016b]. Furthermore, we noticed that some DhMPs might be related with distal regulatory elements, as it could be the case for the 5hmC region associated with *TET3* (Supplementary Figure S9) which colocalizes with an enhancer for adult liver and overlaps with H3K4me1 and H3K27ac histone mark signals in HepG2 cells, as reported on the Epigenome Road Map Consortium and ENCODE, respectively.

In order to understand if acquisition of 5hmC is a key factor for differentiation, we assessed the effect of an adenosine derivative, IFC-305, which is able to modulate 5mC and 5hmC levels during experimental cirrhosis [Rodriguez-Aguilera et al., 2018]. We round that the hydroxymethylome of HepaRG cells exposed to IFC-305 presents an intermediate state between proliferative and differentiating cells (Figures 4 and 5, Supplementary Figure S13). This could be explained by the capacity of IFC-305 to increase SAM levels (Supplementary Figure S15E). SAM increase favours a methylating environment which could compete with DNA demethylation, therefore bringing a lower enrichment of 5hmC associated with attenuated differentiation. Contrary to our approach where cells are exposed to a SAM stimulating compound, a mouse model of methionine-choline-deficient diet which reduces SAM availability, did not cause a significant reduction of 5mC levels, instead inducing an up-regulation of Tet2, Tet3, thymine DNA glycosylase and apurinic/apyrimidic-endonuclease 1, and increased expression of Dnmt1 and Dnmt3a [Takumi et al., 2015]. Thus, while methylation dynamics could overcome SAM

deficiency, SAM increase leads to reduced 5hmC enrichment with the consequent delay in differentiation evident at longer culture time (Supplementary Figure S13).

The possibility to modulate differentiation through regulation of 5hmC represents a relevant tool. In this sense, some studies indicate that one of the early alterations in HCC is a significant decrease of global genomic 5hmC, a behaviour also observed in hepatitis B virus infection [Liu et al., 2018], cirrhosis [Rodriguez-Aguilera et al., 2018], and during HSCs *trans*-differentiation to miofibroblast [Page et al., 2016]. Altered patterns of 5hmC are not only detectable in tumour-normal tissue pairs from resections or biopsies, but also in circulating DNA from cancer patients [Pfeifer and Szabo, 2018] suggesting that 5hmC is a potential biomarker for early cancer detection. Moreover, the possibility to modify cell identity through regulation of 5hmC distribution and levels represents an innovative pharmacological method to prevent or reverse certain pathologies.

Conclusions

Our findings illustrate how differentiation of liver progenitor cells involves a demethylation process as well as a genome-wide increase in 5hmC. This 5hmC increase matches the enrichment of the same modified cytosine on promoter P1 of hepatocyte differentiation master regulator, *HNF4A*, and the activation of a liver transcriptional program at 1 week of differentiation. Moreover, a fraction of enriched 5hmC sites could be associated with over-expressed genes in differentiating cells. Furthermore, we found that cells exposed to an adenosine derivative presented lower 5hmC and did not reach levels of hepatocyte-expression markers observed in differentiating cells as well as presenting a less-differentiated phenotype. These results suggest a physiological role of 5hmC in acquisition of cell identity and support this modified cytosine as a potential biomarker for early detection of liver pathologies related with de-differentiation processes such as liver cancer.

Methods

Chemicals

Reagents were from Sigma Chemical Co. (St. Louis, MO). IFC-305 is the aspartate salt of adenosine: 2-aminosuccinic acid-2-(6-amino-9*H*-purin-9-yl)-5-(hydroxymethyl) tetrahydrofuran-3,4-diol (1:1). It was synthesized in the laboratory in agreement with UNAM patent 207422.

HepaRG cell culture

Human HepaRG cells (Biopredic) were cultured as follows. Differentiating cells ($4.4 \times 10^4/cm^2$) were grown for 1 week in William's E medium (Gibco 12551-032) supplemented with 10% fetal bovine serum (Eurobio CVFSVF0001), 1x penicillin/streptomycin (Gibco 10378016), 5 µg/mL insulin (Sigma I9278) and 3×10^{-5} mM hydrocortisone (Sigma H0888) in 6 well plates (Figure 1), medium was replaced 24 h after seeding and once more after 3 days. For proliferative conditions, cells were seeded at low confluence, avoiding cell to cell contact to prevent cell differentiation. Treatment with IFC-305 began 24 h after cell seeding, and cells were re-treated at 3 day of culture when medium was replaced; this compound was directly solubilised in William's E medium (Figure 1). Cells were harvested 7 days after seeding.

Transcriptome analysis

RNA was isolated, directly from culture plate, with TRIzol (Invitrogen 15596018) and treated with DNase (Invitrogen 18068-015). Using the Illumina TotalPrep-96 RNA Amp Kit (Ambion 4393543), 500 ng of RNA was reverse transcribed into cDNA, which undergoes second strand synthesis to become a template for T7 RNA polymerase and thereby labelled with biotin-UTP. Hybridization of 2000 ng of labelled cDNA to the Illumina HumanHT-12 v3 (Illumina) were processed according to the manufacturer's protocol. Slides were scanned immediately using Illumina BeadStation iScan (Illumina). Assays were performed in two independent cell cultures/condition.

Quantitative RT-PCR

cDNA synthesis was performed from 2 µg of total RNA using M-MLV Reverse Transcriptase (Invitrogen 28025-013) and random primers. All quantitative PCR assays were performed independently in 3 cell cultures/condition in duplicate, with the delta-delta Ct method, using Mesa green qPCR 2x MasterMix Plus (Eurogentec 05-SY2X-06+WOU) on a CFX96 PCR system (Bio-Rad). Primers were described previously [Ancey et al., 2017].

Cell survival evaluation

Differentiating and IFC-305 treated HepaRG cells cultured for 1 week were trypsinized and counted using TC20 automated cell counter (Bio-Rad) with dual chamber slides and trypan blue (Bio-Rad 1450003). Total cell and live cell numbers were determined automatically and % survival was determined by comparing live cells in each condition, with the mean of non-treated live cells which was considered as 100 %.

Immunofluorescence

400 000 HepaRG cells/well were seeded in 6-wells plate with 4 coverslips/well, and were treated according to differentiation model with or without IFC-305. 100 000 cells were seeded in the same conditions during 24 h and were designated as proliferative cells. At different time points cells were washed with PBS, fixed in 4 % formaldehyde and washed twice with PBS. Primary antibodies for immunofluorescence were anti-HNF4α (Cell signalling 3113S), anti-5hmC (Active Motif 39769). After secondary antibodies, coverslips were washed and mounted on a slide with a mounting medium containing DAPI (Vectashield). Fluorescence was visualized with an Olympus Inverted Microscope model IX71 and images captured with Evolution/QImaging Digital Camera (Cybernetics). Data analysis was performed using ImageJ (National Institutes of Heatlh).

Oxidative Bisulfite and Methylation Bead Arrays

For genomic DNA isolation, 500 µL of lysis buffer (50 Mm Tris-HCl pH 8, 100 mM EDTA, 100 mM NaCl, 1% SDS and 0.5 mg/mL proteinase K) were added to wells from 6-well plates, previously washed twice with PBS 1x. Cells were detached by pipetting and suspension was incubated 2 h

at 55°C. 200 µL of 6 M NaCl was added, sample was mixed and centrifuged 10 min at full speed. Supernatant was recovered and DNA was precipitated with 500 µL isopropanol, washed with 500 µL 70% ethanol and dried by inverting the tube on a tissue. DNA was resuspended with 25 µL injectable water. 1000 ng DNA was oxidative bisulfite- and conventional bisulfite-converted using TrueMethyl Seq Kit (Cambridge Epigenetix) according to manufacturer's instructions. This technique oxidises 5hmC to 5fC which is read as thymine (non-modified cytosine and 5mC are read as thymine and cytosine respectively, as in conventional bisulfite) [Booth et al., 2013]. Converted DNA was analysed with MethylationEPIC arrays (Illumina) using recommended protocols for amplification, labelling, hybridization, and scanning. For proliferative and differentiating cells, each methylation analysis was performed in two independent culture wells and for IFC-305 treatment in triplicates.

Bioinformatic Analyses

Raw expression and methylation data were imported and processed using R/Bioconductor packages for Illumina bead arrays [Du et al., 2008]. Data quality was inspected using boxplots for the distribution of expression signals, and inter-sample relationship using multidimensional scaling plots and unsupervised clustering. For methylation data, we removed low quality probes with a detection P value > 0.01 in more than 10% of the samples. Following swan (Subset-quantile Within Array) normalization [Maksimovic et al., 2012] implemented in the minfi package [Aryee et al., 2014], 5hmC "peaks" were identified by subtracting the signal of oxidative bisulfite from the signal of conventional bisulfite. Next, we performed Maximum Likelihood Estimate (MLE) of 5mC and 5hmC (oxBS.MLE) with the ENmix package [Xu et al., 2016]. Using a binomial model at each CpG locus in each sample, oxBS.MLE outputs a matrix of MLEs of 5mC levels and a matrix of MLEs of 5hmC levels, setting as NA any negative value. To define differentially expressed genes (DEGs), differentially methylated positions (DMPs) and differentially hydroxymethylated positions (DhMPs), we modelled experimental conditions as categorical variables in a linear regression using an empirical Bayesian approach [Smyth, 2004]. Differentially methylated and hydroxymethylated regions (DMRs and DhMRs, respectively) were identified with the DMRcate package using the recommended proximity-based criteria [Peters

et al., 2015]. Comparisons with an FDR-adjusted P value below 0.05 were considered statistically significant. In addition, only DhMPs with at least 10% change in 5hmC were considered as significant for any given comparison, as this has been suggested as a threshold for the sensitivity of this technique [Skvortsova et al., 2017]. DEGs, DMPs, and DMRs were further analyzed to determine functional pathways and ontology enrichment using EnrichR [Chen et al., 2013]. Genomic context annotations, including chromatin states (ChromHMM) were performed with the ChIPseeker [Yu et al., 2015] and Annotatr [Cavalcante and Sartor, 2017] packages. EnrichedHeatmap package [Gu et al., 2018] was used for summary heatmaps of genomic context. All expression and methylation data will be deposited to the Gene Expression Omnibus repository.

DNA immunoprecipitation

80 uL of aqueous genomic DNA (100 ng/uL) were sonicated in Covaris microTUBE AFA Fiber Pre-Slit Snap-Cap 6x16mm with Covaris sonicator S220 to obtain fragments between 400-800 bp (Temperature < 7°C, peak power 105.0, duty factor 5.0, Cycles/Burst 200 and time 40 s). 130 ng DNA was used per immunoprecipitation. Auto hMeDIP kit (Diagenode C02010033) was used according to manufacturer instructions. Precipitation was adjusted to 15 h for mixing at 4°C and middle mix speed; for washes mixing time was 8 min, at 4°C and middle mix speed. Immunoprecipitations were performed independently in 3 cell cultures/condition. 5 uL of immunoprecipitated hydroxymethyl DNA was analysed for enriched 5hmC regions according to oxBS data (regions with at least 3 CpGs containing a DhMP with 10 % difference between proliferative and differentiating cells (Delta 10%)), *SFRS4* gene promoter was used as control of non-5hmC enrichment. All quantitative PCR assays were performed in duplicate with Mesa green qPCR 2x MasterMix Plus (Eurogentec 05-SY2X-06+WOU) on a CFX96 PCR system (Bio-Rad) using primers indicated in Supplementary Table S1. 5hmC enrichment was determined as % (hmeDNA-IP/ Total input) as follows: % (hmeDNA-IP/ Total input) = 2^[(Ct(10%input) - 3.32) - Ct(hmeDNA-IP)]x 100%, where 2 is the amplification efficiency; Ct (hmeDNA-IP) and Ct (10%input) are threshold values obtained from exponential phase of qPCR for the

hydroxymethyl DNA sample and input sample respectively; the compensatory factor (3.32) is used to take into account the dilution 1:10 of the input.

Adenosine, S-adenosylmethionine and S-adenosylhomocysteine quantification by HPLC

Adenosine, SAM and SAH levels were determined modifying protocols previously described [Hernandez-Munoz et al., 1984; Korinek et al., 2013]. Briefly, $10*10^6$ proliferating HepaRG cells were seeded in a 15 cm Petri dish; 24h after seeding, cells were either cultured with or without IFC-305 for 1 week to get differentiate, or collected for the Proliferative condition. Next, cells were frozen with liquid nitrogen and preserved at -70°C. Frozen cells were harvested with 1.5 mL 0.03% trifluoroacetic acid in 90% MeOH. Samples were incubated 10 min at room temperature and passed through a Dounce homogenizer. Obtained solutions were sonicated twice for 1 min in a Bransonic 220 and centrifuged at 16 000 g for 13 min at 4°C. Supernatants were recovered and centrifuged until dry in a speedvac at 45°C. Samples were reconstituted with 200 µL MilliQ water and protein concentration was determined by Bradford assay. Samples were diluted to 1.2 ug/uL protein and 100 µL 1.6 M $HClO_4$ was added to 300 µL of diluted sample (0.4 M $HClO_4$ final concentration) before incubating for 10 min on ice. 10 µL of 5 M K_2CO_3 was added to samples and incubated for 10 min on ice. Sample dilutions were centrifuged at 14 000 rpm during 5 min in a Eppendorf 5415C Micro-Centrifuge. Recovered supernatants were filtered using Phenex PTFE 4 mm syringe filters and 95 µL supernatant + 5 µL of 400 mM adenosine and 400 mM SAM standards mix were injected to HPLC Knauer E4310 (SAM standard contains SAH contamination, which was determined using SAH standard curve (data not shown)). Samples were separated in an ACE 5 C 18 column (150 x 4.6 mm) (Advanced Chromatpgraphy Technologies LTD) using a mobile phase consisting of 8 mM sodium heptanesulfonate, 40 mM ammonium phosphate monobasic and 15 % methanol pH 3 without gradient, at 1 mL/min flux, detection was measured at 254 nm absorbance, and separation total runtime of 60 min. Peaks were analyzed using EUROCHROME for windows version 3.05 (Knauer GmbH).

Abbreviations

5mC: 5-methylchytosine, 5hmC: 5-hydroxymethylcytosine, BS: bisulfite sequencing, CGI: CpG island, DMP: differentially methylated position, DMR: differentially methylated region, DNMTs: DNA methyl-transferases, HCC: Hepatocellular carcinoma, iCCA: intrahepatic cholangiocarcinoma, oxBS: oxidative bisulfite sequencing, SAM: s-adenosylmethionine, SAH: S-adenosylhomocysteine, TETs: Tet Methylcytosine Dioxigenases, TF: transcription factor, TSS: transcription start sites.

Availability of data and material

Datasets generated during the current study will be uploaded to the GEO repository.

Ethics approval and consent to participate

Not applicable.

Consent for publication

Not applicable.

Competing interests

The authors declare that they have no competing interests.

Funding

This work was supported by the Agence Nationale de Recherches sur le SIDA et les Hépatites Virales (ANRS, Reference No. ECTZ47287 and ECTZ50137); the Institut National du Cancer AAP PLBIO 2017 (project : *T cell tolerance to microbiota and colorectal cancers*); La Ligue Nationale Contre Le Cancer Comité d'Auvergne-Rhône-Alpes AAP 2018; Dirección General de Asuntos del Personal Académico/Programa de Apoyo a Proyectos de Investigación e Innovación Tecnológica (DGAPA/PAPIIT-UNAM Grant number IN9082015); PhD Fellowship from Consejo Nacional de Ciencia y Tecnología to JRRA (CONACyT CVU 508509); International Research Internship Support

to JRRA from Programa de Apoyo a los Estudios de Posgrado del Programa de Maestría y Doctorado en Ciencias Bioquímicas (PAEP-UNAM No. Cta. 30479367-5), CONACyT (Beca Mixta CVU 508509), Stipend Supplement from IARC (Ref. STU. 2052), and *Aide au logement* from CAF (No Allocataire: 4384941 W) and ROAL660122.

Authors' contributions

JRRA carried out the experiments and co-wrote the first draft of the manuscript; SE performed sample preparations for HT-12 array and advice in MeDIP assays; MPC performed immunofluorescence assays and provided technical assistance in the progenitor differentiation experiments and qPCR assays; CG performed additional validations and co-wrote the first draft of the manuscript; MDL standardized and provided technical assistance in HPLC experiments; NGC and RPCV performed additional differentiation assays and contributed to HPLC experiments; IC and FRT contributed to discussion of results and provided conceptual assistance; VCS conceived the study, provided conceptual assistance and supervised experiments; HHV conceived the study, carried out statistical and bioinformatics analysis, supervised experiments, coordinated the project and wrote the manuscript. All authors discussed the results and manuscript text.

Acknowledgements

The authors thank Cyrille Cuenin (Epigenetics Group, IARC, Lyon) and Severine Croze (Claude Bernard, University Lyon 1) for their help with the HT-12 array and MethylEPIC assays. The authors also thank Florence Le Calvez-Kelm and Geoffroy Durand (Genetic Cancer Susceptibility Group, IARC, Lyon) for Covaris Sonicator supply, Zdenko Herceg (Epigenetics Group, IARC, Lyon) for facilitating the infrastructure to realize hMeDIP experiments, Ramón González García-Conde (Research Center on Cellular Dynamics, UAEM, Mexico) for HepaRG cell line donation for preliminary assays, Emilio-Rojas del Castillo (Department of Genomic Medicine and Environmental Toxicology, IIB-UNAM, Mexico) for his advice during JRRA PhD studies, Pedro Valencia Mayoral (Planning Direction, Hospital Infantil de México "Federico Gómez") for training JRRA on liver histopathology during PhD Studies, Athena Sklias and Andrea Halaburkova

(Epigenetics Group, IARC, Lyon) for their enriching discussions during laboratory work, and Aurelie Salle (Epigenetics Group, IARC, Lyon), Georgina Guerrero-Avendaño and Rosario Pérez-Molina (Department of Molecular Genetics, IFC-UNAM, Mexico) for their technical assistance.

References

Ancey PB, Ecsedi S, Lambert MP, Talukdar FR, Cros MP, Glaise D, Narvaez DM, Chauvet V, Herceg Z, Corlu A, Hernandez-Vargas H. 2017. TET-Catalyzed 5-Hydroxymethylation Precedes HNF4A Promoter Choice during Differentiation of Bipotent Liver Progenitors. Stem Cell Reports 9:264-278.

Aryee MJ, Jaffe AE, Corrada-Bravo H, Ladd-Acosta C, Feinberg AP, Hansen KD, Irizarry RA. 2014. Minfi: a flexible and comprehensive Bioconductor package for the analysis of Infinium DNA methylation microarrays. Bioinformatics 30:1363-9.

Auta J, Zhang H, Pandey SC, Guidotti A. 2017. Chronic Alcohol Exposure Differentially Alters One-Carbon Metabolism in Rat Liver and Brain. Alcoholism, Clinical and Experimental Research 41:1105-1111.

Booth MJ, Ost TW, Beraldi D, Bell NM, Branco MR, Reik W, Balasubramanian S. 2013. Oxidative bisulfite sequencing of 5-methylcytosine and 5-hydroxymethylcytosine. Nat Protoc 8:1841-51.

Castelli G, Pelosi E, Testa U. 2017. Liver Cancer: Molecular Characterization, Clonal Evolution and Cancer Stem Cells. Cancers (Basel) 9.

Cavalcante RG, Sartor MA. 2017. annotatr: genomic regions in context. Bioinformatics 33:2381-2383.

Chagoya de Sanchez V, Hernandez-Munoz R, Sanchez L, Vidrio S, Yanez L, Suarez J. 1991. Twenty-four-hour changes of S-adenosylmethionine, S-adenosylhomocysteine adenosine and their metabolizing enzymes in rat liver; possible physiological significance in phospholipid methylation. Int J Biochem 23:1439-43.

Chagoya de Sanchez V, Martinez-Perez L, Hernandez-Munoz R, Velasco-Loyden G. 2012. Recovery of the Cell Cycle Inhibition in CCl(4)-Induced Cirrhosis by the Adenosine Derivative IFC-305. Int J Hepatol 2012:212530.

Chapman CG, Mariani CJ, Wu F, Meckel K, Butun F, Chuang A, Madzo J, Bissonette MB, Kwon JH, Godley LA. 2015. TET-catalyzed 5-hydroxymethylcytosine regulates gene expression in differentiating colonocytes and colon cancer. Sci Rep 5:17568.

Chen EY, Tan CM, Kou Y, Duan Q, Wang Z, Meirelles GV, Clark NR, Ma'ayan A. 2013. Enrichr: interactive and collaborative HTML5 gene list enrichment analysis tool. BMC Bioinformatics 14:128.

Du P, Kibbe WA, Lin SM. 2008. lumi: a pipeline for processing Illumina microarray. Bioinformatics 24:1547-8.

Dubois-Chevalier J, Oger F, Dehondt H, Firmin FF, Gheeraert C, Staels B, Lefebvre P, Eeckhoute J. 2014. A dynamic CTCF chromatin binding landscape promotes DNA hydroxymethylation and transcriptional induction of adipocyte differentiation. Nucleic Acids Res 42:10943-59.

Ecsedi S, Rodríguez-Aguilera JR, Hernández-Vargas H. 2018. 5-Hydroxymethylcytosine (5hmC), or How to Identify Your Favorite Cell. Epigenomes 2:3.

Ervik M, Lam F, Ferlay J, Mery L, Soerjomataram I, Bray F. 2016. Cancer Today editor^editors Lyon, France: World Health Organization, International Agency for Research on Cancer.

Garcea R, Daino L, Pascale R, Simile MM, Puddu M, Ruggiu ME, Seddaiu MA, Satta G, Sequenza MJ, Feo F. 1989. Protooncogene methylation and expression in regenerating liver and preneoplastic liver nodules induced in the rat by diethylnitrosamine: effect of variations of S-adenosylmethionine:S-adenosylhomocysteine ratio. Carcinogenesis 10:1183-92.

Gu Z, Elis R, Schlesner M, Ishaque N. 2018. EnrichedHeatmap: an R/Bioconductor package for comprehensive visualization of genomic signal associations. BMC Genomics 4;19(1):234.

Hahn MA, Qiu R, Wu X, Li AX, Zhang H, Wang J, Jui J, Jin SG, Jiang Y, Pfeifer GP, Lu Q. 2013. Dynamics of 5-hydroxymethylcytosine and chromatin marks in Mammalian neurogenesis. Cell Rep 3:291-300.

Hernandez-Munoz R, Glender W, Diaz Munoz M, Adolfo J, Garcia-Sainz JA, Chagoya de Sanchez V. 1984. Effects of adenosine on liver cell damage induced by carbon tetrachloride. Biochem Pharmacol 33:2599-604.

Kharbanda KK. 2007. Role of transmethylation reactions in alcoholic liver disease. World J Gastroenterol 13:4947-54.

Kim R, Sheaffer KL, Choi I, Won KJ, Kaestner KH. 2016. Epigenetic regulation of intestinal stem cells by Tet1-mediated DNA hydroxymethylation. Genes and Development 30:2433-2442.

Korinek M, Sistek V, Mladkova J, Mikes P, Jiracek J, Selicharova I. 2013. Quantification of homocysteine-related metabolites and the role of betaine-homocysteine S-methyltransferase in HepG2 cells. Biomedical Chromatography 27:111-21.

Kriaucionis S, Heintz N. 2009. The nuclear DNA base 5-hydroxymethylcytosine is present in Purkinje neurons and the brain. Science 324:929-30.

Li L, Li C, Mao H, Du Z, Chan WY, Murray P, Luo B, Chan AT, Mok TS, Chan FK, Ambinder RF, Tao Q. 2016a. Epigenetic inactivation of the CpG demethylase TET1 as a DNA methylation feedback loop in human cancers. Sci Rep 6:26591.

Li W, Qin J, Wang H, Chen LB. 2018. Research progress of epigenetic biomarkers in the early diagnosis and treatment of human diseases. Yi Chuan 40:104-115.

Li X, Liu Y, Salz T, Hansen KD, Feinberg A. 2016b. Whole-genome analysis of the methylome and hydroxymethylome in normal and malignant lung and liver. Genome Research 26:1730-1741.

Li X, Yao B, Chen L, Kang Y, Li Y, Cheng Y, Li L, Lin L, Wang Z, Wang M, Pan F, Dai Q, Zhang W, Wu H, Shu Q, Qin Z, He C, Xu M, Jin P. 2017. Ten-eleven translocation 2 interacts with forkhead box O3 and regulates adult neurogenesis. Nat Commun 8:15903.

Lin IH, Chen YF, Hsu MT. 2017. Correlated 5-Hydroxymethylcytosine (5hmC) and Gene Expression Profiles Underpin Gene and Organ-Specific Epigenetic Regulation in Adult Mouse Brain and Liver. PLoS One 12:e0170779.

Liu J, Jiang J, Mo J, Liu D, Cao D, Wang H, He Y. 2018. Global DNA 5-hydroxymethylcytosine and 5-formylcytosine contents are decreased in the early stage of hepatocellular carcinoma. Hepatology.

Maksimovic J, Gordon L, Oshlack A. 2012. SWAN: Subset-quantile within array normalization for illumina infinium HumanMethylation450 BeadChips. Genome Biol 13:R44.

Manco R, Clerbaux LA, Verhulst S, Bou Nader M, Sempoux C, Ambroise J, Bearzatto B, Gala JL, Horsmans Y, van Grunsven L, Desdouets C, Leclercq I. 2019. Reactive cholangiocytes differentiate into proliferative hepatocytes with efficient DNA repair in mice with chronic liver injury. Journal of Hepatology.

Mato JM, Corrales FJ, Lu SC, Avila MA. 2002. S-Adenosylmethionine: a control switch that regulates liver function. FASEB Journal 16:15-26.

Mu X, Espanol-Suner R, Mederacke I, Affo S, Manco R, Sempoux C, Lemaigre FP, Adili A, Yuan D, Weber A, Unger K, Heikenwalder M, Leclercq IA, Schwabe RF. 2015. Hepatocellular carcinoma originates from hepatocytes and not from the progenitor/biliary compartment. Journal of Clinical Investigation 125:3891-903.

Page A, Paoli P, Moran Salvador E, White S, French J, Mann J. 2016. Hepatic stellate cell transdifferentiation involves genome-wide remodeling of the DNA methylation landscape. Journal of Hepatology 64:661-73.

Perez-Cabeza de Vaca R, Dominguez-Lopez M, Guerrero-Celis N, Rodriguez-Aguilera JR, Chagoya de Sanchez V. 2018. Inflammation is regulated by the adenosine derivative molecule, IFC-305, during reversion of cirrhosis in a CCl4 rat model. Int Immunopharmacol 54:12-23.

Perez-Carreon JI, Martinez-Perez L, Loredo ML, Yanez-Maldonado L, Velasco-Loyden G, Vidrio-Gomez S, Ramirez-Salcedo J, Hernandez-Luis F, Velazquez-Martinez I, Suarez-Cuenca JA, Hernandez-Munoz R, de Sanchez VC. 2010. An adenosine derivative compound, IFC305, reverses fibrosis and alters gene expression in a pre-established CCl(4)-induced rat cirrhosis. Int J Biochem Cell Biol 42:287-96.

Peters TJ, Buckley MJ, Statham AL, Pidsley R, Samaras K, R VL, Clark SJ, Molloy PL. 2015. De novo identification of differentially methylated regions in the human genome. Epigenetics Chromatin 8:6.

Pfeifer GP, Szabo PE. 2018. Gene body profiles of 5-hydroxymethylcytosine: potential origin, function and use as a cancer biomarker. Epigenomics 10:1029-1032.

Recillas-Targa F. 2014. Interdependency between genetic and epigenetic regulatory defects in cancer. Methods Mol Biol 1165:33-52.

Rodriguez-Aguilera JR, Guerrero-Hernandez C, Perez-Molina R, Cadena-Del-Castillo CE, Perez-Cabeza de Vaca R, Guerrero-Celis N, Dominguez-Lopez M, Murillo-de-Ozores AR, Arzate-Mejia R, Recillas-Targa F, Chagoya de Sanchez V. 2018. Epigenetic Effects of an Adenosine Derivative in a Wistar Rat Model of Liver Cirrhosis. Journal of Cellular Biochemistry 119:401-413.

Rodríguez-Aguilera JR, Pérez-Cabeza-de-Vaca R, Guerrero-Celis N, Velasco-Loyden G, Domínguez-López M, Recillas-Targa F, Chagoya-de-Sánchez V. 2019. Molecular and cellular aspects of cirrhosis and how an adenosine derivative could revert fibrosis. In Tsoulfas G, editor^editors. Liver Cirrhosis - Debates and Current Challenges. United Kingdom: InctechOpen.

Shin S, Wangensteen KJ, Teta-Bissett M, Wang YJ, Mosleh-Shirazi E, Buza EL, Greenbaum LE, Kaestner KH. 2016. Genetic lineage tracing analysis of the cell of origin of hepatotoxin-induced liver tumors in mice. Hepatology 64:1163-1177.

Sia D, Villanueva A, Friedman SL, Llovet JM. 2017. Liver Cancer Cell of Origin, Molecular Class, and Effects on Patient Prognosis. Gastroenterology 152:745-761.

Skvortsova K, Zotenko E, Luu PL, Gould CM, Nair SS, Clark SJ, Stirzaker C. 2017. Comprehensive evaluation of genome-wide 5-hydroxymethylcytosine profiling approaches in human DNA. Epigenetics Chromatin 10:16.

Smyth GK. 2004. Linear models and empirical bayes methods for assessing differential expression in microarray experiments. Stat Appl Genet Mol Biol 3:Article3.

Tahiliani M, Koh KP, Shen Y, Pastor WA, Bandukwala H, Brudno Y, Agarwal S, Iyer LM, Liu DR, Aravind L, Rao A. 2009. Conversion of 5-methylcytosine to 5-hydroxymethylcytosine in mammalian DNA by MLL partner TET1. Science 324:930-5.

Takumi S, Okamura K, Yanagisawa H, Sano T, Kobayashi Y, Nohara K. 2015. The effect of a methyl-deficient diet on the global DNA methylation and the DNA methylation regulatory pathways. Journal of Applied Toxicology 35:1550-6.

Tehlivets O, Malanovic N, Visram M, Pavkov-Keller T, Keller W. 2013. S-adenosyl-L-homocysteine hydrolase and methylation disorders: yeast as a model system. Biochimica et Biophysica Acta 1832:204-15.

The L. 2018. GLOBOCAN 2018: counting the toll of cancer. Lancet 392:985.

Velasco-Loyden G, Perez-Carreon JI, Aguero JF, Romero PC, Vidrio-Gomez S, Martinez-Perez L, Yanez-Maldonado L, Hernandez-Munoz R, Macias-Silva M, de Sanchez VC. 2010. Prevention of in vitro hepatic stellate cells activation by the adenosine derivative compound IFC305. Biochem Pharmacol 80:1690-9.

Velasco-Loyden G, Perez-Martinez L, Vidrio-Gomez S, Perez-Carreon JI, Chagoya de Sanchez V. 2017. Cancer chemoprevention by an adenosine derivative in a model of cirrhosis-hepatocellular carcinoma induced by diethylnitrosamine in rats. Tumour Biology 39:1010428317691190.

Xu Z, Taylor JA, Leung YK, Ho SM, Niu L. 2016. oxBS-MLE: an efficient method to estimate 5-methylcytosine and 5-hydroxymethylcytosine in paired bisulfite and oxidative bisulfite treated DNA. Bioinformatics 32:3667-3669.

Yoo Y, Park JH, Weigel C, Liesenfeld DB, Weichenhan D, Plass C, Seo DG, Lindroth AM, Park YJ. 2017. TET-mediated hydroxymethylcytosine at the Ppargamma locus is required for initiation of adipogenic differentiation. Int J Obes (Lond) 41:652-659.

Yu G, Wang LG, He QY. 2015. ChIPseeker: an R/Bioconductor package for ChIP peak annotation, comparison and visualization. Bioinformatics 31:2382-3.

Zhong X, Wang QQ, Li JW, Zhang YM, An XR, Hou J. 2017. Ten-Eleven Translocation-2 (Tet2) Is Involved in Myogenic Differentiation of Skeletal Myoblast Cells in Vitro. Sci Rep 7:43539.

Zhu J, Adli M, Zou JY, Verstappen G, Coyne M, Zhang X, Durham T, Miri M, Deshpande V, De Jager PL, Bennett DA, Houmard JA, Muoio DM, Onder TT, Camahort R, Cowan CA, Meissner A, Epstein CB, Shoresh N, Bernstein BE. 2013. Genome-wide chromatin state transitions associated with developmental and environmental cues. Cell 152:642-54.

epigenomes

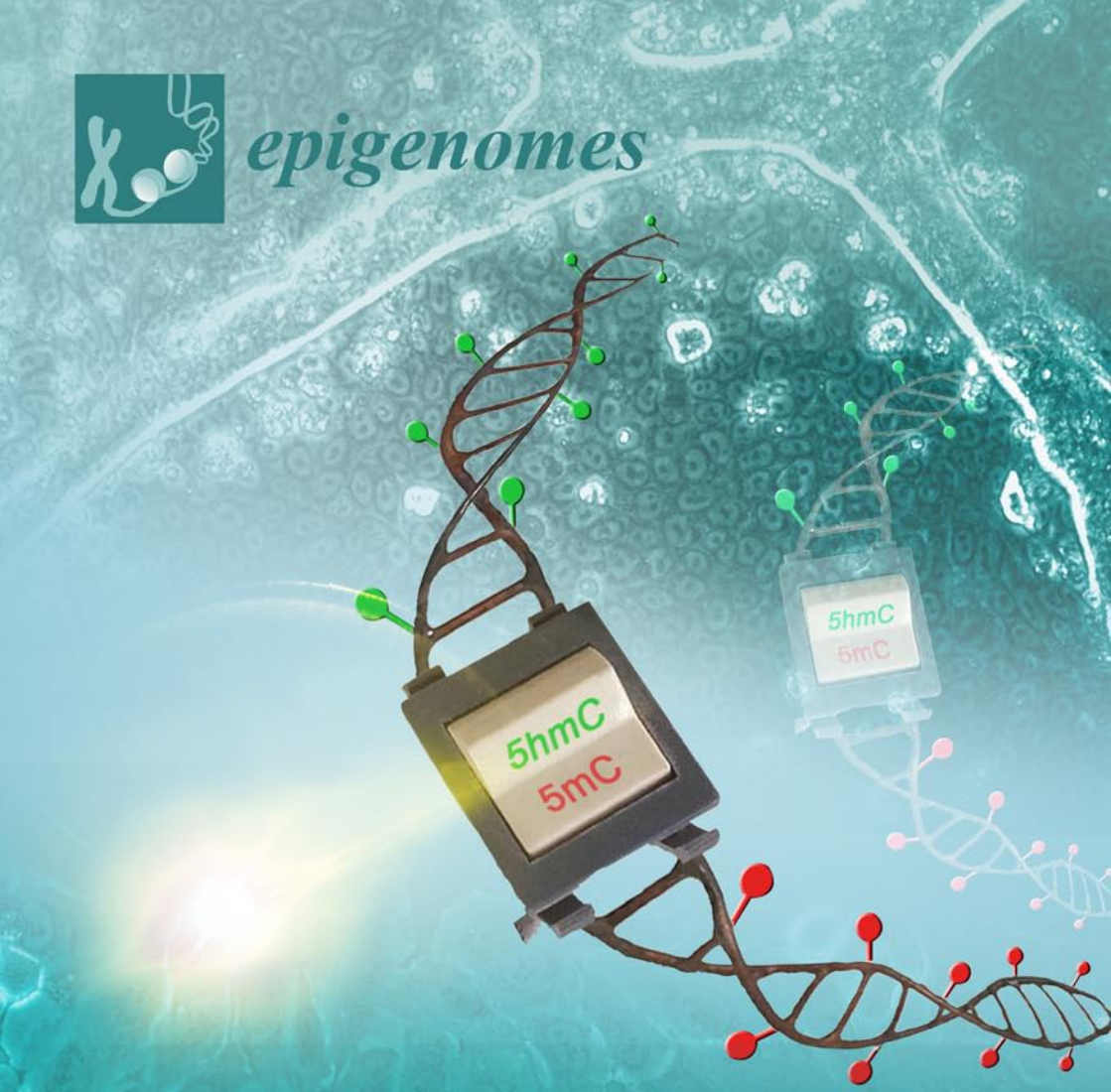

5hmC, an Imprint of Cell Fate

Volume2 · Issue 1 | March 2018

MDPI

mdpi.com/journal/epigenomes
ISSN 2075-4655

epigenomes

MDPI

Perspective

5-Hydroxymethylcytosine (5hmC), or How to Identify Your Favorite Cell

Szilvia Ecsedi [1], Jesús Rafael Rodríguez-Aguilera [2] and Héctor Hernandez-Vargas [3,*]

[1] Institute of Biology Valrose (iBV), The National Center for Scientific Research (CNRS)—National Institute of Health and Medical Research (Inserm), Université Côte d'Azur, 06108 Nice, France; szilvia.ecsedi@unice.fr
[2] Laboratory 305-Sur, Department of Cellular Biology and Development, Institute of Cellular Physiology, National Autonomous University of Mexico (UNAM), Coyoacán, 04510 Ciudad de México, Mexico; jesusr_rodagu@comunidad.unam.mx
[3] Cancer Research Centre of Lyon (CRCL), Inserm U 1052, CNRS UMR 5286, Centre Léon Bérard, Université de Lyon, 28 rue Laennec, 69373 Lyon CEDEX 08, France
* Correspondence: hector.hernandez@inserm.fr; Tel.: +33-046-985-6186

Received: 20 December 2017; Accepted: 23 January 2018; Published: 30 January 2018

Abstract: Recently described as the sixth base of the DNA macromolecule, the precise role of 5-hydroxymethylcytosine (5hmC) is the subject of debate. Early studies indicate that it is functionally distinct from cytosine DNA methylation (5mC), and there is evidence for 5hmC being a stable derivate of 5mC, rather than just an intermediate of demethylation. Moreover, 5hmC events correlate in time and space with key differentiation steps in mammalian cells. Such events span the three embryonic germ layers and multiple progenitor cell subtypes, suggesting a general mechanism. Because of the growing understanding of the role of progenitor cells in disease origin, we attempted to provide a detailed summary on the currently available literature supporting 5hmC as a key player in adult progenitor cell differentiation. This summary consolidates the emerging role for 5hmC in defining cellular fate.

Keywords: DNA methylation; progenitor cells; differentiation; 5mC; 5hmC

1. Introduction

Like evidence in a crime scene, cytosine DNA methylation (5mC) can reconstitute diverse information about the origin and context of the host cell [1]. While sex can be easily identified from 5mC data, algorithms designed in recent years use 5mC to also extract information about the major tissue types in which a given cell resides and the age of the donor [2]. Even in complex samples such as blood, DNA methylation can be used to infer the proportion of major cell subpopulations [3], illustrating the tissue- and cell-specificity of 5mC. More recently, several studies showed that, at the level of progenitor cell differentiation, it is the loss of 5mC at particular intragenic regions that precedes a switch in cell identity, as we will show throughout this study. The improved knowledge of how this DNA demethylation occurs is leading to a redefinition of DNA methylation dynamics.

Presence of 5-hydroxymethylcytosine (5hmC) in the genome was suggested in 1972, in rat's brain and liver DNA [4]. However, it was not until 2009 when 5hmC was identified as an unusual nucleotide when comparing the abundance of 5mC in Purkinje and granule cells [5]. In parallel, Tet Methylcytosine Dioxygenase 1 (TET1) was first described as an enzyme able to convert 5mC to 5hmC by oxidation [6]. Increasing the complexity of this field, additional oxidized derivatives of 5mC (i.e., 5-carboxylcytosine (5caC) and 5-formylcytosine (5fC) [7] and two new members of the TET family (i.e., TET2 and TET3) have been described [8,9]. Although with a slightly distinct chemical construction, all three TET proteins are considered as 5hmC "writers" [8,9], while all three oxidized

derivatives of 5mC were initially defined as intermediaries in the active process of DNA demethylation (Figure 1).

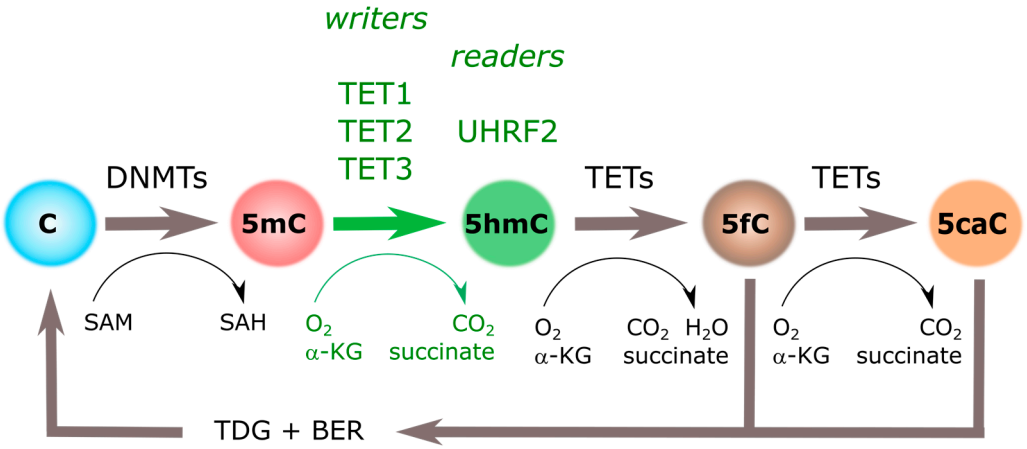

Figure 1. Cytosine methylation cycle. Cytosine DNA methylation (5mC) groups introduced by DNA Methyl-Transferases (DNMTs) can be iteratively oxidized to 5-hydroxymethylcytosine (5hmC), 5-formylcytosine (5fC), and 5-carboxylcytosine (5caC) by the action of Tet Methylcytosine Dioxygenases (TETs). Three "writers" (i.e., TET1, TET2, and TET3), and at least one "reader" (i.e., UHRF2), have been identified for 5hmC. α-KG: α-ketoglutarate; BER: base excision repair; SAH: *S*-adenosylhomocysteine; SAM: *S*-adenosylmethionine; TDG: thymine DNA glycosylase.

Ever since the discovery of the "sixth base", strenuous efforts have been made to characterize the precise role of 5hmC in development. Such roles are becoming more evident as we learn about 5hmC specific genomic localization, its relative stability, and its recognition by other proteins. Based on the available evidence, we illustrate here how 5hmC is consistently found as a dynamic mark during the establishment of cell identity in multiple model systems.

2. 5-Hydroxymethylcytosine: "Localized, Stable and Readable"

Mapping 5hmC location represented a first step in deciphering its function. Early methods such as immunofluorescence (IF) and mass spectrometry (MS) allowed researchers to assess global levels of 5hmC, and high-performance liquid chromatography-mass spectrometry (HPLC-MS) is still the most accurate method for 5hmC global detection [10]. However, the development of locus-specific methods has played a pivotal role in our comprehension of the functional role of 5hmC. In general, affinity-based enrichment methods are widely used and can be easily combined with genome-wide profiling. Affinity-based applications can be divided into antibody and chemical capture-based methods, with both approaches providing highly reproducible results [11], and the vast majority of information on the distribution of 5hmC has been generated by antibody-based methods as 5hmC immunoprecipitation (hMeDIP) [12]. Regarding chemical labelling enrichment technics, those based on β-glycosyltransferase (βGT)-catalyzed 5hmC glycosylation such as glycosylation labelled sequencing (hMe-Seal), glucosylation, periodate oxidation and biotinylation (GLIB), and J-binding protein 1 sequencing (JBP-1) have also been extensively used; however, they are claimed to exhibit relatively low resolution compared to the antibody-based methods [11,13]. More recently, oxidative bisulfite sequencing (oxBS-Seq) [14] and TET assisted bisulfite sequencing (TAB-Seq) [15] were published and, starting now, they will be widely used methods in order to provide single resolution maps of 5hmC. However, both techniques require excessive chemical treatments and therefore can cause DNA damage. Furthermore, oxBS-seq and TAB-Seq require at least 30x sequencing depths to provide reliable, quantitative results.

Globally, 5hmC was shown by IF to be enriched in the euchromatin compartment [16]. Although exposed and accessible to anti-5hmC antibodies in euchromatin, the presence of 5hmC in heterochromatin seems to be hindered by binding proteins under non-denaturizing IF conditions [17]. Novel chemical methods allowed researchers to precisely map the genomic distribution of 5hmC and distinguish it from other cytosine variants. Immunoprecipitation with 5hmC antibodies followed by sequencing (hMeDIP-Seq) provided the first genome-wide map of 5hmC distribution, and confirmed its association with active transcription, CpG islands, 5′ regions of LINE1, CTCF, and pluripotency transcription factor (TF) binding sites and, in general, regions marked by 5mC decrease and active chromatin marks [16]. Upon differentiation from embryonic stem cells (ESCs) into embryonic bodies, the levels of 5hmC decreased. As will be discussed below, with the exception of neurogenesis, this distribution and global decrease of 5hmC is consistent across many models of differentiation. Also in ESCs, 5hmC was described in association with bivalent promoters (i.e., simultaneously occupied by histone marks H3K4me3 and H3K27me3). In this sense, it was recently shown that TET enzymes block aberrant hypermethylation in this type of promoter, ensuring robust lineage-specific transcription upon differentiation [18]. Another type of "bivalency" has been recently described at later stages of differentiation, in which genes simultaneously display promoter 5mC and gene body 5hmC at developmentally important genes [19]. Finally, Ficz et al. also described 5hmC association with non-CpG methylation resulting in strand bias that increased as a response of TET1/2 silencing. Interestingly, whenever 5hmC and 5mC occurred in parallel, gene expression was higher compared to regions in which 5mC occurred alone [16].

Growing evidence confirms the distribution and dynamics of 5hmC during embryonic cell development, outlining that it is functionally distinct from 5mC. However, the relatively low levels of 5hmC in the human genome, as well as the presence of other oxidized cytosine variants (5fC and 5caC), raised fundamental questions regarding the stability of the novel mark. Indirectly, genome-wide acquisition of 5hmC during neurogenesis in the absence of a major 5mC drop suggested that rather than an intermediate of demethylation, 5hmC serves as a stable signal on its own [20,21]. In addition, direct evidence of 5hmC stability in different cell types was obtained from ultrasensitive analytical liquid chromatography-tandem mass spectrometry (LC-MS/MS), showing no change in the levels of 5hmC over cell cycle phases [22]. Moreover, data suggested that 5mC oxidation does not occur on the nascent strand but must be formed in the double-stranded DNA produced immediately after replication [22]. Although several fundamental questions remain to be explained regarding TET binding and interaction affinities, a single, remarkable study described 5hmC-DNA interactions as much more stable and less prone than 5mC-DNA to further oxidation [23]. Favoring the idea that 5hmC is a persistent mark, compared to 5fC and 5caC, 5hmC is a poor substrate for TETs, thus protecting 5hmC from further oxidation [23,24] (reviewed in [25]). In a similar way, 5fC and 5caC are more efficiently recognized by thymine-DNA glycosylase (TDG) for removal and subsequent base excision repair (BER) leading to demethylation [26] (Figure 1). Together, higher affinities of TETs and TDG for 5fC and 5caC ensure a relative abundance and recognition of 5hmC in the genome.

In addition to confined genomic location and biochemical stability, a characteristic of other chromatin marks such as histone modifications is their capacity to be read and interpreted by specific proteins. A computational method that combined 139 published assays (chromatin immunoprecipitation sequencing (ChIP-Seq), MeDIP-Seq and glucosylation, periodate oxidation and biotinylation sequencing (GLIB-Seq), involving 77 chromatin features (3 cytosine modifications, 13 histone marks, and 61 chromatin related proteins), revealed four different co-evolutionary associations of 5hmC with chromatin related proteins: SIN3A/LSD1, TET1/MBD2, MBD2/MLL2, and OGT/TAF1 [27]. The associations of these 5hmC writers/erasers (i.e., TET1, OGT, and LSD1) do not reflect direct physical interactions of the protein pairs but rather their roles in the control of cytosine modifications and gene regulation. Although early studies described several molecules as potential readers of 5hmC, further mass spectrometry (MS) measurements failed to provide direct evidence on binding to 5hmC (reviewed by [28]). A single MS study revealed that the Set and Really

Interesting New Gene (RING) finger-associated (SRA) domain of UHRF2 specifically interacts with 5hmC [29]. This discovery was subsequently supported by a structural and biochemical study [30], which demonstrated that the UHRF2-SRA domain, unlike the equivalent domain in UHRF1, does not preferentially bind to hemi-methylated DNA. Instead, it binds to fully hydroxymethylated and hemi-hydroxymethylated DNA 3.2- and 1.5-fold more tightly than it does to hemi-methylated DNA, respectively. In addition, the Chromatin target of Prmt1 (CHTOP)-methylosome complex, which methylates H4R3, has been recently described as a novel molecular interactor of 5hmC in a study conducted in gliomas [31,32].

Interestingly, 5fC and 5caC seem to be associated with numerous molecular readers [28,33–35]. Of note, these methylated variations have been shown to cause pause at the transcription rate generated by RNA Polymerase II (Pol II) binding. No similar mechanism has been detected for 5hmC so far, which is in line with the previously described phenomenon that 5hmC is a hallmark of active gene expression.

3. Specific 5-Hydroxymethylcytosine Enrichment Identifies Blood Cell Subtypes

In agreement with its relative stability and readability, recent studies provide ample evidence of the importance of the "sixth base" during differentiation and lineage commitment of several adult cell types. Given the existence of relatively easy approaches to perform in vitro differentiation and selection of well-characterized types of hematopoietic cells, substantial data has been accumulated to favor the role of 5hmC in transcriptional programming of myeloid and lymphoid differentiation (Table 1).

Table 1. 5-hydroxymethylcytosine (5hmC) and blood cell subtypes.

Cell Type	Organism	Model System	5hmC Technique	5hmC Enrichment	5hmC Writer	Authors
Myeloid & Lymphoid						
HSCs	*Hs*	umbilical cord CD34+ cells	RRHP + NGS	exons, promoters, enhancers	no data	Tekpli et al., 2016
HSCs	*Mm*	Tet2 and Dnmt3a knockout mice	CMS-IP + sequencing	promoters and gene bodies of highly expressed genes	Dnmt3a, Tet2	Zhang et al., 2016
Myeloid						
Macrophages, Osteoclasts	*Hs*	in vitro differentiation	OxBS + HM450	enhancers, 5hmC changes at promoters and gene bodies	TET2, TDG, AID	Garcia-Gomez et al., 2017
Macrophages	*Hs*	monocyte elutriation and differentiation	OxBS + sequencing	Demethylation at nucleosome-free loci that gain active enhancer marks	TET2	Wallner et al., 2016
Dendritic cells	*Hs*	in vitro differentiation	hMedIP (and glycosylation-sensitive restriction) + qPCR	candidate gene promoters	TET2	Klug et al., 2013
Mast cells	*Mm*	Tet2 knockout mice + in vitro differentiation	GLIB-Seq	TSS distal (enhancers), gene bodies	Tet2	Montagner et al., 2016
Erythrocytes	*Hs*	in vitro culture of HSCs	hMe-Seal; TAB-Seq	TF binding sites, gene bodies of overexpressed genes	TET2, TET3	Madzo et al., 2014
Erythrocytes	*Hs*	cultured cord blood CD34+ cells	LC-MS	global loss of 5hmC	TET2, TET3	Yan et al., 2017
Lymphoid						
B cells	*Hs*	in vitro activation of human naïve B cells	hMe-Seal	enhancers, gene bodies. B cell identity genes lose whereas Plasma Cell identity genes gain 5hmC	no data	Caron et al., 2015
B cells	*Mm*	mice deficient for Tet2 and Tet3 in early B cells	CMS-IP + sequencing	B cell enhancers, chromatin-accessible regions	Tet2, Tet3	Lio et al., 2016
T cells	*Mm*	purified naïve and in vitro differentiated T cell subtypes	CMS-IP + sequencing	gene bodies of highly expressed genes, active tissue-specific enhancers	no data	Tsagaratou et al., 2014
T cells	*Mm*	sorted mouse cell subpopulations	βGT catalyzed restriction enzyme protection + qPCR; OxBS + qPCR	candidate gene approach (CD4 locus)	no data	Sellars et al., 2015

Table 1. *Cont.*

Cell Type	Organism	Model System	5hmC Technique	5hmC Enrichment	5hmC Writer	Authors
Tfh cells	*Mm*	in vivo-generated Tfh cells from Bcl6-RFP reporter mice	hMedIP-Seq	5hmC loss in Tfh cells at Bcl6 binding sites compared to naïve T cells	Tet1	Liu et al., 2016
Tfh cells	*Hs*	human PBMCs, and lupus prone mice	DNA dot plot, MedIP-Seq	global 5hmC gain, no genome context data	TET2, TET3	Wu et al., 2016
CD4 T cells	*Hs*	human CD4+ T cell differentiation ex vivo	Methyl/Hydroxymethyl sensitive qPCR (EpiMark)	gene body enrichment and TSS depletion, actively transcribed genes	TET1	Nestor et al., 2016
CD4 T cells	*Mm*	mouse T cell subtypes	hMedIP + sequencing	introns and intergenic regions, lineage-specific TFs	Tet2	Ichiyama et al., 2015
CD8 T cells	*Mm*	mouse CD8+ T cells with low or high HIF signalling	hMedIP + qPCR	overall reduction of 5hmC	Tet2	Tyrakis et al., 2016
iNKT cells	*Mm*	Tet2-Tet3 DKO mice	CMS-IP + sequencing	chromatin accessible-regions associated with iNK T cell development	Tet2, Tet3	Tsagaratou et al., 2017
Treg cells	*Mm*	H2S-deficient (Cbs−/−) mice	dot blot; hMedIP + qPCR	*Foxp3* promoter and CNS2	Tet1, Tet2	Yang et al., 2015
Treg cells	*Mm*	Tet2-Tet3 DKO mice	OxBS + sequencing	*Foxp3* CNS1 and CNS2	Tet2, Tet3	Yue et al., 2016

Hs: *Homo Sapiens*; *Mm*: *Mus Musculus*; HSC: Hematopoietic stem cells; iNKT cells: Invariant natural killer T cells; Peripheral blood mononuclear cells (PBMCs); HIF: Hypoxia-inducible factors; DKO: Double knock-out; RRHP: reduced representation of hydroxymethylation profiling; NGS: next-generation sequencing; CMS-IP: cytosine-5-methylenesulphonate immunoprecipitation; OxBS: oxidative bisulfite; HM450: Infinium 450K bead arrays; hMeDIP: 5hmC immunoprecipitation; hMeDIP-Seq: hMeDIP Sequencing; qPCR: Quantitative polymerase chain reaction; GLIB: glycosylation, periodate oxidation, and biotinylation; GLIB-Seq: GLIB-Sequencing; hMe-Seal: βGT-catalyzed 5hmC glycosylation labelled sequencing; TAB-Seq: Tet-assisted bisulfite sequencing; LC-MS: liquid chromatography mass spectrometry; TSS: transcription start site; TF: Transcription factor; CNS: Conserved non-coding sequences; TDG: thymine DNA glycosylase, AID: activation-induced deaminase.

Globally, a drop in 5hmC levels has been described during differentiation from hematopoietic stem cells (HSCs) [36], except for one study showing overall 5hmC increase (without genome context data) [37]. Despite this global reduction, 5hmC remains enriched at particular loci, matching the distribution shown by earlier studies (i.e., promoters and gene bodies). In addition, 5hmC enrichment has been described in enhancers [19,36,38–41] and lineage-specific TF binding sites [42,43]. In line with this, 5hmC changes are overrepresented in highly transcribed genes. For example, chromatin-accessible-regions are associated with T cell [36,44] and induced natural killers (iNK) T cell development [45], Treg FoxP3 activation [46,47], B cell identity genes [39,41], or Bcl6 binding sites in T follicular helper (Tfh) cells [48] (Figure 2 and Table 1). During mast cell development, it was shown that Tet2 knockout caused differential 5hmC levels in genes enriched with leukocyte differentiation and proliferation, malignant transformation, and mast cell-related processes [40]. Hypo-hydroxymethylated loci overlapped with enhancer regions, suggesting that 5hmC had a role in transcriptional programming [40].

Many of these studies provide mechanistic data supporting the role of TETs in cell differentiation. This is the case for Tet2 (and to a lesser degree Tet3), which is consistently reported in murine models [39,40,43,45–47,49] and human cells [37,38,42,50–52]. Of note, the role of Tet2 in mast cell differentiation described above [40] is partially independent of 5hmC, as rescuing mast cell developmental changes upon Tet2 knockout was only possible by the re-expression of Tet2 independently of its catalytic activity, which assumes that Tet2 possibly interacts with other complexes (something similar has been shown between TET1 and the SIN3A co-repressor complex [53]).

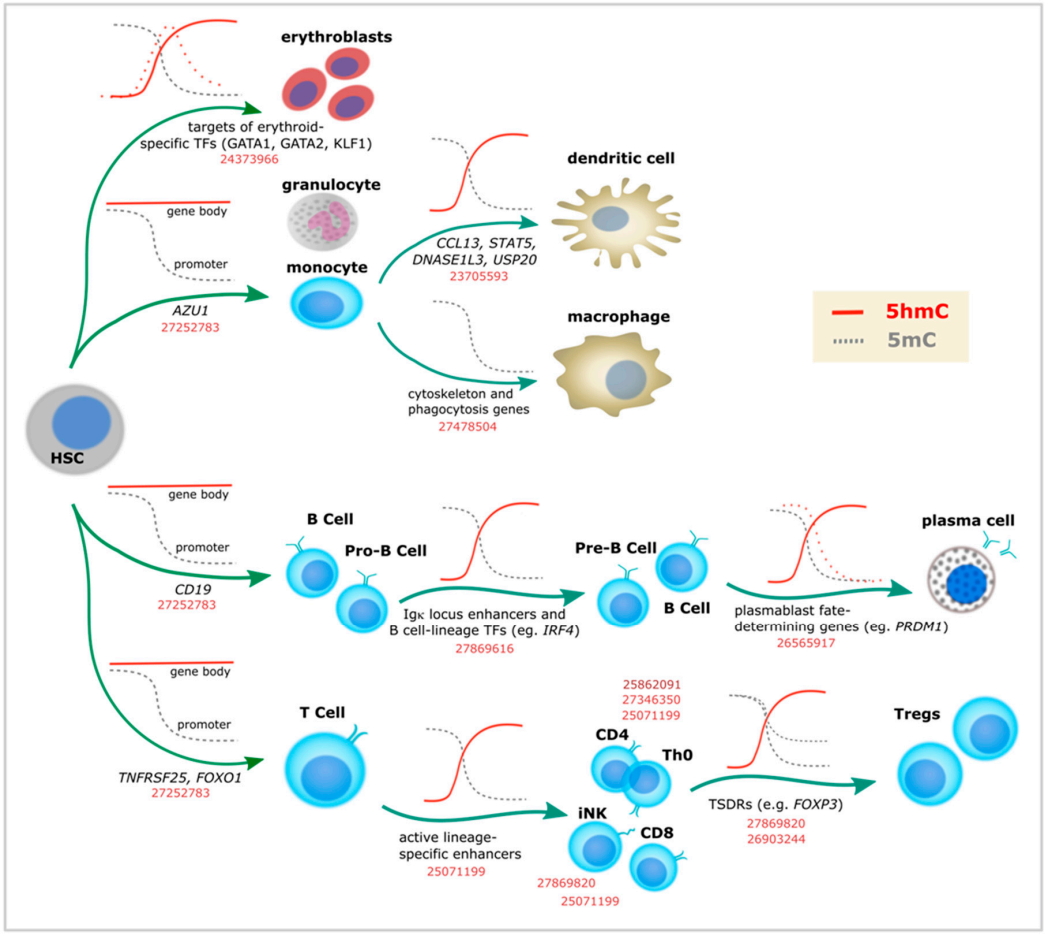

Figure 2. 5-Hydroxymethylcytosine dynamics during blood cell differentiation. Evidence for dynamic changes in 5mC (gray lines) or 5hmC (red lines) at the indicated loci, as associated with immune lineage commitment. Dashed lines represent additional evidence. Corresponding PubMed PMIDs for each study are shown in red. TSDRs: Treg-specific demethylated regions. Th0: naïve T helper cells.

3.1. Myeloid Lineage

In addition to mast cells, specific redistribution of 5hmC has been described during differentiation of monocytes into macrophages or into dendritic cells [50,51]. Moreover, a unique role of 5hmC in red blood cell development seems well established according to a study that provided a comprehensive view of 5hmC distribution at stem/early progenitors, primitive erythroid progenitors, basophilic, polychromatic, orthochromatic, and reticulocytes [42].

Initially, by mass spectrometry measurements, using both in vitro as well as in vivo models, the authors described a general increase of 5hmC during commitment to the erythroid lineage, followed by remarkable decrease during the subsequent steps of differentiation [42]. In contrast to the dynamic fluctuation of 5hmC, 5mC exhibited modest decrease. Besides negligible levels of TET1 and TET3, TET2 seemed to be involved in the differentiation process, being the highest at the time point of specific erythroid lineage commitment. As for other cell types, in parallel with the overall decrease, elevated levels of 5hmC were detected at particular loci [42]. As erythropoiesis is a replication dependent process, this argues in favor of a stable 5hmC mark at given DNA regions that overlaps with TF binding sites and activating histone marks (i.e., H3K4me1, H3K4me3, H3K9ac, and H3K27ac).

3.2. Lymphoid Lineage

On a pioneer study of 5hmC and T-cell lineage commitment, deep sequencing was performed on purified samples (double positive, CD4 single positive, CD8 single positive, naïve CD4, naïve CD8, and CD4-differentiated Th1 and Th2 T helper cells) enriched by cytosine-5-methylenesulfonate-based immunoprecipitation [36]. In all cell types, 5hmC was found to be highest at promoters and intragenic regions, without enrichment for transcription start sites (TSS). On average, naive T-cells showed higher global 5hmC compared to the previous stage of differentiation, followed by a drop at the later stages (Th1 and Th2). As the reduction of 5hmC was replication-dependent, this initially suggested that 5hmC had been passively diluted in a cell cycle manner. However, in contrast to 5mC, gene body 5hmC exhibited significant positive correlation with gene expression accompanied with Pol II occupancy and enrichment for active histone marks. Moreover, 5hmC was suggested to mark long-range interactions between enhancers and other regulatory regions at the transition points of T-cell development. More recently, using Tet2-Tet3 double knock-out (DKO) mice, the same group showed that TET proteins are essential for maturation of invariant natural killer T cells (iNKT), and its absence generates a T cell antigen receptor (TCR)-mediated expansion of these cells and a lethal lymphocytic infiltrate in lung and liver [45]. Transcriptomic evaluation identified a characteristic profile of natural killer NKT17 cells (expressing RAR-related orphan receptor γ (RORγt) and Interleukin 17) and genes related with malignant transformation.

Of note, studies supporting a role of 5mC/5hmC in immune cell development have been performed in both mouse and human cells (Table 1). For example, analogous DNA methylation dynamics are observed during differentiation of human naive B cells into plasma cells [41]. Most differentially methylated loci identified in this process were demethylated and enriched for enhancers, with demethylation becoming particularly pronounced at terminal stages of development. Initial assessment by selective chemical labeling followed by dot blot showed global loss of 5hmC during differentiation, accompanied by decrease in TETs expression. However, 5hmC was found to be enriched at specific DNA regions, particularly at B-cell identity genes with enhancer chromatin marks (i.e., H3K4me1 and H3K27ac) (Figure 2). As mentioned above, 5hmC at gene bodies correlated with gene expression.

Therefore, 5hmC events take place at all stages of lymphoid cell differentiation, from HSCs to highly specialized cell types (Figure 2). For example, 5hmC seems to define the transition to the lymphoid lineage, the choice between B and T cell types, and between CD4 and CD8 T cells [36]. Furthermore, 5hmC enrichment at specific loci has been described for each of the well specialized fates of naïve T helper (Th0) cells (i.e., Th1, Th2, Th17, Thf, and Treg). Indeed, studies of Treg cell differentiation represent a good example of what has been done in other systems in terms of linking 5hmC to cell identity. Defined as the master TF of Treg programming almost 15 years ago [54], *Foxp3* was later shown to be demethylated in particular loci called Treg-specific demethylated regions (TSDRs) (Figure 2). TSDRs were described as the most reliable criterion for natural Treg identification long before the first 5hmC studies became available [55,56]. In addition, TSDRs were suggested as a requirement for lineage stabilization [55–58] and a way to distinguish Tregs from different origins (i.e., thymic vs. periphery vs. in vitro) [56–60]. While TSDRs were associated with intragenic conserved non-coding sequences (CNS) in the *Foxp3* loci displaying a particular chromatin landscape [57], additional TSDRs were found in mice in other immune-related genes as well (i.e., *Ctla4*, *Il2ra*, *Ikzf4*, and *Tnfrsf18*) [61]. After several additional studies highlighted that CNS2 is specifically demethylated in Tregs [62,63], subsequent work demonstrated that TET proteins were necessary for *Foxp3* 5hmC enrichment [46,47]. More recently, one additional CNS loci (CNS0) has been described as a FoxP3 super-enhancer and a binding site for the chromatin organizer Satb1 [64].

Overall, mouse and human studies agree on a dynamic redistribution of 5hmC in myeloid and lymphoid differentiation (including both T and B cells). Also, in mice and humans, 5hmC is enriched in gene bodies and enhancers of the corresponding cell identity genes. In addition, in line with its role in blood cell development, TETs mutations are often detected in lymphoid and myeloid malignancies [65].

Indeed, the frequency of frameshift and nonsense mutations in *TET2* is estimated to be as high as 45% in patients with chronic myelomonocytic leukemia [66]. Although this places TET mutations as driver events in leukemia, it is worth mentioning that TET2 mutations alone have proven insufficient to cause cancer [65]. Future studies aimed at elucidating a more comprehensive role of TET mutations in the 5mC-5hmC balance may shed light on the dynamic interplay between genetic and epigenetic machinery in disease development, rather than considering mutations as master regulators.

4. 5-Hydroxymethylcytosine Is Redistributed during Terminal Differentiation from All Germ Layers

In addition to most blood cell subtypes, 5hmC has been associated with differentiation into other cell types from mesodermal origin. Moreover, examples also exist for the endodermal and ectodermal germ layers, as described below (Table 2).

Table 2. 5-hydroxymethylcytosine and non-blood cell subtypes.

Cell Type	Organism	Model System	5hmC Technique	5hmC Enrichment	5hmC Writer	Authors
Endoderm						
Hepatocytes	*Hs*	human fetal and adult liver tissues	LC-MS; IF; hMedIP + sequencing	global 5hmC gain, occupancy in active catabolic and metabolic genes	no data	Ivanov et al., 2013
Hepatocytes	*Hs*	bipotent liver progenitors	hMedIP + qPCR	alternative HNF4A promoters	TET1, TET2	Ancey et al., 2017
Colonocytes	*Hs*	T84 colon cancer cells, primary colonocytes	dot blot; hMe-Seal; TAB-Seq	5-hmC gain at promoters and gene bodies; highly expressed and induced genes	TET1	Chapman et al., 2015
Enterocytes	*Mm*	Lgr5+ and intestinal villus epithelial cells	IHC; hMedIP combined with qPCR and sequencing	promoters and gene bodies of highly expressed genes. eightfold 5hmC signal gain in differentiated relative to Lgr5+ cells	Tet1	Kim et al., 2016
Mesoderm						
Chondriocytes	*Mm*	embryonic growth plate; ATDC5 progenitors	hMe-Seal	gene bodies, near TSS	Tet1	Taylor et al., 2016
Cardiomyocytes	*Mm*	embryonic, neonatal, adult and hypertrophic cardiomyocytes	hMedIP-Seq, TAB-Seq, biotin-glucosyl tagging	introns and intergenic regions; body of highly expressed genes and distal regulatory regions	Tet2	Greco et al., 2016
Cardiomyocytes	*Mm*	newborn and adult cardiomyocytes	ELISA; hMe-Seal	gene bodies and low methylated enhancers; positively associated with gene expression	no data	Kranzhofer et al., 2016
Myocytes	*Mm*	murine C2C12 myoblast in vitro differentiation	IS	global 5hmC gain in differentiated myotubes. gradual 5hmC gain with differentiation	Tet2	Zhong et al., 2017
Adipocytes	*Mm*	mouse 3T3-L1 pre-adipocytes and primay adipocytes	hMedIP-Seq, hMeDIP-qPCR	CTCF-associated enhancers activated during adipogenesis	Tet1, Tet2	Dubois-Chevalier et al., 2014
Adipocytes	*Mm*	Murine 3T3-L1 preadipocytes	GC-MS; MassARRAY; hMeDIP,	5hmC gain, globally and at the Pparγ locus	Tet2	Yoo et al., 2017
Sertoli cells	*Rn*	rat Sertoli cells	LC-MS; IS; hMe-Seal	global 5hmC gain during puberty; correlated with gene expression	no data	Landfors et al., 2017

Table 2. *Cont.*

Cell Type	Organism	Model System	5hmC Technique	5hmC Enrichment	5hmC Writer	Authors
Ectoderm						
Neurons	*Mm*	mouse Nestin+/Sox2+ adult neural stem cells (aNSC)	dot blot; IS; hMe-Seal; LC-MS	global gain; positive correlation with transcriptional upregulation	Tet2	Li et al., 2017
Neurons	*Hs*	human fetal brain samples	OxBS combined + HM450	CpG island shores and shelves, flanking TSS and gene bodies	no data	Spiers et al., 2017
Neurons	*Mm*	mouse cerebellum and hippocampus	dot blot; hMe-Seal; IS; hMeDIP-qPCR	developmentally activated gene bodies; repetitive loci; 60% of DhMRs intragenic and enriched in exons	MeCP2, no TET data	Szulwach et al., 2011
Neurons	*Mm*	transgenic mice with dual reporter for neural progenitors and progeny	IS; LC-MS; hMe-Seal labelled NimbleGen 2.1M arrays; TAB-Seq	global 5hmC gain; promoters, gene bodies, intragenic regions, during neurogenesis. associated with higher transcription	Tet2, Tet3	Hahn et al., 2013
Retina	*Dr*	zebrafish retinal neurogenesis	IS; ELISA; hMe-Seal enzyme protection + sequencing	body of one candidate gene	Tet2, Tet3	Seritrakul et al., 2017

Rn: Rattus norvegicus; *Dr: Danio rerio;* ATDC5: chondroprogenitor cell line; TAB-Seq: Tet-assisted bisulfite sequencing; GC-MS: Gas chromatography mass spectrometry; IF: immunofluorescence; IHC: Immunohistochemistry; IS: Immunostaining; ELISA: Enzyme-linked immunosorbent assay.

4.1. Endoderm

Endoderm gives rise to many of the cell types that form the gastrointestinal tract and related organs. The adult liver is relatively rich in 5hmC content, and global redistributions of 5mC [67–69] and 5hmC [70] have been described during the fetal to adult liver transition. Specifically, liquid chromatography mass spectrometry (LC-MS) estimations indicate that 5hmC increases from 0.125% to 1% of the total cytosine content. In adult livers, such 5hmC occupancy is overrepresented at genes involved in active catabolic and metabolic processes [71] (Figure 3). While these studies suggest a role of 5hmC in liver physiology, a recent report described a specific 5hmC event during hepatocyte differentiation [72]. TET-dependent 5hmC activation preceded activation of the HNF4A P1 promoter, a master TF of hepatocyte identity (Figure 3). In the same model of hepatocyte differentiation from a bipotent progenitor, we recently profiled 5mC/5hmC using oxidative bisulfite (OxBS) coupled to HumanMethylationEPIC arrays (Illumina, San Diego, CA, USA), and noticed that this process involves 5mC reduction and 5hmC gain partially associated with the acquisition of hepatocyte expression profile (unpublished results). Of note, liver tumor development has been associated with reduced TET activity and 5hmC in human samples [73], as well as in mouse [71] and in vitro models, suggesting 5hmC could be used as a biomarker of hepatocarcinogenesis [74].

Although 5hmC accumulation at the HNF4A P1 promoter seems to be transient, global higher levels in adult liver suggest stable 5hmC occupancy. In addition, stable accumulation of 5hmC has been described for enterocyte differentiation in well-known TF binding sites and targets involved in this process [75,76]. This contrasts with the pattern shown for blood cell subtypes, at least at earlier stages of blood cell differentiation (i.e., from HSCs) [19], in which there is a more general presence of 5hmC followed by a global drop that respects lineage-related loci, as described above. Interestingly, both in blood cells and endoderm differentiation, 5hmC redistribution was accompanied by a drop in 5mC (compare 5mC kinetics in Figures 2 and 3). Also, in both cases, loss of gene expression in committed cells correlated with a significant decrease in gene body 5hmC levels.

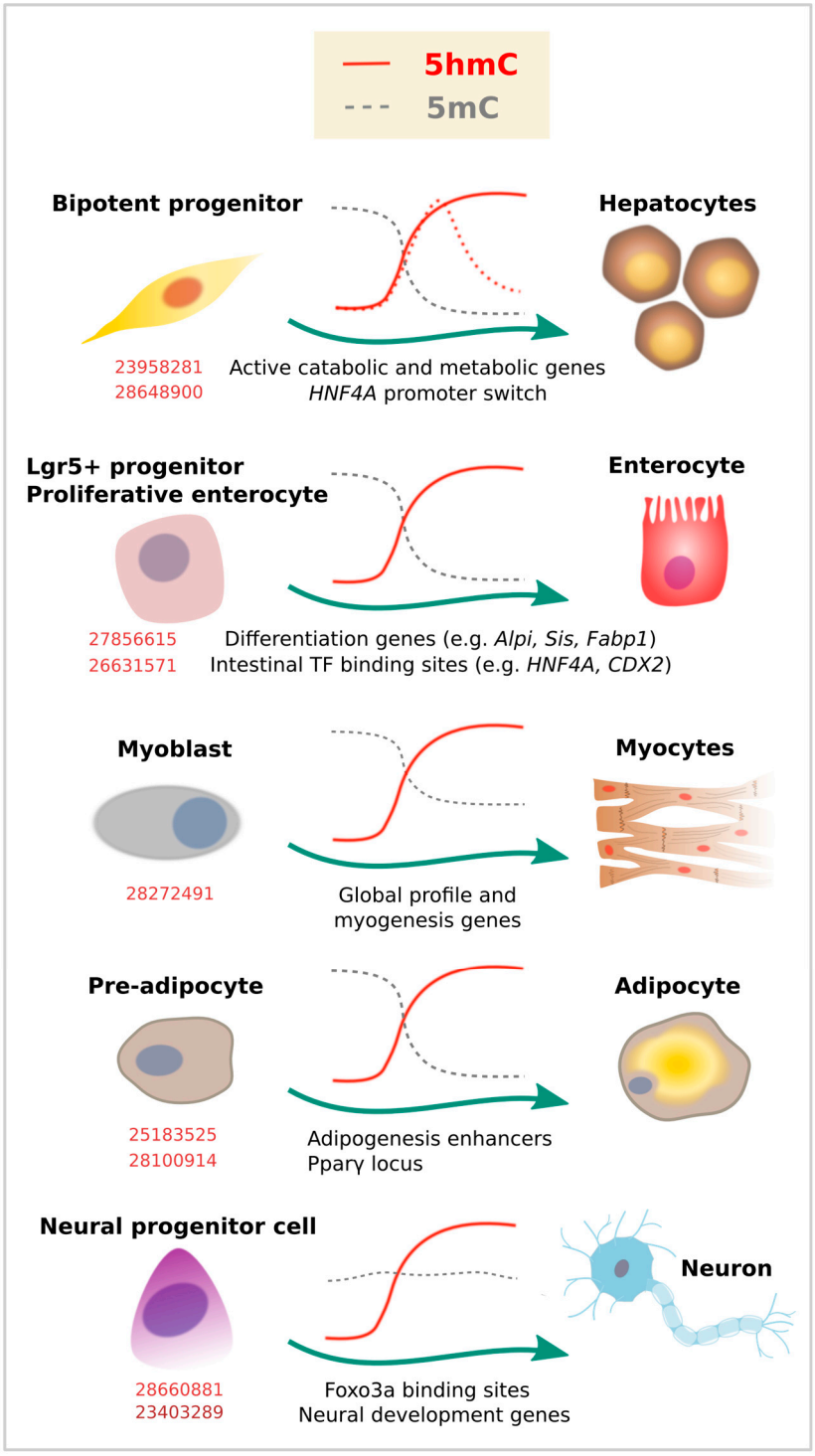

Figure 3. 5-Hydroxymethylcytosine dynamics during cell differentiation. Evidence for dynamic changes in 5mC (gray lines) or 5hmC (red lines) at the indicated loci, as associated with lineage commitment. Dashed lines represent additional evidence. Corresponding PubMed PMIDs for each study are shown in red.

4.2. Mesoderm (Other Than Blood Cells)

Besides blood cells, a more recent base resolution study suggests an important role of 5hmC during terminal chondriocyte differentiation. An increase in global 5hmC IF signal was observed at

the first stage of chondrogenic differentiation, followed by decrease at a later stage [77]. Using β-Glucosyltransferase-based chemical labelling and sequencing, the authors benefited from the previously established ATDC5 chondroprogenitor model system and found 5hmC enrichment near TSSs. In a similar way to what was described in immune cell subtypes, the increase in 5hmC was even more evident in gene bodies of key chondrogenic lineage-specific factors (Sox9, 5, and 6, Runx2, and Col2a1) and was associated with transcriptional activation.

Global and localized enrichment of 5hmC has also been described for myocyte [78] and cardiomyocyte development [79,80]. 5hmC enrichment was mainly found at gene bodies and distal regulatory regions, marking active genes enriched for Pol II occupancy, as well as active histone marks. The transition from embryonic into adult heart development was characterized by 5hmC peaks in genes related to heart development, such as actin-filament-based process and regulation of heart contraction. In addition, Tet2 has been implicated in both cardiomyocyte and myocyte development. Tet2 knockout resulted in 5hmC depletion at specific cardiomyocyte gene loci [80]. In a similar way, knockdown of Tet2, but not Tet1, significantly reduced myocyte gene expression (myogenin, Myf6, and myomaker) and impaired myoblast differentiation [78].

At least two studies have shown 5hmC enrichment during adipocyte development, using murine 3T3-L1 preadipocytes as a model (Figure 3). In the first study, the chromatin insulator CTCF was found to interact with TET enzymes to promote 5hmC deposition at adipogenic transcriptional enhancers [81]. In the second study, also TET proteins (and particularly TET2) were shown to be required for adipogenesis by increasing 5hmC at the Pparγ locus and inducing Pparγ gene expression [82].

Finally, a recent study has shown that 5hmC is also redistributed in Sertoli cells, mesodermal cells that are required for spermatogenesis. LC-MS evaluation of primary isolates of rat Sertoli cells from juvenile (7 days) and adult animals showed a puberty-associated reduction of 5mC and increase of 5hmC [83]. 5hmC peaks gained during maturation were related to cell transport, catabolic process, mitochondrion, and endocytosis, which go hand in hand with the fact that adult Sertoli cells have a diverse and highly active metabolism with an abundance of mitochondria.

Similar to blood cell types, these studies relate the differentiation process to an enrichment of 5hmC, suggesting that a general 5hmC shift in genomic distribution could be associated with the upregulation of genes that define cell state.

4.3. Ectoderm

At the time of 5hmC rediscovery, using a wide range of biochemical methods, the newly identified 5-hydroxymethyl-2′-deoxycytidine was shown to constitute 0.6% of total nucleotides in Purkinje cells [5]. Being highly abundant in brain, 5hmC was immediately suggested to have a role in the genomic control of neural functions. Therefore, together with ESCs, neurons of various types, anatomical locations, and levels of differentiation have been some of the best-studied cell types in terms of 5mC/5hmC content, distribution, and function. We refer the readers to specialized reviews in 5hmC and brain function [84,85], and only outline here some of the major findings in the context of dynamic models of neurogenesis.

Similar to other tissue types, 5hmC is enriched in the bodies of actively transcribed genes in postmitotic neurons, and accumulates at the flanking region of enhancers and TF binding sites [15,85,86]. In addition, 5hmC was found to accumulate in adult neurons as synaptogenesis occurs, although its content and distribution varies among different kind of neurons [20]. In line with this, the three TET proteins are expressed in the mammalian brain, and are all involved in neurogenesis and brain physiology [85]. Particularly, neural progenitor cells (NPC) have been reported to be affected by the absence of Tet1 with consequences at the functional level, including in learning and memory [87,88]. Similarly, loss of Tet2 was shown to reduce 5hmC levels (particularly at neurogenic genes) and partially block 5hmC gain upon differentiation [89]. It was also shown that forkhead box O3 (Foxo3a) physically interacts with Tet2 and regulates the expression of genes related to neural stem/progenitor proliferation [89] (Figure 3). Therefore, 5hmC and TETs control the expression of

genes and pathways related to neural programs, many of which are developmentally regulated [90]. Specific 5hmC enrichment has been observed at sequences adjacent to p300 sites in genes critical for neuronal differentiation [21], or Notch and Wnt pathway genes in retinal neurogenesis [91].

Another fact that increased the interest for 5hmC was the possibility of methylcytosine binding protein 2 (MeCP2) as a 5hmC reader [53], as this protein was previously associated with neurodevelopmental disorders [92] (reviewed in [93]). Indeed, it was recently shown that distribution of 5hmC in CG and non-CpG dinucleotides is distinct and reflects the binding specificity and genome occupancy of MeCP2 [86]. In addition, loss of MeCP2 led to specific reduction of 5hmC signals in dynamically hydroxymethylated intragenic non-CpGs involved in gene activation [20]. However, while the role of MeCP2 as a reader needs to be further validated [28], other candidate readers have been suggested in the context of neurogenesis and adult brain [29,94].

Therefore, dynamic models of neurogenesis are consistent with an important role of 5hmC, not only during differentiation, but also later in adult neuron life. Contrary to other tissues, 5mC depletion does not necessarily precede 5hmC acquisition [21] (Figure 3). Moreover, the high levels of 5hmC in adult neurons (and capacity to further increase), and the specific distribution across cell types and brain regions, indicate an important functional role in addition to preserving cell identity. Recent studies showing that demethylation occurs rapidly after neuronal or behavioral stimulation [95–97], and that 5hmC is dynamically regulated during aging [20], are helping to elucidate such role.

5. Perspectives and Concluding Remarks

Cell identity is acquired through the sequential and combinatorial activity of TFs on lineage-specific enhancers [98]. A global picture is emerging in which, in joint action with TFs and enhancers, TET-catalyzed 5hmC marks identity genes at key differentiation checkpoints. In most cases, global 5hmC seems to be progressively reduced from progenitor to differentiated state, but remains (or is acquired) at relevant lineage-specific loci or at genes related to adult cell function. As illustrated here, examples exist for all embryonic layers, and both epithelial and mesenchymal phenotypes, suggesting a general mechanism. In a time when cell subtypes are being systematically redefined [99], 5hmC promises to be an exquisite marker of cell identity. Moreover, as has been shown for the FoxP3 CNS loci in Treg cells, 5hmC may be able not only to identify a cell subtype, but also its origin, something that gene expression alone cannot do [57,62,63].

Although proliferation status seems to be critical for global 5hmC [22], this does not explain the specificity of 5hmC occupancy during differentiation. Recent studies are shedding light into such mechanisms. For example, interaction between TET proteins and lineage-specific TFs such as the FOXA family have been described [72,89,100]. Although this is better supported at the level of pioneer factors, it is feasible that other TFs involved in lineage commitment are also able to recruit TETs to specific genomic loci. While several TFs are involved in DNA demethylation by interacting with TET proteins (e.g., Nanog during establishment of pluripotency [101], the hematopoiesis-related RUNX1 [102] and EBF1 [103], PU.1 in osteoclast differentiation [104], and PPARγ in adipogenesis [105]), screening systems suggest that many others may share this property [106]. Alternatively, enhancer elements that distinguish cell types may be specifically targeted by TETs based on their chromatin conformation and histone mark profile. Indeed, based on their abundance in gene bodies of active genes and poised enhancers, TETs have been suggested as general transcriptional activators that recruit other proteins to demethylate enhancers [25].

Whether related or not to the preservation of cell identity, this oxidative form of methylated cytosine is emerging as a novel marker in many disorders [107]. Studies assessing 5mC and 5hmC content in different neurodegenerative pathologies, including Alzheimer's and Huntington's diseases, haven been reviewed in past years [108]. The levels of 5hmC in brain increase progressively from birth until death [108], and this age-associated increase was significantly higher in an Alzheimer transgenic mice model [109], while there is a disease-associated decrease of 5hmC levels in different brain regions in patients with the same condition [108]. One example that illustrates the importance of

5hmC in maintaining cell phenotype is liver fibrosis. In this pathology, chronic inflammatory injury triggers an adipogenic-to-fibrogenic phenotype switch in hepatic stellate cells, eventually leading to cirrhosis [110]. During different stages of chronic liver injury, 5hmC was found reduced, while hepatic stellate cells became transdifferentiated [111]. Consistent with these data, global 5hmC was shown to be reduced in a rat model of CCl4-induced cirrhosis [112]. It is important to note the recent availability of liver methylome and hydroxymethylome data on Wistar and Sprague-Dawley rats, as well as the genome-wide distribution of enhancer related chromatin marks (i.e., H3K4me1 and H3K27ac), which could represent a baseline reference for future studies of liver pathology [113].

An obvious context in which 5hmC occupancy is expected to be dysregulated is malignant disease (specialized reviews on cancer and TET-dependent 5hmC have been recently published [114–118]). Indeed, while Tet deletions/mutations have been shown to predispose to blood malignancies, cancer was initially associated with a global loss of 5hmC in various tissues [65,66]. Although such reports revealing 5hmC decrease in cancer lacked genome-wide or base-level resolution, studies consistently show that 5hmC profiles are able to distinguish malignant tissues, even under cell culture conditions [119]. If 5hmC does indeed preserve cellular phenotypes, it would be expected to have a protective role against cancer. In line with this, it was suggested that 5hmC is a hallmark from the early intestinal development that prevents neoplastic DNA hypermethylation events [120]. In addition, 5hmC was recently shown to correlate with lower regional CpG > T mutation frequency in cancers from various tissues (i.e., brain, kidney, and blood), also suggesting a protective role [121].

Finally, it has been suggested for years that DNA methylation may represent an interphase between environment and disease. The debate has been centered around which genomic locations are more dynamic or sensitive to external factors, and high interest has been placed on DNA methylation fluctuations at enhancer elements. Nowadays, emerging work suggests an important role of the oxidized forms of 5m—in particular, of 5hmC and the enzymes that establish it. For example, TETs are able to control differentiation into immune cell subtypes in response to specific inflammatory signals and are sensors of diverse metabolic processes. Another interesting example could be the critical role of oxygen concentration (as a co-factor) that influences TET activity and hence regulating cellular differentiation and fate in embryogenesis in which there are graded levels of molecular oxygen [122]. In a similar way, as α-ketoglutarate-dependent dioxygenases, the activity of TETs can be inhibited by 2-hydroxyglutarate in pathological conditions such as aberrant liver progenitor differentiation in presence of IDH1/2 mutations [123], or $CD8^+$ T cell fate under hypoxia [49]. Moreover, TET activity has been shown to be influenced by the availability of vitamins C [46,124,125] and A [125], and hydrogen sulphide [47].

In conclusion, the data sets presented throughout this study lead us to suggest that previously published studies that lack discriminated detection of 5mC and 5hmC (such as the widely used bisulphite conversion) have to be carefully revisited. Furthermore, approaches that are able to distinguish between DNA methylation intermediates should be superior in the future. Evidence points towards 5hmC (rather than 5mC) as a more likely interphase between the environment and dynamic gene expression changes, and most importantly, it seems to regulate the directors of cell fate. Therefore, its distribution in the genome could be used as a "fingerprint" to clearly indicate cell identity. This new potential of the 5hmC not only opens the door to deeper studies of cell differentiation and tissue development, but could also provide a useful tool for early detection and prevention of several conditions associated with the loss of cellular identity such as cancer.

Acknowledgments: We apologize to our colleagues whose works were not directly covered or cited here. S.E. is supported by the French Government, under a grant from the Agence Nationale de la Recherche (Project Investissements d'Avenir UCAJEDI, No. ANR-15-IDEX-01). J.R.R.-A. is the recipient of Fellowships from Consejo Nacional de Ciencia y Tecnología (CONACyT) (CVU 508509) and Programa de Apoyo a los Estudios de Posgrado-Universidad Nacional Autónoma de México (PAEP-UNAM) (No. Cta. 30479367-5). H.H.-V. studies on 5hmC in progenitor and immune cell identity are currently supported by grants from the Agence Française de Recherches sur le VIH/Sida et les Hépatites Virales (ANRS) (grants No. ECTZ47287 and ECTZ50137), and the Institut National du Cancer (INCA) (Grant No. PLBIO17-317, Inserm Plan Cancer No. C14088CS). The authors declare no conflicts of interest.

Author Contributions: S.E., J.R.R.-A. and H.H.-V. wrote jointly this manuscript.

Conflicts of Interest: The authors declare no conflict of interest.

References

1. Schübeler, D. Function and information content of DNA methylation. *Nature* **2015**, *517*, 321–326. [CrossRef] [PubMed]
2. Horvath, S. DNA methylation age of human tissues and cell types. *Genome Biol.* **2013**, *14*, R115. [CrossRef] [PubMed]
3. Houseman, E.A.; Accomando, W.P.; Koestler, D.C.; Christensen, B.C.; Marsit, C.J.; Nelson, H.H.; Wiencke, J.K.; Kelsey, K.T. DNA methylation arrays as surrogate measures of cell mixture distribution. *BMC Bioinform.* **2012**, *13*, 86. [CrossRef] [PubMed]
4. Penn, N.W.; Suwalski, R.; O'Riley, C.; Bojanowski, K.; Yura, R. The presence of 5-hydroxymethylcytosine in animal deoxyribonucleic acid. *Biochem. J.* **1972**, *126*, 781–790. [CrossRef] [PubMed]
5. Kriaucionis, S.; Heintz, N. The nuclear DNA base 5-hydroxymethylcytosine is present in Purkinje neurons and the brain. *Science* **2009**, *324*, 929–930. [CrossRef] [PubMed]
6. Tahiliani, M.; Koh, K.P.; Shen, Y.; Pastor, W.A.; Bandukwala, H.; Brudno, Y.; Agarwal, S.; Iyer, L.M.; Liu, D.R.; Aravind, L.; et al. Conversion of 5-methylcytosine to 5-hydroxymethylcytosine in mammalian DNA by MLL partner TET1. *Science* **2009**, *324*, 930–935. [CrossRef] [PubMed]
7. Ito, S.; Shen, L.; Dai, Q.; Wu, S.C.; Collins, L.B.; Swenberg, J.A.; He, C.; Zhang, Y. Tet proteins can convert 5-methylcytosine to 5-formylcytosine and 5-carboxylcytosine. *Science* **2011**, *333*, 1300–1303. [CrossRef] [PubMed]
8. Koh, K.P.; Yabuuchi, A.; Rao, S.; Huang, Y.; Cunniff, K.; Nardone, J.; Laiho, A.; Tahiliani, M.; Sommer, C.A.; Mostoslavsky, G.; et al. Tet1 and Tet2 regulate 5-hydroxymethylcytosine production and cell lineage specification in mouse embryonic stem cells. *Cell Stem Cell* **2011**, *8*, 200–213. [CrossRef] [PubMed]
9. Huang, Y.; Chavez, L.; Chang, X.; Wang, X.; Pastor, W.A.; Kang, J.; Zepeda-Martínez, J.A.; Pape, U.J.; Jacobsen, S.E.; Peters, B.; et al. Distinct roles of the methylcytosine oxidases Tet1 and Tet2 in mouse embryonic stem cells. *Proc. Natl. Acad. Sci. USA* **2014**, *111*, 1361–1366. [CrossRef] [PubMed]
10. Qing, Y.; Tian, Z.; Bi, Y.; Wang, Y.; Long, J.; Song, C.-X.; Diao, J. Quantitation and mapping of the epigenetic marker 5-hydroxymethylcytosine. *BioEssays News Rev. Mol. Cell. Dev. Biol.* **2017**, *39*. [CrossRef] [PubMed]
11. Thomson, J.P.; Hunter, J.M.; Nestor, C.E.; Dunican, D.S.; Terranova, R.; Moggs, J.G.; Meehan, R.R. Comparative analysis of affinity-based 5-hydroxymethylation enrichment techniques. *Nucleic Acids Res.* **2013**, *41*, e206. [CrossRef] [PubMed]
12. Song, C.-X.; Yi, C.; He, C. Mapping recently identified nucleotide variants in the genome and transcriptome. *Nat. Biotechnol.* **2012**, *30*, 1107–1116. [CrossRef] [PubMed]
13. Rivera, C.M.; Ren, B. Mapping human epigenomes. *Cell* **2013**, *155*, 39–55. [CrossRef] [PubMed]
14. Booth, M.J.; Branco, M.R.; Ficz, G.; Oxley, D.; Krueger, F.; Reik, W.; Balasubramanian, S. Quantitative sequencing of 5-methylcytosine and 5-hydroxymethylcytosine at single-base resolution. *Science* **2012**, *336*, 934–937. [CrossRef] [PubMed]
15. Yu, M.; Hon, G.C.; Szulwach, K.E.; Song, C.-X.; Zhang, L.; Kim, A.; Li, X.; Dai, Q.; Shen, Y.; Park, B.; et al. Base-resolution analysis of 5-hydroxymethylcytosine in the mammalian genome. *Cell* **2012**, *149*, 1368–1380. [CrossRef] [PubMed]
16. Ficz, G.; Branco, M.R.; Seisenberger, S.; Santos, F.; Krueger, F.; Hore, T.A.; Marques, C.J.; Andrews, S.; Reik, W. Dynamic regulation of 5-hydroxymethylcytosine in mouse ES cells and during differentiation. *Nature* **2011**, *473*, 398–402. [CrossRef] [PubMed]
17. Zhong, S.; Li, Z.; Jiang, T.; Li, X.; Wang, H. Immunofluorescence imaging strategy for evaluation of the accessibility of DNA 5-hydroxymethylcytosine in chromatins. *Anal. Chem.* **2017**, *89*, 5702–5706. [CrossRef] [PubMed]
18. Verma, N.; Pan, H.; Doré, L.C.; Shukla, A.; Li, Q.V.; Pelham-Webb, B.; Teijeiro, V.; González, F.; Krivtsov, A.; Chang, C.-J.; et al. TET proteins safeguard bivalent promoters from de novo methylation in human embryonic stem cells. *Nat. Genet.* **2017**. [CrossRef]

19. Tekpli, X.; Urbanucci, A.; Hashim, A.; Vågbø, C.B.; Lyle, R.; Kringen, M.K.; Staff, A.C.; Dybedal, I.; Mills, I.G.; Klungland, A.; et al. Changes of 5-hydroxymethylcytosine distribution during myeloid and lymphoid differentiation of $CD34^+$ cells. *Epigenet. Chromatin* **2016**, *9*, 21. [CrossRef] [PubMed]
20. Szulwach, K.E.; Li, X.; Li, Y.; Song, C.-X.; Wu, H.; Dai, Q.; Irier, H.; Upadhyay, A.K.; Gearing, M.; Levey, A.I.; et al. 5-hmC–mediated epigenetic dynamics during postnatal neurodevelopment and aging. *Nat. Neurosci.* **2011**, *14*, 1607–1616. [CrossRef] [PubMed]
21. Hahn, M.A.; Qiu, R.; Wu, X.; Li, A.X.; Zhang, H.; Wang, J.; Jui, J.; Jin, S.-G.; Jiang, Y.; Pfeifer, G.P.; et al. Dynamics of 5-hydroxymethylcytosine and chromatin marks in mammalian neurogenesis. *Cell Rep.* **2013**, *3*, 291–300. [CrossRef] [PubMed]
22. Bachman, M.; Uribe-Lewis, S.; Yang, X.; Williams, M.; Murrell, A.; Balasubramanian, S. 5-Hydroxymethylcytosine is a predominantly stable DNA modification. *Nat. Chem.* **2014**, *6*, 1049–1055. [CrossRef] [PubMed]
23. Hu, L.; Lu, J.; Cheng, J.; Rao, Q.; Li, Z.; Hou, H.; Lou, Z.; Zhang, L.; Li, W.; Gong, W.; et al. Structural insight into substrate preference for TET-mediated oxidation. *Nature* **2015**, *527*, 118–122. [CrossRef] [PubMed]
24. He, Y.-F.; Li, B.-Z.; Li, Z.; Liu, P.; Wang, Y.; Tang, Q.; Ding, J.; Jia, Y.; Chen, Z.; Li, L.; et al. Tet-mediated formation of 5-carboxylcytosine and its excision by TDG in mammalian DNA. *Science* **2011**, *333*, 1303–1307. [CrossRef] [PubMed]
25. Szyf, M. The elusive role of 5′-hydroxymethylcytosine. *Epigenomics* **2016**, *8*, 1539–1551. [CrossRef] [PubMed]
26. Hashimoto, H.; Hong, S.; Bhagwat, A.S.; Zhang, X.; Cheng, X. Excision of 5-hydroxymethyluracil and 5-carboxylcytosine by the thymine DNA glycosylase domain: its structural basis and implications for active DNA demethylation. *Nucleic Acids Res.* **2012**, *40*, 10203–10214. [CrossRef] [PubMed]
27. Juan, D.; Perner, J.; Carrillo de Santa Pau, E.; Marsili, S.; Ochoa, D.; Chung, H.-R.; Vingron, M.; Rico, D.; Valencia, A. Epigenomic co-localization and co-evolution reveal a key role for 5hmC as a communication hub in the chromatin network of ESCs. *Cell Rep.* **2016**, *14*, 1246–1257. [CrossRef] [PubMed]
28. Song, J.; Pfeifer, G.P. Are there specific readers of oxidized 5-methylcytosine bases? *BioEssays News Rev. Mol. Cell. Dev. Biol.* **2016**, *38*, 1038–1047. [CrossRef] [PubMed]
29. Spruijt, C.G.; Gnerlich, F.; Smits, A.H.; Pfaffeneder, T.; Jansen, P.W.T.C.; Bauer, C.; Münzel, M.; Wagner, M.; Müller, M.; Khan, F.; et al. Dynamic readers for 5-(hydroxy)methylcytosine and its oxidized derivatives. *Cell* **2013**, *152*, 1146–1159. [CrossRef] [PubMed]
30. Zhou, T.; Xiong, J.; Wang, M.; Yang, N.; Wong, J.; Zhu, B.; Xu, R.-M. Structural basis for hydroxymethylcytosine recognition by the SRA domain of UHRF2. *Mol. Cell* **2014**, *54*, 879–886. [CrossRef] [PubMed]
31. Fanis, P.; Gillemans, N.; Aghajanirefah, A.; Pourfarzad, F.; Demmers, J.; Esteghamat, F.; Vadlamudi, R.K.; Grosveld, F.; Philipsen, S.; van Dijk, T.B. Five friends of methylated chromatin target of protein-arginine-methyltransferase[prmt]-1 (chtop), a complex linking arginine methylation to desumoylation. *Mol. Cell. Proteom. MCP* **2012**, *11*, 1263–1273. [CrossRef] [PubMed]
32. Takai, H.; Masuda, K.; Sato, T.; Sakaguchi, Y.; Suzuki, T.; Suzuki, T.; Koyama-Nasu, R.; Nasu-Nishimura, Y.; Katou, Y.; Ogawa, H.; et al. 5-Hydroxymethylcytosine plays a critical role in glioblastomagenesis by recruiting the CHTOP-methylosome complex. *Cell Rep.* **2014**, *9*, 48–60. [CrossRef] [PubMed]
33. Hashimoto, H.; Olanrewaju, Y.O.; Zheng, Y.; Wilson, G.G.; Zhang, X.; Cheng, X. Wilms tumor protein recognizes 5-carboxylcytosine within a specific DNA sequence. *Genes Dev.* **2014**, *28*, 2304–2313. [CrossRef] [PubMed]
34. Wang, L.; Zhou, Y.; Xu, L.; Xiao, R.; Lu, X.; Chen, L.; Chong, J.; Li, H.; He, C.; Fu, X.-D.; et al. Molecular basis for 5-carboxycytosine recognition by RNA polymerase II elongation complex. *Nature* **2015**, *523*, 621–625. [CrossRef] [PubMed]
35. Jin, S.-G.; Zhang, Z.-M.; Dunwell, T.L.; Harter, M.R.; Wu, X.; Johnson, J.; Li, Z.; Liu, J.; Szabó, P.E.; Lu, Q.; et al. Tet3 Reads 5-Carboxylcytosine through Its CXXC Domain and Is a Potential Guardian against Neurodegeneration. *Cell Rep.* **2016**, *14*, 493–505. [CrossRef] [PubMed]
36. Tsagaratou, A.; Äijö, T.; Lio, C.-W.J.; Yue, X.; Huang, Y.; Jacobsen, S.E.; Lähdesmäki, H.; Rao, A. Dissecting the dynamic changes of 5-hydroxymethylcytosine in T-cell development and differentiation. *Proc. Natl. Acad. Sci. USA* **2014**, *111*, E3306–E3315. [CrossRef] [PubMed]
37. Wu, H.; Huang, X.; Qiu, H.; Zhao, M.; Liao, W.; Yuan, S.; Xie, Y.; Dai, Y.; Chang, C.; Yoshimura, A.; et al. High salt promotes autoimmunity by TET2-induced DNA demethylation and driving the differentiation of Tfh cells. *Sci. Rep.* **2016**, *6*, 28065. [CrossRef] [PubMed]

38. Garcia-Gomez, A.; Li, T.; Kerick, M.; Català-Moll, F.; Comet, N.R.; Rodríguez-Ubreva, J.; de la Rica, L.; Branco, M.R.; Martín, J.; Ballestar, E. TET2- and TDG-mediated changes are required for the acquisition of distinct histone modifications in divergent terminal differentiation of myeloid cells. *Nucleic Acids Res.* **2017**, *45*, 10002–10017. [CrossRef] [PubMed]
39. Lio, C.-W.; Zhang, J.; González-Avalos, E.; Hogan, P.G.; Chang, X.; Rao, A. Tet2 and Tet3 cooperate with B-lineage transcription factors to regulate DNA modification and chromatin accessibility. *eLife* **2016**, *5*, e18290. [CrossRef] [PubMed]
40. Montagner, S.; Leoni, C.; Emming, S.; Chiara, G.D.; Balestrieri, C.; Barozzi, I.; Piccolo, V.; Togher, S.; Ko, M.; Rao, A.; et al. TET2 Regulates Mast Cell Differentiation and Proliferation through Catalytic and Non-catalytic Activities. *Cell Rep.* **2016**, *15*, 1566–1579. [CrossRef] [PubMed]
41. Caron, G.; Hussein, M.; Kulis, M.; Delaloy, C.; Chatonnet, F.; Pignarre, A.; Avner, S.; Lemarié, M.; Mahé, E.A.; Verdaguer-Dot, N.; et al. Cell-Cycle-Dependent Reconfiguration of the DNA Methylome during Terminal Differentiation of Human B Cells into Plasma Cells. *Cell Rep.* **2015**, *13*, 1059–1071. [CrossRef] [PubMed]
42. Madzo, J.; Liu, H.; Rodriguez, A.; Vasanthakumar, A.; Sundaravel, S.; Caces, D.B.D.; Looney, T.J.; Zhang, L.; Lepore, J.B.; Macrae, T.; et al. Hydroxymethylation at Gene Regulatory Regions Directs Stem/Early Progenitor Cell Commitment during Erythropoiesis. *Cell Rep.* **2014**, *6*, 231–244. [CrossRef] [PubMed]
43. Ichiyama, K.; Chen, T.; Wang, X.; Yan, X.; Kim, B.-S.; Tanaka, S.; Ndiaye-Lobry, D.; Deng, Y.; Zou, Y.; Zheng, P.; et al. The methylcytosine dioxygenase Tet2 promotes DNA demethylation and activation of cytokine gene expression in T cells. *Immunity* **2015**, *42*, 613–626. [CrossRef] [PubMed]
44. Nestor, C.E.; Lentini, A.; Hägg Nilsson, C.; Gawel, D.R.; Gustafsson, M.; Mattson, L.; Wang, H.; Rundquist, O.; Meehan, R.R.; Klocke, B.; et al. 5-Hydroxymethylcytosine Remodeling Precedes Lineage Specification during Differentiation of Human CD4+ T Cells. *Cell Rep.* **2016**, *16*, 559–570. [CrossRef] [PubMed]
45. Tsagaratou, A.; González-Avalos, E.; Rautio, S.; Scott-Browne, J.P.; Togher, S.; Pastor, W.A.; Rothenberg, E.V.; Chavez, L.; Lähdesmäki, H.; Rao, A. TET proteins regulate the lineage specification and TCR-mediated expansion of iNKT cells. *Nat. Immunol.* **2017**, *18*, 45–53. [CrossRef] [PubMed]
46. Yue, X.; Trifari, S.; Äijö, T.; Tsagaratou, A.; Pastor, W.A.; Zepeda-Martínez, J.A.; Lio, C.-W.J.; Li, X.; Huang, Y.; Vijayanand, P.; et al. Control of Foxp3 stability through modulation of TET activity. *J. Exp. Med.* **2016**, *213*, 377–397. [CrossRef] [PubMed]
47. Yang, R.; Qu, C.; Zhou, Y.; Konkel, J.; Shi, S.; Liu, Y.; Chen, C.; Liu, S.; Liu, D.; Chen, Y.; et al. Hydrogen sulfide promotes Tet1- and Tet2-mediated Foxp3 demethylation to drive regulatory T cell differentiation and Maintain Immune Homeostasis. *Immunity* **2015**, *43*, 251–263. [CrossRef] [PubMed]
48. Liu, X.; Lu, H.; Chen, T.; Nallaparaju, K.C.; Yan, X.; Tanaka, S.; Ichiyama, K.; Zhang, X.; Zhang, L.; Wen, X.; et al. Genome-wide analysis identifies Bcl6-controlled regulatory networks during T follicular helper cell differentiation. *Cell Rep.* **2016**, *14*, 1735–1747. [CrossRef] [PubMed]
49. Tyrakis, P.A.; Palazon, A.; Macias, D.; Lee, K.L.; Phan, A.T.; Veliça, P.; You, J.; Chia, G.S.; Sim, J.; Doedens, A.; et al. The immunometabolite S-2-hydroxyglutarate regulates CD8+ T-lymphocyte fate. *Nature* **2016**, *540*, 236–241. [CrossRef] [PubMed]
50. Wallner, S.; Schröder, C.; Leitão, E.; Berulava, T.; Haak, C.; Beißer, D.; Rahmann, S.; Richter, A.S.; Manke, T.; Bönisch, U.; et al. Epigenetic dynamics of monocyte-to-macrophage differentiation. *Epigenet. Chromatin* **2016**, *9*, 33. [CrossRef] [PubMed]
51. Klug, M.; Schmidhofer, S.; Gebhard, C.; Andreesen, R.; Rehli, M. 5-Hydroxymethylcytosine is an essential intermediate of active DNA demethylation processes in primary human monocytes. *Genome Biol.* **2013**, *14*, R46. [CrossRef] [PubMed]
52. Yan, H.; Wang, Y.; Qu, X.; Li, J.; Hale, J.; Huang, Y.; An, C.; Papoin, J.; Guo, X.; Chen, L.; et al. Distinct roles for TET family proteins in regulating human erythropoiesis. *Blood* **2017**, *129*, 2002–2012. [CrossRef] [PubMed]
53. Williams, K.; Christensen, J.; Pedersen, M.T.; Johansen, J.V.; Cloos, P.A.C.; Rappsilber, J.; Helin, K. TET1 and hydroxymethylcytosine in transcription and DNA methylation fidelity. *Nature* **2011**, *473*, 343–348. [CrossRef] [PubMed]
54. Fontenot, J.D.; Gavin, M.A.; Rudensky, A.Y. Foxp3 programs the development and function of CD4+CD25+ regulatory T cells. *Nat. Immunol.* **2003**, *4*, 330–336. [CrossRef] [PubMed]
55. Baron, U.; Floess, S.; Wieczorek, G.; Baumann, K.; Grützkau, A.; Dong, J.; Thiel, A.; Boeld, T.J.; Hoffmann, P.; Edinger, M.; et al. DNA demethylation in the human FOXP3 locus discriminates regulatory T cells from activated FOXP3+ conventional T cells. *Eur. J. Immunol.* **2007**, *37*, 2378–2389. [CrossRef] [PubMed]

56. Floess, S.; Freyer, J.; Siewert, C.; Baron, U.; Olek, S.; Polansky, J.; Schlawe, K.; Chang, H.-D.; Bopp, T.; Schmitt, E.; et al. Epigenetic control of the foxp3 locus in regulatory T cells. *PLoS Biol.* **2007**, *5*, e38. [CrossRef] [PubMed]
57. Zheng, Y.; Josefowicz, S.; Chaudhry, A.; Peng, X.P.; Forbush, K.; Rudensky, A.Y. Role of conserved non-coding DNA elements in the Foxp3 gene in regulatory T-cell fate. *Nature* **2010**, *463*, 808–812. [CrossRef] [PubMed]
58. Toker, A.; Engelbert, D.; Garg, G.; Polansky, J.K.; Floess, S.; Miyao, T.; Baron, U.; Düber, S.; Geffers, R.; Giehr, P.; et al. Active demethylation of the Foxp3 locus leads to the generation of stable regulatory T cells within the thymus. *J. Immunol.* **2013**, *190*, 3180–3188. [CrossRef] [PubMed]
59. Kim, H.-P.; Leonard, W.J. CREB/ATF-dependent T cell receptor-induced Foxp3 gene expression: A role for DNA methylation. *J. Exp. Med.* **2007**, *204*, 1543–1551. [CrossRef] [PubMed]
60. Polansky, J.K.; Kretschmer, K.; Freyer, J.; Floess, S.; Garbe, A.; Baron, U.; Olek, S.; Hamann, A.; von Boehmer, H.; Huehn, J. DNA methylation controls Foxp3 gene expression. *Eur. J. Immunol.* **2008**, *38*, 1654–1663. [CrossRef] [PubMed]
61. Ohkura, N.; Hamaguchi, M.; Morikawa, H.; Sugimura, K.; Tanaka, A.; Ito, Y.; Osaki, M.; Tanaka, Y.; Yamashita, R.; Nakano, N.; et al. T cell receptor stimulation-induced epigenetic changes and Foxp3 expression are independent and complementary events required for Treg cell development. *Immunity* **2012**, *37*, 785–799. [CrossRef] [PubMed]
62. Li, X.; Liang, Y.; LeBlanc, M.; Benner, C.; Zheng, Y. Function of a Foxp3 cis-element in protecting regulatory T cell identity. *Cell* **2014**, *158*, 734–748. [CrossRef] [PubMed]
63. Feng, Y.; Arvey, A.; Chinen, T.; van der Veeken, J.; Gasteiger, G.; Rudensky, A.Y. Control of the inheritance of regulatory T cell identity by a cis element in the Foxp3 locus. *Cell* **2014**, *158*, 749–763. [CrossRef] [PubMed]
64. Kitagawa, Y.; Ohkura, N.; Kidani, Y.; Vandenbon, A.; Hirota, K.; Kawakami, R.; Yasuda, K.; Motooka, D.; Nakamura, S.; Kondo, M.; et al. Guidance of regulatory T cell development by Satb1-dependent super-enhancer establishment. *Nat. Immunol.* **2017**, *18*, 173–183. [CrossRef] [PubMed]
65. Chiba, S. Dysregulation of TET2 in hematologic malignancies. *Int. J. Hematol.* **2017**, *105*, 17–22. [CrossRef] [PubMed]
66. Patnaik, M.M.; Zahid, M.F.; Lasho, T.L.; Finke, C.; Ketterling, R.L.; Gangat, N.; Robertson, K.D.; Hanson, C.A.; Tefferi, A. Number and type of TET2 mutations in chronic myelomonocytic leukemia and their clinical relevance. *Blood Cancer J.* **2016**, *6*, e472. [CrossRef] [PubMed]
67. Bonder, M.J.; Kasela, S.; Kals, M.; Tamm, R.; Lokk, K.; Barragan, I.; Buurman, W.A.; Deelen, P.; Greve, J.-W.; Ivanov, M.; et al. Genetic and epigenetic regulation of gene expression in fetal and adult human livers. *BMC Genom.* **2014**, *15*, 860. [CrossRef] [PubMed]
68. Huse, S.M.; Gruppuso, P.A.; Boekelheide, K.; Sanders, J.A. Patterns of gene expression and DNA methylation in human fetal and adult liver. *BMC Genom.* **2015**, *16*. [CrossRef] [PubMed]
69. Wilson, A.A.; Ying, L.; Liesa, M.; Segeritz, C.-P.; Mills, J.A.; Shen, S.S.; Jean, J.; Lonza, G.C.; Liberti, D.C.; Lang, A.H.; et al. Emergence of a stage-dependent human liver disease signature with directed differentiation of alpha-1 antitrypsin-deficient iPS cells. *Stem Cell Rep.* **2015**, *4*, 873–885. [CrossRef] [PubMed]
70. Ivanov, M.; Kals, M.; Kacevska, M.; Barragan, I.; Kasuga, K.; Rane, A.; Metspalu, A.; Milani, L.; Ingelman-Sundberg, M. Ontogeny, distribution and potential roles of 5-hydroxymethylcytosine in human liver function. *Genome Biol.* **2013**, *14*. [CrossRef] [PubMed]
71. Thomson, J.P.; Ottaviano, R.; Unterberger, E.B.; Lempiäinen, H.; Muller, A.; Terranova, R.; Illingworth, R.S.; Webb, S.; Kerr, A.R.W.; Lyall, M.J.; et al. Loss of Tet1-associated 5-hydroxymethylcytosine is concomitant with aberrant promoter hypermethylation in liver cancer. *Cancer Res.* **2016**, *76*, 3097–3108. [CrossRef] [PubMed]
72. Ancey, P.-B.; Ecsedi, S.; Lambert, M.-P.; Talukdar, F.R.; Cros, M.-P.; Glaise, D.; Narvaez, D.M.; Chauvet, V.; Herceg, Z.; Corlu, A.; et al. TET-Catalyzed 5-Hydroxymethylation Precedes HNF4A Promoter Choice during Differentiation of Bipotent Liver Progenitors. *Stem Cell Rep.* **2017**, *9*, 264–278. [CrossRef] [PubMed]
73. Yang, H.; Liu, Y.; Bai, F.; Zhang, J.-Y.; Ma, S.-H.; Liu, J.; Xu, Z.-D.; Zhu, H.-G.; Ling, Z.-Q.; Ye, D.; et al. Tumor development is associated with decrease of TET gene expression and 5-methylcytosine hydroxylation. *Oncogene* **2013**, *32*, 663–669. [CrossRef] [PubMed]
74. Thomson, J.P.; Hunter, J.M.; Lempiäinen, H.; Müller, A.; Terranova, R.; Moggs, J.G.; Meehan, R.R. Dynamic changes in 5-hydroxymethylation signatures underpin early and late events in drug exposed liver. *Nucleic Acids Res.* **2013**, *41*, 5639–5654. [CrossRef] [PubMed]

75. Kim, R.; Sheaffer, K.L.; Choi, I.; Won, K.-J.; Kaestner, K.H. Epigenetic regulation of intestinal stem cells by Tet1-mediated DNA hydroxymethylation. *Genes Dev.* **2016**, *30*, 2433–2442. [CrossRef] [PubMed]
76. Chapman, C.G.; Mariani, C.J.; Wu, F.; Meckel, K.; Butun, F.; Chuang, A.; Madzo, J.; Bissonette, M.B.; Kwon, J.H.; Godley, L.A. TET-catalyzed 5-hydroxymethylcytosine regulates gene expression in differentiating colonocytes and colon cancer. *Sci. Rep.* **2015**, *5*, 17568. [CrossRef] [PubMed]
77. Taylor, S.E.B.; Li, Y.H.; Smeriglio, P.; Rath, M.; Wong, W.H.; Bhutani, N. Stable 5-hydroxymethylcytosine (5hmC) acquisition marks gene activation during chondrogenic differentiation. *J. Bone Miner. Res. Off. J. Am. Soc. Bone Miner. Res.* **2016**, *31*, 524–534. [CrossRef] [PubMed]
78. Zhong, X.; Wang, Q.-Q.; Li, J.-W.; Zhang, Y.-M.; An, X.-R.; Hou, J. Ten-eleven translocation-2 (Tet2) is involved in myogenic differentiation of skeletal myoblast cells in vitro. *Sci. Rep.* **2017**, *7*, 43539. [CrossRef] [PubMed]
79. Kranzhöfer, D.K.; Gilsbach, R.; Grüning, B.A.; Backofen, R.; Nührenberg, T.G.; Hein, L. 5′-hydroxymethylcytosine precedes loss of CpG methylation in enhancers and genes undergoing activation in cardiomyocyte maturation. *PLoS ONE* **2016**, *11*, e0166575. [CrossRef] [PubMed]
80. Greco, C.M.; Kunderfranco, P.; Rubino, M.; Larcher, V.; Carullo, P.; Anselmo, A.; Kurz, K.; Carell, T.; Angius, A.; Latronico, M.V.G.; et al. DNA hydroxymethylation controls cardiomyocyte gene expression in development and hypertrophy. *Nat. Commun.* **2016**, *7*. [CrossRef] [PubMed]
81. Dubois-Chevalier, J.; Oger, F.; Dehondt, H.; Firmin, F.F.; Gheeraert, C.; Staels, B.; Lefebvre, P.; Eeckhoute, J. A dynamic CTCF chromatin binding landscape promotes DNA hydroxymethylation and transcriptional induction of adipocyte differentiation. *Nucleic Acids Res.* **2014**, *42*, 10943–10959. [CrossRef] [PubMed]
82. Yoo, Y.; Park, J.H.; Weigel, C.; Liesenfeld, D.B.; Weichenhan, D.; Plass, C.; Seo, D.-G.; Lindroth, A.M.; Park, Y.J. TET-mediated hydroxymethylcytosine at the Pparγ locus is required for initiation of adipogenic differentiation. *Int. J. Obes. (2005)* **2017**, *41*, 652–659. [CrossRef] [PubMed]
83. Landfors, M.; Johansen, J.; Aronsen, J.M.; Vågbø, C.B.; Doré, L.C.; He, C.; Sjaastad, I.; Sætrom, P.; Fedorcsák, P.; Dahl, J.A.; et al. Genome-wide profiling of DNA 5-hydroxymethylcytosine during rat Sertoli cell maturation. *Cell Discov.* **2017**, *3*, 17013. [CrossRef] [PubMed]
84. Sun, W.; Zang, L.; Shu, Q.; Li, X. From development to diseases: the role of 5hmC in brain. *Genomics* **2014**, *104*, 347–351. [CrossRef] [PubMed]
85. Wen, L.; Tang, F. Genomic distribution and possible functions of DNA hydroxymethylation in the brain. *Genomics* **2014**, *104*, 341–346. [CrossRef] [PubMed]
86. Mellén, M.; Ayata, P.; Heintz, N. 5-hydroxymethylcytosine accumulation in postmitotic neurons results in functional demethylation of expressed genes. *Proc. Natl. Acad. Sci. USA* **2017**, *114*, E7812–E7821. [CrossRef] [PubMed]
87. Zhang, R.-R.; Cui, Q.-Y.; Murai, K.; Lim, Y.C.; Smith, Z.D.; Jin, S.; Ye, P.; Rosa, L.; Lee, Y.K.; Wu, H.-P.; et al. Tet1 regulates adult hippocampal neurogenesis and cognition. *Cell Stem Cell* **2013**, *13*, 237–245. [CrossRef] [PubMed]
88. Rudenko, A.; Dawlaty, M.M.; Seo, J.; Cheng, A.W.; Meng, J.; Le, T.; Faull, K.F.; Jaenisch, R.; Tsai, L.-H. Tet1 is critical for neuronal activity-regulated gene expression and memory extinction. *Neuron* **2013**, *79*, 1109–1122. [CrossRef] [PubMed]
89. Li, X.; Yao, B.; Chen, L.; Kang, Y.; Li, Y.; Cheng, Y.; Li, L.; Lin, L.; Wang, Z.; Wang, M.; et al. Ten-eleven translocation 2 interacts with forkhead box O3 and regulates adult neurogenesis. *Nat. Commun.* **2017**, *8*, 15903. [CrossRef] [PubMed]
90. Spiers, H.; Hannon, E.; Schalkwyk, L.C.; Bray, N.J.; Mill, J. 5-hydroxymethylcytosine is highly dynamic across human fetal brain development. *BMC Genom.* **2017**, *18*, 738. [CrossRef] [PubMed]
91. Seritrakul, P.; Gross, J.M. Tet-mediated DNA hydroxymethylation regulates retinal neurogenesis by modulating cell-extrinsic signaling pathways. *PLoS Genet.* **2017**, *13*, e1006987. [CrossRef] [PubMed]
92. Amir, R.E.; Van den Veyver, I.B.; Wan, M.; Tran, C.Q.; Francke, U.; Zoghbi, H.Y. Rett syndrome is caused by mutations in X-linked MECP2, encoding methyl-CpG-binding protein 2. *Nat. Genet.* **1999**, *23*, 185–188. [CrossRef] [PubMed]
93. Qiu, Z. Deciphering MECP2-associated disorders: disrupted circuits and the hope for repair. *Curr. Opin. Neurobiol.* **2017**, *48*, 30–36. [CrossRef] [PubMed]
94. Frauer, C.; Hoffmann, T.; Bultmann, S.; Casa, V.; Cardoso, M.C.; Antes, I.; Leonhardt, H. Recognition of 5-hydroxymethylcytosine by the Uhrf1 SRA domain. *PLoS ONE* **2011**, *6*, e21306. [CrossRef] [PubMed]

95. Martinowich, K.; Hattori, D.; Wu, H.; Fouse, S.; He, F.; Hu, Y.; Fan, G.; Sun, Y.E. DNA methylation-related chromatin remodeling in activity-dependent BDNF gene regulation. *Science* **2003**, *302*, 890–893. [CrossRef] [PubMed]
96. Ma, D.K.; Jang, M.-H.; Guo, J.U.; Kitabatake, Y.; Chang, M.-L.; Pow-Anpongkul, N.; Flavell, R.A.; Lu, B.; Ming, G.-L.; Song, H. Neuronal activity-induced Gadd45b promotes epigenetic DNA demethylation and adult neurogenesis. *Science* **2009**, *323*, 1074–1077. [CrossRef] [PubMed]
97. Chen, W.G.; Chang, Q.; Lin, Y.; Meissner, A.; West, A.E.; Griffith, E.C.; Jaenisch, R.; Greenberg, M.E. Derepression of BDNF transcription involves calcium-dependent phosphorylation of MeCP2. *Science* **2003**, *302*, 885–889. [CrossRef] [PubMed]
98. Adam, R.C.; Fuchs, E. The Yin and Yang of chromatin dynamics in stem cell fate selection. *Trends Genet. TIG* **2016**, *32*, 89–100. [CrossRef] [PubMed]
99. Regev, A.; Teichmann, S.A.; Lander, E.S.; Amit, I.; Benoist, C.; Birney, E.; Bodenmiller, B.; Campbell, P.; Carninci, P.; Clatworthy, M.; et al. Human Cell Atlas Meeting Participants The Human Cell Atlas. *eLife* **2017**, *6*. [CrossRef]
100. Yang, Y.A.; Zhao, J.C.; Fong, K.-W.; Kim, J.; Li, S.; Song, C.; Song, B.; Zheng, B.; He, C.; Yu, J. FOXA1 potentiates lineage-specific enhancer activation through modulating TET1 expression and function. *Nucleic Acids Res.* **2016**, *44*, 8153–8164. [CrossRef] [PubMed]
101. Costa, Y.; Ding, J.; Theunissen, T.W.; Faiola, F.; Hore, T.A.; Shliaha, P.V.; Fidalgo, M.; Saunders, A.; Lawrence, M.; Dietmann, S.; et al. NANOG-dependent function of TET1 and TET2 in establishment of pluripotency. *Nature* **2013**, *495*, 370–374. [CrossRef] [PubMed]
102. Suzuki, T.; Shimizu, Y.; Furuhata, E.; Maeda, S.; Kishima, M.; Nishimura, H.; Enomoto, S.; Hayashizaki, Y.; Suzuki, H. RUNX1 regulates site specificity of DNA demethylation by recruitment of DNA demethylation machineries in hematopoietic cells. *Blood Adv.* **2017**, *1*. [CrossRef] [PubMed]
103. Guilhamon, P.; Eskandarpour, M.; Halai, D.; Wilson, G.A.; Feber, A.; Teschendorff, A.E.; Gomez, V.; Hergovich, A.; Tirabosco, R.; Fernanda, A.M.; et al. Meta-analysis of IDH-mutant cancers identifies EBF1 as an interaction partner for TET2. *Nat. Commun.* **2013**, *4*, 2166. [CrossRef] [PubMed]
104. de la Rica, L.; Rodríguez-Ubreva, J.; García, M.; Islam, A.B.M.M.K.; Urquiza, J.M.; Hernando, H.; Christensen, J.; Helin, K.; Gómez-Vaquero, C.; Ballestar, E. PU.1 target genes undergo Tet2-coupled demethylation and DNMT3b-mediated methylation in monocyte-to-osteoclast differentiation. *Genome Biol.* **2013**, *14*, R99. [CrossRef] [PubMed]
105. Fujiki, K.; Shinoda, A.; Kano, F.; Sato, R.; Shirahige, K.; Murata, M. PPARγ-induced PARylation promotes local DNA demethylation by production of 5-hydroxymethylcytosine. *Nat. Commun.* **2013**, *4*, 2262. [CrossRef] [PubMed]
106. Suzuki, T.; Maeda, S.; Furuhata, E.; Shimizu, Y.; Nishimura, H.; Kishima, M.; Suzuki, H. A screening system to identify transcription factors that induce binding site-directed DNA demethylation. *Epigenet. Chromatin* **2017**, *10*. [CrossRef] [PubMed]
107. Liang, J.; Yang, F.; Zhao, L.; Bi, C.; Cai, B. Physiological and pathological implications of 5-hydroxymethylcytosine in diseases. *Oncotarget* **2016**, *7*, 48813–48831. [CrossRef] [PubMed]
108. Sherwani, S.I.; Khan, H.A. Role of 5-hydroxymethylcytosine in neurodegeneration. *Gene* **2015**, *570*, 17–24. [CrossRef] [PubMed]
109. Cadena-del-Castillo, C.; Valdes-Quezada, C.; Carmona-Aldana, F.; Arias, C.; Bermúdez-Rattoni, F.; Recillas-Targa, F. Age-dependent increment of hydroxymethylation in the brain cortex in the triple-transgenic mouse model of Alzheimer's disease. *J. Alzheimer's Dis. JAD* **2014**, *41*, 845–854. [CrossRef]
110. Tsuchida, T.; Friedman, S.L. Mechanisms of hepatic stellate cell activation. *Nat. Rev. Gastroenterol. Hepatol.* **2017**, *14*, 397–411. [CrossRef] [PubMed]
111. Page, A.; Paoli, P.; Moran Salvador, E.; White, S.; French, J.; Mann, J. Hepatic stellate cell transdifferentiation involves genome-wide remodeling of the DNA methylation landscape. *J. Hepatol.* **2016**, *64*, 661–673. [CrossRef] [PubMed]
112. Rodríguez-Aguilera, J.R.; Guerrero-Hernández, C.; Pérez-Molina, R.; Cadena-Del-Castillo, C.E.; Pérez-Cabeza de Vaca, R.; Guerrero-Celis, N.; Domínguez-López, M.; Murillo-de-Ozores, A.R.; Arzate-Mejía, R.; Recillas-Targa, F.; et al. Epigenetic effects of an adenosine derivative in a wistar rat model of liver cirrhosis. *J. Cell. Biochem.* **2017**. [CrossRef]

113. Thomson, J.P.; Ottaviano, R.; Buesen, R.; Moggs, J.G.; Schwarz, M.; Meehan, R.R. Defining baseline epigenetic landscapes in the rat liver. *Epigenomics* **2017**, *9*, 1503–1527. [CrossRef] [PubMed]
114. An, J.; Rao, A.; Ko, M. TET family dioxygenases and DNA demethylation in stem cells and cancers. *Exp. Mol. Med.* **2017**, *49*, e323. [CrossRef] [PubMed]
115. Chen, Z.; Shi, X.; Guo, L.; Li, Y.; Luo, M.; He, J. Decreased 5-hydroxymethylcytosine levels correlate with cancer progression and poor survival: a systematic review and meta-analysis. *Oncotarget* **2017**, *8*, 1944–1952. [CrossRef] [PubMed]
116. Koivunen, P.; Laukka, T. The TET enzymes. *Cell. Mol. Life Sci.* 2017. [CrossRef] [PubMed]
117. Liang, G.; Weisenberger, D.J. DNA methylation aberrancies as a guide for surveillance and treatment of human cancers. *Epigenetics* **2017**, *12*, 416–432. [CrossRef] [PubMed]
118. Jeschke, J.; Collignon, E.; Fuks, F. Portraits of TET-mediated DNA hydroxymethylation in cancer. *Curr. Opin. Genet. Dev.* **2016**, *36*, 16–26. [CrossRef] [PubMed]
119. Foksinski, M.; Zarakowska, E.; Gackowski, D.; Skonieczna, M.; Gajda, K.; Hudy, D.; Szpila, A.; Bialkowski, K.; Starczak, M.; Labejszo, A.; et al. Profiles of a broad spectrum of epigenetic DNA modifications in normal and malignant human cell lines: Proliferation rate is not the major factor responsible for the 5-hydroxymethyl-2′-deoxycytidine level in cultured cancerous cell lines. *PLoS ONE* **2017**, *12*. [CrossRef] [PubMed]
120. Uribe-Lewis, S.; Stark, R.; Carroll, T.; Dunning, M.J.; Bachman, M.; Ito, Y.; Stojic, L.; Halim, S.; Vowler, S.L.; Lynch, A.G.; et al. 5-hydroxymethylcytosine marks promoters in colon that resist DNA hypermethylation in cancer. *Genome Biol.* **2015**, *16*, 69. [CrossRef] [PubMed]
121. Tomkova, M.; McClellan, M.; Kriaucionis, S.; Schuster-Boeckler, B. 5-hydroxymethylcytosine marks regions with reduced mutation frequency in human DNA. *eLife* **2016**, *5*. [CrossRef] [PubMed]
122. Burr, S.; Caldwell, A.; Chong, M.; Beretta, M.; Metcalf, S.; Hancock, M.; Arno, M.; Balu, S.; Kropf, V.L.; Mistry, R.K.; et al. Oxygen gradients can determine epigenetic asymmetry and cellular differentiation via differential regulation of Tet activity in embryonic stem cells. *Nucleic Acids Res.* 2017. [CrossRef] [PubMed]
123. Saha, S.K.; Parachoniak, C.A.; Ghanta, K.S.; Fitamant, J.; Ross, K.N.; Najem, M.S.; Gurumurthy, S.; Akbay, E.A.; Sia, D.; Cornella, H.; et al. Mutant IDH inhibits HNF-4α to block hepatocyte differentiation and promote biliary cancer. *Nature* **2014**, *513*, 110–114. [CrossRef] [PubMed]
124. Sasidharan Nair, V.; Song, M.H.; Oh, K.I. Vitamin C Facilitates Demethylation of the Foxp3 Enhancer in a Tet-Dependent Manner. *J. Immunol.* **2016**, *196*, 2119–2131. [CrossRef] [PubMed]
125. Hore, T.A.; von Meyenn, F.; Ravichandran, M.; Bachman, M.; Ficz, G.; Oxley, D.; Santos, F.; Balasubramanian, S.; Jurkowski, T.P.; Reik, W. Retinol and ascorbate drive erasure of epigenetic memory and enhance reprogramming to naïve pluripotency by complementary mechanisms. *Proc. Natl. Acad. Sci. USA* **2016**, *113*, 12202–12207. [CrossRef] [PubMed]

ARTICLE
Journal of Cellular Biochemistry 9999:1–13 (2017)

Journal of Cellular Biochemistry

Epigenetic Effects of an Adenosine Derivative in a Wistar Rat Model of Liver Cirrhosis

Jesús Rafael Rodríguez-Aguilera,[1] Carlos Guerrero-Hernández,[1] Rosario Pérez-Molina,[2] Carla Elizabeth Cadena-del-Castillo,[2] Rebeca Pérez-Cabeza de Vaca,[1] Nuria Guerrero-Celis,[1] Mariana Domínguez-López,[1] Adrián Rafael Murillo-de-Ozores,[1] Rodrigo Arzate-Mejía,[2] Félix Recillas-Targa,[2] and Victoria Chagoya de Sánchez [1]*

[1]*Departamento de Biología Celular y Desarrollo, Instituto de Fisiología Celular, UNAM, Circuito Exterior s/n Ciudad Universitaria, Coyoacán 04510, Cd.Mx., México*

[2]*Departamento de Genética Molecular, Instituto de Fisiología Celular, UNAM, Circuito Exterior s/n Ciudad Universitaria, Coyoacán 04510, Cd.Mx., México*

ABSTRACT

The pathological characteristic of cirrhosis is scarring which results in a structurally distorted and dysfunctional liver. Previously, we demonstrated that *Col1a1* and *Pparg* genes are deregulated in CCl_4-induced cirrhosis but their normal expression levels are recovered upon treatment with IFC-305, an adenosine derivative. We observed that adenosine was able to modulate S-adenosylmethionine-dependent *trans*-methylation reactions, and recently, we found that IFC-305 modulates *HDAC3* expression. Here, we investigated whether epigenetic mechanisms, involving DNA methylation processes and histone acetylation, could explain the re-establishment of gene expression mediated by IFC-305 in cirrhosis. Therefore, Wistar rats were CCl_4 treated and a sub-group received IFC-305 to reverse fibrosis. Global changes in DNA methylation, 5-hydroxymethylation, and histone H4 acetylation were observed after treatment with IFC-305. In particular, during cirrhosis, the *Pparg* gene promoter is depleted of histone H4 acetylation, whereas IFC-305 administration restores normal histone acetylation levels which correlates with an increase of *Pparg* transcript and protein levels. In contrast, the promoter of *Col1a1* gene is hypomethylated during cirrhosis but gains DNA methylation upon treatment with IFC-305 which correlates with a reduction of *Col1a1* transcript and protein levels. Our results suggest a model in which cirrhosis results in a general loss of permissive chromatin histone marks which triggers the repression of the *Pparg* gene and the upregulation of the *Col1a1* gene. Treatment with IFC-305 restores epigenetic modifications globally and specifically at the promoters of *Pparg* and *Col1a1* genes. These results reveal one of the mechanisms of action of IFC-305 and suggest a possible therapeutic function in cirrhosis. J. Cell. Biochem. 9999: 1–13, 2017.

KEY WORDS: LIVER; DNA METHYLATION; CHROMATIN; *Col1a1*; HEPATOPROTECTOR

Cirrhosis originates from different mechanisms of liver injury that lead to necroinflammation and fibrogenesis. Histologically, it is characterized by diffuse nodular regeneration surrounded by dense fibrotic septa with subsequent parenchymal extinction and collapse of liver structures, with pronounced distortion of hepatic vascular architecture [Tsochatzis et al., 2014]. Fibrosis is largely asymptomatic and its progression to cirrhosis is slow, developing over 20–40 years in patients with chronic liver injury. The scarring response of liver includes activation of hepatic stellate cells (HSCs), which represent resident mesenchymal cells, into contractile myofibroblasts that encapsulate the injury, and induce loss of vitamin A droplets. These activated cells enhance migration and

ABBREVIATIONS: 5mC, 5-methylcytosine; 5hmC, 5-hydroxymethylcytosine; H4ac, histone H4 acetylation; H3K27me3, histone H3 lysine 27 trimethylation; PTM, post-translational modification.

Conflicts of interest: The authors who have taken part in this study declared that they do not have anything to disclose regarding conflict of interest with respect to this manuscript.

Grant sponsor: Dirección General de Asuntos del Personal Académico, Universidad Nacional Autónoma de México; Grant numbers: IN201114, IN203811, IN207012, IN225909; Grant sponsor: Consejo Nacional de Ciencia y Tecnología; Grant numbers: 128464, 220503; Grant sponsor: PAEP-UNAM, Programa de Maestría y Doctorado en Ciencias Bioquímicas, UNAM; Grant number: 30479367-5; Grant sponsor: PhD Fellowship from CONACyT; Grant number: CVU 508509.

*Correspondence to: Victoria Chagoya de Sánchez, Circuito Exterior s/n, Ciudad Universitaria, Coyoacán, 04510 México, Cd.Mx., México. E-mail: vchagoya@ifc.unam.mx

Manuscript Received: 27 February 2017; Manuscript Accepted: 6 June 2017

Accepted manuscript online in Wiley Online Library (wileyonlinelibrary.com): 07 June 2017

DOI 10.1002/jcb.26192 • © 2017 Wiley Periodicals, Inc.

deposition of extracellular matrix components, like collagen I, the principal protein that triggers fibrosis [Hernandez-Gea and Friedman, 2011]. A widely used model to study cirrhosis is chronic administration of CCl_4 into rats [Paquet and Kamphausen, 1975] which has been considered an acceptable model to study human cirrhosis.

Chronic CCl_4-intoxication of rats results in cirrhosis at 8–12 weeks [Iredale, 2007]. The CCl_4 metabolism produces lipid peroxidation and membrane damage, which are the main causes of hepatocellular alteration [Varela-Moreiras et al., 1995]. Furthermore, it causes chromosome instability suggesting involvement of DNA damage [Michalopoulos, 1990]. Previously, we demonstrated in this animal model that treatment with IFC-305, an adenosine derivative, reverses liver fibrosis and ameliorates hepatic function [Perez-Carreon et al., 2010]. At the cellular level, it prevents HSC activation in vivo and in vitro [Perez-Carreon et al., 2010; Velasco-Loyden et al., 2010], promotes recovery of the cell cycle inhibition [Chagoya de Sanchez et al., 2012], and re-establishes the expression of around 150 genes deregulated in cirrhosis, among them *Col1a1* and *Pparg* [Perez-Carreon et al., 2010].

With an increased understanding of chromatin organization of the eukaryotic genome, it has become clear that not only genetic but also epigenetic processes influence both normal biology and diseases [Recillas-Targa, 2014]. The peroxisome proliferator-activated receptor gamma (PPARγ) is one of those factors whose activity is diminished in activated HSCs; in fact, its expression, per se, even maintains HSCs in a quiescent state [Hazra et al., 2004a]. PPARγ can be regulated by the methyl-CpG-binding protein 2 (MeCP2), which co-localizes with the deposition of the histone modification H3K27me3 and forms a repressive chromatin structure in the coding region of *Pparg* gene [Mann et al., 2010]. One of the most antifibrotic effects of PPARγ is its ability to inhibit collagen I gene transcription. This inhibition is mediated by the ability of the nuclear receptor to compete with NF-I/p300 association to the *Col1a1* gene promoter in HSCs [Yavrom et al., 2005].

As IFC-305 affects the expression of a sub-set of genes during fibrosis reversion, we decided to evaluate if epigenetic mechanisms are involved. To this aim, we first evaluated global levels of methylated DNA (5mC), 5-hydroxymethylcytosine (5hmC), and histone H4 acetylation (H4ac). In addition, we analyzed the deposition of histone H4ac and H3K27me3 marks in the *Pparg* gene promoter and the DNA methylation state of the *Col1a1* gene promoter. We found that IFC-305 exerts its effect by regulating chromatin marks globally and in some genes directly involved in the fibrogenic process. We propose a key role of IFC-305 in fibrosis reversion that involves an increase in DNA methylation around the transcription start site of *Col1a1* gene and the acquisition of a transcriptional favoring combination of histone post-translational modifications (PTMs) at the *Pparg* gene promoter. These results can be understood as the molecular basis of hepatoprotective properties of IFC-305, and suggest it might have the potential to function as a therapeutic alternative for cirrhosis treatment; moreover, here we highlight the importance of epigenetic changes in cirrhosis establishment in vivo.

RESULTS

IFC-305 PROTECTS FROM CCl_4-INDUCED LIVER FIBROSIS

The CCl_4-mediated liver surface distortion was observed both in rats treated with the toxic compound for 10 weeks and in rats receiving in addition saline for another 5 weeks after CCl_4 (Supplementary Fig. S1B). We found nodules, an increment in alanine aminotransferase activity (ALT), and hepatomegaly (Fig. S1B–D). Treatment of cirrhotic rats for 5 weeks with IFC-305 triggered a rescue with a liver phenotype similar to animals without cirrhosis (Supplementary Fig. S1B). IFC-305 treatment also led to a decrease in ALT activity (Supplementary Fig. S1C), which suggests a hepatoprotective function by IFC-305 as it has been previously reported [Perez-Carreon et al., 2010]. Interestingly, the treatment of healthy rats with IFC-305 over 10 weeks does not generate any physiological effect denoted by no alteration of ALT as a biochemical parameter (Supplementary Fig. S1C: 10IFC). These results indicate that IFC-305 is capable of normalizing the hepatic function altered by cirrhosis and to accelerate the recovery of the liver macroscopic phenotype shown before the 5-week treatment.

To demonstrate that alterations in the liver phenotype can be attributed to collagen accumulation, mimicking human cirrhosis, we performed Western blot assays against collagen I, and found that there is a nearly 50% increment of collagen I in cirrhosis (Supplementary Fig. S2A). Treatment with IFC-305 diminished the amount of the protein as compared to the cirrhosis and saline groups. A similar effect was observed with Masson Trichrome staining (Supplementary Fig. S2B). Together, these data confirmed that IFC-305 has hepatoprotective properties and reduces the amount of collagen I in the liver.

IFC-305 REGULATES S-ADENOSYLMETHIONINE (SAM) LEVELS AND DNA METHYLATION

We have previously shown that adenosine can modulate *trans*-methylation reactions, like methylation of phospholipids, via regulation of SAM levels [Chagoya de Sanchez et al., 1991]. Therefore, to assess if IFC-305 has an impact on DNA methylation, we first quantified the level of SAM and found that the amount of this molecule is diminished in cirrhosis, whereas IFC-305 treatment restored the physiological levels (Fig. 1A).

The effects of cirrhosis at the epigenetic level are little understood, but there are few studies that have demonstrated that the DNA methylation status was reduced throughout the genome because of CCl_4 treatment in the early-stage liver fibrosis [Varela-Moreiras et al., 1995; Komatsu et al., 2012]. To determine whether the hepatoprotective effects of IFC-305 involve changes in DNA methylation, we evaluated global DNA methylation levels in the cirrhosis model. We found a reduction in DNA methylation at the cirrhosis state and a regaining of the 5mC modification with the treatment with IFC-305 (Fig. 1B and C). These samples were analyzed by ELISA which revealed a twofold increase in the level of DNA methylation, when comparing IFC-305 treatment against healthy and cirrhotic liver states (Fig. 1D). These results demonstrate that IFC-305, as adenosine itself, regulates the *trans*-methylation reactions through modulating the levels of SAM and suggest an epigenetic effect of IFC-305 in cirrhotic rats.

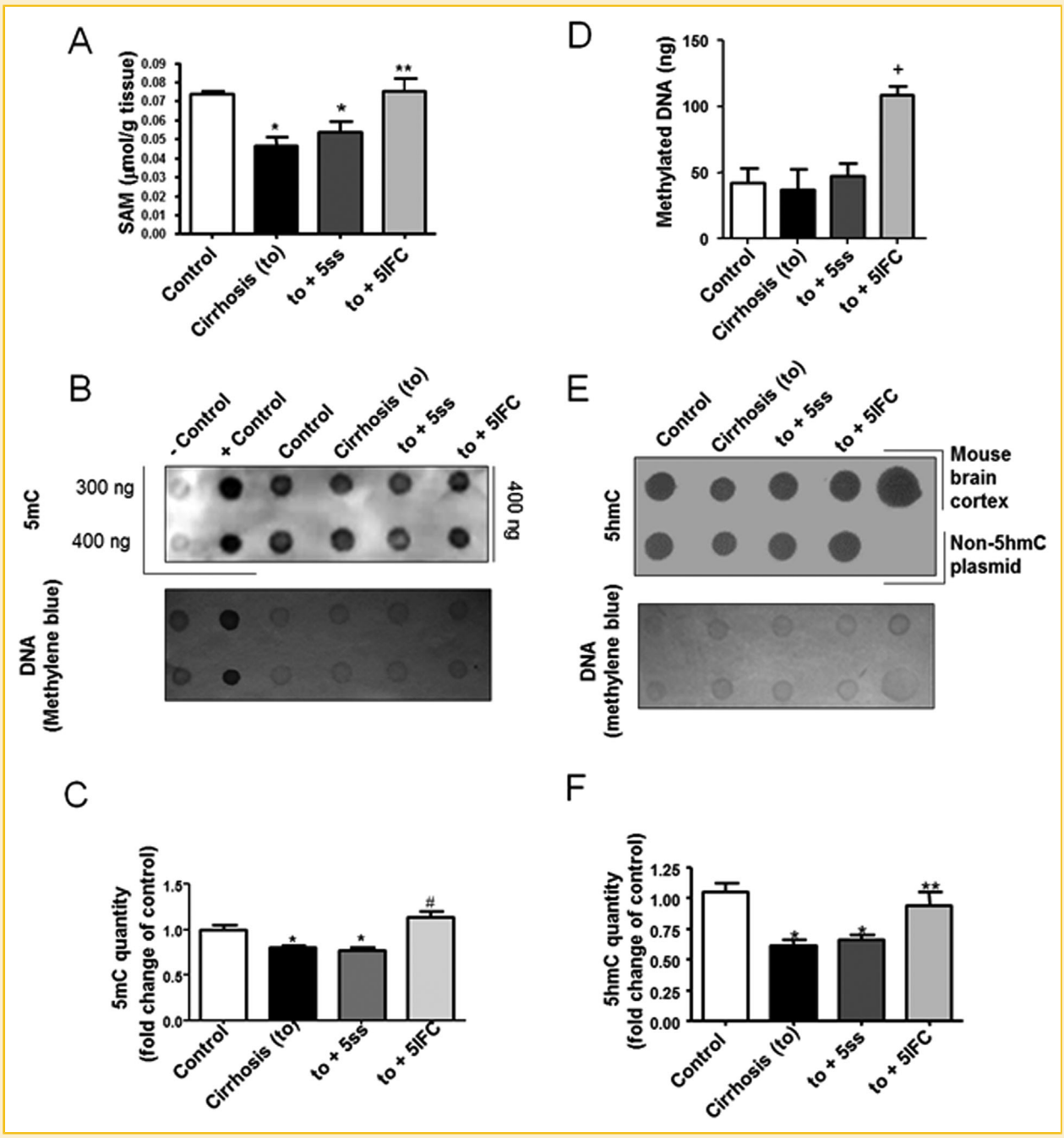

Fig. 1. Timelapse analysis of SAM levels and DNA methylation dynamics in the CCl_4-induced cirrhosis model. (A) SAM quantification. (B) Global DNA methylation analysis. Upper panel shows a representative image of a biological triplicate of dot-blot; Lower panel represents the membrane stained with methylene blue. (C) 5mC dot-blot quantification. (D) DNA methylation analysis by ELISA assay (E) 5hmC quantification. Upper panel shows a representative image of a biological triplicate; Lower panel represents the membrane stained with methylene blue. (F) 5hmC dot-blot quantification. Data represent mean ± SEM from three rats/group. *Statistical difference ($P < 0.05$) compared to Control group. **Statistical difference ($P < 0.05$) when compared to Cirrhosis (to). #Statistical difference ($P < 0.05$) compared to Cirrhosis (to) and to +5ss. +Statistical difference ($P < 0.05$) compared to Control, Cirrhosis (to) and to +5ss.

5-HYDROXYMETHYLCYTOSINE IS REDUCED DURING CIRRHOSIS AND IFC-305 RESTORES ITS PHYSIOLOGICAL LEVELS

Next, we decided to decipher in more detail other epigenetic processes in response to IFC-305 treatment. The presence of DNA methylation has been considered a synonym of gene expression silencing and repressive chromatin structure [Recillas-Targa, 2014]. The discovery of an active DNA demethylation pathway, that involves the conversion of 5mC to oxidized forms, like 5hmC, and DNA repair through the base excision system, incorporates a dynamic reversibility of DNA methylation

[Kriaucionis and Heintz, 2009; Tahiliani et al., 2009; Bhutani et al., 2011; Kohli and Zhang, 2013]. Considering the significant number of genes modified during cirrhosis [Perez-Carreon et al., 2010] and the effect of IFC-305 on global DNA methylation (Fig. 1B–D), we analyzed global levels of 5hmC.

We performed dot-blot assays using an anti-5hmC antibody and found that 5hmC is diminished in cirrhosis. Interestingly, we observed a rescue of 5hmC levels with IFC-305 treatment in cirrhotic rats similar to the one observed in control rats (Fig. 1E and F). Consequently, it seems that IFC-305 can modulate the active DNA demethylation process, thereby restoring the amount of 5hmC to levels found in healthy liver. Taken together, these data suggest that IFC-305 treatment results in a restoration of 5hmC to physiological levels, while increasing the amount of 5mC genome wide.

HISTONE H4 ACETYLATION DECREASES IN CIRRHOSIS AND IFC-305 REESTABLISHES ITS PHYSIOLOGICAL LEVEL

DNA methylation is associated with gene silencing and the establishment of a close chromatin conformation, in part, by modulation of histone acetylation levels. Our previous transcriptome analysis showed that HDAC3, a histone deacetylase, is overexpressed in cirrhotic liver in rats [Perez-Carreon et al., 2010]. Administration of IFC-305 for 5 weeks triggers a 30% decrease of the HDAC3 expression level [Perez-Carreon et al., 2010], which suggests that IFC-305 could restore histone acetylation levels in part by down regulating *HDAC3* gene expression. To validate this, we first quantified HDAC3 protein levels and found a twofold increase in the cirrhotic state compared to non-treated rats and healthy rats treated for 10 weeks with IFC-305 (10IFC). In contrast, we found that the amount of HDAC3 after treating the cirrhotic state for 5 weeks with IFC-305 was similar to the one observed in a healthy liver (Fig. 2A). To investigate if the HDAC3 protein levels correlate with changes in histone acetylation we carried out Western blots of nuclear protein extracts using an antibody against acetylated histone H4. Importantly, we found a correlation between increased levels of HDAC3 and diminishment of hyperacetylated histone H4 in cirrhosis, while IFC-305 was able to restore the healthy liver level of this histone mark (Fig. 2B). This change is HDAC3 specific as no differences in the protein level of HDAC1 could be observed in cirrhosis or 5 weeks of treatment with IFC-305 (Supplementary Fig. S4). Together, these data demonstrate that treatment of cirrhotic rats with IFC-305 modulates the level of DNA methylation modifications 5mC and 5hmC, as well as the PTM histone H4ac, which regulate epigenetically gene expression.

THE OVEREXPRESSION OF *Pparg* GENE BY IFC-305 IS MEDIATED BY THE GENERATION OF OPEN CHROMATIN IN THE GENE PROMOTER

Once we established that cirrhosis generates global chromatin alterations which are to some extent reversed by IFC-305 administration, we decided to analyze in detail the chromatin configuration of gene promoters that exhibit an altered expression in cirrhosis and are involved in the fibrogenic process, such as *Col1a1* and *Pparg*.

A few years ago, it has been demonstrated that PPARγ is a negative regulator of *Col1a1* gene expression in HSCs [Yavrom et al., 2005]. Taking this into account, we first analyzed by Western blot the amount of nuclear receptor in the cirrhotic model and found that protein levels correlated with transcript levels previously described [Perez-Carreon et al., 2010]. In cirrhosis we observed a decrease of the protein level, whereas IFC-305 increased its concentration beyond the normal liver level (Fig. 3A). In order to know which type of cells were responsible for the expression changes of PPARγ, we performed immunofluorescence assays and found that PPARγ signal was detected in a considerable number of cells in healthy liver. In

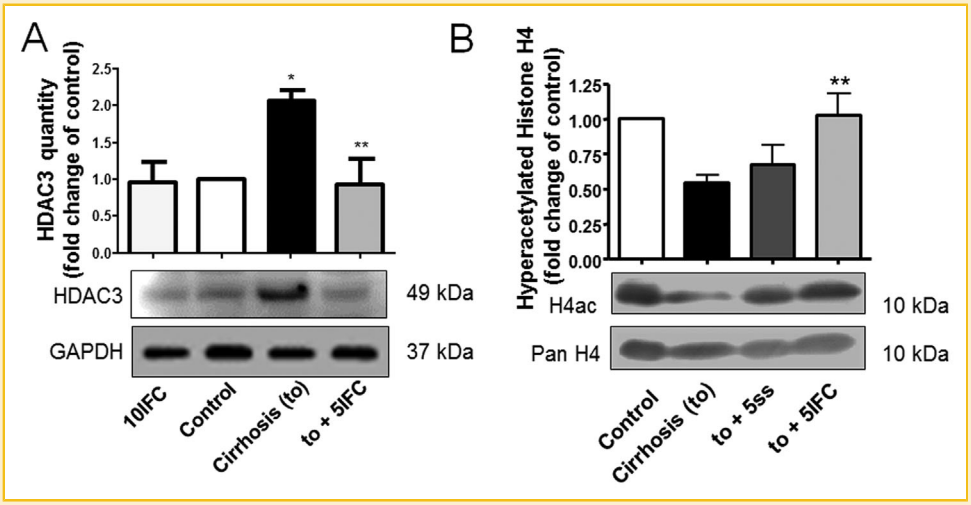

Fig. 2. Histone H4 acetylation levels are recovered after IFC-305 treatment of cirrhotic rats. (A) HDAC3 protein levels in CCl_4 model. Representative Western blots are shown at the bottom of densitometric analysis. GAPDH immunodetection was used as a loading control. Data represent mean ± SEM from three rats/group. (B) Immunodetection of global hyperacetylated histone H4 levels. Representative Western blot images are shown at the bottom of densitometric analysis. Total H4 immunodetection using a pan-Histone H4 antibody was used as a loading control. Data represent mean ± SEM from three rats/group. *Statistical difference ($P < 0.05$) compared to Control group. **Statistical difference ($P < 0.05$) when compared to Cirrhosis (to).

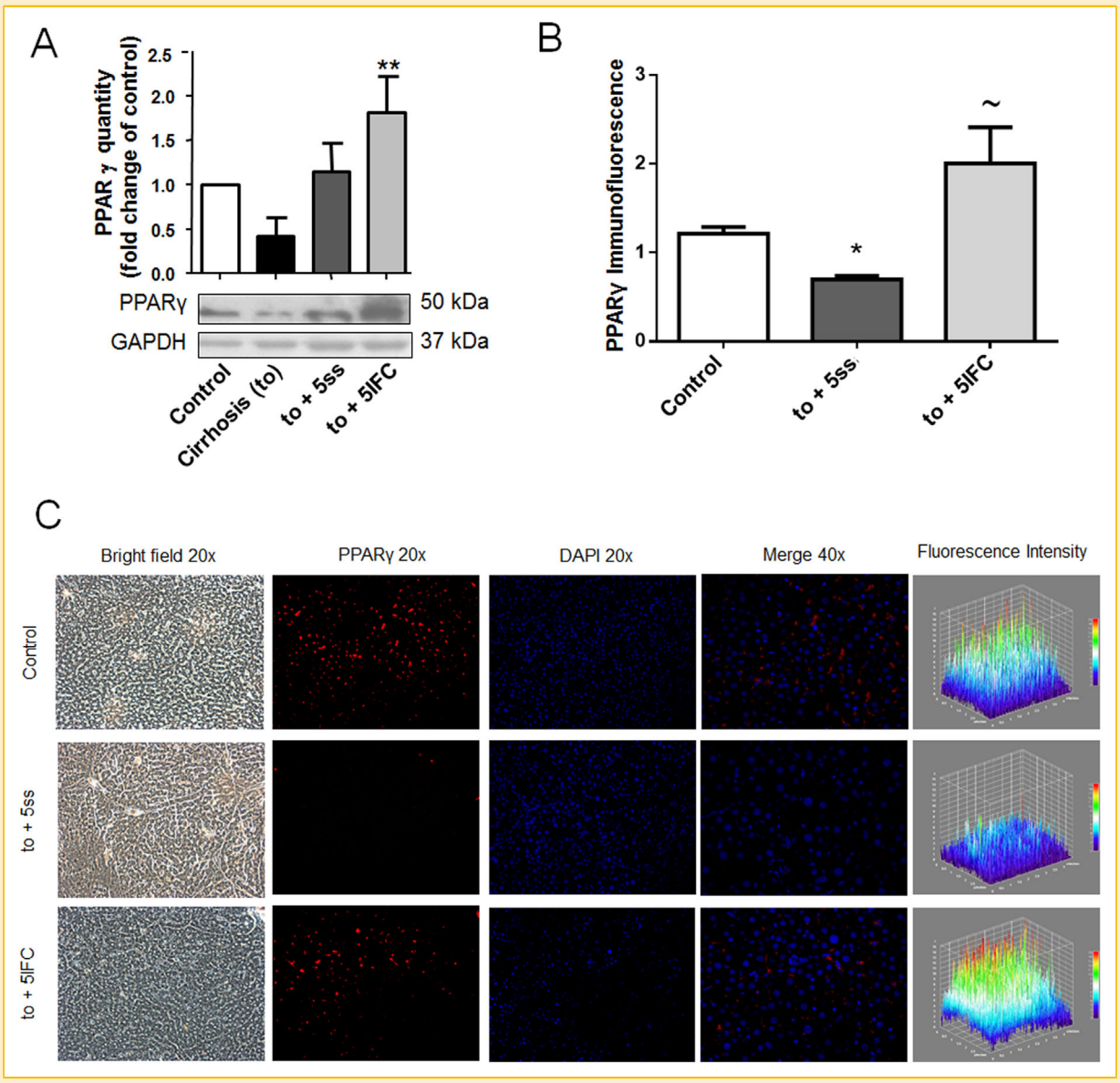

Fig. 3. The nuclear receptor PPARγ levels increase in cirrhotic liver treated with IFC-305. (A) Representative Western blot images are shown at the bottom of densitometric analysis. Data represent mean ± SEM from four rats/group. **Statistical difference ($P < 0.05$) when compared to Cirrhosis (to). (B) Quantification of immunofluorescence of the positive signal to PPARγ. Data represent mean ± SEM from three fields/group. *Statistical difference ($P < 0.05$) when compared to control group. ~Statistical difference ($P < 0.05$) when compared to +5ss. (C) Immunofluorescence of PPARγ in whole liver histological sections. Representative images are shown.

case of the cirrhotic liver (to +5ss) the positive signal decreases strongly, whereas the IFC-305 treatment leads to a recovery of the levels of PPARγ signal (Fig. 3B and C). Analyzing the location of cells with a positive PPARγ signal in the to +5IFC condition, we observed that immunoreactive cells were found in regions where there is not residual of fibrosis septa. When we immunostained sections of fibrotic tissue with an antibody against αSMA, a marker of activated HSCs, we observed in to +5ss an enrichment of αSMA positive cells around the fibrosis septa, but with the IFC-305 treatment the immunoreactivity decreased (Supplementary Fig. S3). The localization of αSMA positive cells is consistent with our previous data [Perez-Carreon et al., 2010].

To determine if the increased amount of PPARγ after treatment of cirrhotic rats with IFC-305 is mediated by changes of histone PTM at the *Pparg* gene promoter, we performed chromatin immunoprecipitations (ChIP) using an antibody against acetylated histone H4. We observed that the acetylated histone H4 mark decreased in the liver of cirrhotic rats, whereas in rats treated with IFC-305, the histone H4ac modification recovered reaching normal levels (Fig. 4A). Additionally, we analyzed chromatin samples from a group of healthy rats treated with IFC-305 over 10 weeks (10 IFC), and we did not observe a significant difference compared with control rats, only when compared with cirrhosis (to) (Fig. 4A: 10 IFC). Together, these data suggest that the increase in

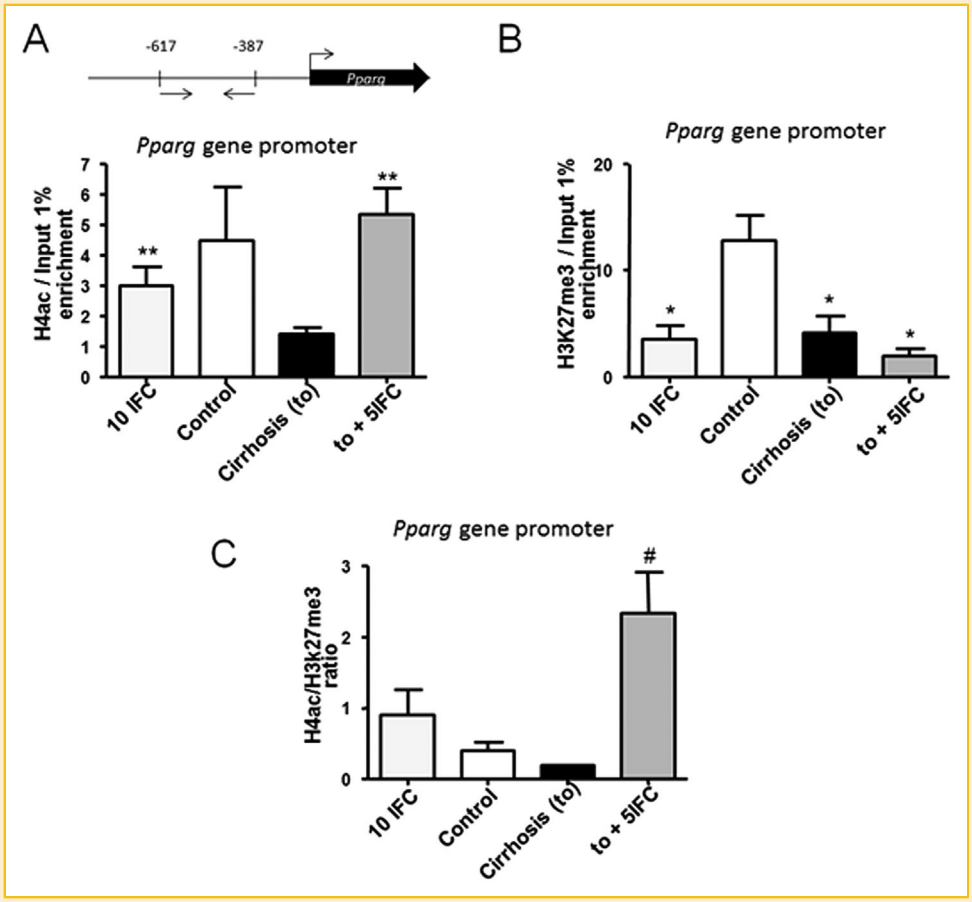

Fig. 4. Combination histone PTMs on the *Pparg* gene promoter and deposition of PPARγ at the *Col1a1* gene promoter in the CCl_4–induced cirrhosis model. (A) Scheme of *Pparg* gene promoter depicting the positions of primers used in A–C; enrichment of permissive hyperacetylated histone H4 mark on *Pparg* gene promoter in a pre-established cirrhosis treated with the IFC-305 compound. (B) Deposition of repressive histone mark H3K27me3 on *Pparg* gene promoter. (C) Ratio of H4ac and H3K27me3 histone marks enrichment. Data represent mean ± SEM of two biological samples analyzed in triplicate. *Statistical difference ($P < 0.05$) compared to Control (to) group. **Statistical difference ($P < 0.05$) when compared to Cirrhosis (to). #Statistical difference ($P < 0.05$) when compared to Control and Cirrhosis (to).

transcription and consequently in PPARγ protein levels result from a restoration of open chromatin marks at the promoter of the *Pparg* gene mediated by IFC-305 treatment of the cirrhotic liver (Fig. 4A: to +5IFC). To further validate the open chromatin state of the *Pparg* gene promoter we performed ChIP assays using an antibody against the repressive histone mark H3K27me3 deposited by the Polycomb repressive complex 2. H3K27me3 ChIP assays revealed a reduction in the deposition of the repressive histone mark on the *Pparg* gene promoter region in all treatments compared to the healthy liver (Fig. 4B). We calculated the ratio of enrichment between H4ac and H3K27me3, and determined that the *Pparg* promoter is preferentially found in a transcriptionally permissive chromatin structure in the cirrhotic liver treated with IFC-305 (Fig. 4C: to +5IFC).

Next, we evaluated the DNA methylation state of the promoter and 5′ region of the *Pparg* gene, that includes a segment of the first exon, by sodium bisulfite conversion and sequencing. Previously, the group of Mann et al. [2010] described that in myofibroblasts derived from HSCs the promoter and first exon of the *Pparg* are enriched for MeCP2 binding, and the first exon additionally for MBD2 and HP1α, proteins directly linked to DNA methylation and heterochromatin, respectively. Under our experimental conditions promoter and 5′ region of the *Pparg* gene were not DNA methylated (Supplementary Fig. S5). Therefore, these results suggest that over expression of the *Pparg* gene induced by IFC-305 [Perez-Carreon et al., 2010], in a pre-established cirrhosis, is mediated not by DNA methylation, but mainly by histone modifications, favoring its transcription.

REPRESSION OF THE *Col1a1* GENE BY IFC-305 IS MAINLY MEDIATED BY AN INCREMENT IN DNA METHYLATION AROUND THE TRANSCRIPTION START SITE OF THE GENE

Previous work published by Tsukamoto and coworkers demonstrated that PPARγ suppresses the proximal *Col1a1* promoter [Yavrom et al., 2005]. When we evaluated the deposition of nuclear receptor on the *Col1a1* gene promoter, we found in cirrhosis no difference in the deposition of the nuclear receptor as compared to a healthy liver (Supplementary Fig. S6). These data suggest that the repression mechanism of *Col1a1* gene expression mediated by PPARγ is particular for HSCs, as previously shown [Yavrom et al., 2005].

To investigate whether the cause for collagen I over expression during cirrhosis is related to a reduction of DNA methylation on its gene promoter we applied sodium bisulfite conversion and sequencing to the *Col1a1* gene promoter (Fig. 5). This regulatory sequence is known to contain two protected footprints as determined by DNase footprinting analysis of activated HSCs (−133 to −79 bp) [Nehls et al., 1991; Rippe et al., 1995; Yavrom et al., 2005]. Furthermore, it contains the sites via which PPARγ renders a mayor inhibitory effect on the promoter and in vitro the transcription factors NF-1 and Sp1 bind to it in activated HSCs [Yavrom et al., 2005] (Fig. 5A). We found that in the *Col1a1* gene promoter and first exon, the CpGs in positions 1, 11, and 17 lose DNA methylation in cirrhosis (Fig. 5B: Cirrhosis [to]). Interestingly, the loss of 5mC is sustained during the next 5 weeks in the absence of CCl_4 (Fig. 5B; to +5ss; CpGs 1, 4, 11, and 17). On the other hand, treatment with IFC-305 increased CpG methylation around the transcription start site (TSS) and fostered recovery of CpG methylation at the first position (Fig. 5B; to +5IFC; CpG 1). The previously described behavior at specific CpG dinucleotides is represented by the trend line in the graphic of % of DNA methylation, which depicts the level of methylation of each CpG dinucleotide. Comparing the percentage of DNA methylation in this trend line, we observed that the treatment with IFC-305 triggers a significant increment in DNA methylation compared with to +5ss (Fig 5B: % of DNA methylation, trend line). This suggests that *Col1a1* gene expression which is overexpressed in cirrhosis and returns to control levels with IFC-305 treatment [Perez-Carreon et al., 2010] shows an inverse correlation with the DNA methylation status in the *Col1a1* gene promoter in the used cirrhosis model.

THE PREVENTION OF IN VITRO HSC ACTIVATION BY IFC-305 APPEARS TO BE COORDINATED BY EPIGENETIC MECHANISMS

The liver tissue is composed of different cell types, whereby the hepatocytes represent the vast majority of the cells of the organ. Taking this into account, it is probable that the observations described above result from changes that occur primarily in these parenchymal cells. Moreover, the cells that are mainly responsible for the development of fibrosis are HSCs, which represent 8% of the cellular population of the liver. Therefore, in order to validate the origin of epigenetic changes mediated by IFC-305 treatment we assessed the levels of hyperacetylated histone H4 on a global level in a previously described model of prevention of HSC activation in vitro [Velasco-Loyden et al., 2010].

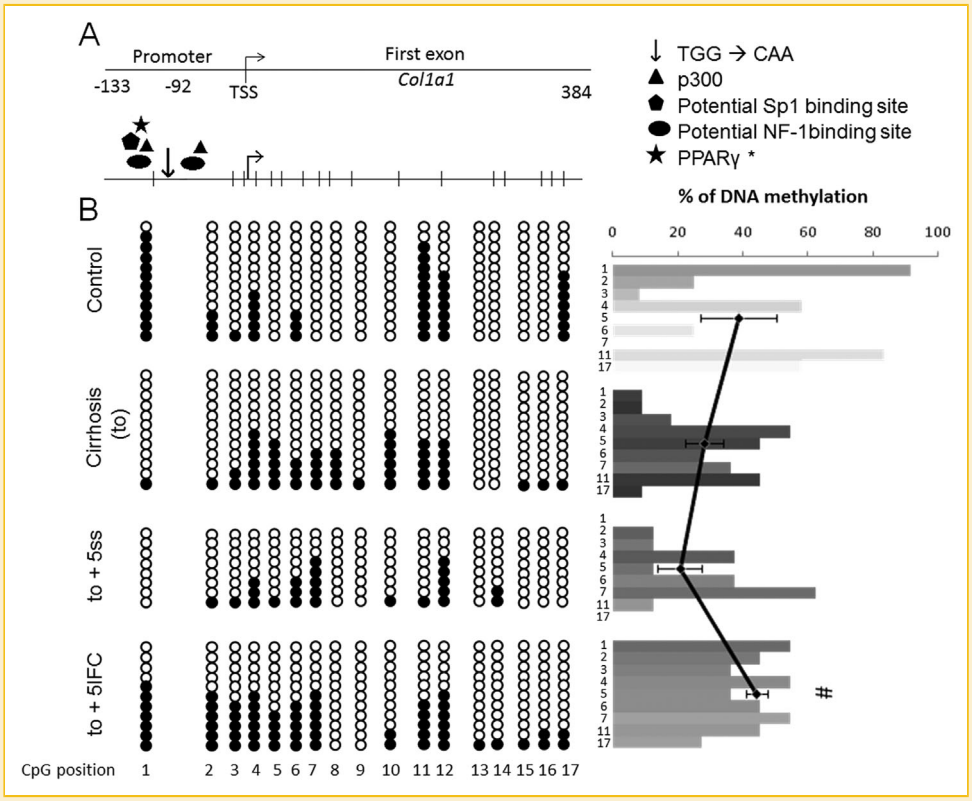

Fig. 5. DNA methylation analysis of the *Col1a1* gene promoter and first exon. (A) Scheme of the analyzed region of the *Col1a1* gene promoter. Pentagon and oval indicate putative Sp1- and NF-1-binding sites, respectively; the triangle denotes the region to which p300 is recruited and the star corresponds to the region where PPARγ inhibits p300-facilitated NF-1 binding to DNA in HSCs to abrogate *Col1a1* gene expression. Vertical arrow marks a sequence which is critical for promoter function, a 3-nucleotide mutation results in an almost complete loss of promoter activity [Nehls et al., 1991; Yavrom et al., 2005]. (B) Left panel: DNA methylation status, white (○) and black (●) dots represent unmethylated and methylated CpG, respectively. Columns represent each CpG site and rows show all individual clones analyzed. For the scheme two independent biological samples were analyzed. Right panel: Percentage of DNA methylation, which was calculated as the ratio between methylated CpGs and the number of analyzed clones for each condition. The trend line was obtained from the mean of ratios of all analyzed CpGs of each condition. #Statistical difference ($P < 0.05$) compared to Cirrhosis (to) and to +5ss.

In this model we have previously demonstrated that IFC-305 prevents the activation of isolated HSCs [Velasco-Loyden et al., 2010]. Here, we isolated primary cultures of HSCs and observed that the activation process directs an increment of hyperacetylated histone H4. Additionally, we found an enrichment of this histone modification at 7 days of activation, whereas the culture treated with 5 mM IFC-305 prevented an acquisition of the histone H4 acetylation (Supplementary Fig. S7). These results propose that the in vitro activation of HSC presents a different behavior compared to the whole liver. Due to this and considering the localization of PPARγ detected by immunofluorescence in liver sections, it is most likely that the epigenetic changes observed in the cirrhosis model can be mainly attributed to hepatocytes.

DISCUSSION

Cirrhosis is the 14th cause of death worldwide [Tsochatzis et al., 2014] and today no curative treatment exists, except for liver transplantation. We propose IFC-305, an adenosine derivative compound, as a promising alternative to treat liver injury. The aim of the present study is to explore the mechanism of action of IFC-305 in cirrhotic rats and the contribution of epigenetic mechanisms implicated in fibrosis reversion.

Based on our cirrhotic model we observed in dot-blot assay, a diminishment in DNA methylation during cirrhosis which is in concordance with other reports [Varela-Moreiras et al., 1995; Komatsu et al., 2012]. On the other hand, we obtained restoration of global genomic DNA methylation levels with the administration of the hepatoprotector IFC-305 (Fig. 1B and C). In contrast, in ELISA assay we observed a hypermethylation of the genomic DNA in response to IFC-305 treatment (Fig. 1D). It is conceivable that this variation can be attributed to the difference in DNA samples used for both assays, as the DNA for the first assay was sonicated to enhance the recognition of the antibody to the 5mC epitope and for the ELISA assay integral DNA was used as the kit's manufacturer indicates. One possible explanation for the regulation of DNA methylation by IFC-305 lies in its ability to restore SAM levels decreased at cirrhosis (Fig. 1A). From its chemical structure the IFC-305 compound is a derivative of adenosine, which has previously been shown to have a role in the regulation of SAM-dependent methylation reactions [Chagoya de Sanchez et al., 1991]. Furthermore, it may be explained by the increment of energy charge in hepatocytes mediated by adenosine [Chagoya de Sanchez et al., 1972] favoring ATP-dependent reactions such as transformation of methionine to SAM by methionine adenosyltransferases. In addition, there are reports that indicate that treatment of preneoplastic rats with hepatic nodules with SAM triggers a modification of DNA methylation leading to changes in gene expression [Garcea et al., 1989]. Therefore, the increase in DNA methylation induced by IFC-305 administration could be mediated through a regulation of SAM levels (Fig. 1A). Both increments mediated by IFC-305 could counteract the depletion of DNA methylation in the cirrhotic tissue, which is linked to a decrease of genomic instability, that is a characteristic of cirrhosis [Michalopoulos, 1990] and contributes to carcinogenesis [Hamilton, 2011].

In an attempt to find a correlative relationship with DNA methylation, we analyzed the incorporation of 5hmC and found a decrease of this DNA modification in cirrhotic samples, an effect that was abrogated by IFC-305 administration (Fig. 1E and F). As an approach to gain an insight into the effects caused by IFC-305 on an epigenetic level, we used assays to detect global 5mC and 5hmC levels that revealed an average of all the changes taking place genome wide, and did not give us information about the alterations of these DNA modifications at specific loci. For this reason, as we observe a mean increment in both marks in response to IFC-305 treatment, instead of a negative correlation, we suppose that the changes of each cytosine variant occur in different regions of the genome. It is possible, as suggested by the group of Mann, that specific CpGs become de novo methylated in order to recruit chromatin remodeling complexes that silence gene expression, while other CpGs become de novo methylated to subsequently become hydroxymethylated which would then instead lead to transcriptional activation or an increase in transcriptional elongation [Page et al., 2016]. However, oxidative bisulfite assays coupled to next-generation sequencing are needed to prove this hypothesis. Furthermore, it is important to keep in mind that during cirrhosis we observed a decrease in SAM, which is the universal donor of methyl groups, and therefore, this change may reflect a diminishment of methyl groups that are available for DNA methyltransferases (DNMTs). Thus, we can argue that the diminishment of 5mC can be attributed to the deficiency of SAM and not to active demethylation. This could also explain the levels of 5hmC which is generated from 5mC, a DNA modification that is already low under this condition. The initial description of 5hmC incorporation to DNA was reported in the liver and brain of rat [Penn et al., 1972], and recently a global reduction of 5hmC and its regulatory enzymes that accompany liver fibrosis and HSC *trans*-differentiation was documented [Page et al., 2016]. When we view cirrhosis as a preneoplasic state, reduction of 5hmC is consistent with studies in patients where hepatic, breast, lung, and pancreas cancer samples present a drop in 5hmC levels compared to adjacent tissue or healthy tissue samples [Yang et al., 2013].

The quantification of acetylated histone H4 revealed a 50% reduction during cirrhosis and IFC-305 treatment led to a recovery to normal levels (Fig. 2B). Histone acetylation generates an open chromatin structure that facilitates the association of transcription factors to their DNA binding sites in gene regulatory regions favoring controlled gene expression [Recillas-Targa, 2014]. Thus, this could be a mechanism by which IFC-305 treatment reduces the amount of deregulated genes in cirrhotic rats from 413 to 263 [Perez-Carreon et al., 2010]. The histone acetylation dynamics in our cirrhosis model could be particularly explained by the altered transcription [Perez-Carreon et al., 2010] and protein levels of HDAC3, as the amount of enzyme increases in cirrhosis and decreases with IFC-305 administration about 50% (Fig. 2A). Notably, the treatment of healthy rats with IFC-305 for 10 weeks generates a decrease in HDAC1 protein levels (Fig. S4: 10 IFC). Interestingly, however, no alteration of the liver physiology can be observed, when IFC-305 is administered to healthy rats, despite the global change in HDAC1 levels (Supplementary Fig. S1C: 10IFC).

The study of deposition of histone marks in the *Pparg* gene promoter demonstrated that, in cirrhosis, the chromatin presents a combinatorial code of histone PTMs at this regulatory sequence that does not favor transcription, in comparison to a healthy liver. In contrast, the treatment with IFC-305 triggers a ratio between the active histone mark H4ac and the repressive histone modification H3K27me3 (Fig. 4C) that matches with a permissive chromatin structure and correlates with an increase of transcription [Perez-Carreon et al., 2010] and protein levels of the *Pparg* gene (Fig. 3A). Importantly, our results are in agreement with a previously published report that described the enrichment of repressive histone marks (H3K27me2 and H3K9me3) on the *Pparg* promoter and gene in myofibroblast derived from *trans*-differentiated HSC, an in vitro cell system that is to a certain extent equivalent to cirrhosis [Mann et al., 2010].

In addition, we evaluated the DNA methylation status of the *Pparg* gene promoter and found that this region is devoid of DNA methylation under all conditions of the CCl_4 model (Supplementary Fig. S5). This result goes hand in hand with the fact that H3K27me3 and DNA methylation are mutually exclusive marks on CpG islands [Brinkman et al., 2012]. We also addressed the PPARγ deposition on the *Col1a1* gene promoter, where the nuclear receptor inhibits *trans*-activation of the fibrogenic gene in HSC. We found no changes in the deposition of PPARγ between healthy and cirrhotic rats. Interpreting this observation we have to take into account that the HSC population corresponds only to approximately 8%, while the hepatocytes are the most abundant cells in the liver. PPARγ positive immunoreactivity in response to IFC-305 treatment was detected in the latter cell type, as the signal was present (Fig. 3C) in non-septa regions (that were negative for the activated HSC marker αSMA [Supplementary Fig. S3]). It is possible that the mechanism of *Pparg* gene regulation, involving DNA methylation, as well as the PPARγ-mediated regulation of *Col1a1* are HSC-specific. Therefore, as the parenchymal cells outnumber the HSCs, mechanisms that take place only in HSCs are hidden, when analyzing the whole tissue. Our results suggest that on an epigenetic level transcription of the *Pparg* gene in CCl_4-induced cirrhosis are mediated principally by histone PTMs. It is important to mention that the levels of PPARγ protein are similar to the control when CCl_4 is suspended (Fig. 3A: to +5ss), nevertheless the collagen quantity is equivalent to cirrhosis in this state (Supplementary Fig. S2: to +5ss). Maybe the PPARγ overproduction mediated by the IFC-305 (Fig. 3A: to +5IFC) is necessary to trigger the binding of the nuclear receptor to the *Col1a1* gene promoter in activated HSCs to abrogate the *Col1a1* overexpression. In this context, it has been described that PPARγ is necessary to revert activated HSCs to a quiescent state, and inhibit the expression of collagen I, TGFβ, and αSMA in HSCs [Hazra et al., 2004b; Tsuchida and Friedman, 2017].

Concerning the DNA methylation pattern of the *Col1a1* gene promoter, we identified four CpG dinucleotides which specifically decreased their DNA methylation level in cirrhosis (Fig. 5B). The difference in DNA methylation correlates with an over-expression of the transcript [Perez-Carreon et al., 2010] and an increment in the protein level of collagen I (Supplementary Fig. S2). It is noteworthy that CpG at position 1 is in close proximity to some relevant regulatory sequences, like the NF-I binding site, and the relevant TGG-triplet that is critical for *Col1a1* gene expression, which is abrogated when mutated to CCA (Fig. 5A: vertical arrow) [Yavrom et al., 2005]. At this CpG we identified the strongest reduction in DNA methylation in cirrhosis that was largely recovered by IFC-305 treatment (Fig. 5B; CpG 1). Furthermore, we want to point out that the administration of IFC-305 to cirrhotic rats triggers an increase of DNA methylation at the CpGs surrounding the *Col1a1* gene TSS. Therefore, it would be interesting to investigate the dynamics of histone PTMs in this region to understand if they cooperate with DNA methylation to regulate *Col1a1* gene expression.

In order to know if HSC is the cell type that is responsible for the changes described in the cirrhosis model, we determined the global levels of histone H4 acetylation. We observed that contrary to the cirrhosis state, which is characterized by a loss of histone H4 acetylation, there is a gain of this epigenetic modification in the activated state of HSCs (7d), (Supplementary Fig. S7). It has been described previously that the developmental cell specification is accompanied by a progressive chromatin restriction as the default state transitions from dynamic remodeling to generalized compaction [Zhu et al., 2013]. Since the activation process of HSCs can be considered a *trans*-differentiation process from a specialized cell to a myofibroblast, it is understandable that the chromatin of these cells acquires characteristics of decompaction, such as histone H4 acetylation. Previously, we showed that culturing HSCs in the presence of IFC-305 blocks their activation in vitro [Velasco-Loyden et al., 2010]. When we analyzed the histone H4 acetylation in this context, we noticed that the hepatoprotective drug retains the HSCs in an intermediate state with H4ac levels between the ones of a recently isolated cell (3 h) and an activated HSC (7 d). This suggests that the activation impairment mediated by IFC-305 is partially linked to chromatin modifications. Interestingly, the global changes described on whole tissue differed from the observations made in HSCs in vitro. The most likely explanation for this discrepancy is that data obtained from the whole liver tissue will primarily reflect changes that occur in the most abundant cell type, namely parenchymal cells, whereas HSCs only account for 8% of the total cell population in the liver. Thus, if IFC-305 is able to generate different chromatin changes depending on the metabolism characteristics of the cell type, it would be relevant to explore other functions of the adenosine derivative in different liver cell types.

In summary, we propose a model which suggests that changes in gene expression observed during treatment with the hepatoprotector IFC-305 are driven by epigenetic mechanisms, like DNA methylation and histone H4 acetylation, at a global scale, as well as in specific genes critical for cirrhosis development, such as *Pparg* and *Col1a1* (Fig. 6). The model further proposes that chromatin modulation coordinated by the adenosine derivative plays a role in the prevention of HSC activation in vitro. These findings raise further questions concerning the molecular mechanisms involved in the regulation of other genes and hepatic functions altered during cirrhosis, which need to be addressed in future studies.

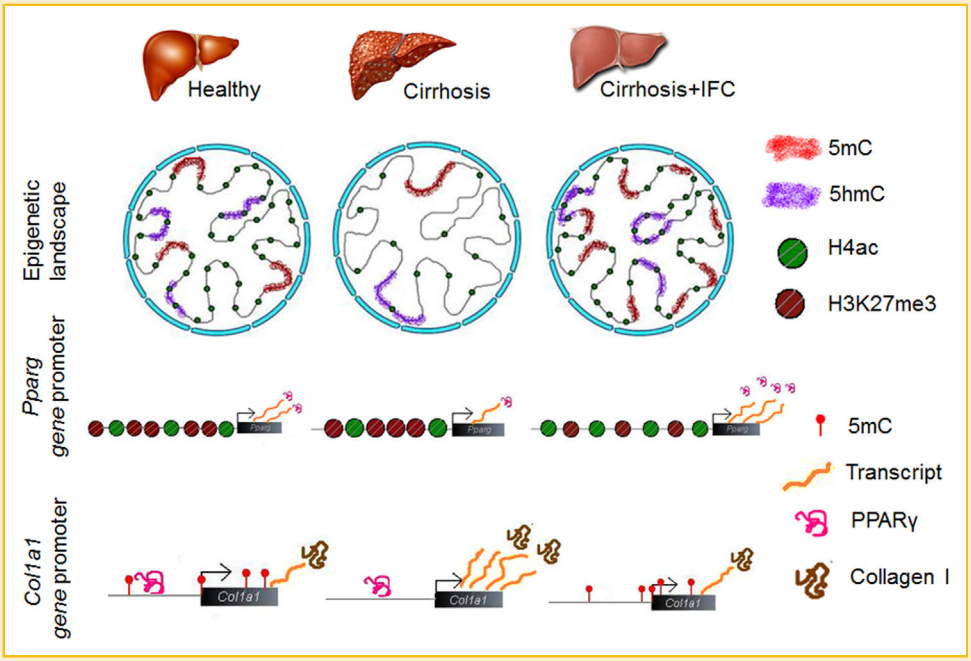

Fig. 6. Integrative model of the effects of the hepatoprotector IFC-305 in the CCl_4-induced cirrhosis rat model. Top panel: Global epigenetic changes; in cirrhosis there is a decrease in global DNA methylation (5mC), 5hmC, and histone H4 acetylation levels; IFC-305 treatment increases DNA methylation and re-establishes the levels of 5hmC and histone H4 acetylation. Middle panel: Changes in the *Pparg* gene promoter; in cirrhosis, the chromatin configuration of the promoter is more compact than in the control liver and this correlates with decreased transcript and protein levels. In contrast, administration of the hepatoprotector IFC-305 triggers chromatin relaxation at the *Pparg* gene promoter, mediating transcript and protein over expression. Bottom panel: Changes in the *Col1a1* gene promoter; four methylated CpG dinucleotides in the healthy liver were found to lose DNA methylation in cirrhosis, this change correlates with an increment of *Col1a1* transcription and as a consequence generates fibrosis. Administration of IFC-305 induces an increase in CpG methylation around the TSS and at the CpG at position 1.

CONCLUSIONS

This study provides a general description of dynamics of DNA methylation and histone PTMs (H4ac and H3K27me3) in a CCl_4-induced cirrhosis animal model and the changes that occur upon treatment with the adenosine derivative IFC-305 (Fig. 6). We find a decrease of SAM levels, as well as global 5mC, 5hmC, and histone H4 acetylation modifications in cirrhosis. Treatment with IFC-305 restores levels of SAM, 5hmC, and histone H4 acetylation to physiological levels and increases the amount of 5mC. The hepatoprotector establishes a combination of histone PTMs at the *Pparg* gene promoter that triggers an increment of its transcription and protein levels. However, further studies are required in order to decipher the global dynamics of chromatin conformation in cirrhosis and upon administration of IFC-305. Finally, we propose that the reduction of collagen I, mediated by IFC-305, is induced by a recovery of DNA methylation in the *Col1a1* gene promoter, and this could be a key mechanism of action to reverse cirrhosis. Thus, the results of this study provide an important foundation to understand the fibrosis process at a molecular level.

MATERIALS AND METHODS

CHEMICALS

CCl_4 was purchased from Merk® México (México). IFC-305 is the aspartate salt of adenosine: 2-aminosuccinic acid-2-(6-amino-9*H*-purin-9-yl)-5-(hydroxymethyl) tetrahydrofuran-3,4-diol (1:1). It was synthesized in the laboratory in agreement with UNAM patent 207422. Salts were from MP Biomedicals, LLC (Illkirch, France) and MP Biomedicals, Inc. (Eschwege, Germany).

ANIMAL TREATMENT AND INDUCTION OF CIRRHOSIS WITH CCl_4

Male Wistar rats (n = 20) weighing 100–110 g were rendered cirrhotic by chronic treatment with CCl_4. Animals were intraperitoneally injected with a solution of 1:6 of CCl_4 in vegetable oil (0.4 g/kg weight) for 10 weeks. Cirrhosis-induced rats were divided in three groups, one was euthanized after CCl_4 withdrawal (Cirrhosis [to]), while other groups were treated with saline solution (to +5ss) or with IFC-305 (to +5IFC) for 5 weeks (50 mg/kg weight, three times/week), a group of non-treated rats was used as control and an additional group of healthy rats treated for 10 weeks with IFC-305 (10 IFC) were used in some assays to compare the effect of the drug with CCl_4 (Supplementary Fig. S1A). Animals were euthanized with sodium pentobarbital (Sedalpharma, Pets Pharma de México S.A. de C.V.). Liver was photographed (Supplementary Fig. S1B), recovered, weighed, and frozen or fixed with formaldehyde, and routinely processed for Masson Trichrome staining (Supplementary Fig. S2B). Animals were obtained from animal care facility of the Instituto de Fisiología Celular, UNAM. All procedures were conducted according to institutional guidelines for care and use of laboratory animals and were approved with protocol number VCHH53-14, valid to October 2019.

SEROLOGICAL PARAMETERS OF LIVER FUNCTION

Alanine aminotransferase (ALT, EC 2.6.1.2) activity was determined as previously described [Hernandez-Munoz et al., 1984].

S-ADENOSYLMETHIONINE QUANTIFICATION

SAM levels were determined as previously described [Hernandez-Munoz et al., 1984].

TOTAL LIVER AND NUCLEAR PROTEINS ISOLATION

Liver tissue (100 mg) was manually homogenized in a Potter tube with a Teflon pistil with 1 mL PBS 1× and a protease inhibitors cocktail (Complete, Roche; PMSF, Sigma), incubated 20 min on ice, and centrifuged at 14,000 rpm, 4°C for 5 min (GS-15R Centrifuge, F2402H rotor, Beckman). The supernatant was recovered and centrifuged a second time. The nuclear fraction was obtained as previously described [Chagoya de Sanchez et al., 2012].

WESTERN BLOT ANALYSIS

Total liver proteins or nuclear proteins were quantified with the Bradford reagent (Bio-Rad), and 30 μg of protein/well was run by electrophoresis in SDS-polyacrylamide gels (12% for total protein extracts and 20% for nuclear protein extracts) and transferred (1 h for total protein extracts and 30 min for nuclear protein extracts in humidity chamber) to an Immobilon®-P transfer membrane (Millipore). The blots were incubated with primary antibodies anti-collagen I (Santa Cruz Biotechnology sc-25974, Lot #F1207, RRID:AB_2081880), anti-PPARγ (Santa Cruz Biotechnology sc-7196, Lot #E0611, RRID:AB_654710), anti-GAPDH (Millipore MAB374, Lot #NG1722294, RRID:AB_2107445), anti-HDAC3 (Abcam ab47237, Lot #GR29265-1, RRID:AB_732779), anti-HDAC1 (Cell Signaling #5356, RRID:AB_10612242, kindly donated by Dr. Alfonso León del Rio, IIB-UNAM) for total proteins and anti-hyperacetylated Histone H4 (Millipore 06-946, Lot #29860, RRID: AB_310310) and anti-histone H4 (Millipore 04-858, Lot #1951953, RRID:AB_1977264) for nuclei proteins and detected with the respective secondary antibody. Protein bands were visualized by using SuperSignal® West Femto (Thermo Scientific). Densitometric analyses of bands were done with Quantity One software (Bio-Rad®, Hercules, CA). The biological replicates of Western blots were performed independently and each series-assay was normalized to its own liver control and then compared between replicates.

DOT-BLOT ANALYSIS

Genomic DNA was isolated from 200 mg of frozen rat liver [Strauss, 1998], then, genomic DNA was sonicated to obtain 100–12,000 kb DNA fragments and 400 ng were used per assay. For 5mC detection we used as positive control commercially available methylated-DNA (Zymo Research D5325-5-1) and for 5hmC we employed genomic DNA isolated from mice brain cortex. Plasmid DNA was used as negative control for both assays. Each DNA was hybridized onto a DNA hybridization membrane (HybondN+ GE) and then cross-linked using UV light [Valdes-Quezada et al., 2013]. The membrane was incubated overnight with antibody against 5mC (Zymo Research A3001-30, Lot #ZRC175458) or 5hmC (ActiveMotif® 39769, Lot #10310001, RRID:AB_10013602) and detected with secondary antibody. DNA dots were visualized with SuperSignal® West Femto (Thermo Scientific®). The membrane was methylene blue stained as loading control. Densitometric analyses of dots were done with the Quantity One software (Bio-Rad®).

QUANTITATIVE EVALUATION OF GLOBAL GENOMIC DNA METHYLATION

Global DNA methylation was determined by using 100 ng of genomic DNA with the Imprint Methylated DNA Quantification Kit (Sigma® MDQ1) following the manufacturer's instruction.

CHROMATIN IMMUNOPRECIPITATION ASSAY

Briefly, 200 mg of frozen liver tissue was fractionated and treated with 1% formaldehyde in PBS 1× and protease inhibitors in agitation for 10 min. The crosslinking was stopped with 125 mM glycine for 10 min, centrifuged 5 min at 5,000 rpm at 4°C (GS-15R Centrifuge, F2402H rotor, Beckman) [Valdes-Quezada et al., 2013]. The sonicated chromatin fragments were between 500 and 800 bp. The samples were diluted 1:5 in a dilution buffer and the diluted chromatin was pre-cleared [Valdes-Quezada et al., 2013]; 800 μg of chromatin were incubated with 4 μg of antibodies anti-hyperacetylated histone H4 (Millipore 06-946, Lot #29860, RRID: AB_310310), anti-H3K27me3 (Abcam® AB6002, Lot #GR137554-2, RRID:AB_305237), anti-PPARγ (Abcam® AB41928, Lot #GR26030-60, RRID:AB_777392), normal rabbit anti-IgG (Millipore 12-370) and normal mouse anti-IgG (Millipore 12-371). The recovered DNA was assayed by qPCR (StepOne™ detection system, Applied Biosystems) using the following primers: *Pparg* gene promoter previously described by Mann et al. [2010]; we used the *GAPDH* gene as a positive control of an open chromatin region, forward 5′-GGCACTGCACAAGAAGATG-3′, reverse 5′-GTAAAGCCGCGAG-TAGCTG-3′; and a satellite repeated sequence as a positive control of a compacted chromatin region [Hernandez-Hernandez et al., 2008]; PPARγ response element in *aP2* gene, as positive control of PPARγ binding region, and *Col1a1* gene promoter were taken from Tsukamoto's group report [Yavrom et al., 2005]. For the open chromatin histone mark (acetylated histone H4), the enrichment was calculated over a rat satellite region. Inversely, for the repressive chromatin histone mark (H3K27me3), the enrichment was calculated over a constitutively open region corresponding to the *GAPDH* gene. For PPARγ the enrichment was calculated over GAPDH region, where the nuclear receptor is not bound. The enrichment calculations were performed as follows: Enrichment = antibody $(Ct_T - Ct_C)$/Input 1% $(Ct_T - Ct_C)$; where Ct_T = amplification of the test region and Ct_C = amplification of the negative control region.

SODIUM BISULFITE DNA CONVERSION AND SEQUENCING

Genomic DNA (3 μg) was processed with sodium bisulfite [Valdes-Quezada et al., 2013], DNA fragments of interest were PCR-amplified using the following primers: *Pparg* gene promoter and first exon 5′-end, forward 5′-GGTTATGGGTATTTGTTTGAGG-3′, reverse 5′-ATCAAAAAATAACTTCTCAACCC-3′; *Pparg* first exon, forward 5′-GGGTTGAGAAGTTATTTTTTGAT-3′, reverse 5′-TAAA AAAAAC CTAAAATAACTCCAC-3′; *Col1a1* gene promoter, forward 5′-GAG GGTT TAGTTATATTTAGTGAT-3′, reverse 5′-CAAAACTCCACTTC-TAAAATCTAC-3′. The amplified DNA fragments were cloned into

the pGEM-T Easy system (Promega®), and sequenced using SP6 sequence primers.

HEPATIC STELLATE CELL ISOLATION AND CULTURE

HSCs were isolated from normal male Wistar rats (600–800 g body weight) by in situ enzymatic digestion of the liver with collagenase/pronase and density gradient ultracentrifugation with Accudenz® (Accurate Chemical, Westbury, NY) as previously described [Velasco-Loyden et al., 2010]. HSCs were cultured on plastic cell culture dishes in DMEM low glucose (LG) (Invitrogen, Carlsbad, CA) containing 10% fetal bovine serum (FBS), Antibiotic-Antimycotic, and 2 μg/mL gentamicin (Gibco, Life Technologies, Grand Island, NY) (DMEM LG 10% FBS AB/AM + genta). We seeded 250,000 cells (3 h, 1 day [1 d] and 7 days with IFC-305 5 mM [7 d + 5IFC]) or 125,000 cells (7 days [7 d]) by duplicate in a 12 wells plate. For 7 d and 7 d + 5IFC, after 24 h of isolation, the culture medium was replaced with DMEM LG 10% FBS AB/AM + genta, containing the indicated concentration of IFC-305. The medium was changed every other day for a total of 7 days.

IMMUNOFLUORESCENCE

Histological sections of liver were used for PPARγ and α-smooth muscle actin (αSMA) immunofluorescence, with anti-PPARγ (Santa Cruz Biotechnology sc-7196, Lot #E0611, RRID:AB_654710) diluted at 1:50, incubating overnight (4°C), with anti-αSMA (clone 1A4 Sigma Chemical Co. A 2547, Lot 035K4846, RRID:AB_476701) diluted at 1:700 and secondary Alexa Fluor 568 goat anti-rabit IgG (Invitrogen) antibody diluted 1:400 for anti-PPARγ, and secondary Fluorescein horse anti-mouse IgG (Vector Laboratories, Inc., Burlingame, CA) antibody diluted 1:400 for anti-αSMA, incubating for 2 h in obscurity at room temperature. We used the components of DAKO EnVision + System, HRP (DAB) (DAKO Corporation, Carpinteira, CA. K400711) to block the proteins and to dilute the antibodies. Coverslips were mounted on the histological sections with mounting medium for fluorescence with DAPI (Vectashield, Burlingame, CA). Fluorescence was visualized with an Olympus Inverted Microscope model IX71 and images captured with Evolution/QImaging Digital Camera (Media Cybernetics, Bethesda, MD). Data analysis was performed using ImageJ (National Institutes of Health, Bethesda, MD).

For cell cultures, once the growing times have elapsed, HSC were washed twice with PBS 1×, fixed with 4% paraformaldehyde for 5 min, and washed three more times. The wells were blocked with block solution (1% Triton X-100 and albumin fraction V from bovine blood (USB Corporation, Cleveland, OH) in PBS 1×) for 20 min. The cells were washed once with block solution without Triton X-100. Cells were incubated overnight at 4°C with 1:400 primary antibody anti-hyperacetylated histone H4 in block solution without Triton X-100 (Millipore 06-946, Lot #29860, RRID:AB_310310). Then, the cells were incubated 1 h at room temperature, washed three times, and then incubated with 1:400 anti-rabbit Alexa Fluor goat anti-rabbit IgG (Invitrogen) in PBS 1× or block solution in accordance with primary antibody solution. Finally the cells were washed three times and a circle coverslip was mounted on the well with mounting medium for fluorescence with DAPI (Vectashield). Fluorescence was visualized with an Olympus Inverted Microscope model IX71 and images captured with Evolution/QImaging Digital Camera (Media Cybernetics). Data analysis was performed using ImageJ (National Institutes of Health).

STATISTICAL ANALYSIS

Statistical analysis was performed using the unpaired, Student's *t*-test, using Graph Pad Prism 5.0 (Graph Pad Software, Inc., La Jolla, CA) for Windows.

AUTHORS' CONTRIBUTIONS

JRRA: Performed the great majority of experiments and prepared the manuscript. CAGH: Provided the conceptual framework and performed some experimental assistance. RPM: Provided experimental assistance performing sodium bisulfite DNA conversion, chromatin immunoprecipitation assay and comments on the manuscript. CECC: Provided assistance for dot blot assay and comments on the manuscript. RPCV: Was responsible for animal experimental procedures, immunohistochemistry, Western blot assay and comments on the manuscript. NGC: Contributed to some experiments and comments on the manuscript. MDL: Performed enzymatic assay determination, technical assistance in HPLC and comments on the manuscript. ARMO: Contributed to some experiments and comments on the manuscript. RAM: Contributed with bioinformatics analysis and made remarks on the manuscript. FRT: Contributed to design of epigenetic experiments, discussions of the results and comments on the manuscript. VCS: Provided insights and design of the project and prepared the manuscript with assistance from JRRA and FRT.

ACKNOWLEDGMENTS

We acknowledge the technical assistance of Lucía Yáñez-Maldonado, Lidia Martínez-Pérez, Susana Vidrio-Gómez, Gabriela Velasco-Loyden, Georgina Guerrero-Avendaño, Fernando Suaste-Olmos, and the Molecular Biology Unit of IFC-UNAM. We thank Alberto Aranda-Fraustro and Olga Lidia Pérez Reyes from the Instituto Nacional de Cardiología "Ignacio Chávez" for obtaining the histological sections for this work. We wish to thank Emilio Rojas del Castillo, Mónica Liliana Guzmán-López, Karin Meier, and the members of the Recillas-Targa research group for their constant comments and suggestions. JRRA appreciates the article shared by Dr. James P. Hamilton. JRRA dedicates this work to his PhD advisor, Dr. Victoria Chagoya, within the framework of the celebration of the 50th years of her studies about adenosine and to his co-advisor Dr. Félix Recillas-Targa. This work has been supported by DGAPA-UNAM, grant numbers: IN225909 and IN207012 to VCS; IN203811 and IN201114 to FRT; CONACyT México, grant numbers: 128464 and 220503 to FRT; Fellowship: PAEP-UNAM, Programa de Maestría y Doctorado en Ciencias Bioquímicas, UNAM; No. Cta. 30479367-5 to JRRA; fellowship: PhD Fellowship from CONACyT; CVU 508509 to JRRA.

REFERENCES

Bhutani N, Burns DM, Blau HM. 2011. DNA demethylation dynamics. Cell 146:866–872.

Brinkman AB, Gu H, Bartels SJ, Zhang Y, Matarese F, Simmer F, Marks H, Bock C, Gnirke A, Meissner A, Stunnenberg HG. 2012. Sequential ChIP-bisulfite sequencing enables direct genome-scale investigation of chromatin and DNA methylation cross-talk. Genome Res 22:1128–1138.

Chagoya de Sanchez V, Brunner A, Pina E. 1972. In vivo modification of the energy charge in the liver cell. Biochem Biophys Res Commun 46:1441–1445.

Chagoya de Sanchez V, Hernandez-Munoz R, Sanchez L, Vidrio S, Yanez L, Suarez J. 1991. Twenty-four-hour changes of S-adenosylmethionine, S-adenosylhomocysteine adenosine and their metabolizing enzymes in rat liver; possible physiological significance in phospholipid methylation. Int J Biochem 23:1439–1443.

Chagoya de Sanchez V, Martinez-Perez L, Hernandez-Munoz R, Velasco-Loyden G. 2012. Recovery of the cell cycle inhibition in CCl(4)-induced cirrhosis by the adenosine derivative IFC-305. Int J Hepatol 2012:212530.

Garcea R, Daino L, Pascale R, Simile MM, Puddu M, Ruggiu ME, Seddaiu MA, Satta G, Sequenza MJ, Feo F. 1989. Protooncogene methylation and expression in regenerating liver and preneoplastic liver nodules induced in the rat by diethylnitrosamine: Effect of variations of S-adenosylmethionine: S-adenosylhomocysteine ratio. Carcinogenesis 10:1183–1192.

Hamilton JP. 2011. Epigenetics: Principles and practice. Dig Dis 29:130–135.

Hazra S, Miyahara T, Rippe RA, Tsukamoto H. 2004a. PPAR gamma and hepatic stellate cells. Comp Hepatol 3:S7.

Hazra S, Xiong S, Wang J, Rippe RA, Krishna V, Chatterjee K, Tsukamoto H. 2004b. Peroxisome proliferator-activated receptor gamma induces a phenotypic switch from activated to quiescent hepatic stellate cells. J Biol Chem 279:11392–11401.

Hernandez-Gea V, Friedman SL. 2011. Pathogenesis of liver fibrosis. Annu Rev Pathol 6:425–456.

Hernandez-Hernandez A, Rincon-Arano H, Recillas-Targa F, Ortiz R, Valdes-Quezada C, Echeverria OM, Benavente R, Vazquez-Nin GH. 2008. Differential distribution and association of repeat DNA sequences in the lateral element of the synaptonemal complex in rat spermatocytes. Chromosoma 117:77–87.

Hernandez-Munoz R, Glender W, Diaz Munoz M, Adolfo J, Garcia-Sainz JA, Chagoya de Sanchez V. 1984. Effects of adenosine on liver cell damage induced by carbon tetrachloride. Biochem Pharmacol 33:2599–2604.

Iredale JP. 2007. Models of liver fibrosis: Exploring the dynamic nature of inflammation and repair in a solid organ. J Clin Invest 117:539–548.

Kohli RM, Zhang Y. 2013. TET enzymes, TDG and the dynamics of DNA demethylation. Nature 502:472–479.

Komatsu Y, Waku T, Iwasaki N, Ono W, Yamaguchi C, Yanagisawa J. 2012. Global analysis of DNA methylation in early-stage liver fibrosis. BMC Med Genomics 5:5.

Kriaucionis S, Heintz N. 2009. The nuclear DNA base 5-hydroxymethylcytosine is present in Purkinje neurons and the brain. Science 324:929–930.

Mann J, Chu DC, Maxwell A, Oakley F, Zhu NL, Tsukamoto H, Mann DA. 2010. MeCP2 controls an epigenetic pathway that promotes myofibroblast transdifferentiation and fibrosis. Gastroenterology 138:705–714,714 e1–e4.

Michalopoulos GK. 1990. Liver regeneration: Molecular mechanisms of growth control. FASEB J 4:176–187.

Nehls MC, Rippe RA, Veloz L, Brenner DA. 1991. Transcription factors nuclear factor I and Sp1 interact with the murine collagen alpha 1 (I) promoter. Mol Cell Biol 11:4065–4073.

Page A, Paoli P, Moran Salvador E, White S, French J, Mann J. 2016. Hepatic stellate cell transdifferentiation involves genome-wide remodeling of the DNA methylation landscape. J Hepatol 64(3):661–673.

Paquet KJ, Kamphausen U. 1975. The carbon-tetrachloride-hepatotoxicity as a model of liver damage. First report: Long-time biochemical changes. Acta Hepatogastroenterol (Stuttg) 22:84–88.

Penn NW, Suwalski R, O'Riley C, Bojanowski K, Yura R. 1972. The presence of 5-hydroxymethylcytosine in animal deoxyribonucleic acid. Biochem J 126:781–790.

Perez-Carreon JI, Martinez-Perez L, Loredo ML, Yanez-Maldonado L, Velasco-Loyden G, Vidrio-Gomez S, Ramirez-Salcedo J, Hernandez-Luis F, Velazquez-Martinez I, Suarez-Cuenca JA, Hernandez-Munoz R, de Sanchez VC. 2010. An adenosine derivative compound, IFC305, reverses fibrosis and alters gene expression in a pre-established CCl(4)-induced rat cirrhosis. Int J Biochem Cell Biol 42:287–296.

Recillas-Targa F. 2014. Interdependency between genetic and epigenetic regulatory defects in cancer. Methods Mol Biol 1165:33–52.

Rippe RA, Almounajed G, Brenner DA. 1995. Sp1 binding activity increases in activated Ito cells. Hepatology 22:241–251.

Strauss WM. 1998. Preparation of genomic DNA from mammalian tissue. Curr Protoc Mol Biol (Suppl42):2.2.1–2.2.3.

Tahiliani M, Koh KP, Shen Y, Pastor WA, Bandukwala H, Brudno Y, Agarwal S, Iyer LM, Liu DR, Aravind L, Rao A. 2009. Conversion of 5-methylcytosine to 5-hydroxymethylcytosine in mammalian DNA by MLL partner TET1. Science 324:930–935.

Tsochatzis EA, Bosch J, Burroughs AK. 2014. Liver cirrhosis. Lancet 383:1749–1761.

Tsuchida T, Friedman SL. 2017. Mechanisms of hepatic stellate cell activation. Nat Rev Gastroenterol Hepatol https://doi.org/10.1038/nrgastro.2017.38 [Epub ahead of print].

Valdes-Quezada C, Arriaga-Canon C, Fonseca-Guzman Y, Guerrero G, Recillas-Targa F. 2013. CTCF demarcates chicken embryonic alpha-globin gene autonomous silencing and contributes to adult stage-specific gene expression. Epigenetics 8:827–838.

Varela-Moreiras G, Alonso-Aperte E, Rubio M, Gasso M, Deulofeu R, Alvarez L, Caballeria J, Rodes J, Mato JM. 1995. Carbon tetrachloride-induced hepatic injury is associated with global DNA hypomethylation and homocysteinemia: Effect of S-adenosylmethionine treatment. Hepatology 22:1310–1315.

Velasco-Loyden G, Perez-Carreon JI, Aguero JF, Romero PC, Vidrio-Gomez S, Martinez-Perez L, Yanez-Maldonado L, Hernandez-Munoz R, Macias-Silva M, de Sanchez VC. 2010. Prevention of in vitro hepatic stellate cells activation by the adenosine derivative compound IFC305. Biochem Pharmacol 80:1690–1699.

Yang H, Liu Y, Bai F, Zhang JY, Ma SH, Liu J, Xu ZD, Zhu HG, Ling ZQ, Ye D, Guan KL, Xiong Y. 2013. Tumor development is associated with decrease of TET gene expression and 5-methylcytosine hydroxylation. Oncogene 32:663–669.

Yavrom S, Chen L, Xiong S, Wang J, Rippe RA, Tsukamoto H. 2005. Peroxisome proliferator-activated receptor gamma suppresses proximal alpha1(I) collagen promoter via inhibition of p300-facilitated NF-I binding to DNA in hepatic stellate cells. J Biol Chem 280:40650–40659.

Zhu J, Adli M, Zou JY, Verstappen G, Coyne M, Zhang X, Durham T, Miri M, Deshpande V, De Jager PL, Bennett DA, Houmard JA, Muoio DM, Onder TT, Camahort R, Cowan CA, Meissner A, Epstein CB, Shoresh N, Bernstein BE. 2013. Genome-wide chromatin state transitions associated with developmental and environmental cues. Cell 152:642–654.

SUPPORTING INFORMATION

Additional supporting information may be found in the online version of this article at the publisher's web-site.

International Immunopharmacology 54 (2018) 12–23

Contents lists available at ScienceDirect

International Immunopharmacology

journal homepage: www.elsevier.com/locate/intimp

Inflammation is regulated by the adenosine derivative molecule, IFC-305, during reversion of cirrhosis in a CCl_4 rat model

Rebeca Pérez-Cabeza de Vaca, Mariana Domínguez-López, Nuria Guerrero-Celis, Jesús R. Rodríguez-Aguilera, Victoria Chagoya de Sánchez*

Instituto de Fisiología Celular, UNAM, Departamento de Biología Celular y Desarrollo, Laboratorio 305-Sur, Circuito Exterior s/n Ciudad Universitaria, Coyoacán, 04510 Mexico City, Mexico.

ARTICLE INFO

Keywords:
Cirrhosis
CCl_4
Hepatotoxicity
Hepaprotective molecule
Liver immune response
Inflammation
Anti-inflammatory response
Liver immune response
Inflammation

ABSTRACT

Cirrhosis is a liver pathology originated by hepatocytes, Kupffer and hepatic stellate cells interactions and transformations. This pathology is associated with inflammation and fibrosis, originated by molecular signals secreted by immunological and parenchymal cells, such as cytokines and chemokines, like IL-1β, IL-6, TNF-α or MCP-1, driven by Kupffer cells signals. As part of inflammation resolution, the same activated Kupffer cells contribute to anti-inflammatory effects with IL-10 and MMP-9 secretion. In a Wistar rat model, cirrhosis induced with CCl_4 is characterized by increased inflammatory cytokines, IL-6, IL-1β, MCP-1, and TNF-α, in plasma and liver tissue. The IFC-305 compound, an adenosine derivative salt, reverses the cirrhosis in this model, suggesting that immune mechanisms related to inflammation should be explored. The IFC-305 reduced inflammatory cytokines, supporting the anti-inflammatory effects induced by the elevation of IL-10, as well as the reduction of M1 inflammatory macrophages ($CD11b/c^+/CD163^+$) and the increase of M2 anti-inflammatory macrophages ($HIS36^+/CD11b^+$), measured by flow cytometry. Furthermore, the IFC-305 enhances the metabolic activity of arginase and moderates the inducible nitric oxide synthetase, evaluated through biochemical and immunohistochemical methods. These results contribute to understand the function of the IFC-305, which modulates the immune response in the Wistar rat model of CCl_4-induced cirrhosis and support the hepatic protective action through an anti-inflammatory effect, mainly mediated by Kupffer cells.

1. Introduction

Cirrhosis is a pathological condition that represents the 14th most common cause of death worldwide [1]. In recent years, many studies have been conducted to understand the mechanisms involved in the development of this disease and its resolution, at cellular and molecular levels. It has been demonstrated that the immune response is one of the main mechanisms involved in the progression and repair of this liver pathology [2].

Liver injuries provide a proper model of inflammation and repair, showing a complex interaction of epithelial cells, myofibroblasts, and the extracellular matrix (ECM), all are components of the mammalian wound-healing response. In almost all etiologies, cirrhosis is preceded by fibrosis and inflammation, with elements of innate and adaptive immune response that are crucial in regulating these processes [3]. The most common etiologies for cirrhosis are: hepatitis B and C alcohol abuse [4,5], non-alcoholic steatohepatitis [6], and chronic infection with parasites such as *Schistosoma mansoni* and *Schistosoma japonicum* [7]. The efforts to confront these fibrotic diseases are focused on finding specific marks that transform an acute inflammation to a chronic one, and to use them as therapeutic aims for treatment and reversion of these phenomena [8]. The immune response plays an essential role in this transformation, mainly due to diverse cellular phenotypes [9]. This dynamic environment in the complex hepatic structure and intercellular communication produces an irreversible tissue fibrosis, cirrhosis, and, in many cases, hepatocellular carcinoma [10]. The participation of immune cells, such as Kupffer cells (KC) as initial effectors, is responsible for cirrhosis development [11,12], and they represent an immune cell population related to liver fibrosis treatment.

The resident liver macrophages and KC present diverse activation phenotypes: M1 related to inflammation and M2 anti-inflammation [13], both are regulated by extracellular signals, such as adenosine [14]. This activation has been described as a product of the signals related to inflammation and resolution of inflammation processes [15,16].

In liver diseases, the phenomenon, in a canonical way, occurs when

* Corresponding author.
E-mail address: vchagoya@ifc.unam.mx (V. Chagoya de Sánchez).

http://dx.doi.org/10.1016/j.intimp.2017.10.019
Received 17 January 2017; Received in revised form 3 October 2017; Accepted 17 October 2017
Available online 28 October 2017

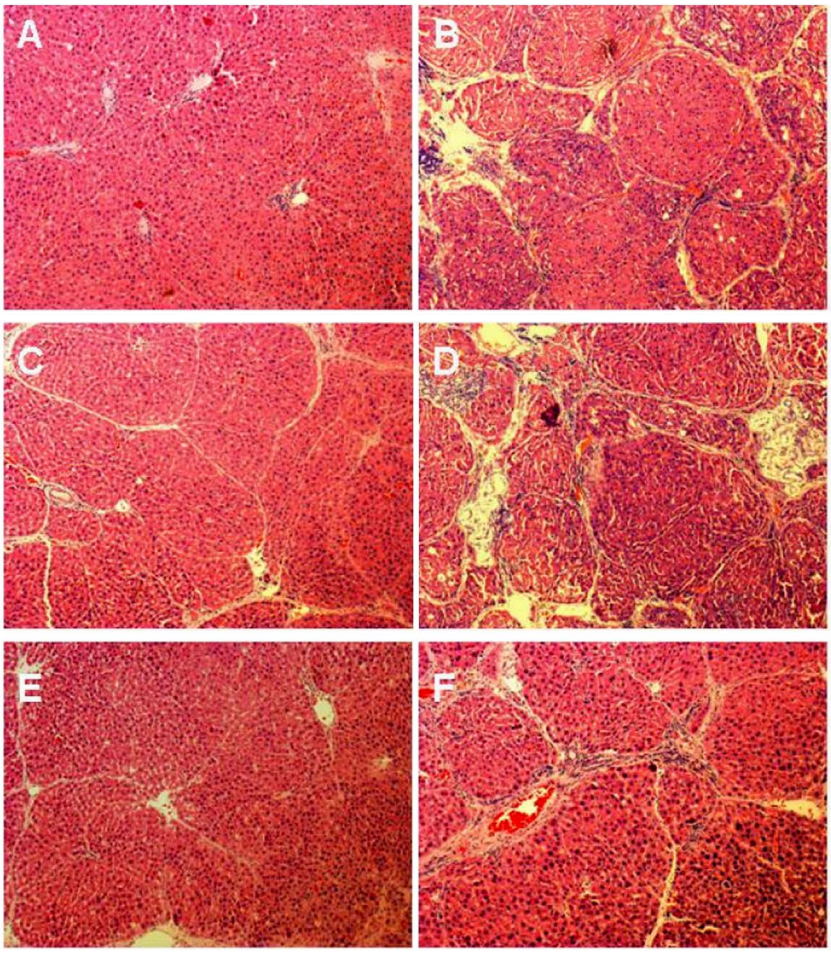

Fig. 1. Effects of IFC-305 on liver tissue samples stained with haematoxylin. (10X). (A) HC; (B) Ci; (C) Ci IFC 5w; (D) Ci SS 5w; (E) Ci IFC 10w; (F) Ci SS 10w.

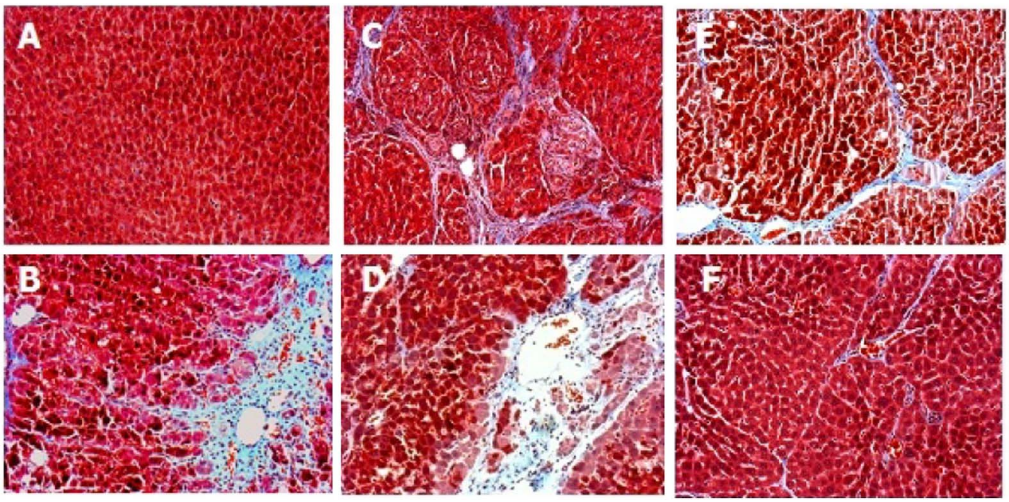

Fig. 2. Effects of IFC-305 on liver tissue samples stained with Masson's trichrome 10X. (A) HC, (B) Ci, (C) Ci SS 5w, (D) Ci SS 10w, (E) Ci IFC 5w, (F) Ci IFC 10w.

the activated Kupffer cells regulate the activation of hepatic stellate cells (HSC) and other molecular and cell interactions associated to the establishment of cirrhosis [17,18]. KC also interact with other cells, like neutrophils, hepatocytes, etc., mainly through molecules directly associated to inflammation and fibrosis, like cytokines and chemokines, such as IL-1β, IL-6, TNF-α, and MCP-1 [19]; KC could be contributing to anti-inflammatory effects with IL-10 and other cytokines involved in tissue repair [20]. Cytokines are hormone-like molecular mediators that are synthesized by a variety of cells in response to various stimuli, including inflammation and tissue damage. The liver is the main organ that produces and removes cytokines; all cell types in the liver, parenchymal and non-parenchymal, are capable of cytokines production [21,22].

Besides the knowledge of the pathological mechanisms involved, the therapeutic options for the treatment of liver diseases, such as cirrhosis, are limited. We have previously reported that the IFC-305 compound, an adenosine derivative salt, was shown to be able to reverse cirrhosis induced by CCl_4 in a rat model [23]. Part of these effects has been associated with the inhibition of HSC activation [24] and regulation of the cell cycle and the proliferative capacity of the liver

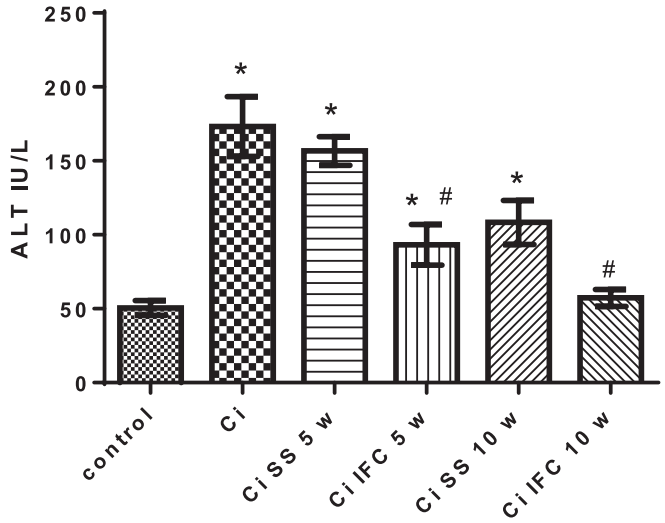

Fig. 3. ALT activity, 10 weeks of administration with CCl_4 (Ci), 5 and 10 weeks with IFC-305 and SS, respectively. Values are shown as times over control of Kupffer cells ± SEM $^{*}p \leq 0.5$ vs. control rat, $^{\#}p \leq 0.5$ IFC-305 vs. SS treatment.

tissue [25]. This compound also functions as a metabolic effector, participating in the recovery of the energetic and redox states including antioxidant defences [26].

In order to determine if the IFC-305 compound exerts an effect on the immune response that contributes to cirrhosis reversion, we studied changes in cellular and molecular factors linked to HSC activation, such as Kupffer cells and cytokines, as well as the perpetuation of inflammation, fibrosis, and irreversible cirrhosis.

2. Materials and methods

2.1. Experimental model

Male Wistar rats ($n = 42$) weighing 120–150 g were rendered cirrhotic as previously described in Pérez-Carreón et al. [23]. Briefly, animals were administered with CCl_4 (0.4 g/kg) during 10 weeks. Cirrhotic-induced rats were divided in five groups: the cirrhotic rats (**Ci**); two groups treated with saline solution (SS), and two more with the experimental molecule IFC-305. For the groups **Ci, SS, 5w,** and **Ci, SS, 10w,** saline solution was administrated IP, three times per week, for 5 and 10 weeks, respectively; and two different groups received the IFC-305 molecule at pre-established doses of 50 mg/kg [27] (IP, three times per week; diluted at a concentration of 20 mg/mL in saline solution with a pH = 7.4), denominated **Ci IFC 5w** and **Ci IFC 10w**. All the experiments included an additional group of control rats without any treatment, named **Healthy Control (HC)**.

Animals were housed under a circadian cycle (light/dark = 12:12 h), in temperature-controlled rooms (21 °C ± 2°) and allowed food and water ad libitum. All animals were obtained from the Instituto de Fisiología Celular at the Universidad Nacional Autónoma de México (UNAM). All animal procedures followed the Biomedical-Ethics protocol of UNAM for the care and use of laboratory animals and the institutional protocols and approval with the VCHH53–14 number valid until October 2019.

At the end of the administration weeks, animals were weighed and anaesthetised (sodium pentobarbital 120 mg/kg, IP injection, Sedalpharma®). Between 9 and 12 mL of blood were obtained by myocardial heart puncture, with EDTA as anticoagulant. The liver was isolated and fractionated in pieces for histological analysis and kept at − 70 °C until used for further determinations. The rest of the liver was perfused in situ to get the non-parenchymal cells (NPC) for flow cytometry assays.

2.2. IFC-305 molecule preparation

IFC-305 is the aspartate salt of adenosine prepared with adenosine free base (MP Biomedicals, LLC, Illkirch, France) and L-aspartic acid (MP Biomedicals, Inc., Eschwege, Germany) as described (Patent No. MX220780; US 8507, 459B2. [28]) Doses were calculated based on the animal weights and the aspartate salt was dissolved in saline solution as vehicle for its administration.

2.3. Histology and immunohistochemical studies

Liver tissue samples were paraffin-embedded and slices (5 μm) were stained with haematoxylin-eosin and Masson's trichrome according to standard protocols. For immunostaining, we employed arginase I antibody (H-52): sc-20150 (1:100); CD163 antibody (ED2): sc-58965 (1:500); iNOS NOS_2 antibody (C-11): sc-7271 (1:200); and DAKO® HRP-DAB system.

2.4. Alanine transaminase (ALT) enzyme activity

Alanine transaminase (ALT; EC 2.6.1.2) as parameter of liver function was determined in plasma as previously described (Hernandez-Munoz et al., 1990).

2.5. Kupffer and non-parenchymal cells extraction

Anaesthetised and punctured rats with a ventral midline incision over the peritoneal cavity were tubed with a cannula into the portal vein. The liver was perfused in situ with calcium-free Hank's buffered salt solution (HBSS) at pH 7.4 and 37 °C, to remove blood from the tissue at a flow rate of 15 mL/min. Afterwards, the washing solution was replaced by collagenase solution (2.0 mg/mL) and the liver was perfused at a flow rate of 10 mL/min for 10 min at 37 °C. After perfusion, the liver was removed and gently dispersed. Liver cell suspension was incubated under continuous agitation at 37 °C for 15 min with collagenase solution (1.0 mg/mL) in 50 mL polypropylene tubes. Hereafter, all experiments were performed at 4 °C. The liver cell suspension was filtered through nylon gauze and placed in 50 mL of HBSS and centrifuged at 600 rpm for 5 min, two more times. A second centrifugation of the supernatant was performed to obtain a NPC pellet. The pellet was placed in 10 mL buffer and layered on top of a gradient (50%/25%) of Percoll Plus GE®. The cells at the interphase, which were mostly sinusoidal cells, were suspended in buffer and washed twice by centrifugation at 250 rpm for 5 min. The pellet was suspended with phosphate buffer solution (PBS) and the cells were counted in a Neubauer chamber to proceed with the staining for flow cytometry [29–31].

2.6. Flow cytometry analysis

NPC were separated from the digested livers through Percoll density gradient. The cells (1×10^6) were incubated 1 h with the next antibodies: Kupffer cells population was characterized as double positive marker CD11b/c (Millipore®), which reacts with the CR3 complement (C3bi) receptor found in most monocytes, granulocytes, and macrophages; CD163 (eBioscience®); HIS36 (tissue macrophage receptor ED-2), which is known as ED2-like antigen expressed by thioglycolate-elicited peritoneal cells and tissue macrophages, used as a marker for total rat tissue macrophages. After 1 h of incubation, cells were washed with PBS, fixed with 1% paraformaldehyde and flow cytometric analysis was performed by fluorescence-activated cell sorting (FACS, FACS-Calibur flow cytometer, Becton-Dickinson; performed at the Instituto de Investigaciones Biomédicas, UNAM).

Undyed-macrophages were gated by forward and scatter, and located in the Dot Plot as Kupffer control undyed cells; subsequently, cells with simple staining of each antibody were located in the

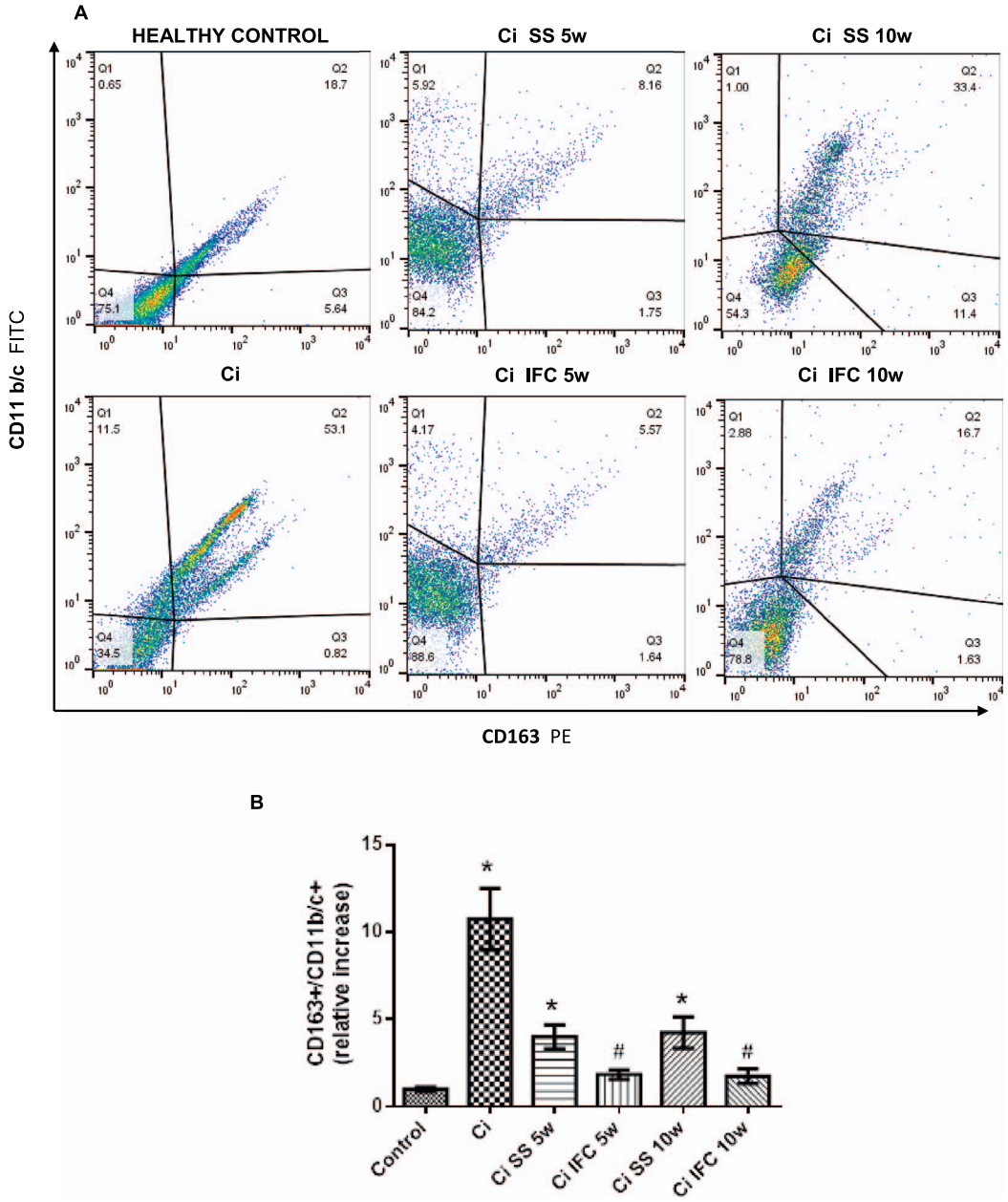

Fig. 4. Effect of IFC-305 on activated Kupffer cells ($CD163^+/CD11b/c^+$) of cirrhotic livers evaluated by flow cytometry ($n = 5$ rats per group), 10 weeks of administration with CCl_4 (Ci), 5 and 10 weeks with IFC-305 and SS, respectively. (A) Representative examples of dot plots from the different groups. (B) Quantification of ($CD163^+/CD11b/c^+$) percentage of gate Q2 are shown as times over respective control of Kupffer cells ± SEM $^*p \leq 0.5$ vs. control rat, $^{\#}p \leq 0.5$ IFC-305 vs. SS treatment.

corresponding quadrants of simple staining. The stained cells with both antibodies were compensated to observe the positive double cells in the upper right quadrant; from all comparisons of these double stained cells it was possible to compare all treatments with the control. Data were collected for 10,000 events, stored in a list mode, and subsequently analyzed using Flow Jo software®. Results of these experiments are expressed as the mean values ± standard error of the mean (SEM) of triplicate samples.

2.7. Nitric oxide assay

Nitric oxide (NO) was measured by the cadmium reduction method as nitrite product, using the Griess reagent [32]. Briefly, a volume of serum or tissue homogenate was mixed with 100 µL of 1% sulphanilamide, 0.1% naphthyl ethylenediamine dihydrochloride, and 2.5% H_3PO_4. Absorbance was detected at 540 nm in an ELISA microplate reader (VERSAmax®). Results of these experiments are expressed as the mean values ± SEM of triplicate samples.

2.8. Arginase activity

Arginase activity was measured in liver homogenates, as previously described [32]. Tissue and serum were treated and diluted with reaction buffer that contained (25 mM of Tris-HCl and 5 mM $MnCl_2$ at pH 7.4). The enzyme was then activated by heating for 10 min at 56 °C. Arginine hydrolysis came from incubating at a 1:1 v/v with 0.5 M arginine, pH 9.7, at 37 °C for 60 min. The reaction was stopped with 400 µL of acidic mixture (H_2SO_4, H_3PO_4 and H_2O, 1:3:7 v/v). The urea was measured at 540 nm after addition of 9% α-isonitrosopropiophenone (dissolved in absolute ethanol) and heating at 100 °C for 45 min. Absorbance was detected on an ELISA microplate reader (VERSAmax®). Results of these experiments are presented as the

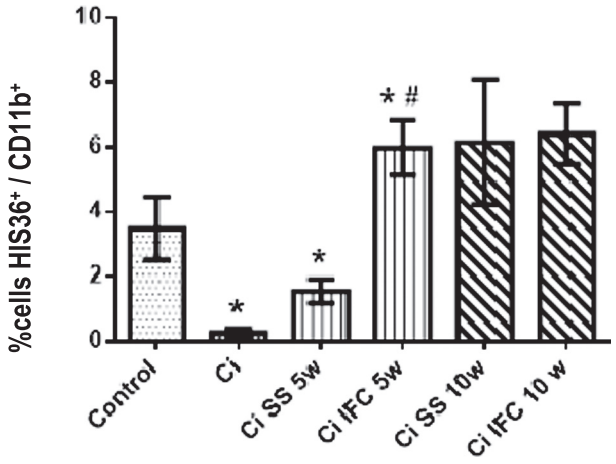

Fig. 5. Effect of IFC-305 treatment on liver non-parenchymal cells of cirrhotic rats, stained with CD11b and HIS36 and analyzed using flow cytometry ($n = 5$ rats per group), 10 weeks of CCl_4 administration (Ci), 5 and 10 weeks with IFC-305 and SS, respectively. Values are shown as mean percentage (%) of Kupffer cells ± SEM $^{*}p \leq 0.5$ CCl_4 vs. control rat; $^{\#}p \leq 0.5$ IFC-305 vs. SS treatment.

mean values ± SEM of triplicate samples.

2.9. Measurement of liver and serum cytokine levels

The blood samples obtained with EDTA (0.25 M, pH 8.0) were centrifuged at 2500 rpm for 10 min. The liver tissue samples were thawed and homogenized with RIPA buffer with protease inhibitors. Cytokines levels, IL-1β, IL-4, IL-12, IL-10, MCP-1, TNF-α, and INF-γ, were determined in samples with a commercially available kit (MILLIPLEX MAP Millipore®) according to manufacturer's instructions, and IL-6 was determined with ELISA (PEPROTEC®). Results of these experiments are expressed as the mean values ± SEM of triplicate samples.

3. Results

3.1. IFC-305 molecule reduces fibrosis and inflammatory cells infiltration leading to recovery of the hepatic function and structure

The aim of this study was to determine the grade of inflammation generated by CCl_4 and the participation of the immune response in the anti-inflammatory response, liver tissue repair, and cirrhosis reversion by IFC-305.

Inflammatory and fibrotic deposits were observed mainly in periportal regions, as shown in Fig. 1; animals with experimental cirrhosis after 10 weeks of CCl_4 treatment (Fig. 1B) exhibited remarkable changes in the liver architecture in slices stained with haematoxylin-eosin, showing a clear inflammatory infiltrate compared to healthy controls (HC) (Fig. 1A). Furthermore, IFC-305 treatment for 5 weeks after the development of experimental cirrhosis (Fig. 1C) induced a higher ordered distribution of the parenchyma in comparison to the animals treated with saline solution only (Fig. 1D). A similar effect occurred when the animals were treated for 10 weeks with IFC-305 (Fig. 1E) compared with the corresponding saline solution treatment (Fig. 1F). These results suggest that IFC-305 induces reversion of the disrupted hepatic architecture induced by experimental cirrhosis in rats.

Slices with Masson's trichrome staining (Fig. 2) show that the histological section of HC rats (Fig. 2A) does not have fibrosis and the parenchymal tissue is ordered (stained in red), compared to the CCl_4 treatment that affected the structure and showed a high deposition of collagen fibres (blue stained); whereas slices from IFC-305-treated rats for 5 and 10 weeks (Fig. 2E and F) revealed less deposition of collagen fibres (stained in blue) and a more homogeneous parenchymal tissue and a smaller amount of oxidized structures, as inferred from the less intense red colour compared to the SS-treated group (Fig. 2C and D). At the histological level, IFC-305 was able to restore the parenchyma's distribution in liver tissue and diminish recruiting of inflammatory cells.

To confirm that CCl_4 affects not only liver tissue but also liver function, as shown by results obtained in previous publications [23], alanine transaminase (ALT) activity was measured as a marker of liver function and it was observed that Ci SS 5w and Ci SS 10w had a significant increment of enzyme activity with respect to HC. The IFC-305 treatment for 5 and 10 weeks tended to decrease the ALT activity as compared to those treated with SS, confirming the IFC-305 effect on the recovery of liver function (Fig. 3).

ALT activity was determined as a marker of liver function. It was observed that Ci, Ci SS 5w and Ci SS 10w are significantly different respect to the control, and treatment with IFC-305 at 5 to 10 weeks tended to decrease ALT value, confirming the ability of IFC-305 to recover liver function.

3.2. The IFC-305 molecule regulates macrophages M1 ($CD11b/c^+$/$CD163^+$) infiltration to the cirrhotic liver

To analyze the macrophages in the liver and their phenotype by flow cytometry, CD11b/c, as mononuclear cell marker, and CD163, for the classic activation marker of Kuppfer cells [33,34], were used; both surface markers were considered indicative of inflammatory macrophage phenotype M1. Flow cytometry results of dot plots (Fig. 4A) are representative images of the total NPC acquired for each group and their respective controls, observing that the IFC-305 treatment reduced the M1 double positive cells ($CD11b/c^+/CD163^+$). On fig. 4B, the analysis reveals a significant 11-fold increase of Kupffer cells ($CD11b/c^+/CD163^+$), in the Ci group treated with CCl_4 administration with respect to the HC group, demonstrating the IFC-305 effect over KC.

These results agree with other reports that describe the capacity of CD163 cells to trigger inflammatory mediators, such as NO, TNF-α, IL-1β, and IL-6 [35]. These cells were significantly increased with chronic administration of CCl_4 and this increase is directly related to the liver damage observed [11]. After 5 and 10 weeks of SS administration, the percentage of $CD11b/c^+/CD163^+$ cells decreased significantly as compared to Ci, but this percentage is still higher than the one found in the livers of HC rats. By treating cirrhotic rats for 5 and 10 weeks with the IFC-305, the $CD11b/c^+/CD163^+$ cells decreased significantly reaching levels almost equal to those presented by the HC liver, which relates directly to the recovery of the liver structure and function. These observations on the modulating action exerted on $CD11b/c^+/CD163^+$ cells by IFC-305 (Fig. 4A–B) are substantial evidence of its effect on the immune response of the liver.

To study the anti-inflammatory macrophages phenotype M2, we analyzed the percentage of $HIS36^+/CD11b^+$ (Fig. 5). These double positive cells significantly decreased in the cirrhotic group with respect to the control rats. Something similar happened after induction of cirrhosis and in the animals treated for 5 weeks with SS, but not with the treatment for 10 weeks, where a significant increase in the amount of $HIS36^+/CD11b^+$ cells occurred. Furthermore, the IFC-305 induced a significant increase in $HIS36^+/CD11b^+$ KC population at 5 and 10 weeks of treatment, showing a direct effect on the number of KC anti-inflammatory phenotype M2.

These results indicate that the compound has effect on cirrhotic liver resident macrophages. It firstly decreases the percentage of inflammatory Kupffer cells respect to cirrhotic rats; on the other hand, it increases the anti-inflammatory macrophage phenotype, demonstrating an immunomodulatory effect of the compound on the NPC population in the liver, which has a direct effect on the recovery of cirrhosis.

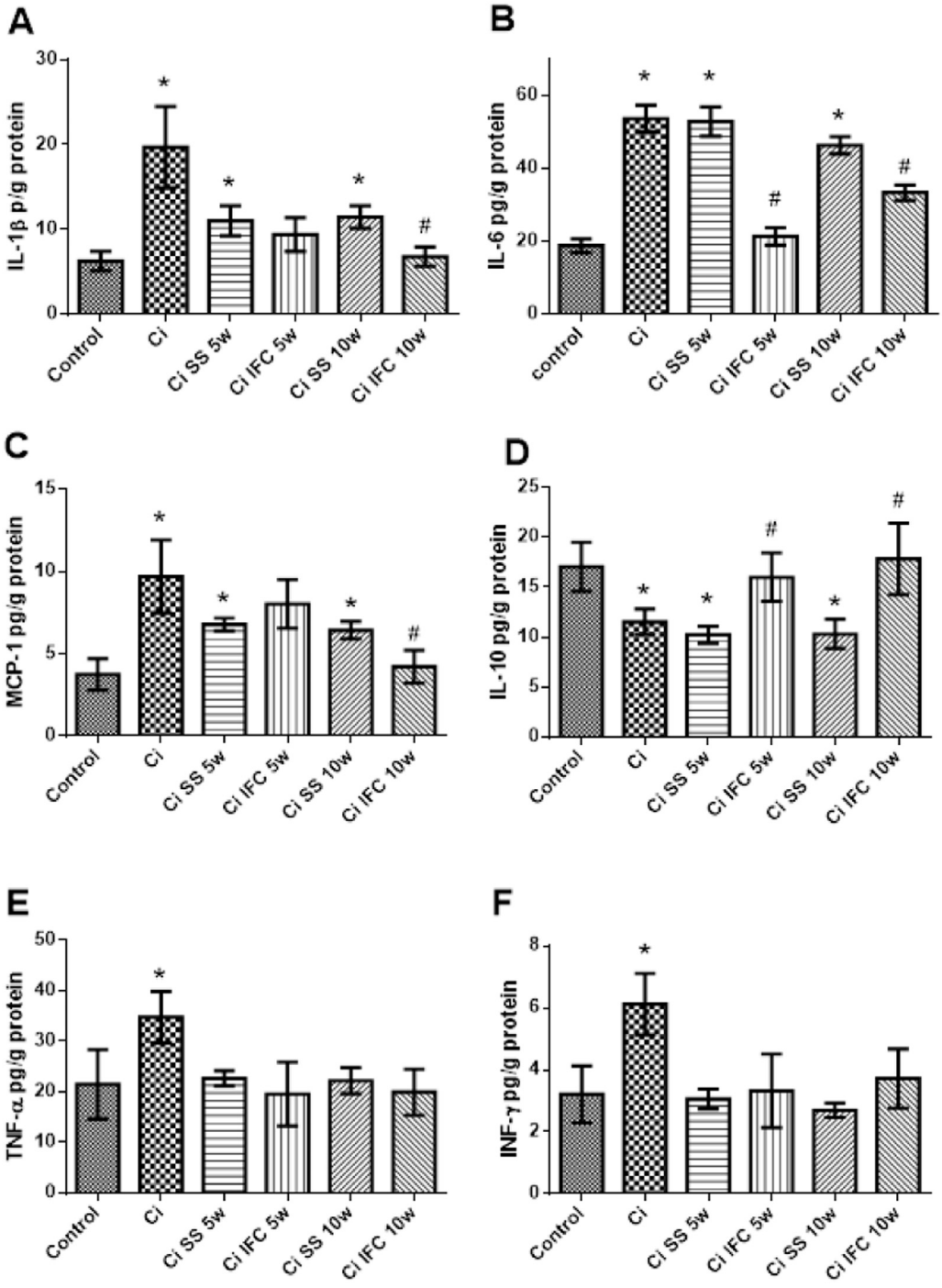

Fig. 6. Cytokines in liver homogenates of cirrhotic rats with IFC-305 treatment, 10 weeks of CCl_4 administration (Ci), 5 and 10 weeks with IFC-305 and SS, respectively. Levels of cytokines (A) IL-6 were measured by ELISA, (B) IL-1β, (C) MCP-1, (D) IL-10, (E) TNF-α, (F) INF-γ (pg/g protein) were measured using luminex-multiplex cytokine assay® ($n = 4$ rats per group), Values are shown as mean concentration ± SEM $^{*}p \leq 0.5$ vs. control rat; $^{\#}p \leq 0.5$ IFC-305 vs. SS treatment.

3.3. Local liver anti-inflammatory effects produced by IFC-305. Diminishing of IL-1β, IL-6, MCP-1 cytokines levels and raising of IL-10 contribute to the cirrhosis reversion mechanism

The pro-inflammatory cytokine, IL-1β, plays an essential role in the signaling of cirrhosis; recently, it was demonstrated that its action in vivo is directly related to the activation of HSCs for the establishment of hepatic fibrosis [36]. In the liver (Fig. 6A), IL-1β is significantly increased compared to the control after CCl_4 administration (Ci), as has been reported [37]. After 5 and 10 weeks, the levels of IL-1β decreased significantly respect to Ci in the groups treated with saline solution, but did not reach the values of the controls, including the group treated with IFC-305 for 5 weeks. The treatment with IFC-305 for 10 weeks recovered the levels of IL-1β to the HC group values, this shows that persistence of the damage had been defined by high levels of this inflammatory cytokine in the liver, as its decrease reached normal values only with the IFC-305 treatment lasting 10 weeks. This shows that its role in the recovery process of the cirrhotic liver is related to its modulatory activity of the inflammatory response.

The cytokine IL-6 is a major pro-fibrogenic cytokine that is produced continuously during the chronic progress of cirrhosis [38,39]. This cytokine is increased in the liver (Fig. 6B) with CCl_4 administration and is maintained at the same level at 5 and 10 weeks of SS administration. IFC-305 was capable of reducing its levels at 5 weeks, reaching HC group values; for the 10 weeks administration of IFC-305, the value of IL-6 is significantly lower as compared to the 10 weeks of SS administration. This shows that the IFC-305 is able to decrease this fibrogenic cytokine and that this activity may be one of the main action

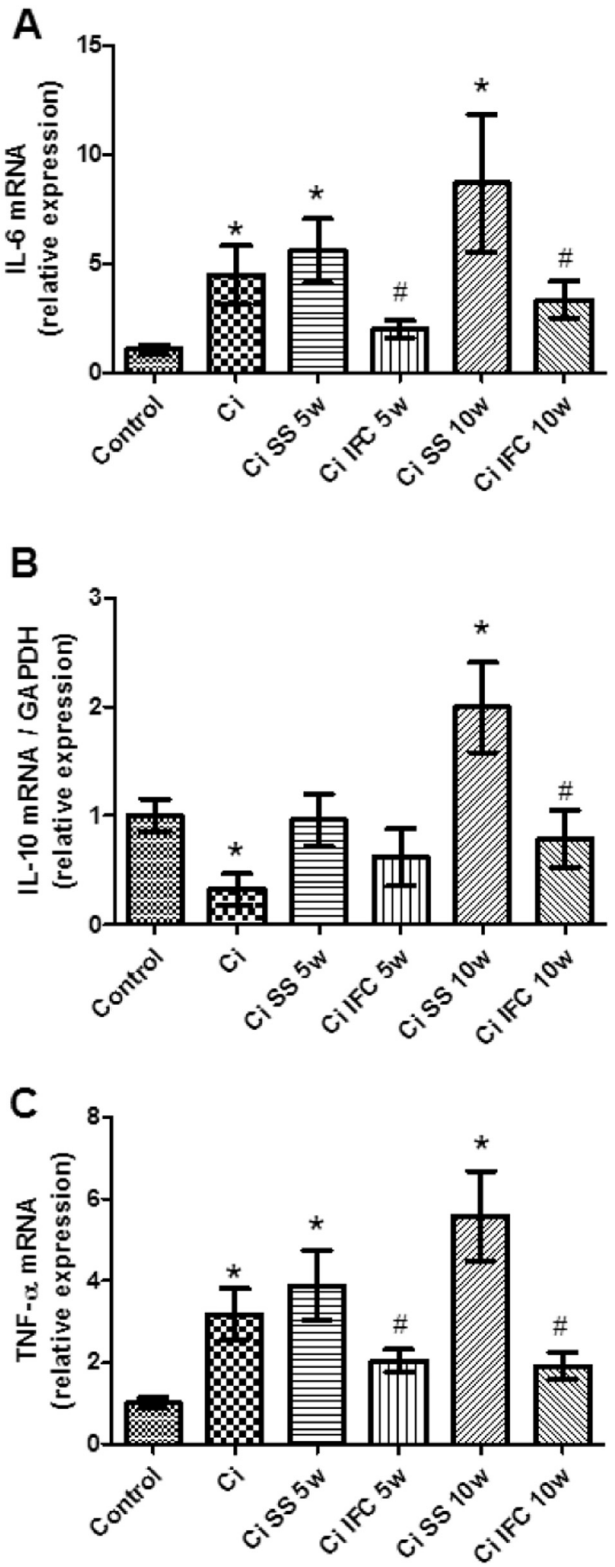

Fig. 7. Cytokines mRNA expression in liver homogenates of cirrhotic rats with IFC-305 and SS treatment; 10 weeks of CCl_4 administration (Ci), 5 and 10 weeks with SS and IFC-305, respectively. Levels of mRNA cytokines, (A) IL-6, (B) IL-10, and (C) TNF-α, were analyzed by real-time PCR (n = 5–7 rats per group), GAPDH was used as control gene, Values are shown as mean of relative expression ± SEM-fold increase compared to the control group $^{*}p \leq 0.5$ vs. control group; $^{\#}p \leq 0.5$ IFC-305 vs. SS treatment group.

mechanisms on liver tissue.

The MCP-1 cytokine, which has chemo-attractant activity and activates monocytes [40], remains at high levels during the 5 weeks with either SS or IFC-305 administration, but after 10 weeks with IFC treatment the levels of MCP-1 reached the control group values (Fig. 6C). Its increase in SS groups reflects the behaviour of macrophages in the liver, which presumably is regulated by this cytokine's effect on the liver damage caused by CCl_4 administration.

Studies by Huang Y. et al. [41], in which cirrhosis was induced with CCl_4, have established that the anti-inflammatory effects of the IL-10 cytokine, on hepatic regeneration occur 3 weeks after administration of CCl_4. These data agree with those obtained in the present work (Fig. 6D), in which the level of the IL-10 anti-inflammatory cytokine was lower in the liver homogenate of the Ci group compared to the control group. The IL-10 levels in the liver decreased at 5 weeks after SS and significantly increased with IFC-305 treatment, reaching the levels found in livers of control rats. The restoration of this cytokine reveals the anti-inflammatory effects of the compound, thus contributing to its hepatoprotective action on liver tissue.

We evaluated two other inflammatory cytokines: TNF-α and IFN-γ (Fig. 6E and F), as well as the cytokine IL-1β, all of them were significantly elevated by CCl_4 administration with respect to HC, as reported by Fu Y et al. [42]; however, these cytokines decreased to control levels with SS administration, without any apparent activity of the IFC-305 compound on their regulation.

3.4. IL-6, IL-10, and TNF-α mRNA cytokine levels are controlled by IFC-305 as part of its anti-inflammatory effect

It has been previously reported that the levels of cytokines, such as IL-6, IL-10, among others, are expressed differently, depending on the cirrhosis progress and they are directly related to the level of the mRNA products. For IL-6, a significant increase has been reported from week 6 of CCl_4 administration until 12 weeks of continuous administration [18]; these results are consistent with data obtained in our laboratory (Fig. 7A). Additionally, the mRNA level of IL-6 remained high after CCl_4 administration. Remarkably, treatment with the anti-cirrhotic compound IFC-305 reduced the transcription level of IL-6 mRNA, the main fibrogenic cytokine, as happened with the protein expression.

The liver expression of IL-10 mRNA cytokine decreased with 10 weeks CCl_4 administration, Ci group (Fig. 7B), as happened with the protein in liver homogenates (Fig. 6D), observing a relationship between the mRNA and the IL-10 protein amount at this time. Five weeks of treatment with either SS or IFC-305 did not show IL-10 mRNA differences between treatments. At 10 weeks of SS administration, an increase of IL-10 mRNA was observed, which significantly decreased with the IFC-305 compound. The level observed in the liver protein suggests that the increased protein of this anti-inflammatory cytokine could result from the mRNA increase that generates more protein or by avoiding its degradation in the liver.

The expression of TNF-α in the liver was significantly enhanced with CCl_4 administration relative to control (Fig. 7C); these levels were still high at 5 and 10 weeks of SS administration. At 5 and 10 weeks of IFC-305 treatment, TNF-α mRNA levels decreased contrary to the protein level detected in liver, suggesting an additional mechanism that involves deregulation of the degradation or TNF-α protein accumulation in the tissue.

3.5. Systemic inflammation is modulated by IFC-305 in cirrhosis reversion, controlling IL-1β and IL-10 serum levels

Cytokines levels were also measured in serum. For the IL-1β cytokine in serum we observed a similar behaviour to that of the liver (Fig. 8A), a significant decrease was observed at 5 weeks, and a reduction with IFC-305 treatment as compared to SS at 10 weeks, although it was not significant.

IL-6 (Fig. 8B) remained increased at 5 and 10 weeks compared to the control and the anti-cirrhotic compound IFC-305 significantly reduced IL-6 at 5 and 10 weeks of treatment.

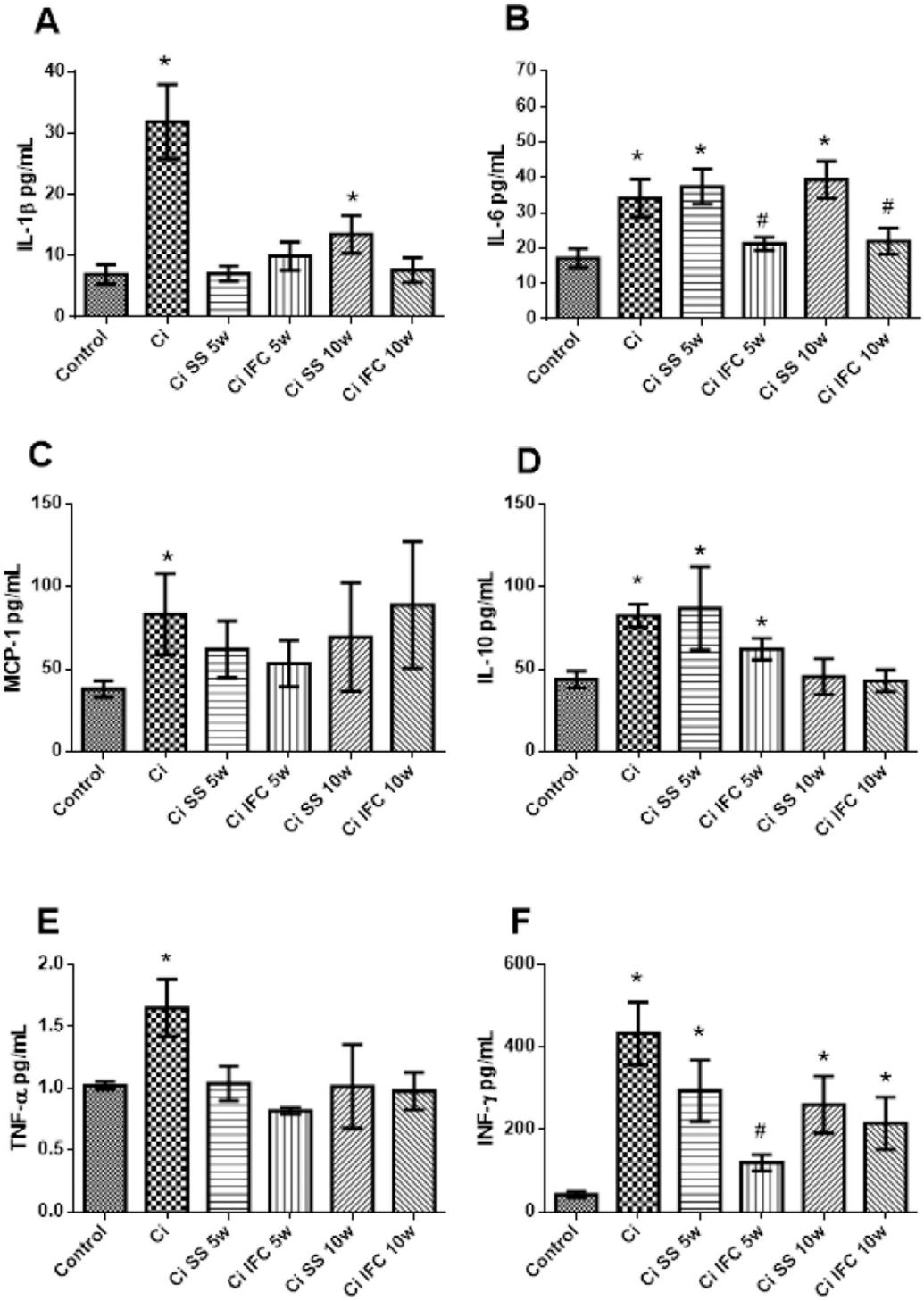

Fig. 8. Cytokines levels in serum of cirrhotic rats with IFC-305 treatment, 10 weeks of administration with CCl_4 (Ci), 5 and 10 weeks with SS and IFC-305, respectively. Levels of cytokines (A) IL-6 were measured by ELISA, (B) IL-1β, (C) MCP-1, (D) IL-10, (E) TNF-α, (F) INF-γ (pg/mL) were measured using Luminex® Multiplex cytokine assay® ($n = 4$ rats per group), Values are shown as mean concentration ± SEM $^{*}p \leq 0.5$ vs. control rat; $^{\#}p \leq 0.5$ IFC-305 vs. its own SS treatment.

The cytokine MCP-1, main monocyte chemo-attractant and stimulator of macrophages, in serum, increased in the Ci group respect to the HC, but it did not diminish with any treatment at 5 or 10 weeks (Fig. 8C).

The levels of the serum cytokine, IL-10 (Fig. 8D), were increased in the Ci group and went in parallel with the information published by Yu et al., 2004 [43], this cytokine's levels remained high at 5 weeks of treatment; at 10 weeks of either SS or IFC-305 it decreased reaching values similar to those of the HC. These results suggest that the immunomodulatory effect of this anti-inflammatory cytokine is mainly exerted on the liver (Fig. 6D).

TNF-α values in serum increased in the Ci group and decreased independently of IFC-305 treatments at 5 and 10 weeks (Fig. 8E), as observed in the liver (Fig. 6E), highlighting that this inflammatory cytokine in this model is induced by the chronic administration of CCl_4, and decreases due to its own anti-inflammatory mechanisms.

Levels of INF-γ were diminished at 5 weeks of IFC-305 administration respect to Ci SS 5w, showing that the systemic anti-inflammatory effect, at this time, is mainly regulated by this cytokine, otherwise no changes were observed at 10 weeks of treatment, suggesting that the hepatoprotective effect is mediated by other mechanisms (Fig. 8F).

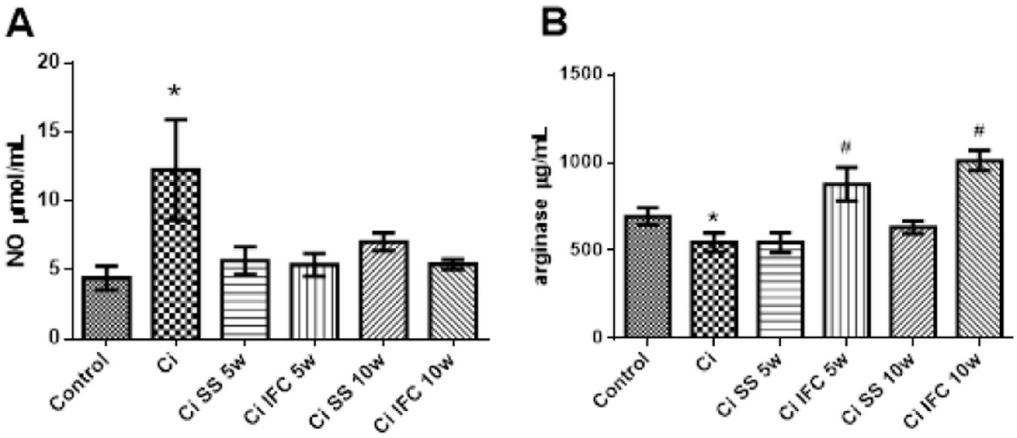

Fig. 9. (A) Nitric oxide by Griess method, and (B) levels of arginase were determined by ELISA in cirrhotic rats serum with IFC-305 treatment, 10 weeks of administration with CCl_4 (Ci), 5 and 10 weeks with SS and IFC-305, respectively. Levels of nitric oxide ($n = 3$ rats per group), values are shown as mean concentration (µmol/mL) ± SEM $^{*}p \leq 0.5$ vs. control rat; $^{\#}p \leq 0.5$ IFC-305 vs. its own SS treatment.

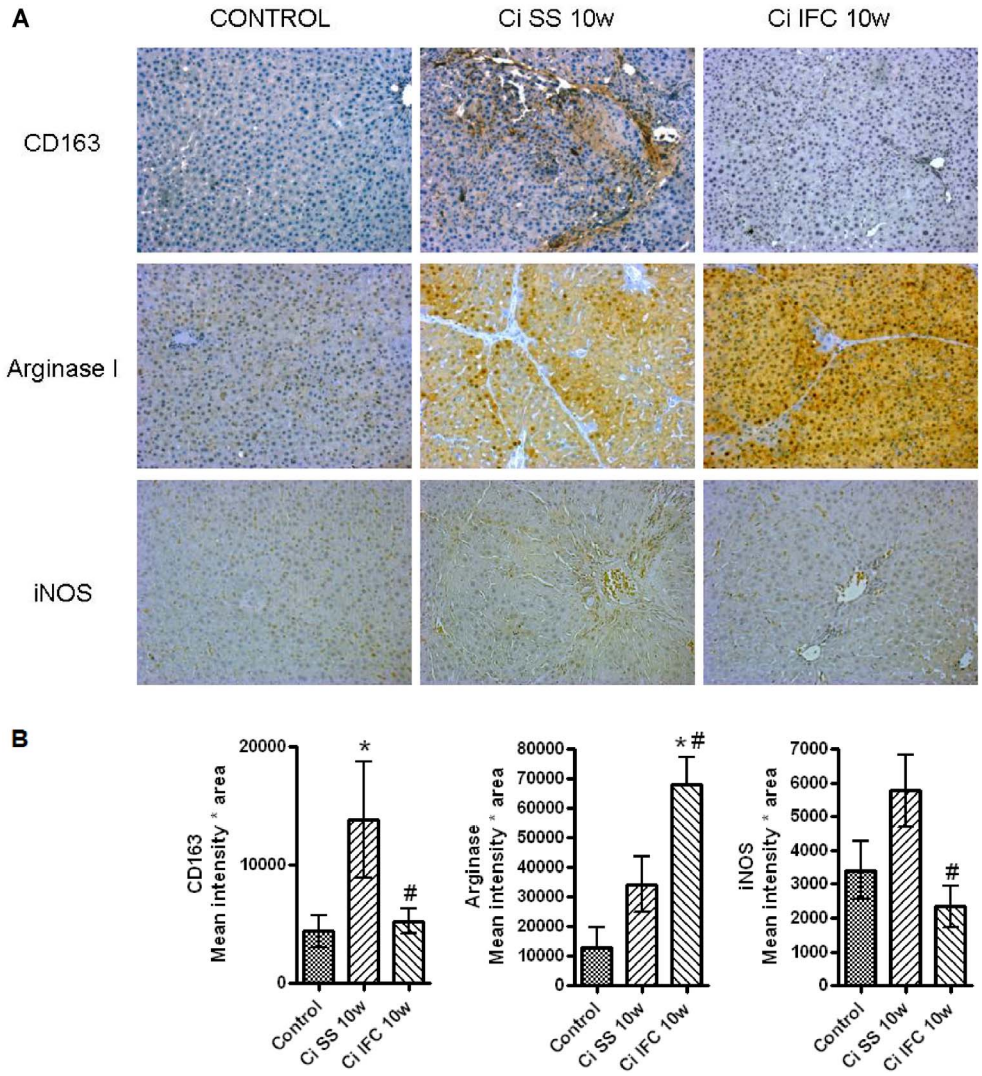

Fig. 10. (A) Effects of the IFC-305 on liver tissue samples immunostained with CD163, Arginase I and iNOS 40X. 1) Control, 2) Ci IFC 10w, 3) Ci SS 10w. (B) IMH quantification (Mean intensity* area) ± SEM $^{*}p \leq 0.5$ vs. control rat; $^{\#}p \leq 0.5$ IFC-305 vs. its own SS treatment.

3.6. The IFC-305 molecule mediates the equilibrium between iNOS and arginase activity

Nitric oxide is related to various mechanisms, control of liver blood flow, action on vascular tone, and there is a close relationship with the release of pro-inflammatory cytokines. Determination of NO in serum (Fig. 9A) shows that its value was increased in the Ci group, relative to the control group, and that its levels reached normal values at 5 and 10 weeks with IFC-305 and SS treatments. To compare the contrary effect to NO release, arginase activity was quantified. Arginase is an enzyme that competes with inducible-nitric oxide synthase (iNOS, main NO producer in inflammatory processes) for the arginine. The metabolism of arginine substrate by iNOS produces nitric oxide and by arginase activity produces urea. Measurements show that arginase increases in the serum of IFC-305-treated rats at 5 and 10 weeks respect to its corresponding SS. In previous results [23], we demonstrated that

urea cycle function is unregulated in cirrhosis stages and IFC-305 is capable of inducing it, this last action triggers the availability of arginine, which is used for arginase activity (Fig. 9B), reducing the NO production due to the competence with iNOS.

To evaluate this hypothesis experimentally, the iNOS protein levels were measured, through immunostaining (Fig. 10A) of the 10-week group samples, with comparative expression of CD163, we observed that arginase I and iNOS values increased in the SS 10w, whereas the IFC-305 treatment increased arginase I and reduced iNOS and CD163 levels.

4. Discussion

According to previous studies, the adenosine derivative IFC-305 compound reverses the cirrhosis induced in rats by CCl_4 [23]. Employing this model, the purpose of this work was to study the regulation exerted by IFC-305 over some immune response mechanisms involved in cirrhosis and its reversion. To confirm the activity of IFC-305, histological studies were performed (Figs. 1 and 2) and ALT levels (Fig. 3) were determined, observing that this compound is able to restore parenchyma distribution in liver tissue and reduce the recruiting of inflammatory cells.

Immune response cells and cytokines are involved in the development of CCl_4 liver damage, liver inflammation, progression of fibrosis, cirrhosis, and cancer. One type of these immune cells are the resident and circulating macrophages involved in the progression of liver damage, but also in tissue repair and inflammation resolution [2]. In the particular case of cirrhosis, an acute inflammation is unchained by the etiological source of liver damage [44]. This acute inflammation is transformed to a chronic one by a long-term (months or even years) exposure to the damaging agent. This mechanism is mediated by Kupffer cells and HSC activation [45] due to a cascade of signals, producing oxidant stress and cytokines [46]. Kupffer cells M1 proinflammatory subtype activation and HSC transformation to myofibroblasts generate ECM accumulation, parenchyma rearrangement, immunological and metabolic liver dysfunction. These markers have been described not only during the development of cirrhosis in animal models [47], but also as markers of high clinical relevance in cirrhotic patients [48]. Besides the inflammatory response associated with cirrhosis, at a metabolic level there are diverse mechanisms that also represent dysfunction in cirrhotic patients and in experimental models [35]. It is clear that the urea cycle is lost during liver damage [49]; arginase activity, as a consequence, brings a deregulation of arginine and nitric oxide metabolism [50].

In CCl_4-induced cirrhotic rats, adenosine could work as a cirrhosis reversion agent [23,51,52]. Cronstein and Haskó's research groups suggested an important role of adenosine and its receptors in the inflammatory regulation response [14,53,54]. In particular, it has been described that adenosine mediates macrophage plasticity to an M2 polarization (anti-inflammatory phenotype), which could contribute to tissue regeneration and repair. Adenosine increases the general liver arginase activity [55], suggesting that extracellular adenosine is an important pro-resolving mediator of inflammation [25,56], regulated by A2a and A2b receptors that induce arginase activity and the tissue inhibitor of matrix metalloproteinase-1 (TIMP-1), promoting tissue restitution.

Analysis of the IFC-305 adenosine derivate effect on CCl4 cirrhosis reversion model with flow cytometry (Figs. 4 and 5) showed that the compound IFC-305 modulates cirrhotic liver resident macrophages; firstly, by decreasing the percentage of inflammatory Kupffer cells (M1) with respect to those found in cirrhotic rats and, secondly, by increasing the anti-inflammatory macrophage phenotype (M2).

Besides the KC actions [52], the anti-cirrhotic effects of the IFC-305 compound [23] and the regulation of the A2a receptor and cell cycle [25] are essential for the immunological fibrosis reversion effects on the CCl_4-induced cirrhosis model in rats. Previous results suggested that the mechanism of the IFC-305 is mediated by the intracellular adenosine transport that induces liver regeneration through hepatocytes proliferation and recovery of the cell cycle during cirrhosis [25]. Relevantly, a microarray analysis of this CCl_4 and IFC-305 model revealed that 12.10% of the deregulated genes are involved in immunity and defense [23]. Some of them, such *Tgf-β, Csf1* (colony stimulating factor) also known as macrophage colony-stimulating factor (M-CSF), and *Cxcr4*, a chemokine that defines bone marrow monocytes heterogeneity and regulates their function in peripheral tissues. Meanwhile M-CSF and CXCR4 must be related to KC activation and recruiting balance, TGF-β is a cytokine directly related to the activation of HSC and the fibrogenic process progression to cirrhosis, which was decreased by IFC-305 treatment of the cirrhotic liver, as previously reported [23]. TGF-β and IL-6 are the two major fibrogenic cytokines and both are involved in cirrhosis development mediated by KC and HSC activation in the CCl_4 model [38]. Fig. 7 shows, at 8 to 10 weeks, a predominant inflammatory condition, caused by chronic administration of CCl_4, triggering cirrhosis. Serum and liver IL-6 protein and mRNA levels increased also in SS treatments at 5 and 10 weeks later.

As shown (Figs. 7 and 8), IFC-305 decreased production and reversed IL-6 level at baseline, suggesting that one of the main mechanisms of cirrhosis reversal occurs at the level of inhibiting fibrogenic cytokines, such as IL-6 and TGF–β [9,10].

Analysis of a group of characteristically inflammatory cytokines (IL-1β, INF-γ, MCP-1, and TNF-α) in the liver, which could be related also with inflammation (Fig. 6), revealed that their highest levels were reached with chronic administration of CCl_4; whereas, IL-10 decreased.

As shown by Tiegs et al. [57], IL-10 decreased by the effect of INF-γ, TNF-α, IL-6, and other cytokines, but it is relevant that, in this case, INF-γ recovered the liver protein baseline values at 5 and 10 weeks of SS administration, in an independent regulatory mechanism, possibly due to inherent mechanisms of liver repair, but it is not contributing to the full recovery of the cirrhotic liver by IFC-305.

Regarding TNF-α level, no changes were observed at serum and liver tissue proteins, but there was a clear difference in the TNF-α mRNA level. These results suggest that the protein could not be stable to be detected at the cirrhosis stage or that it was rapidly degrade, a mechanism that should be considered, because IFC-305 in fact decreased the expression of the TNF-α transcript, related to the recovery of the cirrhotic liver (Fig. 7).

Anti-inflammatory IL-10 is secreted by monocytes, macrophages, lymphocytes, and NK cells [58,59]; in the liver, IL-10 is mainly produced by Kupffer cells [59] and hepatocytes [60] and represents a master regulatory cytokine that inhibits the synthesis of other pro-inflammatory cytokines. The regulatory mechanisms are mediated by high levels of IL-10 to maintain a homeostatic immune response after some inflammatory processes. At shown (Fig. 6), IL-10 decreased in Ci and in the SS-treated groups for 5 and 10 weeks, but IFC-305 treatment recovered the HC levels, showing that the regulation of this IL-10 impacts the decreased IL-1β and MCP-1 pro-inflammatory cytokine levels (Fig. 6). All of them have been related with the activation M2 of macrophages, which can be the cellular source of the anti-inflammatory activity of IL-10.

As part of the mechanism some changes in NO and arginase functions were explored. It has been reported that NO synthesis is upregulated in hepatocytes and in non-parenchymal cells after CCl_4 intoxication, as a result of the oxidative stress, contributing to the liver injury [61]. In these experiments, NO levels and iNOS expression increased in the CCl_4 Ci group (Figs. 9 and 10), and IFC-305 treatment decreased iNOS protein level. As mentioned above, arginase biochemistry could also be linked to liver regeneration by IFC-305, It is known that during regeneration states, arginase expression contributes to restore the homeostatic cellular level of arginine, limiting the activity of both arginase and iNOS. Arginase competes with inducible nitric oxide synthase (iNOS) for its substrate and the balance between these two enzymes plays a crucial role in regulating immune responses and

macrophage activation. Reported data have identified a clear link between Kupffer cell activation and hepatic steatosis by demonstrating that selective depletion of Kupffer cells in Arg2 −/− mice resulted in a reversal of hepatic steatosis [62]. An imbalance in the iNOS/arginase ratio has been postulated as a crucial regulation of immune responses and macrophage activation. Arginase deficiency is related to the activation of Kupffer cells towards a classically M1 pro-inflammatory state [62]. As observed, IFC-305 treatment attenuated iNOS expression, (Fig. 10) and activated arginase enzymatic activity and protein expression (Figs. 9 and 10), Both phenomena are regulated by the reduction of general oxidative stress, contributing to liver regeneration, suppressing chronic inflammation and fibrosis [63].

In addition, the IFC-305 compound has the metabolic ability to increase the amount of arginase activity reducing NO production, reflecting an antioxidant and anti-inflammatory activity. In parallel, the lower levels of Kupffer cells (M1), related to the cytokines profile of IFC-305-treated animals, suggests that the anti-inflammatory effects could be driven by IL-10 and arginase activity, highlighting that the IFC-305 reverses cirrhosis by modulating the secretion of these molecules, but also by mediating the activation of cells directly related to the immune response, such as Kupffer cells.

As has been described by other authors, the modulation of the macrophage phenotypes, M1 and M2, could be regulated by adenosine receptors [14] and epigenetic changes have also been described, such as chromatin regulation in this phenotype transformation, mediated by DNA methylation [64]; mechanisms in which the IFC-305 could be also involved and should be studied further in more detail.

Results from the cytokines profiles, the reduction of M1 macrophages and iNOS and arginase activity, and M2 macrophages activation could be linked to the other results of TGF-β [23], HSC activation [24], and cell cycle control, revealing that the A2a receptor protein level increased with the CCl_4 and was reduced by IFC-305 [25]. These findings, in combination with the immunomodulatory IFC-305 effects, could be mediated through adenosine receptors expression, but also by adenosine metabolism through cell membrane transporters, and their respective signal transduction pathways, which should be studied further in the immune response cells.

In conclusion, the results of this study show that the anti-cirrhotic effect of the IFC-305 compound is mediated by an immunomodulatory response in the model of CCl_4-induced cirrhosis through regulation of inflammation, which opens the possibility to study its mechanism in the immune responses related to other chronic inflammatory processes, such as cancer, obesity, keratoconus, Alzheimer, among others.

Acknowledgments

We thank for the financial support of ICyTDF project 312/2009 and DGAPA-UNAM project IN225909 and fellowship from CONACyT (Rebeca Pérez Cabeza de Vaca CVU: 298432) and PAEP-UNAM [2009-2015]; Nora Gabriela Velasco Loyden, Susana Vidrio Gómez†, Lidia Martínez Pérez†, Carlos Alberto Guerrero Hernández, Rosario Villaseñor, Jesús Salgado, Unidad de Biología Molecular, IFC-UNAM; Eduardo García Zepeda†, Carlos Castellanos, Instituto de Biomédicas, UNAM; Alberto Aranda Fraustro, Benito Chávez Rentería. Departamento de Patología del Instituto Nacional de Cardiología “Ignacio Chávez”; Jorge Antonio García Álvarez, Facultad de Ciencias, UNAM.

References

[1] E.A. Tsochatzis, J. Bosch, A.K. Burroughs, Liver cirrhosis, Lancet 383 (2014) 1749–1761.
[2] F. Heymann, F. Tacke, Immunology in the liver - from homeostasis to disease, Nat. Rev. Gastroenterol. Hepatol. 13 (2016) 88–110.
[3] A. Pellicoro, P. Ramachandran, J.P. Iredale, J.A. Fallowfield, Liver fibrosis and repair: immune regulation of wound healing in a solid organ, Nat. Rev. Immunol. 14 (2014) 181–194.
[4] E. Vezali, A. Aghemo, M. Colombo, A review of the treatment of chronic hepatitis C virus infection in cirrhosis, Clin. Ther. 32 (2010) 2117–2138.
[5] A.M. Miller, N. Horiguchi, W.I. Jeong, S. Radaeva, B. Gao, Molecular mechanisms of alcoholic liver disease: innate immunity and cytokines, Alcohol. Clin. Exp. Res. 35 (2011) 787–793.
[6] R. Bataller, K. Rombouts, J. Altamirano, F. Marra, Fibrosis in alcoholic and non-alcoholic steatohepatitis, Best Pract. Res. Clin. Gastroenterol. 25 (2011) 231–244.
[7] Z.A. Andrade, Schistosomiasis and liver fibrosis, Parasite Immunol. 31 (2009) 656–663.
[8] A. Mallat, S. Lotersztajn, Cellular mechanisms of tissue fibrosis. 5. Novel insights into liver fibrosis, Am. J. Phys. Cell Phys. 305 (2013) C789–99.
[9] F. Tacke, T. Luedde, C. Trautwein, Inflammatory pathways in liver homeostasis and liver injury, Clin Rev Allergy Immunol 36 (2009) 4–12.
[10] V. Hernandez-Gea, S.L. Friedman, Pathogenesis of liver fibrosis, Annu. Rev. Pathol. 6 (2011) 425–456.
[11] P. Muriel, Y. Escobar, Kupffer cells are responsible for liver cirrhosis induced by carbon tetrachloride, J. Appl. Toxicol. 23 (2003) 103–108.
[12] M.J. Edwards, B.J. Keller, F.C. Kauffman, R.G. Thurman, The involvement of Kupffer cells in carbon tetrachloride toxicity, Toxicol. Appl. Pharmacol. 119 (1993) 275–279.
[13] J. Wan, M. Benkdane, F. Teixeira-Clerc, S. Bonnafous, A. Louvet, F. Lafdil, F. Pecker, A. Tran, P. Gual, A. Mallat, S. Lotersztajn, C. Pavoine, M2 Kupffer cells promote M1 Kupffer cell apoptosis: a protective mechanism against alcoholic and nonalcoholic fatty liver disease, Hepatology 59 (2014) 130–142.
[14] G. Hasko, B. Cronstein, Regulation of inflammation by adenosine, Front. Immunol. 4 (2013) 85.
[15] L.J. Dixon, M. Barnes, H. Tang, M.T. Pritchard, L.E. Nagy, Kupffer cells in the liver, Comp. Physiol. 3 (2013) 785–797.
[16] P. Ramachandran, J.P. Iredale, Macrophages: central regulators of hepatic fibrogenesis and fibrosis resolution, J. Hepatol. 56 (2012) 1417–1419.
[17] G. Kolios, V. Valatas, E. Kouroumalis, Role of Kupffer cells in the pathogenesis of liver disease, World J. Gastroenterol. 12 (2006) 7413–7420.
[18] S.W. Luckey, D.R. Petersen, Activation of Kupffer cells during the course of carbon tetrachloride-induced liver injury and fibrosis in rats, Exp. Mol. Pathol. 71 (2001) 226–240.
[19] G. Ramadori, T. Armbrust, Cytokines in the liver, Eur. J. Gastroenterol. Hepatol. 13 (2001) 777–784.
[20] A.M. Diehl, Cytokine regulation of liver injury and repair, Immunol. Rev. 174 (2000) 160–171.
[21] H.G. Hsieh, H.C. Huang, F.Y. Lee, C.Y. Chan, J.Y. Lee, S.D. Lee, Kinetics of cytokine expression in cirrhotic rats, J. Chin. Med. Assoc. 74 (2011) 385–393.
[22] L. Llorent, Y. Richaud-Patin, N. Alcocer-Castillejos, R. Ruiz-Soto, M.A. Mercado, H. Orozco, A. Gamboa-Dominguez, J. Alcocer-Varela, Cytokine gene expression in cirrhotic and non-cirrhotic human liver, J. Hepatol. 24 (1996) 555–563.
[23] J.I. Perez-Carreon, L. Martinez-Perez, M.L. Loredo, L. Yanez-Maldonado, G. Velasco-Loyden, S. Vidrio-Gomez, J. Ramirez-Salcedo, F. Hernandez-Luis, I. Velazquez-Martinez, J.A. Suarez-Cuenca, R. Hernandez-Munoz, V.C. de Sanchez, An adenosine derivative compound, IFC305, reverses fibrosis and alters gene expression in a pre-established CCl(4)-induced rat cirrhosis, Int. J. Biochem. Cell Biol. 42 (2010) 287–296.
[24] G. Velasco-Loyden, J.I. Perez-Carreon, J.F. Aguero, P.C. Romero, S. Vidrio-Gomez, L. Martinez-Perez, L. Yanez-Maldonado, R. Hernandez-Munoz, M. Macias-Silva, V.C. de Sanchez, Prevention of in vitro hepatic stellate cells activation by the adenosine derivative compound IFC305, Biochem. Pharmacol. 80 (2010) 1690–1699.
[25] V. Chagoya de Sanchez, L. Martinez-Perez, R. Hernandez-Munoz, G. Velasco-Loyden, Recovery of the cell cycle inhibition in CCl(4)-induced cirrhosis by the adenosine derivative IFC-305, Int. J. Hepatol. 2012 (2012) 212530.
[26] R. Hernandez-Munoz, M. Diaz-Munoz, V. Lopez, F. Lopez-Barrera, L. Yanez, S. Vidrio, A. Aranda-Fraustro, V. Chagoya de Sanchez, Balance between oxidative damage and proliferative potential in an experimental rat model of CCl4-induced cirrhosis: protective role of adenosine administration, Hepatology 26 (1997) 1100–1110.
[27] V. Chagoya-de-Sánchez, F. Hernández-Luis, M. Díaz-Muñoz, R. Hernández-Muñoz, Role of the energy state of liver cell in cirrhosis development and treatment, in: L.M. Miranda (Ed.), Liver Cirrhosis Causes, Diagnosis and Treatment, Nova Science Publishers, Inc, 2012, pp. 31–58.
[28] Chagoya de Sánchez V, Hernández-Muñoz R. 2004. México Patent No. MX220780.
[29] G. Kolios, V. Valatas, P. Manousou, C. Xidakis, G. Notas, E. Kouroumalis, Nitric oxide and MCP-1 regulation in LPS activated rat Kupffer cells, Mol. Cell. Biochem. 319 (2008) 91–98.
[30] D.P. Praaning-Van Dalen, D.L. Knook, Quantitative determination of in vivo endocytosis by rat liver Kupffer and endothelial cells facilitated by an improved cell isolation method, FEBS Lett. 141 (1982) 229–232.
[31] N.E. Reiner, Methods in molecular biology. Macrophages and dendritic cells. Methods and protocols. Preface, Methods Mol. Biol. 531 (2009) v–vi.
[32] I.M. Corraliza, G. Soler, K. Eichmann, M. Modolell, Arginase induction by suppressors of nitric oxide synthesis (IL-4, IL-10 and PGE2) in murine bone-marrow-derived macrophages, Biochem. Biophys. Res. Commun. 206 (1995) 667–673.
[33] H. Gronbaek, T.D. Sandahl, C. Mortensen, H. Vilstrup, H.J. Moller, S. Moller, Soluble CD163, a marker of Kupffer cell activation, is related to portal hypertension in patients with liver cirrhosis, Aliment. Pharmacol. Ther. 36 (2012) 173–180.
[34] L.K. Weaver, K.A. Hintz-Goldstein, P.A. Pioli, K. Wardwell, N. Qureshi, S.N. Vogel, P.M. Guyre, Pivotal advance: activation of cell surface toll-like receptors causes shedding of the hemoglobin scavenger receptor CD163, J. Leukoc. Biol. 80 (2006) 26–35.

[35] M.M. Polfliet, B.O. Fabriek, W.P. Daniels, C.D. Dijkstra, T.K. van den Berg, The rat macrophage scavenger receptor CD163: expression, regulation and role in inflammatory mediator production, Immunobiology 211 (2006) 419–425.
[36] R.G. Gieling, K. Wallace, Y.P. Han, Interleukin-1 participates in the progression from liver injury to fibrosis, Am. J. Physiol. Gastrointest. Liver Physiol. 296 (2009) G1324-31.
[37] G. D'Argenio, D.C. Amoruso, G. Mazzone, P. Vitaglione, A. Romano, M.T. Ribecco, M.R. D'Armiento, E. Mezza, F. Morisco, V. Fogliano, N. Caporaso, Garlic extract prevents CCl(4)-induced liver fibrosis in rats: the role of tissue transglutaminase, Dig. Liver Dis. 42 (2010) 571–577.
[38] S. O'Reilly, M. Ciechomska, R. Cant, T. Hugle, J.M. van Laar, Interleukin-6, its role in fibrosing conditions, Cytokine Growth Factor Rev. 23 (2012) 99–107.
[39] I. Choi, H.S. Kang, Y. Yang, K.H. Pyun, IL-6 induces hepatic inflammation and collagen synthesis in vivo, Clin. Exp. Immunol. 95 (1994) 530–535.
[40] J. Marsillach, J. Camps, N. Ferre, R. Beltran, A. Rull, B. Mackness, M. Mackness, J. Joven, Paraoxonase-1 is related to inflammation, fibrosis and PPAR delta in experimental liver disease, BMC Gastroenterol. 9 (2009) 3.
[41] Y.H. Huang, M.N. Shi, W.D. Zheng, L.J. Zhang, Z.X. Chen, X.Z. Wang, Therapeutic effect of interleukin-10 on CCl4-induced hepatic fibrosis in rats, World J. Gastroenterol. 12 (2006) 1386–1391.
[42] Y. Fu, S. Zheng, J. Lin, J. Ryerse, A. Chen, Curcumin protects the rat liver from CCl4-caused injury and fibrogenesis by attenuating oxidative stress and suppressing inflammation, Mol. Pharmacol. 73 (2008) 399–409.
[43] Yu XH, J.S. Zhu, Yu HF, L. Zhu, Immunomodulatory effect of oxymatrine on induced CCl4-hepatic fibrosis in rats, Chin. Med. J. 117 (2004) 1856–1858.
[44] W.C. Zhou, Q.B. Zhang, L. Qiao, Pathogenesis of liver cirrhosis, World J. Gastroenterol. 20 (2014) 7312–7324.
[45] E. Seki, R.F. Schwabe, Hepatic inflammation and fibrosis: functional links and key pathways, Hepatology 61 (2015) 1066–1079.
[46] F. Marra, F. Tacke, Roles for chemokines in liver disease, Gastroenterology 147 (2014) 577–594 (e1).
[47] L. Hammerich, F. Tacke, Interleukins in chronic liver disease: lessons learned from experimental mouse models, Clin. Exp. Gastroenterol. 7 (2014) 297–306.
[48] A. Albillos, M. Lario, M. Alvarez-Mon, Cirrhosis-associated immune dysfunction: distinctive features and clinical relevance, J. Hepatol. 61 (2014) 1385–1396.
[49] E. Mezey, Liver disease and protein needs, Annu. Rev. Nutr. 2 (1982) 21–50.
[50] F. Scaglia, N. Brunetti-Pierri, S. Kleppe, J. Marini, S. Carter, P. Garlick, F. Jahoor, W. O'Brien, B. Lee, Clinical consequences of urea cycle enzyme deficiencies and potential links to arginine and nitric oxide metabolism, J. Nutr. 134 (2004) (2775S-82S; discussion 96S-97S).
[51] B.P. Vaughn, S.C. Robson, M.S. Longhi, Purinergic signaling in liver disease, Dig. Dis. 32 (2014) 516–524.
[52] R. Hernandez-Munoz, M. Diaz-Munoz, J.A. Suarez-Cuenca, C. Trejo-Solis, V. Lopez, L. Sanchez-Sevilla, L. Yanez, V.C. De Sanchez, Adenosine reverses a preestablished CCl4-induced micronodular cirrhosis through enhancing collagenolytic activity and stimulating hepatocyte cell proliferation in rats, Hepatology 34 (2001) 677–687.
[53] G. Hasko, J. Linden, B. Cronstein, P. Pacher, Adenosine receptors: therapeutic aspects for inflammatory and immune diseases, Nat. Rev. Drug Discov. 7 (2008) 759–770.
[54] G. Hasko, B.N. Cronstein, Adenosine: an endogenous regulator of innate immunity, Trends Immunol. 25 (2004) 33–39.
[55] G. Hasko, P. Pacher, Regulation of macrophage function by adenosine, Arterioscler. Thromb. Vasc. Biol. 32 (2012) 865–869.
[56] B. Csoka, Z. Selmeczy, B. Koscso, Z.H. Nemeth, P. Pacher, P.J. Murray, D. Kepka-Lenhart, S.M. Morris Jr., W.C. Gause, S.J. Leibovich, G. Hasko, Adenosine promotes alternative macrophage activation via A2A and A2B receptors, FASEB J. 26 (2012) 376–386.
[57] G. Tiegs, A.W. Lohse, Immune tolerance: what is unique about the liver, J. Autoimmun. 34 (2010) 1–6.
[58] K.W. Moore, A. O'Garra, R. de Waal Malefyt, P. Vieira, T.R. Mosmann, Interleukin-10, Annu. Rev. Immunol. 11 (1993) 165–190.
[59] P. Knolle, J. Schlaak, A. Uhrig, P. Kempf, K.H. Meyer zum Buschenfelde, G. Gerken, Human Kupffer cells secrete IL-10 in response to lipopolysaccharide (LPS) challenge, J. Hepatol. 22 (1995) 226–229.
[60] Alfrey EJ, Most D, Wang X, Lee LK, Holm B, Krieger NR, Sibley RK, Huie P, Dafoe DC. 1995. Interferon-gamma and interleukin-10 messenger RNA are up-regulated after orthotopic liver transplantation in tolerant rats: evidence for cytokine-mediated immune dysregulation. Surgery 118: 399–404; (discussion -5).
[61] E.A. Minin, I.B. Buchwalow, M. Wellner, D. Palmes, H.U. Spiegel, J. Neumann, W. Boecker, H. Herbst, L-Arginine-NO-cGMP signaling following acute liver injury in the rat, Exp. Toxicol. Pathol. 57 (2005) 161–171.
[62] L.A. Navarro, A. Wree, D. Povero, M.P. Berk, A. Eguchi, S. Ghosh, B.G. Papouchado, S.C. Erzurum, A.E. Feldstein, Arginase 2 deficiency results in spontaneous steatohepatitis: a novel link between innate immune activation and hepatic de novo lipogenesis, J. Hepatol. 62 (2015) 412–420.
[63] T.A. Wynn, L. Barron, R.W. Thompson, S.K. Madala, M.S. Wilson, A.W. Cheever, T. Ramalingam, Quantitative assessment of macrophage functions in repair and fibrosis, Curr. Protoc. Immunol. (2011) (Chapter 14: Unit14 22).
[64] O. Takeuch, S. Akira, Epigenetic control of macrophage polarization, Eur. J. Immunol. 41 (2011) 2490–2493.

1521-0103/361/2/292–302$25.00
THE JOURNAL OF PHARMACOLOGY AND EXPERIMENTAL THERAPEUTICS

https://doi.org/10.1124/jpet.116.239301
J Pharmacol Exp Ther 361:292–302, May 2017

Functional, Metabolic, and Dynamic Mitochondrial Changes in the Rat Cirrhosis-Hepatocellular Carcinoma Model and the Protective Effect of IFC-305[S]

Enrique Chávez, María Guadalupe Lozano-Rosas, Mariana Domínguez-López, Gabriela Velasco-Loyden, Jesús Rafael Rodríguez-Aguilera, Concepción José-Nuñez, Marietta Tuena de Gómez-Puyou, and Victoria Chagoya de Sánchez

Departamento de Biología Celular y Desarrollo, Instituto de Fisiología Celular, Universidad Nacional Autónoma de México, Mexico City, Mexico (E.C., M.G.L.-R., M.D.-L., G.V.-L., J.R.R.-A., V.C.S.); and Departamento de Bioquímica y Biología Estructural, Instituto de Fisiología Celular, Universidad Nacional Autónoma de México, Mexico City, Mexico (C.J.-N., M.T.G.-P.)

Received November 29, 2016; accepted February 13, 2017

ABSTRACT

Background: Mitochondrion is an important metabolic and energetic organelle that regulates several cellular processes. Mitochondrial dysfunction has been related to liver diseases including hepatocellular carcinoma. As a result, the energetic demand is not properly supplied and mitochondrial morphologic changes have been observed, resulting in an altered metabolism. We previously demonstrated the chemopreventive effect of the hepatoprotector IFC-305. *Aim:* In this work we aimed to evaluate the functional, metabolic, and dynamic mitochondrial alterations in the sequential model of cirrhosis-hepatocellular carcinoma induced by diethylnitrosamine in rats and the possible beneficial effect of IFC-305. *Methods:* Experimental groups of rats were formed to induce cirrhosis-hepatocellular carcinoma and to assess the IFC-305 effect during cancer development and progression through the evaluation of functional, metabolic, and dynamic mitochondrial parameters. *Results:* In this experimental model, dysfunctional mitochondria were observed and suspension of the diethylnitrosamine treatment was not enough to restore them. Administration of IFC-305 maintained and restored the mitochondrial function and regulated parameters implicated in metabolism as well as the mitochondrial dynamics modified by diethylnitrosamine intoxication. *Conclusion:* This study supports IFC-305 as a potential hepatocellular carcinoma treatment or as an adjuvant in chemotherapy.

Introduction

Mitochondria are organelles responsible for most of the energetic metabolism in eukaryotic cells. As an integral part of ATP production, through the oxidative phosphorylation, the tricarboxylic acid cycle (TCA) donates electrons to the electron transport chain (ETC), which consists of five complexes (I-V), where complex I is the electron entry site for NADH and generates NAD^+ and complex V is in charge of ATP synthesis. The ability of mitochondria to regulate the energetic, redox state and metabolism of the cells could result in the production of epigenetic intermediates, point them out as a major therapeutic target because mitochondrial dysfunction is involved in several diseases including cancer (Mughal et al., 2012; Boland et al., 2013).

Studies have revealed several metabolic alterations in liver diseases including modifications in energy supply (Hernandez-Munoz et al., 1991; Hernandez-Munoz and Chagoya de Sanchez, 1994). Otto Warburg suggests that mitochondria from tumor cells supply the energetic demand, through the glycolytic flux because of the lack of oxygen or due to genetic-epigenetic alterations that affect the oxidative metabolism (Wallace and Fan, 2010). In fact, metabolic alterations and some anti-apoptotic proteins such as BCL-K_L reduce the acetyl-CoA level (Ac-CoA) (Yi et al., 2011); this intermediate also plays an important role as a signal transducer and gene expression modulator (Pietrocola et al., 2015). Oxidative stress diminishes oxidative metabolism flux, which includes TCA enzymes such as isocitrate dehydrogenase (IDH) and malate dehydrogenase (MDH). Indeed, studies have identified mutations in IDH producing an oncometabolite in different tumor types (Dang et al., 2016). A good indicator of the mitochondrial redox state is the NAD^+/NADH ratio and if it is correctly regulated, an efficient ETC activity is possible; as shown in the limitation of breast tumor growth (Santidrian et al., 2013). Previously our research group demonstrated the ability of adenosine to maintain the energetic and redox state of the cell (Hernandez-Munoz et al., 1978; Hernandez-Munoz et al., 1987). In addition to the metabolic role of NAD^+, it participates in the

This work was supported by Consejo Nacional de Ciencia y Tecnología (240315). E. Chávez was a fellow of DGAPA-UNAM Mexico.
https://doi.org/10.1124/jpet.116.239301.
[S] This article has supplemental material available at jpet.aspetjournals.org.

ABBREVIATIONS: Ac-CoA, acetyl-CoA; CP, cancer progression; DEN, diethylnitrosamine; DRP1, dynamin-related protein 1; ETC, electron transport chain; HCC, hepatocellular carcinoma; IDH, isocitrate dehydrogenase; MDH, malate dehydrogenase; MFN-2, mitofusin-2; PARP-1, poly(ADP-ribose) polymerase 1; PGC-1α, peroxisome proliferator-activated receptor γ-coactivator 1α; Sirt-1, -3, sirtuin-1, -3; TCA, tricarboxylic acid cycle.

activity of multiple enzymes. According to this, Sirtuin-1 (Sirt-1), a NAD^+-dependent protein and a member of class III histone deacetylase, targets several transcription factors including the peroxisome proliferator-activated receptor γ-coactivator 1α (PGC-1α). The latter coactivates major transcription factors involved in mitochondrial and nuclear gene expression directing the complex program of mitochondrial biogenesis (Finley and Haigis, 2009). However, Sirt-1 and PGC-1α have been found overexpressed in hepatocellular carcinoma (HCC) and are related to defective mitochondrial accumulation (Chen et al., 2012; Boland et al., 2013). Another NAD^+-dependent protein is PARP-1[Poly(ADP-ribose)[polymerase-1 whose activity modulates transcription and DNA repair; nevertheless, overexpression and increased activity of PARP-1 have been found in HCC and has been considered as a cancer hallmark (Hanahan and Weinberg, 2011).

Mitochondria are not static organelles; their dynamism depends, at least in part, on the fission and fusion phenomena that determine their shape. Mitochondrial fusion requires polarized mitochondrial membrane and the activity of proteins such as mitofusin 1 and 2 (MFN 1, 2); this process promotes cristae integrity and oxidative phosphorylation. Mitochondrial fission is induced by different kinds of stress and requires proteins such as the dynamin-related protein 1 (DRP1); membrane depolarization is observed during fission and, if the membrane potential is not recovered, mitochondria are targeted to autophagy (Boland et al., 2013). Altered mitochondrial fission and fusion have been observed in tumor cells mainly due to increased DRP1 and decreased MFN-2 expression (Rehman et al., 2012).

Our research group demonstrated the hepatoprotective effects of IFC-305, an adenosine-derived compound (Perez-Carreon et al., 2010; Velasco-Loyden et al., 2010; Chagoya de Sanchez et al., 2012; Velasco-Loyden, 2016); this compound has been evaluated in a diethylnitrosamine (DEN)-induced sequential rat model of cirrhosis-HCC, where it inhibited preneoplastic lesion development in comparison with DEN-treated groups. The chemopreventive effect was associated with the reduction of the expression of collagen, thymidylate synthase, the tumor marker γ-glutamyl transferase, the hepatocyte growth factor, and the induction of the cell cycle inhibitor p27 expression (Velasco-Loyden, 2016).

In this work we evaluated the mitochondrial alterations in the sequential cirrhosis-hepatocellular carcinoma model, previously described by Schiffer et al. (2005), and the possible beneficial effects of the hepatoprotector IFC-305 during HCC development and progression on mitochondrial function, metabolism, and dynamics. We measured the mitochondrial function through the respiratory quotient, membrane potential, complex I activity, and ATP synthesis. The activity of the malate-aspartate shuttle, IDH and MDH, and the level of Ac-CoA and lactate were determined as metabolic parameters. Dynamic mitochondrial proteins were determined to evaluate the morphology and biogenesis; electron microscopy was also used for morphology studies.

Materials and Methods

Chemicals

IFC-305 is the aspartate salt of adenosine prepared with adenosine free base (MP Biomedicals, LLC, Illkirch, France) and L-aspartic acid (MP Biomedicals, Inc., Eschwege, Germany) is as described (Patent No. MX220780; MX 207422; US 8,507,459 B2) (Chagoya de Sanchez, 2002,2004, 2013). Diethylnitrosamine, sucrose, EDTA, Trisma base, KCl, $MgCl_2$, glutamate, ADP, rhodamine 123, HEPES, EGTA, cyclosporine A, valinomycin, succinate, 2,6-dicholorindophenol, ATP, NAD. NADH, acetophenone were purchased from the Sigma Chemical Company (St. Louis, MO).

Animal Treatment and Experimental Groups

Male Wistar rats (weighing 200 g) were obtained from and housed at the Animal Facility of the National Autonomous University of Mexico (UNAM), and all procedures were conducted according to our institutional guidelines for the care and use of laboratory animals. Groups of rats (n = 6, each group) were divided in two different schemes: hepatocellular carcinoma (HCC) and cancer progression (CP). These were treated as follows: 1) the HCC groups were injected with DEN (Sigma-Aldrich) at 50 mg/kg body weight i.p., once a week and saline solution or IFC-305 at 50 mg/kg body weight i.p., 3 times weekly (HCC+IFC-305) for 16 weeks plus 2-weeks wash out; 2) the CP groups were administered DEN at 50 mg/kg body weight i.p., once a week for 16 weeks and then received saline solution or IFC-305 (CP+IFC-305) at 50 mg/kg body weight i.p., 3 times weekly during 6 weeks (Table 1). To euthanize animals, a lethal dose of sodium pentobarbital was used and the liver was removed.

Mitochondrial Function

Mitochondria Isolation and Oxygen Uptake. Liver samples were homogenized (1:10 w/v) in a medium containing 250 mM sucrose, 1 mM EDTA, 10 mM Trizma base, and 0.1% BSA, pH 7.3. The tissue homogenate was centrifuged at 755 g for 5 minutes to remove nuclei and plasma membrane fragments. The supernatant was filtered through organza fabric and centrifuged at 8400 g for 10 minutes to obtain the mitochondrial pellet. Mitochondria were resuspended in 250 mM sucrose, 1 mM EDTA, 10 mM Trizma base, pH 7.3. Mitochondrial respiration was recorded polarographically with a Clark-type oxygen electrode in 3 ml of a medium containing 250 mM sucrose, 10 mM KCl, 5 mM $MgCl_2$, 10 mM potassium phosphate, 10 mM Trizma base; 10 mM glutamate, and malate were used as substrates for site I. Mitochondrial state 3 was initiated by adding 226 μM ADP (final concentration).

Mitochondrial Membrane Potential. The mitochondrial membrane potential was determined according to Baracca et al. (2003). Briefly, a calibration curve was done by plotting rhodamine 123 fluorescence against the membrane potential calculated through the Nerst equation. To determine the mitochondrial membrane potential, 0.15 mg of mitochondria were added to a medium containing 250 mM sucrose, 10 mM HEPES, 100 μM EGTA, 2 mM $MgCl_2$, 4 mM KH_2PO_4, pH 7.4, and 10 mM sucrose and 2.5 U hexokinase. Then, 1 μg/ml of 33 nM cyclosporine A and 0.1 mM ADP were added. Finally, rhodamine (50 nM) fluorescence was measured in the presence of 20 mM succinate.

TABLE 1

Experimental groups design

Five experimental groups (n = 6) were formed as indicated. Control group received saline solution only. DEN was administered at 50 mg/kg i.p. once a week for 16 weeks and the IFC-305 compound at 50 mg/kg i.p. 3 times weekly during the DEN intoxication (HCC+IFC-305) or 6 weeks after DEN administration was stopped (CP+IFC-305).

Group	Treatment	
	16 weeks	6 weeks
Control	Saline solution	
HCC	DEN + saline solution	
HCC+IFC-305	DEN + IFC-305	
CP	DEN	Saline solution
CP+IFC-305	DEN	IFC-305

HCC, hepatocellular carcinoma; CP, cancer progression.

Complex I Activity. The 2,6-dichloroindophenol reduction was used to determine complex I activity in mitochondria isolated from the liver. Briefly, 1 mg of mitochondrial protein was added to a medium containing 0.25 M sucrose, 1 mM EDTA, 0.1% BSA, 100 μM KCN, 10 mM glutamate as substrate, and 152 μM rotenone. The absorbance was followed at 600 nm and the activity was calculated using the 2,6-dichloroindophenol extinction coefficient (21 $mM^{-1} \cdot cm^{-1}$).

Determination of the ATPase Activity and the Content of the $\alpha\beta$ Subunits. Rat liver mitochondria (2 mg) were resuspended in different volumes of the mitochondrial preparation medium. Mitochondria were centrifuged at 180 *g* for 10 minutes at 4°C. The mitochondrial pellet was resuspended in 50 μl of 250 mM sucrose and 1 mM $MgCl_2$ and centrifuged in an air-driven ultracentrifuge at 5249 *g* at 10 psi. The pellet was resuspended in a medium containing 50 mM NaCl, 50 mM imidazole, 1 mM EDTA, 2 mM aminocaproic acid, and 0.66 mg digitonin/mg mitochondria. The suspension was centrifuged at 9860 *g* at 22 psi for 5 minutes. The supernatant was used for protein determination with first dimension blue native PAGE and second dimension SDS-PAGE.

First dimension: Protein extracted with digitonin (100 μg) was mixed with 10 μl buffer 3× (1.5 M 6-aminocaproic acid, 150 mM Bis-Tris) plus serva blue G (7 μg/μl stock serva blue G in 1.5 M 6-aminocaproic acid) (final concentration, 30 ng serva blue/1 μg protein). The sample was charged to a 3.5–11% linear blue native-PAGE and electrophoresis was performed at 70 V for 2 hour and 100 V for 8 hour at 4°C. ATPase activity was identified by incubating the first dimension gel in a preincubation-solution containing 35 mM Tris, 250 mM glycine, pH 8.3. Then, the gel was stirred and incubated for 1 and 2 hours at 37°C with 5 mM ATP, 5 mM $MgCl_2$, 0.15% (w/v) lead acetate, and 150 mM glycine, pH 8.3. After that, the gel was stirred and incubated at room temperature for 24 hours. Monomer and dimer bands with dark background were scanned at 1, 2, and 24 hours. Monomer bands were read at 1, 2, and 24 hours, with Image J software.

Metabolic Evaluation

Malate-Aspartate Shuttle. The activity of the malate-aspartate shuttle was determined using the assay previously described for Scholz et al. (1998). Briefly, 50 μl of mitochondrial suspension was mixed with 2 ml of 300 mM mannitol, 10 mM potassium phosphate, 10 mM Tris, 10 mM KCl, 5 mM $MgCl_2$, 2 mM aspartate, 2 mM ADP, and 0.14 mM NADH, pH 7.4. Then, 2 IU/ml of AST was added, and basal oxidation of NADH was followed at 340 nm at 37°C for 4 minutes. The shuttle activity was started with the addition of 4 mM malate and 4 mM glutamate. Oxidation of NADH was followed at 340 nm for 4 minutes at 37°C.

Isocitrate Dehydrogenase and Malate Dehydrogenase Activities. Isocitrate dehydrogenase and malate dehydrogenase activities were estimated using the following commercial kits: Isocitrate Dehydrogenase Activity Assay Kit (Cat. MAK062) and Malate Dehydrogenase Assay Kit (Cat. MAK196) following the instructions provided by the manufacturer (Sigma-Aldrich).

Acetyl-CoA, 3-Hydroxybutyric Acid, and Lactate Determination. The levels of acetyl-CoA, 3-hydroxybutyric acid, acetoacetate, and lactate were determined using the following commercial kits: Acetyl-Coenzyme A Assay Kit (Cat. MAK039, Sigma-Aldrich); Acetoacetate Colorimetric Assay Kit (Cat. MAK199); EnzyChrom Ketone Body Assay Kit (Cat. EKBD-100, Hayward, CA). The instructions provided by the manufacturers were followed.

PARP-1 Enzymatic Activity. The PARP-1 enzymatic activity was determined according to (Putt and Hergenrother, 2004). Briefly, liver samples were homogenized in a buffer containing 50 mM Tris, 2 mM $MgCl_2$, pH 8.0, and protease inhibitors cocktail (Roche Diagnosis, Indianapolis, IN). The tissue homogenate was centrifuged at 13,700 *g* for 10 minutes at 4°C. The supernatant was separated and protein content was determined by the Bradford method (Bio-Rad, Laboratories, Inc., Hercules, CA). A DNA sample was obtained from the control liver tissue through a modified salt extraction method described by Lopera-Barrero (2008). Briefly, 20 μl of 100 μM NAD^+ was added to the plate; subsequently, 30 μg of protein and DNA (at 12.5 μg/ml), previously activated with UV irradiation, was added. The plate was incubated at room temperature for 20 minutes, and the amount of NAD^+ present was determined by the addition of 10 μl of 2 M KOH and 10 μl of 20% acetophenone (in ethanol). The plate was incubated at 4°C for 10 minutes. Finally, 45 μl of 88% formic acid was added, and the plate was incubated at 110°C for 5 minutes. The plate was allowed to cool and was read at 378 nm. To quantitate the NAD^+, absorbances were interpolated in a NAD^+ calibration curve, previously performed.

Evaluation of Mitochondrial Dynamics

Nuclear Protein Extraction. The isolation of intact and stable nuclei consisted in an iso-osmotic lysis procedure, as reported by Dyer and Herzog (1995). With this lysis procedure, the nuclear envelope remained intact even during further manipulations of washing, freezing, and ultracentrifugation and provided nuclear protein extract. Briefly, 0.8 g of liver tissue was homogenized in 1.6 ml of buffer containing 0.25 M sucrose, 0.05 M Tris-Cl, 0.005 M KCl_2. The homogenate was filtered and supplemented with 3 ml of a 2.3 M sucrose solution to increase the homogenate's density. Then, the sucrose gradient was created by adding 1.5 ml of a 2.3 M sucrose solution to the bottom of the tube containing the homogenate. The nucleus was isolated by centrifugation for 30 minutes at 4°C at 255,000 *g*. After the isolation, nuclear lysis was performed by incubating and stirring with a hypotonic and hypertonic solution. The nuclear extract protein was determined by the Bradford method and used for the corresponding assays.

Total Protein Extraction. Liver samples were homogenized with RIPA buffer (100 mg of tissue/ml buffer) containing protease and phosphatase inhibitors (Roche Diagnostics Corp.). The homogenate was centrifuged at 16,000 *g* for 10 minutes at 4°C; the supernatant was used as total liver homogenate.

Western Blot Assays. Mitochondrial, nuclear, and total protein extracts were used as corresponding. Volumes equivalent to 50 μg of protein were electrophoresed on 12% polyacrylamide gel (20% polyacrylamide for histones); separated proteins were transferred onto PVDF (Immobilon P). Next, blots were blocked with 5% skim milk and 0.05% Tween-20 for 30 minutes at room temperature and independently incubated overnight at 4°C with selective antibodies (dilution 1:1000) against PGC-1α (MAB 1032 from Chemicon Int. Inc.), Sirt-1, Drp-1, Sirt-3, Mfn-2 (Santa Cruz Biotechnology sc-15404, sc-32898, sc-99143, sc-50331, respectively), H4ac, Hsp60, H3, H4 (06-946, MAB 3844, 06-755, 04-858 from Millipore, respectively), as appropriate. On the following day, the membranes were washed and then exposed to a secondary peroxidase-labeled antibody at dilution 1:10,000 (Jackson ImmunoResearch) in the blocking solution for 1 hour at room temperature. Blots were washed and protein was developed using the ECL detection system. Densitometric analyses of bands were performed with Quantity One software (Bio-Rad Laboratories).

Electron Microscopy. Liver samples for electron microscopy were fixed with glutaraldehyde (6%) and stained with osmium tetroxide (1% phosphate-buffered saline solution) according to Mascorro and Yates (1976).

Statistical Analysis

Data are expressed as mean values ± standard error of the mean (S.E.M.). Comparisons were carried out by analysis of variance, followed by Tukey's test, as appropriate, using Graph Pad Prism 5.0 (Graph Pad Software Inc, La Jolla, CA) for Windows. Differences were considered statistically significant when $P < 0.05$.

Results

IFC-305 Treatment was Helpful to Maintain and Recover the Mitochondrial Function that Was Altered in the Sequential Model of Cirrhosis-Hepatocellular Carcinoma

Mitochondria are the main source of energy and act as an energy modulator to orchestrate their physiologic responses.

For this reason, we decided to evaluate some parameters that reflect the mitochondrial function in the sequential model of cirrhosis-hepatocellular carcinoma in the rat and the effect of IFC-305 treatment. The respiratory quotient was obtained from the state 3 and state 4 ratio. Chronic treatment with DEN induced an increased oxidation of glutamate in the absence of ADP (state 4) and a lower response for ADP (state 3), resulting in a diminished respiratory quotient in the HCC and CP groups compared with the control group (Table 2); the IFC-305 treatment prevented and reversed this alteration as seen in the HCC+IFC-305 and CP+IFC-305 groups. Moreover, there was a significant decrease in ATP synthesis in the groups treated with DEN that was not restored even in the CP group, and the beneficial effect of IFC-305 to prevent and reverse the damage caused by DEN can be observed in the groups receiving IFC-305 (Table 2). A significant reduction in the complex I activity in the HCC and CP groups and the beneficial effect of the IFC-305 treatment can be observed, which was able to reverse this alteration to the normal level. Mitochondrial membrane potential provides an electrochemical gradient required to regulate mitochondrial function. We found important changes in this parameter; depolarization was observed in mitochondria from HCC and CP groups and a tendency to prevent and reverse this effect can be observed in groups HCC+IFC-305 and CP+IFC-305 (Table 2). These results clearly indicate the functional impairment due to the chronic intoxication with DEN and the improvement effect exerted by the IFC-305 treatment.

Considering the aforementioned findings, we evaluated complex V, which is in charge of ATP synthesis as an integral part of the mitochondrial function. Through the isolation of the F1F0 complex from samples at week 22, we evaluated its ability to hydrolyze ATP. In this approach, we observed that the ATPase activity remained lower in the CP group than in the control one. The IFC-305 treatment restored this activity, which became higher at 24 hours (Fig. 1A). Moreover, the absence of the dimeric form of the F1F0 complex was seen the DEN intoxication even after it had been suspended (CP group); the control group and that treated with the IFC-305 compound (CP+IFC-305 group) revealed the presence of the dimeric form of the F1F0 complex (Fig. 1B). Similar results were obtained through the monomer quantification in blue gel and Coomassie staining and, the $\alpha\beta$ subunits content (Supplemental Fig. 1). These findings support the IFC-305 beneficial effect on the $\alpha\beta$ ATPase subunits.

The mitochondrial function was damaged in the HCC and CP groups; as it was previously mentioned, the suspension of DEN did not recovered mitochondrial functionality but the IFC-305 compound helps to maintain mitochondrial integrity.

The Hepatoprotector Improved the Metabolic Alterations Generated by Dysfunctional Mitochondria

Because of the previously described results, we decided to evaluate parameters that could show metabolic modifications. As seen in Fig. 2A, the malate-aspartate shuttle activity is decreased in preparations obtained from HCC and CP groups; IFC-305 treatment inhibited the effect of DEN and restored the activity of this shuttle, HCC+IFC-305, and CP+IFC-305, respectively. From the levels of 3-hydroxybutyric acid and acetoacetate we calculated the NAD^+/NADH ratio. Mitochondria isolated from the HCC and CP groups had a marked diminution of the mitochondrial NAD^+/NADH ratio. In the HCC+IFC-305 group, small protection against this damage was observed and the CP+IFC-305 group reached the control value (Fig. 2B).

Because we observed alterations in the NAD^+ mitochondrial regulation, we decided to evaluate the activity of two NAD^+-dependent enzymes that participate in the TCA cycle, IDH and MDH. As shown in Fig. 2C, IDH activity did not change significantly when it was compared with the control group. Nevertheless, treatment with IFC-305 increased the activity of this enzyme compared with the HCC and CP groups, respectively. MDH activity of HCC and HCC+IFC-305 is similar to the control group. In the CP group, the MDH activity decreased but the treatment with IFC-305 tended to reverse this effect (Fig. 2D). The impaired IDH and MDH activity suggest an altered TCA function due to DEN administration; IFC-305 treatment improved mainly the IDH activity, possibly related to the increase in redox potential.

As mentioned in the introduction, the experimental model used in this study is associated with HCC and because we found modifications in mitochondrial function, we determined the level of hepatic lactate as an indicator of metabolic adaptation. Chronic administration of DEN increased the amount of lactate in the liver and it did not return to the control level 6 weeks after the DEN treatment had been suspended as shown in the HCC and CP groups (Fig. 3). IFC-305 treatment significantly decreased the level of lactate

TABLE 2
Effect of DEN and IFC-305 administration on the mitochondrial respiratory quotient, ATP synthesis, complex I activity, and membrane potential
Values are expressed as mean ± S.E.

Group	State III/State IV	ATP Synthesis	Complex I Activity	ΔΨm
		nmol/min/mg	*μmol/min/mg*	*ml*
Control	8.39 ± 0.62	171.60 ± 22.01	20.16 ± 3.03	163.77 ± 11.17
HCC	2.98 ± 1.43[a]	100.27 ± 24.61[a]	1.62 ± 0.76[a]	58.29 ± 7.19[a]
HCC+IFC-305	6.13 ± 0.55[b]	173.46 ± 17.27[b]	4.46 ± 1.30[a]	100.55 ± 13.94[a,b]
CP	4.86 ± 1.39[a]	125.02 ± 4.18[a]	6.96 ± 2.17[a]	67.01 ± 8.46[a]
CP+IFC-305	7.80 ± 1.25	174.94 ± 12.81[c]	17.57 ± 3.70[c]	102.19 ± 15.65[a,c]

[a]Significant difference versus control.
[b]Significant difference versus HCC.
[c]Significant difference versus CP.
Isolated mitochondria were used to determine the respiratory quotient with glutamate plus malate as substrates ($P<0.05$), complex I activity ($P<0.01$), and mitochondrial membrane potential (ΔΨm) ($P<0.001$). ATP synthesis was calculated from data obtained in the oximetry analysis in the presence of glutamate plus malate (state III X ADP/O) (*$P<0.05$).

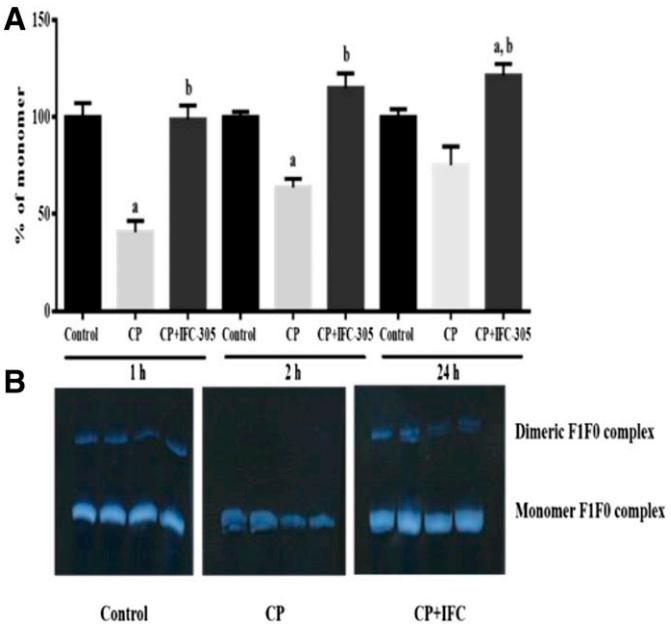

Fig. 1. Changes in ATPase activity and determination of the monomeric and dimeric F1F0 ATPase complex in mitochondria. (A) Monomer F1F0-ATPase activity quantification at 1, 2, and 24 hours in digitonin mitochondrial extracts in gradient blue native gels. Optical density data were normalized taking the control group as 100%. Each bar represents the mean of each group ± SE. [a]Statistical significant difference versus control; [b]significant difference versus CP group ($P < 0.05$). (B) Monomer and dimer F1F0-ATPase at 24 hour sin digitonin mitochondrial extracts from four different samples in blue native gels.

(HCC+IFC-305), suggesting metabolic adaptation in response to recuperated mitochondrial function.

Another intermediate that depends on mitochondrial energetics is Ac-CoA. DEN administration had no significant effect on the amount of Ac-CoA in both groups, HCC and CP, but IFC-305 treatment significantly increased Ac-CoA levels in the HCC+IFC-305 and CP+IFC-305 groups (Fig. 4A) consequently to the recuperation of mitochondrial function. Previous studies showed the ability of IFC-305 to modulate some epigenetic modifications including histone acetylation (Rodríguez-Aguilera, 2015). Thanks to this and considering the increased level of this metabolic intermediate, we decided to determine this posttranslational modification because Ac-CoA is a required cofactor for histone acetyltransferases. Diminution of H4ac was observed in the HCC and CP groups; an increment trend was observed in HCC+IFC-305 and CP+IFC-305 groups (Fig. 4, B and C), suggesting Ac-CoA availability. This result could be important because it might establish a link between mitochondrial function and epigenetic control of gene expression.

In addition to the mitochondrial alterations, other enzyme activities could be modified, dependent, at least in part, on mitochondrial integrity and functionality. Specifically, PARP-1 overexpression and overactivation have been shown to be a characteristic of HCC. The PARP-1 activity is dependent on NAD^+ and Fig. 5 shows a significant increment in the CP group, whereas the CP+IFC-305 group revealed the IFC-305 ability to decrease it. The overactivation of PARP-1 obtained in the DEN-intoxicated groups could be the cause of the diminution of NAD^+ level previously described in Fig. 2B.

IFC-305 Treatment Was Beneficial to Avoid and Recover the Altered Mitochondrial Dynamics Induced by DEN Intoxication

The interplay between the mitochondrion and the nucleus is relevant in the regulation of the mitochondrial response to stress, and PGC-1α and Sirt-1 are proteins involved in this process. The nuclear amount of both proteins was increased by DEN treatment, even in the CP group, as compared with the control (Fig. 6, A and B). The pharmacological treatment with IFC-305, HCC+IFC-305, and CP+IFC-305, reduced the nuclear content of both Sirt-1 and PGC-1α, suggesting a diminution of mitochondrial stress induced by DEN.

Mitochondrial networks determined by fission and fusion cycle were evaluated through the mitochondrial level of proteins regulating this process. Figure 7 shows the effect of DEN and IFC-305 on mitochondrial localization of three important proteins related to fission and fusion processes. DRP-1, required for mitochondrial fission by pinching them off into smaller fragmented mitochondria, was induced in HCC and CP groups and it was prevented by the hepatoprotector (Fig. 7A). Figure 7B shows no significant differences in the MFN-2 content between the experimental groups; however, a tendency to increase this protein in the HCC group can be seen. However, when the DRP-1/MFN-2 ratio was determined (Fig. 7C), an important increase in this parameter was observed in the CP group, reflecting a predominance of the fission process. This alteration was not observed in the CP+IFC-305 group.

Until now important mitochondrial alterations were observed, but we wanted to know if there were changes in mitochondrial content of Sirt-3, a NAD^+-dependent deacetylase, that would be indicative of a correlation between mitochondrial dynamics and metabolic function. The progressive damage, observed when the toxicant was suspended, induced a decreased in mitochondrial Sirt-3 (CP group) and the administration of IFC-305 increased Sirt-3 level (CP+IFC-305), even more than the control group (Fig. 7D). The upregulation in the presence of the compound could be related to the improved mitochondrial redox state. Mitochondrial modifications prompted us to obtain liver slices to observe the changes in mitochondrial morphology through electron microscopy. The control group depicted mainly elongated mitochondria. Circular shaped mitochondria were abundant in HCC and CP groups (Fig. 8, B and D), and elongated shape was observed in groups receiving IFC-305 (Fig. 8, C and E). As well as the altered mitochondrial shape, altered cristae were observed in the HCC and CP groups, whereas the IFC-305-treated groups maintained and recovered cristae. An important observation is the large amount of ribosomes observed in the slices from the HCC+IFC-305 and CP+IFC-305 groups marked with black arrows (Supplemental Fig. 2). To appreciate better these effects, in Supplemental Fig. 2 mitochondria can be observed in a more amplified size than in Fig. 8. This observation supports the previous observations in mitochondrial functions, metabolism. and dynamic.

Discussion

This study shows that mitochondria from the liver of DEN-treated rats underwent alterations resulting in decreased respiratory quotient, which means that uncoupled mitochondria

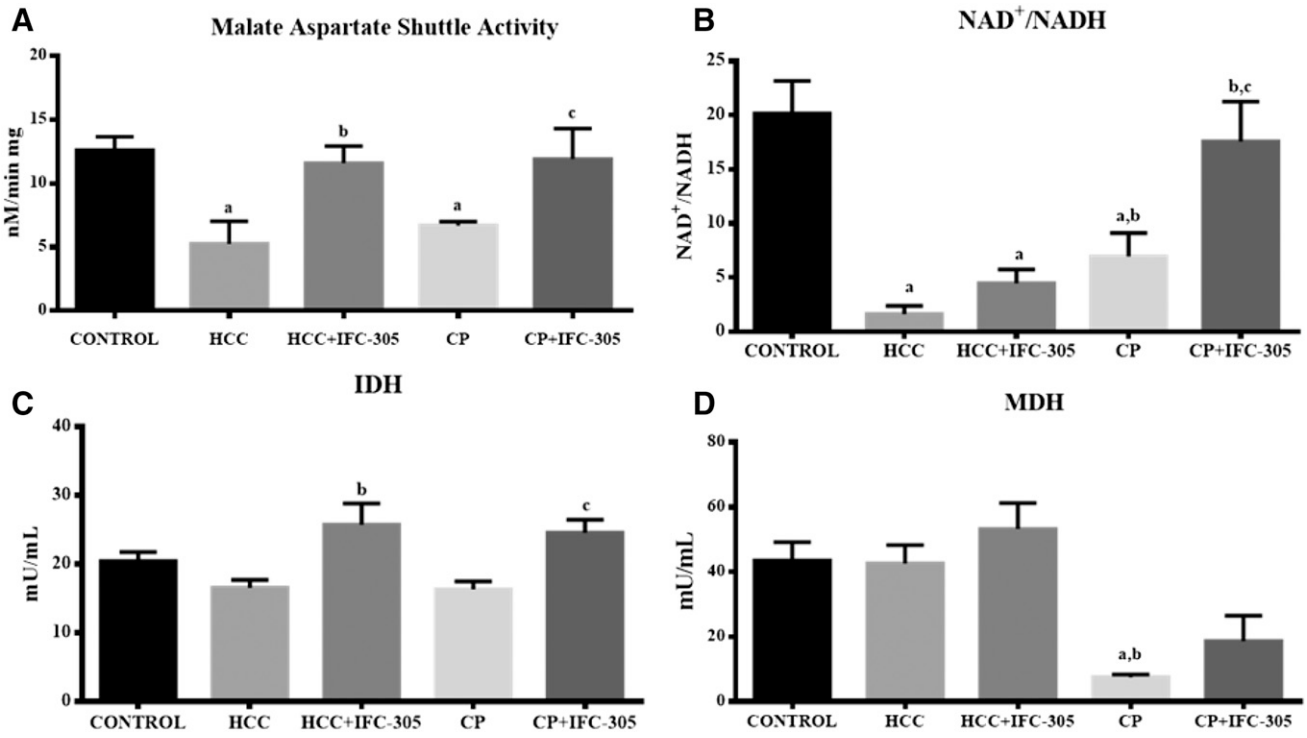

Fig. 2. Metabolic mitochondrial parameters evaluated in isolated mitochondria from the liver in the different experimental groups. (A) Malate-aspartate shuttle ($P<0.05$); (B) NAD+/NADH ratio ($P<0.001$); (C) isocitrate dehydrogenase activity ($P<0.01$); and (D) malate dehydrogenase activity ($P<0.001$). Values are expressed as means ± S.E. [a]Significant difference versus Control; [b]statistical significant difference versus HCC group; [c]significant difference versus CP group.

with low phosphorylating capacity depicted lower ATP synthesis probably because of the altered ΔΨm and complex I activity (Table 2). Moreover, ATP synthase plays an essential role in energy metabolism, because it is in charge of ATP synthesis; the dimeric and oligomeric ATP synthase complexes increase its stability and promote the formation of mitochondrial cristae (Garcia-Trejo and Morales-Rios, 2008; Couoh-Cardel et al., 2010). The regeneration of the dimeric form of the F1F0 ATPase is an indicator that the mitochondrial energetic machinery and morphology of cristae were recovered with IFC-305 administration to the CP. Previously, the sensitivity of the ETC complex I to the hepatotoxic action of CCl_4, ethanol, and DEN had been demonstrated; for DEN, this effect is attributed to the inhibition of NAD^+-linked respiration at this site (Cederbaum et al., 1974; Schilling and Reitz, 1980; Boitier et al., 1995). The malate-aspartate shuttle maintains appropriate NADH equivalents, and its intermediates are coupled to the TCA cycle. The activity of this system was diminished in mitochondria from DEN-treated rats (Fig. 2A), supporting the idea that mitochondria are the site for DEN-induced damaged. As mentioned before, the treatment with IFC-305 improved the mitochondrial redox state damaged by DEN. Mitochondrial function requires an optimal NAD^+/NADH ratio to be efficient. The ability to restore the mitochondrial NAD^+/NADH ratio was achieved when the IFC-305 was given after the discontinuation of DEN injection (CP+IFC-305 group) (Fig. 2B). The maintenance of this ratio allowed the correct supply of electrons to complex I and the proper function of mitochondria. The decreased ΔΨm in the DEN-treated rats was expected because of the alterations previously mentioned. These results demonstrate relevant mitochondrial function impairment induced by DEN and the beneficial effects of IFC-305 to maintain the mitochondrial function, supporting the previously mentioned adenosine findings, which is the base molecule of the compound studied in this work (Hernandez-Munoz et al., 1978).

IDH and MDH are mitochondrial TCA enzymes coupled to the mitochondrial redox potential. IDH activity is decreased in patients with chronic liver injury after several years of alcohol abuse and in rats treated with DEN (Suresh et al., 2013; Popov et al., 2014). We found a tendency to diminish the IDH activity by DEN intoxication and its increased activity by

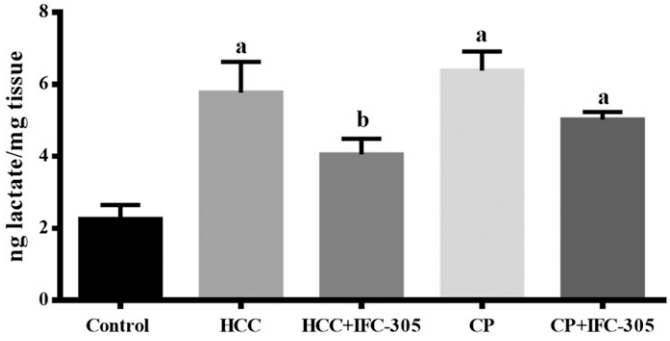

Fig. 3. Lactate level in the liver as an indicator of metabolic adaptation. Perchloric extracts from the liver were obtained to determine the levels of lactate. Values are expressed as means ± S.E. [a]Significant difference versus Control; [b]statistical significant difference versus HCC group; [c]significant difference versus CP group ($P<0.01$).

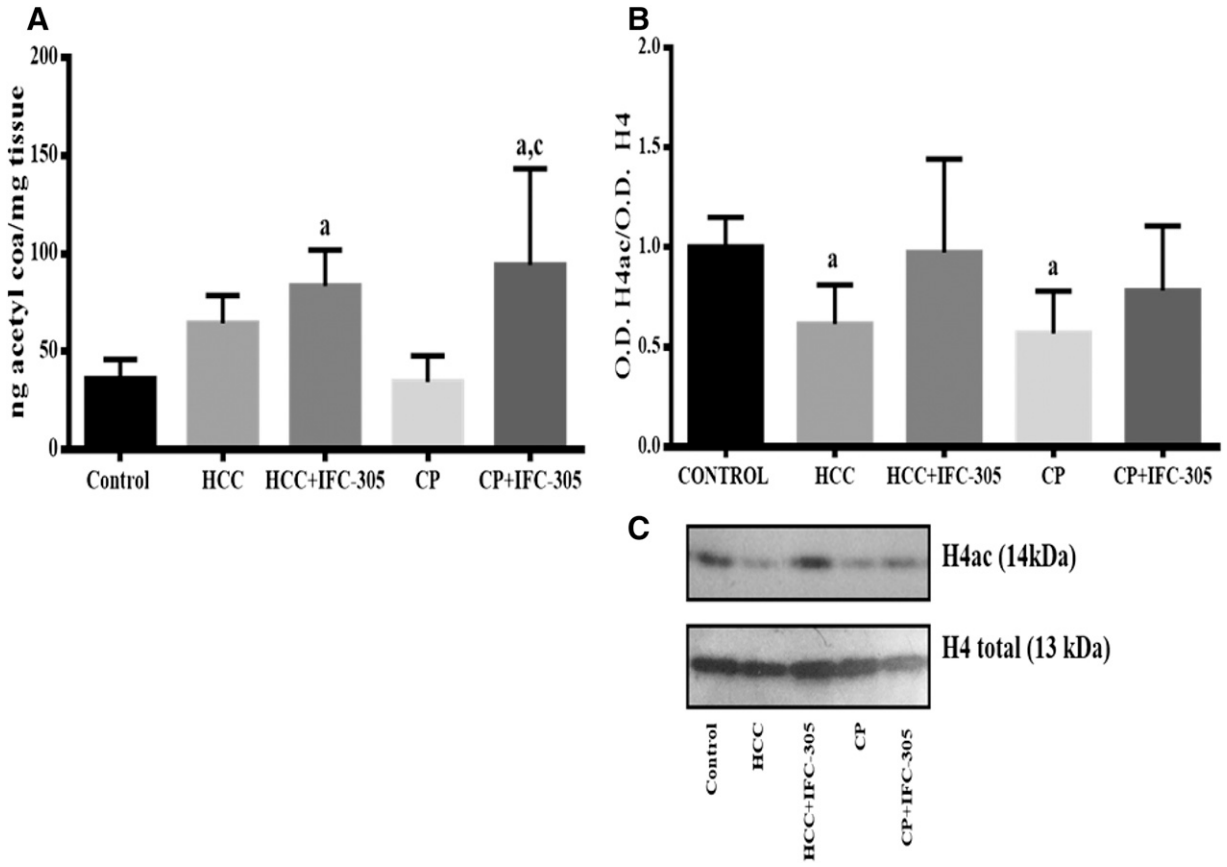

Fig. 4. Changes in the mitochondrial amount of Ac-CoA might reflect mitochondrial dysfunction and epigenetic changes. (A) Ac-CoA determined with a commercial kit in mitochondria isolated following manufacturer's instructions ($P<0.001$). (B) Densitometric analysis of the acetylated H4, Western blot normalized respect to H4 ($P<0.05$). (C) Representative Western blot of (B). [a]Significant difference versus Control; [c] statistically significant difference versus CP group ($P < 0.05$).

IFC-305-treatment (Fig. 2C). This compound might promote the correct function of mitochondrial enzymes by modulating the redox state as we mentioned above. A similar effect was seen in MDH activity in the CP scheme.

The PARP-1 enzyme activity consists in the poly-adenosine diphosphate ribosylation [poly(ADP-ribosyl)ation] of different substrates, and there is evidence of increased PARP-1 expression and auto-poly(ADP-ribosyl)ation in HCC and cirrhosis (Nomura et al., 2000; Shiobara et al., 2001; Shimizu et al., 2004). Here, we demonstrated an increased PARP-1 activity in the liver of rats treated with DEN. and this result correlates with the diminution of the NAD^+/NADH ratio, suggesting depletion in NAD^+ content. The IFC-305 compound prevented PARP-1 activation by DEN as previously was showed in the presence of adenosine (Jagtap et al., 2004). This result favored the NAD^+ availability and contributed to the maintenance of the redox state.

Mitochondrial changes affect the cytosolic redox state and, hence, metabolic alterations such as lactate production. It has been suggested the aerobic glycolysis is the main source of energy in cancer (Linehan and Rouault, 2013). In this context, glucose metabolism produces lactate. Here, we found an induction of high levels of lactate with DEN even 6 weeks after intoxication was stopped. This metabolic adaptation was inhibited and reversed with the IFC-305 compound (Fig. 3). Probably the source of energy became glycolysis dependent because of the altered mitochondrial function observed in the DEN-treated rats; the beneficial effect of IFC-305 treatment could be explained by its ability to maintain mitochondrial integrity.

The synthesis of Ac-CoA, a carbon donor in anabolic reactions, is altered by mitochondrial dysfunction (Wellen and Thompson, 2012). Moreover, it represents the link between pyruvate and the mitochondrial TCA cycle and ETC; thus, it might reflect the mitochondrial energetic supply. In addition to its energetic role, Ac-CoA represents

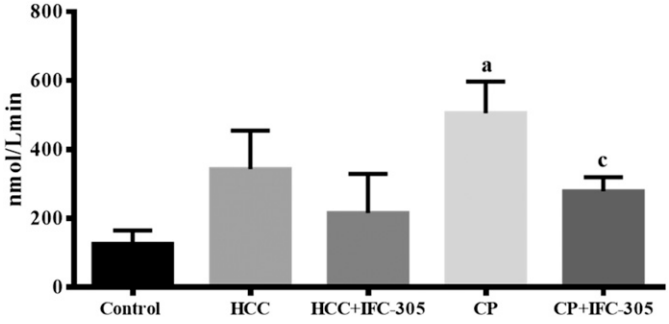

Fig. 5. Enzymatic activity of PARP-1, a NAD^+-dependent enzyme. This parameter was determined in liver slices through the consumption of NAD^+ in presence of DNA previously activated. Values are expressed as means ± S.E. [a]Statistically significant difference versus, Control; [c]significant difference versus CP group ($P<0.01$).

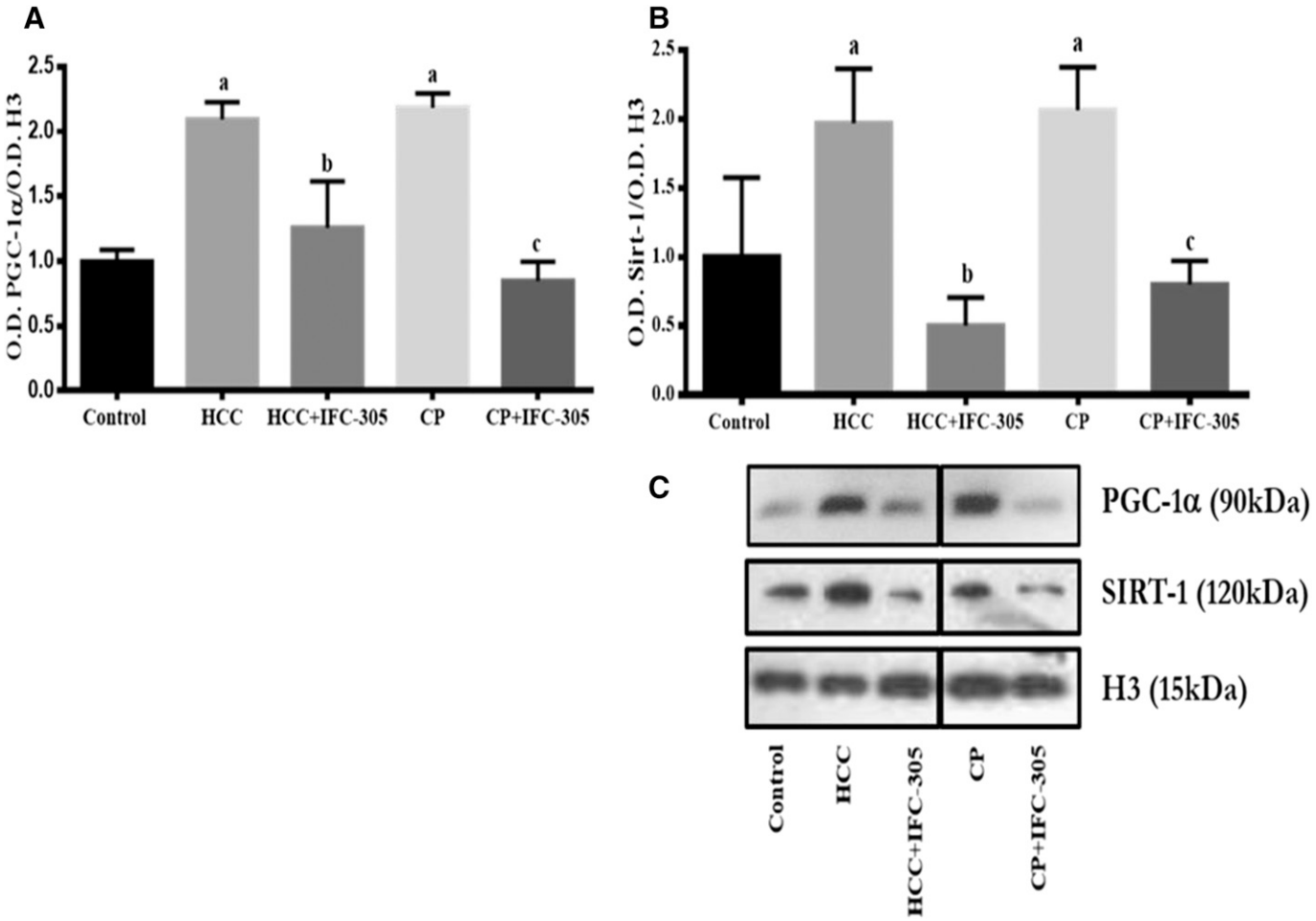

Fig. 6. Changes in the nuclear amount of proteins implicated in mitochondrial biogenesis. (A) PGC-1α and (B) Sirt-1; the bars correspond to the densitometric analysis. Values are expressed as means ± S.E. [a]Significant difference versus Control; [b]significant difference versus HCC group; [c]significant difference versus CP group ($P<0.001$). (C) Representative Western blot of (A) and (B).

availability of the substrate for acetylation reactions; it is important in the nucleus to modulate the gene expression through acetylation of histone lysines in DNA-binding proteins reducing the protein-DNA interaction (Wallace and Fan, 2010). Although DEN did not significantly change the Ac-CoA level with respect to the control group, IFC-305 treatment did change it (Fig. 4A); moreover, we observed a tenuous and not significant increased H4ac induced by IFC-305, suggesting that Ac-CoA levels regulated by IFC-305 might affect the mark of histones acetylation (Fig. 4B). In cancer cells, Ac-CoA is ectopically synthesized in the nucleus and is involved in cell cycle progression and DNA replication (Comerford et al., 2014). However, our results show Ac-CoA from mitochondria, indicating that the source of this metabolite is from the normal glycolytic flux through pyruvate, β-oxidation, and the catabolism of amino acids. These results confirm the ability of IFC-305 to increase the energy status of the liver and to improve the mitochondrial integrity. Possibly, H4ac allowed the transactivation of genes involved in growth and replication and it must be considered that the experimental model used implies cirrhosis, i.e., the whole liver, was affected by the administration of DEN. Further studies are necessary to test if replication of healthy hepatocytes is facilitated in this experimental model by IFC-305, as we previously reported in the CCl_4 model (Chagoya de Sanchez et al., 2012).

The diminished Sirt-3 mitochondrial content obtained with DEN reflects the inability to control the redox state and the metabolic activity. Recently, Sultana et al. (2016) demonstrated the protective effect of Sirt-3 on the mitochondrial function, probably by the oxidative stress modulation through the mitochondrial antioxidant enzymes such as Mn-SOD. Moreover, some authors have demonstrated downregulation of Sirt-3 in human HCC, suggesting that this pattern is associated with differentiation and tumor multiplicity (Xiong et al., 2016). Our results suggest a role of Sirt-3 in the mitochondrial effects of the IFC-305 compound possibly by deacetylation of the ATPase and complex I subunits (Vassilopoulos et al., 2014). Further studies are needed to demonstrate this. Overexpression of Sirt-3 induces apoptosis in HCC culture cells through mitochondrial translocation of the Bcl-2-associated X protein (Zhang and Zhou, 2012; Song et al., 2015). The transcriptional coactivator PGC-1α and Sirt-1 are considered important inducers of mitochondrial biogenesis through nuclear-encoded mitochondrial genes. Sirt-1 maintains PGC-1α in a deacetylated active state, promoting its transcriptional activity (Gerhart-Hines et al., 2007). Our results suggest the ability of IFC-305 to inhibit the activation of PGC-1α, at least in part, to maintain

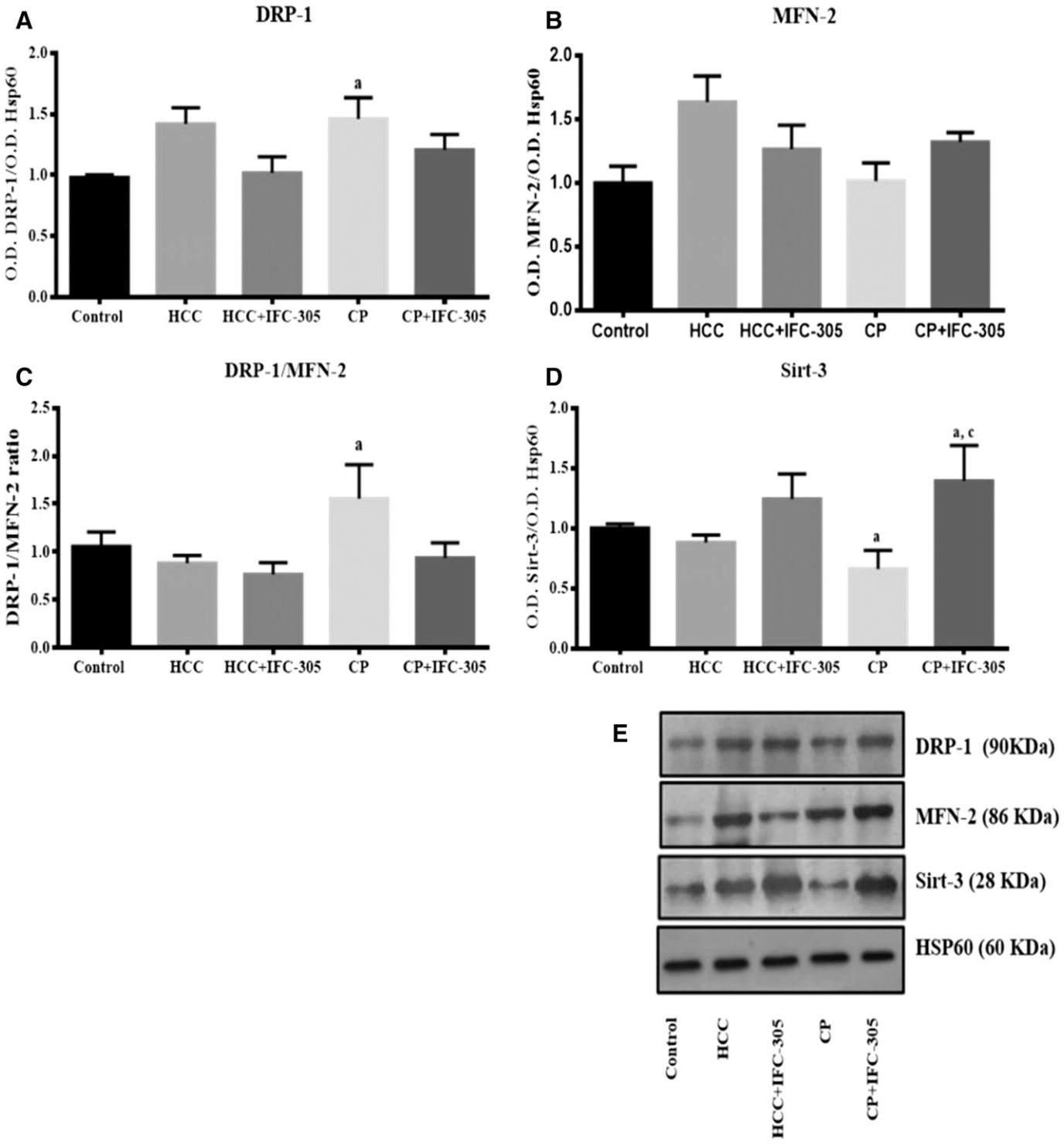

Fig. 7. Level of proteins related to the mitochondrial dynamics determined by Western blot. (A) DRP-1 ($P<0.05$), (B) MFN-2, (C) DRP-1/MFN-2 ratio ($P<0.05$), and (D) Sirt-3 ($P<0.001$) (*$P<0.05$). Bars correspond to the densitometric analysis. Values are expressed as means ± S.E.. [a]Significant difference versus Control; [b]means significant difference versus HCC group; [c]means significant difference versus CP group. (E) Representative Western blot of each protein.

the Ac-CoA levels and the decreased nuclear amount of Sirt-1. This effect allows us to explain the lower accumulation of dysfunctional mitochondria. Additionally, Sirt-1 has been linked to tumorigenesis and its depletion inhibits proliferation of HCC cells by cellular senescence or apoptosis (Chen et al., 2012). The nuclear localization of both proteins is increased in the rats intoxicated with DEN compared with the control group (Fig. 4). The IFC-305 compound was able to decrease the nuclear content of both Sirt-1 and PGC-1α. It is suggested that biogenesis induced by PGC-1α is tumor promoting, but production of new healthy mitochondria could be tumor suppressive (Boland et al., 2013).

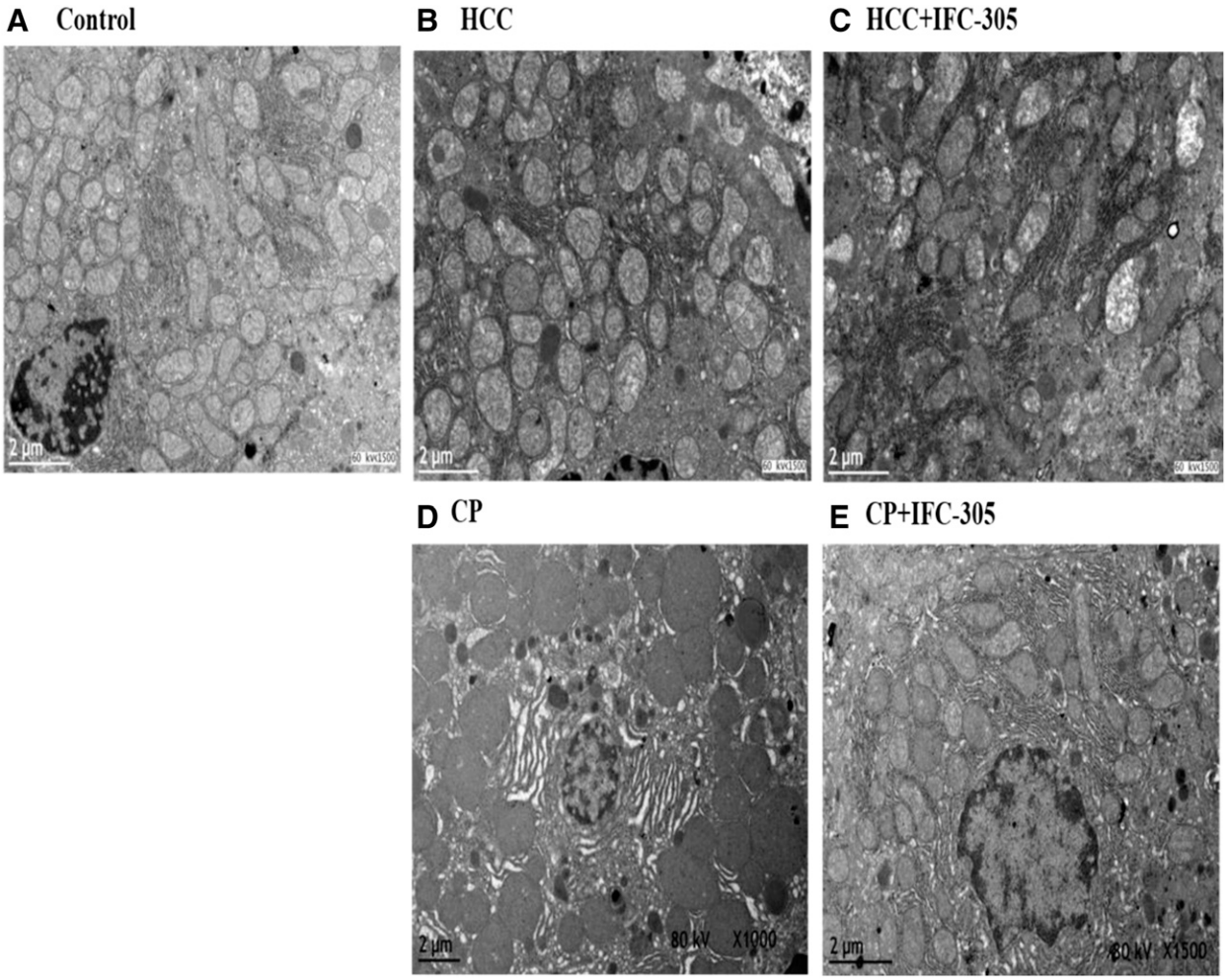

Fig. 8. Morphologic changes evaluated through electron microscopy. Each panel is representative of each group. Liver slices were fixed with glutaraldehyde and stained with osmium tetroxide. The square in the right inferior border represents a magnification of a mitochondrion. (A) Control; (B) HCC; (C) HCC+IFC-305; (D) CP; (E) CP+IFC-305.

Mitochondria are dynamic organelles to maintain their correct functionality and morphology. DRP1 regulates mitochondrial fission through scission of the outer mitochondrial membrane. Mitochondrial fusion is regulated by MFN-1 and -2, which facilitates binding of the outer mitochondrial membrane of different mitochondria (Dhingra and Kirshenbaum, 2014). According to this, small and fragmented mitochondria have been found in mice with reduced levels of MFN-2, but when this protein is restored, the normal mitochondria phenotype is obtained (Liesa et al., 2008). Here, we show that DEN intoxication induces important changes in the DRP-1/MFN-2 ratio 6 weeks after DEN administration was suspended. This alteration indicates a predominance fission over fusion. The mitochondrial morphology observed by electronic microscopy corroborates these results, because those isolated from HCC and CP groups depicted a circular shape instead of the elongated phenotype shown by the control and those receiving IFC-305 treatment. These results support the idea that mitochondrial shape regulates their function and integrity and that the hepatoprotector IFC-305 favors the fusion process promoting the functional mitochondria.

We conclude that chronic DEN intoxication induces mitochondrial alterations favoring the establishment of liver damage, resulting in abnormal mitochondrial accumulation and cellular behavior. The damage with DEN had been established for 16 weeks and, according to the results, it continued even after the insult had been stopped. IFC-305 maintains and restores the mitochondrial activity damaged by DEN and probably allows mitochondria to be repaired. The beneficial effects of IFC-305 reveal an integrative effect of the compound between mitochondrion and nucleus. This study demonstrated the mitochondrial impairment through functional, metabolic, and dynamic alterations in the sequential model of cirrhosis-hepatocellular carcinoma and the hepatoprotector IFC-305 helps to repair them, supporting its use as a potential hepatocellular carcinoma treatment or as an adjuvant in chemotherapy.

Acknowledgments

The authors dedicate this work to the memory of Dr. Armando Gómez-Puyou, one of the initiators of Bioenergetic in Mexico.

Authorship Contributions

Participated in the research design: Chávez, Tuena de Gómez-Puyou, and Chagoya de Sánchez.

Conducted experiments: Chávez, Lozano-Rosas, Rodríguez-Aguilera, Domínguez-López, Velasco-Loyden, and José-Nuñez.

Performed data analysis: Chávez, Lozano-Rosas, and Chagoya de Sánchez.

Wrote or contributed to the writing of the manuscript: Chávez and Chagoya de Sánchez.

References

Baracca A, Sgarbi G, Solaini G, and Lenaz G (2003) Rhodamine 123 as a probe of mitochondrial membrane potential: evaluation of proton flux through F(0) during ATP synthesis. *Biochim Biophys Acta* **1606**:137–146.

Boitier E, Merad-Boudia M, Guguen-Guillouzo C, Defer N, Ceballos-Picot I, Leroux JP, and Marsac C (1995) Impairment of the mitochondrial respiratory chain activity in diethylnitrosamine-induced rat hepatomas: possible involvement of oxygen free radicals. *Cancer Res* **55**:3028–3035.

Boland ML, Chourasia AH, and Macleod KF (2013) Mitochondrial dysfunction in cancer. *Front Oncol* **3**:292.

Cederbaum AI, Lieber CS, and Rubin E (1974) Effects of chronic ethanol treatment of mitochondrial functions damage to coupling site I. *Arch Biochem Biophys* **165**: 560–569.

Comerford SA, Huang Z, Du X, Wang Y, Cai L, Witkiewicz AK, Walters H, Tantawy MN, Fu A, Manning HC, et al. (2014) Acetate dependence of tumors. *Cell* **159**: 1591–1602.

Couoh-Cardel SJ, Uribe-Carvajal S, Wilkens S, and García-Trejo JJ (2010) Structure of dimeric F1F0-ATP synthase. *J Biol Chem* **285**:36447–36455.

Chagoya de Sánchez V, Martínez-Pérez L, Hernández-Muñoz R, and Velasco-Loyden G (2012) Recovery of the Cell Cycle Inhibition in CCl(4)-Induced Cirrhosis by the Adenosine Derivative IFC-305. *Int J Hepatol* **2012**:212530.

Chagoya de Sanchez VH-M (2002) Método para preparar aspartato de adenosina a partir de la adenosina, composición farmacéutica que las contiene y uso de las mismas en el tratamiento de enfermedades hepáticas fibrosantes., in.

Chagoya de Sanchez VH-M (2004) Uso de la adenosina para preparar medicamentos para el tratamiento de enfermedades hepáticas fibrosantes., in.

Chagoya de Sanchez VH-M, R; Villa-Treviño, S. (2013) Use of adenosine Aspartate for the preparation of pharmaceutical products for the treatment of liver cancer., in.

Chen J, Zhang B, Wong N, Lo AW, To KF, Chan AW, Ng MH, Ho CY, Cheng SH, Lai PB, et al. (2012) Sirtuin 1 is upregulated in a subset of hepatocellular carcinomas where it is essential for telomere maintenance and tumor cell growth. *Cancer Res* **72**:4138–4149.

Dang L, Yen K, and Attar EC (2016) IDH mutations in cancer and progress toward development of targeted therapeutics. *Ann Oncol* **27**:599–608.

Dhingra R and Kirshenbaum LA (2014) Regulation of mitochondrial dynamics and cell fate. *Circulation* **78**:803–810.

Dyer RB and Herzog NK (1995) Isolation of intact nuclei for nuclear extract preparation from a fragile B-lymphocyte cell line. *Biotechniques* **19**:192–195.

Finley LW and Haigis MC (2009) The coordination of nuclear and mitochondrial communication during aging and calorie restriction. *Ageing Res Rev* **8**:173–188.

García-Trejo JJ and Morales-Ríos E (2008) Regulation of the F1F0-ATP synthase rotary nanomotor in its monomeric-bacterial and dimeric-mitochondrial forms. *J Biol Phys* **34**:197–212.

Gerhart-Hines Z, Rodgers JT, Bare O, Lerin C, Kim SH, Mostoslavsky R, Alt FW, Wu Z, and Puigserver P (2007) Metabolic control of muscle mitochondrial function and fatty acid oxidation through SIRT1/PGC-1alpha. *EMBO J* **26**: 1913–1923.

Hanahan D and Weinberg RA (2011) Hallmarks of cancer: the next generation. *Cell* **144**:646–674.

Hernández-Muñoz R and Chagoya de Sánchez V (1994) In vivo correlation between liver and blood energy status as evidenced by chronic treatment of carbon tetrachloride and adenosine to rats. *Can J Physiol Pharmacol* **72**: 1252–1256.

Hernández-Muñoz R, Díaz-Muñoz M, and Chagoya de Sánchez V (1987) In vivo and in vitro adenosine stimulation of ethanol oxidation by hepatocytes, and the role of the malate-aspartate shuttle. *Biochim Biophys Acta* **930**: 254–263.

Hernández-Muñoz R, Glender W, Díaz-Muñoz M, Suárez J, Lozano J, and Chagoya de Sánchez V (1991) Alterations of ATP levels and of energy parameters in the blood of alcoholic and nonalcoholic patients with liver damage. *Alcohol Clin Exp Res* **15**:500–503.

Hernández-Muñoz R, Santamaría A, García-Sáinz JA, Piña E, and Chagoya de Sánchez V (1978) On the mechanism of ethanol-induced fatty liver and its reversibility by adenosine. *Arch Biochem Biophys* **190**:155–162.

Jagtap PG, Southan GJ, Baloglu E, Ram S, Mabley JG, Marton A, Salzman A, and Szabó C (2004) The discovery and synthesis of novel adenosine substituted 2,3-dihydro-1H-isoindol-1-ones: potent inhibitors of poly(ADP-ribose) polymerase-1 (PARP-1). *Bioorg Med Chem Lett* **14**:81–85.

Liesa M, Borda-d'Agua B, Medina-Gómez G, Lelliott CJ, Paz JC, Rojo M, Palacín M, Vidal-Puig A, and Zorzano A (2008) Mitochondrial fusion is increased by the nuclear coactivator PGC-1beta. *PLoS One* **3**:e3613.

Linehan WM and Rouault TA (2013) Molecular pathways: Fumarate hydratase-deficient kidney cancer–targeting the Warburg effect in cancer. *Clin Cancer Res* **19**: 3345–3352.

Lopera-Barrero NP, Ribeiro RP, Gomes PC, Jacometo CB, and da Silva Lopes T. (2008) Comparación de protocolos de extracción de ADN con muestras de aleta y larva de peces: extracción modificada con cloruro de sodio. *Cienc Investig Agrar* **35**: 77–86.

Mascorro JALM and Yates RD(1976) Rapid infiltration of biological tissues nucleoside. The latter could be particularly true regarding utilizing h-hexenyl succinic anhydride (HXSA)/vinyl ciclohexane dioxthe formation of the extracellular matrix,7 which is similar ide (VCD), and ultra-low viscosity embedding medium. Proc Ann Meeting Soc Am **34**:346-347.

Mughal W, Dhingra R, and Kirshenbaum LA (2012) Striking a balance: autophagy, apoptosis, and necrosis in a normal and failing heart. *Curr Hypertens Rep* **14**: 540–547.

Nomura F, Yaguchi M, Togawa A, Miyazaki M, Isobe K, Miyake M, Noda M, and Nakai T (2000) Enhancement of poly-adenosine diphosphate-ribosylation in human hepatocellular carcinoma. *J Gastroenterol Hepatol* **15**:529–535.

Pérez-Carreón JI, Martínez-Pérez L, Loredo ML, Yañez-Maldonado L, Velasco-Loyden G, Vidrio-Gómez S, Ramírez-Salcedo J, Hernández-Luis F, Velázquez-Martínez I, Suárez-Cuenca JA, et al. (2010) An adenosine derivative compound, IFC305, reverses fibrosis and alters gene expression in a pre-established CCl(4)-induced rat cirrhosis. *Int J Biochem Cell Biol* **42**:287–296.

Pietrocola F, Galluzzi L, Bravo-San Pedro JM, Madeo F, and Kroemer G (2015) Acetyl coenzyme A: a central metabolite and second messenger. *Cell Metab* **21**: 805–821.

Popov SS, Shulgin KK, Pashkov AN, and Agarkov AA (2014) The effect of melaxen on the activity of caspases and the glutathione antioxidant system in toxic liver injury. *Acta Naturae* **6**:110–118.

Putt KS and Hergenrother PJ (2004) An enzymatic assay for poly(ADP-ribose) polymerase-1 (PARP-1) via the chemical quantitation of NAD(+): application to the high-throughput screening of small molecules as potential inhibitors. *Anal Biochem* **326**:78–86.

Rehman J, Zhang HJ, Toth PT, Zhang Y, Marsboom G, Hong Z, Salgia R, Husain AN, Wietholt C, and Archer SL (2012) Inhibition of mitochondrial fission prevents cell cycle progression in lung cancer. *FASEB J* **26**:2175–2186.

Rodríguez-Aguilera JR (2015) Estudio de las modificaciones epigenéticas en un modelo de cirrosis experimental y su reversión por el hepatoprotector IFC-305, *Biología Celular y Desarrollo, Instituto de Fisiología Celular*, Universidad Nacional Autónoma de México, México.

Santidrian AF, Matsuno-Yagi A, Ritland M, Seo BB, LeBoeuf SE, Gay LJ, Yagi T, and Felding-Habermann B (2013) Mitochondrial complex I activity and NAD+/NADH balance regulate breast cancer progression. *J Clin Invest* **123**:1068–1081.

Schiffer E, Housset C, Cacheux W, Wendum D, Desbois-Mouthon C, Rey C, Clergue F, Poupon R, Barbu V, and Rosmorduc O (2005) Gefitinib, an EGFR inhibitor, prevents hepatocellular carcinoma development in the rat liver with cirrhosis. *Hepatology* **41**:307–314.

Schilling RJ and Reitz RC (1980) A mechanism for ethanol-induced damage to liver mitochondrial structure and function. *Biochim Biophys Acta* **603**:266–277.

Scholz TD, Koppenhafer SL, tenEyck CJ, and Schutte BC (1998) Ontogeny of malate-aspartate shuttle capacity and gene expression in cardiac mitochondria. *Am J Physiol* **274**:C780–C788.

Shimizu S, Nomura F, Tomonaga T, Sunaga M, Noda M, Ebara M, and Saisho H (2004) Expression of poly(ADP-ribose) polymerase in human hepatocellular carcinoma and analysis of biopsy specimens obtained under sonographic guidance. *Oncol Rep* **12**:821–825.

Shiobara M, Miyazaki M, Ito H, Togawa A, Nakajima N, Nomura F, and Morinaga N, and Noda M (2001) Enhanced polyadenosine diphosphate-ribosylation in cirrhotic liver and carcinoma tissues in patients with hepatocellular carcinoma. *J Gastroenterol Hepatol* **16**:338–344.

Song CL, Tang H, Ran LK, Ko BC, Zhang ZZ, Chen X, Ren JH, Tao NN, Li WY, Huang AL, et al. (2015) Sirtuin 3 inhibits hepatocellular carcinoma growth through the glycogen synthase kinase-3beta/BCL2-associated X protein-dependent apoptotic pathway. *Oncogene* **35**:631–641.

Sultana MR, Bagul PK, Katare PB, Anwar Mohammed S, Padiya R, and Banerjee SK (2016) Garlic activates SIRT-3 to prevent cardiac oxidative stress and mitochondrial dysfunction in diabetes. *Life Sci* **164**:42–51.

Suresh V, Anbazhagan C, Thangam R, Senthilkumar D, Senthilkumar N, Kannan S, Rengasamy R, and Palani P (2013) Stabilization of mitochondrial and microsomal function of fucoidan from Sargassum plagiophyllum in diethylnitrosamine induced hepatocarcinogenesis. *Carbohydr Polym* **92**:1377–1385.

Vassilopoulos A, Pennington JD, Andresson T, Rees DM, Bosley AD, Fearnley IM, Ham A, Flynn CR, Hill S, Rose KL, et al. (2014) SIRT3 deacetylates ATP synthase F1 complex proteins in response to nutrient- and exercise-induced stress. *Antioxid Redox Signal* **21**:551–564.

Velasco-Loyden G, Pérez-Carreón JI, Agüero JF, Romero PC, Vidrio-Gómez S, Martínez-Pérez L, Yáñez-Maldonado L, Hernández-Muñoz R, Macías-Silva M, and de Sánchez VC (2010) Prevention of in vitro hepatic stellate cells activation by the adenosine derivative compound IFC305. *Biochem Pharmacol* **80**:1690–1699.

Velasco-Loyden G, Pérez-Martínez L, Vidrio-Gómez S, Pérez-Carreón JI, and Chagoya de Sánchez V (2016) Cancer chemoprevention by an adenosine derivative in a model of cirrhosis-hepatocellular carcinoma induced by diethylnitrosamine in rats. *Tumour Biol*. DOI: 10.1177/1010428317691190.

Wallace DC and Fan W (2010) Energetics, epigenetics, mitochondrial genetics. *Mitochondrion* **10**:12–31.

Wellen KE and Thompson CB (2012) A two-way street: reciprocal regulation of metabolism and signalling. *Nat Rev Mol Cell Biol* **13**:270–276.

Xiong Y, Wang M, Zhao J, Han Y, and Jia L (2016) Sirtuin 3: A Janus face in cancer. *Int J Oncol* **49**:2227–2235.

Yi CH, Pan H, Seebacher J, Jang IH, Hyberts SG, Heffron GJ, Vander Heiden MG, Yang R, Li F, Locasale JW, et al. (2011) Metabolic regulation of protein N-alpha-acetylation by Bcl-xL promotes cell survival. *Cell* **146**:607–620.

Zhang YY and Zhou LM (2012) Sirt3 inhibits hepatocellular carcinoma cell growth through reducing Mdm2-mediated p53 degradation. *Biochem Biophys Res Commun* **423**:26–31.

Address correspondence to: Victoria Chagoya de Sánchez, Departamento de Biología Celular y Desarrollo, Instituto de Fisiología Celular, Universidad Nacional Autónoma de México. Ciudad de México, México. C.P. 04510. E-mail: vchagoya@ifc.unam.mx

LA N6-METILADENINA: UNA POTENCIAL MARCA DE REGULACIÓN EPIGENÉTICA EN EUCARIONTES*

Adrián Rafael Murillo-de-Ozores, Jesús Rafael Rodríguez-Aguilera

Departamento de Biología Celular y Desarrollo, Instituto de Fisiología Celular, UNAM. CDMX, México. Ambos autores contribuyeron por igual a la elaboración del presente trabajo. Correo E: jesusr_rodagu@comunidad.unam.mx

RESUMEN

La N6-metiladenina en el ADN (6mA), -la que fue descrita originalmente como un factor de protección para el ADN bacteriano en contra de las enzimas de restricción- recientemente ha cobrado importancia ya que en tres publicaciones en organismos eucariontes que incluyen a la mosca de la fruta *Drosophila melanogaster*, al gusano *Caenorhabditis elegans* y al alga verde *Chlamydomonas reinhardtii*, identificaron variaciones en los niveles de esta modificación así como en las enzimas que la establecen y remueven. Dichas variaciones se correlacionan con alteraciones funcionales en estos organismos por lo que la 6mA resurge, ahora en eucariontes, como una potencial marca de regulación epigenética.

PALABRAS CLAVE:

Metilación del ADN, Epigenética, *Drosophila melanogaster, Caenorhabditis elegans, Chlamydomonas reinhardtii*.

ABSTRACT

The modified nucleotide N6-methyladenine in DNA (6mA), -which was described originally as a mechanism of protection for the bacterial DNA against the restriction enzymes- recently it has become important because three reports in eukaryotic organisms, the fruit fly *Drosophila melanogaster*, the worm *Caenorhabditis elegans* and the green algae *Chlamydomonas reinhardtii*, identified variations in the levels of this modification as well as in the enzymes that establish and remove it. These variations correlate with the functional alterations of these three organisms and therefore, the 6mA reappears as a potential epigenetic mark.

KEY WORDS:

DNA methylation, Epigenetics, *Drosophila melanogaster, Caenorhabditis elegans, Chlamydomonas reinhardtii.*

MÁS ALLÁ DE LA GENÉTICA, LA EPIGENÉTICA

Las células de un organismo eucarionte son genéticamente idénticas pero son estructural y funcionalmente heterogéneas debido a que en cada tipo celular se expresan diferentes genes. Estas diferencias pueden surgir durante el desarrollo, la diferenciación celular o en la enfermedad. La regulación de la expresión génica es mediada por tres principales mecanismos que actúan en conjunto: el primero se basa en los factores de transcripción que se unen a secuencias específicas y que regulan a un grupo determinado de genes; el segundo involucra mecanismos de regulación epigenética que ayudan a establecer el estado de diferenciación de una célula y su progenie; el tercero está relacionado con la organización de la cromatina nuclear.

La regulación epigenética está definida como todos aquellos cambios heredables en la expresión de los genes y en la función del genoma que ocurren sin afectar la secuencia del ADN (1). Dentro de los procesos epigenéticos que más correlacionan con la actividad génica y que se han estudiado mejor, resaltan: la metilación del ADN, las modificaciones post-traduccionales de histonas, los complejos remodeladores de la cromatina dependientes de ATP y los complejos represor Polycomb y activador Trithorax. Asimismo, en años recientes también se ha observado la acción coordinada de ARNs no-codificantes para proteínas, en la modulación de la estructura de la cromatina.

*Recibido: 11 de diciembre de 2015 Aceptado: 2 de marzo de 2016

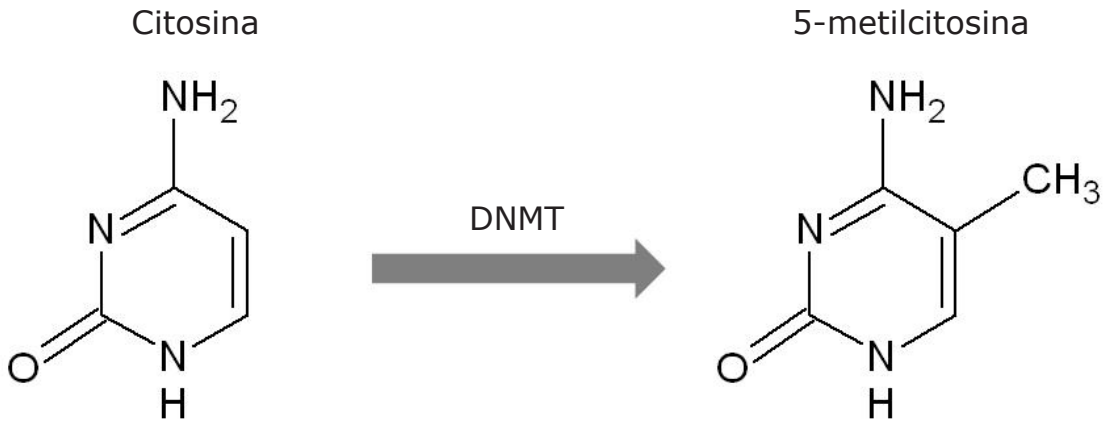

Figura 1. *Metilación del DNA en CpGs de eucariontes. La reacción está dada por la actividad enzimática de DNA metiltransferasas (DNMT) (2).*

LA METILACIÓN DEL ADN EN EUCARIONTES: LA 5-METILCITOSINA

La 5-metilcitosina (5mC) consiste en la incorporación de un grupo metilo en la posición 5 de la citosina (Fig. 1) (2). Esta modificación del ADN se ha descrito ampliamente en organismos eucariontes y está relacionada con la regulación de varios procesos celulares incluyendo el desarrollo embrionario, la transcripción, la inactivación del cromosoma X, la impronta genómica y la estabilidad cromosómica (1).

La metilación del ADN puede regular la expresión genética por impedimento estérico de los factores de transcripción con sus secuencias blanco, evitando así su activación o mediante el reclutamiento de proteínas que reconocen al ADN metilado, uniendo co-represores que provocan la compactación de la cromatina, principalmente mediante la acción de desacetilasas de histonas (1).

Se ha propuesto que este proceso es dinámico, pues mientras las metiltransferasas de ADN establecen y mantienen la presencia de 5mC, las dioxigenasas de citosina "ten-eleven translocation" (TET) oxidan a la 5mC hacia 5-hidroximetilcitosina (5hmC), 5-formilcitosina (5fC) y 5-carboxicitosina (5caC) las cuales pueden ser removidas por el sistema de reparación de ADN por escisión de bases (BER) para restaurar una citosina sin modificar (3).

LA ADENINA TAMBIÉN PUEDE SER METILADA

La adición de un grupo metilo en la posición 6 de la adenina resulta en la N6-metiladenina (6mA), la cual se ha encontrado en el ADN de virus, bacterias, protistas, hongos y algas. Otra modificación en la adenina ocurre por la metilación en la primera posición del anillo de purinas (1mA) y que en conjunto con la metilación en la posición 3 del anillo de pirimidina de la citosina (3mC) son consideradas como eventos de daño por metilación en el ADN, ya que impide la correcta formación del puente de hidrógeno con la base complementaria (4).

En bacterias, la 6mA fue inicialmente señalada como componente de los sistemas de restricción/modificación que corresponden a los mecanismos de defensa de estos organismos contra fagos y plásmidos y que les permiten distinguir entre el ADN propio y el del invasor (4). En otras palabras, el ADN del microorganismo con adeninas metiladas, se protege de la digestión de enzimas capaces de cortar en sitios metilados, mientras que el ADN externo al no contar con dicha marca, es cortado por estas enzimas una vez que entra a la célula.

En años recientes, la 6mA ha sido utilizada para identificar los sitios de interacción de proteínas con el genoma eucarionte *in vivo* a través de la tecnología denominada DamID (Fig. 2) (5), la cual es un método basado en la fusión de la proteína de interés con la metiltransferasa de adenina de *Escherichia coli* ("dam", por las siglas en inglés de metiltransferasa de ADN). La expresión de esta proteína de fusión *in vivo* conduce a la metilación de adeninas en el ADN alrededor de los sitios nativos de unión de la proteína a la cual esta fusionada la "dam", lo que permite la identificación de dichos sitios de unión (6).

Aunque se han propuesto ciertas funciones de esta modificación en procariontes, como la replicación y reparación del ADN o la expresión génica, no se ha descrito la función que pudiera desempeñar en eucariontes, o incluso si se encuentra o no en el genoma de algunos de éstos organismos. En

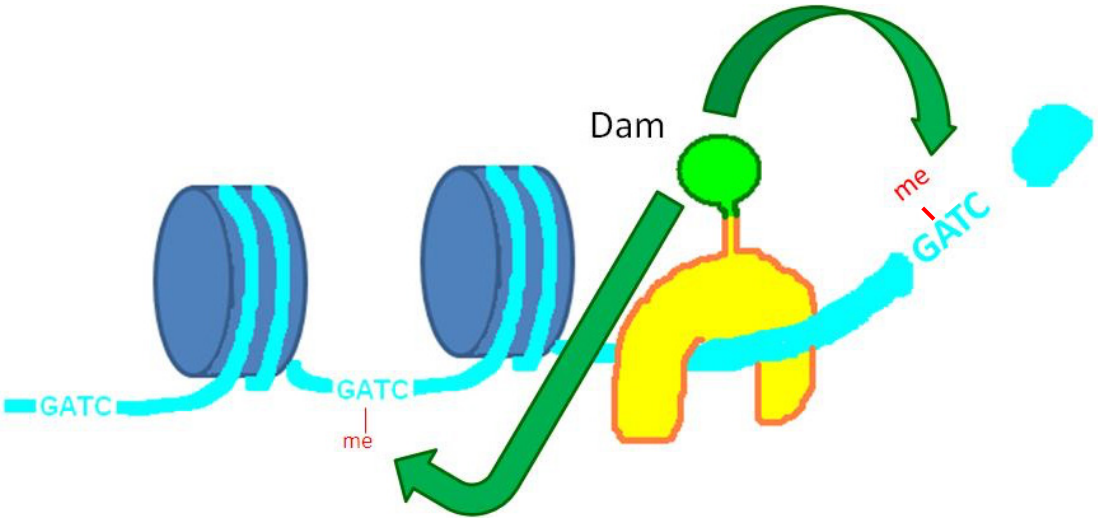

Figura 2. *Principio de DamDI. El esquema muestra un fragmento de cromatina (se observa el DNA y dos nucleosomas). La enzima Dam (verde) fusionada con la proteína de interés (amarillo) es reclutada por ésta última a sus sitios de unión nativos en la cromatina lo que resultará en la metilación local de las adeninas la cual funcionará como una etiqueta única en el genoma que podrá detectarse utilizando enzimas de restricción. Modificado de (5).*

este sentido, tres estudios recientes publicados en la revista Cell, demuestran la 6mA en *Drosophila melanogaster* (7), *Caenorhabditis elegans* (8) y *Chlamydomonas reinhardtii* (9), y aportan información sobre su distribución espacio-temporal y su papel en la biología celular de estos organismos.

La detección precisa de bajas cantidades de 6mA en el genoma de eucariontes fue posible gracias al desarrollo de técnicas más refinadas y sensibles. Dichas técnicas de última generación incluyen a la cromatografía líquida de alta resolución acoplada a espectrometría de masas de triple cuadrupolo, la inmunoprecipitación de la 6mA seguida de secuenciación masiva y la secuenciación basada en enzimas de restricción o la secuenciación SMRT ("single-molecule real-time"), capaz de distinguir entre bases modificadas (10).

LA 6mA JUEGA UN PAPEL IMPORTANTE EN EL DESARROLLO DE *Drosophila*

Los bajos niveles de 5mC en la mosca de la fruta han sugerido que las diferentes modificaciones post-traduccionales (PTM) de histonas y sus reguladores son los principales determinantes en la configuración tridimensional del genoma de la *Drosophila*. Sin embargo, la reciente descripción de la desmetilación activa del ADN en vertebrados motivó la búsqueda de nuevas modificaciones del ADN, con la premisa de encontrar la desmetilasa responsable de remover esa modificación, abatirla y así poder detectar un aumento en los niveles de dicha modificación.

Chen y sus colaboradores (7) pudieron detectar 6mA en el genoma de embriones de *Drosophila*, mientras que en etapas posteriores del desarrollo no se encontró esta modificación, lo que sugiere un papel importante en el desarrollo temprano de la mosca. También se demostró que la presencia de extractos nucleares puede inducir la desmetilación de la 6mA en el ADN, lo que estableció las bases para la búsqueda bioinformática de una desmetilasa de ADN codificada en el genoma de la mosca. Se encontró que el gen CG2083 de *Drosophila melanogaster* codifica para una proteína con ciertas regiones altamente conservadas: como un dedo de zinc CXXC, el cual permite a la proteína interactuar con el ADN; un dominio rico en Cys y un tercer dominio DSBH ("double stranded beta helix"), característico de oxigenasas y probable responsable de la actividad enzimática de esta proteína. Estas tres regiones también se encuentran en las proteínas TET de mamíferos, mientras que la desmetilasa bacteriana de ADN AlkB, responsable de re-establecer la adenina a partir de 6mA, sólo contiene la región DSBH. El grupo de investigación llamó a esta proteína DMAD (*Drosophila* DNA 6mA "demethylase") y la caracterizó.

DMAD se expresa en niveles bajos durante las primeras etapas del desarrollo embrionario, pero su expresión aumenta durante las etapas embriogénicas tardías. Debido a que DMAD se expresa de manera inversamente proporcional a la cantidad de 6mA, se sugiere que su función es la desmetilación de la 6mA en el ADN. Mediante ensayos de pérdida de función a través de ARN de doble

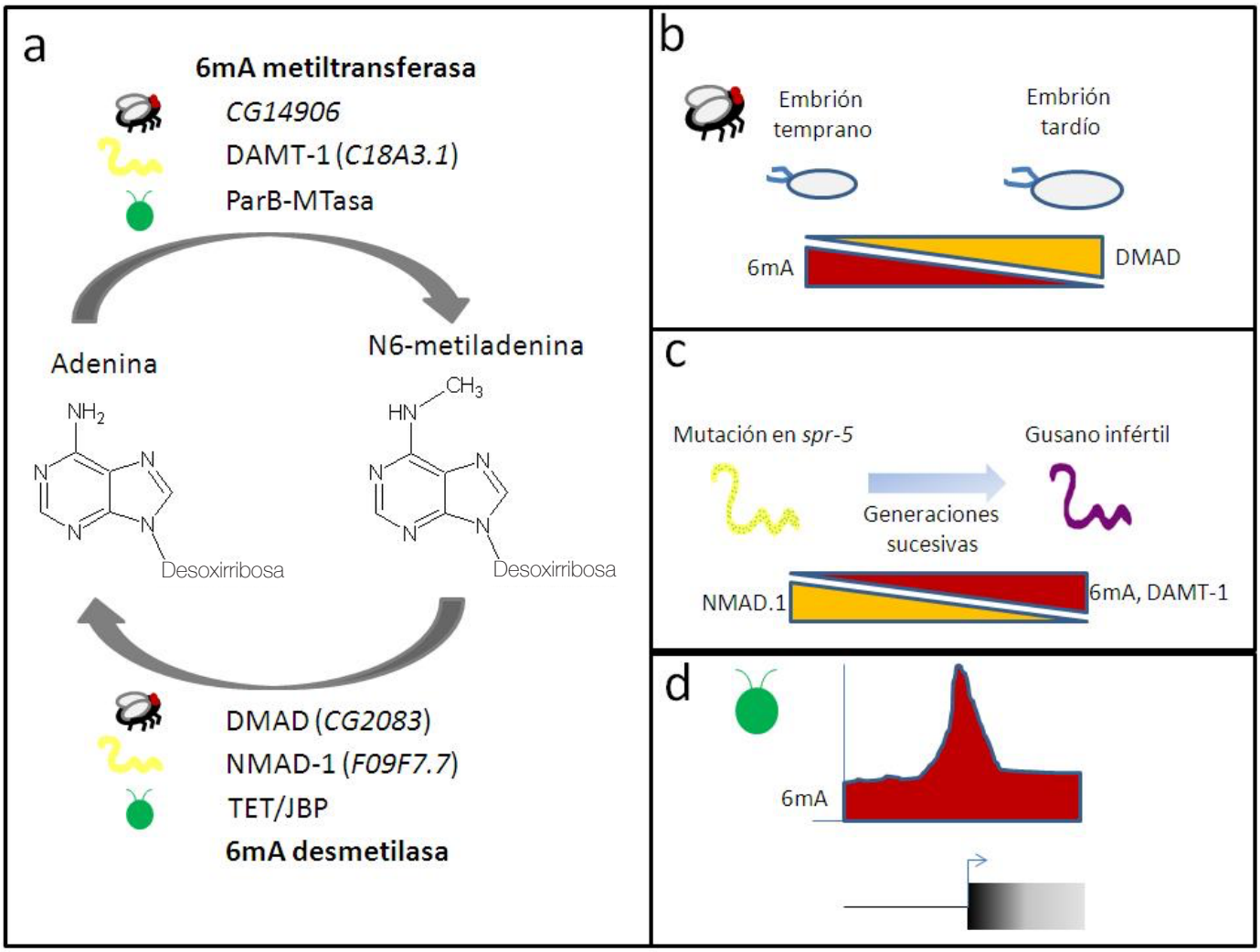

Figura 3. *La 6mA y su comportamiento en eucariontes. a) Las bases de adenina en el DNA son modificadas por las N6-metiladenina (6mA) metiltransferasas y 6mA desmetilasa. Las enzimas modificadoras están conservadas en los super-reinos de la vida con actividad putativa también en Homo sapiens. b) Comportamiento de la 6mA y de la 6mA desmetilasa de Drosophila durante el desarrollo. c) Abundancia de la 6mA y de sus enzimas modificadoras a través de las generaciones de C. elegans con mutación en spr-5 que las lleva a la infertilidad. d) Enriquecimiento de 6mA alrededor del TSS de la mayoría de los genes de Chamydomonas. Modificado de (7).*

cadena (dsRNA) y la herramienta de edición del genoma CRISPR/Cas9, se encontró que la proteína DMAD es esencial para el desarrollo de la mosca, pues su ausencia ocasiona letalidad en las últimas etapas embrionarias, lo cual está precedido por un aumento en la 6mA en su genoma (Fig. 3).

Mediante el uso de inmunoprecipitación del ADN, se encontró que este aumento se da principalmente en regiones del genoma que corresponden a transposones (7). Por lo tanto, es probable que la letalidad causada por la ausencia de DMAD pueda deberse a la inestabilidad genómica producida por la expresión de ciertos elementos genéticos transponibles.

6mA Y LA INFERTILIDAD DE *C. elegans* ¿QUÉ METILA Y QUÉ DESMETILA A LA ADENINA?

Durante varios años se pensó que el genoma de *Caenorhabditis elegans* no presentaba metilación, ya que no había sido posible replicar los experimentos que indicaban que la marca de 5mC incrementaba en función del envejecimiento además que este organismo no presenta homólogos de las metiltransferasas de ADN.

El grupo de Shi (8) se dio a la tarea de investigar las formas de metilación en el genoma del nematodo, encontrando a la 6mA como la única forma detectable. La 6mA está presente en el organismo

completo así como en embriones y líneas germinales exceptuando el núcleo del esperma (8). Esto último indican los autores, puede atribuirse a la gran compactación de la cromatina en estas células lo que impide su detección o ser un indicativo de un borrado paterno de la marca.

La 6mA se encuentra en menos del 1% del total de las adeninas en el genoma de *C. elegans*, sin embargo, a diferencia de la metilación en la posición 5 de la citosina, que se presenta en el contexto CpG en varios eucariontes, la 6mA se encontró en motivos GAGG y AGAA. Esto indica que la metilación de la adenina ocurre en una sola cadena del ADN (8), debido a que no hay adenina en la cadena complementaria a estos motivos. Es decir, dichas secuencias no son complementarias, a diferencia de la citosina y la guanina, donde ambas cadenas tienen un sito CpG en el mismo *locus*, por lo que la metilación o está presente en ambas cadenas o en ninguna.

En esa investigación se encontró además, una correlación entre la mutante para la desmetilasa de lisina 4 de la histona H3 (spr-5, ortóloga de LSD1/KDM1A), el incremento de 6mA de manera transgeneracional y la infertilidad del gusano (Fig. 3) (8).

Teniendo esto como antecedente, el grupo estudió a la familia de enzimas desalquilantes ALKB e identificó que mutantes para F09F7.7 aceleraban el proceso de infertilidad en mutantes para spr-5. Se evaluó la actividad desmetilante de F09F7.7 *in vitro* encontrando que la enzima era capaz de desmetilar oligonucleótidos con 6mA y 3mC. Esta actividad se verificó en gusanos mutantes para la desmetilasa, encontrando niveles elevados de 6mA, pero no de 3mC en estos organismos. Estos hallazgos sugieren que se trata de la principal desmetilasa de 6mA *in vivo*, por lo que se renombró como N6-metiladenina desmetilasa 1 (nmad-1) (8).

Una vez identificada la enzima que se encarga de remover a la 6mA en *C. elegans*, Shi y sus colaboradores se interesaron en identificar a la enzima responsable de colocar a dicha modificación. Un candidato interesante era C18A3.1 que es parte del complejo Ime4/Kar4 de la familia MTA-70 y que en levadura codifica a una metilasa de ARNm. Encontraron que la expresión de C18A3.1 en células SF9 conducía a un mayor nivel de 6mA en el ADN genómico y la mutación de aminoácidos del sitio de reconocimiento de sustrato abatía la cantidad de 6mA. Para comprobar que esta enzima actuara *in vivo*, realizaron "knockdowns" en gusanos silvestres y en mutantes para spr-5 y encontraron en ambos casos una disminución de 6mA y que además se suprimía el fenotipo transgeneracional de baja fertilidad. Esto sugería que la enzima es la 6mA metiltransferasa de *C. elegans* (Fig. 3) y se renombró como ADN N6 adenina metiltransferasa 1 (damt-1) (8).

Finalmente ese estudio encontró una intercomunicación entre la marca de H3K4me2 y la 6mA ya que la remoción de damt-1 reduce los niveles de H3K4me2 en gusanos mutantes para spr-5 así como el "knockdown" de eap-1 (proteína de unión a H3K9me) misma que también disminuye a la 6mA (8). Estos resultados sugieren una regulación recíproca de H3K4 y la N6 metilación de adenina, así como una relación entre los reguladores de la metilación de adenina y de histonas.

Chlamydomonas REVELA UNA POSIBLE FUNCIÓN DE LA 6mA EN LA REGULACIÓN TRANSCRIPCIONAL

Desde 1978 se había descrito que el alga verde *Chlamydomonas reinhardtii* presentaba altos niveles de 6mA (~0.3-0.5 mol%) en el ADN nuclear; por lo que con el interés de determinar la distribución, así como una posible función de esta marca, el grupo encabezado por He (9) desarrolló diferentes métodos para localizar a la 6mA en ADN genómico.

Para determinar la dinámica de la 6mA a lo largo del crecimiento celular, el grupo sincronizó células del alga para que crecieran durante la fase de luz (fase G1) y posteriormente tuvieran rondas de replicación del ADN y divisiones celulares (fases S/M) al entrar a la fase de oscuridad. Encontraron que los niveles de 6mA disminuían dramáticamente durante la replicación del ADN y que había una rápida recuperación de estos niveles, lo que indica que la marca se instala en el ADN recién sintetizado en un periodo corto de tiempo después de la replicación (9).

Al analizar la distribución de la 6mA de algas cultivadas en luz u oscuridad constante, se encontró una coincidencia en 88% en los picos de la modificación a lo largo del genoma, lo que sugiere que la instalación/mantenimiento de la marca se da en lugares específicos y se observó que el enriquecimiento se daba alrededor del sitio de inicio de la transcripción (TSS) en 84 % de los genes de *Chlamydomonas*. Dichos genes estaban relacionados con regiones altamente transcritas (Fig. 3); el resto de los sitos no presentaba un patrón de enriquecimiento y se encontraba tanto en el cuerpo de los genes como en regiones intergénicas (9).

Para identificar las secuencias a las que estaba asociada la 6mA, el grupo de He desarrolló un método con una resolución de ~33 pb que permi-

tió identificar que el enriquecimiento de la marca se asociaba a secuencias que contenían motivos con dinucleótidos ApT. La validación de sitios individuales de metilación permitió identificar dos motivos asociados a la metilación de adenina: CATG y GATC (9).

Tomando en cuenta que la marca de 6mA se encuentra alrededor del TSS, los autores decidieron evaluar la correlación de esta marca con la posición de nucleosomas y encontraron que los sitios de 6mA se localizan entre dos nucleosomas adyacentes, es decir en el ADN "linker". Además propusieron que si dos sitios adyacentes de 6mA se encuentran separados por una distancia mayor a 150 pb, entonces un nucleosoma se encontrará entre ambas y si la distancia es menor, entonces se originará un sitio libre de nucleosomas entre ellos, que indica que la 6mA puede coordinar el posicionamiento nucleosomal (9).

Considerando que en el alga también está presente la marca de 5mC, el grupo comparó la distribución de ésta con los sitios enriquecidos para 6mA y no encontró correlación lo que indica que ambas marcas tienen función diferente en este organismo. Por lo anterior, el grupo propuso que la 6mA puede estar contribuyendo a estructuras cromatínicas que permiten el inicio de la transcripción mientras que la 5mC contribuye al silenciamiento de transposones, impronta la definición de exones y regula la elongación de la transcripción (9).

CONCLUSIONES

Los tres trabajos describen papeles importantes de la 6mA (7-9): primero, un mecanismo que favorece la transcripción en el alga verde (9); segundo, la dinámica de dicha marca durante el desarrollo de la mosca de la fruta (7) y por último, su relevancia para la fertilidad en *C. elegans* (8). Dichas propiedades podrían ser el inicio del descubrimiento de una variedad de funciones de la 6mA, descrita originalmente en procariontes y que ahora podría representar una nueva marca de regulación epigenética para organismos eucariontes.

Es importante comentar que aunque la modificación de la 6mA únicamente se ha descrito -para el caso de eucariontes- en los tres organismos comentados, y que en comparación con la 5mC su distribución es mucho menor, no hay que descartar su trascendencia. Es posible que en el futuro las nuevas tecnologías con mayor sensibilidad de detección, puedan identificar esta marca en otros eucariontes o bien, describir un mayor número de funciones asociadas a la 6mA. Para una revisión más extensa sobre esta modificación del ADN y su posible papel en la regulación epigenética se sugiere consultar los trabajos de Luo *et al* (11), Sun *et al* (12), Summerer (13) y Huang *et al* (14).

AGRADECIMIENTOS

Agradecemos el apoyo brindado para la redacción de este escrito a la M. en C. Rosario Pérez-Molina, a la M en C. Rebeca Pérez Cabeza de Vaca y a la Lic. María Elena Rodríguez-Aguilera así como a la Dra. Victoria Chagoya de Sánchez y al Dr. Félix Recillas-Targa quienes nos han permitido formar parte de sus equipos de investigación al realizar nuestros proyectos de licenciatura y doctorado.

REFERENCIAS

1. Recillas-Targa F (2014) Interdependency between genetic and epigenetic regulatory defects in cancer. Meth Mol Biol 1165: 33-52.
2. Griffiths AJF, Wessler SR, Lewontin RC, Carroll SB (2008) Genética, 9ª Ed. Mc Graw Hill. España.
3. Bhutani N, Burns DM, Blau HM (2011) DNA demethylation dynamics. Cell 146: 866-872.
4. Arber W, Dussoix D (1962) Host specificity of DNA produced by Escherichia coli. I. Host controlled modification of bacteriophage lambda. J Mol Biol 5: 18-36.
5. van Steensel lab: DamID info. Netherlands Cancer Institute. [Información en Intenet] 2013 [acceso 31 de Julio de 2015] Disponible en http://research.nki.nl/vansteensellab/DamID_FAQ.htm
6. Greil F, Moorman C, van Steensel B (2006) DamID: mapping of in vivo protein-genome interactions using tethered DNA adenine methyltransferase. Meth of Enzimol 410: 342-357.
7. Zhang G, Huang H, Liu D, Cheng Y, Liu X, Zhang W, Yin R, Zhang D, Zhang P, Liu J, Li C, Liu B, Luo Y, Zhu Y, Zhang N, He S, He C, Wang H, Chen D (2015) N(6)-methyladenine DNA modification in Drosophila. Cell 161: 893-906.

8. Greer EL, Blanco MA, Gu L, Sendinc E, Liu J, Aristizabal-Corrales D, Hsu CH, Aravind L, He C, Shi Y (2015) DNA Methylation on N(6)-Adenine in C elegans. Cell 161: 868-878.
9. Fu Y, Luo GZ, Chen K, Deng X, Yu M, Han D, Hao Z, Liu J, Lu X, Dore LC, Weng X, Ji Q, Mets L, He C (2015) N(6)-methyldeoxyadenosine marks active transcription start sites in chlamydomonas. Cell 161: 879-892.
10. Heyn H, Esteller M (2015) An adenine Code for DNA: A Second Life for N6-methyladenine. Cell 161:710-713.
11. Luo GZ, Blanco MA, Greer EL, He C, Shi Y (2015)DNA N(6)-methyladenine: a new epigenetic mark in eukaryotes? Nature reviews. Mol Cell Biol 16:705-710.
12. Sun Q, Huang S, Wang X, Zhu Y, Chen Z, Chen D (2015) N(6)-methyladenine functions as a potential epigenetic mark in eukaryotes. Bioassays 37:1155-1162.
13. Summerer D (2015) N(6)-Methyladenine: A Potential Epigenetic Mark in Eukaryotic Genomes. Angew Chem Int Ed Engl 54: 10714-10716.
14. Huang S, Chen D (2015) N6-methyladenine: a potential epigenetic mark I eukaryotes. Oncotarget 6:15744-15745.

10072–10085 *Nucleic Acids Research, 2019, Vol. 47, No. 19* *Published online 6 September 2019*
doi: 10.1093/nar/gkz762

Human mitochondrial DNA is extensively methylated in a non-CpG context

Vibha Patil [1,*], Cyrille Cuenin[1], Felicia Chung[1], Jesus R. Rodriguez Aguilera[1], Nora Fernandez-Jimenez[2], Irati Romero-Garmendia[2], Jose Ramon Bilbao[2], Vincent Cahais[1], Joseph Rothwell[3] and Zdenko Herceg [1,*]

[1]Epigenetics Group, International Agency for Research on Cancer (IARC), 69372 Lyon Cedex 08, France, [2]Department of Genetics, Physical Anthropology and Animal Physiology, University of the Basque Country (UPV/EHU), Biocruces-Bizkaia Health Research Institute, Leioa, Basque Country 48940, Spain and [3]Nutritional Epidemiology Group, International Agency for Research on Cancer (IARC), 69372 Lyon Cedex 08, France

Received May 3, 2019; Revised August 19, 2019; Editorial Decision August 21, 2019; Accepted August 23, 2019

ABSTRACT

Mitochondrial dysfunction plays critical roles in cancer development and related therapeutic response; however, exact molecular mechanisms remain unclear. Recently, alongside the discovery of mitochondrial-specific DNA methyltransferases, global and site-specific methylation of the mitochondrial genome has been described. Investigation of any functional consequences however remains unclear and debated due to insufficient evidence of the quantitative degree and frequency of mitochondrial DNA (mtDNA) methylation. This study uses WGBS to provide the first quantitative report of mtDNA methylation at single base pair resolution. The data show that mitochondrial genomes are extensively methylated predominantly at non-CpG sites. Importantly, these methylation patterns display notable differences between normal and cancer cells. Furthermore, knockdown of DNA methyltransferase enzymes resulted in a marked global reduction of mtDNA methylation levels, indicating these enzymes may be associated with the establishment and/or maintenance of mtDNA methylation. DNMT3B knockdown cells displayed a comparatively pronounced global reduction in mtDNA methylation with concomitant increases in gene expression, suggesting a potential functional link between methylation and gene expression. Together these results demonstrate reproducible, non-random methylation patterns of mtDNA and challenge the notion that mtDNA is lowly methylated. This study discusses key differences in methodology that suggest future investigations must allow for techniques that assess both CpG and non-CpG methylation.

INTRODUCTION

Mitochondria maintain cellular homeostasis by generating metabolic energy via oxidative phosphorylation (OXPHOS) as well as regulating apoptotic pathways. Mitochondrial dysfunction in a wide range of human malignancies is well documented and targeting mitochondria remains a promising avenue for the development of novel strategies for cancer treatment (1).

Mitochondrial DNA (mtDNA) is a double helical molecule composed of a heavy and light strand that encodes for 13 protein subunits that make up the complexes required for OXPHOS, transfer RNAs that carry specific amino acids for protein synthesis as well as ribosomal RNAs also involved in protein synthesis (2). A 1200-bp non-coding region of the mitochondrial genome, called the Displacement Loop (D-Loop), controls mitochondrial replication and transcription of its encoded genes (2) through a number of different start sites and promoter regions (3–5). However, exact molecular mechanisms involved in transcriptional control of the mitochondrial genome remain unclear.

The existence of mtDNA methylation has been reported previously via a large array of techniques, while some studies have reported an absence of mtDNA methylation (6,7), the majority have detected it (8–11). Older studies reported human fibroblast cultures and cell lines to have 2–5% of all mtDNA molecules fully methylated at specific CpG regions analysed via the method involving restriction digestion (12). Similar findings were reported using radioactive labelling in mouse fibroblast and hamster kidney cell cultures (13). Later studies confirmed the presence of mtDNA methylation in mouse brain tissue using ELISA (14), in lymphoblastoid cells of Down Syndrome children using

*To whom correspondence should be addressed. Tel: + 61410808636; Email: veepatill@gmail.com
Correspondence can also be addressed to Zdenko Herceg. Tel: +33 4 72 73 83 98; Fax: +33 4 72 73 83; Email: hercegz@iarc.fr

mass spectrometry (15) as well as in human colorectal cancer cell lines (10) and human brain tissue (16) using immunoprecipitation. Pyrosequencing and bisulfite sequencing have also detected site specific mtDNA methylation in human blood cells (17–19). In addition, methylation-specific PCR techniques have detected substantial mtDNA methylation in liver tumour samples (11). Furthermore, the biological relevance of mtDNA methylation was suggested by a study showing that DNMT1 contains a targeted sequence upstream of its TSS that allows translocation into the mitochondria where it binds to the D-Loop (10). Elevated levels of DNMT1 correlated with increased expression of some mitochondrial genes adding weight to the notion that DNMT1 may have functional capacity in the mitochondria (10). Recently, DNMTIso3 (an isoform of DNMT1) was shown to be more concentrated in the mitochondria than DNMT1; suggesting that certain isoforms of DNA methyltransferases are mitochondria specific (20). Two independent studies reported the presence of DNMT1, DNMT3A and DNMT3B enzymes in the mitochondrial protein fraction of mouse skeletal muscle (21) and mouse embryonic stem cells (17). Finally, a more recent study utilized CpG and GpC methyltransferases to target mitochondrial DNA and concluded that increased GpC methylation decreased the abundance of mitochondrial encoded transcripts (22). Collectively these findings suggest the existence of mtDNA methylation, which may have a biological relevance, however mtDNA methylation remains debated largely due to contradictory reports from bisulfite sequencing studies (6,23). Since a genome-wide quantitative approach has not been demonstrated successfully for comprehensive mapping of mtDNA methylation patterns, exploration of the biological relevance of mtDNA methylation remains impeded.

Recently, several reports in the field aimed at improving techniques to be used for identification of mtDNA methylation however these studies focused primarily on CpG methylation (23–26). The present study builds on those findings by addressing key methodological adaptations which are required for investigating mtDNA methylation via whole genome bisulfite sequencing. This study presents the first report of genome-wide mitochondrial DNA methylation across different cell lines and tissue samples at single nucleotide resolution. The results show non-random, reproducible patterns of mtDNA methylation predominantly in a non-CpG context. Differences in global methylation for normal versus cancer cells derived from both liver and breast cancer are observed. Finally, the data implicates DNMT1, DNMT3A and DNMT3B to be associated with mtDNA methylation.

MATERIALS AND METHODS

Cell line selection

Normal breast epithelial cells MCF10A were maintained in DMEM (Invitrogen No. 11039-047) with 10% FBS, 1% penicillin-streptomycin, 20 ng/ml epidermal growth factor (Peprotech 1 mg), 0.5 μg/ml hydrocortisone (Sigma No. H-0888), 100 ng/ml cholera toxin (Sigma No. C-8052) and 10 μg/ml insulin (Sigma No. I-1882). Human breast cancer cells MCF7 were maintained in DMEM (Invitrogen No. 11039-047) with 10% FBS, 1% penicillin-streptomycin, sodium pyruvate (1 mM) and glutamine (2 mM). Human hepatocarcinoma cells HepG2 were maintained in DMEM (Invitrogen No. 11039-047) with 10% FBS and 1% penicillin-streptomycin. All cells were maintained in an atmosphere of 5% CO_2 at 37°C. Frozen pellets of primary derived human breast cancer cells (HMEC) were a gift from the Jiri Zavadil's lab and primary human hepatocytes were a gift from Prof. Michel Rivoire - Centre Léon Bérard (CLB), INSERM U1032, Lyon, France.

Mitochondrial DNA extraction

Frozen cell pellets (1×10^7 cells) were resuspended in 500 μl ice-cold homogenization buffer (100 mM Tris-HCl pH 7.4, 250 mM sucrose, 10 mmM EDTA) on ice. The cell pellet was homogenized with a 30G syringe and centrifuged (Eppendorf Centrifuge 5424 R) at 4°C, 1500 *g* for 10 min to collect debris. The supernatant was then transferred to a new tube and centrifuged again at 4°C, 10 000 *g* for 10 min. The pellet containing mitochondria was resuspended in 50 μl high-salt buffer (10 mM Tris-HCl pH 7.6, 10 mM KCl, 10 mM $MgCl_2$, 0.4M NaCl, 2 mM EDTA). About 8 μl of 10% SDS was then added to the homogenate and the homogenate was incubated for 7 min at 55°C to denature and solubilize proteins. Proteins were then removed by addition of 20 μl of 5 M NaCl and centrifugation at 11 300 *g* for 20 min at room temperature. The supernatant was collected into a new 1.5 ml Eppendorf tube. Twice the volume of 100% ethanol was added and the supernatant was centrifuged for 10 min at 10 000 *g* for precipitation of the mtDNA pellet. The pellet was resuspended in 50 μl of milliQ H20 and immediately processed with phenol-chloroform method for clean-up. An equal volume of phenol/chloroform/isoamyl alcohol (25:24:1) was added and sample was mixed gently by inverting the tube. The tube was then centrifuged at room temperature for 5 min at 12 000 *g*. The top aqueous layer was carefully collected and the same process was repeated with chloroform/isoamyl alcohol (24:1). To the upper aqueous layer, collected in a fresh tube, 1/10th volume of 3 M NaOAc (pH 5.2), 2 μl glycogen (15 mg/ml Ambion) and 2.5× volume of absolute ethanol was added and mixed by gently inverting the tube. The mixture was incubated overnight at −20°C or for 2 h at −80°C. The crude mitochondrial pellet was obtained by centrifugation at 4°C for 15 min, 12 000 *g*. The pellet was resuspended in 20 μl MilliQ grade H20 and concentration of mtDNA was assessed using Qubit fluorometer. Multiple pellets of the same cell type were processed this way and mtDNA was pooled until a minimum 2 μg concentration was achieved for bisulfite modification.

DNA quality check

Relative enrichment of mtDNA to nuclear DNA of all extractions was assessed with qPCR to ensure the extractions were not contaminated with nuclear DNA. Primers specific to the mitochondrial genome, Forward Primer (5′-GCTC AACACCCACTACCTAAA-3′), Reverse Primer (5′-TG ATCTGACGCAGGCTTATG-3′) as well as primers specific to nuclear encoded gene GAPDH, Forward Primer (5′-CCCTTCATACCCTCACGTATTC-3′), Reverse Primer

(5′-CCATTCTGTCTTCCACTCACTC-3′) were used to amplify the mtDNA extraction. The quality of the extraction was assessed by comparing the fold change of mitochondrial genome versus nuclear genome using the ΔC_t method.

Mitochondrial DNA pre-processing

Linearization of 700 ng of HepG2 mtDNA was achieved via a 10-min incubation of mtDNA at 65 degrees to encourage uncoiling followed by a 9-h incubation with 2U of BamHI restriction enzyme and NEB Buffer. Linearization was confirmed by visualization on 1% Agarose gel. Subsequently, sonication was selected as a better method since this has been shown to improve library preparation quality specifically for NGS in the context of plasmid DNA (27). Since mtDNA is of a similar structure to plasmid DNA, all mtDNA samples were sonicated with the Diagenode bioruptor Next Gen until fragments between 100 and 10 000 bp was achieved. MtDNA from each cell type was diluted to an appropriate concentration determined experimentally and sonicated with different conditions ranging from 3 cycles on the HIGH setting to 25 cycles on HIGH setting with a sonication time of 30 s per cycle. Fragment sizes of HepG2 cells were initially assessed on the BioAnalayser as well as 1% Agarose gel to confirm the method works. All other samples were subsequently checked on 1% Agarose gel to ensure no visible secondary structure remained. The mtDNA was then bisulfite modified using the EZ DNA Methylation Gold Kit (Zymo Research, USA), and the bisulfite modified DNA was quantified on Nano Drop using the ssDNA setting.

Pyrosequencing

Bisulfite modified DNA was amplified with previously published pyrosequencing primers ((19); Supplementary Table S1) in a 50 μl reaction. Following visualization of amplicon via gel agarose, 45 μl of PCR product was used with the PyroMark Kit (QIAGEN Cat. No. 972804) for each sequencing reaction as per manufacturer instructions. Briefly, DNA was immobilized on to streptavidin-coated beads in binding buffer for 10 min. The biotin-labeled template was purified using the pyrosequencing vacuum prep tool and incubated with 10 pmol/reaction sequencing primer in annealing buffer (20 mM Tris-acetate, 2 mM $MgAc_2$; pH 7.6). The DNA strands were denatured at 80°C for 2 min and reannealed at room temperature for 10 min. Sequencing was performed according to manufacturer instructions.

Library preparation and next-generation sequencing

Library preparation of the extracted, phenol-chloroform cleaned, sonicated and bisulfite modified mtDNA was then performed using the TruSeq DNA Methylation Kit (Illumina, EGMK81312) according to manufacturer instructions. Briefly, 200 ng of bisulfite-converted mtDNA was ligated to adapters and amplification indexes from the TruSeq Indexes Kit (Illumina) were introduced during PCR amplification. Adapter-Tagged libraries were purified using AMPure beads (Beckman Coulter). Libraries were assessed on Bioanalyser for quality assurance. Libraries were then subjected to 150 bp paired-end sequencing using the Illumina MiSeq instrument.

Bioinformatics—data filtering and alignment

For all WGBS runs, internal controls showed greater than 95% of all reads were detected by the MiSeq to be ≥ Q30. Just over 45 million reads passed filter for all samples. All reads that passed filter from the MiSeq were then further assessed through FastQC v0.11.3 for standard quality control. Reads were trimmed with Trimgalore version 0.4.4 with a minimum quality cut off of 28 bp and a minimum length cut off of 30 bp. Following adapter trimming, all reads below a QC threshold of 30 were discarded. Mapping and methylation calls were done using BSMAP v2.42 (28).

For MeDIP runs, TrimGalore software was used to http://www.bioinformatics.babraham.ac.uk/projects/trim_galore/) (29) to remove the custom adapters of the paired-end sequences, and 20 additional nucleotides from each 3-prime end, due to the specific requirements of the sequencing kit. The custom adapters were GCCAAT, CAGATC, CTTGTA and AGTCAA, for both read files of sample 'HepG2', 'HepG2-replicate', 'Hepatocyte' and 'Hepatocyte-replicate', respectively. The NC_012920.1 mitochondrial genome was used as the reference genome for the alignment that was done by bowtie2 software (30). The same software was used to perform the paired-end alignment and obtained SAM files. After replacing 'NC_012920.1' by 'chrM', sorted BAM files were generated with samtools (31) and the indexes were obtained of each file using the command index. Next, the BAM files were uploaded into the Integrative Genome Viewer (IGV) software to obtain the read profile of each sample and their plots and calculated the differential methylation across the mitochondrial chromosome by using the default parameters of the MEDIPS R package (32). Briefly, we used chromosome M of the 'BSgenome.Hsapiens.UCSC.hg38' library as a reference genome and fixed a P value = 1e-3 as a maximum of stacked reads per genomic position, extending all reads to a length of 300 nucleotides according to the given strand information and dividing the genome into adjacent windows of length = 100 nucleotides.

Noise filtering of mitochondrial DNA methylation sequencing data

Conventional methods used for assessing bisulfite conversion efficiency of nuclear DNA (33), which require spiking samples with λ DNA, were unsuccessful for sequencing of mtDNA (data not shown). Hence, in order to assess the quality of the sequencing reads, apart from standard read filtering methods described above, a 100% unmethylated plasmid DNA (ThermoFisher Scientific Cat. No SD0021) sample was processed and sequenced alongside the samples of interest. The amount of potential incorrect methylation calls was assessed from these data to determine the threshold of sequencing reads that need to be considered for avoiding potential false positive methylation calls. The following formula was used:

$$\text{False Positive Rate} = \left[\left(\frac{\#\text{methylated cytosines in plasmid genome}}{\text{total \# cytosines in plasmid genome}}\right) * 100\right]$$

From this analysis, we found that including data points under the threshold of 10 reads and all cytosines with methylation levels under 9% considerably increased the false positive detection of methylation, decreasing the accuracy to <97%. Therefore, for all datasets, all sites with coverage of <10 reads as well as all sites with methylation levels under 9% were removed. This ensured that the methylation calls from the data are at least 98.95% accurate.

Methylation calculations

Descriptive Statistics on the global patterns of methylation across the four cell lines was conducted in order to compare between cell lines. The following formulas were used to determine the methylation ratio at individual cytosines, methylation index (MI) and proportion of methylation across the mitochondrial genome:

$$\text{Methylation Ratio} = \left[\frac{\#\text{ of reads identified as methylated for CpN site}}{\text{total }\#\text{ of reads aligned to that CpN site}}\right]$$

$$\text{Methylation Index Over a Region} = \left[\left(\frac{\text{sum of all mCpN sites}}{\text{total }\#\text{ of CpN sites}}\right) * 100\right]$$

$$\text{Proportion of Methylation} = \left[\left(\frac{\#\text{ of methylated cytosines}}{16597}\right) * 100\right]$$

Non-parametric, paired and unpaired Wilcox *T*-test was used to calculate significant differences between mean methylation of functionally relevant genomic regions between cell types.

Methylated DNA immunoprecipitation

A total of 1.2 μg of mtDNA per reaction was extracted as outlined in the 'Mitochondrial DNA Extraction' section above from HepG2 and hepatocyte cells. Cell lines were processed in technical duplicate using the Auto MagMeDIP Kit (Diagenode #C02010013) as per instructions. Briefly, extracted mtDNA was sonicated, quantified and assessed for fragment size and quality via Qubit and BioAnalyser. Immunoprecipitation was conducted by pre-set protocols on the IP-Star Compact robot (Diagenode) that performed the necessary antibody incubation and washing steps required. Library preparation for sequencing of the MeDIP output mtDNA was then performed using the ACCEL-NGS Methyl-Seq DNA Library Kit (Swift Bioscience #30024) as per manufacturer instructions.

RNA interference-mediated knockdown of DNMT enzymes

Small interfering RNAs (siRNAs) were introduced into MCF10A cells by transfection using the Lipofectamine® RNAiMAX Reagent (Invitrogen) according to the manufacturer instructions. Cells were transfected with 100 nM of the following human ON-TARGET*plus* SMARTpools (Dharmacon): DNMT1 (ON-TARGET plus SMARTpool siDNMT1, L-004605-00-0005), DNMT3a (ON-TARGET plus SMARTpool siDNMT3a, L-006672-01-0005), DNMT3b (ON-TARGET plus SMARTpool siDNMT3b, L-006395-00-0005) or ON-TARGET plus non-targeting pool (D-001810-10-05) that was used as a negative control. Cells were harvested 96 h post-transfection and protein was extracted to validate the silencing with western blot.

Western blot analysis of DNMT enzymes

Whole cell protein lysates were extracted using ice-cold RIPA buffer supplemented with protease inhibitors. Protein (50 μg) was subjected to SDS-PAGE followed by immunoblotting. Primary antibodies against DNMT3a (ab13888, 1:500) and DNMT3b (ab13604, 1:500) were obtained from Abcam. Monoclonal antibodies against DNMT1 (MAB0079, 1:1000) and β-actin (Clone C4, 1:1000) were obtained from Abnova and MP Biomedicals, respectively.

Relative protein levels were quantified by ImageJ (https://imagej.nih.gov/ij/). The relative intensity was calculated for each DNMT band with respect to the siControl and normalized to the relative intensity of actin in each sample.

Mitochondrial DNA content assessment

Whole cell DNA and RNA extractions were performed using the All Prep DNA/RNA Mini Kit (Qiagen, REF80204) according to manufacturer instructions. The mitochondrial DNA content in each cell type was determined using qPCR on whole cell DNA extractions. Primers specific to the mitochondrial genome, Forward Primer (5′-GCTCAACACC CACTACCTAAA-3′), Reverse Primer (5′-TGATCTGA CGCAGGCTTATG-3′) as well as primers specific to nuclear encoded gene GAPDH, Forward Primer (5′-CCCTTC ATACCCTCACGTATTC-3′), Reverse Primer (5′-CCAT TCTGTCTTCCACTCACTC-3′) were used to amplify the whole cell DNA extraction. The mtDNA content of the extraction was assessed by comparing the fold change in expression of mitochondrial genome versus nuclear genome using the ΔC_t method.

mRNA expression analysis

Following cDNA synthesis from the above RNA extractions, relative enrichment of mRNA expression of mitochondrial encoded genes was assessed with qPCR using previously published primers (see Supplementary Table S1). GAPDH, Forward Primer (5′AACGGGAAGCTTGTCA TCAA-3′), Reverse Primer (5′TGGACTCCCACGACGT ACTCA-3′), was used as housekeeping gene for breast cell types. SFRS4, Forward Primer(5′-GGCTACGGGA AGATCCTGGA-3′), Reverse Primer (5′-TGCATCACGC AGATCATCAA-3′), was used as housekeeping gene for liver cell types (34). In order to compare mRNA expression between cell lines, mRNA expression was normalized to the mtDNA content in each cell in order to account for vastly differing mitochondrial DNA content between cell types:

$$\text{Gene Expression Normalized} = \frac{\Delta\text{Ct mRNA Expression relative to housekeeping gene}}{\Delta\text{Ct Mitochondrial DNA amount relative to nuclear DNA}}$$

RESULTS

Development of NGS methodology for high-resolution DNA methylation analysis specifically for the mitochondrial genome

To investigate genome-wide mtDNA methylation patterns at single base pair resolution in human normal and can-

cer cell lines and tissues, we aimed to optimize the method that combines bisulfite conversion with NGS. To this end, the mtDNA enrichment achieved from the extraction protocol was confirmed by qPCR analysis using mitochondrial and nuclear specific primers (Figure 1A). Based on previous studies, mtDNA was initially extracted from HepG2 cells and linearized with restriction enzyme BamHI in order to avoid bisulfite conversion inefficiency as previously described (24). This was then followed by deep sequencing using the MiSeq platform. The degree of methylation detected at each cytosine position was compared to the sequencing depth achieved for that position (Figure 1B). In line with previous reports, the data showed that only small methylation values had high sequencing depth and that reads exhibiting higher methylation values had low sequencing depth (23). Moreover, the ratio of sequencing reads (not shown) which aligned to the H-strand compared to the L-strand was also uneven (0.08), suggesting some amplification bias. However, mtDNA that was fragmented mechanically prior to bisulfite modification and sequencing, eliminated this strand bias (ratio = 1.16) (Figure 1C). Furthermore, the cells that were sonicated prior to sequencing also produced far better coverage (Figure 1E). Hence, all further samples were fragmented before bisulfite modification and subsequent sequencing.

To ensure quality methylation calls, 100% unmethylated plasmid DNA was processed and sequenced simultaneously alongside the mtDNA samples (Figure 1F). When all methylation calls with <10× coverage and <9% methylation were excluded, 378 cytosines remained false positive out of a potential 24 182 cytosines. Hence 98.44% accuracy in methylation calls can be achieved with minimum 10× coverage and a detection threshold of 9% methylation. All reads not matching this threshold criteria were excluded as background noise (see 'Materials and Methods' section).

To further confirm that these results are not the consequence of bisulfite conversion-related false positives, mitochondrial DNA of HepG2 cells and primary hepatocytes were processed via a bisulfite-free method to confirm that the mtDNA is methylated. MeDIP-seq assay performed on technical replicates of two cell lines also showed that the mitochondrial genome was globally methylated, hence complementing the WGBS data (Supplementary Figure S1A).

The results indicate this stringent approach allows adequate investigation of mtDNA methylation at single base pair resolution that accounts for both CpG and non-CpG methylation.

Mitochondrial DNA within normal and cancer liver cells exhibit significantly different methylation patterns that are primarily in a non-CpG context

In order to establish baseline methylation patterns within the mitochondrial genome, normal liver cells derived from primary human liver (hepatocytes) and liver cancer cells (HepG2) were assessed first. Globally, in both cases, the L-strand displayed a higher degree and frequency of methylation compared to the H-strand (Figure 2A and B). Hepatocytes had 37% of all cytosines were methylated, whereas HepG2 had 44% of their mitochondria methylated (Figure 2C). Interestingly, in contrast to nuclear DNA, a substantial amount of methylation in the hepatocyte and HepG2 mitochondrial genome was detected in CpT, CpC and CpA contexts. The highest frequency of methylation (around 30%) was detected within a CpT and CpC dinucleotide context, whereas methylation of CpG sites had the lowest methylation frequency (12% and 5%, respectively) (Figure 2C). A striking difference in methylation was observed across tRNA encoding regions. Specifically, hepatocytes are completely devoid of methylation on the L-strand within tRNAs which carry the amino acids arginine and lysine (Arg and Lys MI = 0%) (Figure 2D); however, these same regions are methylated in HepG2 cells (MI = 11.4%) (Figure 2D). Significant differences in mean methylation across almost all gene encoding regions in both strands of HepG2 was detected compared to hepatocytes (P value < 0.001; Figure 2E). In addition, the distribution of methylation values across the displacement loop in each cell type was compared since this region contains multiple promoters and functionally relevant transcriptional start sites. Hepatocytes showed a bimodal distribution of methylation values indicating both highly and lowly methylated regions across the D-Loop, whereas HepG2 showed a right skewed distribution indicating the D-Loop is mostly highly methylated (Figure 2F). Methylation across the L-strand promoter region (392–435 bp) was compared to the level of ND6 mRNA expression in each cell type. Finally, the higher methylation across the L-strand promoter region detected in HepG2 was associated with lower expression of ND6 mRNA compared to hepatocytes (Figure 2G).

To ensure biological relevance of mtDNA methylation in the disease context, primary tissue resections of normal liver and hepatocellular carcinoma samples were also examined (Supplementary Figure S2). Similar to the cell line samples, significant differences (P value < 0.001) in mean methylation of both global and some gene-encoding regions across both strands was observed (Supplementary Figure S2A and C). Both primary samples showed a bimodal distribution of methylation values across the D-Loop, however in line with methylation patterns observed in cell line samples (Figure 2D), this distribution was slightly skewed toward the right in tumour cells (Supplementary Figure S2B).

Together these results show that specific mtDNA methylation profiles across biologically relevant genomic regions can be observed among different normal and cancer cell types.

Baseline mitochondrial methylation patterns of normal and cancer breast cell lines differ significantly

To test the generality of mitochondrial genome methylation, baseline mtDNA methylation patterns were next examined in an independent cell type. MtDNA isolated from normal mammary epithelial cells (MCF10A) and breast cancer cells (MCF7) were assessed and compared. Similar to the liver context, globally in both cases, the L-strand displayed a higher degree and frequency of methylation compared to the H-strand (Figure 3A and B). MCF10A had 43% of the entire mitochondrial genome methylated, whereas MCF7 had 38% of their mitochondria methylated (Figure 3C). In contrast to nuclear DNA, and much like what was observed in liver cells, a substantial amount of

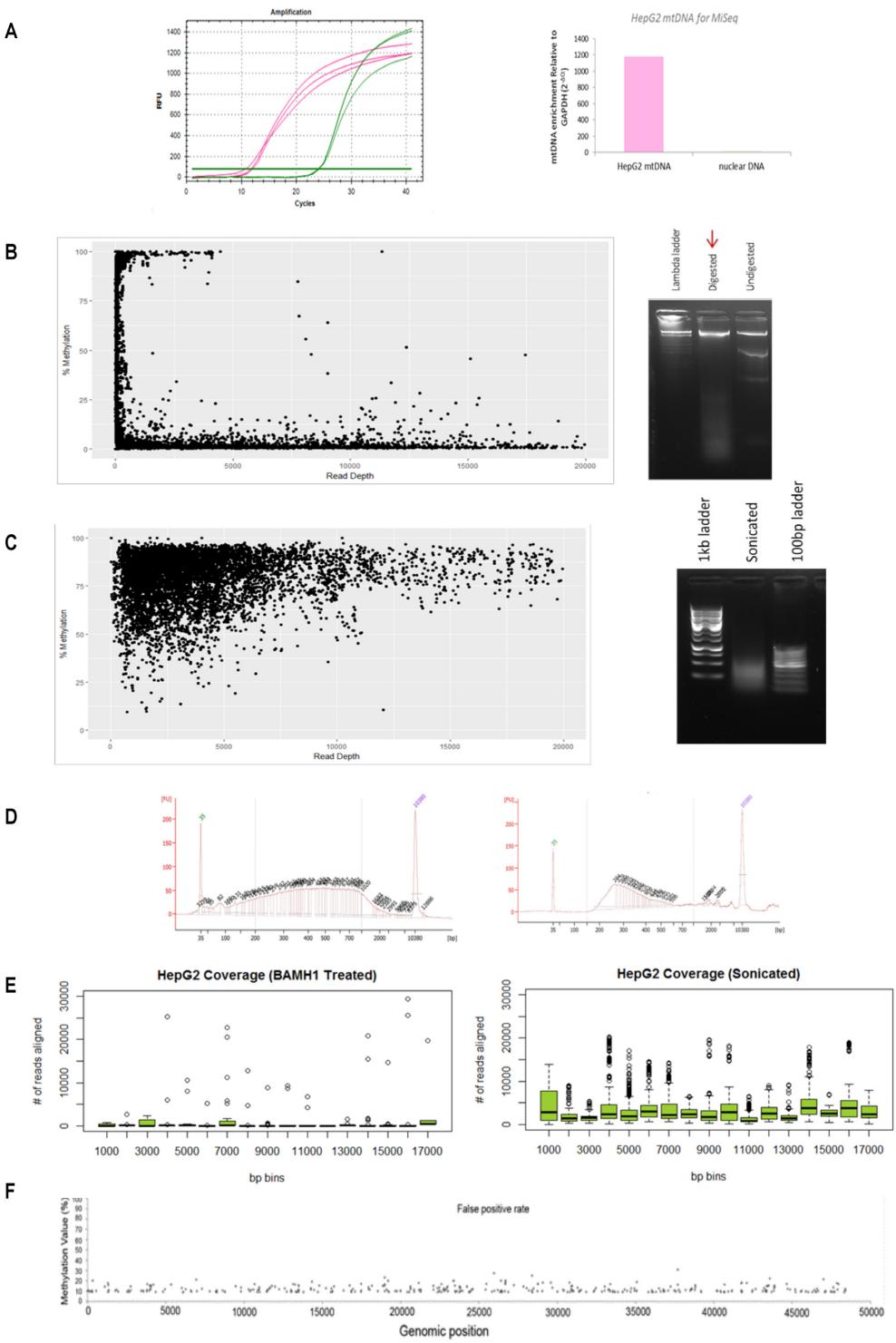

Figure 1. Mitochondrial DNA sequencing requires method adjustments. (**A**) Raw amplification cycles of mtDNA enrichment assessed with qPCR of a mitochondrial specific genomic region compared to nuclear specific GAPDH genomic region (left panel). Relative fold enrichment of mtDNA to nuclear DNA ($2^{-\Delta Ct}$) for HepG2 mtDNA extractions is indicated (right panel). The lack of nuclear DNA enrichment confirms the quality of mtDNA extraction. (**B**) Cytosine methylation compared to sequencing read depth (left panel) of HepG2 mtDNA which was digested with 2U of *BamHI* overnight at 37°C and visualised on agarose gel (right panel). (**C**) Cytosine methylation compared to sequencing read depth (left panel) of HepG2 mtDNA that was fragmented via sonication (100–7000 bp) and visualized on agarose gel (right panel). (**D**) HepG2 sonicated mtDNA (left panel) and bisulfite modified mtDNA (right panel) was assessed on the BioAnalyser to ensure sonication was efficient and that modified mtDNA produced the standard expected curve. (**E**) Average number of reads aligning to the mitochondrial genome per 1000 bp. HepG2 sample that was sonicated prior to sequencing showed an improvement in coverage compared to the BamHI-treated HepG2 sample. (**F**) A 100% unmethylated plasmid DNA control was processed and sequenced alongside mtDNA samples to ensure an appropriate false positive threshold can be used for data analysis. The *X*-axis represents the genomic position of the plasmid genome (48 kb). The *Y*-axis represents the methylation value detected at each cytosine. The dots represent the 1.56% false detection rate.

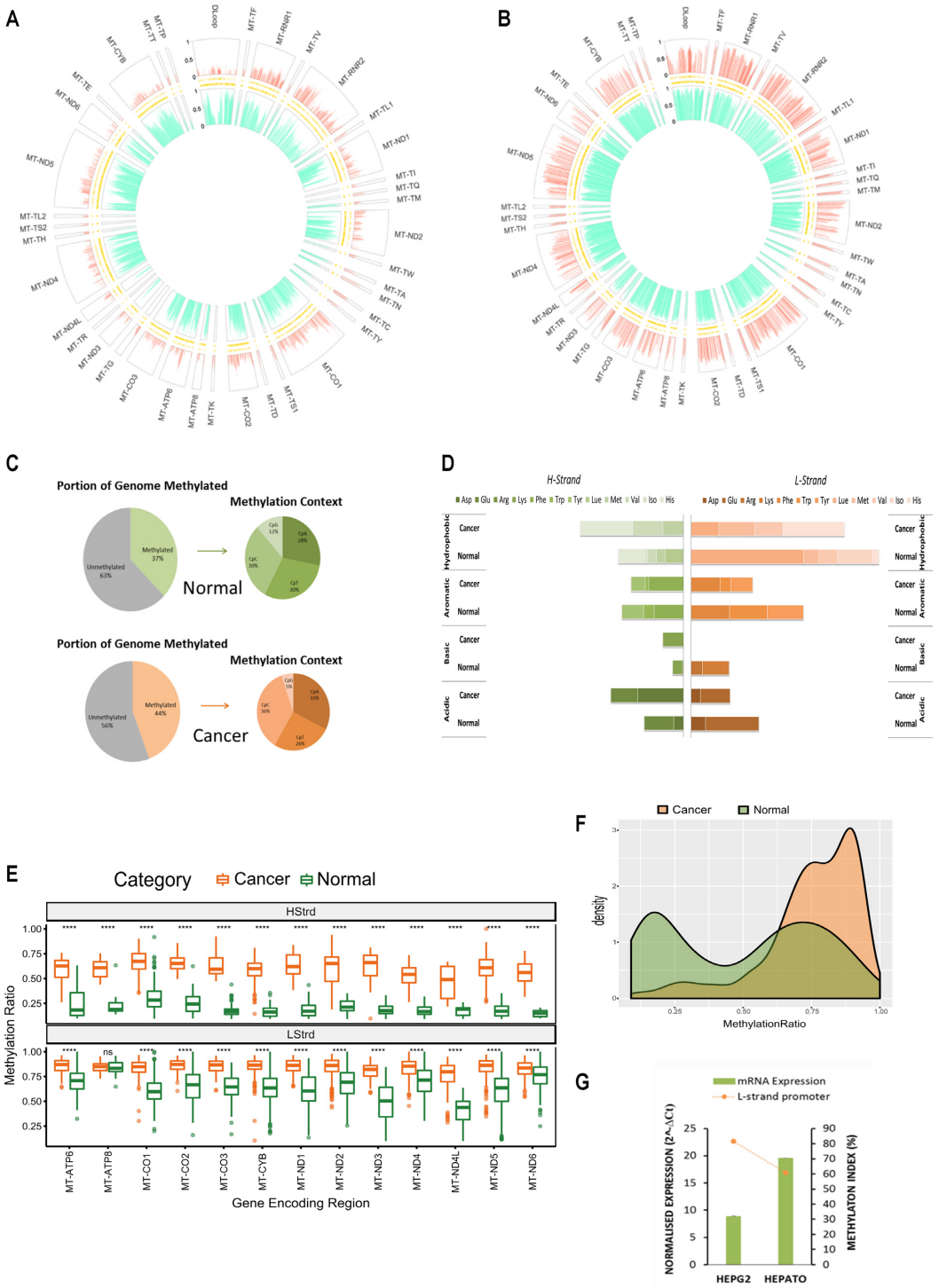

Figure 2. Baseline patterns of the mitochondrial methylome in normal and cancer liver cells. (**A** and **B**) MtDNA isolated from hepatocytes and liver cancer cells (HepG2) that was sequenced using the NSG MiSeq platform as described in Figure 1. The circular plot represents genomic position (1–16 kb) of all methylated cytosines with respect to sequence order. Each segment of the circle represents a separate functionally relevant region, tRNA, rRNA, gene or D-Loop. The *Y*-axis indicating that methylation level is represented on the left-hand side of the D-Loop segment. The large outer ring displays methylation at each cytosine within the H-Strand, whereas the large inner ring displays methylation at each cytosine on the L-Strand. Thin inner bands indicate the genomic position of all cytosines within the H-Strand and L-Strand sequence. Global mtDNA methylation patterns differ between hepatocytes and cancer cells and are also strand specific. (**C**) Summary statistics of the frequency of mitochondrial mCpN context in liver cells. (**D**) Methylation Index across tRNA encoding regions in liver cancer versus normal cells. Each horizontal segment compares the MI within tRNAs that have been grouped according to the amino acid they carry (acidic, basic, aromatic or hydrophobic). The left panel indicates MI across H-Strand and right panel indicates MI across L-Strand. (**E**) Comparative boxplots indicating significant ($P < 0.001$) difference of mean methylation across gene encoding regions of normal versus cancer cells in each strand. (**F**) Density plot of the distribution of methylation values along the D-Loop region. (**G**) Relative ND6 mRNA expression normalized to mtDNA amount compared with methylation index across the LSP. High LSP methylation associates with low ND6 expression.

Figure 3. Baseline patterns of the mitochondrial methylome in normal and cancer breast cells. MtDNA was sequenced using the NSG MiSeq platform. The circular plot represents genomic position (1–16 kb) of all methylated cytosines with respect to sequence order. Each segment of the circle represents a separate functionally relevant region, tRNA, rRNA, gene or DLoop. The *Y*-axis indicating methylation level is represented on the left-hand side of the D-Loop segment. The large outer ring displays methylation at each cytosine within the H-Strand whereas the large inner ring displays methylation at each cytosine on the L-Strand. Thin inner bands indicate the genomic position of all cytosines within the H-Strand, L-Strand sequence. Global mtDNA methylation patterns differ between these cell types and are also strand specific. (**A**) Normal breast epithelial cells (MCF10A); (**B**) Cancer epithelial cells (MCF7); (**C**) Summary statistics of the frequency of mitochondrial mCpN context in liver cells and (**D**) Methylation Index across tRNA encoding regions in breast cancer versus normal. Each horizontal segment compares the MI within tRNAs that have been grouped according to the amino acid they carry (acidic, basic, aromatic or hydrophobic). The left panel indicates MI across H-Strand and right panel indicates MI across L-Strand. (**E**) Comparative boxplot indicating significant ($P < 0.001$) difference of mean methylation across gene encoding regions of normal versus cancer cells in each strand. (**F**) Density plot of the distribution of methylation values along the D-Loop region. (**G**) Relative ND6 mRNA expression normalized to mtDNA amount compared with methylation index across the LSP. High LSP methylation associates with low ND6 expression

methylation in the MCF10A and MCF7 mitochondrial genome was detected in CpT, CpC and CpA contexts. Again, the highest frequency of methylation was detected within a CpT or CpC dinucleotide context, whereas methylation of CpG sites was the least frequently methylated dinucleotides (12% and 10%, respectively) (Figure 3C). In breast cells a different pattern of tRNA methylation was observed compared to liver cells. On the H-strand of breast cancer cells (MCF7) (Figure 3D), methylation in tRNA encoding regions, which carry the amino acids arginine, lysine, asparagine and glutamine, is almost completely lost (MI = 0.29%) compared to normal breast (MCF10A) cells (MI = 8.84%) (Figure 3D). The distribution of methylation values across the displacement loop in each cell type was compared since this region contains multiple promoters and functionally relevant transcriptional start sites. MCF7 exhibited a bimodal distribution of methylation values indicating the presence of both highly and lowly methylated regions across the D-Loop, whereas MCF10A showed a right skewed distribution, consistent with high level methylation in the D-Loop (Figure 3F). Methylation levels across the L-strand promoter region (392–435 bp) were then compared with the level of ND6 mRNA expression in each cell type. Higher methylation across the region detected in MCF10A coincided with lower expression of ND6 compared to MCF7 (Figure 3G), these findings were consistent with those observed in liver cells.

To investigate concordance of baseline methylation patterns among cell types, additional normal liver (HepaRG) and normal breast (HMEC) cell lines were subjected to mtDNA methylation profiling. Significant differences in mean methylation of both global as well as some gene encoding regions across both strands was observed between HMEC and MCF10A cells (Supplementary Figure S2D–F) as well as hepatocytes and HepaRG cells (Supplementary Figure S2G–I).

Together these results provide further evidence to the generality of previously mentioned methylation patterns and confirm the methylation patterns are cell type specific.

DNMT3B, DNMT3A and DNMT1 are involved in modulating mtDNA methylation

Since multiple DNMTs have previously been detected in the mitochondria by various independent studies (10,17,20,21), it was important to assess the dependence of mtDNA methylation patterns on different DNMT enzymes. Thus, the impact of knockdown of DNMT1, DNMT3A and DMT3B on mtDNA methylation was assessed using a siRNA approach. Global cellular protein levels of each enzyme were depleted individually in MCF10A cells (Supplementary Figure S3) and was followed by mtDNA methylation analysis. Silencing of all three DNMT enzymes resulted in markedly reduced levels of cytosine methylation globally across the MCF10A mitochondrial genome compared to the control cells (Supplementary Figure S4).

The degree and frequency of methylation were especially affected in the DNMT3B silenced cells (Figure 4A and B) with the L-strand most heavily affected (Figure 4A and B), therefore the impact of DNMT3B knockdown on mtDNA methylation was analysed in further detail. Methylation between DNMT3B knockdown and control cells showed the L-strand in both cases displayed a higher degree and frequency of methylation compared to the H-strand (Figure 4A). Significant decreases (P value < 0.001) were observed in global methylation in the knockdown cells as well as within gene encoding regions on both strands (Figure 4C and E). The distribution of methylation values across the displacement loop in the knockdown cells was also observed to be markedly lower than in control cells (Figure 4D). To assess potential functional impact of the observed mtDNA methylation loss, mRNA expression of a set of mitochondrial genes was analysed in DNMT3B knockdown cells. A drop in methylation in the D-Loop region in DNMT3B knockdown cells, which accounts for a drop in methylation across all promoter regions, resulted in higher mRNA expression of the genes COX1, COX3, ND4, ND4L and ND5 (Figure 4G). Furthermore, similar to previous observations, the drop in global methylation induced by DNMT3B knockdown resulted in reduced methylation of the LSP and this was found to be concomitant with an increase in mRNA expression of the ND6 gene (Figure 4H).

Since knockdown experiments implicated a potential role for DNMTs in mtDNA methylation, whether DNMT enzymes are present in mitochondria was further explored with confocal microscopy. Analysis of 2D images suggest small amounts of all three DNMT1, DNMT3A and DNMT3B may be co-localized in both MCF7 and HepG2 cells (Supplementary Figure S4); however, additional assays such as z-stack imaging are needed to confirm and consolidate these data.

Together these results suggest that DNMT1, DNMT3A and DNMT3B enzymes may be associated with the observed baseline methylation patterns of the mitochondrial genome and there may be a link between mtDNA methylation and gene expression as is the case in the nuclear genome.

DISCUSSION

The present study for the first time combines appropriate stepwise methodology for quantitatively assessing genome-wide mtDNA methylation at both CpG and non-CpG methylation sites with base-pair resolution. This methodology has revealed human mitochondrial genomes can be extensively methylated. Results show that the methylation is cell type specific occurs predominantly in a non-CpG context and is more heavily present on the L-strand than the H-Strand. MtDNA methylation can be modulated by decreasing global protein levels of DNMT1, DNMT3A and DNMT3B enzymes, suggesting an association of these enzymes with mtDNA methylation. A potential functional relevance of this methylation is suggested by the observed association between mtDNA methylation levels within the displacement loop region and mRNA of relevant genes encoded on the mitochondrial DNA. Considering the different mitochondrial methylome patterns observed in the normal and cancer cells examined, this study suggests important implications for the role of mtDNA methylation in tumorigenesis.

There are three crucial steps in methodology that is unique and specific for WGBS of mtDNA in this study

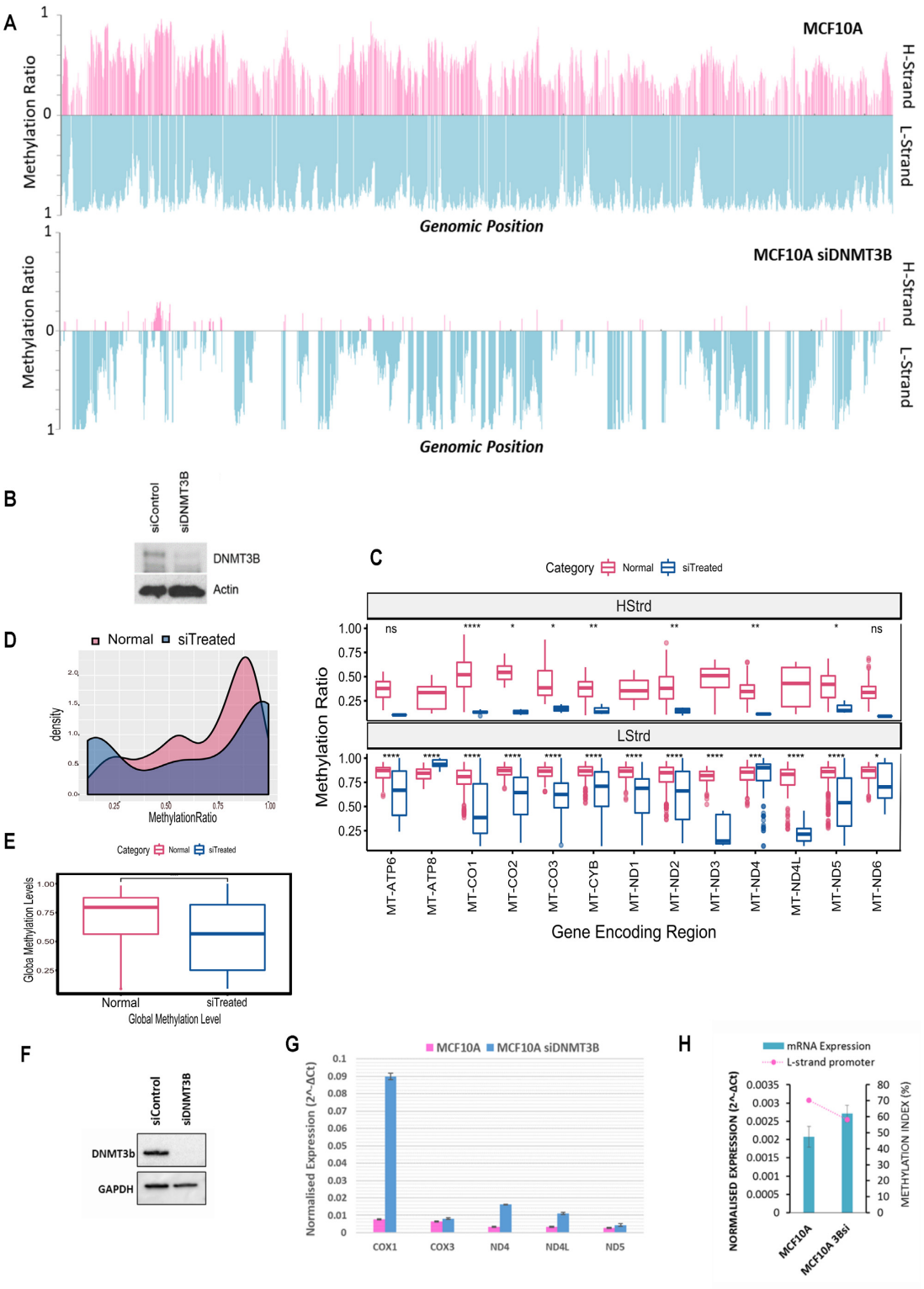

Figure 4. Silencing DNMT3B modulates mitochondrial DNA methylation concomitant to expression changes of mitochondrial transcripts. (**A**) MtDNA methylation in MCF10A cells exposed to a 96-h treatment of DNMT3B siRNA compared to control. A global drop in methylation ratio is observed for H and L strand methylation in DNMT3Bsi treated cells. (**B**) Whole cell protein was assayed for relative amounts of DNMT3B via western blot to confirm assay efficiency. (**C**) Comparative boxplot indicating significant ($P < 0.001$) difference of mean methylation across gene encoding regions of control versus knockdown treated cells in each strand. (**D**) Paired Wilcox *t*-test showing significance of the global drop in methylation between control and treated cells ($P < 0.001$). (**E**) Density plot of the distribution of methylation values along the D-Loop region. (**F**) Whole cell protein of repeat experiment assayed for relative amounts of DNMT3B via western blot to confirm efficiency. (**G**) Relative mRNA expression normalized to mtDNA amount compared of genes encoded on the H-strand. Treated cells show an increase in gene expression compared to control. (**H**) Relative ND6 mRNA expression normalized to mtDNA amount compared with methylation index across the LSP. High LSP methylation associates with low ND6 expression.

(Supplementary Figure S5). These are (i) the separation of mtDNA from nuclear DNA, (ii) removal of excess protein via phenol-chloroform and (iii) finally shearing of the mtDNA to ensure no coiled or secondary structures remain prior to bisulfite sequencing. The following describes how methodology may be a key contributor to underestimation of mtDNA in previous reports.

One of the key issues pertaining to sequencing mtDNA for methylation analysis is in understanding the intrinsic differences of mtDNA function and structure as well as how these differences require adaptation of existing methodologies which have evolved with a primary focus on nuclear DNA and CpG methylation. Liu *et al.*, for instance, showed that the mtDNA needs to be linearized prior to methylation analysis with pyrosequencing to avoid overestimation of methylation values owing to inefficient bisulfite conversion (24) caused by the coiled, circular structures of mtDNA. Results from this study concur with previous findings since in all cell lines analysed via pyrosequencing, linearized mtDNA via sonication showed lower methylation levels compared to unfragmented, circular mtDNA (data not shown). In addition, pyrosequencing detected lower amounts of mtDNA methylation than those detected by NGS (Supplementary Figure S1C). Since global methylation was observed in both methylation results from NGS and MeDIP-seq data of two different cell lines (Supplementary Figure S1A), it is likely that pyrosequencing may underestimate cytosine methylation of mtDNA due to its CpG nucleotide bias (Supplementary Figure S1C). One explanation for the discrepancy between pyrosequencing and NGS results can be attributed to the previously established notion that standard pyrosequencing assays are biased towards CpG methylation (35,36). This is especially relevant to the mitochondrial genome where the sequence is heavily dispersed with repetitive cytosine nucleotides ($n > 3$) throughout the genome. Hence methodology that adequately allows assessment of both CpG and non-CpG methylation is essential for investigating mtDNA methylation; this may be a possible explanation for previous reports that have concluded low or no mitochondrial methylation (6).

The complimentary bisulfite methylation data (Figure 2A and B) and MeDIP data (Supplementary Figure S1A) observed in this study is in line with previous reports that comprehensively showed cytosine methylation within mitochondrial genomes to be present across 39 pre-existing datasets spanning different human cell and tissue types (37). Although our results concur with conclusions made by Ghosh *et al.*, it should be noted that since the paper was first published, a series of methodological processing required to address bisulfite conversion efficiency that is unique for mtDNA has been reported (23,24). This may be another potential factor that has lead to the idea that mtDNA is generally lowly methylated. Pre-existing WGBS datasets were not produced with experimental considerations unique to mtDNA in mind. Hence assessing mtDNA methylation in these databases, although a viable option for exploratory analysis, may underestimate mtDNA methylation levels and this should be considered for future studies (37).

Accurate fragmentation is a key technical adaption that needs to be optimized in order to ensure high quality, reliable methylation reads from sequencing data. Recently, Mechta *et al.* concluded that secondary structures of mitochondrial DNA may have caused hindrance in the bisulfite conversion step leading to false positive methylation values (23). In concordance, results from this study further demonstrate that fragmentation of mtDNA is required for optimal mtDNA accessibility for accurate bisulfite conversion and sequencing (Figure 1). This was further consolidated by the high correlation ($R^2 = 0.97$) observed between biological replicate data (Supplementary Figure S1B). Accessibility needs to be addressed when considering mtDNA for bisulfite sequencing due to the highly coiled form it exists within cells (38). When cells were treated with BamHI and sequenced (Figure 1B), the data showed an almost exact match to the 'read depth versus methylation value' patterns obtained by Mechta *et al.* (23) and we concur this was most likely due to hindrance toward bisulfite conversion from secondary structures post linearisation (23). However, when mtDNA was fragmented through sonication a more even distribution of methylation values and sequencing depth was achieved (Figure 1C). One of the pitfalls of using sonication for fragmentation is the lack of control in obtaining fragment sizes. Each cell line had to be individually optimized (Figure 1D) through a rigorous process of trial and error until an ideal range of fragments were observed on agarose gel (∼100–7000 bp) and these size ranges were then confirmed with BioAnalyser. Since these fragments then underwent a further strenuous process of bisulfite conversion, it is possible that a number of fragments (especially fragments within 100–200 bp size) would have been more vulnerable to degradation, making them impossible to be incorporated in the library preparation stage. Indeed those mitochondrial DNA samples which were sonicated to the point where all fragments were within 100–200 bp range did not produce successful libraries (data not shown). Hence although not perfected, fragmentation via sonication can overcome secondary structure obstructions to bisulfite conversion. The data presented in this study have been validated via a secondary non-bisulfite dependent method (Supplementary Figure S1A) and shown to be reproducible ($R^2 = 0.97$) through cell line biological replicates (Supplementary Figure S1B). This line of evidence provides support that the data is unlikely to be false positive results.

Another key step in the methodology that is crucial for consideration is the phenol-chloroform extraction that immediately followed extraction of the crude mitochondrial DNA pellet (see 'Materials and Methods' section). Using crystal structure imaging, it has been previously shown that the mtDNA transcription factor TFAM binds to both H-Strand promoter, as well as non-specific mtDNA regions, and imposes U-turn shapes on the mtDNA. Hence, transcription factor binding encourages compaction and packaging of mtDNA molecules (38). This combined with the difficulty observed in HepG2 mtDNA double digestion with restriction enzymes BamHI and EcoRI (data not shown), we hypothesized that some protein–DNA interactions may have remained intact during the crude mtDNA extraction protocol. Since phenol-chloroform is a technique used to separate nucleic acids from proteins and lipids (39,40), it was added as a final step in the extraction method. After this step was added to the protocol, complete fragmentation of the mtDNA in subsequent steps was easier as

observed by number of sonication cycles required and visualization on agarose gel (data not shown). Hence there is a chance mtDNA bound transcription factors, and/or any restriction enzymes used for linearization, remain and encourage compaction of mtDNA following extraction methods that have not undergone phenol-chloroform clean up. Hence further investigation is required to confirm results from any reports (26,41) of mtDNA methylation that have relied on restriction enzyme digestion alone as this may be a point of hindrance in efficient bisulfite conversion of mtDNA. These findings show that methodology for bisulfite sequencing needs to be specifically adapted for mitochondrial genomes.

Since the D-Loop consists of promoter regions and is responsible for controlling mtDNA replication, we considered whether the frequency distribution of methylation within this region differs in normal and cancer contexts. A striking shift from the bimodal distribution of methylation frequency in normal liver cells was observed in liver cancer cells, which was strongly right skewed (Figure 2D). A similar but less pronounced pattern was also observed in primary liver and liver tumour resections (Supplementary Figure S2A–C). However, a different distribution of D-Loop methylation was observed in breast cancer and normal cells (Figure 3F). MtDNA content and cancer have been previously implicated in disease prognosis. For example, low mtDNA content was found to be associated with better survival (42) and treatment outcomes (43) for breast cancer patients, whereas low mtDNA content in liver has been associated with higher risk of developing non-alcoholic fatty liver disease, a precursor to cancer development (44). Since the D-Loop region is involved in mtDNA replication, whether D-Loop methylation determined by this study (Figures 2F, 3F and 4D) has direct regulatory consequences for mitochondrial replication should be investigated further. The functional consequences of this could mean a cell type specific layer of regulation concerning mtDNA replication that has remained unexplored.

Because MtDNA is known to insert into the nuclear genome, resulting in 'nuclear DNA sequences of mitochondrial origin' (NUMTs), the presence of NUMTs in some analytical procedures may generate misleading results (6,23). It is estimated that there are between 1000 and 10 000 copies of mtDNA in each mammalian cell (45); hence, the probability of identical sequences in the nuclear genome being amplified when mtDNA is the target sequence is extremely low due to the vast excess of mtDNA (6). Although mtDNA enrichment was confirmed using qPCR, to avoid any complication, data from this study was aligned to the human nuclear genome (Human Genome Assembly GRCh38.p12, June 2018) as well as to the mitochondrial genome alone (revised Cambridge Reference Sequence NC_012920, June 2018). Any reads that aligned to both were excluded to ensure only those reads that uniquely mapped to mtDNA were considered in the analysis. Therefore, the presence of NUMT sequences is highly unlikely to contribute to mtDNA methylation levels and patterns observed in this study.

Previous work investigating non-CpG methylation in the nuclear genome has shown a conservation of methylation context. The trend observed in nuclear genome, i.e. mCpG > mCpA > mCpT > mCpC (36), has been attributed to the observed patterns being non-random and hence biologically significant. Similarly in this study, distinct trends in the frequency of methylation at each dinucleotide, i.e. mCpC>mCpA /mCpT>mCpG, is largely conserved in all cell types. Further studies are warranted to examine the potential biological significance of the consistent occurrence of non-CpG methylation detected in mtDNA. In the nuclear genome, unlike CpG methylation, non-CpG methylation largely occurs asymmetrically and this has been attributed to its acute regulation in response to environmental stimuli/stressors. It has also been shown to regulate the expression of specific genes, in particular PGC-1a (35) which is involved in mitochondrial function and biogenesis. In the nuclear genome, characteristic areas of the genome, such as gene promoter regions, are often aberrantly hypo- or hypermethylated in cancer versus normal cells and this has been directly linked to transcriptional regulation of gene expression (46). Likewise, this study has shown a similar association where higher average promoter methylation of the L-strand has been concomitant with lower expression of ND6 between different cell types (Figures 2E, 3E and 4E). This suggests the detected methylation may play a role in strand specific regulation of gene expression. These results concur with previous investigations where gene expression was associated with induced promoter methylation within GpC dinucleotides (22). It should be noted that GpC methylation from the previous study has been reported as part of the CpN methylation in the present study. It is also noteworthy that in mtDNA, unlike in the nuclear genome, one promoter region such as the Origin of replication (100–441 bp) has been identified to regulate multiple genes (3,5). Previous reports have shown a link between the expression of specific genes, such as ND1, to be associated with induced GpC methylation within specific promoters such as HSP2 (22). To further emphasize this, strand specific methylation of CpG and adjacent CpN sites has been shown across a known transcription factor binding site (523–550 bp) of the mitochondrial genome in Supplementary Figure S4 (47). The complex relationship between multiple H-strand promoters and origins of replication in the D-Loop as well as varying distributions of methylation in the D-Loop between cell types observed in this study should be investigated further to determine any functional links to transcription of genes encoded on the H-strand. The asymmetry of non-CpG methylation has previously been attributed to its high response to environmental stimuli (36). In addition, mitochondria are known to be highly responsive to changing cellular conditions as part of many of their physiological functions such as maintaining cellular energy demands. Hence, it can be postulated that the detected mtDNA methylation could play a role in regulation of specific genes in a transient manner with respect to immediate cellular demand.

Another important finding from this study is that the methylation may be modulated by global cellular DNMT enzymes (Supplementary Figure S3). It is also noteworthy that DNMT3B was the enzyme that severely impacted the global frequency and amount of mtDNA methylation in normal breast cells (Figure 4). It should be noted that a wide variety of nuclear encoded genes are known to have direct, functional effects on mitochondrial processes

as well as mitochondrial DNA compaction and transcription (48). The effects of DNMT knockdown on these nuclear encoded genes and any potential consequential effects on the observed changes in mtDNA methylation cannot be ruled out. Co-operative maintenance of DNA methylation by the DNMT family of enzymes in the nuclear genome has been previously well characterized (49). However, little is known about the consequences of aberrant overexpression of DNMT3B in particular that has been reported for a number of malignancies including breast cancer (50) and colorectal cancer (51,52). Due to its high relevance in disease, there is a need for a better understanding of the complex interplay between the DNMT family of enzymes and how they may be involved in modulating mitochondrial DNA methylation. The complex nature of the nuclear-mitochondrial crosstalk, and how methylation of the two genomes plays a role (48) is another area of future investigation.

In summary, the present study demonstrates, for the first time via NGS-based bisulfite sequencing, that the mitochondrial genome is heavily methylated with predominant non-CpG methylation and that this methylation is associated with multiple DNMT enzymes. Furthermore, the results show that mtDNA methylation patterns are cell type specific and that they may be functionally linked to mitochondrial gene expression. Importantly, this study highlights key methodological requirements for adequate assessment of methylation within mitochondrial DNA. This study implores the importance of adapting methodology to allow assessment of both CpG and non-CpG methylation for future investigations. Future efforts aimed at deciphering the potential functional consequences and biological variances of mtDNA methylation may prove to be highly useful.

DATA AVAILABILITY

Available upon request.

SUPPLEMENTARY DATA

Supplementary Data are available at NAR Online.

ACKNOWLEDGEMENTS

HMEC cells were a gift from Jiri Zavadil's lab (Lyon, France), we would like to thank Dr Mauraj Pandey for optimizing growth conditions for the HMEC cells. Human primary hepatocytes were a gift from Prof. Michel Rivoire - Centre Léon Bérard (CLB), INSERM U1032, Lyon, France. We would like to thank Maud Michelet for technical assistance and isolation of PHHs; F. Zoulim and M. Rivoire for access to liver resections.

FUNDING

Institut National du Cancer (INCa, France); European Commission (EC) Seventh Framework Programme (FP7) Translational Cancer Research (TRANSCAN) Framework; Foundation ARC pour la Recherche sur le Cancer (France); Plan Cancer-Eva-Inserm research grant (to Z.H.); Postdoctoral Fellowship from International Agency for Research on Cancer (to V.P.), partially supported by the EC FP7 Marie Curie Actions – People – Co-funding of regional, national and international programmes (COFUND)'. Funding for open access charge: Institut National du Cancer (INCa, France); European Commission (EC) Seventh Framework Programme (FP7) Translational Cancer Research (TRANSCAN) Framework; Foundation ARC pour la Recherche sur le Cancer (France); Plan Cancer-Eva-Inserm research grant (to Z.H.).
Conflict of interest statement. The authors alone are responsible for the views expressed in this article and they do not necessarily represent the views, decisions or policies of the institutions with which they are affiliated.

REFERENCES

1. Porporato,P.E., Filigheddu,N., Pedro,J.M.B., Kroemer,G. and Galluzzi,L. (2018) Mitochondrial metabolism and cancer. *Cell Res.*, **28**, 265–280.
2. Chinnery,P.F. and Hudson,G. (2013) Mitochondrial genetics. *Br. Med. Bull.*, **106**, 135–159.
3. Tapper,D.P. and Clayton,D.A. (1981) Mechanism of replication of human mitochondrial DNA. Localization of the 5′ ends of nascent daughter strands. *J. Biol. Chem.*, **256**, 5109–5115.
4. Crews,S., Ojala,D., Posakony,J., Nishiguchi,J. and Attardi,G. (1979) Nucleotide sequence of a region of human mitochondrial DNA containing the precisely identified origin of replication. *Nature*, **277**, 192–198.
5. Fish,J., Raule,N. and Attardi,G. (2004) Discovery of a major D-loop replication origin reveals two modes of human mtDNA synthesis. *Science*, **306**, 2098–2101.
6. Hong,E.E., Okitsu,C.Y., Smith,A.D. and Hsieh,C.L. (2013) Regionally specific and genome-wide analyses conclusively demonstrate the absence of CpG methylation in human mitochondrial DNA. *Mol. Cell Biol.*, **33**, 2683–2690.
7. Maekawa,M., Taniguchi,T., Higashi,H., Sugimura,H., Sugano,K. and Kanno,T. (2004) Methylation of mitochondrial DNA is not a useful marker for cancer detection. *Clin. Chem.*, **50**, 1480–1481.
8. Gao,J., Wen,S., Zhou,H. and Feng,S. (2015) De-methylation of displacement loop of mitochondrial DNA is associated with increased mitochondrial copy number and nicotinamide adenine dinucleotide subunit 2 expression in colorectal cancer. *Mol. Med. Rep.*, **12**, 7033–7038.
9. Feng,S., Xiong,L., Ji,Z., Cheng,W. and Yang,H. (2012) Correlation between increased ND2 expression and demethylated displacement loop of mtDNA in colorectal cancer. *Mol. Med. Rep.*, **6**, 125–130.
10. Shock,L.S., Thakkar,P.V., Peterson,E.J., Moran,R.G. and Taylor,S.M. (2011) DNA methyltransferase 1, cytosine methylation, and cytosine hydroxymethylation in mammalian mitochondria. *Proc. Natl. Acad. Sci. U.S.A.*, **108**, 3630–3635.
11. Pirola,C.J., Gianotti,T.F., Burgueño,A.L., Rey-Funes,M., Loidl,C.F., Mallardi,P., Martino,J.S., Castaño,G.O. and Sookoian,S. (2013) Epigenetic modification of liver mitochondrial DNA is associated with histological severity of nonalcoholic fatty liver disease. *Gut*, **62**, 1356–1363.
12. Shmookler Reis,R.J. and Goldstein,S. (1983) Mitochondrial DNA in mortal and immortal human cells. Genome number, integrity, and methylation. *J. Biol. Chem.*, **258**, 9078–9085.
13. Nass,M.M. (1973) Differential methylation of mitochondrial and nuclear DNA in cultured mouse, hamster and virus-transformed hamster cells. In vivo and in vitro methylation. *J. Mol. Biol.*, **80**, 155–175.
14. Dzitoyeva,S., Chen,H. and Manev,H. (2012) Effect of aging on 5-hydroxymethylcytosine in brain mitochondria. *Neurobiol. Aging*, **33**, 2881–2891.
15. Infantino,V., Castegna,A., Iacobazzi,F., Spera,I., Scala,I., Andria,G. and Iacobazzi,V. (2011) Impairment of methyl cycle affects mitochondrial methyl availability and glutathione level in Down's syndrome. *Mol. Genet. Metab.*, **102**, 378–382.

16. Devall,M., Smith,R.G., Jeffries,A., Hannon,E., Davies,M.N., Schalkwyk,L., Mill,J., Weedon,M. and Lunnon,K. (2017) Regional differences in mitochondrial DNA methylation in human post-mortem brain tissue. *Clin. Epigenetics*, **9**, 47.
17. Bellizzi,D., D'Aquila,P., Scafone,T., Giordano,M., Riso,V., Riccio,A. and Passarino,G. (2013) The control region of mitochondrial DNA shows an unusual CpG and non-CpG methylation pattern. *DNA Res.*, **20**, 537–547.
18. Byun,H.M., Colicino,E., Trevisi,L., Fan,T., Christiani,D.C. and Baccarelli,A.A. (2016) Effects of air pollution and blood mitochondrial DNA methylation on markers of heart rate variability. *J. Am. Heart Assoc.*, **5**, e003218.
19. Baccarelli,A.A. and Byun,H.M. (2015) Platelet mitochondrial DNA methylation: a potential new marker of cardiovascular disease. *Clin Epigenetics*, **7**, 44.
20. Saini,S.K., Mangalhara,K.C., Prakasam,G. and Bamezai,R.N.K. (2017) DNA Methyltransferase1 (DNMT1) Isoform3 methylates mitochondrial genome and modulates its biology. *Sci. Rep.*, **7**, 1525.
21. Wong,M., Gertz,B., Chestnut,B.A. and Martin,L.J. (2013) Mitochondrial DNMT3A and DNA methylation in skeletal muscle and CNS of transgenic mouse models of ALS. *Front. Cell Neurosci.*, **7**, 279.
22. van der Wijst,M.G., van Tilburg,A.Y., Ruiters,M.H. and Rots,M.G. (2017) Experimental mitochondria-targeted DNA methylation identifies GpC methylation, not CpG methylation, as potential regulator of mitochondrial gene expression. *Sci. Rep.*, **7**, 177.
23. Mechta,M., Ingerslev,L.R., Fabre,O., Picard,M. and Barrès,R. (2017) Evidence Suggesting Absence of Mitochondrial DNA Methylation. *Front. Genet.*, **8**, 166.
24. Liu,B., Du,Q., Chen,L., Fu,G., Li,S., Fu,L., Zhang,X., Ma,C. and Bin,C. (2016) CpG methylation patterns of human mitochondrial DNA. *Sci. Rep.*, **6**, 23421.
25. Mechta,M., Ingerslev,L.R. and Barres,R. (2018) Methodology for accurate detection of mitochondrial DNA methylation. *J. Visual. Exp.*, **135**, doi:10.3791/57772.
26. Owa,C., Poulin,M., Yan,L. and Shioda,T. (2018) Technical adequacy of bisulfite sequencing and pyrosequencing for detection of mitochondrial DNA methylation: Sources and avoidance of false-positive detection. *PLoS One*, **13**, e0192722.
27. Thompson,M., Aukema,K., O'Bryan,D., Rader,S. and Murray,B. (2008) Plasmid sonication improves sequencing efficiency and quality in the Beckman Coulter CEQ system. *BioTechniques*, **45**, 327–329.
28. Xi,Y. and Li,W. (2009) BSMAP: whole genome bisulfite sequence MAPping program. *BMC Bioinformatics*, **10**, 232.
29. Martin,M. (2011) Cutadapt removes adapter sequences from high-throughput sequencing reads. *EMBnet. J.*, **17**, 10–12.
30. Langmead,B. and Salzberg,S.L. (2012) Fast gapped-read alignment with Bowtie 2. *Nat. Methods*, **9**, 357–359.
31. Robinson,J.T., Thorvaldsdottir,H., Winckler,W., Guttman,M., Lander,E.S., Getz,G. and Mesirov,J.P. (2011) Integrative genomics viewer. *Nat. Biotechnol.*, **29**, 24–26.
32. Lienhard,M., Grimm,C., Morkel,M., Herwig,R. and Chavez,L. (2014) MEDIPS: genome-wide differential coverage analysis of sequencing data derived from DNA enrichment experiments. *Bioinformatics*, **30**, 284–286.
33. Wang,Q., Gu,L., Adey,A., Radlwimmer,B., Wang,W., Hovestadt,V., Bähr,M., Wolf,S., Shendure,J., Eils,R. *et al.* (2013) Tagmentation-based whole-genome bisulfite sequencing. *Nat. Protoc.*, **8**, 2022–2032.
34. Waxman,S. and Wurmbach,E. (2007) De-regulation of common housekeeping genes in hepatocellular carcinoma. *BMC Genomics*, **8**, 243.
35. Barrès,R., Osler,M.E., Yan,J., Rune,A., Fritz,T., Caidahl,K., Krook,A. and Zierath,J.R. (2009) Non-CpG methylation of the PGC-1alpha promoter through DNMT3B controls mitochondrial density. *Cell Metab.*, **10**, 189–198.
36. Patil,V., Ward,R.L. and Hesson,L.B. (2014) The evidence for functional non-CpG methylation in mammalian cells. *Epigenetics*, **9**, 823–828.
37. Ghosh,S., Sengupta,S. and Scaria,V. (2014) Comparative analysis of human mitochondrial methylomes shows distinct patterns of epigenetic regulation in mitochondria. *Mitochondrion*, **18**, 58–62.
38. Ngo,H.B., Lovely,G.A., Phillips,R. and Chan,D.C. (2014) Distinct structural features of TFAM drive mitochondrial DNA packaging versus transcriptional activation. *Nat. Commun.*, **5**, 3077.
39. Gedamu,L., Iatrou,K. and Dixon,G.H. (1978) A simple procedure for the isolation and purification of protamine messenger ribonucleic acid from trout testis. *Biochem. J.*, **171**, 589–599.
40. Green,M.R. and Sambrook,J. (2017) Isolation of high-molecular-weight DNA using organic solvents. *Cold Spring Harb Protoc.*, **2017**, doi:10.1101/pdb.prot093450.
41. Morris,M.J., Hesson,L.B., Poulos,R.C., Ward,R.L., Wong,J.W.H. and Youngson,N.A. (2018) Reduced nuclear DNA methylation and mitochondrial transcript changes in adenomas do not associate with mtDNA methylation. *Biomarker research*, **6**, 37.
42. Weerts,M.J., Sieuwerts,A.M., Smid,M., Look,M.P., Foekens,J.A., Sleijfer,S. and Martens,J.W. (2016) Mitochondrial DNA content in breast cancer: Impact on in vitro and in vivo phenotype and patient prognosis. *Oncotarget*, **7**, 29166–29176.
43. Weerts,M.J.A., Hollestelle,A., Sieuwerts,A.M., Foekens,J.A., Sleijfer,S. and Martens,J.W.M. (2017) Low tumor mitochondrial DNA content is associated with better outcome in breast cancer patients receiving Anthracycline-Based chemotherapy. *Clin. Cancer Res.*, **23**, 4735–4743.
44. Kamfar,S., Alavian,S.M., Houshmand,M., Yadegarazari,R., Seifi Zarei,B., Khalaj,A., Shabab,N. and Saidijam,M. (2016) Liver mitochondrial DNA copy number and deletion levels may contribute to nonalcoholic fatty liver disease susceptibility. *Hepat Mon*, **16**, e40774.
45. Lightowlers,R.N., Chinnery,P.F., Turnbull,D.M. and Howell,N. (1997) Mammalian mitochondrial genetics: heredity, heteroplasmy and disease. *Trends Genet.*, **13**, 450–455.
46. Baylin,S.B. and Jones,P.A. (2016) Epigenetic determinants of cancer. *Cold Spring Harb Perspect Biol*, **8**, doi:10.1101/cshperspect.a019505.
47. Fisher,R.P., Topper,J.N. and Clayton,D.A. (1987) Promoter selection in human mitochondria involves binding of a transcription factor to orientation-independent upstream regulatory elements. *Cell*, **50**, 247–258.
48. Sun,X., Vaghjiani,V., Jayasekara,W.S.N., Cain,J.E. and St John,J.C. (2018) The degree of mitochondrial DNA methylation in tumor models of glioblastoma and osteosarcoma. *Clin Epigenetics*, **10**, 157.
49. Jin,B. and Robertson,K.D. (2013) DNA methyltransferases, DNA damage repair, and cancer. *Adv. Exp. Med. Biol.*, **754**, 3–29.
50. Roll,J.D., Rivenbark,A.G., Jones,W.D. and Coleman,W.B. (2008) DNMT3b overexpression contributes to a hypermethylator phenotype in human breast cancer cell lines. *Mol. Cancer*, **7**, 15.
51. Rhee,I., Bachman,K.E., Park,B.H., Jair,K.W., Yen,R.W., Schuebel,K.E., Cui,H., Feinberg,A.P., Lengauer,C., Kinzler,K.W. *et al.* (2002) DNMT1 and DNMT3b cooperate to silence genes in human cancer cells. *Nature*, **416**, 552–556.
52. Nosho,K., Shima,K., Irahara,N., Kure,S., Baba,Y., Kirkner,G.J., Chen,L., Gokhale,S., Hazra,A., Spiegelman,D. *et al.* (2009) DNMT3B expression might contribute to CpG island methylator phenotype in colorectal cancer. *Clin. Cancer Res.*, **15**, 3663–3671.

frontiers in Immunology

ORIGINAL RESEARCH
published: 03 March 2017
doi: 10.3389/fimmu.2017.00219

Methylation of FOXP3 TSDR Underlies the Impaired Suppressive Function of Tregs from Long-term Belatacept-Treated Kidney Transplant Patients

*Evelyn Katy Alvarez Salazar[1], Arimelek Cortés-Hernández[1], Germán Rodrigo Alemán-Muench[1], Josefina Alberú[2], Jesús R. Rodríguez-Aguilera[3], Félix Recillas-Targa[3], Victoria Chagoya de Sánchez[3], Eric Cuevas[2], Eduardo Mancilla-Urrea[4], María Pérez García[4], Guillermo Mondragón-Ramírez[5], Mario Vilatobá[2], Ian Bostock[2], Erick Hernández-Méndez[2], David De Rungs[2], Eduardo A. García-Zepeda[1] and Gloria Soldevila[1]**

[1] Departmento de Inmunología, Instituto de Investigaciones Biomédicas, Universidad Nacional Autónoma de México, Ciudad de México, Mexico, [2] Departmento de Trasplantes, Instituto Nacional de Ciencias Médicas y Nutrición Salvador Zubirán, Ciudad de México, Mexico, [3] Departamento de Genética Molecular, Instituto de Fisiología Celular, Universidad Nacional Autónoma de México, Ciudad de México, Mexico, [4] Departamento de Nefrología, Instituto Nacional de Cardiología Ignacio Chávez, Ciudad de México, Mexico, [5] Instituto Mexicano de Trasplantes, Morelos, Mexico

OPEN ACCESS

Edited by:
Martin Johannes Hoogduijn,
Erasmus University
Rotterdam, Netherlands

Reviewed by:
Paolo Puccetti,
University of Perugia, Italy
Fleur Peters,
Erasmus University
Rotterdam, Netherlands

***Correspondence:**
Gloria Soldevila
soldevi@unam.mx

Specialty section:
This article was submitted to Alloimmunity and Transplantation, a section of the journal Frontiers in Immunology

Received: 12 December 2016
Accepted: 15 February 2017
Published: 03 March 2017

Citation:
Alvarez Salazar EK, Cortés-Hernández A, Alemán-Muench GR, Alberú J, Rodríguez-Aguilera JR, Recillas-Targa F, Chagoya de Sánchez V, Cuevas E, Mancilla-Urrea E, Pérez García M, Mondragón-Ramírez G, Vilatobá M, Bostock I, Hernández-Méndez E, De Rungs D, García-Zepeda EA and Soldevila G (2017) Methylation of FOXP3 TSDR Underlies the Impaired Suppressive Function of Tregs from Long-term Belatacept-Treated Kidney Transplant Patients. Front. Immunol. 8:219. doi: 10.3389/fimmu.2017.00219

Regulatory T cells (Tregs) are considered key players in the prevention of allograft rejection in transplanted patients. Belatacept (BLT) is an effective alternative to calcineurin inhibitors that appears to preserve graft survival and function; however, the impact of this drug in the homeostasis of Tregs in transplanted patients remains controversial. Here, we analyzed the phenotype, function, and the epigenetic status of the Treg-specific demethylated region (TSDR) in FOXP3 of circulating Tregs from long-term kidney transplant patients under BLT or Cyclosporine A treatment. We found a significant reduction in the proportion of $CD4^+CD25^{hi}CD127^{lo/-}FOXP3^+$ T cells in all patients compared to healthy individual (controls). Interestingly, only BLT-treated patients displayed an enrichment of the $CD45RA^+$ "naïve" Tregs, while the expression of Helios, a marker used to identify stable $FOXP3^+$ thymic Tregs remained unaffected. Functional analysis demonstrated that Tregs from transplanted patients displayed a significant reduction in their suppressive capacity compared to Tregs from controls, which is associated with decreased levels of FOXP3 and CD25. Analysis of the methylation status of the FOXP3 gene showed that BLT treatment results in methylation of CpG islands within the TSDR, which could be associated with the impaired Treg suppression function. Our data indicate that analysis of circulating Tregs cannot be used as a marker for assessing tolerance toward the allograft in long-term kidney transplant patients. Trial registration number IM103008.

Keywords: transplantation, tolerance, belatacept, Cyclosporine A, Treg, suppression

Abbreviations: CNI, calcineurin inhibitors; CsA, Cyclosporine A; BLT, belatacept; Tregs, regulatory T cells; FOXP3, Forkhead box P3; IL-2, interleukin 2; APC, antigen-presenting cell; CTLA-4, cytotoxic T-lymphocyte-associated antigen 4; PBMCs, Peripheral blood mononuclear cells; CFSE, Carboxy fluorescein succinimidyl ester; FBS, fetal bovine serum.

INTRODUCTION

Kidney transplantation is considered the treatment of choice for patients with end-stage renal failure. The use of calcineurin inhibitors (CNI) such as Cyclosporine A (CsA) and tacrolimus reduce allograft rejection (1); however, the toxic effect produced by the prolonged use of these immunosuppressive drugs, has aimed researchers to develop new drugs that prevent allograft rejection without the side effects of CNI (2). Among them, belatacept (BLT), a human fusion protein combining a modified extracellular portion of cytotoxic T-lymphocyte-associated antigen 4 (CTLA-4) with the constant-region fragment (Fc) of human IgG1, was approved in 2011 by US Food and Drug Administration as therapeutic agent for the prevention of allograft rejection. BLT mediates its function by interacting with costimulatory ligands CD80/CD86 on the antigen-presenting cell (APC), thereby blocking the costimulatory signal (second signal) required for naive T cell activation and resulting in anergy or apoptosis (3). A lower incidence of chronic allograft nephropathy, favoring BLT compared to patients under CsA treatment was documented by 12 months post-transplantation (4, 5). Although, it has been reported an increase of acute rejection episodes and post-transplant lymphoproliferative disorders in BLT-treated patients (4), clinical studies have shown that 7 years after transplantation kidney transplant patients under BLT treatment have a significantly better patient and graft survival, as well as mean estimated glomerular filtration rate than patients under CsA (6).

Regulatory T cells (Tregs) are cells with immunosuppressive capacity that are important in tolerance maintenance after organ transplantation (7). These cells are characterized by the expression of the transcription factor FOXP3, considered the master regulator of their development and function, as well as high levels of surface CD25, and low levels of CD127 ($CD4^+CD25^{hi}CD127^{lo/-}FOXP3^+$). Therefore, several studies have addressed the potential effects of immunosuppressive therapy on Tregs from transplanted patients.

Some studies have claimed that BLT, rather than acting as immunosuppressor, plays a role as immunomodulator. This was supported by studies showing an increase of $CD16^+IDO^+$ cells and Tregs in peripheral blood and in intragraft $FOXP3^+$ cells, proposed to generate a tolerant profile to renal allograft in those patients (8, 9). Other studies showed no differences in the percentage of $CD4^+CD25^{hi}$ and in FOXP3 levels in the $CD4^+$ subpopulation between BLT and CsA patients after 6 months of treatment (10) or showed no long-term negative impact of BLT on circulating Tregs (11). By contrast, other studies reported a lower percentage of $CD4^+CD25^{hi}$ cells in peripheral blood and a reduced intragraft level of FOXP3 mRNA compared to CsA (12). However, it was argued that the negative effect of BLT might be the result of short-term effect of the basiliximab used in the induction therapy. Therefore, the effect of this drug on Tregs remains controversial [reviewed in Ref. (13)].

As BLT is a costimulation blocker, it could interfere with signaling pathways (CD28 and CTLA-4) important for the development, homeostasis, and function of Tregs (14, 15). As these cells are important in tolerance maintenance after organ transplantation (7), it is necessary to study not only their frequency but also their suppressor function and FOXP3 epigenetic status, in transplanted patients under long-term therapy. Thus, the aim of the present study was to analyze the impact of long-term therapy with BLT or CsA on the phenotype, suppressive function, and the epigenetic status of the FOXP3 TSDR from peripheral Tregs of kidney transplant patients with stable graft function. Our data indicate that analysis of circulating Tregs cannot be used as a marker for assessing tolerance toward the allograft in long-term kidney transplant patients.

MATERIALS AND METHODS

Kidney Transplant Patients

Thirty-five primary kidney transplant patients included in this sub-study participated in the clinical trial BENEFIT (IM103008 study), which continue on their original study drug arm, BLT ($n = 24$) or CsA ($n = 11$). All patients received induction therapy with basiliximab, and adjunctive maintenance therapy with mycophenolate mofetil and prednisone. BLT was administered at a dose of 5 mg/kg every 4 weeks and CsA in an adequate dosage to maintain a blood level of 100–200 ng/dl (current mean blood level of 132.8 ± 40.1, 65.6–189.4). The current daily dose for mycophenolate mofetil and prednisone in both groups was 1 g/day and 5 mg/day, respectively. The daily exposure to mycophenolate mofetil and prednisone was comparable in both groups.

This sub-study was conducted with authorization of Bristol-Myers Squibb (protocol IM103-351) and approval from the Committees Medical Ethics at the Instituto de Investigaciones Biomédicas (UNAM), the Instituto Nacional de Ciencias Médicas y Nutrición Salvador Zubirán (Reference number 1535), the Instituto Nacional de Cardiología Ignacio Chávez, and the Instituto Mexicano de Trasplantes, and performed in accordance with the revised Declaration of Helsinki content, the Declaration of Istanbul, and Good Clinical Practice Guidelines. All patients provided written informed consent to participate in the study.

The transplanted individuals had stable graft function and with no clinical/biochemical evidence of rejection. Transplanted individuals in this sub-study had a mean of 7 years post-transplant. Buffy coat preparations of normal blood donors (control group) were provided by the Blood Bank, Instituto Nacional de Enfermedades Respiratorias, México DF.

Reagents

Anti-CD127-PECy7, anti-CD25-PECy5, anti-CD45RA-APCH7, anti-CD19-FITC, and anti-CD3-APCCy7 were purchased from BD Biosciences (San Jose, CA, USA). Anti-CD4-PE and anti-CD8-PECy7 were purchased from Tonbo Biosciences (San Diego, CA, USA). Anti-FOXP3-AlexaFluor647 was purchased from Beckman Coulter (Brea, CA, USA). Carboxy fluorescein succinimidyl ester (CFSE) was purchased from Life Technologies (Eugene, OR, USA).

For intracellular staining, FOXP3/Transcription Factor Staining Buffer Set (eBiosciences, San Diego, CA, USA) was used. All staining were performed in RPMI 1640 (Gibco, Carlsbad, CA, USA) with 10% fetal bovine serum (FBS), 2 mM glutamine, 10 mM HEPES, and 10 mM antibiotic-anti-mycotic (Gibco).

Cell Isolation, Antibody Staining, and Cell Sorting

Peripheral blood mononuclear cells (PBMCs) were isolated from blood of patients or from the buffy coat preparations of healthy donors by standard Ficoll-Paque™ Plus density-gradient centrifugation (GE Healthcare). PBMCs were labeled with anti-CD4, anti-CD127, anti-CD25, and anti-CD45RA monoclonal antibodies, incubated at 4°C in the dark for 20 min. For intracellular staining, cells were permeabilized with 150 µL of fixation/permeabilization solution at 4°C for 12 h. After two washes with permeabilization buffer 1×, PBMCs were incubated with anti-FOXP3 and anti-Helios for 30 min at 4°C in the dark. Samples were acquired with an Attune® Acoustic Focusing Cytometer (Life Technologies) and FlowJo 7.6.2 software (Tree Star, Ashland, OR, USA) was used for data analysis. A total of 100,000 events were acquired for analysis, after gating of lymphocytes based on the FSC/SSC dot plot.

For sorting, 50×10^6 PBMCs were washed once and resuspended in media (RPMI/10% FBS) at 100×10^6 per ml. Cells were incubated with anti-CD4 and anti-CD25 at 4°C for 30 min, washed twice and resuspended in PBS 1×. Labeled cells were sorted using a FACs Aria I sorter (BD Biosciences). For Treg isolation, a $CD4^+CD25^{veryhi}$ gate was used and sorted cells were collected in media (RPMI/20% FBS), washed once and resuspended in culture media until ready to be plated in the suppression assay.

T Cell Suppression Assays

As a significant percentage of the patient's Tregs did not express low levels of CD127, we were unable to use the conventional $CD4^+CD25^{hi}CD127^{lo}$ region to purify Tregs, and instead a $CD4^+CD25^{veryhi}$ gate (containing >85% of $Foxp3^+$ T cells) was used to isolate Tregs from both healthy subjects or kidney transplant patients (see Figure S3 in Supplementary Material). Sorted Tregs were cocultured with $CD3^+$ cells (Tresp) from the same individuals. $CD3^+$ T cells were isolated by negative selection using a Pan T cell Isolation Kit (Miltenyi Biotec, San Diego, CA, USA) according to the manufacturer's instructions, then labeled with 2.5 µM of CFSE at 37°C for 15 min, and finally washed three times with RPMI 10% FBS. In all assays, 5×10^4 CFSE-labeled Tresp were cocultured with Tregs at ratios Tregs:Tresp (0:1, 1:2, 1:4, 1:8, and 1:16) in RPMI media supplemented with 10% human AB serum and in the presence of Human Treg Suppression Inspector beads (Miltenyi Biotec) at a bead:Tresp ratio of 1:1. After 5 days, cells were stained with antibodies to CD4 and CD8, and cells were acquired with an Attune® Acoustic Focusing Cytometer and FlowJo 7.6.2 software was used for data analysis. The percentage of proliferating Tresp cells was determined by CFSE dilution and unlabeled CFSE-negative Tregs were excluded. Suppression was calculated as relative inhibition using the following formula: [(Tresp proliferation without Tregs − Tresp proliferation with Tregs)/Tresp proliferation without Tregs] × 100, for each individual.

Cytokine Production Assay

The levels of the cytokines IL-2 and IFN-γ in the culture supernatants from suppression assay were measured using LEGENDplex bead-based immunoassay KIT (Biolegend), according to the recommended procedure. Briefly, the samples were incubated with a panel of capture beads, then mixed with biotinylated detection antibody and subsequently with streptavidin–phycoerythrin, providing flourescent signals that were quantified on a flow cytometer. The concentrations of the cytokines were determined using a standard curve generated in the same assay. The experiments were performed in quadruplicate and repeated two times.

DNA Methylation Analysis of the FOXP3 TSDR

Methylation of Treg-specific demethylated region (TSDR) of FOXP3 gene was evaluated in isolated $CD4^+CD25^{hi}$ from transplanted patients and controls previously used for suppression assays ($CD4^+CD25^{veryhi}$ gate). As negative controls, $CD4^+CD25^-CD45RA^+$ T cells from controls were included. Sodium bisulfite modification of genomic DNA was carried out using the EZ DNA Methylation direct Kit (Zymo Research Corp., USA) according to the manufacturer's protocol. Bisulfite-treated DNA was PCR amplified using the following primers: *p*-5′-TGTTTGGGGGTAGAGGATTT-3′ and *o*-5′-TATCACCCCACCTAAACCAA-3′. Amplified DNA product was gel purified using QIAEX II gel extraction kit (Qiagen, Germany) and cloned into pGEM-T easy vector (Promega). *Escherichia coli* competent cells were transformed with recombinant vector 10 individual positive bacterial colonies were selected from which recombinant plasmid DNA was purified and sequenced with 3500 Genetic Analyzer (Applied Biosystems, USA). Sequences were interpreted using the Bioedit Software 7.2.5 (Ibis Biosciences, USA).

Statistical Analysis

The statistical analysis was performed using Prism 5.0 software (GraphPad Software, San Diego, CA, USA). Values were expressed as mean ± SEM. The Kolmogorov–Smirnov test was used to evaluate the distribution of each parameter. Only the control group followed a normal distribution. Differences between three groups were calculated using the Kruskal–Wallis test and comparison between two groups were made using the two tailed, Mann–Whitney non-parametric *U* test. A value of $p < 0.05$ was considered significant.

RESULTS

Kidney Transplant Patients

Twenty-four patients were included in the BLT group and 11 patients were in the CsA group. Clinic and demographic characteristics of the patients included in the study are shown in **Table 1**. As observed in this Table, no differences were found in donor and patients characteristics, although patients under BLT treatment maintained significantly better and stable graft function (both serum creatinine and cGFR) compared to patients under CsA. All patients were included at comparable years after transplantation. There were no differences in the total number of

HLA mismatches. The control group consisted of a group of nine healthy individuals (eight males and one female) closely matched with kidney transplant patients for age, with a mean of 35 years (24–54 years). Furthermore, the current number of peripheral blood lymphocytes was comparable between both transplant groups ($3.2 \pm 1.7 \times 10^3$ cells/μl blood and $2.5 \pm 1.0 \times 10^3$ cells/μl blood for BLT and CsA, respectively) and to controls ($2.5 \pm 0.5 \times 10^3$ cells/μl blood).

Patients under BLT Treatment Present High Frequency of Circulating CD4$^+$CD45RA$^+$ T Lymphocytes

No significant differences were found between the frequencies of peripheral lymphocytes (CD3$^+$, CD3$^+$CD4$^+$, CD3$^+$CD8$^+$, and CD19$^+$ cells) among patients with BLT and CsA compared with controls (**Figure 1A**). Although the frequency of CD4$^+$ T

TABLE 1 | Clinic and demographic characteristics of kidney transplant patients and controls.

	Belatacept (n = 24)	CsA (n = 11)	Control (n = 9)	p value
Age (years)	31.08 ± 10.1 (18–57)	28.9 ± 10.7 (18–50)	35 ± 10.5 (24–54)	0.565
Gender (F/M)	10/14	3/8	1/8	0.478
Donor age (years)	36.12 ± 9.47 (21–54)	37.81 ± 9.34 (23–52)	NA	0.625
Donor gender (F/M)	17/7	6/5	NA	0.451
Haplotypes (2-H/1-H/0-H)	2/14/8	2/6/3	NA	0.755
ESRD cause	Unk: 18	Unk: 9	NA	0.672
	DM: 3	DM: 0		
	GMN: 3	GMN: 2		
1-year SCr post-KT (mg/dl)	1.05 ± 0.19 (0.7–1.4)	1.34 ± 0.27 (0.95–1.83)	NA	0.0011
Current SCr (mg/dl)	1.03 ± 0.304 (0.66–2.03)	1.48 ± 0.43 (0.9–2.1)	NA	0.0012
1-year post-KT cGFR (ml/min) by MDRD	79.01 ± 15.6 (56.1–126.2)	63.81 ± 9.1 (50.9–78.9)	NA	0.0056
Current cGFR (ml/min) by MDRD	79.6 ± 16.5 (40.1–107.7)	56.8 ± 13.6 (38.1–76.1)	NA	0.0004
1-year post-KT serum CsA blood level (ng/ml)	NA	155.9 ± 36.2 (112–228.7)	NA	
Current serum CsA blood level (ng/ml)	NA	132.8 ± 40.1 (65.6–189.4)	NA	
Time since transplantation (years)	7.28 ± 0.91 (5.9–8.67)	7.11 ± 0.83 (5.9–8.22)	NA	0.606
Peripheral blood lymphocytes (cells/μl blood)	$3.2 \pm 1.7 \times 10^3$	$2.5 \pm 1.0 \times 10^3$	$2.5 \pm 0.5 \times 10^3$	0.478

ESRD, end-stage renal disease; Unk, unknown; GMN, glomerulonephritis; DM, diabetes mellitus; SCr, serum creatinine; KT, kidney transplant; cGFR, glomerular filtration rate; MDRD, modification of diet in renal disease; CsA, cyclosporine A; NA, not available.

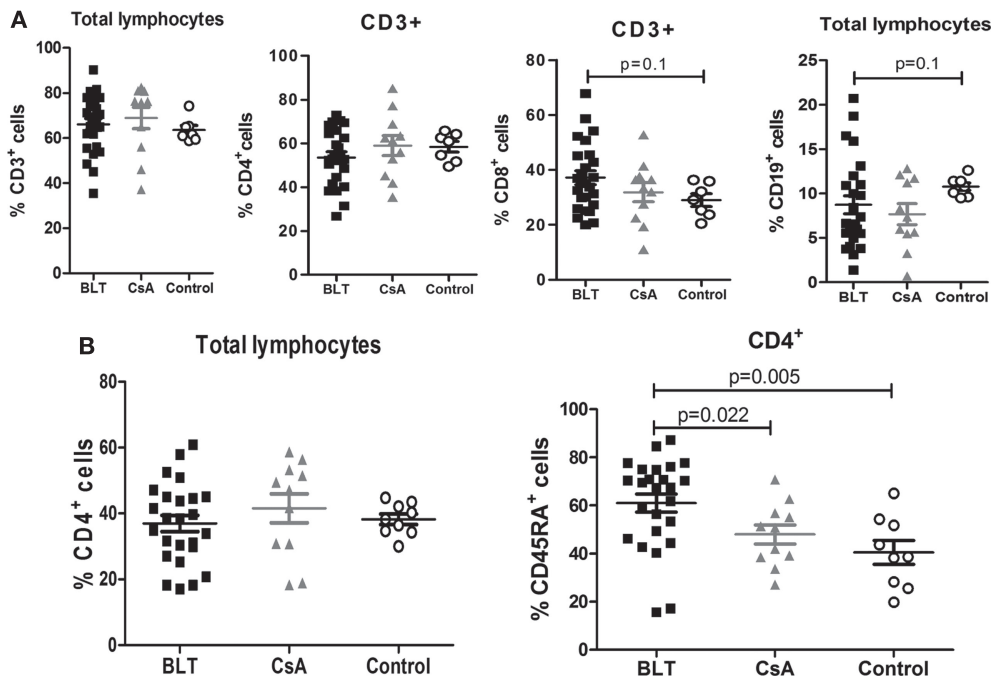

FIGURE 1 | Increased frequency of naïve CD4$^+$ T cells in BLT-treated patients. **(A)** Normal percentages of CD3$^+$, CD4$^+$, and CD8$^+$ cells are found in BLT- (n = 24) and CsA- (n = 11) treated patients compared to control (n = 9), and a slight reduction of B (CD19$^+$) cells is observed in BLT-treated patients. **(B)** Analysis of naïve T cell populations by the expression of CD45RA marker shows a significant increase in the frequency of CD4$^+$CD45RA$^+$ naïve T cells in BLT compared to CsA-treated kidney transplant patients and controls. Statistical analysis was performed using non-parametric Mann–Whitney test, two tailed. BLT, belatacept; CsA, Cyclosporine A. Control group was composed by healthy individuals.

cells was similar between all groups (**Figure 1B**, left), patients on long-term BLT treatment presented significantly higher percentages of circulating $CD4^+CD45RA^+$ T lymphocytes compared with CsA and control groups (BLT = 61.04 ± 3.74; CsA = 48.03 ± 3.97; control = 40.56 ± 4.92; $p < 0.05$) (**Figure 1B**, right).

Decreased Frequency of FOXP3$^+$ and Reduced Expression of FOXP3 and CD25 Inside of Total CD4$^+$ T Cells from BLT-Treated Patients

To examine the effect of BLT versus CsA on the frequency of circulating Tregs in kidney transplant patients, we first analyzed the expression of FOXP3 in total $CD4^+$ T cells. Within the $CD4^+$ T cell population, the percentage of $FOXP3^+$ cells in both transplanted patients was significantly reduced compared with control group (BLT = 5.81 ± 0.47; CsA = 4.57 ± 0.32; control = 7.94 ± 0.48; $p < 0.01$) (**Figure 2A**). In addition, the expression [mean fluorescence intensity (MFI)] of FOXP3 in $CD4^+FOXP3^+$ T cells from BLT-treated patients was lower than those of CsA and controls groups (BLT = 28,731 ± 3,639; CsA = 42,362 ± 6,687; control = 49,964 ± 3,108; $p < 0.005$) (**Figure 2B**, upper panel). As high expression of CD25 characterizes Tregs, we next analyzed CD25 within the $CD4^+$ $FOXP3^+$ T cells population and found that this marker was significantly reduced in BLT-treated patients compared with CsA and control groups. There was no difference of CD25 MFI between CsA and controls (BLT = 12,509 ± 839.1; CsA = 18,612 ± 2,728; control = 16,111 ± 808.6; $p < 0.05$) (**Figure 2B**, lower panel).

Frequency of Peripheral $CD4^+CD25^{hi}CD127^{lo/-}$ Tregs from Kidney Transplant Patients Are Reduced and Express Lower Levels of FOXP3 and CD25

Some reports indicate that a $CD25^{hi}$ and $CD127^{lo/-}$ phenotype on $CD4^+$ T cells allows more accurately to distinguish Tregs from activated $CD25^+$ conventional T cells, particularly in human samples (16). As shown in **Figure 3A**, the proportion of $CD25^{hi}CD127^{lo/-}$ T cells within the $CD4^+$ region was significantly reduced in both BLT- and CsA-treated patients compared with the control group (BLT = 3.31 ± 0.25; CsA = 3.83 ± 0.51; control = 5.28 ± 0.36; $p < 0.05$). As a result, the frequency of $CD25^{hi}CD127^{lo/-}FOXP3^+$ T cells among $CD4^+$ cells was significantly reduced in both treatment groups compared with controls (BLT = 2.81 ± 0.22; CsA = 2.97 ± 0.44; control = 4.69 ± 0.36; $p < 0.05$) (**Figure 3B**). In addition, the expression of FOXP3 in $CD4^+CD25^{hi}CD127^{lo/-}FOXP3^+$ T cells of transplanted patients was lower than those of controls (BLT = 29,099 ± 5,020; CsA = 36,840 ± 9,520; control = 65,997 ± 5,026; $p < 0.05$) (**Figure 3C**, upper panel). Expression of CD25 within the $CD4^+CD25^{hi}CD127^{lo/-}FOXP3^+$ population was significantly reduced in BLT-treated patients compared with CsA and control groups (BLT = 20,701 ± 1,363; CsA = 28,447 ± 3,859; control = 24,389 ± 1,154; $p < 0.05$) (**Figure 3C**, lower panel).

Moreover, in order to examine whether the reduced expression of FOXP3 and CD25 is the result of changes in the composition of the total Treg pool, we determined the frequency of $CD45RA^+$ and $Helios^+$ within the $CD4^+CD25^{hi}CD127^{lo/-}FOXP3^+$ T cells of kidney transplant patients and controls. Similarly to what was observed for total $CD4^+$ T cells, BLT-treated patients showed a significantly increased frequency of $CD4^+CD25^{hi}CD127^{lo/-}FOXP3^+CD45RA^+$ T cells ("naïve" Tregs) compared with control group (BLT = 50.76 ± 3.89; CsA = 43.34 ± 5.19; control = 30.78 ± 5.41; $p = 0.009$) (**Figure 4A**). Interestingly, both $CD45RA^+$ and $CD45RA^-$ Tregs from BLT-treated patients display lower levels of FOXP3 compared to the controls (**Figures 4B,C**), so that our results are not a consequence of the accumulation of Tregs with naïve phenotype.

No differences between groups were observed regarding the frequency of $Helios^+$ Tregs (**Figure 5A**) within the $CD4^+CD25^{hi}CD127^{lo/-}FOXP3^+$ subpopulation. Furthermore, FOXP3 was similarly downregulated in BLT-treated patients among $Helios^+$ and $Helios^-$ Tregs compared to controls (**Figures 5B,C**). This transcription factor has been recently shown to cooperate with FOXP3 to promote Treg suppression function, suggesting that it could be a useful marker for the identification of stable Foxp3 (+) Tregs that are primarily generated in the thymus (tTregs) (17). Therefore, FOXP3 and CD25 expression is reduced in Tregs from BLT-treated patients independently of Helios expression.

Interestingly, within the $CD4^+CD25^{hi}CD127^{lo/-}$ region, we found that only patients under CsA treatment showed a reduced percentage of $FOXP3^+$ cells compared to controls (76.80 ± 2.83 versus 88.46 ± 1.20; $p = 0.002$); while the percentage of $FOXP3^+$ cells within this region was not significantly altered in kidney transplant patients under BLT treatment compared to controls (83.29 ± 2.39 versus 88.46 ± 1.20; $p = 0.07$). Furthermore, some CsA-treated patients (three out of seven) showed a proportion of $FOXP3^+$ cells outside the characteristic $CD4^+CD25^{hi}CD127^{lo/-}$ region (Figure S1 in Supplementary Material).

Tregs from BLT-Treated Patients Display Impaired Suppressive Function

To determine whether the long-term immunosuppressive therapies had any effect in Treg function, $CD4^+CD25^{hi}$ T cells were purified from each group for *in vitro* suppression assays. As the percentage of $CD25^+FOXP3^+$ cells within the $CD4^+$ subpopulation was reduced in kidney transplant patients (Figure S2 in Supplementary Material), for the suppression assays a gate was set to sort Tregs containing >85% of $CD4^+CD25^{hi}FOXP3^+$ T cells similar to the control group ($CD4^+CD25^{veryhi}$ gate, Figure S3A in Supplementary Material). $CD4^+CD25^{hi}$ T cells from controls were able to suppress proliferation of both autologous $CD4^+$ and $CD8^+$ T cells at all evaluated ratios. By contrast, $CD4^+CD25^{hi}$ T cells isolated from CsA- and BLT-treated patients showed reduced suppression even at high ratios of Tregs to $CD4^+$ T cells (BLT = 19.52 ± 5.16; CsA = 17.74 ± 6.81; control = 51.03 ± 5.52

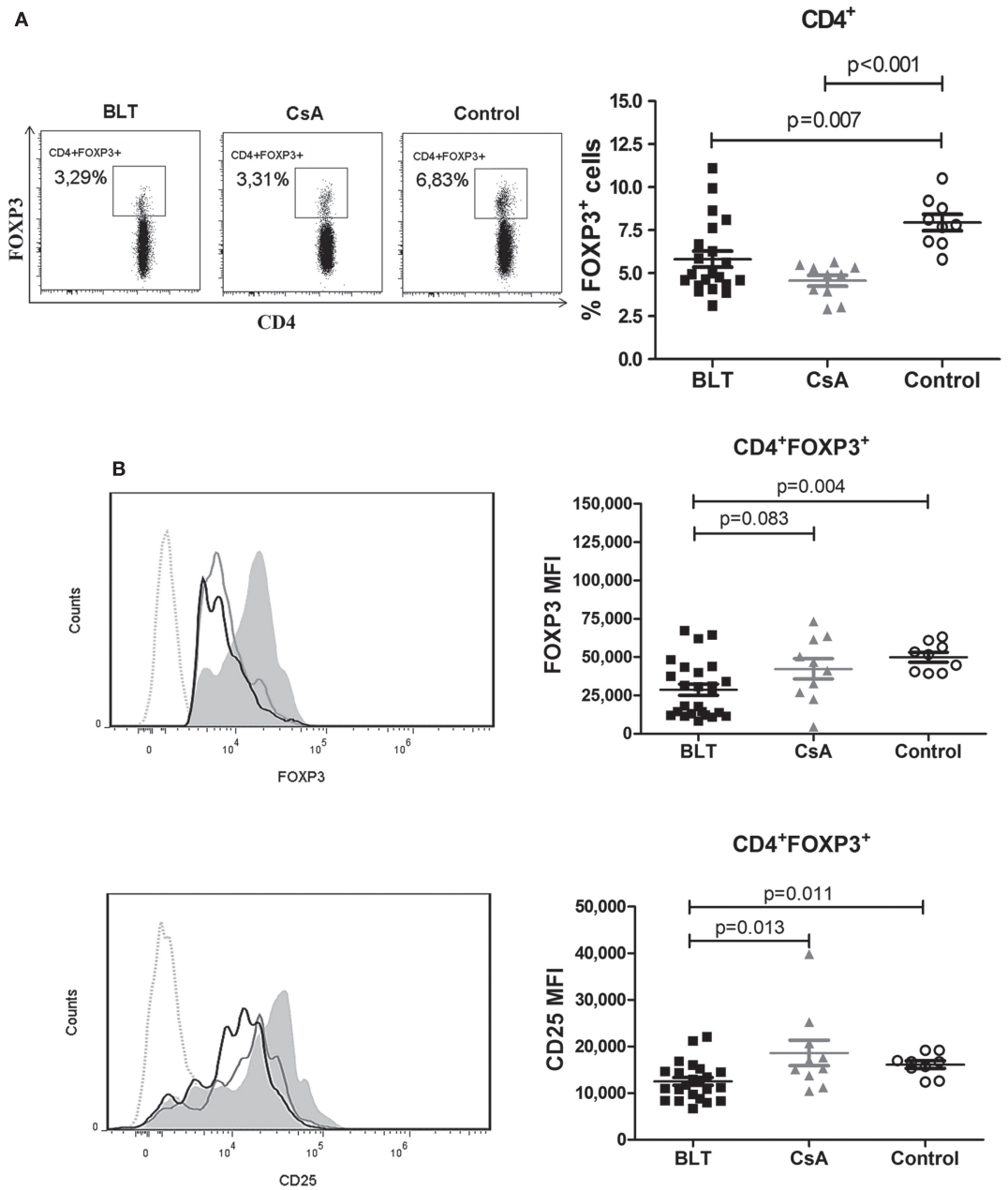

FIGURE 2 | **CD4⁺ T cells from BLT-treated patients show a diminished frequency of FOXP3⁺ subset with reduced levels of FOXP3 and CD25**. **(A)** A reduced frequency of CD4⁺FOXP3⁺ T cells was found in patients under BLT ($n = 21$) and CsA ($n = 10$) treatment compared to controls ($n = 9$). Lefts panels show representative dot plots from patients and controls. **(B)** Levels of FOXP3 and CD25 expression within the CD4⁺ subpopulations, were calculated as mean fluorescence intensity (MFI), showing a significant reduction in BLT-treated patients compared to CsA and control group. Left panels show representative histograms from BLT (black solid line), CsA (gray solid line), and control (filled histogram) individual; dotted line denotes fluorescence minus one control. MFI values from each individual were calculated by subtracting the MFI values of the non-expressing subpopulation for each marker from the corresponding expressing subpopulation. Statistical analysis was performed using non-parametric Mann–Whitney test, two tailed. BLT, belatacept; CsA, Cyclosporine A. Control group was composed by healthy individuals.

at 1:2 ratio; $p < 0.01$) and CD8⁺ T cells (BLT = 17.31 ± 4.83; CsA = 21.67 ± 3.20; control = 53.31 ± 5.66 at ratio 1:2 ratio; $p < 0.01$) (**Figure 6**), being associated with the reduced levels of FOXP3 and CD25 observed in the isolated $CD4^+CD25^{hi}$ T cells of all kidney transplant patients (Figure S3B in Supplementary Material). The suppressive capacity of Tregs was not significantly different between BLT- and CsA-treated patients. Of note, in the absence of Tregs, T cells from patients were equally able to proliferate after anti-TCR stimulation (Figure S4 in Supplementary Material).

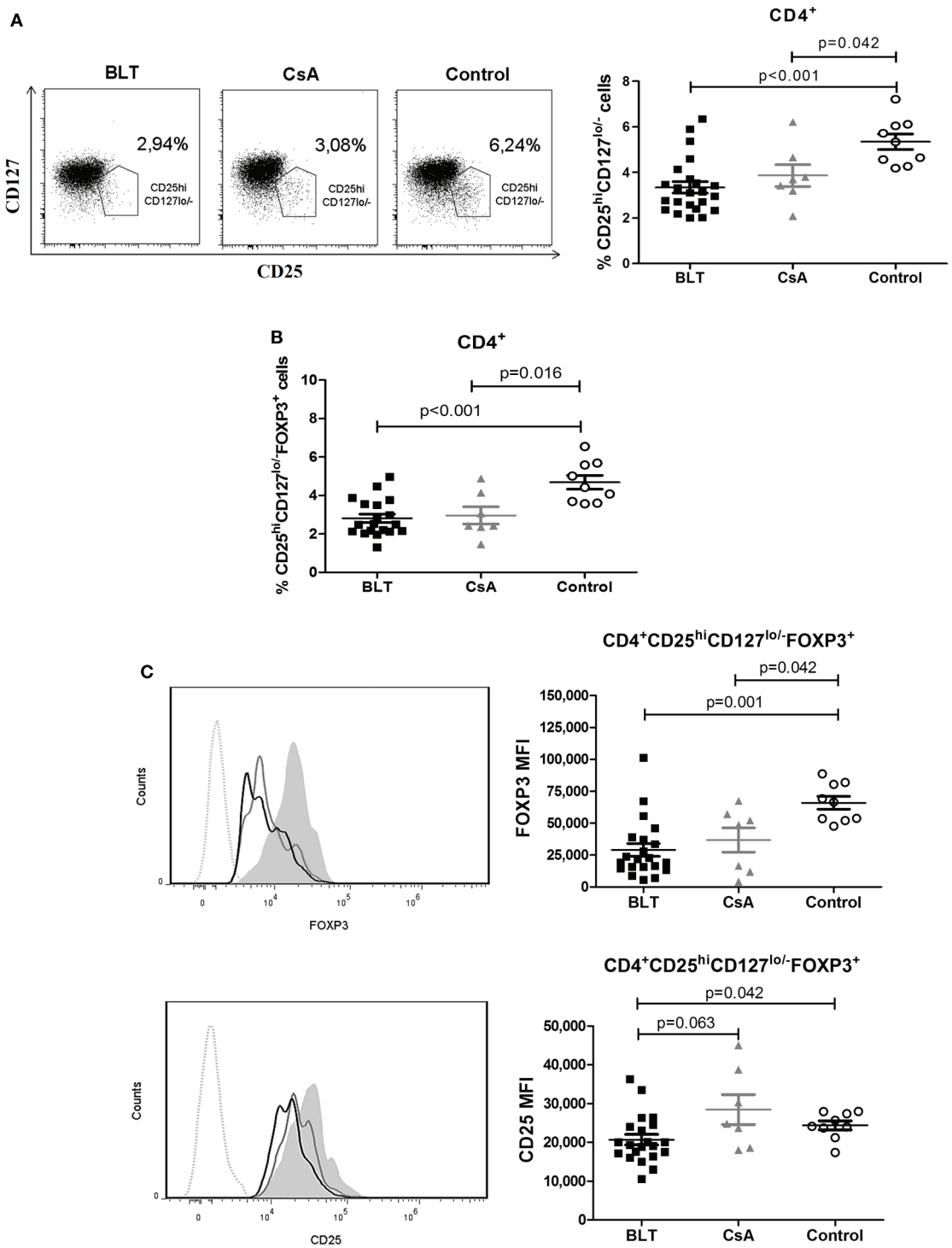

FIGURE 3 | Peripheral CD4$^+$CD25^{hi}CD127$^{lo/-}$FOXP3$^+$ T cells [regulatory T cells (Tregs)] from kidney transplant patients showed a reduction in frequency and expression levels of FOXP3. **(A)** Reduced frequency of CD4$^+$CD25^{hi}CD127$^{lo/-}$ T cells in long-term kidney transplant patients (BLT = 12 and CsA = 7) versus controls (n = 9). Right panels show representative dot plots from patients and controls. **(B)** Reduction in the percentage of CD4$^+$CD25$^+$CD127$^{lo/-}$FOXP3$^+$ T cells in compared to controls. **(C)** Expression of markers characteristic of the Treg phenotype demonstrates a significant reduction of FOXP3 and CD25 in Tregs from BLT-treated patients. Left panels show representative histograms from BLT (black solid line), CsA (gray solid line), and control (filled histogram) individual; dotted line is a fluorescence minus one control. Mean fluorescence intensity (MFI) values from each individual were calculated by subtracting the MFI values of the non-expressing subpopulation for each marker from the corresponding expressing subpopulation. Statistical analysis was performed using non-parametric Mann–Whitney test, two tailed. BLT, belatacept; CsA, Cyclosporine A; control group was composed by healthy individuals.

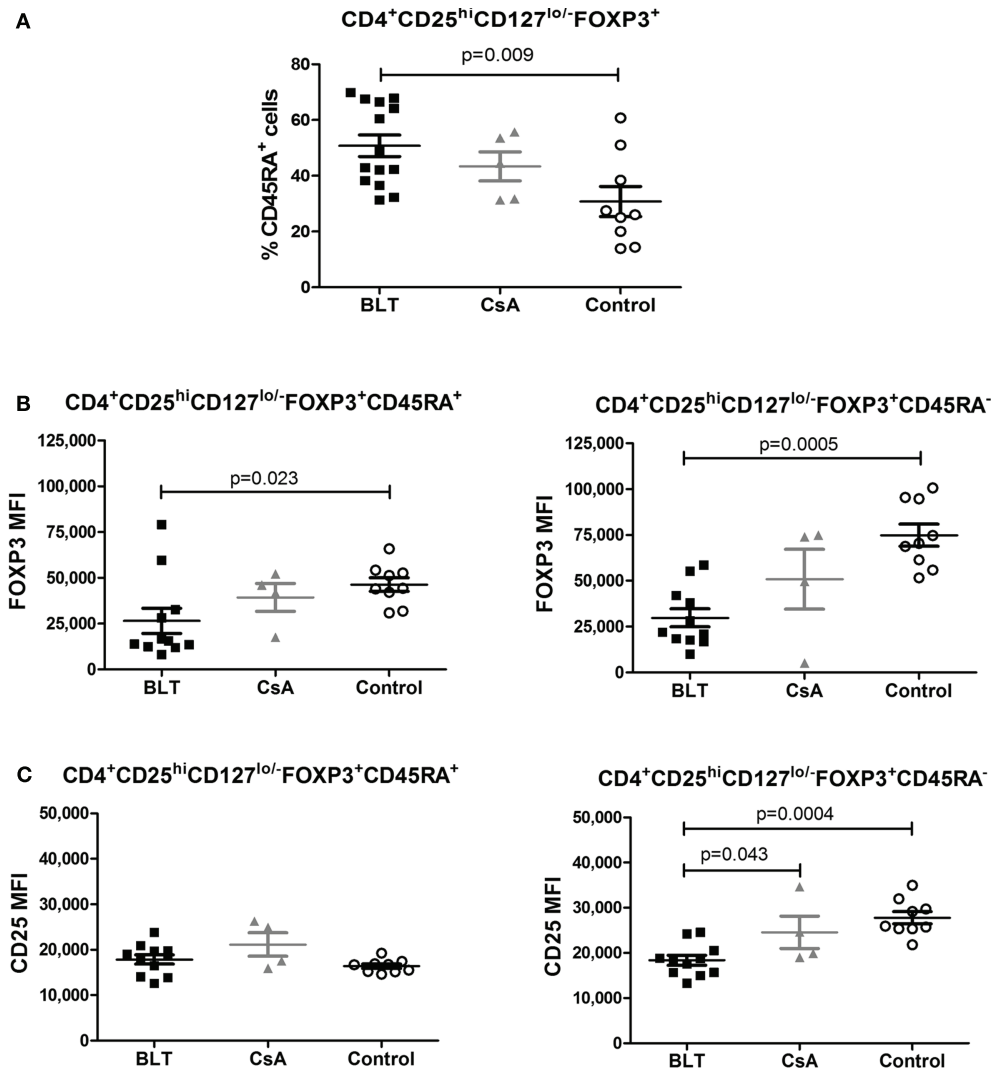

FIGURE 4 | Reduced FOXP3 expression on BLT regulatory T cells (Tregs) is not a consequence of the accumulation of Tregs with naïve phenotype. Patients under BLT treatment showed an increase frequency of naïve Tregs **(A)**; however, a reduced expression of FOXP3 **(B)** was found in both naïve ($CD45RA^+$) and activated ($CD45RA^-$) Tregs from patients under BLT ($n = 14$) treatment compared to CsA ($n = 4$) and controls ($n = 9$). **(C)** CD25 expression was significantly reduced in activated but not naïve Tregs from BLT patients. Statistical analysis was performed using non-parametric Mann–Whitney test, two tailed. BLT, belatacept; CsA, Cyclosporine A. Control group was composed by healthy individuals.

Tregs from BLT-Treated Patients Slightly Reduced IFN-γ by Activated T Cells

To investigate whether the impaired ability of Tregs from patients to inhibit T cell proliferation was accompanied by a reduced production of cytokines by responders T cells, we analyzed the cytokine secretion in the culture supernatants of the same suppression assays. As shown in **Figure 7A**, we found a decrease in the production of IFN-γ in the cocultures compared to responders T cells alone when patient's Tregs were used. This reduction was lower in BLT-treated patients to that observed in cultures of CsA and controls. Interestingly, although the production of IL-2 in responder T cells alone was similar between controls and BLT-treated patients, the levels of IL-2 were not significantly reduced in the cocultures from these patients compared to controls (**Figure 7B**). By contrast, a reduced production of IL-2 was found in responders T cells alone and cocultures from CsA-treated patients.

FOXP3 TSDR Is Methylated in Tregs from BLT- and CsA-Treated Patients

It has been previously reported that stable expression of FOXP3 is important to maintain Treg function (18), therefore we next analyzed the methylation state of the FOXP3 TSDR from isolated $CD4^+CD25^{hi}$ T cells of transplanted patients and controls, which were previously used for suppression assays ($CD4^+CD25^{veryhi}$ gate, Figure S3A in Supplementary Material). As FOXP3 gene is located into X chromosome, we evaluated only male individuals and the results were reported as percentage of methylated CpG

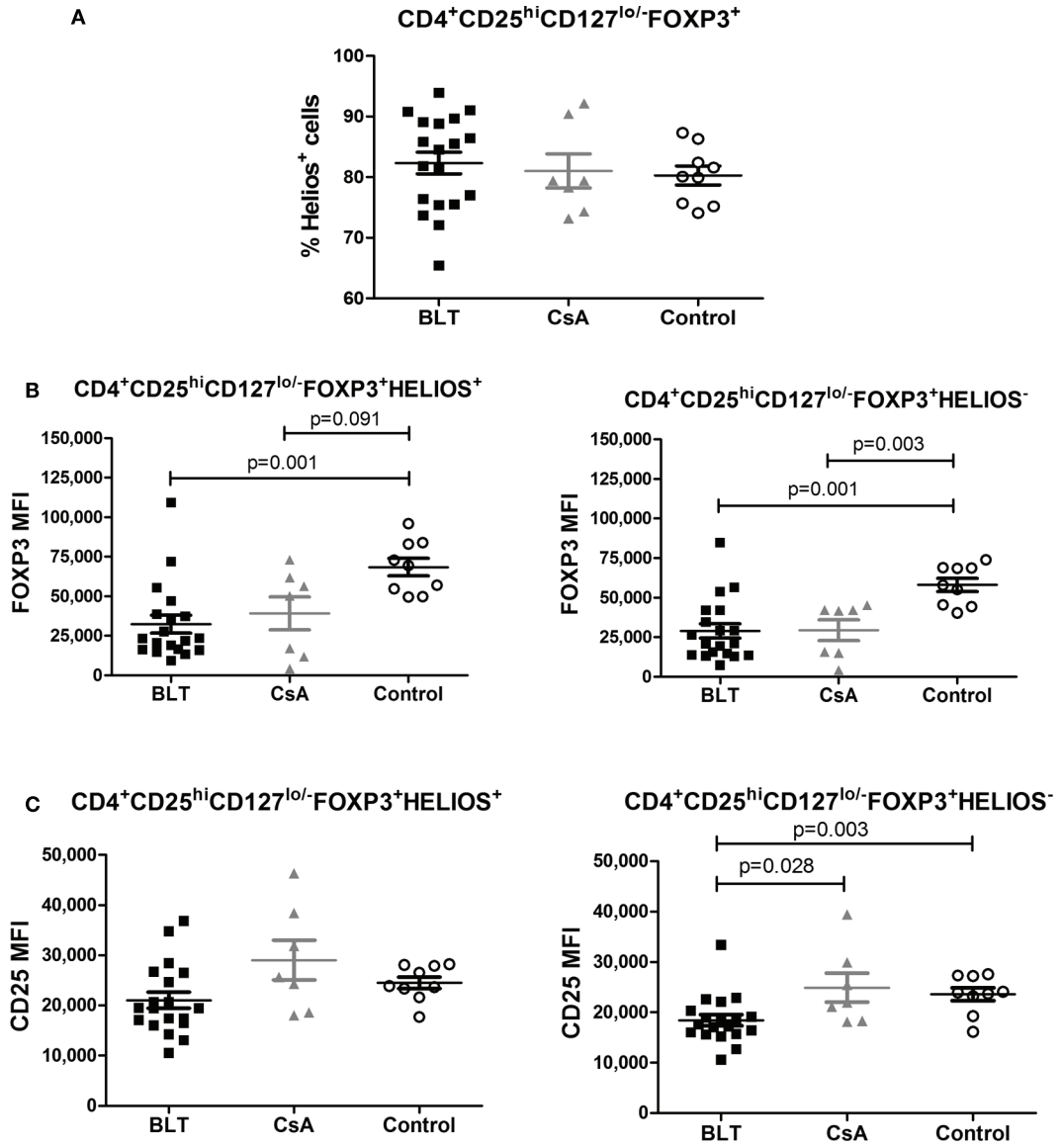

FIGURE 5 | FOXP3 expression is reduced in regulatory T cells (Tregs) from BLT-treated patients independently of Helios expression. **(A)** No differences in the frequency of Helios$^+$ on Tregs population from the three evaluated groups. **(B)** Reduced expression of FOXP3 within Helios$^+$ (left panel) or Helios$^-$ Tregs (right panel) of transplanted patients (BLT = 19 and CsA = 7) compared with control group (n = 9). **(C)** CD25 expression was significantly reduced in Helios$^-$ but not in Helios$^+$ Tregs from BLT patients. Statistical analysis was performed using non-parametric Mann–Whitney test, two tailed. BLT, belatacept; CsA, Cyclosporine A. Control group was composed by healthy individuals.

(of a total of 15) from five positive clones obtained from each individual. When we analyzed the percentage of methylation from all CpG sites sequenced, we observed a variability in kidney transplant patients, where some patients were almost all methylated (BLT2 and CsA2) and others showed a full demethylation (BLT3 and CsA1) independently of immunosuppressive treatment, compared to controls where almost all clones sequenced were demethylated (**Figure 8B**). As a result, the complete analysis of all patients showed a significant increase in the percentage of methylation in the FOXP3 TSDR in Tregs from BLT- and CsA-treated patients compared to controls (**Figure 8C**). This enhanced methylation could be associated with the reduced of suppression observed in Tregs from transplanted patients (**Figure 6**).

DISCUSSION

Regulatory T cells have been implicated in tolerance induction to allogeneic organ transplantation (13). Thus, it is important to ensure that immunosuppressive drugs do not interfere in Treg development and/or function (19). Studies have reported that kidney transplant patients under BLT treatment show a better renal function and less chronic nephropathy in comparison to those

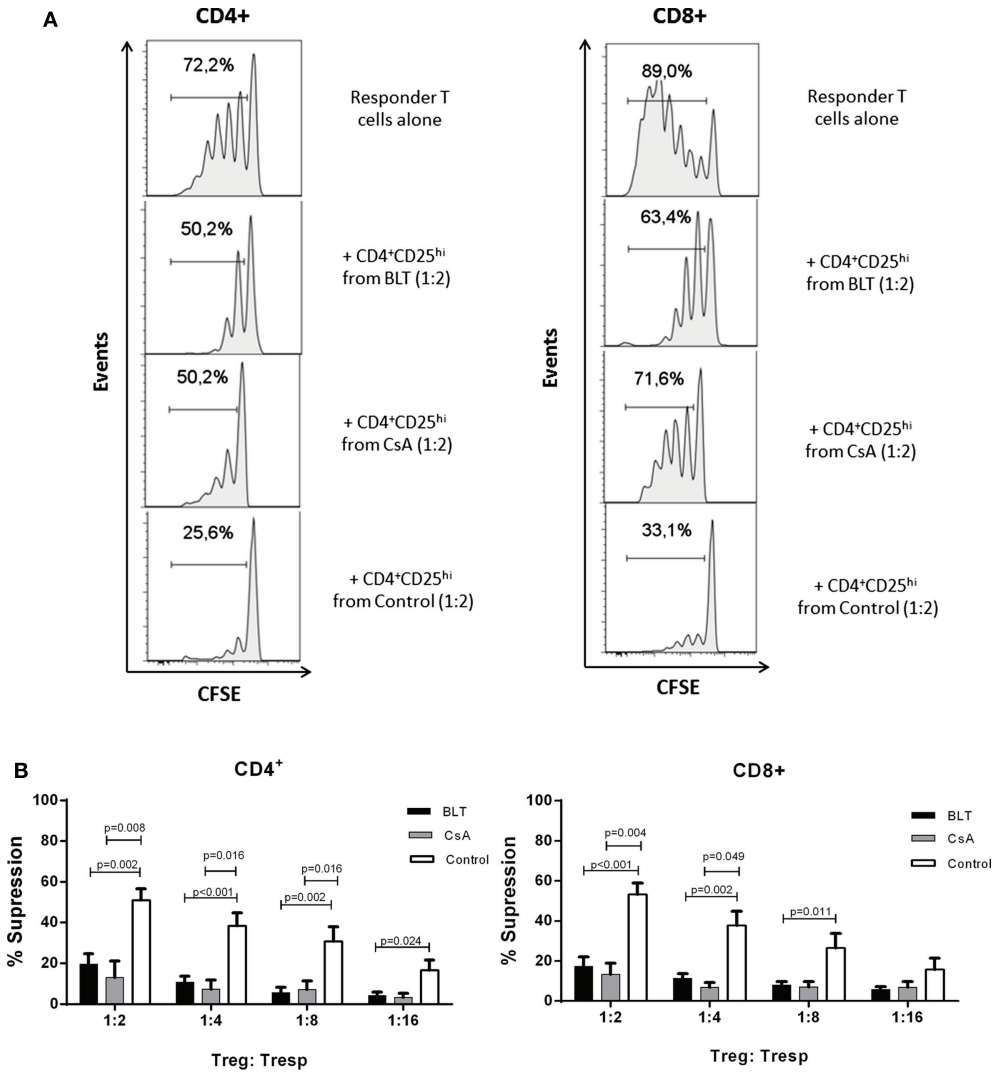

FIGURE 6 | **Impaired suppressive function of regulatory T cells (Tregs) from kidney transplant patients. (A)** Histograms show cells proliferation of carboxy fluorescein succinimidyl ester (CFSE)-labeled CD3+ T cells in the absence (responder T cells alone) or presence of Tregs ($CD4^+CD25^{veryhi}$ gated) from kidney transplant patients (BLT and CsA) or healthy subjects (control), numbers indicate the percentage of dividing cells. One representative experiment is presented. **(B)** $CD4^+CD25^{hi}$ T cells (Treg) isolated from BLT- (black bars, $n = 9$) or CsA- (gray bars, $n = 4$) treated patients showed impaired suppression of both autologous responder $CD4^+$ and $CD8^+$ T cell (Tresp) proliferation at all evaluated Tregs:Tresp ratios, compared to controls (white bars, $n = 8$). There were no significant differences between Tregs from BLT- and CsA-treated patients. Suppression was calculated as relative inhibition using the following formula: [(Tresp proliferation without Tregs − Tresp proliferation with Tregs)/Tresp proliferation without Tregs] × 100. Statistical analysis was performed using non-parametric Mann–Whitney test, two tailed. BLT, belatacept; CsA, Cyclosporine A.

under CsA treatment (4, 6, 20). Some studies claim that Treg frequency in peripheral blood and transplanted organs are increased in patients under BLT treatment (9, 21); however, other studies claim the opposite (12). Such differences may be caused by inconsistent parameters used for the characterization of the total Treg pool, different gating strategies and small numbers of participants in many studies. In the present study, we found no differences in the frequency of Treg ($CD4^+CD25^{hi}CD127^{lo/-}FOXP3^+$), between patients under BLT and CsA treatment, although they were lower than those found in healthy individuals. In this study, we used, besides the $CD25^+$ and $FOXP3^+$ markers, the low expression of CD127 to identify Tregs that were evaluated in 35 patients with a mean time of 7 years since transplantation. By contrast, analysis of Tregs in other studies was based on CD25 and FOXP3 expression (9), two markers that are transiently expressed in activated humans T cells (22), and other results were limited by the small numbers of patients included in the study (21).

Helios was initially reported as a marker of Treg generated in the thymus and was used to differentiate tTregs from those generated in the periphery (23). However, recent reports have shown that Helios can be expressed in peripherally induced Tregs and is associated with T cell activation and cell division

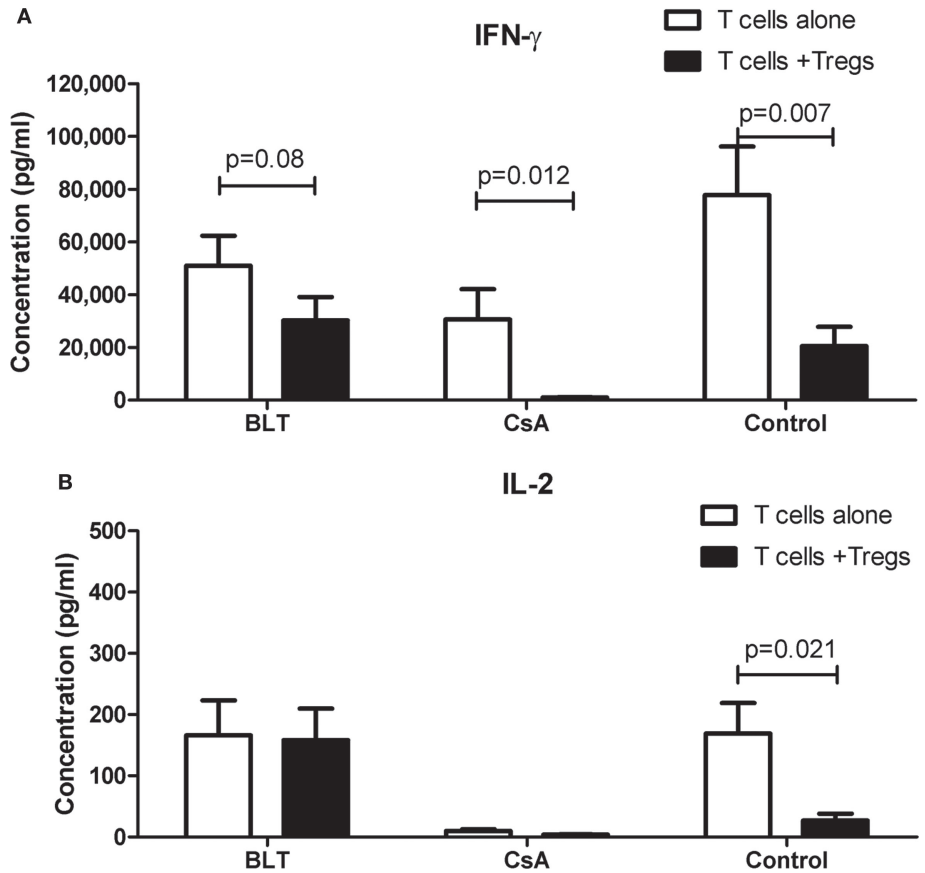

FIGURE 7 | **IFN-γ and IL-2 production in suppression cocultures from kidney transplant patients**. Cytokines were measured in the supernatant cultures of suppression assays from kidney transplant patients (BLT = 3 and CsA = 4) and controls (n = 4), after a stimulus with beads CD3/CD28 (responder T cells alone) or cocultured with autologous regulatory T cells (Tregs) by 4 days. **(A)** Responder T cells alone from transplanted individuals produce IFN-γ after CD3/CD28 stimulus in the same way of controls, and this production is reduced in the presence of autologous Tregs. Tregs from BLT-treated patients slightly reduced IFN-γ production by activated T cells. **(B)** Alterations in IL-2 production were observed in transplanted individuals compared with controls. Responder T cells alone from BLT but not CsA-treated patients produce normal levels of IL-2. Statistical analysis was performed using non-parametric Mann–Whitney test, two tailed. BLT, belatacept; CsA, Cyclosporine A. Control group was composed by healthy individuals.

(24). Interestingly, it was reported that FOXP3$^+$Helios$^+$ Tregs represent a much more stable population as they differ from FOXP3$^+$Helios$^-$ Tregs in their epigenetic status of the FOXP3 locus and their capacity to produce effector cytokines (25). Our results suggest that Helios expression is not responsible for the levels of FOXP3, as this marker was similarly downregulated in Helios$^+$ and Helios$^-$ Tregs from kidney transplant patients, compared to controls (**Figure 5**). Similarly, an accumulation of "naïve" Tregs cannot account for the reduced expression of FOXP3 on Tregs from BLT-treated patients, as it was affected in both "naïve" (CD45RA$^+$) and "activated" (CD45RA$^-$) Tregs (**Figure 4**).

It has been argued that the immunosuppressive drugs used to maintain graft acceptance in kidney transplant patients may be affecting both the development, homeostasis, and function of Tregs (26); BLT blocks T cell signaling by inhibiting the CD28 costimulatory pathway while CsA inhibits the synthesis of NFAT-dependent cytokines such as IL-2. Previous studies have shown that both CD28 and IL-2 pathways signaling are essential for sustained expression of FOXP3 in Treg cells and maintenance of a stable phenotype in the periphery (27, 28). In this study, transplanted patients showed a lower MFI of FOXP3, which is associated with lower suppressor function *in vitro* (**Figure 6**).

Besides of blocking proliferation, Tregs are able to inhibit the production of cytokines and prevent the differentiation of immune cells. We observed that Tregs from BLT-treated patients slightly reduced IFN-γ production despite their impaired suppressive function on T cell proliferation (**Figure 7A**). In this context, it has been reported that Tregs can inhibit IFN-γ production without blocking the proliferation of CD4$^+$ T cells (29). Moreover, their suppressor effects on TCR signaling, IL-2/IFN-γ transcription as well as IFN-γ production were retained in conventional T cells after the removal of Tregs (30). So, it is probable that Tregs require a more prolonged cellular contact to be able in suppress the proliferation of immune cells (31). A reduction or alteration of membrane markers as CTLA-4 or defects in expression of receptors to IL-2 (CD25) could explain the lack of suppression of proliferation observed in our transplanted patients. In this context, Tregs from BLT-treated patients showed diminished CD25

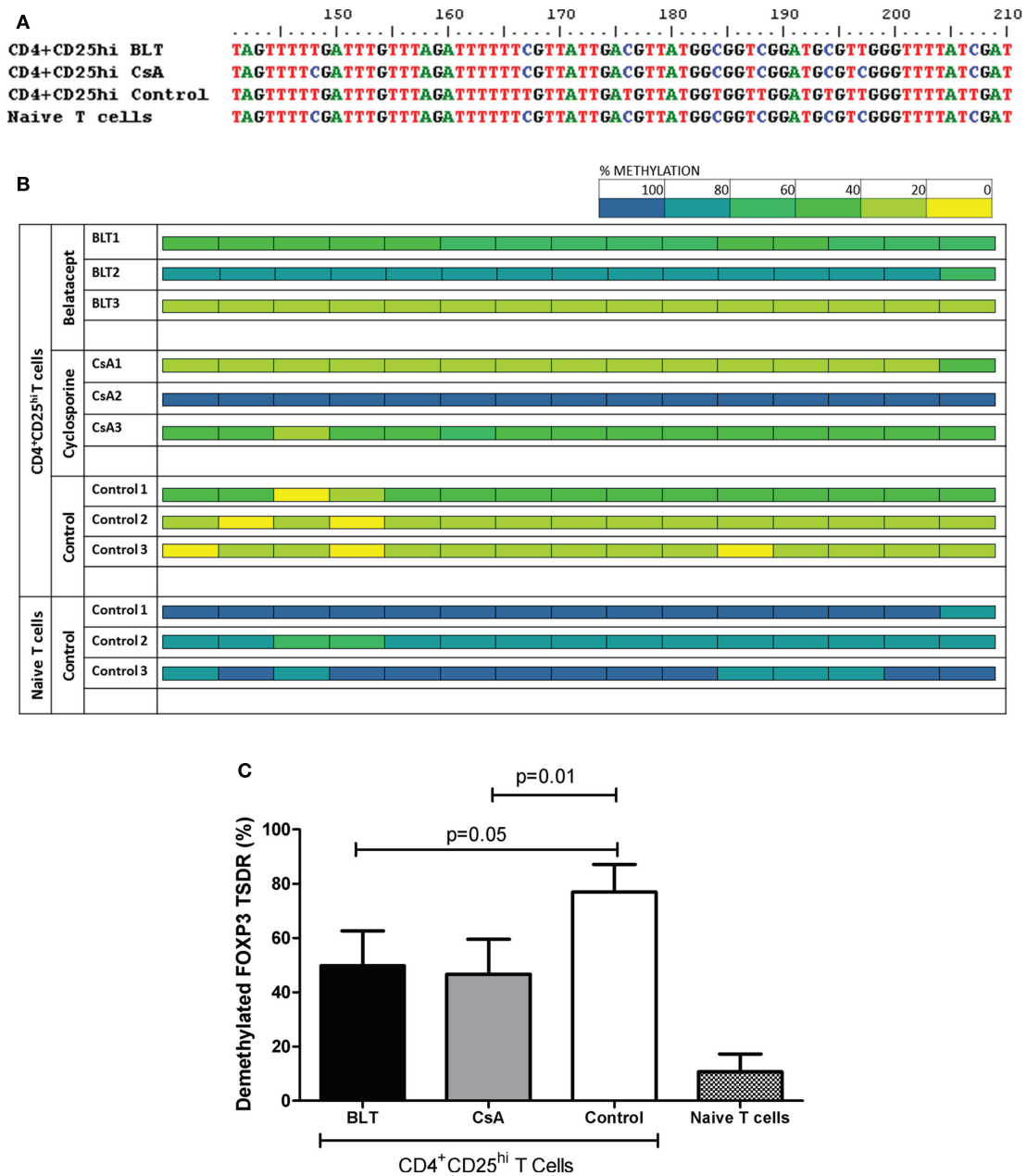

FIGURE 8 | **Altered methylation in the regulatory T cell (Treg) FOXP3 TSDR from kidney transplant patients**. Sequence analysis of the TSDR region of the FOXP3 gene from BLT, CsA, or controls (three male individuals per group, five clones per individual). **(A)** After bisulfite treatment, all demethylated CpG cytosines (blue) convert to thymines (red), as seen with $CD4^+CD25^{hi}$ Tregs from the control ($CD4^+CD25^{veryhi}$ gated). By contrast, naïve T cells display a completely methylated TSDR and were used as negative control. Data from representative individuals from each group are shown. **(B)** The panel shows the methylation status of the TSDR FOXP3 in the indicated T cells from the three evaluated groups (three individuals per group). Each square represents one CpG analyzed, data are presented as mean percentage methylation of five clones per individual. Methylation color code ranges from yellow (0% methylation) to blue (100% methylation) according to the color scale (upper right). **(C)** Percentage of demethylation from each evaluated group, represented as the ratio between the numbers of demethylated cytosines and the total number of sequenced CpG sites within the TSDR region.

expression (**Figure 3C**) which could affect the "consumption" of IL-2 by Tregs, explaining the lack of IL-2 depletion observed in the cocultures with Tregs from these patients (**Figure 7B**).

Many reports have claimed the "division of labour" between distinct Treg subpopulations in the maintenance of tolerance (32). In the context of allospecific tolerance, it has been claimed that tTregs may participate in the inhibition of T-effector cell trafficking to the target organ while antigen-specific iTregs primarily prevent T-cell priming by acting on antigen-presenting dendritic cells (33). Therefore, it would be relevant to analyze the impact

of inmunosuppressors in the percentage and/or function of both subpopulations. Our data showed a decrease in percentage and suppressor function of circulating Tregs; however, no specific markers are currently available to reliably distinguish thymic versus peripherally induced Treg populations (24).

Although there is a previous study claiming that neither BLT nor CsA affect the normal function of Treg cells (11), the current study analyzed the patient's Treg suppressor capacity on responder T cells from the same kidney transplant patients, while the former one used responder T cells from their respective donors. Interestingly, we were unable to detect strong direct alloreactive responses from our transplanted patients toward their donors APCs, even in the presence of exogenous IL-2 (data not shown), which suggests a possible deletion of direct allospecific T cells. In addition, in long-term kidney transplant patients as those included in this study, alloreactive T cells may likely recognize alloantigens by an indirect pathway (34), and thus suppression function of Tregs on alloreactive T cells activated by this pathway should be pursued. Therefore, we cannot exclude the possibility that Tregs cells with an indirect pathway of allospecificity may have a normal suppressor function. It is not clear whether the relevant allospecific Treg subpopulation of long-term kidney transplant patients can be found in peripheral blood or rather it has migrated to the transplanted organ to accomplish its function, as has been suggested (8).

Our study showed that some transplanted patients display a low frequency and decreased expression of FOXP3 within $CD4^+CD25^{hi}CD127^{lo/-}$ region (**Figure 3**), which was previously reported for CsA-treated patients (35). In addition to affecting the generation or homeostasis of the Treg pool, this reduction may be caused by the fact that some Tregs might lose its FOXP3 expression due to the action of the immunosupressors on FOXP3 stability, that is controlled by epigenetic and post-translational modifications (36, 37). In this context, demethylated TSDR (Treg-specific demethylation region) of the FOXP3 gene is indicative of stable FOXP3 expression and Treg lineage commitment (36). Unlike other studies which analyzed the methylation state of total PBMC by real time PCR (38), here we decided to sequence the whole TSDR region of sorted Tregs to obtain a more complete information about the epigenetic status of the FOXP3 TSDR in this subpopulation. Interestingly, our data showed that transplanted patients under BLT or CsA treatment presented partial methylation of the CpG islands present in the TSDR (**Figure 8**), which is associated with the impaired suppressor function from Tregs of these patients. Thus, the loss of demethylation in TSDR region might be responsible for the reduced FOXP3 expression observed in these patients, and lower levels of FOXP3-dependent markers such as CD25 and CTLA-4 (39, 40), where its upregulation is associated with enhanced Treg activity (28, 41). It has been reported that ten–eleven translocation (TET) enzymes might participate in the demethylation of FOXP3 (42). TET enzymes catalyzes the conversion of 5-methylcytosine (5mC) to 5-hydroxymethylcytosine that are intermediates in the process of DNA demethylation. High expression of these enzymes was observed in thymic $FOXP3^+$ Treg subsets and a deletion of TET enzymes led to FOXP3 hypermethylation (43). In addition, high expression of TET enzymes have been observed after TCR signaling and IL-2 was necessary to maintain their expression (44) and, it was shown that (IL-2)-activated Stat5 facilitated Tet1 and Tet2 binding to FOXP3. On other hand, CD28 signaling in Tregs is required for stabilization of FOXP3 mRNA in thymic Treg precursors (45). Therefore, the block of these pathways by immunosuppressive drugs could explain the methylation in the FOXP3 TSDR observed in transplanted patients under BLT and CsA treatment.

The variability found in the percentages of GpG island demethylation from the TSDR region of patients under immunosuppressive treatment suggests that the impaired suppressor function of Tregs from transplanted patients may also be caused by FOXP3-independent factors, such as IL-10, TGFβ, granzyme B, and galectin-1 (46). Therefore, although our results are suggestive of the impact of BLT and CsA on TSDR methylation, it is necessary to include other phenotypic and functional analysis to determine the mechanism underlying the alterations of Tregs in long-term transplanted patients.

Our findings suggest that circulating Tregs are no solely responsible for the quiescence immune state achieved in stable long-term patients. In this context, a recent study showed BLT-treated patients have increased cellular populations with regulatory function such that $IL\text{-}10^+$ B cells and IDO^+ cells (9, 47), which could promote tolerance during transplantation and facilitate the long-term survival and function of allografts.

In summary, this study has shown that even in patients with stable graft function, treatment with BLT can have an advertent effect on Treg, suggesting that the beneficial effects reported by BLT cannot be only explained by circulating Tregs. However, we cannot exclude the immunomodulatory role of Tregs, as allospecific Treg function has not directly been evaluated. Interestingly, a report showed that combination of T cell depletion, BLT, and Sirolimus favored Treg expansion and abrogation of T-cell alloreactive anti-donor responses *in vitro*, although the study was performed only at 12 months of transplantation (48). Whether the drug effects on Tregs have an impact on the ultimate outcome of renal allografts remains unclear. Therefore, the effects of long-term immunosuppression on Tregs should be taken into account in the design of new Treg-based therapy.

AUTHOR CONTRIBUTIONS

GS supervised the research, analyzed the data, wrote the manuscript, and obtained funding. EA-S performed experiments, analyzed data, and wrote the manuscript. AC-H, GA-M, and JRR-A performed experiments and revised manuscript. JA designed the study, obtained patient consentment to participate, followed-up the patients, and reviewed the manuscript. FR-T contributed with reagents and revised manuscript. VCS contributed with reagents. EC, MG, IB, and EH-M gathered clinical information and blood samples. EM-U, GM-R, MV, and DR obtained patient consentment to participate, followed-up the patients, and reviewed the manuscript. EG-Z provided reagents and analyzed data, and reviewed the manuscript.

ACKNOWLEDGMENTS

The authors thank QFB Carlos Castellanos, Dr. Andrea Bedoya, and Erick Espindola M.Sc. from the LABNALCIT-UNAM/CONACYT for technical assistance with FACS sorting. The authors also thank Lorena Villaseñor (Instituto Mexicano de Trasplantes) for providing update clinical data of their patients. This study was supported by CONACyT Grants #180288 and #272518 and Fundación Miguel Alemán Valdés (Mexico). EAS is a student of the PhD program: Doctorado en Ciencias Biomédicas, Universidad Nacional Autónoma de México and a recipient of a doctoral fellowship from CONACyT (#508108). EAH is a student of the PhD program: Doctorado en Ciencias Bioquímicas, Universidad Nacional Autónoma de México and was supported by a fellowship from CONACyT (#549444).

SUPPLEMENTARY MATERIAL

The Supplementary Material for this article can be found online at http://journal.frontiersin.org/article/10.3389/fimmu.2017.00219/full#supplementary-material.

REFERENCES

1. Nankivell BJ, Alexander SI. Rejection of the kidney allograft. *N Engl J Med* (2010) 363(15):1451–62. doi:10.1056/NEJMra0902927
2. Saeed B. Pediatric renal transplantation. *Int J Organ Transplant Med* (2012) 3(2):62–73.
3. Sayegh MH, Turka LA. The role of T-cell costimulatory activation pathways in transplant rejection. *N Engl J Med* (1998) 338(25):1813–21. doi:10.1056/NEJM199806183382506
4. Vincenti F, Charpentier B, Vanrenterghem Y, Rostaing L, Bresnahan B, Darji P, et al. A phase III study of belatacept-based immunosuppression regimens versus cyclosporine in renal transplant recipients (BENEFIT study). *Am J Transplant* (2010) 10(3):535–46. doi:10.1111/j.1600-6143.2009.03005.x
5. Masson P, Henderson L, Chapman JR, Craig JC, Webster AC. Belatacept for kidney transplant recipients. *Cochrane Database Syst Rev* (2014) 11:CD010699. doi:10.1002/14651858.CD010699.pub2
6. Vincenti F, Rostaing L, Grinyo J, Rice K, Steinberg S, Gaite L, et al. Belatacept and long-term outcomes in kidney transplantation. *N Engl J Med* (2016) 374(4):333–43. doi:10.1056/NEJMoa1506027
7. Joffre O, Santolaria T, Calise D, Al Saati T, Hudrisier D, Romagnoli P, et al. Prevention of acute and chronic allograft rejection with CD4+CD25+Foxp3+ regulatory T lymphocytes. *Nat Med* (2008) 14(1):88–92. doi:10.1038/nm1688
8. Furuzawa-Carballeda J, Lima G, Uribe-Uribe N, Avila-Casado C, Mancilla E, Morales-Buenrostro LE, et al. High levels of IDO-expressing CD16+ peripheral cells, and Tregs in graft biopsies from kidney transplant recipients under belatacept treatment. *Transplant Proc* (2010) 42(9):3489–96. doi:10.1016/j.transproceed.2010.08.037
9. Furuzawa-Carballeda J, Bostock IC, Lima G, Mancilla-Urrea E, Mondragón G, Reyes-Acevedo R, et al. Immunophenotyping of peripheral immunoregulatory as well as Th17A and Th22 cell subpopulations in kidney transplant recipients under belatacept or cyclosporine treatment. *Transpl Immunol* (2014) 30(2–3):107–13. doi:10.1016/j.trim.2014.02.002
10. Chavez H, Beaudreuil S, Abbed K, Taoufic Y, Kriaa F, Charpentier B, et al. Absence of CD4CD25 regulatory T cell expansion in renal transplanted patients treated in vivo with belatacept mediated CD28-CD80/86 blockade. *Transpl Immunol* (2007) 17(4):243–8. doi:10.1016/j.trim.2007.01.005
11. Bluestone JA, Liu W, Yabu JM, Laszik ZG, Putnam A, Belingheri M, et al. The effect of costimulatory and interleukin 2 receptor blockade on regulatory T cells in renal transplantation. *Am J Transplant* (2008) 8(10):2086–96. doi:10.1111/j.1600-6143.2008.02377.x
12. Grimbert P, Audard V, Diet C, Matignon M, Plonquet A, Mansour H, et al. T-cell phenotype in protocol renal biopsy from transplant recipients treated with belatacept-mediated co-stimulatory blockade. *Nephrol Dial Transplant* (2011) 26(3):1087–93. doi:10.1093/ndt/gfq453
13. Pilat N, Wekerle T. Belatacept and Tregs: friends or foes? *Immunotherapy* (2012) 4(4):351–4. doi:10.2217/imt.12.13
14. Golovina TN, Mikheeva T, Suhoski MM, Aqui NA, Tai VC, Shan X, et al. CD28 costimulation is essential for human T regulatory expansion and function. *J Immunol* (2008) 181(4):2855–68. doi:10.4049/jimmunol.181.4.2855
15. Sojka DK, Hughson A, Fowell DJ. CTLA-4 is required by CD4+CD25+ Treg to control CD4+ T-cell lymphopenia-induced proliferation. *Eur J Immunol* (2009) 39(6):1544–51. doi:10.1002/eji.200838603
16. Banham AH. Cell-surface IL-7 receptor expression facilitates the purification of FOXP3(+) regulatory T cells. *Trends Immunol* (2006) 27(12):541–4. doi:10.1016/j.it.2006.10.002
17. Takatori H, Kawashima H, Matsuki A, Meguro K, Tanaka S, Iwamoto T, et al. Helios enhances Treg cell function in cooperation with FoxP3. *Arthritis Rheumatol* (2015) 67(6):1491–502. doi:10.1002/art.39091
18. Floess S, Freyer J, Siewert C, Baron U, Olek S, Polansky J, et al. Epigenetic control of the foxp3 locus in regulatory T cells. *PLoS Biol* (2007) 5(2):e38. doi:10.1371/journal.pbio.0050038
19. De Serres SA, Yeung MY, Mfarrej BG, Najafian N. Effect of biologic agents on regulatory T cells. *Transplant Rev (Orlando)* (2011) 25(3):110–6. doi:10.1016/j.trre.2010.11.002
20. Vincenti F, Larsen C, Durrbach A, Wekerle T, Nashan B, Blancho G, et al. Costimulation blockade with belatacept in renal transplantation. *N Engl J Med* (2005) 353(8):770–81. doi:10.1056/NEJMoa050085
21. Vondran FW, Timrott K, Kollrich S, Klempnauer J, Schwinzer R, Becker T. Decreased frequency of peripheral CD4(+) CD161(+) Th(17)-precursor cells in kidney transplant recipients on long-term therapy with belatacept. *Transpl Int* (2012) 25(4):455–63. doi:10.1111/j.1432-2277.2012.01441.x
22. Allan SE, Crome SQ, Crellin NK, Passerini L, Steiner TS, Bacchetta R, et al. Activation-induced FOXP3 in human T effector cells does not suppress proliferation or cytokine production. *Int Immunol* (2007) 19(4):345–54. doi:10.1093/intimm/dxm014
23. Thornton AM, Korty PE, Tran DQ, Wohlfert EA, Murray PE, Belkaid Y, et al. Expression of Helios, an Ikaros transcription factor family member, differentiates thymic-derived from peripherally induced Foxp3+ T regulatory cells. *J Immunol* (2010) 184(7):3433–41. doi:10.4049/jimmunol.0904028
24. Akimova T, Beier UH, Wang L, Levine MH, Hancock WW. Helios expression is a marker of T cell activation and proliferation. *PLoS One* (2011) 6(8):e24226. doi:10.1371/journal.pone.0024226
25. Kim YC, Bhairavabhotla R, Yoon J, Golding A, Thornton AM, Tran DQ, et al. Oligodeoxynucleotides stabilize Helios-expressing Foxp3+ human T regulatory cells during in vitro expansion. *Blood* (2012) 119(12):2810–8. doi:10.1182/blood-2011-09-377895
26. De Serres SA, Sayegh MH, Najafian N. Immunosuppressive drugs and Tregs: a critical evaluation! *Clin J Am Soc Nephrol* (2009) 4(10):1661–9. doi:10.2215/CJN.03180509
27. Huynh A, Zhang R, Turka LA. Signals and pathways controlling regulatory T cells. *Immunol Rev* (2014) 258(1):117–31. doi:10.1111/imr.12148
28. Mahmud SA, Manlove LS, Farrar MA. Interleukin-2 and STAT5 in regulatory T cell development and function. *JAKSTAT* (2013) 2(1):e23154. doi:10.4161/jkst.23154
29. Sojka DK, Fowell DJ. Regulatory T cells inhibit acute IFN-gamma synthesis without blocking T-helper cell type 1 (Th1) differentiation via a compartmentalized requirement for IL-10. *Proc Natl Acad Sci U S A* (2011) 108(45):18336–41. doi:10.1073/pnas.1110566108
30. Schmidt A, Oberle N, Weiss EM, Vobis D, Frischbutter S, Baumgrass R, et al. Human regulatory T cells rapidly suppress T cell receptor-induced Ca(2+), NF-kappaB, and NFAT signaling in conventional T cells. *Sci Signal* (2011) 4(204):ra90. doi:10.1126/scisignal.2002179
31. Schmidt A, Oberle N, Krammer PH. Molecular mechanisms of Treg-mediated T cell suppression. *Front Immunol* (2012) 3:51. doi:10.3389/fimmu.2012.00051

32. Curotto de Lafaille MA, Lafaille JJ. Natural and adaptive foxp3+ regulatory T cells: more of the same or a division of labor? *Immunity* (2009) 30(5):626–35. doi:10.1016/j.immuni.2009.05.002
33. Shevach EM, Thornton AM. tTregs, pTregs, and iTregs: similarities and differences. *Immunol Rev* (2014) 259(1):88–102. doi:10.1111/imr.12160
34. Ali JM, Bolton EM, Bradley JA, Pettigrew GJ. Allorecognition pathways in transplant rejection and tolerance. *Transplantation* (2013) 96(8):681–8. doi:10.1097/TP.0b013e31829853ce
35. Akimova T, Kamath BM, Goebel JW, Meyers KE, Rand EB, Hawkins A, et al. Differing effects of rapamycin or calcineurin inhibitor on T-regulatory cells in pediatric liver and kidney transplant recipients. *Am J Transplant* (2012) 12(12):3449–61. doi:10.1111/j.1600-6143.2012.04269.x
36. Li X, Zheng Y. Regulatory T cell identity: formation and maintenance. *Trends Immunol* (2015) 36(6):344–53. doi:10.1016/j.it.2015.04.006
37. van Loosdregt J, Coffer PJ. Post-translational modification networks regulating FOXP3 function. *Trends Immunol* (2014) 35(8):368–78. doi:10.1016/j.it.2014.06.005
38. Wieczorek G, Asemissen A, Model F, Turbachova I, Floess S, Liebenberg V, et al. Quantitative DNA methylation analysis of FOXP3 as a new method for counting regulatory T cells in peripheral blood and solid tissue. *Cancer Res* (2009) 69(2):599–608. doi:10.1158/0008-5472.CAN-08-2361
39. Camperio C, Caristi S, Fanelli G, Soligo M, Del Porto P, Piccolella E. Forkhead transcription factor FOXP3 upregulates CD25 expression through cooperation with RelA/NF-kappaB. *PLoS One* (2012) 7(10):e48303. doi:10.1371/journal.pone.0048303
40. Wu Y, Borde M, Heissmeyer V, Feuerer M, Lapan AD, Stroud JC, et al. FOXP3 controls regulatory T cell function through cooperation with NFAT. *Cell* (2006) 126(2):375–87. doi:10.1016/j.cell.2006.05.042
41. Read S, Greenwald R, Izcue A, Robinson N, Mandelbrot D, Francisco L, et al. Blockade of CTLA-4 on CD4+CD25+ regulatory T cells abrogates their function in vivo. *J Immunol* (2006) 177(7):4376–83. doi:10.4049/jimmunol.177.7.4376
42. Toker A, Engelbert D, Garg G, Polansky JK, Floess S, Miyao T, et al. Active demethylation of the Foxp3 locus leads to the generation of stable regulatory T cells within the thymus. *J Immunol* (2013) 190(7):3180–8. doi:10.4049/jimmunol.1203473
43. Yang R, Qu C, Zhou Y, Konkel JE, Shi S, Liu Y, et al. Hydrogen sulfide promotes Tet1- and Tet2-mediated Foxp3 demethylation to drive regulatory T cell differentiation and maintain immune homeostasis. *Immunity* (2015) 43(2):251–63. doi:10.1016/j.immuni.2015.07.017
44. Nair VS, Oh KI. Down-regulation of Tet2 prevents TSDR demethylation in IL2 deficient regulatory T cells. *Biochem Biophys Res Commun* (2014) 450(1):918–24. doi:10.1016/j.bbrc.2014.06.110
45. Nazarov-Stoica C, Surls J, Bona C, Casares S, Brumeanu TD. CD28 signaling in T regulatory precursors requires p56lck and rafts integrity to stabilize the Foxp3 message. *J Immunol* (2009) 182(1):102–10. doi:10.4049/jimmunol.182.1.102
46. Sugimoto N, Oida T, Hirota K, Nakamura K, Nomura T, Uchiyama T, et al. Foxp3-dependent and -independent molecules specific for CD25+CD4+ natural regulatory T cells revealed by DNA microarray analysis. *Int Immunol* (2006) 18(8):1197–209. doi:10.1093/intimm/dxl060
47. Leibler C, Matignon M, Pilon C, Montespan F, Bigot J, Lang P, et al. Kidney transplant recipients treated with belatacept exhibit increased naïve and transitional B cells. *Am J Transplant* (2014) 14(5):1173–82. doi:10.1111/ajt.12721
48. Bestard O, Cassis L, Cruzado JM, Torras J, Franquesa M, Gil-Vernet S, et al. Costimulatory blockade with mTor inhibition abrogates effector T-cell responses allowing regulatory T-cell survival in renal transplantation. *Transpl Int* (2011) 24(5):451–60. doi:10.1111/j.1432-2277.2011.01223.x

Conflict of Interest Statement: The authors declare that the research was conducted in the absence of any commercial or financial relationships that could be construed as a potential conflict of interest.

The reviewer FP and handling editor declared their shared affiliation, and the handling editor states that the process nevertheless met the standards of a fair and objective review.

Chapter

Molecular and Cellular Aspects of Cirrhosis and How an Adenosine Derivative Could Revert Fibrosis

Jesús Rafael Rodríguez-Aguilera, Rebeca Pérez-Cabeza de Vaca, Nuria Guerrero-Celis, Gabriela Velasco-Loyden, Mariana Domínguez-López, Félix Recillas-Targa and Victoria Chagoya de Sánchez

Abstract

Hepatic fibrosis occurs in response to persistent liver damage and is characterized by an excessive accumulation of extracellular matrix. When the damage is prolonged, there is a chronic inflammation and persistent hepatic fibrosis eventually leads to cirrhosis, where in addition to the scar, there is an important vascular remodeling associated with portal hypertension and, if decompensated, leads to death or can develop hepatocellular carcinoma. We have been studying the pharmacologic functions of adenosine, finding that a derivative of this nucleoside, IFC-305, shows hepatoprotective effects in a CCl_4-induced rat cirrhosis model where it reverses liver fibrosis through modulation of fibrosis-related genes and by ameliorating hepatic function. Furthermore, this compound has the property to rescue cell cycle inhibition *in vivo*, prevents hepatic stellate cell activation, modulates anti-inflammatory macrophage polarization, and favors a chromatin context that could decrease the genomic instability and characteristics of cirrhosis, enabling the recovery of gene expression profile. Here we show results that contribute to the comprehension of molecular and cellular mechanism of cirrhosis, give the opportunity to suggest biomarkers to the early diagnostic of this pathology, and constitute the fundaments to suggest IFC-305 as a coadjuvant for treatment of this disease.

Keywords: liver fibrosis reversion, adenosine, Kupffer cells, hepatic stellate cells, cell cycle, epigenetics

1. Introduction

Cirrhosis is the 14th dead cause worldwide in adults [1]; this pathology represents an hepatocellular alteration, which is defined histologically by a vascular remodeling that triggers formation of fibrotic interconnected septum that wraps the entire liver tissue and divides the parenchyma in nodules [2]; as a consequence, there is a reduction in hepatocellular mass as well as liver function and blood flow alterations. These pathologic characteristics are independent of disease etiology, which mainly could be alcoholic, biliary, and directed by viral or chronic hepatitis [3].

In the past, cirrhosis was considered as an irreversible illness, but there is evidence, which suggests that when there is an arrest of the viral or nonviral mayor cirrhotic-generator insult, it is possible to resolve fibrosis [4–9]. This is evident in successfully chronic hepatitis C treatment, in fibrosis resolution in hemochromatosis patients with effective treatment, and also in alcoholic liver illness patient who has suspended alcohol consumption [10]. A group of histopathological injuries of "reverted cirrhosis" has been described in the "hepatic reparatory complex" [9] including a thin, incomplete and perforated septum, through which hepatocytes are evident; there is a hepatocyte growing in terminal hepatic venules and little cumulus of thick collagen fibers in the parenchymal sinusoids [2]. Nevertheless, this disease could be considered as a pre-neoplastic state considering that 80% of hepatocellular carcinoma originated from cirrhosis [11].

This pathology is a silence one; generally it courses without symptoms, whereby its development confers a significant morbidity and mortality risk, and progression to this terminal state of chronic liver injury is slow, around 20–40 years [12]. Thanks to advances in the understanding of chromatin organization and rapid progress in sequencing technology, it has been clear that not only genetics but also epigenetics influence both normal human biology and diseases [13]; the combinatorial of these both factors could influence on speed of disease development, generating changes in chromatin, an inflammatory process and hepatic stellate cell (HSC) activation, triggering a pro-fibrotic environment and if it is perpetuated, the cirrhosis establishment. In this section, we will get deep into molecular and cellular aspects of cirrhosis and how an adenosine derivative could reverse this pathology through generating an anti-inflammatory environment and blocking HSC activation, modulating cell cycle and mediating epigenetic changes which reduce altered expressed genes.

2. Biochemical and physiological alteration of liver during cirrhosis and hepatoprotective effects of an adenosine derivative

Cirrhosis has a complex cellular and molecular dynamic that should be approached using laboratory models that could be animal or cell cultures. One of the most studied cirrhotic models employs carbon tetrachloride (CCl_4) to generate the pathology. This compound is a hepatic and renal toxic, whose effect is produced by two different mechanisms: the first one is related with the alteration of hepatocyte capacity to bind triacylglycerides to transporter lipoproteins, triggering an intracellular lipid accumulation and fatty degeneration of the liver; the second mechanism consists in the formation of metabolites extremely toxic, which lead to cell death and centrilobular hepatic necrosis [14]. This toxic compound is a substrate of P450 cytochrome that transforms it into $CCl_3\cdot$ radicals, and these radicals generate $CCl_3OO\cdot$ when it reacts with molecular oxygen. Since $CCl_3\cdot$ radicals react with cell membranes inducing lipid peroxidation, it has been proposed that the main cause of hepatic illness by CCl_4 is the membrane damage by the free radical chain reaction, and probably, the initial event is related with mitochondrion membrane damage [15]. Nevertheless, it is important to say that this model, unlike what happens in the human, progresses to hepatocellular carcinoma with low frequency, so that it permits only the evaluation of cirrhotic state.

Rats are intraperitoneal treated with 0.04 g/kg body weight of CCl_4 three times per week, during 10 weeks. After this time it is possible to observe a liver distortion, the formation of nodules, bilirubin accumulation and hepatomegaly [16], the generation of a fibrotic area of 16% of the tissue, and a reduction in parenchyma surface to around 78%. As a consequence of these liver architecture changes, there are alterations of liver function: serum samples of cirrhotic rats display elevated AST,

ALT, and bilirubin levels and albumin are relatively reduced [17]. Furthermore, there is a reduction in ATP level with slow recovery after 5 weeks with saline. All of these altered parameters reflect chronic hepato-biliary injury.

Since 1967, our laboratory has been studying the pharmacologic effects of adenosine on hepatic metabolism [18], finding that this nucleoside increases hepatocyte energetic charge [19], an effect which is able to increase metabolic fluxes [20]; it increases glycogen synthesis, blocks fatty acid oxidation [21], and maintains cell redox state. Some of the pharmacologic effects of adenosine on hepatotoxicity are: prevention of fatty liver disease [21], recovery of basal energetic state which was reduced by toxic agents [22], maintenance of redox balance between cytosol and mitochondrion [23], prevention of CCl_4-induced necrosis [24], avoiding free radical propagation during CCl_4 metabolism [25], and modulation of the blood flux of hepatic artery [23]. Furthermore, adenosine is able to reduce 50% collagen accumulation in a cirrhosis prevention model, thanks to the increase of liver collagenolytic activity hand by hand with an improvement of liver function [26–31]. These findings allowed us to propose adenosine as possible treatment to reverse cirrhosis.

In order to understand the mechanism of action of adenosine, we generated several derivatives and compared their hepatoprotective properties against adenosine, because this nucleoside is subject of an active metabolism within the cell resulting in a short half-life of the nucleoside but with capability of metabolic modulation; it could be phosphorylated by adenosine kinase, deaminated to inosine by adenosine deaminase, or transformed to S-adenosylhomocysteine by S-adenosylhomocysteine hydrolase [32].We found that aspartic salt of this nucleoside, now denominated IFC-305, presents a better protection against lethal dose of CCl_4 using a fourth of the dose than the parental compound; this effect could be understandable because IFC-305 presented a delay in the maximal absorption than adenosine (20 vs. 30 min), but adenosine level rapidly declined to practically undetectable levels between 60 and 120 min, while IFC-305 presented a significant liver concentration even 120 min after its administration; this behavior could be explained by a 20% diminution of the activity of the adenosine deaminase, in the presence of IFC-305, an enzyme responsible to transform adenosine to inosine. These results suggest that IFC-305 clearance is much slower than that of adenosine [33]. With these results, we decided to explore the hepatoprotective properties of this adenosine compound, treating rats (50 mg/kg body weight, three times per week) during 5 weeks after cirrhosis induction with CCl_4.

Cirrhotic rats treated with IFC-305 present a healthy-like liver phenotype compared with cirrhotic rats and also with cirrhotic rats treated with saline during 5 weeks after cirrhosis induction. Besides, decreased fibrosis was evident in response to IFC-305 treatment, accelerating fibrosis resolution, leaving only 4% of fibrotic area, while increasing parenchymal liver area from 87 to 90%, and collagen was decreased to half-level as compared to saline-treated rats. This improvement in liver architecture was in accordance with liver physiological amelioration; IFC-305 reduced significantly bilirubin and serum transaminase activities [17], and ATP levels were equivalent to those of healthy liver [34], corroborating that IFC-305 presents the same hepatoprotective properties reverting cirrhosis than adenosine but with a lower dose.

3. Cell cycle inhibition during cirrhosis and its recovery by IFC-305

Liver has a well-known capability to regenerate after resection [35]; the severity of liver fibrosis is considered to be related with impaired regenerative capacity, suggesting the arrest of cell cycle [36]. The fibrogenesis process is accompanied by

energetic imbalance as well as oxidative damage generated by oxygen species that could result in chromosomal instability, which induces injury in the check points of the cellular cycle triggering an impaired regenerative capacity [34].

Cell cycle molecules play essential roles in hepatocyte proliferation. Specifically, G1-phase related molecules are important because they are a requisite to enter into cell cycle from quiescent state [34]. Considering adenosine is able to increase DNA synthesis as well as the mitotic index and the expression of proliferating cell nuclear antigen (PCNA) in a pre-established cirrhosis [31], over and above accelerating progression of cell cycle during liver regeneration in rats subjected to one-third hepatectomy [37], we have explored cell cycle state during cirrhosis and changes mediated by IFC-305.

During cirrhosis, there is no evident change on PCNA, which is an auxiliary protein of DNA polymerase delta and is an excellent marker of cell proliferation and it is present at the beginning of the S phase; but IFC-305 treatment generates a 10-fold increase of this protein, supporting the effect on proliferation activation mediated by this compound; this result was validated by immunohistochemistry [34]. Regarding cell cycle cyclins, cyclin D1 levels in cirrhotic state was not altered, but treatment with IFC-305 showed a 77% protein increase; this behavior correlates with expression levels of that cyclin. On the other hand, Cyclin B1 did not change in cirrhotic rats, but IFC-305 treatment reduces by 30% the protein level [34]. Cyclin D1 belongs to G1 phase and is fundamental to initiate cell cycle and requires the association with cyclin-dependent kinase 4 or 6 (CDK4/CDK6) to form an active complex and allows the progression of cell cycle to S phase, whereas degradation of cyclin B1 is important for metaphase-anaphase transition and progression of cell cycle [38]. Evaluating the levels of CDK4, we did not find changes in cirrhosis but IFC-305 generates a high increment of this protein. In the case of CDK6, the protein is present in cirrhosis, the cessation of CCl_4 and saline solution administration reduces its levels, meanwhile IFC-305 treatment maintains elevated the presence of CDK6 [33]. These results suggest that both CDK4 and CDK6 could form a complex with Cyclin D1 and favor cell cycle progress in response to IFC-305 treatment. The complex Cyclin D/CDK4/6 is responsible for Rb protein phosphorylation, promoting the release of E2F1, which can induce transcription of several genes involved in cell cycle entry into S phase and induction or inhibition of apoptosis [39]. In livers from cirrhotic rats, there is a reduction of phospho-Rb (Ser 795), and IFC-305 restores the healthy levels; *Rb* gene expression correlates with protein levels. Analysis of E2F1 protein levels reveals a decrease of this protein in cirrhotic livers and administration with saline solution during 5 weeks after cirrhosis inductions partially reestablishes the levels of that protein but IFC-305 generates a higher increment than the one reached with saline; this increment together with Rb gain supports the reactivation of cell cycle, suggesting the entry to S phase of cell cycle [34].

Another level to regulate cell cycle progression is related with its inhibitors; with regard to this, p21 is reduced 40% in cirrhotic animals and IFC-305 is able to reassemble the healthy liver levels; p27, another cell cycle inhibitor, did not show effects that could be related with cirrhosis establishment neither to IFC-305 treatment during 5 weeks [34], so it is possible to suggest that one of the key cell cycle inhibitors in cirrhosis development is p21.

Trying to understand which could be the signal that generates this reactivation of cell cycle, we evaluated hepatocyte growth factor (HGF) levels in serum and liver; HGF originally identified and cloned as a potent mitogen for hepatocytes, is a strong protective and trophic factor for many tissues and organs [40]. Since HGF is produced mainly by mesenchymal cells and c-Met, its specific receptor tyrosine kinase is expressed in most epithelial, endothelial, and somatic stem cells [41]. In cirrhosis, there is a little increment of HGF in serum but in liver, there are no

significant changes; meanwhile, rats treated with IFC-305 trigger a threefold increase of serum HGF versus healthy animals and a 35% increase versus cirrhotic animals; in liver, there is a trend to increase the levels of HGF compared with both healthy and cirrhotic rats. On the other hand, c-Met receptors present a 25% increase in cirrhotic animals with further increase after 5 weeks of progress, but treatment with IFC-305 induced a diminution in relation with cirrhotic rats administered with saline [34]. With these results, we could suggest that IFC-305 is able to increase HGF levels in serum of cirrhotic rats, which could interact with c-Met in liver, being the mitogenic signal which could trigger the reactivation of cell cycle recovery.

4. Inflammation, the beginning of liver disease and a key of IFC-305-mediated cirrhosis resolution

In recent years, it has been demonstrated that the immune response is one of the main mechanisms involved in the progression and repair of liver pathologies [42].

Liver injuries provide a proper model of inflammation and repair, showing a complex interaction of parenchymal, no-parenchymal cells and the extracellular matrix, all of them, components of the mammalian wound-healing response. In almost all etiologies, cirrhosis is preceded by fibrosis and inflammation, with elements of innate and adaptive immune response that are crucial in regulating these processes [43]. Recent efforts to confront these fibrotic diseases are focused on finding specific marks that transform an acute inflammation to a chronic one, and to use them as therapeutic aims for treatment and reversion of this phenomenon [44]. The immune response plays an essential role in this transformation, mainly by diverse cellular phenotypes [45]. The participation of immune cells, such as Kupffer cells (KCs), the liver macrophages, as initial effectors, is one of the main responsible of cirrhosis development [46, 47]. They are antigen presenting cells and represent an immune cell population related to liver fibrosis treatment.

The KCs present diverse activation phenotypes: M1 related to inflammation and M2 anti-inflammation related with resolution of inflammation processes [48–50], both are regulated by extracellular signals such as adenosine [51] and are directly connected with other immune cells types as B and T cells.

In liver diseases, the phenomenon, in a canonical way, occurs when the activated KCs regulate the hepatic stellate cells and other molecular and cell interactions associated with the establishment of cirrhosis [52, 53]. KCs also interact with other cells, like neutrophils, hepatocytes, etc., mainly through molecules directly associated with inflammation, tissue damage, and fibrosis, like cytokines and chemokines, such as IL-1β, IL-6, TNF-α, and MCP-1 [54] or ROS (reactive oxygen species) which promote the inflammatory response; KCs could be contributing to anti-inflammatory effects with IL-10 and other cytokines involved in tissue repair [55]. The liver is the main organ that produces and removes cytokines; all cell types in the liver are capable of cytokine production, parenchymal and non-parenchymal cells [56, 57].

By their destructiveness, macrophages guide the course of the inflammatory response and are involved in the synthesis and repair of damaged tissue during the inflammatory process, participating actively in the resolution of inflammation [58]. There are two proposed macrophage subtypes; activated by two ways: the classical pathway (M1) or the alternative pathway (M2) [59]. These different polarization states will depend on the microenvironment and the source of damage that has occurred. The classical activation is critical for the initiation and maintenance of the inflammatory process and to the response against pathogens and immune response.

Classical activation or M1 is produced by the interaction of TLR4 receptor with PAMPs such as LPS, from Gram-negative bacteria wall or by specific cytokines such as TNF-α or γ-IFN. This group of classically activated macrophages produces large amounts of proinflammatory cytokines such as TNF-α, interleukins (IL-1β, IL-6, and IL-12), proinflammatory chemokines such as MCP-1, and nitric oxide (NO), promoting activation, migration of other cells, and tissue damage [58].

In the case of alternative activation, the Th2 cells secrete cytokines such as IL-4 or IL-13 and induce the macrophage alternative M2 phenotype [60]. These M2 macrophages have very little capacity to present antigens while secrete high levels of anti-inflammatory cytokines such as IL-10. Unlike classical activation, these macrophages are not able to produce nitric oxide from L-arginine and also fail to control the growth of intracellular pathogens [61]. However, they are capable of producing a high quantity of arginase 1 enzyme that metabolizes L-arginine to produce proline, glutamate, and polyamines promoting tissue repair [62].

We have demonstrated that in the experimental model of CCl_4-induced cirrhosis, the IFC-305 treatment generates several changes in the inflammatory process, mediated by cytokines and immune cells [63]. During the development of cirrhosis, we observed an increment in the liver inflammatory cytokines, IL-6, IL-1β, MCP-1, and TNF-α, in plasma and liver tissue, as well as an increment of M1 macrophages (CD163+/CD11b+). The IFC-305 treatment decreased these inflammatory cytokines, reduced the M1 inflammatory macrophages, and increased the M2 anti-inflammatory macrophages (HIS36+/CD11b+). The anti-inflammatory role of IFC-305 was also supported by elevation of IL-10, an enhanced metabolic activity of arginase, reduction of NO levels in serum rats, a diminution of the protein levels of inducible nitric oxide synthetase, and an increment of the protein levels of arginase 1 in the liver. These results suggest that the IFC-305 modulates the immune response in cirrhosis and supports the hepatic protective action through an anti-inflammatory role, mainly mediated by Kupffer cells [64].

5. Hepatic stellate cells, generators of extracellular matrix components which trigger fibrosis and its activation prevention by IFC-305

Liver fibrosis is characterized by an accumulation of collagen types I and III that are secreted by liver myofibroblast. These cells are originated mainly from hepatic stellate cells (HSCs) and in a less number from the periportal fibroblast or bone marrow cells. In normal liver, HSCs represent almost 10% of all resident cells of the liver. They are quiescent cells specialized in lipid storage, mostly retinyl esters. When there is a liver damage, the HSC become activated or transdifferentiate to myofibroblast phenotype, characterized for being proliferative, pro-inflammatory, and contractile and for increased synthesis of ECM proteins [65].

The activation of HSCs is promoted by stimuli from resident and infiltrating inflammatory cells that produce fibrogenic, proliferative, and inflammatory cytokines such as TGF-β, PDGF, and TNF-α, among others, in addition to reactive oxygen species [65].

In order to clarify the hepatoprotector role of IFC-305 in the CCl_4-induced liver fibrosis at a molecular and cellular level, we explored the effect of IFC-305 on the activation of HSCs. These cells isolated from normal rat livers become activated *in vitro* after 7 days in culture, in a similar manner that occurs *in vivo* after a liver injury. We isolated HSCs from normal rat livers and cultured them for 7 days. We found that IFC-305 treatment suppresses their activation, determined by the inhibition of *Col1a1* mRNA expression, prevention of Rho activation, inhibition of

PDGF-stimulated proliferation, and increased expression of anti-fibrogenic genes such as *Pparg*, *Smad7*, and *Mmp-13* [66].

Hepatic fibrosis is characterized by ECM deposition, specially the type I collagen protein. The excess of ECM is due to an imbalance between its production and its degradation. ECM degradation is carried out by matrix metalloproteinases (MMPs), whose activity is negatively regulated by tissue inhibitors of matrix metalloproteinases (TIMPs). During progression of liver fibrosis, activated HSCs produce an excess of ECM and increase the expression of TIMP-1 and TIMP-2, resulting in an excess of ECM deposition. In rodents, the MMP-13 is the principal matrix metalloproteinase that degrades type I collagen [67]. Treatment of HSCs with IFC-305 inhibited the production of *Col1a1* mRNA but also increased the expression of *Mmp13* mRNA, which may result in an important decrease of collagen deposition.

The main fibrogenic cytokine is TGF-β, which signals into the cell through membrane kinase TGF-type I and type II receptors, which activate the intracellular Smad proteins and transduce the TGF-α signal to the nucleus. The Smad 7 acts as a negative regulator of this pathway [65]. The *Smad7* mRNA expression induced by IFC-305 could result in the inhibition of TGF-β signaling and inhibition of HSC activation.

Peroxisome Proliferator Activated Receptor gamma (PPARγ) regulates cellular fatty acid storage and adipogenesis of fibroblast. Another very important effect of IFC-305 on HSC is an increase of *Pparg* mRNA expression. PPARγ is expressed in quiescent HSC, and its expression is rapidly decreased during HSC activation *in vitro* and *in vivo* [68]. It is well documented that expression of PPARγ or treatment with its natural or synthetic ligands inhibits HSC activation or can reverse the activated HSC phenotype to the quiescent one [69]. The increased expression of *Pparg* mRNA with IFC305 in HSCs could be contributing to maintain their quiescent phenotype.

The IFC-305 also inhibited the PDGF-BB-stimulated proliferation of HSC; exploring the mechanism, we found that this effect was independent of adenosine receptors, but required their uptake into cells by adenosine transporters followed by their intracellular conversion to AMP by adenosine kinase, leading to increased levels of AMP, pyrimidine starvation, and inhibition of DNA synthesis [66].

In summary, we demonstrated that HSCs are an important target of the anti-fibrotic role of IFC-305 contributing to its hepatoprotective effect on liver fibrosis.

6. Gene expression deregulation in cirrhosis and IFC-305 modulation beyond genetics

With the interest to have a general view of molecular changes occurring in cirrhosis, we assessed the transcriptome evaluation of both cirrhotic and cirrhotic livers treated with IFC-305 and found 413 deregulated genes in cirrhosis, and IFC-305 treatment reduces the genes with deregulated expression to 263; making a gene ontology, we noticed that the highest proportion of deregulated genes is related with signal transduction, and interestingly, some of these deregulated genes are involved in TGF-β signaling pathway, lipid metabolism, urea cycle, and fibrogenesis.

Validating some of these differential expressed genes, we found an over-expression of *Fn1* (fibronectin 1) and *Col1a1* in cirrhosis; both of them are regulated by TGF-β signaling pathway, and importantly, *Col1a1* gene encodes a component of type I collagen called the pro-α1(I) chain that constitutes one of the main ECM proteins in the fibrotic liver. In fact, expression of *Tgfb1* gene was also increased in cirrhosis, and other two genes with the same behavior were the complement *C9* and

Apoa1 [17]. PPARγ has anti-fibrogenic activity inhibiting collagen I transcription [70]; there was a reduction in transcript levels of *Pparg* gene in cirrhosis state, in concordance with other reports [71, 72]. Transcriptome analysis also revealed three genes involved in ornithine and urea metabolism; the transcript level of *Ass1* gene was reduced as well as *Cps1* gene. Making a deeper analysis of the transcriptome data, we could identify a chromatin-related gene deregulated in cirrhosis; *HDAC3* histone deacetylase is over-expressed during cirrhosis. IFC-305 is able to reduce the levels to healthy-like levels for three fibrogenic genes (*Fn1*, *Col1a1*, and *Tgfb1*), *C9, Apob1* and *Hdac3;* meanwhile, this compound generates the increasing expression of *Pparg* and *Cps1* recovering the levels of the healthy liver and partially restoring the levels of *Ass1* [17]. Analyzing proteins, we could identify an increment in collagen I and HDAC3 and a reduction of PPARγ during cirrhosis, and the treatment with IFC-305 resembles the healthy-like levels of these three proteins [16]. Thus, through this quantitative analysis of expression and protein levels, IFC-305 shows capabilities to modulate the gene expression of some important genes involved in liver fibrogenesis.

During CCl_4-induced cirrhosis, besides hepatocellular damage previously mentioned, there is chromosome instability [73] that could be induced by hypomethylation on DNA, and contributes to carcinogenesis [74]. Considering cirrhosis as a pre-neoplastic state (because 80% of hepatocellular carcinoma cases are preceded by cirrhosis) [11], it is possible that the big changes in gene expression could be directed by chromosomal instability generated by CCl_4, but beyond the genetic alterations that probably are occurring, many of these changes could be related to regulation of gene expression at epigenetic level even more because chromosomal instability could be occurring by DNA hypomethylation. Also, it is important to remember that HDAC3 was incremented in cirrhosis, so some changes in gene expression could also be modified by changes in chromatin.

Every process which is able to influence in heritable gene expression without affecting DNA sequence is considered as an epigenetic regulation process [75]. DNA methylation is probably the most studied epigenetic modification [76, 77]; it consists in the incorporation of methyl group in 5 position of cytosine from CpG dinucleotide. This incorporation does not modify DNA sequence and can influence directly in transcriptional activity [78]. Methylated DNA distribution along genome shows an enrichment on noncoding regions, repetitive elements [75], and further, it inactivates mobile elements of the genome as transposons and sequences of viral origin, having a function in genome stability maintenance, blocking undesired recombination events [76]. On the other hand, on CpG islands of active genes, there is no enrichment of this DNA modification [75] and participates in permanent gene silencing in different steps of development [78, 79]. DNA methylation is directed by DNA methyltransferase enzymes which use S-adenosylmethionine (SAM) as methyl donor from methionine cycle and the product of this reaction is S-adenosylhomocysteine (SAH). It is important to mention that one important factor to modulate biological methylation reactions (to DNA, RNA, proteins, and phospholipids) is the hepatocellular ratio SAM/SAH [80].

The discovery of an active DNA demethylation pathway that involves the conversion of 5mC to oxidized forms, like 5hmC, by DNA dioxygenases TETs and DNA repair through the base excision system, incorporates a dynamic reversibility of DNA methylation [81–84]. Ever since the discovery of this dynamics, strenuous efforts have been made to characterize the precise role of 5hmC; such roles are becoming more evident as we learn about 5hmC-specific genomic localization, its relative stability, and recognition by other proteins [85], and current studies have shown that this DNA modification has an antagonic role to 5mC [86].

We have previously shown that adenosine can modulate trans-methylation reactions, like methylation of phospholipids, via regulation of

S-adenosylmethionine (SAM) levels [87], so that we make an approach to SAM levels and found that during cirrhosis, the amount of this molecule is diminished, whereas IFC-305 treatment restored the physiological levels; this suggests that during cirrhosis, it could be an imbalance of methylation reactions, and IFC-305, like adenosine, could also regulate this process [16].

Epigenetic changes in cirrhosis are little understood; some studies demonstrated a reduction on DNA methylation through the genome in CCl_4-induced cirrhosis [15, 88], and analyzing in a global way this modification, we obtained the same behavior. With these results and in order to assess DNA methylation dynamics, 5hmC levels were measured and a similar behavior to the one observed with 5mC, a reduction of 5hmC in cirrhosis in concordance with group of Mann findings, was found [89]. Treatment with IFC-305 triggers a regaining of both 5mC and 5hmC [16]. These results together suggest that there is a perturbation of DNA methylation dynamic during cirrhosis, while IFC-305 is able to modulate this dynamic, possibly reducing chromosome instability.

Another level of epigenetic regulation is related with genome packaging in chromatin, which has a direct repercussion in transcriptional activity, being mandatory its remodeling, space specifically, and in a time defined way to carry out gene expression [90]. Histones are a fundamental component of chromatin structure, being a target of a big variety of post-translational modifications (PTMs), which allows the formation of particular and regulated chromatin states; furthermore these modifications could be inherited post-mitotically [91]. We want to highlight among histone PTMs, lysine acetylation. DNA association with histone *core* is facilitated by electrical charge difference between both molecules, but histone acetylation neutralizes lysine positive charge, weakening nucleosome-DNA interaction and triggering a less compact conformation which favors transcription [92].

Considering the finding that histone deacetylase HDAC3 level was high during cirrhosis, global histone H4 acetylation was assessed, finding a reduction in this histone PTM in cirrhotic livers. Physiological levels of global histone H4 acetylation in cirrhotic rats treated with IFC-305 were recovered [16]. Together, these results suggest that deregulated gene expression during cirrhosis could be related with epigenetic deregulation involving DNA methylation dynamics and changes in histone acetylation; besides, IFC-305 has epigenetic properties being able to modulate 5mC, 5hmC, and histone H4 acetylation in a global way, favoring the recovery of physiological levels of each epigenetic modification and triggering the rescue of healthy-like gene expression in liver.

7. Getting deeper into cirrhosis resolution or epigenetic regulation of *Pparg* and *Col1a1* by IFC-305

Once established that IFC-305 is able to reverse fibrosis, reactivating cell cycle progression in cirrhotic livers, favoring an anti-inflammatory environment, blocking hepatic stellate cell activation, and regulating gene expression through epigenetic modulation, we analyzed the regulation of two of the main genes with modified expression during cirrhosis, *Pparg* and *Col1a1.* Reminding, collagen I is the mayor ECM protein and responsible for liver fibrosis, *Col1a1,* a gene which encodes pro-α1 chain of this protein is over-regulated in cirrhosis, and there is a reduction of nuclear receptor PPARγ in this pathological condition.

PPARγ has antifibrotic properties because it is able to inhibit collagen I gene transcription. This inhibition is mediated by the ability of nuclear receptor to compete with NF-I/p300 association to the *Col1a1* gene in HSC [70]. p300 has a histone acetyltransferase activity that transfers an acetyl group to the lysine residue

[93] generating an open chromatin context in *Col1a1* gene promoter favoring its expression; whether PPARγ replaces p300 in Col1a1 gene promoter, there is a chromatin context change because of the loss of acetylation activity in this region, and the consequent blocking of the gene expression.

On the other hand, regulation of *Pparg* expression is directed by MeCP2 protein in HSC activation like in cirrhosis. MeCP2 binds to regulatory regions of the gene which are CpG enriched and recruits histone H3K9me3 writer enzymes suppressing initial transcription of the gene. Furthermore, MeCP2 is required for polycomb repressor complex 2 EZH2 component that establishes histone H3K27me mark on the downstream coding gene region, blocking transcription elongation [94]. This mechanism could explain the reduction of PPARγ levels in cirrhosis and therefore the over-expression of *Col1a1*in cirrhosis.

Considering that MeCP2 is a methyl binding protein [94], DNA methylation state was evaluated with sodium bisulfite DNA modification on *Pparg* gene promoter, and it was found that both healthy and cirrhotic livers present *Pparg* gene promoter without DNA methylation, and IFC-305 treatment does not modify this nonmethylated state [16]. Evaluating histone H4 acetylation and histone H3K27me3 on *Pparg* gene promoter through chromatin immunoprecipitation assay, we found that in cirrhosis, there is a trend to compact chromatin context mainly dictated by histone H4 acetylation reduction, which correlates with decreased expression and protein levels; after treatment with IFC-305 chromatin, there is an open chromatin context on *Pparg* gene promoter triggered by an increase on histone H4 acetylation and a reduction of histone H3K27me3, going hand by hand with over-expression and increase of protein levels [16]. These findings suggest that reduction of PPARγ on cirrhosis is coordinated by a chromatin compaction on gene promoter, and IFC-305 treatment generates a decompaction of gene promoter with the consequent increase of gene expression.

The next step was to identify if IFC-305 mediated fibrosis reversion is related with *Col1a1* gene expression blocking though PPARγ was to assess nuclear receptor deposition on *Col1a1* gene promoter, but we were not able to find an increment of this interaction in whole cirrhotic tissues treated with IFC-305; rather, we found a diminishment of PPARγ deposition [16]. Further experiments on isolated HSCs treated with IFC-305 are required to know if this molecular mechanism is occurring directly in responsible cells of fibrosis generation. So, we asses DNA methylation state on *Col1a1* gene promoter, to know if this epigenetic mechanism is involved in regulation of gene expression during cirrhosis. In healthy liver, *Col1a1* gene promoter presents a methylated state, which correlates with the absence of collagen I overproduction; in cirrhosis state and progress of the illness, there is an important reduction on methylation state on *Col1a1* gene promoter going hand by hand with accumulation of collagen I; and finally, treatment with IFC-305 generates a remethylation of gene promoter and an enrichment of methylation around transcription start site, associated with collagen reduction.

With these results, we could propose that fibrosis generation could be directed by loss of DNA methylation on *Col1a1* gene promoter, and one of the mechanisms of action that could explain cirrhosis resolution mediated by IFC-305 is the modulation of DNA methylation on *Col1a1* gene.

Blocking the prelude of hepatocellular carcinoma, a key point to avoid chronic liver injury progress.

Along this chapter, some cellular and molecular alterations that characterize cirrhosis have been described: a pathology that results in the combination of factors which alters liver environment, beginning with an immunological response originated by macrophages inflammatory polarization that triggers hepatic stellate cell activation, with alterations at chromatin level resulting in chromosome instability and altered gene expression favoring the fibrogenic process. All these changes, as a whole, could facilitate progress of the illness to hepatocellular carcinoma (HCC),

which is the most common primary carcinoma of the liver. Up to 85% of HCC cases arise in chronically inflamed and subsequently cirrhotic livers [95].

According to GLOBOCAN-IARC datasets [96], liver cancer is estimated to be at the 7th place of cancer incidence and the 4th cancer death cause in 2018. Considering cirrhosis as a prelude of HCC, it is understandable that many liver cancers follow a pattern of pathologic evolution, starting from cirrhosis to low-grade dysplastic nodules, high-grade dysplastic nodules, early HCC, progressed HCC and, finally to advance HCC. Furthermore, this progress of illness involves a more evident imbalance between genetic and epigenetic factors; regarding genetic ones, early dysplastic nodules present a genome with a very limited genetic variation, while advanced HCC has a heterogeneous genome with a range of 72–182 mutations [97, 98]. On the other hand, concerning epigenetic aspects, a genome-wide DNA hypomethylation in HCC has been described, which could be indicative of poor survival [99]. In the same sense, another study described that aberrantly methylated differential expressed genes are related with cell cycle progress, p53 signaling, and MAPK signaling in HCC [100]. Alteration on DNA methylation state could be explained by down-regulation of TET dioxygenases in HCC condition with the consequent reduction of 5hmC levels [101]. In normal tissue there is a characteristic difference between euchromatic and heterochromatic regions that is lost in cancer condition; it has been suggested that lost could be generated by a reduction of 5hmC levels which goes around 70%. Furthermore, the specific relationship between 5hmC and chromatin marks in normal tissue is largely erased in tumors and suggests that 5hmC landscape change in cancer could be associated with chromatin structure alterations and deregulation of gene expression during tumorigenesis [102].

HCC may progress silently in patients with sufficient liver function; due to vague complaints and nonspecific symptoms, HCC diagnosis is usually delayed [103]. Selected patients with localized disease may be treated with curative intents with resection, liver transplantation, or local therapy like radial frequency ablation, chemoembolization or radio-embolization. However, the majority of patients with HCC are not candidates for resection [104, 105]. For patients suffering from advanced HCC, chemotherapy failed to demonstrate a survival advantage [106, 107]; so far, sorafenib is the first and only target orientated agent approved as therapy of HCC [105], but it only extends survival of patients with advanced stage disease for 3 months, and this medication causes considerable adverse events and offers no symptom palliation [108]. This lack of effective treatment and surgical impediment highlights the importance to reinforce molecular target therapies.

Preclinical studies indicated that IFC-305 is not toxic, neither genotoxic, nor teratogenic and it is anti-carcinogenic [33]. Considering this last property, we assessed IFC-305 effects on a chronic model of liver intoxication with diethylnitrosamine and found that it could act as a HCC chemopreventive agent [109, 110]. The above suggests that some anti-fibrotic effects of the compound could prevent cancer development, being an adjuvant in chronic liver disease treatment. Currently we are studying a deep molecular level to identify IFC-305 mechanism of action in prevention of cancer establishment and potential disease reversion.

Considering recent advances in cirrhosis knowledge, we could suggest that in the not long future, drugs targeting specific molecular keys for cirrhotic and HCC will be developed and potentially they could be the first line of treatment even after surgery.

8. Conclusion

Cirrhosis is a complex pathology, which involves deregulation at different levels (**Figure 1**); some insults such as hepatitis viral infections, alcohol, high fat diet, or

even self-immune events could trigger the development of the illness, denoted by biochemical alterations like albumin reduction and increase of transaminases. In our case, we assessed the study of this disease using CCl_4, which generates hepatocellular damage. Once cell membrane is affected by free radicals from CCl_4 metabolism, through epoxide formation, KCs are activated to phagocytose damaged cells; this activation causes an inflammatory process, due to M1 macrophage activation. Whether this inflammation is perpetuated, HSCs could be activated, becoming the main producers of fibrosis (**Figure 1B**). At molecular level, cirrhotic-damaged liver loses the capability to proliferate; there is a reduction in DNA methylation, 5hmC, and histone H4 acetylation, which generates chromosome instability and therefore alteration of gene expression, affecting principally fibrogenic genes. Among important genes involved in the fibrogenic process are *Pparg* and *Col1a1*. Cirrhotic liver presents a compact chromatin context of *Pparg* gene promoter with the consequent reduction of both its transcript and protein; on the other hand, *Col1a1* gene promoter loses DNA methylation, and this correlates with gene overexpression and the increment of protein levels. Adenosine derivative, IFC-305, has hepatoprotective properties (**Figure 1C**); it is able to reduce fibrosis, ameliorate parenchymal area and recover liver function. Treatment with this compound polarizes the macrophages to an anti-inflammatory phenotype M2, increasing the levels of immunosuppressant cytokine IL-10 and arginase 1; the reduction of the inflammatory process facilitates the inhibition of HSC activation and the consequent reduction of fibrosis. At molecular level, high serum levels of HGF, principal liver mitogen, could interact with elevated levels of its receptor, c-Met, and stimulate cell cycle progression, providing once more the regenerative capacity to the liver. IFC-305 could favor a genome instability diminishment as a consequence of the

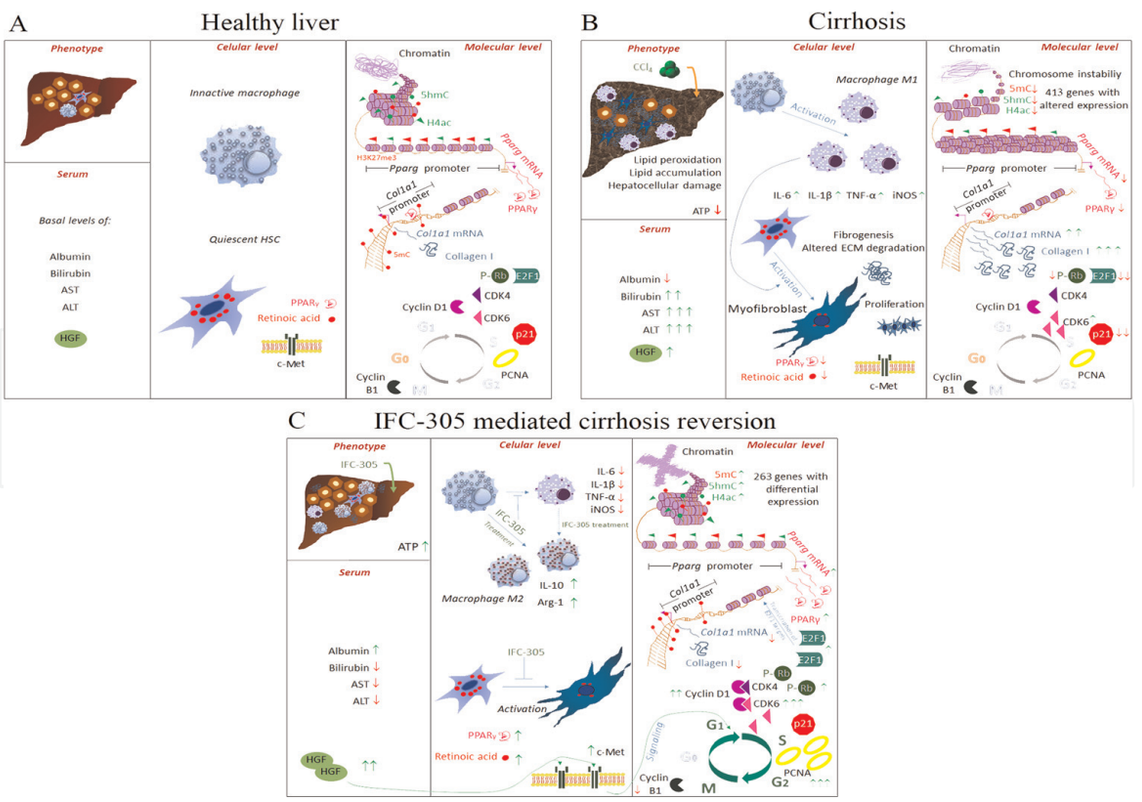

Figure 1.
Architectural, physiological, cellular, and molecular alteration during CCl_4-induced cirrhosis and hepatoprotective effects of IFC-305. We show four different analyzed levels in this section: phenotype, denoting architecture and cell composition of the liver; Serum, biochemical markers related with liver function; cellular level, changes found in non-parenchymal cells; molecular level, changes in cell cycle components, chromatin, and gene expression. (A) Healthy liver; (B) CCl_4-induced cirrhosis state; (C) pre-established cirrhosis treated with IFC-305.

reestablishment of DNA methylation levels and 5hmC and Histone H4 acetylation; these effects on chromatin trigger the recovery of healthy-like gene expression. Fibrosis resolution mediated by IFC-305 could be explained by the generation of an open chromatin context of *Pparg* gene promoter that correlates with its gene and protein up-regulation. High levels of PPARγ could act as a repressor of *Col1a1* expression in HSC; on the other hand, *Col1a1* gene promoter gains DNA methylation on promoter and TSS, this methylation state goes hand by hand with reduction of collagen I expression and protein, favoring a decrease in fibrosis, a key point in cirrhosis resolution. These studies support molecules and cell behavior modified by IFC-305 as a potential target for new drugs to treat cirrhosis, contribute to the understanding of liver fibrosis at epigenetic level, open the door to the exploration of chromatin modifications as a potential biomarker for early detection and intervention of liver diseases, and support the use of IFC-305 as therapy for liver illness. Finally, we highlight the relationship between cirrhosis and HCC, how liver fibrosis is the prelude of HCC and in what manner IFC-305 could be an adjuvant preventing HCC by its anti-cirrhotic and anti-neoplastic effects, and how recent advances could favor development of an effective treatment, preferring a less invasive to surgical one.

Acknowledgements

This work has been supported by DGAPA-UNAM, grant numbers: IN214419 to VCS and IN203917 to FRT; CONACyT, México, grant: *Fronteras de la Ciencia* 290 to FRT; *Fundación Miguel Alemán, México* "*Estímulo a Investigaciones Médicas*" to VCS; PhD Fellowships from CONACyT: CVU 508509 to JRRA, CVU 298432 to RPCV, CVU 580148 to NGC. We acknowledge the assistance of Rosario Pérez-Molina, Georgina Guerrero-Avendaño, Fernando Suaste-Olmos, Enrique Chávez, Rosario Villaseñor Ávila, and Gabriela Valdés Silva.

Conflict of interest

The authors declare no conflict of interest.

Nomenclature

5hmC	5-hydroximethylcytosine
5-LO	5-lipoxygenase
5mC	5-methylcytosine
ALT	alanine aminotransferase
AMP	adenosine monophosphate
AST	aspartate aminotransferase
ATP	adenosine triphosphate
$CCl_3\cdot$	trichloromethane radical
$CCl_3OO\cdot$	trichloromethyl peroxy radical
CCl_4	carbon tetrachloride
CDK4	cyclin-dependent kinase (for example, CDK4, CDK6, etc.)
c-Met	tyrosine-protein kinase Met or hepatocyte growth factor receptor
Col1a1	type I collagen pro-α1(I) chain gene
CpG	cytosine guanine dinucleotide

DNA	deoxyribonucleic acid
E2F1	transcription factor E2F1
ECM	extracellular matrix
H3K27me3	histone H3 trimethyl lysine 27
H4ac	hyperacetylated histone H4
HCC	hepatocellular carcinoma
HDAC	histone deacetylase
HGF	hepatocyte growth factor
HSC	hepatic stellate cells
IFC-305	aspartate salt of adenosine: 2-aminosuccinic acid–2-(6-amino-9H-purin-9-yl)-5-(hydroxymethyl)tetrahydrofuran-3,4-diol (1:1)
IL	interleukin (for example, IL-1β, IL-10, etc.)
iNOS	inducible nitric oxide synthase
KC	Kupffer cells
LPS	lipopolysaccharide
M1	inflammatory macrophages
M2	anti-inflammatory macrophages
MAPK	mitogen-activated protein kinase
MCP-1α	macrophage protein inflammatory 1-alpha
MeCP2	methyl-CpG binding protein 2
MMP9	matrix metalloproteinase 9
mRNA	messenger ribonucleic acid
NO	nitric oxide
p21	cyclin-dependent kinase inhibitor 1
p27	cyclin-dependent kinase inhibitor 1B
P450	CYP450 cytochrome
PAMPs	pathogen associated molecular patterns
PCNA	proliferating cell nuclear antigen
PDGF	platelet-derived growth factor
PPARγ	peroxisome proliferator-activated receptor gamma
PTMs	post-translational modifications
Rb	retinoblastoma protein
RNA	ribonucleic acid
ROS	reactive oxygen species
SAH	S-adenosylhomocysteine
SAM	S-adenosylmethionine
STAT6	signal transducer and activator of transcription 6
TET	DNA dioxygenase ten-eleven translocation
TGF-β	transforming growth factor beta
TIMPs	tissue inhibitors of matrix metalloproteinases
TLR4	Toll-like receptor 4
TNF-α	tumoral necrosis factor alpha
VEGF	vascular endothelial growth factor
α-SMA	alpha smooth muscle actin.

Author details

Jesús Rafael Rodríguez-Aguilera[1], Rebeca Pérez-Cabeza de Vaca[1,2], Nuria Guerrero-Celis[1], Gabriela Velasco-Loyden[1], Mariana Domínguez-López[1], Félix Recillas-Targa[3] and Victoria Chagoya de Sánchez[1]*

1 Department of Cell Biology and Development, Institute of Cellular Physiology, UNAM, Mexico City, Mexico

2 Coordination of Research, National Medical Center "20 de noviembre", ISSSTE, Mexico City, Mexico

3 Department of Molecular Genetics, Institute of Cellular Physiology, UNAM, Mexico City, Mexico

*Address all correspondence to: vchagoya@ifc.unam.mx

References

[1] Tsochatzis EA, Bosch J, Burroughs AK. Liver cirrhosis. Lancet. 2014;**383**: 1749-1761

[2] Ma C, Brunt EM. Histopathologic evaluation of liver biopsy for cirrhosis. Advances in Anatomic Pathology. 2012; **19**:220-230

[3] Fauci A, Kasper D, Longo D, Braunwald E, Hauser S, Jameson L, et al. Harrison Principios de Medicina Interna. 17th ed. China: McGraw-Hill/ Interamericana de México; 2009

[4] Chang TT, Liaw YF, Wu SS, Schiff E, Han KH, Lai CL, et al. Long-term entecavir therapy results in the reversal of fibrosis/cirrhosis and continued histological improvement in patients with chronic hepatitis B. Hepatology. 2010;**52**:886-893

[5] Chen G, Zhang L, Chen L, Wang H, Zhang Y, Bie P. Role of integrin alphavbeta6 in the pathogenesis of ischemia-related biliary fibrosis after liver transplantation. Transplantation. 2013;**95**:1092-1099

[6] Falize L, Guillygomarc'h A, Perrin M, Laine F, Guyader D, Brissot P, et al. Reversibility of hepatic fibrosis in treated genetic hemochromatosis: A study of 36 cases. Hepatology. 2006;**44**: 472-477

[7] Hammel P, Couvelard A, O'Toole D, Ratouis A, Sauvanet A, Flejou JF, et al. Regression of liver fibrosis after biliary drainage in patients with chronic pancreatitis and stenosis of the common bile duct. The New England Journal of Medicine. 2001;**344**:418-423

[8] Pol S, Carnot F, Nalpas B, Lagneau JL, Fontaine H, Serpaggi J, et al. Reversibility of hepatitis C virus-related cirrhosis. Human Pathology. 2004;**35**:107-112

[9] Wanless IR, Nakashima E, Sherman M. Regression of human cirrhosis. Morphologic features and the genesis of incomplete septal cirrhosis. Archives of Pathology and Laboratory Medicine. 2000;**124**:1599-1607

[10] Longo D, Kasper D, Jameson L, Fauci A, Hauser S, Loscalzo J. Harrison Principios de Medicina Interna. 18th ed. México: McGraw-Hill; 2012

[11] Forner A, Hessheimer AJ, Isabel Real M, Bruix J. Treatment of hepatocellular carcinoma. Critical Reviews in Oncology/Hematology. 2006;**60**:89-98

[12] Hernandez-Gea V, Friedman SL. Pathogenesis of liver fibrosis. Annual Review of Pathology. 2011;**6**:425-456

[13] Recillas-Targa F. Interdependency between genetic and epigenetic regulatory defects in cancer. Methods in Molecular Biology. 2014;**1165**:33-52

[14] Medina J. Medicina Ocupacional. Gases y Disolventes. 2011. Available from: http://es.scribd.com/doc/ 57239677/37/Tetracloruro-de-Carbono

[15] Varela-Moreiras G, Alonso-Aperte E, Rubio M, Gasso M, Deulofeu R, Alvarez L, et al. Carbon tetrachloride-induced hepatic injury is associated with global DNA hypomethylation and homocysteinemia: Effect of S-adenosylmethionine treatment. Hepatology. 1995;**22**:1310-1315

[16] Rodriguez-Aguilera JR, Guerrero-Hernandez C, Perez-Molina R, Cadena-Del-Castillo CE, Perez-Cabeza de Vaca R, Guerrero-Celis N, et al. Epigenetic effects of an adenosine derivative in a Wistar rat model of liver cirrhosis. Journal of Cellular Biochemistry. 2018; **119**:401-413

[17] Perez-Carreon JI, Martinez-Perez L, Loredo ML, Yanez-Maldonado L, Velasco-Loyden G, Vidrio-Gomez S,

et al. An adenosine derivative compound, IFC305, reverses fibrosis and alters gene expression in a pre-established CCl(4)-induced rat cirrhosis. The International Journal of Biochemistry and Cell Biology. 2010;**42**: 287-296

[18] Chagoya-de-Sánchez V, Suárez JA, Hernández-Muñoz R. Investigación y desarrollo de un fármaco para el tratamiento de la cirrosis. TIP Revista Especializada en Ciencias Químico-Biológicas. 2005;**8**:106-114

[19] Chagoya de Sanchez V, Brunner A, Pina E. In vivo modification of the energy charge in the liver cell. Biochemical and Biophysical Research Communications. 1972;**46**:1441-1445

[20] Chagoya de Sanchez V, Brunner A, Sanchez ME, Lopez C, Pina E. Utilization of adenosine as a tool in studies on the regulation of liver glycogen biosynthesis. Archives of Biochemistry and Biophysics. 1974;**160**: 145-150

[21] Garcia-Sainz JA, Hernandez-Munoz R, Santamaria A, de Sanchez VC. Mechanism of the fatty liver induced by cycloheximide and its reversibility by adenosine. Biochemical Pharmacology. 1979;**28**:1409-1413

[22] Hernandez-Munoz R, Santamaria A, Garcia-Sainz JA, Pina E, Chagoya de Sanchez V. On the mechanism of ethanol-induced fatty liver and its reversibility by adenosine. Archives of Biochemistry and Biophysics. 1978;**190**: 155-162

[23] Garcia-Sainz JA, Hernandez-Munoz R, Glender W, Pina E, Chagoya de Sanchez V. Effects of adenosine on ethanol-induced modifications of liver metabolism. Role of hepatic redox state, purine and fatty acid metabolism. Biochemical Pharmacology. 1980;**29**: 1709-1714

[24] Hernandez-Munoz R, Glender W, Diaz Munoz M, Adolfo J, Garcia-Sainz JA, Chagoya de Sanchez V. Effects of adenosine on liver cell damage induced by carbon tetrachloride. Biochemical Pharmacology. 1984;**33**:2599-2604

[25] Chagoya de Sanchez V, Hernandez-Munoz R, Yanez L, Vidrio S, Diaz-Munoz M. Possible mechanism of adenosine protection in carbon tetrachloride acute hepatotoxicity. Role of adenosine by-products and glutathione peroxidase. Journal of Biochemical Toxicology. 1995;**10**:41-50

[26] Hernandez-Munoz R, Diaz-Munoz M, Suarez J, Chagoya de Sanchez V. Adenosine partially prevents cirrhosis induced by carbon tetrachloride in rats. Hepatology. 1990;**12**:242-248

[27] Hernandez-Munoz R, Diaz-Munoz M, Chagoya de Sanchez V. Effects of adenosine administration on the function and membrane composition of liver mitochondria in carbon tetrachloride-induced cirrhosis. Archives of Biochemistry and Biophysics. 1992;**294**:160-167

[28] Hernandez-Munoz R, Diaz-Munoz M, Chagoya de Sanchez V. Possible role of cell redox state on collagen metabolism in carbon tetrachloride-induced cirrhosis as evidenced by adenosine administration to rats. Biochimica et Biophysica Acta. 1994; **1200**:93-99

[29] Hernandez-Munoz R, Chagoya de Sanchez V. In vivo correlation between liver and blood energy status as evidenced by chronic treatment of carbon tetrachloride and adenosine to rats. Canadian Journal of Physiology and Pharmacology. 1994;**72**:1252-1256

[30] Hernandez-Munoz R, Diaz-Munoz M, Lopez V, Lopez-Barrera F, Yanez L, Vidrio S, et al. Balance between oxidative damage and proliferative potential in an experimental rat model of CCl4-induced cirrhosis: Protective role of adenosine administration. Hepatology. 1997;**26**:1100-1110

[31] Hernandez-Munoz R, Diaz-Munoz M, Suarez-Cuenca JA, Trejo-Solis C, Lopez V, Sanchez-Sevilla L, et al. Adenosine reverses a preestablished CCl4-induced micronodular cirrhosis through enhancing collagenolytic activity and stimulating hepatocyte cell proliferation in rats. Hepatology. 2001; **34**:677-687

[32] Chagoya de Sanchez V. Circadian variations of adenosine and of its metabolism. Could adenosine be a molecular oscillator for circadian rhythms? Canadian Journal of Physiology and Pharmacology. 1995;**73**: 339-355

[33] Chagoya-de-Sánchez V, Hernández-Luis F, Díaz-Muñoz M, Hernández-Muñoz R. Role of the energy state of liver cell in cirrhosis development and treatment. In: Miranda LM, editor. Liver Cirrhosis Causes, Diagnosis and Treatment. New York, USA: Nova Science Publishers, Inc.; 2012. pp. 31-58

[34] Chagoya de Sanchez V, Martinez-Perez L, Hernandez-Munoz R, Velasco-Loyden G. Recovery of the cell cycle inhibition in CCl(4)-induced cirrhosis by the adenosine derivative IFC-305. International Journal of Hepatology. 2012;**2012**:212530

[35] Kokudo N, Kothary PC, Eckhauser FE, Raper SE. Transforming growth factor-alpha (TGF-alpha) improves hepatic DNA synthesis after hepatectomy in cirrhotic rats. Journal of Surgical Research. 1992;**52**:648-655

[36] Kato A, Bamba H, Shinohara M, Yamauchi A, Ota S, Kawamoto C, et al. Relationship between expression of cyclin D1 and impaired liver regeneration observed in fibrotic or cirrhotic rats. Journal of Gastroenterology and Hepatology. 2005; **20**:1198-1205

[37] Mendieta-Condado E, Pichardo-Olvera M, Sanchez-Sevilla L, Chagoya de Sanchez V, Hernandez-Munoz R. Adenosine administration accelerates progression of the cell cycle during rat liver regeneration induced by one-third hepatectomy. Journal of Pharmacology and Experimental Therapeutics. 2009; **331**:122-132

[38] Fung TK, Siu WY, Yam CH, Lau A, Poon RY. Cyclin F is degraded during G2-M by mechanisms fundamentally different from other cyclins. Journal of Biological Chemistry. 2002;**277**: 35140-35149

[39] Ertosun MG, Hapil FZ, Osman Nidai O. E2F1 transcription factor and its impact on growth factor and cytokine signaling. Cytokine and Growth Factor Reviews. 2016;**31**:17-25

[40] Bellan M, Castello LM, Pirisi M. Candidate biomarkers of liver fibrosis: A concise, pathophysiology-oriented Review. Journal of Clinical and Translational Hepatology. 2018;**6**: 317-325

[41] Fukushima T, Uchiyama S, Tanaka H, Kataoka H. Hepatocyte growth factor activator: A proteinase linking tissue injury with repair. International Journal of Molecular Sciences. 2018;**19**(11):3435

[42] Heymann F, Tacke F. Immunology in the liver—From homeostasis to disease. Nature Reviews. Gastroenterology and Hepatology. 2016; **13**:88-110

[43] Pellicoro A, Ramachandran P, Iredale JP, Fallowfield JA. Liver fibrosis and repair: Immune regulation of wound healing in a solid organ. Nature Reviews. Immunology. 2014;**14**:181-194

[44] Mallat A, Lotersztajn S. Cellular mechanisms of tissue fibrosis. 5. Novel insights into liver fibrosis. American Journal of Physiology. Cell Physiology. 2013;**305**:C789-C799

[45] Tacke F, Luedde T, Trautwein C. Inflammatory pathways in liver

homeostasis and liver injury. Clinical Reviews in Allergy and Immunology. 2009;**36**:4-12

[46] Muriel P, Escobar Y. Kupffer cells are responsible for liver cirrhosis induced by carbon tetrachloride. Journal of Applied Toxicology. 2003;**23**:103-108

[47] Edwards MJ, Keller BJ, Kauffman FC, Thurman RG. The involvement of Kupffer cells in carbon tetrachloride toxicity. Toxicology and Applied Pharmacology. 1993;**119**:275-279

[48] Dixon LJ, Barnes M, Tang H, Pritchard MT, Nagy LE. Kupffer cells in the liver. Comprehensive Physiology. 2013;**3**:785-797

[49] Ramachandran P, Iredale JP. Macrophages: Central regulators of hepatic fibrogenesis and fibrosis resolution. Journal of Hepatology. 2012; **56**:1417-1419

[50] Wan J, Benkdane M, Teixeira-Clerc F, Bonnafous S, Louvet A, Lafdil F, et al. M2 Kupffer cells promote M1 Kupffer cell apoptosis: A protective mechanism against alcoholic and nonalcoholic fatty liver disease. Hepatology. 2014;**59**: 130-142

[51] Hasko G, Cronstein B. Regulation of inflammation by adenosine. Frontiers in Immunology. 2013;**4**:85

[52] Kolios G, Valatas V, Kouroumalis E. Role of Kupffer cells in the pathogenesis of liver disease. World Journal of Gastroenterology. 2006;**12**:7413-7420

[53] Luckey SW, Petersen DR. Activation of Kupffer cells during the course of carbon tetrachloride-induced liver injury and fibrosis in rats. Experimental and Molecular Pathology. 2001;**71**:226-240

[54] Ramadori G, Armbrust T. Cytokines in the liver. European Journal of Gastroenterology and Hepatology. 2001; **13**:777-784

[55] Diehl AM. Cytokine regulation of liver injury and repair. Immunological Reviews. 2000;**174**:160-171

[56] Hsieh HG, Huang HC, Lee FY, Chan CY, Lee JY, Lee SD. Kinetics of cytokine expression in cirrhotic rats. Journal of the Chinese Medical Association. 2011; **74**:385-393

[57] Llorent L, Richaud-Patin Y, Alcocer-Castillejos N, Ruiz-Soto R, Mercado MA, Orozco H, et al. Cytokine gene expression in cirrhotic and non-cirrhotic human liver. Journal of Hepatology. 1996;**24**:555-563

[58] Laskin DL, Laskin JD. Role of macrophages and inflammatory mediators in chemically induced toxicity. Toxicology. 2001;**160**:111-118

[59] Traves PG, Luque A, Hortelano S. Macrophages, inflammation, and tumor suppressors: ARF, a new player in the game. Mediators of Inflammation. 2012; **2012**:568783

[60] Gordon S. Alternative activation of macrophages. Nature Reviews. Immunology. 2003;**3**:23-35

[61] Kropf P, Fuentes JM, Fahnrich E, Arpa L, Herath S, Weber V, et al. Arginase and polyamine synthesis are key factors in the regulation of experimental leishmaniasis in vivo. FASEB Journal. 2005;**19**:1000-1002

[62] Tsunawaki S, Sporn M, Ding A, Nathan C. Deactivation of macrophages by transforming growth factor-beta. Nature. 1988;**334**:260-262

[63] Pérez-Cabeza-de-Vaca R. "Efecto del hepatoprotector IFC-305 en las células de Kupffer en el modelo experimental de cirrosis inducida por CCl_4," Maestría en Ciencias Bioquímicas, Biología Celular y Desarrollo. Instituto de Fisiología Celular: Universidad Nacional Autónoma de México, México; 2012

[64] Perez-Cabeza de Vaca R, Dominguez-Lopez M, Guerrero-Celis N, Rodriguez-Aguilera JR, Chagoya de Sanchez V. Inflammation is regulated by the adenosine derivative molecule, IFC-305, during reversion of cirrhosis in a CCl4 rat model. International Immunopharmacology. 2018;**54**:12-23

[65] Tsuchida T, Friedman SL. Mechanisms of hepatic stellate cell activation. Nature Reviews. Gastroenterology and Hepatology. 2017; **14**:397-411

[66] Velasco-Loyden G, Perez-Carreon JI, Aguero JF, Romero PC, Vidrio-Gomez S, Martinez-Perez L, et al. Prevention of in vitro hepatic stellate cells activation by the adenosine derivative compound IFC305. Biochemical Pharmacology. 2010;**80**: 1690-1699

[67] Schaefer B, Rivas-Estilla AM, Meraz-Cruz N, Reyes-Romero MA, Hernandez-Nazara ZH, Dominguez-Rosales JA, et al. Reciprocal modulation of matrix metalloproteinase-13 and type I collagen genes in rat hepatic stellate cells. The American Journal of Pathology. 2003;**162**:1771-1780

[68] Miyahara T, Schrum L, Rippe R, Xiong S, Yee HF Jr, Motomura K, et al. Peroxisome proliferator-activated receptors and hepatic stellate cell activation. The Journal of Biological Chemistry. 2000;**275**:35715-35722

[69] Hazra S, Xiong S, Wang J, Rippe RA, Krishna V, Chatterjee K, et al. Peroxisome proliferator-activated receptor gamma induces a phenotypic switch from activated to quiescent hepatic stellate cells. The Journal of Biological Chemistry. 2004;**279**: 11392-11401

[70] Yavrom S, Chen L, Xiong S, Wang J, Rippe RA, Tsukamoto H. Peroxisome proliferator-activated receptor gamma suppresses proximal alpha1(I) collagen promoter via inhibition of p300-facilitated NF-I binding to DNA in hepatic stellate cells. The Journal of Biological Chemistry. 2005;**280**: 40650-40659

[71] de Gottardi A, Pazienza V, Pugnale P, Bruttin F, Rubbia-Brandt L, Juge-Aubry CE, et al. Peroxisome proliferator-activated receptor-alpha and -gamma mRNA levels are reduced in chronic hepatitis C with steatosis and genotyp. 3 infection. Alimentary Pharmacology and Therapeutics. 2006; **23**:107-114

[72] Yang L, Chan CC, Kwon OS, Liu S, McGhee J, Stimpson SA, et al. Regulation of peroxisome proliferator-activated receptor-gamma in liver fibrosis. American Journal of Physiology. Gastrointestinal and Liver Physiology. 2006;**291**:G902-G911

[73] Michalopoulos GK. Liver regeneration: Molecular mechanisms of growth control. The FASEB Journal. 1990;**4**:176-187

[74] Hamilton JP. Epigenetics: Principles and practice. Digestive Diseases. 2011; **29**:130-135

[75] Allis CD, Jenuwein T, Reinberg D, Caparros ML. Epigenetics. New York, USA: Cold Spring Harbor Laboratory Press; 2007

[76] Bird A. DNA methylation patterns and epigenetic memory. Genes and Development. 2002;**16**:6-21

[77] Fullgrabe J, Kavanagh E, Joseph B. Histone onco-modifications. Oncogene. 2011;**30**:3391-3403

[78] Klose RJ, Bird AP. Genomic DNA methylation: The mark and its mediators. Trends in Biochemical Sciences. 2006;**31**:89-97

[79] Escamilla-Del-Arenal M, da Rocha ST, Heard E. Evolutionary diversity and developmental regulation of

X-chromosome inactivation. Human Genetics. 2011;**130**:307-327

[80] Kharbanda KK. Role of transmethylation reactions in alcoholic liver disease. World Journal of Gastroenterology. 2007;**13**:4947-4954

[81] Kriaucionis S, Heintz N. The nuclear DNA base 5-hydroxymethylcytosine is present in Purkinje neurons and the brain. Science. 2009;**324**:929-930

[82] Tahiliani M, Koh KP, Shen Y, Pastor WA, Bandukwala H, Brudno Y, et al. Conversion of 5-methylcytosine to 5-hydroxymethylcytosine in mammalian DNA by MLL partner TET1. Science. 2009;**324**:930-935

[83] Bhutani N, Burns DM, Blau HM. DNA demethylation dynamics. Cell. 2011;**146**:866-872

[84] Kohli RM, Zhang Y. TET enzymes, TDG and the dynamics of DNA demethylation. Nature. 2013;**502**: 472-479

[85] Ecsedi S, Rodríguez-Aguilera JR, Hernández-Vargas H. 5-Hydroxymethylcytosine (5hmC), or how to identify your favorite cell. Epigenomes. 2018;**2**(1):3

[86] Mellen M, Ayata P, Dewell S, Kriaucionis S, Heintz N. MeCP2 binds to 5hmC enriched within active genes and accessible chromatin in the nervous system. Cell. 2012;**151**:1417-1430

[87] Chagoya de Sanchez V, Hernandez-Munoz R, Sanchez L, Vidrio S, Yanez L, Suarez J. Twenty-four-hour changes of S-adenosylmethionine, S-adenosylhomocysteine adenosine and their metabolizing enzymes in rat liver; possible physiological significance in phospholipid methylation. The International Journal of Biochemistry. 1991;**23**:1439-1443

[88] Komatsu Y, Waku T, Iwasaki N, Ono W, Yamaguchi C, Yanagisawa J. Global analysis of DNA methylation in early-stage liver fibrosis. BMC Medical Genomics. 2012;**5**:5

[89] Page A, Paoli P, Moran Salvador E, White S, French J, Mann J. Hepatic stellate cell transdifferentiation involves genome-wide remodeling of the DNA methylation landscape. Journal of Hepatology. 2016;**64**:661-673

[90] Arenas-Huertero F, Recillas-Targa F. Chromatin epigenetic modifications in cancer generation. Gaceta Médica de México. 2002;**138**:547-555

[91] Valdes-Quezada C, Arriaga-Canon C, Fonseca-Guzman Y, Guerrero G, Recillas-Targa F. CTCF demarcates chicken embryonic alpha-globin gene autonomous silencing and contributes to adult stage-specific gene expression. Epigenetics. 2013;**8**:827-838

[92] Felsenfeld G, Groudine M. Controlling the double helix. Nature. 2003;**421**:448-453

[93] Yao W, Wang T, Huang F. p300/CBP as a key nutritional sensor for hepatic energy homeostasis and liver fibrosis. BioMed Research International. 2018;**2018**:8168791

[94] Mann J, Chu DC, Maxwell A, Oakley F, Zhu NL, Tsukamoto H, et al. MeCP2 controls an epigenetic pathway that promotes myofibroblast transdifferentiation and fibrosis. Gastroenterology. 2010;**138**:705, 714 e1-714, 714 e4

[95] Bosch FX, Ribes J, Cleries R, Diaz M. Epidemiology of hepatocellular carcinoma. Clinical Liver Disease. 2005; **9**:191-211

[96] The L. GLOBOCAN 2018: Counting the toll of cancer. Lancet. 2018;**392**:985

[97] Marquardt JU, Seo D, Andersen JB, Gillen MC, Kim MS, Conner EA, et al. Sequential transcriptome analysis of

human liver cancer indicates late stage acquisition of malignant traits. Journal of Hepatology. 2014;**60**:346-353

[98] Castelli G, Pelosi E, Testa U. Liver cancer: Molecular characterization, clonal evolution and cancer stem cells. Cancers (Basel). 2017;**9**(9):127

[99] Miyata T, Yamashita YI, Baba Y, Harada K, Yamao T, Umezaki N, et al. Prognostic value of LINE-1 methylation level in 321 patients with primary liver cancer including hepatocellular carcinoma and intrahepatic cholangiocarcinoma. Oncotarget. 2018; **9**:20795-20806

[100] Fan G, Tu Y, Chen C, Sun H, Wan C, Cai X. DNA methylation biomarkers for hepatocellular carcinoma. Cancer Cell International. 2018;**18**:140

[101] Yang H, Liu Y, Bai F, Zhang JY, Ma SH, Liu J, et al. Tumor development is associated with decrease of TET gene expression and 5-methylcytosine hydroxylation. Oncogene. 2013;**32**: 663-669

[102] Li X, Liu Y, Salz T, Hansen KD, Feinberg A. Whole-genome analysis of the methylome and hydroxymethylome in normal and malignant lung and liver. Genome Research. 2016;**26**:1730-1741

[103] Dimitroulis D, Damaskos C, Valsami S, Davakis S, Garmpis N, Spartalis E, et al. From diagnosis to treatment of hepatocellular carcinoma: An epidemic problem for both developed and developing world. World Journal of Gastroenterology. 2017;**23**: 5282-5294

[104] Llovet JM, Schwartz M, Mazzaferro V. Resection and liver transplantation for hepatocellular carcinoma. Seminars in Liver Disease. 2005;**25**:181-200

[105] Nguyen K, Jack K, Sun W. Hepatocellular carcinoma: Past and future of molecular target therapy. Diseases. 2015;**4**(1):1

[106] Deng GL, Zeng S, Shen H. Chemotherapy and target therapy for hepatocellular carcinoma: New advances and challenges. World Journal of Hepatology. 2015;**7**:787-798

[107] Khemlina G, Ikeda S, Kurzrock R. The biology of hepatocellular carcinoma: Implications for genomic and immune therapies. Molecuar Cancer. 2017;**16**:149

[108] Sanoff HK, Chang Y, Lund JL, O'Neil BH, Dusetzina SB. Sorafenib effectiveness in advanced hepatocellular carcinoma. The Oncologist. 2016;**21**: 1113-1120

[109] Velasco-Loyden G, Perez-Martinez L, Vidrio-Gomez S, Perez-Carreon JI, Chagoya de Sanchez V. Cancer chemoprevention by an adenosine derivative in a model of cirrhosis-hepatocellular carcinoma induced by diethylnitrosamine in rats. Tumour Biology. 2017;**39**:1010428317691190

[110] Chavez E, Lozano-Rosas MG, Dominguez-Lopez M, Velasco-Loyden G, Rodriguez-Aguilera JR, Jose-Nunez C, et al. Functional, metabolic, and dynamic mitochondrial changes in the rat cirrhosis-hepatocellular carcinoma model and the protective effect of IFC-305. Journal of Pharmacology and Experimental Therapeutics. 2017;**361** (2):292-302

EL CÁNCER

ES UN CONJUNTO DE ENFERMEDADES RELACIONADAS CON EL PROCESO DE DIVISIÓN CELULAR

Se cree que el médico Hipócrates fué el primero en utilizar el término carcino (referente al cangrejo)

TODOS LOS SERES VIVOS ESTÁN CONFORMADOS POR CÉLULAS

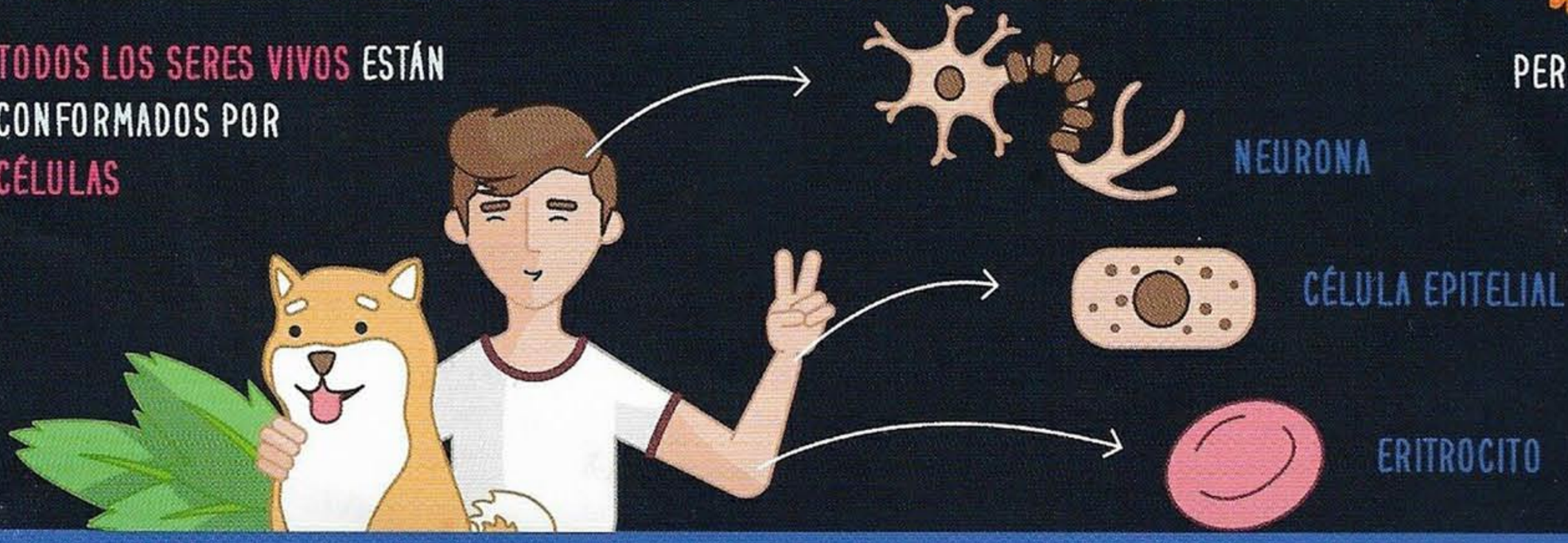

PERO NO TODAS LAS CÉLULAS SON IGUALES Y EXISTEN MUCHAS FORMAS, DE ACUERDO A SU FUNCIÓN

EN MUCHOS TEJIDOS, LAS CÉLULAS SON CAPACES DE DIVIDIRSE PARA SUSTITUIR A CÉLULAS DAÑADAS Y A LAS CÉLULAS QUE MUEREN POR ENVEJECIMIENTO

EN EL CÁNCER SE DESCONTROLA EL PROCESO DE DIVISIÓN CELULAR
NO SE ELIMINAN LAS CÉLULAS DAÑADAS, NO MUEREN LAS CÉLULAS VIEJAS...
Y SE GENERAN CÉLULAS NUEVAS TRANSFORMADAS

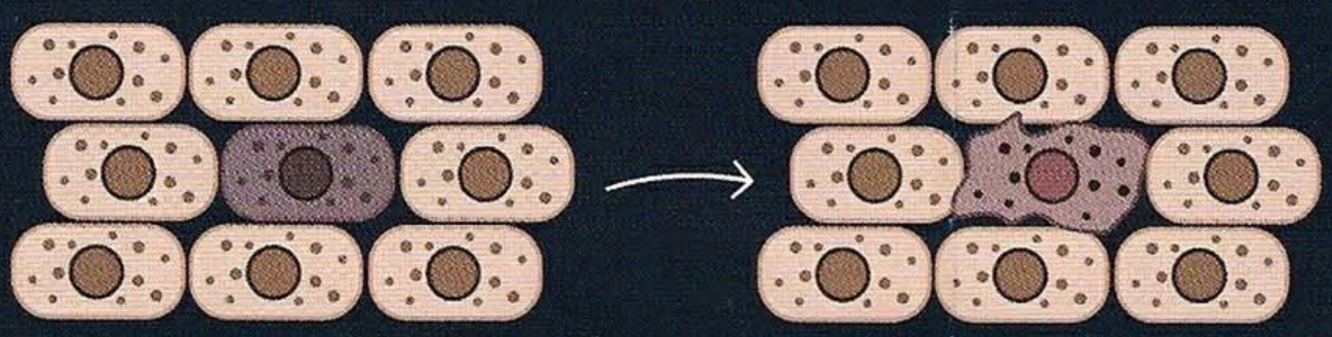

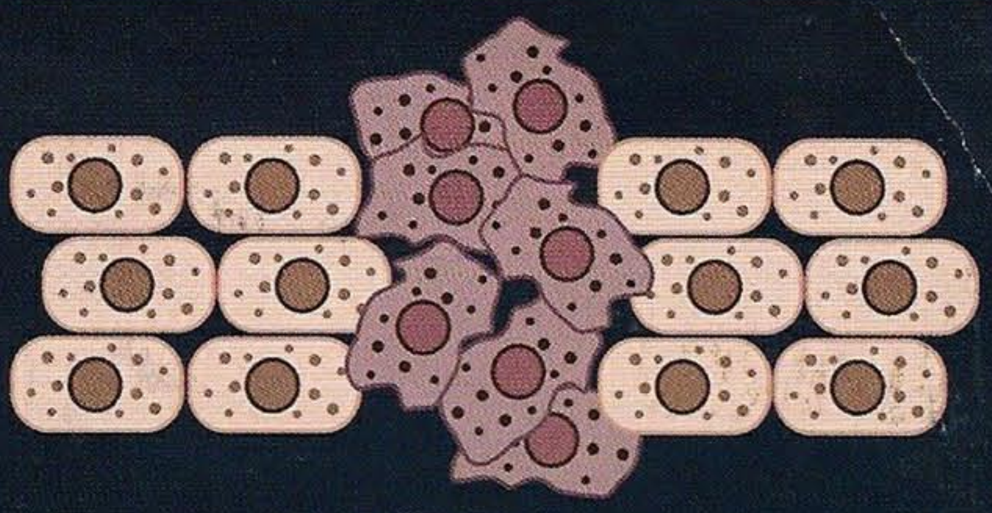

ESTO PRODUCE EL AUMENTO DEL NÚMERO DE CÉLULAS QUE FORMAN MASAS CONOCIDAS COMO TUMORES

LAS CÉLULAS CANCEROSAS TIENEN LA CAPACIDAD PARA INFLUIR SOBRE OTRAS CÉLULAS

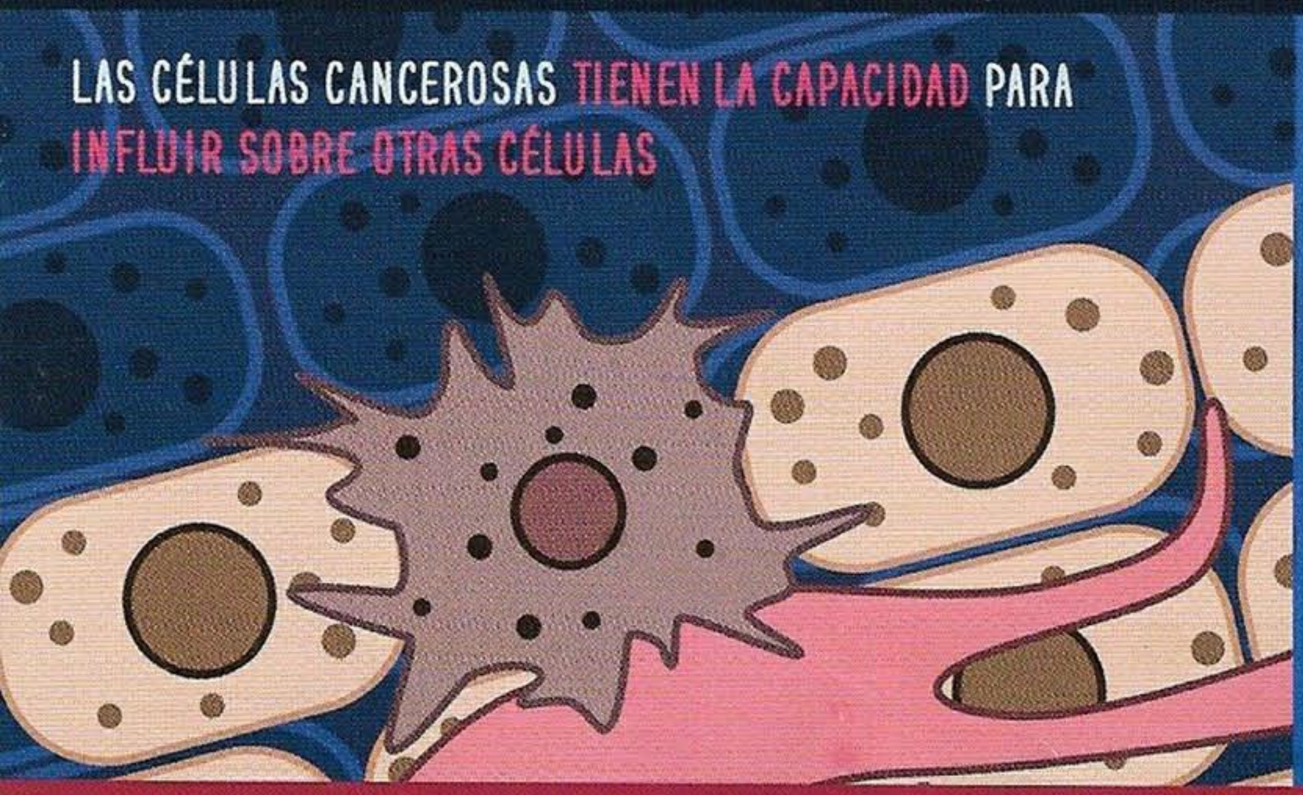

EL CÁNCER SE ORIGINA POR FACTORES GENÉTICOS COMO LOS DAÑOS EN EL ADN (MUTACIONES) PROVOCADOS POR EL AMBIENTE, Y POR FACTORES EPIGENÉTICOS.

LA RADIACIÓN Y SUSTANCIAS TOXICAS FAVORECEN EL ORIGEN DEL MISMO

¿CÓMO PREVENIR?

CONOCE TU CUERPO

EVITA LA EXPOSICIÓN A SUSTANCIAS TÓXICAS
CONOCE LOS ANTECEDENTES FAMILIARES SOBRE LAS ENFERMEDADES
REALÍZATE EXÁMENES MÉDICOS DE FORMA PERIÓDICA
PON ATENCIÓN A SÍNTOMAS COMO LA PÉRDIDA DE PESO DE MANERA INEXPLICABLE O ALGUNOS OTROS MALESTARES

ETAPAS DEL TUMOR

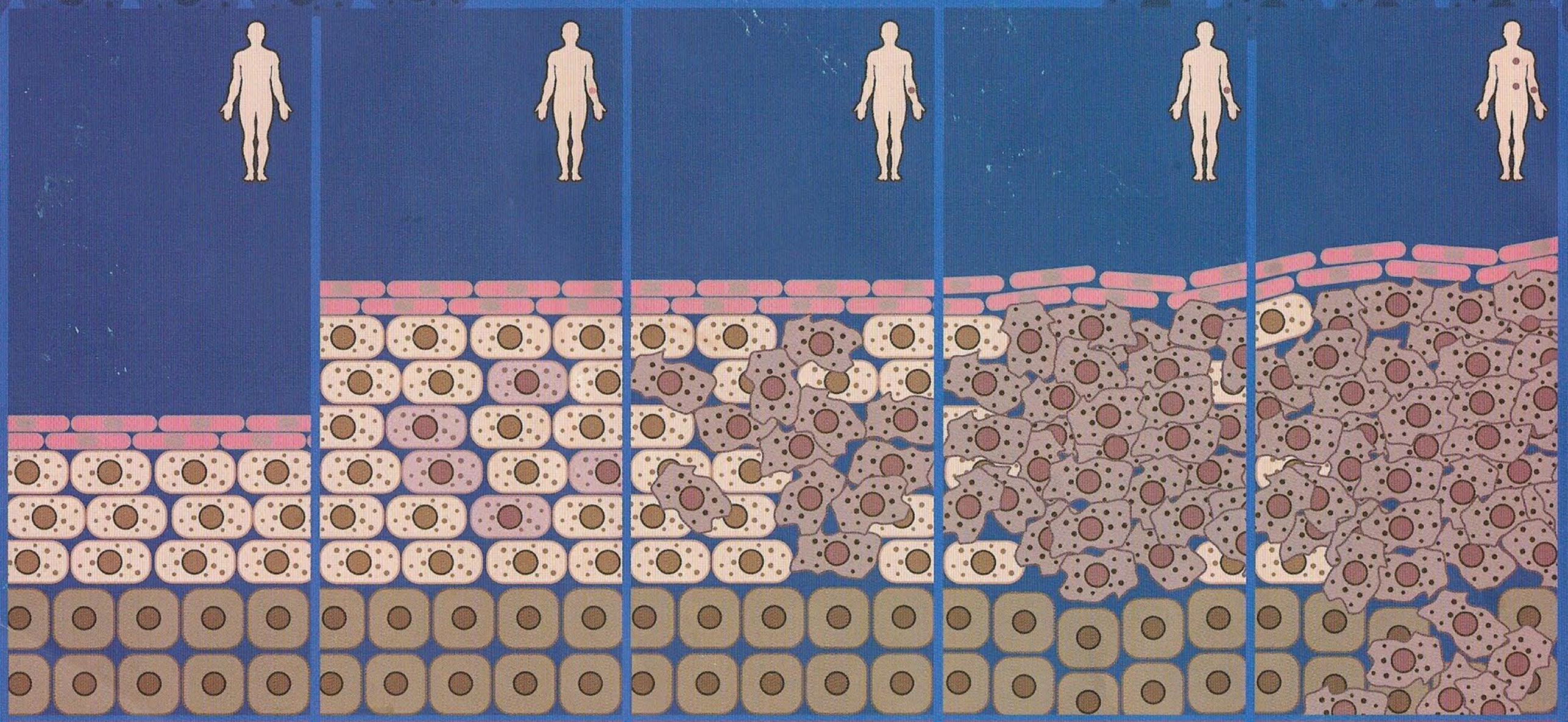

CÉLULAS DE ASPECTO NORMAL

HIPERPLASIA

AUMENTO EN EL NÚMERO DE DIVISIONES CELULARES PERO CON UN ASPECTONORMAL

DISPLASIA

ACUMULACIÓN DE CÉLULAS ADICIONALES, EXISTEN CAMBIOS EVIDENTES

CÁNCER

PROCESO DESMESURADO DE PROLIFERACIÓN DE CÉLULAS CLONALES TRANSFORMADAS

METÁSTASIS

DISEMINACIÓN DE CÉLULAS A LOS TEJIDOS PRÓXIMOS

Instituto de Fisiología Celular, UNAM

Universidad Nacional Autónoma de México
Instituto de Fisiología Celular

Circuito Exterior s/n Ciudad Universitaria,
Coyoacán, 04510 México D.F.

Fax (52) (55) 5616-2282
contacto@ifc.unam.mx
www.ifc.unam.mx

IFC_UNAM

Instituto de Fisiología Celular

Ilustración y Diseño: Eloy Tapia

Redacción: Luz Lazos , Leslie Reyes y Jesús Rafael Rodríguez